Université de Toulouse

THÈSE

En vue de l'obtention du

DOCTORAT DE L'UNIVERSITÉ DE TOULOUSE

Délivré par :

Institut Supérieur de l'Aéronautique et de l'Espace (ISAE)

Présentée et soutenue par :
Vincent BOUSSEMART

le lundi 22 avril 2013

Titre :

Bénéfices de la communication inter-protocoles au niveau applicatif et des ressources pour contrôler les interférences dans les communications satellites

-

On the Benefits of Cross-Layer - Assisted Interference, Resource and Application Management in Satellite-Based Communications

---

École doctorale et discipline ou spécialité :

ED MITT : Réseaux, télécom, système et architecture

Unité de recherche :

Équipe d'accueil ISAE-ONERA SCANR et DLR

Directeur(s) de Thèse :

M. José RADZIK (directeur de thèse)
M. Erich LUTZ (co-directeur de thèse)

Jury :

M. Emmanuel BOUTILLON -Rapporteur
Mme. Maryline HELARD -Examinateur
Mme. Marie-Laure BOUCHERET -Examinateur
M. Matteo BERIOLI -Examinateur
M. Michel BOUSQUET -Examinateur
M. José RADZIK -Directeur de thèse

À tous ceux qui m'ont soutenu pendant cette période parfois, et même souvent, difficile, et qui ont plus que contribué à obtenir ce résultat, plus particulièrement à mes parents Claudine *et* Robert Boussemart*, ma soeur* Virginie*, ainsi qu'à tous les* amis *et* collègues *qui m'ont entouré.*

Abstract

The aim of this Ph.D. work is to investigate the resource management optimisations that can be carried out in the return-link of interference-limited multi-beam satellite systems. Since multi-beam satellite systems can be seen as virtual multiple-input - multiple-output (MIMO) systems, different signal processing techniques can be taken into account so as to improve the system throughput. This Ph.D. focuses on the interference that the users located in different beams generate towards each other, when transmitting data at the same time and on the same frequency. This kind of impairment is also known as co-channel interference (CCI). The number of frequencies (*colours*) present in the satellite system rules the overall bandwidth and therefore the system capacity. On the one hand, when the number of colours becomes low, e.g. considering the particular case of one colour for universal/full frequency reuse, the level of inter-user interference increases dramatically but, on the other hand, the bandwidth available in each beam gets higher. Hence there is a trade off between the number of colours and the level of co-channel interference. Taking this as a reference scenario, the influence of the satellite channel is first practically studied by analysing the uncoded bit error rate (BER) obtained through state-of-the-art interference cancellation (IC) techniques. Furthermore, taking into account the gains achieved using full frequency reuse together with successive interference cancellation (SIC), the Ph.D. moves towards an information theory direction and investigates the impact of the number of colours on the achievable sum rates. The same MIMO-inspired multi-user detection (MUD) schemes are then used to derive the per-user rates, and in particular the max-min criterion is applied to the user rates showing that an improvement of the level of fairness can be achieved between users. The different outcomes of these investigations are used to optimise the resource management where schedule plans are designed specifically to increase the lowest user rates. However, scheduling for large scale MIMO systems, as in the return-links of satellite communications, represents a challenging task, since the search space is prohibitive large. For this reason this Ph.D. also investigates low complexity heuristic algorithms based on graph theory with the aim of finding sub-optimal schedules to better balance the rates that could be offered to the served users. Finally, the number of spot beams and the number of users considered for scheduling are studied so as to propose new algorithms aiming to satisfy quality of service (QoS) constraints.

Contents

Abstract **iii**

Acknowledgment **xi**

Introduction **xiii**

1 Satellite Scenario and Channel Model **1**

1.1 Satellite 2

1.1.1 System Scenario 2

1.1.2 Main Impairments 5

1.1.3 Sources of Interference 6

1.1.4 Sub-Scenarios 13

1.1.5 Beam Pattern Computation 15

1.1.6 Example of Link Budget for the Return-Link 17

1.2 Channel Model 22

1.2.1 Introduction to Simple Input-Output Systems 22

1.2.2 Multiple-Input and Multiple-Output Concept 24

1.2.3 Transmission Block Diagram 27

1.2.4 Absolute Value of the Channel Coefficients 28

1.2.5 Phase of the Channel Coefficients 30

1.3 Summary 31

2 Practical Analysis of the Satellite Channel: Uncoded Bit Error Rate **33**

2.1 Processing of the Received Signal 34

2.1.1 Conventional Receiver 34

2.1.2 Zero Forcing Equaliser 34

2.1.3 Minimum Mean Square Error Operation 35
2.1.4 Optimal Successive Interference Cancellation 36
2.1.5 Successive Interference Cancellation with Maximal Ratio Combining . 37
2.2 Performance Analysis 40
2.2.1 Rayleigh Channel - Validation of the Receivers 40
2.2.2 Satellite Channel - 2×2 System 42
2.2.3 Satellite Channel with Full Frequency Reuse - 7×7 System 47
2.2.4 Satellite Channel with Three Colours - 7×7 System 51
2.2.5 Full Frequency Reuse versus Three Colours 51
2.3 Summary 53

3 Theoretical Analysis of the Satellite Channel: Achievable Rate 55
3.1 Achievable Sum Rate 56
3.1.1 Single-Input - Single-Output (SISO) 56
3.1.2 Single-Input - Multiple-Output (SIMO) 57
3.1.3 Multiple-Input - Multiple-Output (MIMO) 59
3.1.4 Impact of the Phase 62
3.1.5 Impact of the Cluster Size 63
3.1.6 Evaluations with Full Frequency Reuse and Three Colours 64
3.1.7 Analysis of the Sum Rate Results for one and three Colours 66
3.2 Achievable Per-User Rate 69
3.2.1 Successive Interference Cancellation 69
3.2.2 Impact of the Ordering in the Interference Cancellation Process 71
3.2.3 Max-Min Criterion - Maximisation of the Minimum Rate 74
3.2.4 Performance Analysis of the Ordering 80
3.2.5 Statistics on the Single User Rates 82
3.3 Summary 88

4 Scheduling 91
4.1 Basics 92
4.1.1 Introduction 92
4.1.2 Number of Possible Allocations 93
4.1.3 Scheduling and Channel Matrices 95
4.1.4 Impact of Scheduling on the Sum Rate 96
4.2 Invariance of the Sum Rate to Scheduling 97

4.2.1 Scheduling with two Users per Beam 97
4.2.2 Scheduling with three Users per Beam 102
4.2.3 Scheduling with M Users per Beam 104
4.3 Search Algorithms 105
4.3.1 Search over All Possible Allocations 105
4.3.2 Search over All Possible Combinations - B-partite Graph Approach . 107
4.3.3 The Max-Min Criterion - Maximisation of the Minimum Rate 108
4.4 Scheduling Algorithms for Large Scale Systems 112
4.4.1 "Viterbi-Like Algorithm" 112
4.4.2 "Geo-Like Algorithm" 113
4.5 Performance Evaluation of the Different Algorithms 115
4.5.1 Introduction 115
4.5.2 Results 117
4.6 Impact of Scheduling on the Uncoded Bit Error Rate 122
4.6.1 Principle and Process 122
4.6.2 Optimal Allocation 123
4.6.3 Performance Analysis 124
4.7 Summary 126

5 Scheduling with Quality of Service Constraints 129
5.1 Impact of the Number of Beams and Users per Beam 130
5.1.1 Impact of the System Size 130
5.1.2 Impact of the Scheduling Depth 132
5.2 Rate Constraints 133
5.2.1 Free Slot Assignment Concept 134
5.2.2 "Smart Free Slot Assignment Scheduling Algorithm" 137
5.2.3 Performance Analysis 140
5.3 Time Constraints 143
5.3.1 Time Concept with Scheduling 143
5.3.2 "Normal Window Scheduling Algorithm" 144
5.3.3 "Advanced Window Scheduling Algorithm" 147
5.3.4 Performance Analysis 153
5.4 Rate and Time Constraints 155
5.4.1 Principle of the Hybrid Algorithm 155
5.4.2 Performance Analysis 155

5.5 Summary 157

6 Conclusions **159**

Bibliography **163**

List of Figures **177**

List of Tables **180**

A Acronyms and Notations **181**

A.1 Acronyms 181

A.2 Notations 185

A.2.1 Scalars, Vectors and Matrices 185

A.2.2 Operators 185

A.2.3 List of Variables 185

B Useful Mathematical Background **191**

B.1 Mathematical Properties 191

B.1.1 Logarithm 191

B.1.2 Error Function 192

B.1.3 Determinant 192

B.1.4 Trace 193

B.1.5 Expectation 194

B.1.6 Conditional Expectation 195

B.1.7 Hermitian 195

B.2 Mathematical Proofs 195

B.2.1 Trace Derivatives of Real Matrices 196

B.2.2 Trace Derivatives of Complex Matrices 196

C Useful Satellite and Communications Background **201**

C.1 Satellite 202

C.1.1 Beam Border 202

C.1.2 Radiation Pattern 226

C.1.3 Link Budget 233

C.2 Uncoded Bit Error Rate 234

C.2.1 Generation of Vectors and Matrices 234

C.2.2 Theoretical Evaluation of the Error Rate for Phase Shift Modulations 238
C.2.3 Filter Design 245
C.2.4 Simulator Overview and Summary 250
C.2.5 Theoretical Evaluation with Signal Processing 251
C.3 Achievable Rate 255
C.3.1 Considerations 255
C.3.2 Mutual Information 257
C.3.3 Constrained-Capacity 261
C.4 Scheduling 267
C.4.1 Performance of Scheduling with and without Ordering 267
C.4.2 Search Algorithms - Allocations versus Combinations 269
C.4.3 Summary and Dependencies of the Scheduling Algorithms 273

D Additional Side Information 275
D.1 List of Publications, Patents, and Other(s) 275
D.1.1 Conference and Journal Paper(s) 275
D.1.2 Workshops, Summer School and Other(s) 276
D.1.3 Patent(s) 276
D.2 Erratum 276

Acknowledgment

The author would like to gratefully thank his **colleagues** from the **Deutsches Zentrum für Luft- und Raumfahrt (DLR, German Aerospace Centre)**:

– Prof.-Dr. Erich Lutz for his involvement and his support during the Ph.D.,
– Dr. Matteo Berioli for supervising this Ph.D., all the help, the motivation, and his ideas,
– Dr. Francesco Rosetto for all the hints, the explanations, and his availability,
– Dr. Tomaso de Cola for his incredible expertise in mathematics, more particularly in solving integrals (and enjoying it),
– Hartmut Brandt for his knowledge in many, many areas and his personal support,
– Francisco Lazaro Blasco for his knowledge in information theory and the useful discussions we had,
– Zoltan Katona for his expertise in the thermodynamic temperature of satellites,
– Federico Clazzer for his help about cross-polarisation interference,
– Dr. Gianluigi Liva for his expertise in coding and in information theory,
– Dr. Andrea Munari for his help providing and using this LaTeX template,
– and all other colleagues who contributed in making all these working days at DLR more pleasant...

The author would also like to thank the following **persons** working at the **Institut Supérieur de l'Aéronautique et de l'Espace (ISAE)**:

– Dr. José Radzik for accepting supervising this Ph.D.,
– Prof. Michel Bousquet for all the efforts making this Ph.D. between ISAE and DLR possible,
– and all other very nice people like Maryse Herbillon for making administrative procedures between France and Germany easier.

The author thanks the **student Loris Marini**, from the University of Rome "Tor Vergata", for the precious help, involvement, time and effort spent on this topic. The author supervised

this student between mid of August 2011 and mid of April 2012 in the framework of a Master Thesis [Mar12].

Last but not least, a **special thank** to Dr.-Ing. **Nicolas Courville** and his wife **Jessica**, who warmly motivated the author for starting this Ph.D. thesis.

Introduction

Broadband satellite communications enable to cover wide areas over the Earth and therefore to embrace large population densities. This type of communications allows providing access to various services where terrestrial infrastructures are missing for instance because they are not yet deployed, or simply because such infrastructures cannot be installed due to some geographical constraints. In the past the use of satellite communications was not really affordable for public consumers mainly because of the high costs related to the contract, the equipment, the bandwidth and the ratio price over amount of data which was relatively high for instance. Nowadays technological evolutions and new techniques available in satellite communications standards result in cheaper and smaller terminals, higher datarates, and improved Quality of Service (QoS). Hence satellite communications become more and more competitive when compared to conventional terrestrial systems; for instance Internet is now accessible via satellite for almost the same price and conditions as the well-known and spread terrestrial Digital Subscriber Line (DSL). For the different aforementioned reasons, broadband satellite communications are nowadays more attractive and competitive than ever.

Satellite communication systems are actually constrained by the power available onboard the satellite and the overall system bandwidth [MaBo02]. Very first satellite systems were technologically simple and equipped with a single antenna, commonly called beam, designed to cover all users. However such systems had very low system throughput due to the reduced gain of user multiplexing but also of the antenna. Modern satellite systems use the so-called multi-beam technique, where the covered area is divided into radio cells, in order to efficiently serve a large number of users [LuWeJa00]. For this reason the satellite beam footprints, and also the overall system concept, are often compared to conventional terrestrial cellular networks. High frequency bands allow reaching relatively high datarates in multi-beam satellite systems, in the magnitude of megabit/gigabit per second, but small wavelengths suffer from various impairments, mainly due to atmospheric effects and also to different sources of interference. By 2020 horizon, very high capacity broadband satellites

are expected to reach even higher datarate magnitudes and are called “Terabit Satellites” [Gay09], [MEGAAH11]. The migration towards such systems constitutes a big challenge for satellite designers, satellite operators and also for what concerns the development of new satellite communications standards. The aim is to provide more and more bandwidth, higher system efficiency, and also, last but not least, to guarantee sufficient QoS levels to consumers.

This Philosophiae Doctor (Ph.D.) thesis focuses on geostationary (GEO, [Clar45]) multi-beam satellite systems with transparent payload in a star network topology, which are widely used for providing interactive Internet services. In such multi-beam satellite systems the resource space is often discretised in frequency and time slots. The slotted structure of the resource frequency leads to the fact that the system offers parallel channels over which the signals of the users have to be distributed. The reuse of signal frequencies in different beams, however, causes interference such as Co-Channel Interference (CCI).

Current multi-beam satellite systems are impaired by atmospheric conditions. Fade events related to atmospheric disturbances, like clouds and rains, can be counteracted by using fade mitigation techniques (FMTs). The transmission power can be adapted (up-link power control, UPC), a transmission rate different from the nominal one can be selected (dynamic rate assignment, DRA) and/or the modulation and coding (ModCod) can be modified accordingly (adaptive coding and modulation, ACM). These techniques can be implemented in the forward-link, i.e. the link from the gateways towards the satellite terminals, more particularly they are specified in the digital video broadcasting per satellite version 2 (DVB-S2) standard [DVB-S2]. Such techniques are also available in the return-link, i.e. the link from the satellite terminals towards the gateways, as specified in the DVB return channel via satellite version 2 standard (DVB-RCS2) [DVB-RCS2]. The work realised in the framework of this Ph.D. thesis considers the two aforementioned standards as reference.

The purpose of this thesis is to investigate on the limitation of the system due to interference, more particularly to the so-called Co-Channel Interference (CCI), which is directly a consequence of the frequency reuse factor employed in multi-beam satellite systems. Reducing the frequency reuse factor actually permits to increase the overall system bandwidth and consequently the theoretical system capacity, which is of paramount interest, but at the expense of higher interference levels. Multi-beam satellite systems are actually input-output systems equipped with several transmit and receive antennas, and therefore they can realise joint

signal processing and be turned into virtual Multiple-Input and Multiple-Output (MIMO) systems. On the one hand, in the forward-link, which is equivalent to the down-link in terrestrial systems, CCI can be observed when data are transmitted on the same frequency to users located in different beams. Using the MIMO concept, removing this kind of interference at the receiver side, e.g. by using an iterative cancellation approach is not possible, because each user acts as a single receiver, and thus joint decoding of the multiple outputs of the MIMO system is not feasible. For this reason much effort has been made to cancel CCI at the transmitter side, which is not cost-sensitive, e.g. by employing Dirty Paper Coding (DPC) or Tomlinson-Harashima Precoding (THP) [DCMLC07], [PoBeBa09]. However this kind of techniques is difficult to be applied in reality, due to their high complexity, in large scale systems such as multi-beam satellite systems and other joint pre-coding solutions have to be considered [ZCO11-1]. On the other hand, in the return-link, equivalent to the up-link of terrestrial networks, the interference can be cancelled by the entity receiving the users' signals, i.e. the gateway, for which the joint decoding operation is possible, and the complexity is not really a limiting factor. The work presented in this document is exclusively dedicated to this latter point, i.e. to the return-link of multi-beam satellite MIMO systems. It has to be noted that the Internet traffic [Bou05], which is characterised by its high self-similarity (burstiness) [BoGr05], increases considerably. More particularly the data asymmetry between upload and download, respectively return-link and forward-link in a transparent multi-beam satellite system, tends to disappear, mainly due to new emerging and bandwidth consuming interactive services. Hence the return-link is expected to be more and more loaded and solutions for optimising the resources in an efficient way, i.e. rapidly and with low complexity, need to be investigated.

The resource allocation for the return-link builds on, for instance, multi-frequency time-division multiple access (MF-TDMA). In such allocation scheme, a user (satellite terminal) receives in each time frame resources corresponding to a frequency band (carrier) and a time slot. State-of-the art solutions for scheduling users in frequency and time are based on heuristic approaches, since the search of the optimal scheduling is computationally unfeasible. In this thesis a design based on the joint optimisation of the physical layer and the scheduler is carried out, where the scheduler allocates the time-frequency slots to different users located in different beams so as to reduce the level of interference. Additionally, physical layer techniques which are practically implementable and new sub-optimal solutions capable of dealing with large number of users and beams are developed. The purpose of this work is therefore

to optimise the resource management in the return-link of interference-limited multi-beam satellite MIMO systems so as to reduce the level of co-channel interference and to improve the performance of the interference cancellation process at the receiver.

This document is organised as follows. The satellite scenario considered in this study and the corresponding channel model are detailed in Chapter 1. In Chapter 2 the impact of the satellite channel on state-of-the-art receivers, including multi-user detection (MUD), and also on a receiver based on a new heuristic interference cancellation (IC) algorithm, is practically investigated using a bit error rate simulator. Tools provided by information theory are then used in Chapter 3, still considering the multi-beam satellite system as a virtual multiple-input multiple-output (MIMO) system. In this Chapter the total ergodic capacity, i.e. the achievable sum rate, is derived for different input-output (IO) systems, and successive interference cancellation (SIC) is used to derive the achievable per-user rates. In Chapter 4 the notion of scheduling is introduced, search and scheduling algorithms including novel approaches, targeting the maximisation of the minimum per-user rates, and improving the overall level of fairness between users, are described and their performance evaluated. Based on previous results, new scheduling algorithms taking into account QoS constraints are presented in Chapter 5, including the analysis of both simulation results and computational complexity. Finally the conclusions are given in Chapter 6, summarising the main contributions provided by this Ph.D. thesis.

Chapter 1

Satellite Scenario and Channel Model

This chapter is dedicated to the description of the satellite scenario and of the channel model.

The first section presents the necessary background related to broadband satellite communications and also details the different sub-scenarios taken into account in this work. The sub-scenarios are selected so that they are very close to reality and are reasonable enough to constitute a solid framework to the addressed topics. Of course the work presented in this document is not strictly related to these particular scenarios and can be generalised to many other cases. The purpose of this section is mainly to describe step by step the overall system scenario, the impairments, and the sources of interference. It also gives an example of link budget computation in order to better understand the different hypotheses taken into account in this thesis.

The second section introduces the basics of different Input-Output (IO) systems and explains why multi-beam satellite systems can be considered as virtual Multiple-Input and Multiple-Output (MIMO) systems. More particularly the correlation between the return-link of multi-beam satellite systems and MIMO Multiple Access Channel (MAC) is addressed. This section describes the satellite channel model, which is based on a realistic transmission block diagram, and also how the absolute value and the phase of the channel coefficients are computed. This section therefore explains how the channel matrix $\boldsymbol{H}$ is generated, based on realistic beam patterns, and is of utmost importance since all other investigations are based on the channel model described in this chapter.

1.1 Satellite

Satellite-based communications offer an efficient coverage of large and sparsely populated areas and are constrained by several criteria. A satellite is limited in terms of resources, mainly in terms of power and bandwidth available [MaBo02]. Therefore a satellite is limited in throughput. Another typical constraint is the Round-Trip-Time (RTT) which influences the end-to-end delay perceived during transmissions. The RTT is in the magnitude of half a second ($\sim$ 500 ms) with Geostationary (GEO) satellites for instance. Finally satellite-based communications experience high service costs even if nowadays they are becoming cheaper and thus more attractive.

1.1.1 System Scenario

Multi-Beam Concept

Very first satellite systems were technologically simple and were equipped with a single beam covering all users. The single user throughput of the system was very low due to the necessity to perform orthogonal multiplexing of all users and also because of the low gain of the satellite antenna. Modern satellite systems are built with higher power available on board, larger antennas and also provide more bandwidth at higher frequency bands. Modern satellites use many antenna beams which permits to confine the transmit power to smaller areas and therefore to reach higher power efficiency. For this reason modern satellite systems using several antenna beams are called "multi-beam satellite systems" and they are part of the baseline scenario.

Orbit and Topology

We consider as baseline scenario Geostationary (GEO) satellites (altitude of 35 786 km) supporting the transparent star network topology [MaBo02]. The term "star" refers to a gateway which is used to concentrate data coming from/going to the satellite. A satellite star network is generally composed of satellite terminals and one or several gateways which can also play the role of Network Control Centre (NCC) [1]. An example of transparent star network topology is shown in Fig. 1.1.

1. Generally both gateway and NCC are considered as two different entities [DVB-RCS2-P1].

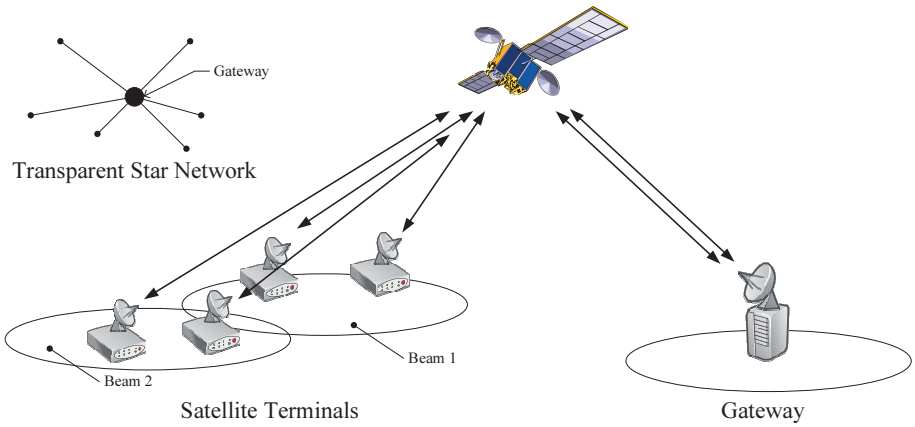


Figure 1.1. *Example of transparent star network topology in a satellite system.*

Links

The star network topology is characterised by the following links:

- From the Gateway to the Satellite Terminal (ST), the so-called Forward-Link (FL) is sub-divided in:
  - The Forward Up-Link (FUL) from the Gateway to the satellite,
  - The Forward Down-Link (FDL) from the satellite to the ST.
- From the ST to the Gateway, the so-called Return-Link (RL) is sub-divided in:
  - The Return Up-Link (RUL) from the ST to the satellite,
  - The Return Down-Link (RDL) from the satellite to the Gateway.
- Between the Gateway and the satellite the link is also called "Feeder Link",
- Between the satellite and the ST the link is also called "User Link".

The different terms described in this paragraph are summarised by Fig. 1.2 and will be used from now on in this document.

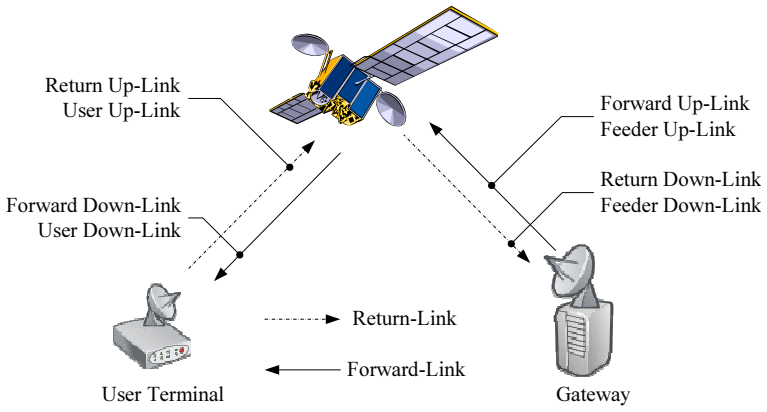


Figure 1.2. *Definition of the satellite links considered in this scenario.*

The frequencies of the links are in the range 20 - 30 GHz and correspond to the Ka-band, widely used in satellite communications and offering high datarates.

This thesis focuses more particularly on the return-link, even if in some sections the forward-link may be considered/mentioned for the sake of a better understanding. Therefore, unless explicitly stated, the Return-Link (RL) constitutes the link of interest in the following.

Cluster Size

The bandwidth available in a multi-beam satellite systems can be split into different frequency bands such that all beams do not necessarily use the same frequency range. The number of different frequency bands, which is defined by K, corresponds to the so-called cluster size [LuWeJa00]. The footprint of the beams can be considered, in an abstracted way, as hexagons like in conventional cellular networks and a colour can be attributed to each of the K frequency bands. The frequency allocation is realised in such a way that adjacent beams do not employ the same frequency and therefore such that the distance between beams using the same frequency increases together with K. An example is given by Fig. 1.3 in which cluster sizes $K = 3$ (left) and $K = 4$ (right) are shown.

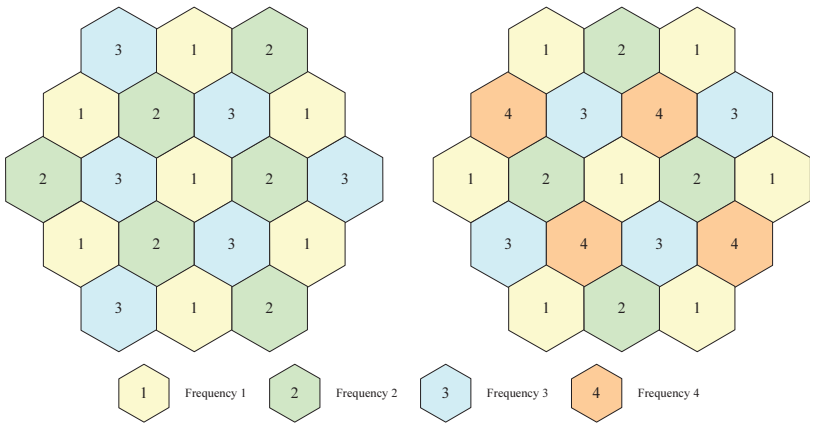


Figure 1.3. *Principle of frequency allocation in beams with cluster size three ($K = 3$, left) and cluster size four ($K = 4$, right).*

The number of possible cluster sizes is [LuWeJa00]:

$$K = i^2 + i\,j + j^2 \tag{1.1}$$

where i and j are integers greater or equal to zero. Expression (1.1) is actually derived from the way the frequency allocation is performed: for this reason cluster sizes such as 2, 5, 6, etc. cannot exist.

Therefore the cluster size K also refers to the number of colours employed in the multi-beam satellite system and in this document it also corresponds to the so-called "frequency reuse factor" [2].

1.1.2 Main Impairments

Different sources contribute to the impairment of the signal within the links. On the one hand bad weather conditions like rain events will have a dramatic impact when using Ka-band. Such events create fluctuation of the signal level (fading events) at a large time scale whereas scintillation, due to the atmosphere, create events at very small time scale (fast fluctuations). Finally the free space loss (FSL), which corresponds to the attenuation of the signal due to the distance between the satellite and the earth, is the highest loss component in the link budget of a satellite system.

Fade Mitigation Techniques

Impairments due to atmospheric events can be counteracted using so-called Fade Mitigation Techniques (FMTs). The purpose is to evaluate the signal level through different mechanisms and to detect when a fading event occurs and also when a fading event disappears. FMTs can be used in both the forward- and the return-links, using the Digital Video Broadcasting via Satellite version 2 (DVB-S2) and Digital Video Broadcasting - Return Channel via Satellite version 2 (DVB-RCS2) standards, respectively [DVB-S2], [DVB-RCS2]. These techniques are already well investigated and aim at adapting the air interface (physical layer) properties according to current channel conditions.

In the return-link the transmit power of the satellite terminals can be modified so that the power received at the satellite remains the same, and therefore, such that the link budget is closed. This technique is called Up-link Power Control (UPC). It has to be remarked that such technique can be implemented/used in a way the power spectral density at the input of the satellite remains the same. For this reason, even in case of a small fade event, if the control loop is correctly implemented and fast enough, the signal level received from a given terminal by the satellite remains almost the same as in clear-sky conditions. When looking at interference, more particularly at Co-Channel Interference (CCI), this implies that the satellite antennas perceive the same interference level even if the transmission power of the terminal

2. This analogy is widely used in literature even if the real definition of the frequency reuse factor should be the one given by [LuWeJa00].

was adjusted. Another technique consists into adapting the transmission rate of the terminal such that the carrier bandwidth is not the same, and this therefore depends on the terminal capabilities. Actually with the same transmission power, this will influence the overall link budget (please refer to Section 1.1.6 for more details). This technique is referred as Dynamic Rate Assignment (DRA). Finally the most popular Fade Mitigation Technique (FMT) consists into selecting the modulation and coding scheme (ModCod) such that to guarantee a given Packet Error Rate (PER) with the current Carrier-to-Noise Ratio (CNR). Changing both modulation and coding impacts the spectral efficiency which is expressed in bit/s/Hz. This latter technique is called Adaptive Coding and Modulation (ACM).

Therefore impairments related to atmospheric events can be controlled using FMTs so that to guarantee a given system availability. Performance analysis realised with a complete satellite system simulator ([BBKNL07], [BoBr08]) has shown the benefit of using ACM in both the forward-link and the return-link of a multi-beam satellite system when compared to Constant Coding and Modulation (CCM) [BoBr09-1], [BoBr09-2]. CCM is actually used in the Digital Video Broadcasting via Satellite (DVB-S) and Digital Video Broadcasting - Return Channel via Satellite (DVB-RCS) standards, respectively [DVB-S], [DVB-RCS].

Interference

In a multi-beam satellite system, the following sources of interference are of interest [MaBo02]:

- Adjacent-Channel Interference (ACI),
- Co-Channel Interference (CCI),
- Cross-Polarisation Channel Interference (CPCI) also called Cross-Polarisation Interference (XPI),
- Inter-Modulation Interference (IMI),
- Inter-Symbol Interference (ISI).

The different sources of interference are described in the next dedicated section (Section 1.1.3) since they constitute the topic of interest in this work.

1.1.3 Sources of Interference

This section presents the different sources of interference which are considered as relevant in satellite communications. There is in principle always interference, of all kind, and all possible combinations; depending on its level an interference may be neglected. In this section the

spectrum of the channels is represented by trapezoidal shapes. In reality the shape of a channel is clearly different but this abstraction is considered for ease of understanding.

Adjacent-Channel Interference

The Adjacent-Channel Interference (ACI) appears in channels which are adjacent in frequency. Typically such interference is present at the beam border if the beams are using adjacent frequency bands and therefore is related to the antenna characteristics. There is also ACI within the beam when two signals are sent in adjacent channels (carriers).

Fig. 1.4 shows an example of carrier organisation involving the presence of adjacent-channel interference. In this example there are three beams such that B_i identifies the i-th beam and the x-axis represents the frequency. As seen the three beams use different frequencies f_1, f_2, and f_3 (center carrier frequencies), therefore the beams do not use the same frequency bands. Each beam supports two sub-carriers, $c_{i,j}$, where i represents the beam identifier (ID), and j the sub-carrier ID within the beam, with identical bandwidths. The shape of the carrier is not perfectly rectangular due to the imperfection of the filter. The filter is actually a raised-cosine filter characterised by the so-called roll-off factor, noted β, and the symbol duration T_s. The carriers are represented with non-vertical lines on the edges due to the roll-factor which is such that $\beta > 0$. The guard band, characterised by the channel spacing coefficient noted α_cs, defines the distance between adjacent carriers or sub-carriers. The guard band can be positive (like within each beam of Fig. 1.4), negative, or even zero (like between beams of Fig. 1.4). On the one hand, the roll-off factor and the guard band are such that within a beam the two sub-carriers do not overlap in theory [3] (for instance $c_{1,1}$ and $c_{1,2}$). Therefore level of ACI can be neglected within the beams. For this reason two users transmitting towards beam B_1, and allocated to each of the two sub-carriers $c_{1,1}$ and $c_{1,2}$, will not really interfere each other. On the other hand, there is no guard bands for the carriers of different beams ($\alpha_\mathrm{cs} = 0$) and this will introduce ACI between adjacent sub-carriers of different beams (for instance between $c_{1,2}$ and $c_{2,1}$) which has to be taken into account. A user allocated in $c_{1,2}$ will generate ACI to the right adjacent sub-carrier present in beam B_2, namely $c_{2,1}$. Reciprocally a user allocated in $c_{2,1}$ will generate ACI to the left adjacent sub-carrier present in beam B_1, namely $c_{1,2}$. The level of interference depends on the geographical position of the users with respect to the beam border, and, as mentioned

3. This is of course not true in reality, the two carriers may overlap but the level of ACI may be negligible.

before, on the characteristics of the antenna.

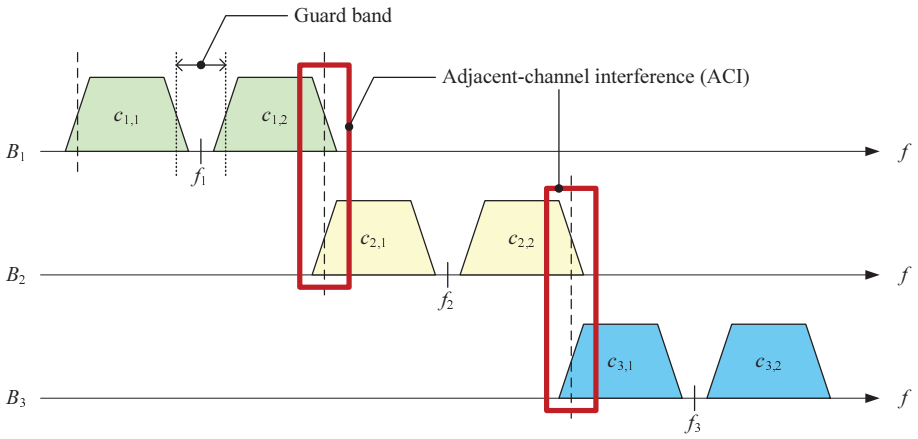


Figure 1.4. *Example of carrier organisation involving adjacent-channel interference.*

The level of ACI is driven by both roll-off factor and guard bands. They can be defined in such a way that ACI can be neglected within the multi-beam satellite system (within the beams and also between the beams). On contrary both parameters can also be adjusted in order to increase the overall bandwidth available, i.e. organising the carriers such that they overlap each other. However doing so increases dramatically the level of ACI and therefore techniques, such as Interference Cancellation (IC), have to be implemented so that to mitigate such kind of impairment [BeGaKa02], [GaVeRi07].

Co-Channel Interference

The Co-Channel Interference (CCI) is directly caused by the non-perfect characteristic of the antennas, more particularly by the presence of side lobes in the radiation pattern. Such interference appears in beams using the same frequency and is thus directly related to the cluster size (please refer to Section 1.1.1 for more details), more particularly to the distance separating beams using the same frequency, which is noted D (the distance D changes according to the the position of the satellite and also to the beam centres coordinates). When focusing on the return-link, CCI appears when two users located in different beams and using the same frequency send their signal simultaneously towards the satellite (Fig. 1.5).

Fig. 1.6 gives an example of carrier organisation which will produce Co-Channel Interference (CCI). The same convention as the one used in the example of Section 1.1.3 is considered. In this particular example all sub-carriers are allocated such that the guard bands are sufficient enough to avoid the presence of ACI both within each beam and also between the

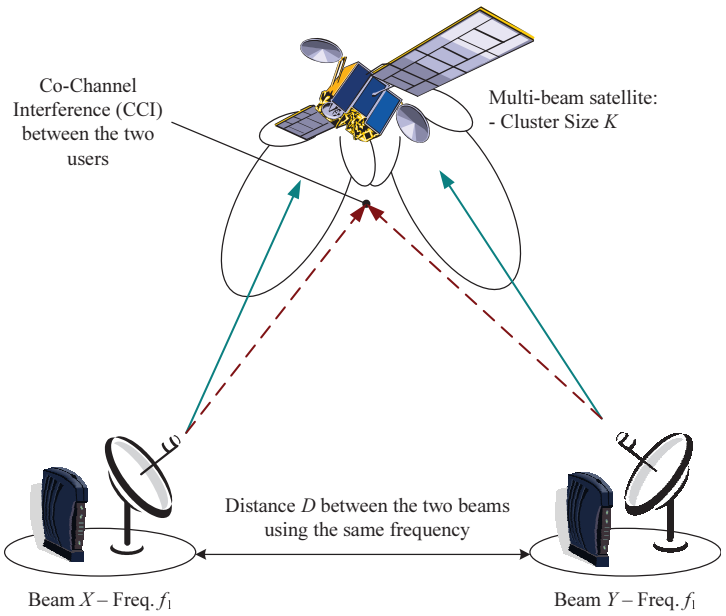


Figure 1.5. *Principle of co-channel interference in the return-link.*

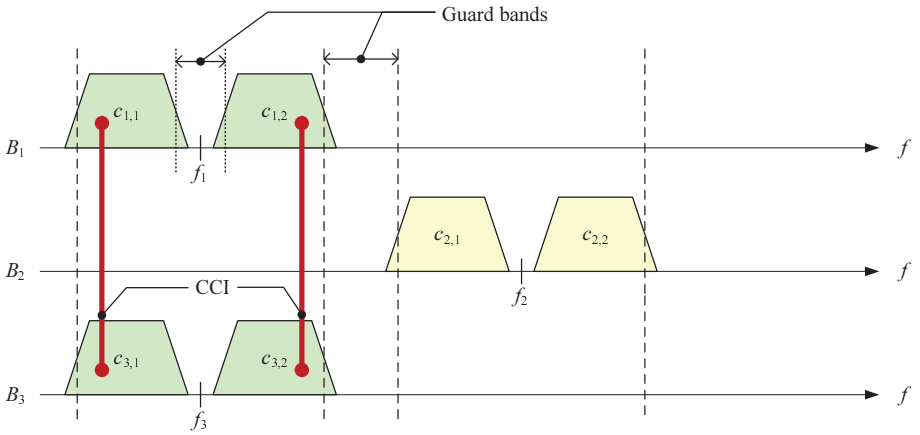


Figure 1.6. *Example of carrier organisation involving co-channel interference.*

beams (the level of ACI is low enough to be neglected). As one can see in Fig. 1.6, both beams B_1 and B_3 use the same frequency band, i.e. $f_1 = f_3$, and more particularly the two sub-carriers present in each beam, $c_{1,1}$ and $c_{1,2}$ in beam B_1 and $c_{3,1}$ and $c_{3,2}$ in beam B_3, have exactly the same properties. For this reason a user allocated in $c_{1,1}$ will create Co-Channel Interference (CCI) to beam B_3, i.e. to the sub-carrier $c_{3,1}$ since they operate at the same frequency, and vice-versa. The same effect holds between sub-carriers $c_{1,2}$ and $c_{3,2}$. As for ACI (Section 1.1.3), the level of CCI depends on the geographical position of the users in each beam and also on the antenna characteristics (side-lobes, please refer to Section 1.1.5 for more details).

The level of CCI in a multi-beam satellite system is related to the antenna side lobes and therefore to the distance D between the beams using the same frequency. The higher the distance, the lower the CCI. Increasing the distance implies using more frequency bands in the system and consequently less bandwidth will be available in each beam. Therefore there is clearly a trade-off between the number of frequency bands, which should be as low as possible, and the level of CCI. As for ACI, techniques such as IC, can be used to limit the impact of this source of interference.

Cross-Polarisation Channel Interference

The so-called Cross-Polarisation Channel Interference (CPCI) (or Cross-Polarisation Interference (XPI)) is related to the utilisation of different polarisations within the same frequency channel. For instance this interference appears if a given frequency channel uses both vertical and horizontal polarisation (linear polarisations), or both left- and right-handed circular polarisations. This interference arises due to the imperfection of the transmit and receive antennas and also because of the atmospheric path present between the transmitter and the receiver [Vas00]. For the latter mainly rain and ice particles tend to modify the polarisation and to convert a part of the initial polarisation into the other, unwanted, polarisation [Ogu83]. Both antenna imperfection and transmission medium will create mutual interference [MaBo02].

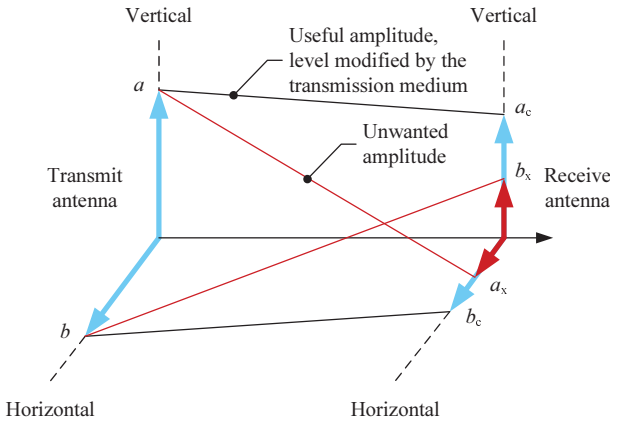


Figure 1.7. *Principle of cross-polarisation interference when using linear polarisations.*

The principle of Cross-Polarisation Channel Interference (CPCI) is explained by Fig. 1.7 when considering linear polarisations. The initial amplitude of the wave is a and b for the vertical and the horizontal polarisation, respectively. The level of these waves will be modified due to the transmission medium and will result into a_c and b_c. An unwanted part of the opposite polarisation will appear and is represented by b_x and a_x for the horizontal and the vertical

polarisation, respectively. The CPCI level when transmitting both polarisations at the same time, is defined by the so-called cross-polarisation isolation, also with acronym XPI, and is such that [MaBo02]:

$$\mathrm{XPI_V} = a_\mathrm{c}/b_\mathrm{x} \quad \leftrightarrow \quad (\mathrm{XPI_V})_\mathrm{dB} = 20\,\log\,(a_\mathrm{c}/b_\mathrm{x}) \tag{1.2}$$

for the vertical polarisation (V) and:

$$\mathrm{XPI_H} = b_\mathrm{c}/a_\mathrm{x} \quad \leftrightarrow \quad (\mathrm{XPI_H})_\mathrm{dB} = 20\,\log\,(b_\mathrm{c}/a_\mathrm{x}) \tag{1.3}$$

for the horizontal polarisation (H) (the polarisation is always according to the direction of the electric field).

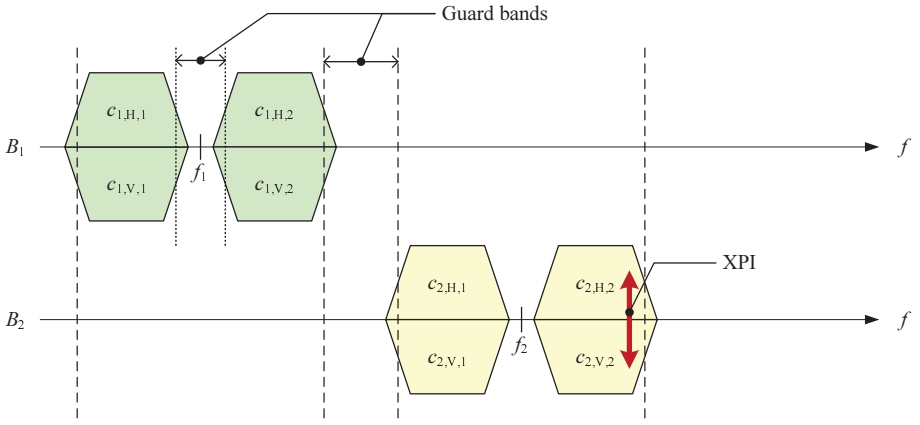


Figure 1.8. *Example of carrier organisation involving cross-polarisation interference.*

The same notation as in Section 1.1.3 and Section 1.1.3 is considered for showing an example of carrier organisation that will involve cross-polarisation interference (Fig. 1.8). On the one hand, in this example there are two sub-carriers per beam and all guard bands, i.e. the guard band within the beam, and the guard band between the beams, are such that ACI can be neglected. In this setup only two beams, B_1 and B_2, are considered and use different frequency bands. Hence CCI can also be neglected. On the other hand, each sub-carrier use two different linear polarisations, horizontal and vertical. The carrier notation is therefore refined into $c_{i,\mathrm{P},j}$, where i represents the beam ID, P the polarisation (H for horizontal and V for vertical), and j the sub-carrier ID. A user allocated in $c_{1,\mathrm{H},1}$ will generate CPCI towards the carrier $c_{1,\mathrm{V},1}$ since the two sub-carriers have the same properties but use orthogonal polarisations. The presence of CPCI holds for all other sub-carriers of each beam.

Using two different polarisations while keeping the same carrier organisation permits to double the capacity of the system (so-called frequency-reuse by orthogonal polarisation). In practice

the presence of CPCI will irreparably introduce interference, reducing the system capacity, and countermeasures such as IC can be taken into account [CeGa10], [ChChOt11].

Inter-Modulation Interference and Inter-Symbol Interference

The Inter-Modulation Interference (IMI) is caused by the non-linearity of the amplifiers which are located on-board the satellite. When two or more radio channels are injected into a non-linear circuit, unwanted sidebands channels, which are products at other positions than the ones of the original channels (frequencies), appear and can therefore possibly generate ACI. The intermodulation products are identified by their order and generally both third order and fifth order products are the most critical ones [Bab52]. This kind of interference is important when the number of carriers is relatively high in a beam for instance (multi-carrier).

Finally Inter-Symbol Interference (ISI) is mainly caused by the non-linear frequency response of a channel which involves that one symbol may interfere with other subsequent symbols. This can happen for instance in a multi-path propagation environment.

Final Considerations

The Inter-Symbol Interference (ISI) is not considered since countermeasures exist and also since a frequency flat channel is assumed in this work. The latter assumption is actually reasonable for satellite systems with static users. The Inter-Modulation Interference (IMI) can be neglected if the number of carriers per beam is low and since the utilisation of filters, and also of both Input Back-Off (IBO) and Output Back-Off (OBO), permit to reduce considerably the effects produced by this kind of interference. The three remaining sources of interference which are Adjacent-Channel Interference (ACI), Co-Channel Interference (CCI) and Cross-Polarisation Channel Interference (CPCI), are all related to the management of the bandwidth in the satellite system.

The utilisation of two polarisations within the same link permits theoretically to double the capacity of this link. At high frequencies CPCI becomes critical and interference cancellation needs to be employed so that to recover the information sent initially in one particular polarisation. However the resulting gains in terms of system capacity are not sufficient to consider this kind of technique. Adjusting the overlapping of carriers also permits theoretically to increase the system capacity. As before IC is mandatory and it is obvious that, when compared to the theoretical increase of capacity which can be achieved when adjusting the

number of colours, investigating CCI will bring higher gains than cancelling ACI (please refer to Section 1.1.4 for more details).

In this thesis we focus on the reduction of the number of colour in the multi-beam satellite system, down to full frequency reuse, also called universal frequency reuse, and therefore on the resulting level of Co-Channel Interference (CCI), considering sufficient guard bands and unique polarisation so that to neglect ACI and CPCI, respectively.

1.1.4 Sub-Scenarios

Number of Colours

The number of colours, which also defines the number of frequencies used in the system, play a significant role on the Co-Channel Interference (CCI). The distance between neighbouring beams employing the same frequency impacts directly the level of interference (please refer to the definition of the cluster size in Section 1.1.1 for more details).

In conventional satellite systems the number of colours K is kept as small as possible. For instance the configuration $K = 4$ limits considerably the amount of CCI but also reduces the bandwidth in each beam. Actually the system capacity is approximately proportional to $(K\,A_\mathrm{b})^{-1}$ where A_b designates the coverage area of a beam [LuWeJa00]. On the one hand with one colour, i.e. cluster size $K = 1$, the capacity is thus theoretically four times the one with four colours but on the other hand CCI is also dramatically increased. The challenge consists in improving the system capacity, i.e. by reducing the number of colours down to full frequency reuse (one single colour), and therefore having a highly interference-limited system, while being able to limit the impact of interference on the performance using different strategies.

In this work we consider three numbers of colour which are one, three and four, i.e. respectively $K = 1$, $K = 3$ and $K = 4$. As already mentioned with four colours CCI is the lowest of the three schemes, i.e. we have a low-interference network, whereas with one single colour CCI is increased, i.e. we have a high interference-limited network. However with the latter the capacity should be improved if countermeasures for interference are employed.

Beam Coverage

The coverage of the beams on ground first depends on the orbital position of the satellite. We focus our investigation on a Geostationary (GEO) satellite at longitude 19.2° East. This satellite covers Europe by the means of 96 beams which is quite a realistic number for modern satellite systems. The position of the satellite and of the beam centres are actually the same as in [Cou06].

Based on [MaBo02] and [LuWeJa00], a method for evaluating the beam coverage was established. The coverage of each beam depends on various criteria, more particularly on the position of the satellite, the location of the beam centre on Earth and the 3 dB beam contour [4]. The purpose is to determine the border of the beams so that the satellite terminals on ground can be placed in the beam of interest. The half-side beam width considered here is $\theta_{3\text{dB}} = 0.2°$ [5]. The investigations realised on this topic targets the derivation of an efficient way, in terms of processing time, for computing the beam border, and for distributing users as fast as possible within the footprints of the beams (please refer to Section C.1.1 in which the complete method is described).

Distributions of the Users

Once the coverage of each beam on Earth is determined, i.e. the footprints of the beams is known, the users can be distributed. The users represent the satellite terminals which are located on ground and receives data from the satellite (forward-link, download) and sends data towards the satellite (return-link, upload).

All computations for what concerns the beam contour, and therefore the coverage area of the beam, are realised based on a grid mapped over the Earth. The resolution of the grid determines the granularity of both latitude and longitude coordinates and the satellite terminals are randomly positioned on this grid. The number of users per beam can either by identical, for instance ten users in each beam, or comprised in a given range (uniformly distributed), for instance between five and ten users per beam. The system takes care of allocating to each beam the desired number of users, taking into account the satellite open angles, to ensure that a given satellite terminal is covered by the beam of interest (such problem arises when

4. A 4.3 dB beam contour can also be taken into account, the purpose being to offer higher beam isolation [LuWeJa00].

5. Sometimes the notation $\theta_{3\text{dB}}$ also refers to the complete beam width [MaBo02] [LuWeJa00].

the position of the user is very close to the beam border). The grid resolution is always equal, unless stated, to one tenth of a degree ($r_{\text{grid}} = 0.1°$).

The location of the satellite terminals can also be defined manually, instead of being generated randomly, by providing the different coordinates. This permits to investigate different scenarios in which the position of the users is perfectly known and therefore in which the level of interference can be foreseen.

System Sizes

Two main system sizes, which depends on the number of beams, noted B, are defined and are considered as sub-scenarios. A small system, composed of seven beams ($B = 7$), and a large system composed of the ninety six beams ($B = 96$, full satellite system). We set as reference beam the beam covering the city of Munich (beam ID 33, i.e. B_{33}, of the ninety six beams system). The seven beams system contains the beam of reference and the direct surrounding beams using the same frequency (therefore six beams). Fig. 1.9 shows the corresponding seven beams system for universal frequency reuse (i.e. $K = 1$) and with two users per beam (beam contours with thin lines). These two users are the so-called "bad users", located close to the beam border in the surrounding beams, and the so-called "good users", located in the centre of each beam (the position of the user in the reference beam is always at the beam centre). Fig. 1.9 also shows the six surrounding beams using the same frequency when considering a three colours system (beam contours with thicker lines). Fig. 1.10 shows the ninety six beams system for three and four colours, i.e. respectively $K = 3$ and $K = 4$. As seen, in the two latter scenarios the beams using the same frequencies are not directly adjacent.

1.1.5 Beam Pattern Computation

The level of Co-Channel Interference (CCI) is directly driven by the characteristics of the antenna on-board. The antenna pattern influences the amount of interferences created by the sending beams to the satellite terminals (forward down-link) and received by the beams from the satellite terminals (return up-link).

The antenna pattern is computed by means of equations derived from [Col85] and [DCMLC07] since the beams of a satellite can be considered as paraboloidal reflector antennas. The next formulae permit to compute the gain for different satellite open-angles (for more details, please

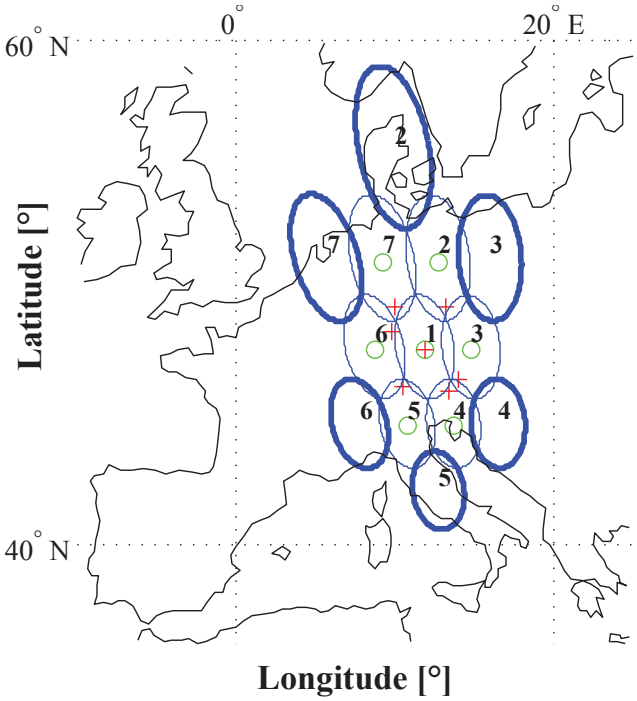


Figure 1.9. *Small system scale for full frequency reuse ($K = 1$) and three colours ($K = 3$). For each colour the system is composed of seven beams ($B = 7$) which are directly adjacent when all beams use the same frequency (thin beam contours) and which are farther for three colours (thicker beam contours). Two users per beam are shown for universal frequency reuse: "bad users" (crosses) and "good users" (circles).*

refer to Section C.1.2 in which the complete derivation of the formula, according to [Col85], is given. Please notice the erratum in the latter reference as indicated in Section D.2.):

$$G(u) = G_{\max}\,\alpha \left(2\,\frac{J_1(u)}{u} + \frac{T}{1-T}\,2^{p+1}\,p!\,\frac{J_{p+1}(u)}{u^{p+1}} \right)^2 \tag{1.4}$$

where J_i is the Bessel function of the first kind and of order i, and:

$$G_{\max,\mathrm{dB}} = 53.23 \text{ dB}, \quad \alpha = \frac{(1-T)\,(p+1)}{(1-T)\,(p+1)+T} \quad \text{and} \quad u = \left(\frac{\pi\, d_{\mathrm{a}}}{\lambda} \right) \sin\theta$$

d_{a} is the diameter of the antenna (reflector), λ is the wavelength and θ represents the open-angle of interest. In this work we considered the following typical values: an antenna efficiency $\eta = 0.6$, a frequency $f = 30$ GHz (return up-link), an aperture edge taper $T = 20$ dB, and the rate at which the aperture field decreases is managed by the coefficient p ($p = 2$). An example is given by Fig. 1.11 in which the radiation pattern of one single beam is shown.

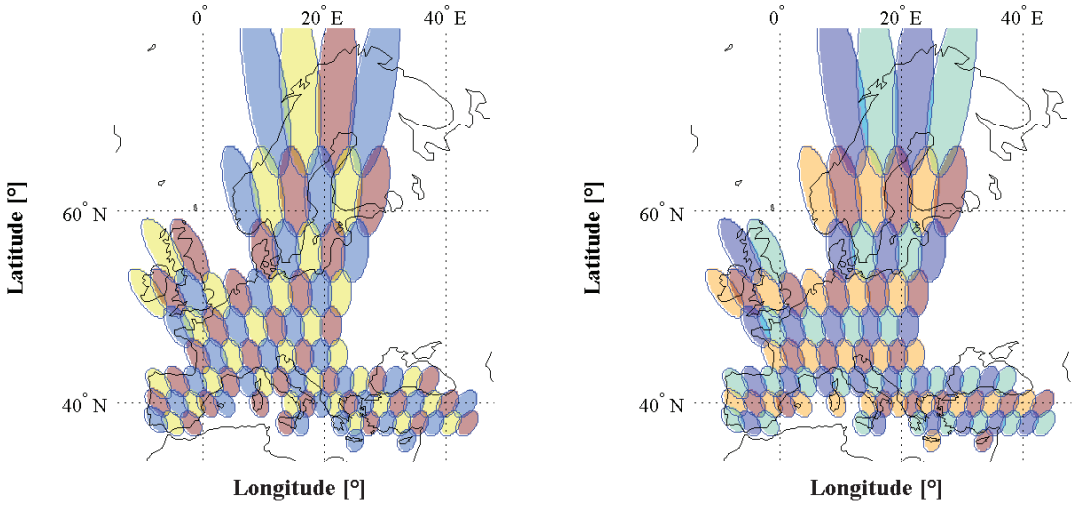


Figure 1.10. *Full system size for three colours ($K = 3$, left) and four colours ($K = 4$, right). The system is composed of ninety six beams ($B = 96$) using three or four different frequencies.*

1.1.6 Example of Link Budget for the Return-Link

This part addresses the computation of the link budget for the Return-Link (RL) of satellite communications. This will help understanding the generation of the channel matrix later on and also permits to get a rough idea of typical signal-to-noise ratios in satellite communications.

Up-Link

The return up-link corresponds to the link from the satellite terminals to the satellite, i.e. from the ground segment to the space segment. The power of the signal received at the satellite from the satellite terminal is noted $P_{\mathrm{Rx,sat}}$ and is obtained using (all terms are expressed in decibels [MaBo02]):

$$P_{\mathrm{Rx,sat}} = P_{\mathrm{Tx,t}} + G_{\mathrm{Tx,t}} - L_{\mathrm{out,t}} - L_{\mathrm{pointing,t}} - L_{\mathrm{OBO,t}} + G_{\mathrm{sat}} - L_{\mathrm{ant,sat}} - L_{\mathrm{FS}} \tag{1.5}$$

where $P_{\mathrm{Tx,t}}$ is the transmit power at the terminal, $G_{\mathrm{Tx,t}}$ the antenna transmit gain of the terminal, $L_{\mathrm{out,t}}$ the output losses of the terminal, $L_{\mathrm{pointing,t}}$ the pointing loss of the terminal, $L_{\mathrm{OBO,t}}$ the output back-off loss of the terminal, G_{sat} the receive gain at the satellite, $L_{\mathrm{ant,sat}}$ the losses of the satellite antenna, and L_{FS} the free space losses. The first part of the equation which is related to the terminal defines the effective isotropic radiated power (EIRP).

Let's consider an example of link budget for the return up-link. The satellite terminals transmits with a power $P_{\mathrm{Tx,t}}$ in the Ka-band at a frequency $f_{\mathrm{U}} = 30$ GHz ("U" stands for

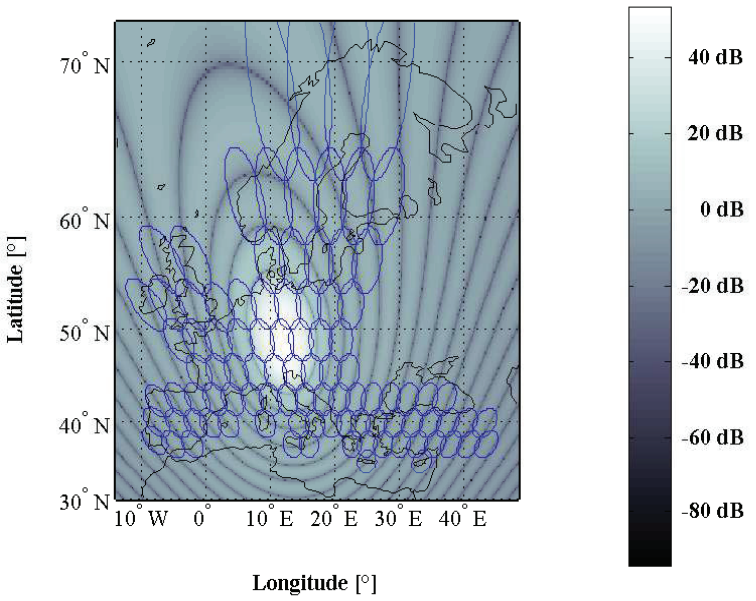


Figure 1.11. *Satellite system and example of beam radiation pattern. The footprints of the ninety six beams considered in the multi-beam satellite scenario are shown. The beam radiation pattern of one single beam is illustrated with the gain in decibels (dB). In this example the highlighted beam has the following centre coordinates: latitude 48.75° North and longitude 11.9° East (beam ID 33).*

up-link) and a bandwidth W. We assume the terminals are equipped with an antenna dish whose diameter is D_{ant}, the resulting transmit gain is:

$$G_{\text{Tx,t}} = \eta \left(\frac{\pi D_{\text{ant}}}{\lambda_{\text{U}}} \right)^2 \tag{1.6}$$

where η is the antenna efficiency, λ_{U} is the wave length and is equal to c/f_{U} ($c = 3 \times 10^8$ m/s).

Typical values for the losses at the terminals are: $L_{\text{out,t}} = 1$ dB, $L_{\text{pointing,t}} = 0.5$ dB and $L_{\text{OBO,t}} = 2$ dB. The latter term is used such that the High-Power Amplifier (HPA) can operate in the linear region. The free space losses depend on both frequency and slant-range, noted S, i.e. the distance between the satellite terminal and the satellite, and is computed according to the well-known Friis formula [MaBo02]:

$$L_{\text{FS}} = \left(\frac{4\pi S}{\lambda_{\text{U}}} \right)^2 \tag{1.7}$$

For a terminal located in Europe (48.75° North and 11.9° East) and a geostationary satellite positioned at 19.2° East the slant-range is $S \simeq 38\,298$ km. The corresponding free space losses are $L_{\text{FS}} \simeq 213.7$ dB.

The following three configurations are considered for computing the return up-link budgets (Table 1.1).

Table 1.1. *Satellite terminal configurations for the return up-link budgets.*

Config. ID	1	2	3
$P_{\mathrm{Tx,t}}$ [W]	1	1.5	2
η	0.55	0.6	0.65
D_{ant} [m]	0.6	0.9	1.2
$G_{\mathrm{Tx,t}}$ [dBi]	42.9	46.8	49.7

Concerning the satellite antenna the following values are realistic: $L_{\mathrm{ant,sat}} = 1$ dB, the pre-low-noise amplifier input loss $L_{\mathrm{ant,sat,lna}} = 1$ dB, the antenna noise temperature $T_{\mathrm{ant,sat}} = 290$ K and the noise figure $\mathrm{NF}_{\mathrm{Rx,sat}} = 3$ dB. The resulting system temperature is $T \simeq 728.5$ K (28.6 dBK, more details are given in Section C.1.3). The receive gain at the satellite is obtained from previous computation (beam pattern) and can be assumed to be: $G_{\mathrm{sat}} \simeq 53.23$ dB (gain in the beam centre).

In this example different bandwidths are considered and the corresponding transmission rates are obtained considering a roll-off factor of 35 % and 11 % channel spacing (Table 1.2, values taken from [ESA-RM]). The next table (Table 1.3) summarises the different values obtained while computing the return up-link budget for the three configurations and in clear sky conditions.

Table 1.2. *Satellite terminal bandwidths and rates for the return up-link budgets.*

Config. ID	1	2	3
W [MHz]	1.5	3	6
R_{s} [Msps]	1	2	4

Down-link

The return down-link corresponds to the link from the satellite to the gateway on ground. For a transparent satellite system (amplify and forward) this link is generally designed such that the carrier-to-noise ratio C/N of the return up-link remains the same.

Table 1.3. *Satellite terminal return up-link budget values.*

Config. ID	1	2	3
$P_{\mathrm{Rx,sat}}$ [dBW]	-122.1	-116.4	-112.3
N [dBW]	-138.2	-135.2	-132.2
C/N [dB]	16.1	18.8	19.9
E_{s}/N_0 [dB]	17.9	20.6	21.7

The power of the signal sent by the satellite and received by the gateway is noted $P_{\mathrm{Rx,gtw}}$ and is obtained using (all terms are expressed in decibels [MaBo02]):

$$P_{\mathrm{Rx,gtw}} = P_{\mathrm{Tx,sat}} + G_{\mathrm{Tx,sat}} - L_{\mathrm{out,sat}} - L_{\mathrm{pointing,sat}} - L_{\mathrm{OBO,sat}} + G_{\mathrm{Rx,gtw}} - L_{\mathrm{ant,gtw}} - L_{\mathrm{FS}} \quad (1.8)$$

where $P_{\mathrm{Tx,sat}}$ is the transmit power at the satellite, $G_{\mathrm{Tx,sat}}$ the transmit gain of the satellite, $L_{\mathrm{out,sat}}$ the output losses of the satellite, $L_{\mathrm{pointing,sat}}$ the pointing loss of the satellite, $L_{\mathrm{OBO,sat}}$ the output back-off at the satellite, $G_{\mathrm{Rx,gtw}}$ the receive gain at the gateway, $L_{\mathrm{ant,gtw}}$ the losses of the gateway antenna, and L_{FS} the free space losses.

As example we consider a frequency $f_{\mathrm{D}} = 18$ GHz for this link ("D" stands for down-link) and assume for what concerns the satellite that the transmit power per beam is $P_{\mathrm{Tx,sat}} = 10$ W, the loss between the amplifier and the antenna $L_{\mathrm{out,sat}} = 1$ dB and the antenna efficiency $\eta = 0.6$. Assuming the gateway as being located in London, the slant-range is about $S \simeq 39\,218$ km. The earth station, i.e. the gateway, is such that the noise figure $\mathrm{NF}_{\mathrm{Tx,gtw}} = 1$ dB, the loss antenna-receiver is $L_{\mathrm{ant,gtw}} = 0.5$ dB, the thermodynamic temperature of the feeder is $T_{\mathrm{F}} = 290$ K, the diameter of the antenna is $D_{\mathrm{ant}} = 9$ m, the maximum pointing error is $\theta_{\mathrm{R}} = 0.1°$ and finally the temperature of the ground is $T_{\mathrm{ground}} = 45$ K. The Effective Isotropic Radiated Power (EIRP) is equal to 67.6 dBW considering $\theta_{3\mathrm{dB}} = 0.2°$. The loss related to the pointing error from the gateway towards the satellite is $L_{\mathrm{pointing,sat}} \simeq 7.1$ dB. The thermodynamic temperature of the down-link, denoted as T_{D}, is $T_{\mathrm{D}} \simeq 164.5$ K assuming that according to the location of the gateway, the elevation of the antenna to point towards the satellite is around 28° and the corresponding temperature of the sky is $T_{\mathrm{sky}} = 20$ K [MaBo02]. The maximum receive gain of the gateway antenna is $G_{\mathrm{Rx,gtw}} \simeq 62.4$ dBi and the figure of merit, $G/T \simeq 32.6$ dBK^{-1}. This leads to a carrier over noise power spectral density $(C/N_0)_{\mathrm{dB}} \simeq 119.4$ dBHz, where the free space losses between the satellite and the gateway located in London is $L_{\mathrm{FS}} \simeq 209.4$ dB. The resulting energy per symbol over noise power spectral densities, E_{s}/N_0, are given in Table 1.4.

Table 1.4. *Satellite terminal return down-link budget values.*

Config. ID	1	2	3
E_s/N_0 [dB]	59.4	56.4	53.4

Total Link Budget

In a transparent satellite we have:

$$\left(\frac{1}{E_s/N_0}\right)_{\text{total}} = \left(\frac{1}{E_s/N_0}\right)_{\text{up}} + \left(\frac{1}{E_s/N_0}\right)_{\text{down}} \tag{1.9}$$

where the left term after the equal sign represents the up-link part and the right term the down-link part (linear terms).

This leads to the total return-link budget values listed in Table 1.5.

Table 1.5. *Satellite terminal total return link budget values.*

Config. ID	1	2	3
E_s/N_0 [dB] - Up	17.9	20.6	21.7
E_s/N_0 [dB] - Down	59.4	56.4	53.4
E_s/N_0 [dB] - Total	17.9	20.6	21.7

As can be seen the total return-link budget is equal to the return up-link budget. For this reason the user link is always considered as the bottleneck in the link budget of a transparent satellite system. The feeder link (i.e. the link between the gateway and the satellite) does not really have an influence on the overall link budget. This property will help later on for deriving the satellite channel model.

It has to be remarked that the different values present in Table 1.5 correspond to a situation where the user is located in the centre of the beam, with clear sky conditions, perfect Line-of-Sight (LoS), no source of interference, in other words to the best link budget one can reach with such configurations. Sources of attenuation like the position of the satellite terminal within the beam footprint, rain, scintillation, ACI, CCI, etc. unavoidably leads to a decrease of the total link budget in the magnitude of several decibels.

1.2 Channel Model

This section describes the channel model, more particularly the generation of the channel matrix. In this section it will be shown that the multi-beam satellite system can be considered as a Multiple-Input and Multiple-Output (MIMO) system.

1.2.1 Introduction to Simple Input-Output Systems

The channel matrix is usually identified by the matrix $\boldsymbol{H}$. The columns j of the channel matrix represent the channel seen by the transmitters and the rows i the channel seen by the receivers. Each element $h_{i,j}$ of the channel matrix $\boldsymbol{H}$ represents the channel between the receiver i and the transmitter j.

$$\boldsymbol{H} = \begin{bmatrix} h_{1,1} & h_{1,2} & \cdots & h_{1,N_{\mathrm{Tx}}} \\ \vdots & \vdots & \ddots & \vdots \\ h_{N_{\mathrm{Rx}},1} & h_{N_{\mathrm{Rx}},2} & \cdots & h_{N_{\mathrm{Rx}},N_{\mathrm{Tx}}} \end{bmatrix} \tag{1.10}$$

Basic Transmission

When transmitting a signal x_j over the channel represented by the matrix $\boldsymbol{H}$ with $j \in \{1, 2, ..., N_{\mathrm{Tx}}\}$, it will be modified by the channel (amplitude and phase) and will be influenced by additional noise. The signal received is noted y_i with $i \in \{1, 2, ..., N_{\mathrm{Rx}}\}$ such that:

$$\begin{aligned} y_1 &= h_{1,1}\, x_1 + h_{1,2}\, x_2 + \cdots + h_{1,N_{\mathrm{Tx}}}\, x_{N_{\mathrm{Tx}}} + \eta_1 \\ y_2 &= h_{2,1}\, x_1 + h_{2,2}\, x_2 + \cdots + h_{2,N_{\mathrm{Tx}}}\, x_{N_{\mathrm{Tx}}} + \eta_2 \\ &\cdots \\ y_{N_{\mathrm{Rx}}} &= h_{N_{\mathrm{Rx}},1}\, x_1 + h_{N_{\mathrm{Rx}},2}\, x_2 + \cdots + h_{N_{\mathrm{Rx}},N_{\mathrm{Tx}}}\, x_{N_{\mathrm{Tx}}} + \eta_{N_{\mathrm{Rx}}} \end{aligned}$$

In the previous equations the additional noise is denoted η_i with $i \in \{1, 2, ..., N_{\mathrm{Rx}}\}$. The previous relations can also be written using vectors and matrices:

$$\boldsymbol{y} = \boldsymbol{H}\boldsymbol{x} + \boldsymbol{\eta} \tag{1.11}$$

The input $\boldsymbol{x}$ is a column vector of size N_{Tx}, i.e. $\boldsymbol{x} = [x_1, x_2, \cdots, x_{N_{\mathrm{Tx}}}]^T$, $\boldsymbol{H}$ is the channel matrix previously defined, $\boldsymbol{\eta}$ and $\boldsymbol{y}$ are column vectors of size N_{Rx}, i.e. $\boldsymbol{\eta} = [\eta_1, \eta_2, \cdots, \eta_{N_{\mathrm{Rx}}}]^T$ and $\boldsymbol{y} = [y_1, y_2, \cdots, y_{N_{\mathrm{Rx}}}]^T$.

Fig. 1.12 shows a basic transmission block diagram. On the left the input signal $\boldsymbol{x}$ enters the system and it results into an output signal $\boldsymbol{y}$. On the right the system is represented by the channel matrix $\boldsymbol{H}$ and the noise $\boldsymbol{\eta}$ added during the transmission.

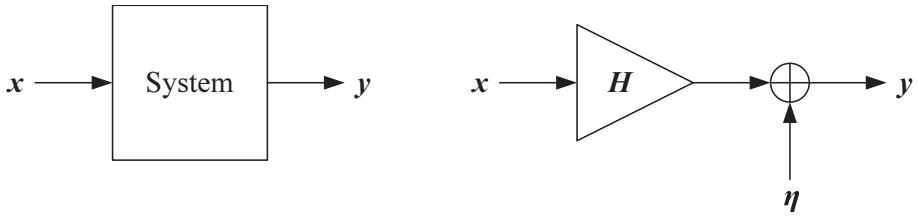


Figure 1.12. *Basic transmission block diagram.*

One Transmitter per Receiver

In the case where one transmitter is associated to one particular receiver, i.e. the number of transmitter equals the number of receiver ($N_{\mathrm{Tx}} = N_{\mathrm{Rx}}$), the channel matrix $\boldsymbol{H}$ is a square matrix. By convention and ease of reading the indexes are identical, i.e. transmitter 1 sends to receiver 1. The diagonal of the channel matrix $\boldsymbol{H}$, i.e. $\mathrm{diag}\{h_{1,1}, h_{2,2}, \cdots, h_{N_{\mathrm{Rx}},N_{\mathrm{Tx}}}\}$, represents therefore the "useful" coefficients.

The coefficient $h_{i,j}$ with $i = j$ thus corresponds to the "useful" channel between the transmitter j and the receiver i. The other coefficients, i.e. $h_{i,j}$ with $i \neq j$, represent the "not-desired" channel. The not-desired channel is also known as interference, for instance $h_{1,2}$ is the interference caused by transmitter 2 on receiver 1.

Power and Symbols

As seen previously the input signal $\boldsymbol{x}$ will be modified by the channel matrix $\boldsymbol{H}$ and also by the noise $\boldsymbol{\eta}$ added during the transmission. The signal is actually composed of complex symbols directly related to the modulation (we assume in-phase and quadrature modulation), i.e. $\boldsymbol{x} \in \mathbb{C}^{N_{\mathrm{Tx}} \times 1}$, and which amplitude depends on the transmit power P, $P \in \mathbb{R}_{>0}$. Therefore (1.11) can thus be also written:

$$\boldsymbol{y} = \sqrt{P}\boldsymbol{H}\boldsymbol{s} + \boldsymbol{\eta} \tag{1.12}$$

where $\boldsymbol{s}$ is a column vector of size N_{Tx} representing the transmitted symbols, i.e. $\boldsymbol{s} = [s_1, s_2, \cdots, s_{N_{\mathrm{Tx}}}]^T$, $\boldsymbol{s} \in \mathbb{C}^{N_{\mathrm{Tx}} \times 1}$, $\boldsymbol{H} \in \mathbb{C}^{N_{\mathrm{Rx}} \times N_{\mathrm{Tx}}}$ and $\boldsymbol{y} \in \mathbb{C}^{N_{\mathrm{Rx}} \times 1}$. In this case the power P is the same among all transmitters. The noise is generally the so-called additive Gaussian noise with $\boldsymbol{\eta} \in \mathbb{C}^{N_{\mathrm{Rx}} \times 1}$, more particularly $\boldsymbol{\eta} \sim \mathcal{CN}(0, N_0 \boldsymbol{I})$ where N_0 is the power spectral density of the Additive White Gaussian Noise (AWGN) and $\boldsymbol{I}$ the identity matrix.

If each transmitter sends with a particular power, then (1.12) is formulated as follows:

$$\boldsymbol{y} = \boldsymbol{H}\boldsymbol{P}\boldsymbol{s} + \boldsymbol{\eta} \tag{1.13}$$

where $\boldsymbol{P} = \text{diag}\{\sqrt{p_1}, \sqrt{p_2}, \cdots, \sqrt{p_{N_{\text{Tx}}}}\}$ such that p_j represent the power of transmitter j. Therefore the input signal represented by the column vector $\boldsymbol{x}$ is such that $\boldsymbol{x} = \boldsymbol{P}\,\boldsymbol{s}$.

1.2.2 Multiple-Input and Multiple-Output Concept

The channel matrix $\boldsymbol{H}$ previously defined can be used to characterise a radio channel for instance. The radio channel can be composed of several inputs (the transmitters) and several outputs (the receivers). The number of inputs - outputs depends on the number of entities, i.e. physical transmitters and receivers, and/or of the number of transmit and receive antennas. The number of inputs and outputs considered in the system determines its type:

– Single-Input and Single-Output (SISO): one transmit antenna and one receive antenna,
– Single-Input and Multiple-Output (SIMO): one transmit antenna and several receive antennas,
– Multiple-Input and Single-Output (MISO): several transmit antennas and one receive antenna,
– Multiple-Input and Multiple-Output (MIMO): several transmit antennas and several receive antennas.

The next figure (Fig. 1.13) shows a basic and common representation of an input - output system with multiple transmitters and multiple receivers.

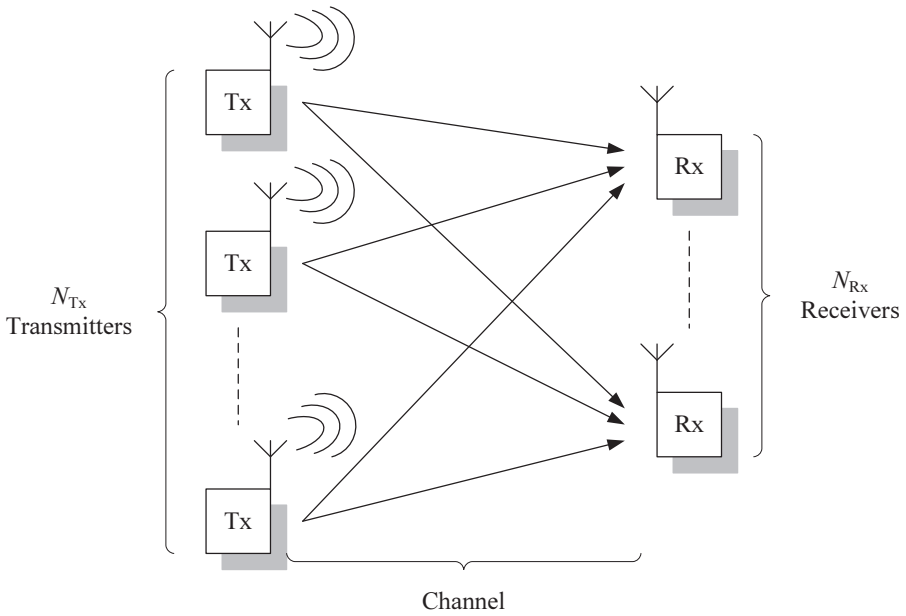


Figure 1.13. *Basic input - output system with multiple transmitters and multiple receivers.*

Receivers with Multiple Antennas

In Fig. 1.13 each transmitter and each receiver are considered as different physical entities and are equipped with a single antenna. It is actually possible for each receiver to be equipped with more than one single antenna. In such a case a dedicated channel matrix is needed to describe the radio channel between the transmitters and each receiver (Fig. 1.14) as in [WuMi06].

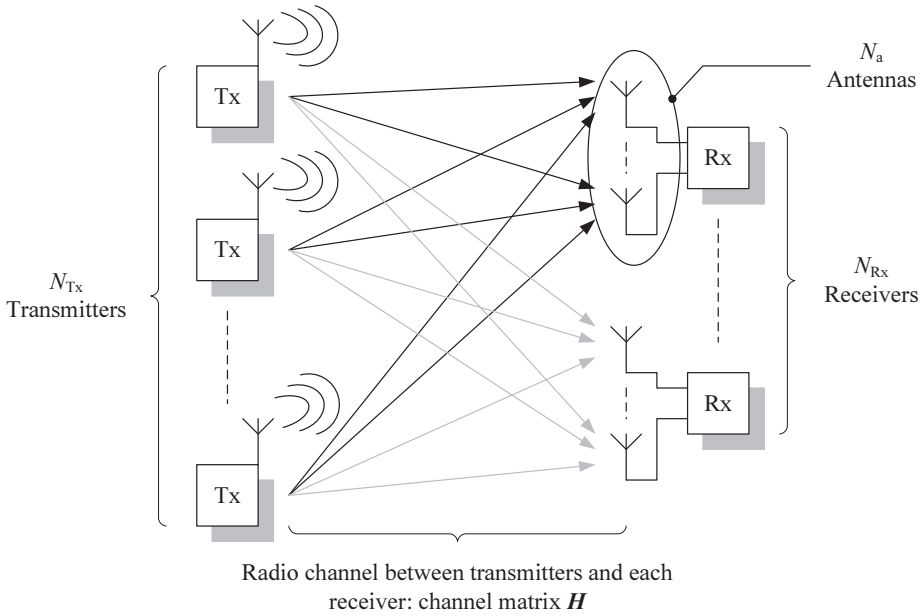


Figure 1.14. *Input - output system with multiple transmitters and multiple receivers equipped with several antennas.*

MIMO Broadcast Channel

On the one hand, a MIMO Broadcast Channel (MIMO BC) corresponds to the down-link of a wireless network in which one transmitter sends to multiple receiver. For instance the sending of information from a Base Station (BS) to several Mobile User Terminal (MUT) in a cellular network can be seen as a MIMO BC. The user information is transmitted by several antennas located at the BS (sector antennas for instance) and can be received via the radio channel by the MUTs equipped with one or several antennas (Fig. 1.15, left). In such a case the signal transmitted by the base station towards a radio cell is received by all users present in this radio cell, and also possibly in neighbouring cells (interference). For this reason the information is broadcast by the base station to several MUTs and the channel is seen as a broadcast channel.

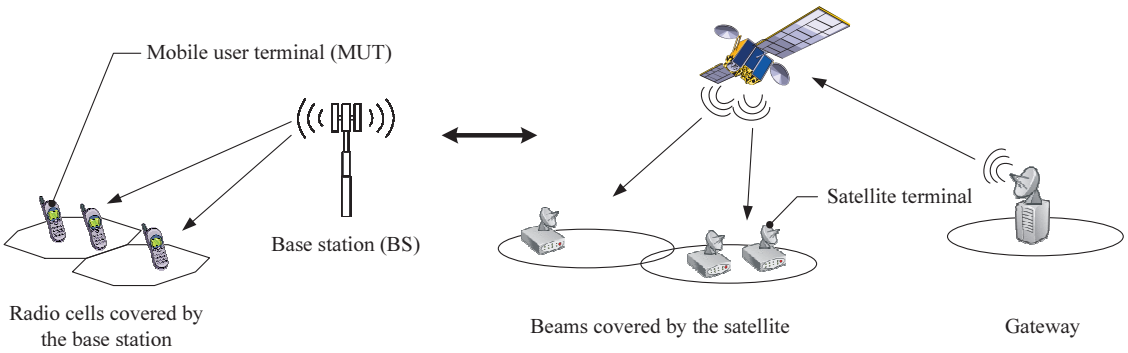


Figure 1.15. *MIMO broadcast channel in a terrestrial system (left) and analogy with a satellite system (right).*

In a multi-beam satellite system the Forward Down-Link (FDL) can be seen as a MIMO Broadcast Channel (MIMO BC) since the satellite is equipped with several transmit antennas (beams) sending data towards Satellite Terminals (STs) located on ground (Fig. 1.15, right).

MIMO Multiple Access Channel

On the other hand, a MIMO Multiple Access Channel (MIMO MAC) represents the up-link of a wireless network in which several transmitters send to one receiver. In such a case the users (MUTs) are equipped with one or multiple antennas and send independent data toward the BS having several antennas (Fig. 1.16, left). In this scenario each MUT transmits information to the base stations and therefore accesses the channel. For this reason the channel is used by several transmitted and is called Multiple Access Channel (MAC).

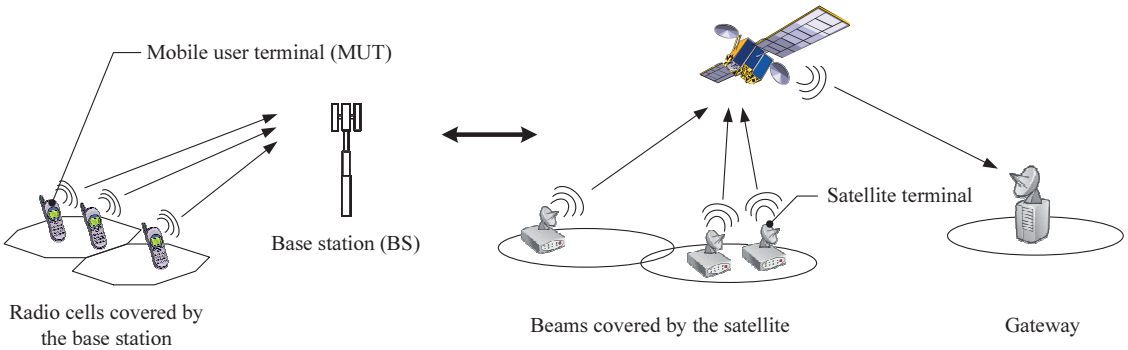


Figure 1.16. *MIMO multiple access channel in a terrestrial system (left) and analogy with a satellite system (right).*

The Return Up-Link (RUL) of a multi-beam satellite system can be considered as a MIMO Multiple Access Channel (MIMO MAC) since several Satellite Terminals (STs) transmit independent data to the satellite which is equipped with multiple antennas (beams, Fig. 1.16, right).

Duality

On the one hand, lot of efforts has been put during last years into solving the optimality transmission problems in MIMO Broadcast Channel (MIMO BC) systems. Actually it has been shown, due to the nature of the transmitted signal in this kind of channel, that the optimisation problems, such as beamforming and power control, are non-convex and therefore cannot be easily solved [SSBHU09], [HeJoUt10]. On the other hand, MIMO Multiple Access Channel (MIMO MAC) systems have the particularity to offer convex problems and therefore optimal optimisations can be found. The duality MIMO BC - MIMO MAC consists into transforming the Broadcast Channel (BC) problem into a MAC problem using the relationship existing between BC and MAC and was first addressed in [RaLiTa98].

1.2.3 Transmission Block Diagram

We assume that the users transmit a sequence of bits which are modulated and represented at a given time by a vector $\boldsymbol{x}$. The elements of the vector $\boldsymbol{x}$, noted x_j with $1 \leq j \leq N_{\mathrm{Tx}}$ where N_{Tx} is the number of transmitters, are sent over the channel which is represented by the inter-beam interference matrix $\boldsymbol{B}$.

Each transmitted symbol x_j is multiplied by the coefficients of the channel matrix. Because of the presence of interferences, a part of x_j will be received by the i-th satellite antenna feed with $i \neq j$. The signal received by the satellite antenna feeds is:

$$\begin{bmatrix} a_1 \\ \vdots \\ a_{N_{\mathrm{a}}} \end{bmatrix} = \begin{bmatrix} b_{1,1} & b_{1,2} & \cdots & b_{1,N_{\mathrm{Tx}}} \\ \vdots & \vdots & \ddots & \vdots \\ b_{N_{\mathrm{a}},1} & b_{N_{\mathrm{a}},2} & \cdots & b_{N_{\mathrm{a}},N_{\mathrm{Tx}}} \end{bmatrix} \begin{bmatrix} x_1 \\ \vdots \\ x_{N_{\mathrm{Tx}}} \end{bmatrix} \tag{1.14}$$

which is the same as writing: $\boldsymbol{a} = \boldsymbol{B}\boldsymbol{x}$, where N_{a} is the number of satellite antenna feeds.

The signal is then handled by the beamformer $\boldsymbol{F}$ and is relayed to N_{b} beams. The signal is frequency-shifted, amplified (transparent payload), and sent back to the gateway. The beamformer is actually highly hardware-oriented and we don't want to focus on a particular one. We thus assume a unitary beamformer and additionally an Additive White Gaussian Noise (AWGN), represented by the vector $\boldsymbol{\eta}$ of size N_{b}, such that the elements η_j have mean value $\mu = 0$ and variance $\sigma^2 = N_0$.

This assumption can be done because of the beamformer properties enunciated previously.

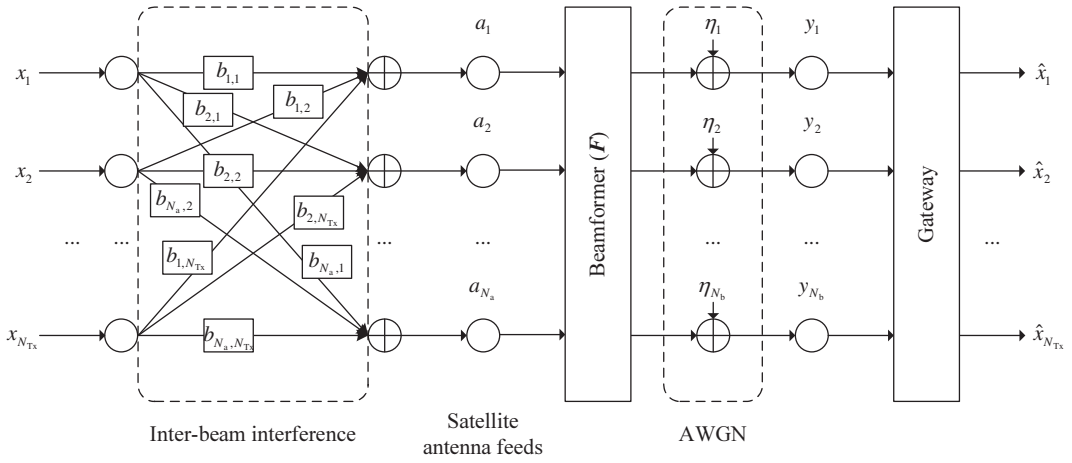


Figure 1.17. *Multi-beam transmission block diagram. It is composed (from the left to the right) of the inter-beam interference block, satellite antenna feeds, satellite spotbeams, the noise block and the gateway. The number of satellite antenna feeds is generally equal or bigger to / than the number of spotbeams.*

The white noise is present at the output knowing it would be coloured because of the beamformer operations. The signal received by the gateway is:

$$\boldsymbol{y} = \boldsymbol{F}\boldsymbol{a} + \boldsymbol{\eta} = \boldsymbol{F}(\boldsymbol{B}\boldsymbol{x}) + \boldsymbol{\eta} \tag{1.15}$$

The distance between the satellite and the gateway is constant. We assume that the signal received by the gateway is proportional to the one received by the satellite (actually the return- down-link of a transparent satellite is designed such a way that the up-link signal-to-noise ratio degrades only marginally as shown in Section 1.1.6). We also assume that the product $\boldsymbol{FB}$ is equivalent to the channel matrix $\boldsymbol{H}$ described in the Section 1.2.1 such that we can write:

$$\boldsymbol{y} = \boldsymbol{H}\boldsymbol{x} + \boldsymbol{\eta} \tag{1.16}$$

where $\boldsymbol{y}$ is thus a vector of N_b elements. The gateway performs different operations in order to estimate the symbols initially transmitted. These estimates are denoted $\hat{\boldsymbol{x}}$. Fig. 1.17 summarises the transmission block diagram previously described.

1.2.4 Absolute Value of the Channel Coefficients

The absolute value of the channel coefficients, that is $|h_{i,j}|$, determines the modification of the amplitude of the transmitted signal between receiver i and transmitter j.

The power of the signal sent by the satellite terminal and received by the satellite is noted

$P_{\mathrm{Rx,sat}}$ and is obtained using [MaBo02], all terms in decibels (equation (1.5) of Section 1.1.6):

$$P_{\mathrm{Rx,sat}} = P_{\mathrm{Tx,t}} + G_{\mathrm{Tx,t}} - L_{\mathrm{out,t}} - L_{\mathrm{pointing,t}} - L_{\mathrm{OBO,t}} + G_{\mathrm{sat}} - L_{\mathrm{ant,sat}} - L_{\mathrm{FS}}$$

We assume the different satellite terminals have identical properties in terms of transmit power, antenna properties, etc. For this reason when performing the link budget (return up-link) all terms remain constant, except the satellite antenna gain (receive gain) and the free space losses which depend directly on the user position on ground. In the return down-link the distance between the satellite and the gateway and the location of the gateway remain the same.

Knowing the position of the users transmitting from the Earth it is possible to compute the satellite antenna gain towards each user for the covering beam but also the "interfering" gains, i.e. the gains of the satellite antenna towards the other users. For each combination beam i - user j we can calculate the corresponding value of the satellite antenna gain.

The link budget also depends on another critical factor for a GEO satellite which is the distance between the user and the satellite (slant range). The slant range varies according to the location of the satellite terminal on the Earth and to the position of the satellite which is assumed here as static. Even if users are transmitting with equal powers they will not be perceived by the satellite the same way. Actually the signal strength will be impaired by the free space losses which are according to the Friis formula [MaBo02]:

$$L_{\mathrm{FS}j} = (4\pi\, S_j/\lambda)^2 \tag{1.17}$$

where $L_{\mathrm{FS}j}$ is the free space loss experienced by user j, S_j the slant range between the satellite and user j, and λ the wave length.

We define a coefficient which is normalised according to the maximum gain and the minimum free space loss, i.e. when the user is perfectly located at the beam centre and with the smallest slant range. In such a case we have the satellite antenna gain $G_{\max}$ and $L_{\mathrm{FS,min}} = \min_j \{L_{\mathrm{FS},j}\}$ the minimum free space loss experienced among the centres of all beams. A given user j will be seen from beam i with a gain $G_{i,j}$ and free space loss $L_{\mathrm{FS},j}$. The coefficient obtained for that user reflects the modification of the amplitude of the signal. This coefficient is noted $|h_{i,j}|$ and is equal to:

$$|h_{i,j}| = \sqrt{\frac{G_{i,j}}{L_{\mathrm{FS},j}} \cdot \frac{L_{\mathrm{FS,min}}}{G_{\max}}} \tag{1.18}$$

If we have N_{Tx} users, then a given user j ($j \in \{1, ..., N_{\mathrm{Tx}}\}$) is seen by N_{Rx} beams and a beam i ($i \in \{1, ..., N_{\mathrm{Rx}}\}$) is seen by N_{Tx} users. We shall consider the case of one user per beam and hence $N_{\mathrm{Tx}} = N_{\mathrm{Rx}}$. We can compute the different coefficients $|h_{i,j}|$ for each combination user - beam such that we obtain a matrix whose size is $N_{\mathrm{Rx}} \times N_{\mathrm{Tx}}$ and which corresponds to the channel matrix $\boldsymbol{H}$. The column j of the matrix describes the channel matrix of the user j in the system (transmitter) and the row i the channel matrix of the beam i in the system (receiver).

The channel matrix $\boldsymbol{H}$ is thus a function of the satellite beam pattern, the position of the users within the beam (different gains) and the distance between the users and the satellite (slant range). In order to simplify the generation of the channel matrix $\boldsymbol{H}$ clear sky conditions (no rain fading events and corresponding scintillation increase) and perfect antenna alignment at the user side are also assumed in the link budget. Finally it has to be remarked that to compute the coefficients of the channel matrix $\boldsymbol{H}$, the radiation pattern of all beams involved in the system have to be taken into account and therefore have to be computed.

1.2.5 Phase of the Channel Coefficients

The channel matrix $\boldsymbol{H}$ is generally composed of complex numbers. The channel coefficient $h_{i,j}$ can also be noted $|h_{i,j}|\,\mathrm{e}^{j\theta_{i,j}}$. The absolute value of the channel coefficient, that is $|h_{i,j}|$, defines how much the amplitude of the transmitted signal will be changed (receiver i - transmitter j, please refer to Section 1.2.4). The phase of the channel coefficient, that is $\theta_{i,j}$, indicates the phase shift applied on the transmitted signal.

The channel matrix $\boldsymbol{H}$ in (1.10) can thus also be written:

$$\boldsymbol{H} = \begin{bmatrix} |h_{1,1}|\,\mathrm{e}^{j\theta_{1,1}} & |h_{1,2}|\,\mathrm{e}^{j\theta_{1,2}} & \cdots & |h_{1,N_{\mathrm{Tx}}}|\,\mathrm{e}^{j\theta_{1,N_{\mathrm{Tx}}}} \\ \vdots & \vdots & \ddots & \vdots \\ |h_{N_{\mathrm{Rx}},1}|\,\mathrm{e}^{j\theta_{N_{\mathrm{Rx}},1}} & |h_{N_{\mathrm{Rx}},2}|\,\mathrm{e}^{j\theta_{N_{\mathrm{Rx}},2}} & \cdots & |h_{N_{\mathrm{Rx}},N_{\mathrm{Tx}}}|\,\mathrm{e}^{j\theta_{N_{\mathrm{Rx}},N_{\mathrm{Tx}}}} \end{bmatrix} \tag{1.19}$$

As already mentioned, in the Return-Link (RL) of satellite systems the transmitters are the satellite terminals on ground and the receivers the beams on board the satellite.

Transmitters

At the transmitter side the signal sent by a satellite terminal toward the satellite will be impacted by a phase shift. Since all the receivers are located in the satellite we can assume

that the phase shift between a given transmitter and all receivers is the same. In other words the phase shift applied for a given column j of the channel matrix $\boldsymbol{H}$ is the same for all rows i with $1 \leq i \leq N_{\mathrm{Rx}}$. Such phase shift can be added to the channel matrix $\boldsymbol{H}$ by considering:

$$\boldsymbol{\Phi}_{\mathrm{Tx}} = \mathrm{diag}\left\{\mathrm{e}^{\mathrm{j}\theta_{\mathrm{Tx},1}}, \mathrm{e}^{\mathrm{j}\theta_{\mathrm{Tx},2}}, \cdots, \mathrm{e}^{\mathrm{j}\theta_{\mathrm{Tx},N_{\mathrm{Tx}}}}\right\} \tag{1.20}$$

and by multiplying it:

$$\boldsymbol{H}_{\Phi_{\mathrm{Tx}}} = \boldsymbol{H}\boldsymbol{\Phi}_{\mathrm{Tx}} \tag{1.21}$$

Receivers

The distance between the feeds on board is fixed meaning that the phase shift between the beams is constant for each realisation of the channel matrix [6]. In other words the phase shift between two receivers, i.e. between two columns of the channel matrix $\boldsymbol{H}$, is the same and does not change over time. In order to apply such a phase shift, while generating the channel matrix, we can build a matrix in which the phase shift between the receivers is stored:

$$\boldsymbol{\Phi}_{\mathrm{Rx}} = \mathrm{diag}\left\{\mathrm{e}^{\mathrm{j}\theta_{\mathrm{Rx},1}}, \mathrm{e}^{\mathrm{j}\theta_{\mathrm{Rx},2}}, \cdots, \mathrm{e}^{\mathrm{j}\theta_{\mathrm{Rx},N_{\mathrm{Rx}}}}\right\} \tag{1.22}$$

and then multiply this matrix with the channel matrix $\boldsymbol{H}$:

$$\boldsymbol{H}_{\Phi_{\mathrm{Rx}}} = \boldsymbol{\Phi}_{\mathrm{Rx}}\boldsymbol{H} \tag{1.23}$$

1.3 Summary

In this Ph.D. thesis we consider geostationary (GEO) satellites with transparent star network topology. We specially focus on the Return-Link (RL), which operating frequency is located in the Ka-band, and assume clear-sky conditions with perfect Line-of-Sight (LoS). For the simulations we take into account a GEO satellite at longitude 19.2° East. This satellite covers Europe by the means of 96 beams, a realistic number for modern satellite systems. Our attention is particularly put on the reduction of the number of colours which permits to increase the per-beam bandwidth and consequently the theoretical capacity.

Three different numbers of colours are considered in this work. The so-called universal frequency reuse ($K = 1$) which is highly interference-limited, three colours ($K = 3$), which increases the distance between beams using the same frequencies, and four colours ($K = 4$), for which the level of Co-Channel Interference (CCI) is the lowest of the three colours (highest

6. It has to be noted that with a frequency of 30 GHz, the wavelength equals 10 cm.

distance between beams using the same frequencies). Two main system sizes are taken into account in order to perform the different investigations. A small scale system which consists of a limited number of seven beams ($B = 7$) and a large scale which corresponds to the "full" ninety six multi-beam satellite system ($B = 96$). The users, also referred as satellite terminals, are randomly generated so that they are located within the coverage area of the beams or manually placed within the spotbeams.

Multi-beam satellite system can actually be regarded as virtual Multiple-Input and Multiple-Output (MIMO) systems. Specially the RL can be considered as a MIMO Multiple Access Channel (MAC) and we assume within this link that all transmitters, i.e. all satellite terminals, have identical properties (in terms of transmit power, antenna properties, etc.). For modelling the satellite channel, the only terms that change the absolute values of the coefficients are the gain of the receiving satellite antenna and the terminal-satellite free space loss, both depending on the user position on ground. The phase of the channel coefficients is modelled by taking into account two effects: the transmitter phase, i.e. the phase shift impacting the signal sent by a satellite terminal toward the satellite, and the receiver phase, i.e. the phase shifts introduced by the beamformer.

Chapter 2

Practical Analysis of the Satellite Channel: Uncoded Bit Error Rate

In this chapter, the purpose is to evaluate the uncoded Bit Error Rate (BER) resulting from a given system which can be depicted by Fig. 2.1.

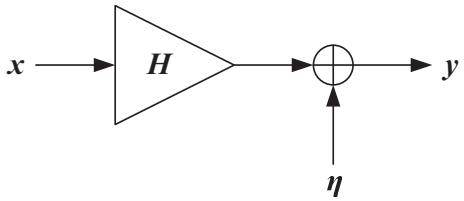


Figure 2.1. *Typical input-output system for bit error rate simulations.*

Measuring the so-called uncoded BER is always very common when realising Multi-User Detection (MUD) and dealing with Interference Cancellation (IC). It permits to be completely independent of any particular coding and decoding scheme like Bose, Chaudhuri, and Hocquenghem (BCH), Low Density Parity Check Code (LDPC), etc.

This chapter presents the different receivers taken into account in this study, including receivers performing interference cancellation. The BER simulator and the receivers are validated using a Rayleigh channel and finally the impact of the satellite channel together with the gains achieved while reducing the number of colours are analysed. Also a novel type of receiver is introduced.

2.1 Processing of the Received Signal

2.1.1 Conventional Receiver

The conventional receiver, referred also as "simple" receiver in this document, consists into evaluating directly from the received signal vector $\boldsymbol{y}$ the transmitted vector $\boldsymbol{x}$. The estimate vector $\hat{\boldsymbol{x}}$ is thus derived from the vector $\boldsymbol{y}$ and therefore for this type of receiver the number of transmitters equals the number of receivers. The channel matrix $\boldsymbol{H}$ is thus a square matrix of size $N_{\mathrm{Rx}} \times N_{\mathrm{Rx}}$ where $N_{\mathrm{Rx}} = N_{\mathrm{Tx}}$. This kind of receiver only assumes phase detection of the users' signal.

2.1.2 Zero Forcing Equaliser

When neglecting the presence of the noise in the system, i.e. when the level of the noise is low, we can simplify the IO system as follows:

$$\boldsymbol{y} = \boldsymbol{H}\,\boldsymbol{x} \tag{2.1}$$

and this remains into having:

$$\hat{\boldsymbol{x}} = \boldsymbol{G}\,\boldsymbol{y} = \boldsymbol{G}\,\boldsymbol{H}\,\boldsymbol{x} \tag{2.2}$$

The best way of estimating the transmitted signal $\boldsymbol{x}$ is thus to simply solve:

$$\boldsymbol{G}\,\boldsymbol{H} = \boldsymbol{I} \tag{2.3}$$

On the one hand, if the channel matrix $\boldsymbol{H}$ is a square matrix , i.e. when the number of transmitters equals the number of receivers, and has full rank, then the system is solved by using:

$$\boldsymbol{G} = \boldsymbol{H}^{-1} \tag{2.4}$$

On the other hand, if the channel matrix $\boldsymbol{H}$ is not square, and has full column rank, then we need to use a generalisation of the inverse which is called "pseudo-inverse". The pseudo-inverse of a matrix $\boldsymbol{A}$, where $\boldsymbol{A} \in \mathbb{R}^{M \times N}$, is written $\boldsymbol{A}^{+}$ and is defined as:

$$\boldsymbol{A}^{+} = \left(\boldsymbol{A}^{\mathrm{T}}\,\boldsymbol{A}\right)^{-1}\boldsymbol{A}^{\mathrm{T}} \tag{2.5}$$

$\boldsymbol{A}^{+}$ is also-called Moore-Penrose pseudo-inverse. In the case of a matrix composed of complex numbers, like our channel matrix $\boldsymbol{H}$, we have:

$$\boldsymbol{H}^{+} = \left(\boldsymbol{H}^{\mathrm{H}}\,\boldsymbol{H}\right)^{-1}\boldsymbol{H}^{\mathrm{H}} = \boldsymbol{W} = \boldsymbol{G}_{\mathrm{ZF}} \tag{2.6}$$

The Moore-Penrose pseudo-inverse of the channel matrix is generally denoted as $\boldsymbol{W}$.

Hence if we know perfectly the channel matrix $\boldsymbol{H}$ at the receiver side, then having a filter which is the pseudo-inverse of the channel matrix permits to find back an estimate the transmitted signal $\boldsymbol{x}$. This filter is called Zero Forcing (ZF) and performs linear operations consisting into nulling the off diagonal elements of the channel matrix, i.e. to remove the interference (this explains the name "Zero Forcing" of this filter). However if we write down again the equation of the system while considering the noise, we obtain:

$$\boldsymbol{G}_{\mathrm{ZF}}\,\boldsymbol{y} = \boldsymbol{W}\,\boldsymbol{y} = \boldsymbol{W}\,(\boldsymbol{H}\,\boldsymbol{x} + \boldsymbol{\eta}) = \boldsymbol{x} + \boldsymbol{W}\,\boldsymbol{\eta} \tag{2.7}$$

As can be seen from the previous equation, the drawback of the Zero Forcing equalisation is the amplification the noise component (through the additional term $\boldsymbol{W}\boldsymbol{\eta}$).

2.1.3 Minimum Mean Square Error Operation

If we consider the Minimum Mean Square Error (MMSE) criterion to design the filter, i.e. finding the filter which minimises the error between the input signal vector $\boldsymbol{x}$ and the estimate vector $\hat{\boldsymbol{x}}$, then we can write:

$$\arg\min_{\boldsymbol{G}} \left\{ \mathrm{E}\left[||\boldsymbol{x} - \hat{\boldsymbol{x}}||_2^2 \right] \right\} = \arg\min_{\boldsymbol{G}} \left\{ \mathrm{E}\left[||\boldsymbol{x} - \boldsymbol{G}\,\boldsymbol{y}||_2^2 \right] \right\} \tag{2.8}$$

The filter we are trying to design is the so-called "MMSE filter" and is represented by the matrix $\boldsymbol{G}_{\mathrm{MMSE}}$.

It can be shown that (please refer to Section C.2.3 to see the complete proof of the following expressions):

$$\boldsymbol{G}_{\mathrm{MMSE}} = \arg\min_{\boldsymbol{G}} \left\{ \mathrm{tr}\left\{\boldsymbol{C}_{\boldsymbol{x}}\right\} - \mathrm{tr}\left\{\boldsymbol{C}_{\boldsymbol{x},\boldsymbol{y}}\,\boldsymbol{G}^{\mathrm{H}}\right\} - \mathrm{tr}\left\{\boldsymbol{G}\,\boldsymbol{C}_{\boldsymbol{x},\boldsymbol{y}}^{\mathrm{H}}\right\} + \mathrm{tr}\left\{\boldsymbol{G}\,\boldsymbol{C}_{\boldsymbol{y}}\,\boldsymbol{G}^{\mathrm{H}}\right\} \right\} \tag{2.9}$$

where $\boldsymbol{C}_{\boldsymbol{x}}$, $\boldsymbol{C}_{\boldsymbol{x},\boldsymbol{y}}$ and $\boldsymbol{G}\,\boldsymbol{C}_{\boldsymbol{y}}$ are respectively the covariance of the transmitted signal vector $\boldsymbol{x}$, the expectation of $\boldsymbol{x}\,\boldsymbol{y}^{\mathrm{H}}$ (i.e. $\mathrm{E}\left[\boldsymbol{x}\,\boldsymbol{y}^{\mathrm{H}}\right]$), and the covariance of the received signal vector $\boldsymbol{y}$.

The solution to this problem is:

$$\boldsymbol{G}_{\mathrm{MMSE}} = \boldsymbol{C}_{\boldsymbol{x},\boldsymbol{y}}\,\boldsymbol{C}_{\boldsymbol{y}}^{-1} \tag{2.10}$$

Exploiting the solution and expressing the different covariance matrices, we obtain:

$$\boldsymbol{G}_{\mathrm{MMSE}} = \boldsymbol{H}^{\mathrm{H}}\left[\boldsymbol{H}\,\boldsymbol{H}^{\mathrm{H}} + N_0\,\boldsymbol{I}\right]^{-1} = \left[\boldsymbol{H}^{\mathrm{H}}\boldsymbol{H} + N_0\,\boldsymbol{I}\right]^{-1}\boldsymbol{H}^{\mathrm{H}} \tag{2.11}$$

where N_0 is the noise power spectral density.

2.1.4 Optimal Successive Interference Cancellation

Successive Interference Cancellation (SIC) can be inserted right after the two filters defined previously, i.e. Zero Forcing (ZF) and Minimum Mean Square Error (MMSE). The principle of SIC is to use consecutively the estimation of the transmitted symbols so that to lower the amount of interference for which they are responsible in the received vector $\boldsymbol{y}$ [TsVi08]. Performing SIC is equivalent to realise Multi-User Detection (MUD) in the return-link of a multi-beam satellite system in which the channel is a multi-user MIMO multiple access channel (MU-MIMO MAC, please refer to Section 1.2.2 for more details). In this section the superscript (i) refers to the i-th realisation of a vector or a matrix.

The optimal SIC consists into taking fully advantage of the MIMO system (Fig. 2.2, [TsVi08]). The initial received signal $\boldsymbol{y}$, that is also $\boldsymbol{y}^{(1)}$, is firstly filtered with $\boldsymbol{G}^{(1)}$ in order to obtain the estimate vector $\hat{\boldsymbol{x}}^{(1)}$. The observable of the strongest user is then decoded and its impact is subtracted from the vector $\boldsymbol{y}^{(1)}$ by using the channel matrix $\boldsymbol{H}$:

$$\boldsymbol{y}^{(2)} = \boldsymbol{y}^{(1)} - \boldsymbol{h}_{j_1^*}\, \hat{x}_{j_1^*}$$

where $\boldsymbol{y}^{(1)}$ corresponds to the first realisation of the received vector and $\boldsymbol{h}_{j_1^*}$ to the j_1^*-th column vector of the initial channel matrix $\boldsymbol{H}$. The output vector is filtered again using $\boldsymbol{G}^{(2)}$ which is a new version of the linear equaliser, computed with the channel matrix which has now $N_{\mathrm{Tx}}-1$ remaining columns. Decision and subtraction are realised for the next strongest user and this operation is performed until all transmitters are detected [TsVi08]. The order with which the detection is done is of paramount importance since an error can spread over the remaining transmitters to be detected. The optimal ordering to be applied depends of course on the filtering performed by the receiver (please refer to Section 3.2.2 for more details).

As can be seen in Fig. 2.2 the transmitters are detected one by one and interference is removed each time. It is obvious that ordering and interference cancellation do not need to be performed for the last transmitter to be decoded. The transmitter indexes which are represented by $j_1^*, j_2^*, ..., j_{N_{\mathrm{Tx}}}^*$ are related to the initial transmitter indexes, i.e. ranging from 1 to N_{Tx}. In terms of computational complexity, both ZF and MMSE linear filtering are in the order of $O\left(N_{\mathrm{Tx}}^3\right)$ and once associated to the SIC operation it reaches an higher order of magnitude, i.e. $O\left(N_{\mathrm{Tx}}^4\right)$ (filtering and cancelling are realised N_{Tx} times) [KaViHa05]. Finally optimal ordering represents an additional complexity in the order of $O\left(N^3\right)$, with $N = N_{\mathrm{Tx}}, N_{\mathrm{Tx}}-1, ..., 1$. Hence the complexity of such receiver grows rapidly with the number

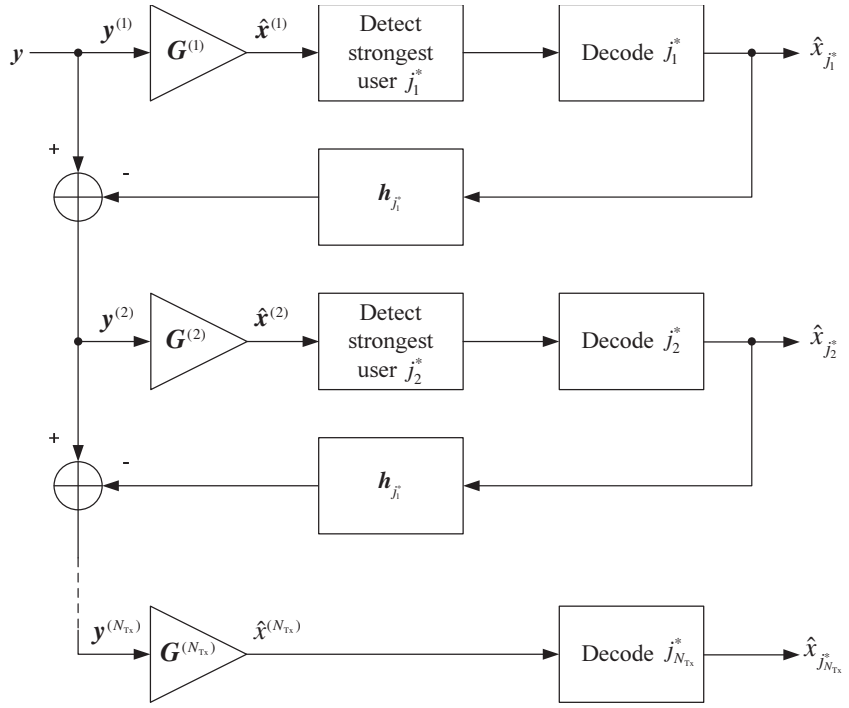


Figure 2.2. *Receiver architecture with optimal SIC.*

of transmitters and a new sub-optimal receiver, with a different architecture, can be designed so as to reduce the overall complexity of the Interference Cancellation (IC) process.

It has to be mentioned that Minimum Mean Square Error (MMSE) with optimal Successive Interference Cancellation (SIC) is capacity achieving, as can be seen in Section 3.2.3, and therefore should offer the best performance.

2.1.5 Successive Interference Cancellation with Maximal Ratio Combining

The previous receiver architecture performs both filtering and ordering operations for each stream (Section 2.1.4). Due to the diagonal structure of the satellite channel (remind that the diagonal elements of the channel matrix $\boldsymbol{H}$ correspond to the "useful" signal), directly related to the strong Line-of-Sight (LoS) components, we could save in complexity by designing a new, but sub-optimal, receiver. This section presents a new heuristic Interference Cancellation (IC) algorithm which is based on the well-known Maximal Ratio Combining (MRC). In this section the superscripts (0) and (1) correspond to the initial version and to the new version of a vector, respectively.

Maximal Ratio Combining (MRC) takes benefit of the presence of the transmitted signal in multiple receivers so that it maximises the equivalent Signal-to-Noise Ratio (SNR). It can be

shown that the SNR in a Single-Input and Multiple-Output (SIMO) system is actually the sum of the SNR present in the different branches of the system (please refer to Section 3.1.2). This receiver uses MRC in order to re-estimate the symbol of a given transmitter [BaMeLe03]. To do so all other estimated symbols are considered; in order to better explain the principle, we consider as example the re-estimation of the symbol sent by the first transmitter. We denote $\hat{\boldsymbol{x}}_{\neq 1}^{(1)}$ the column vector containing all symbols but the one of transmitter 1. Such vector is obtained by performing the following simple operations:

$$\hat{\boldsymbol{x}}_{\neq 1}^{(1)} = \hat{\boldsymbol{x}}^{(0)} - \boldsymbol{e}_1 \circ \hat{\boldsymbol{x}}^{(0)}$$

where $\hat{\boldsymbol{x}}^{(0)}$ corresponds to the first estimate vector, which is also written $\hat{\boldsymbol{x}}'$. $\boldsymbol{e}_j$ is the standard basis vector where $\boldsymbol{e}_j$ is the j-th column of the corresponding identity matrix. The operator "$\circ$" represents the Hadamard product, also known as entrywise product. Here $\boldsymbol{e}_1 = [1 \ldots 0]^T$ thus we can write:

$$\hat{\boldsymbol{x}}_{\neq 1}^{(1)} = [0 \ \hat{\boldsymbol{x}}_2^{(0)} \ \ldots \ \hat{\boldsymbol{x}}_{N_{\mathrm{Tx}}}^{(0)}]^T \tag{2.12}$$

By subtracting the product of $\boldsymbol{H}$ with $\hat{\boldsymbol{x}}_{\neq 1}^{(1)}$ from the received symbol $\boldsymbol{y}$ we have:

$$\boldsymbol{r}_1^{(1)} = \boldsymbol{y} - \boldsymbol{H}\,\hat{\boldsymbol{x}}_{\neq 1}^{(1)} = \begin{bmatrix} h_{1,1}\,x_1 + \eta_1 \\ \ldots \\ h_{N_{\mathrm{Rx}},1}\,x_1 + \eta_{N_{\mathrm{Rx}}} \end{bmatrix} \tag{2.13}$$

One can see that $\boldsymbol{r}_1^{(1)}$ depends only on the transmitted symbol x_1. The j-th column vector of the channel matrix $\boldsymbol{H}$ which plays a role in this equation is noted $\boldsymbol{h}_j$. By multiplying the Hermitian of $\boldsymbol{h}_1$ with $\boldsymbol{r}_1^{(1)}$ we get:

$$\boldsymbol{h}_1^{\mathrm{H}}\,\boldsymbol{r}_1^{(1)} = \boldsymbol{h}_1^{\mathrm{H}}\,\boldsymbol{h}_1\,x_1 + \boldsymbol{h}_1^{\mathrm{H}}\,\boldsymbol{\eta} \tag{2.14}$$

By applying MRC, i.e. maximising the signal-to-noise ratio (SNR), we finally obtain:

$$\hat{x}_1^{(1)} = \frac{\boldsymbol{h}_1^{\mathrm{H}}\,\boldsymbol{r}_1^{(1)}}{\boldsymbol{h}_1^{\mathrm{H}}\,\boldsymbol{h}_1} = \hat{x}_1$$

where $\hat{x}_1^{(1)}$ corresponds to the new estimate of $\hat{x}_1^{(0)}$, more particularly to the final estimate of x_1.

By generalising we can write that re-estimating the symbol x_j using MRC consists in performing the following operations:

$$\hat{\boldsymbol{x}}_{\neq j}^{(1)} = \hat{\boldsymbol{x}}_{\neq j-1}^{(1)} + \boldsymbol{e}_{j-1} \circ \hat{\boldsymbol{x}}^{(1)} - \boldsymbol{e}_j \circ \hat{\boldsymbol{x}}^{(0)} \tag{2.15}$$

then:

$$\boldsymbol{r}_j^{(1)} = \boldsymbol{y} - \boldsymbol{H}\,\hat{\boldsymbol{x}}_{\neq j}^{(1)} \tag{2.16}$$

and finally:

$$\hat{x}_j^{(1)} = \frac{\boldsymbol{h}_j^{\mathrm{H}}\,\boldsymbol{r}_j^{(1)}}{\boldsymbol{h}_j^{\mathrm{H}}\,\boldsymbol{h}_j} = \hat{x}_j \tag{2.17}$$

It has to be remarked that the column vector $\hat{\boldsymbol{x}}^{(1)}$ is initialised with the first version of the estimates, i.e. $\hat{\boldsymbol{x}}^{(0)} = \hat{\boldsymbol{x}}'$. Additionally $\hat{\boldsymbol{x}}_{\neq 0}^{(1)} = \hat{\boldsymbol{x}}^{(1)} = \hat{\boldsymbol{x}}^{(0)}$ and $\boldsymbol{e}_0$ is a zeros column vector.

The corresponding receiver architecture, which is actually a new heuristic Interference Cancellation (IC) algorithm, is summarised in the next figure (Fig. 2.3). The received vector $\boldsymbol{y}$ is the input of a linear filter $\boldsymbol{G}$ which represents either the Zero Forcing filter or the Minimum Mean Square Error filter. The filter outputs N_{Tx} observables which correspond to $\hat{\boldsymbol{x}}'$, the estimates of the transmitted symbols. The "ordering" block indicates in which order the N_{Tx} symbols have to be re-estimated. The SIC process starts with the first stream and using the estimates, the $N_{\mathrm{Tx}} - 1$ interferers for this specific stream are subtracted using the channel matrix. It results into a vector of N_{Rx} replicas of the symbol transmitted by the first user to be re-estimated. The MRC is then used in order to maximise the signal-to-noise ratio and an hard decision is performed. The output of this process is taken into account to update the estimates issued from the filter $\boldsymbol{G}$ and, without changing the initial users' order, the operations continues till the transmitted symbol of all users are re-estimated.

The selection of the symbol to be re-estimated can be improved instead of doing this operation arbitrarily. Actually selecting users having the strongest signal in order to re-estimate the one having the weakest signal would improve the accuracy of the estimations. This is called optimal ordering and can be realised by analysing the content of the channel matrix $\boldsymbol{H}$ (this operation is realised by the "ordering" block present in Fig. 2.3). In this case the ordering depends on the signal level perceived by the receivers, more particularly to the signal-to-interference plus noise ratio (SINR); please refer to the Section 3.2.3 which is dedicated to ordering. This novel approach using SIC-MRC has the advantage of offering low complexity since both filtering and ordering operations are performed only once. The computational complexity of such receiver is therefore in the order of $O\left(N_{\mathrm{Tx}}^3\right)$ for the linear filtering and $O\left(N^3\right)$, with $N = N_{\mathrm{Tx}}$, for the ordering which is performed only once. The complexity of MRC can be neglected with respect to the previous magnitudes since it is realised on a column matrix. Hence this represents a considerable gain in terms of computational complexity when compared to the optimal SIC architecture (Section 2.1.4).

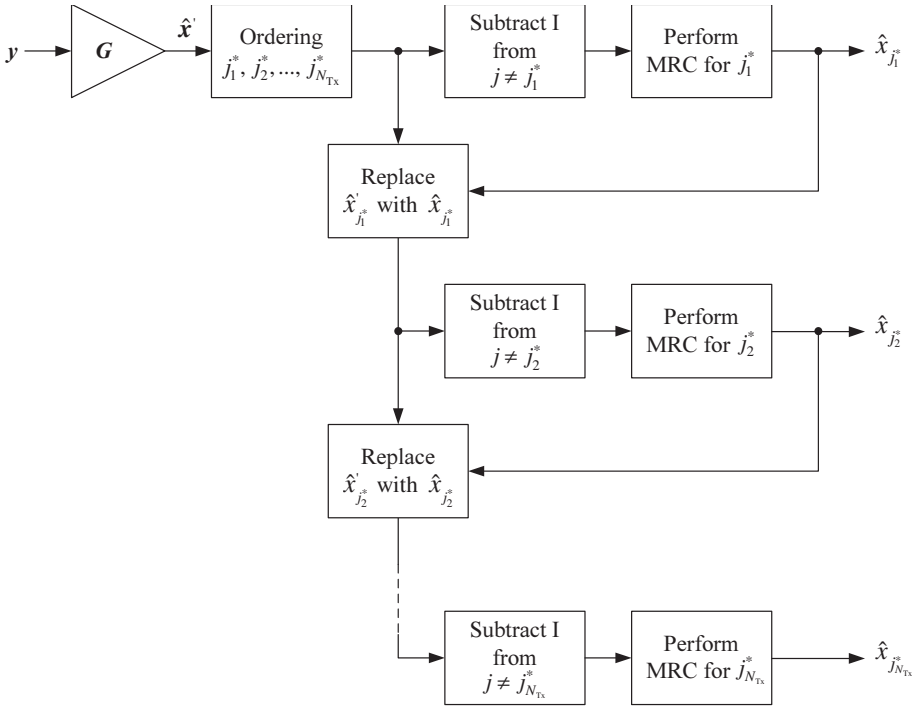


Figure 2.3. *Receiver architecture integrating SIC with MRC.*

2.2 Performance Analysis

This section presents the performance of the different receivers in terms of BER which is first evaluated and assessed with the Rayleigh channel and then with the satellite channel.

2.2.1 Rayleigh Channel - Validation of the Receivers

The Rayleigh channel is assumed to be time-varying meaning that for each sequence of transmitted symbols there is a particular channel realisation. The system is composed of seven transmitters and seven receivers, therefore this is equivalent to a 7×7 MIMO system. The uncoded BER is simulated using the Binary Phase-Shift Keying (BPSK) modulation and the results are averaged among all transmitters.

When analysing the performance of the receivers (Fig. 2.4) we can clearly see that a simple receiver provides 50% of bit error rate over the whole E_b/N_0 range. This behaviour is directly related to the channel type, more particularly to the impact of the multi-path environment, and was expected. A receiver integrating a Zero Forcing (ZF) equalisation already provides great improvements. However when compared with the MMSE receiver we can see, as expected, that the drawback of ZF is the amplification of the noise (difference of about 12 dB

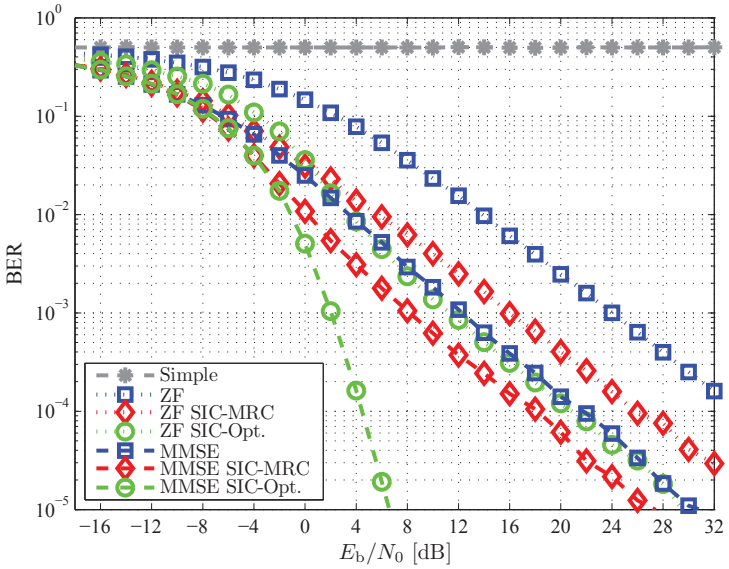


Figure 2.4. *Average BER performance of the receivers with a* 7×7 *Rayleigh channel and BPSK modulation.*

at a BER of 10^{-3} [1]). MRC provides good performance in the noise-limited region since it acts as a matched filter. This can be seen in the results when looking at the curves obtained with the receivers integrating SIC together with MRC. When leaving the noise-limited region SIC helps removing the impact of the interference. Still for a BER equal to 10^{-3} the gain of the SIC-MRC receivers is about 8 and 4 dB respectively for ZF and MMSE. The optimal receiver architecture, i.e. the receiver performing in a recursive manner the filtering, the ordering, the decoding and the interference cancellation, offers the best results. There is however a single exception for what concerns SIC-MRC with ZF. In the noise-limited region MRC permits to obtain better performance than ZF with optimal SIC. For high SNR the gain at 10^{-3} is almost 5 dB for the ZF receiver and 6 dB for the MMSE receiver with respect to the SIC-MRC receiver architecture. However if the gains are almost constant in the interference-limited region among all receivers, the MMSE receiver with optimal SIC distinguishes itself with a stronger waterfall effect where the gain increases from 6 to almost 16 dB respectively at a BER of 10^{-3} and 10^{-4}. Even if the ZF receiver with optimal SIC performs better than MMSE alone for high SNR, the difference between these two receivers is too small (gain less than 1 dB) in view of the complexity imposed by the Interference Cancellation (IC).

The results obtained with the different receivers perfectly match the information theory

1. Theoretically both ZF and MMSE should offer identical performance at high SNR regime, however it is not the case in practice, as investigated in [JiVaLi05].

and therefore validate the simulation environment for the next evaluations with the satellite channel.

2.2.2 Satellite Channel - 2×2 System

No Interference

We first consider the return-link of a 2×2 system, i.e. a system composed of two transmitters (users) and two receivers (beams). The channel matrix $\boldsymbol{H}$ is therefore of size 2×2. We assume the system has no interference, which is actually the case if the two beams use different frequencies. The channel matrix is thus strictly diagonal, i.e. the elements outside the diagonal, also called off-diagonal elements, equal 0, more particularly $h_{1,2} = h_{2,1} = 0$. We focus on a specific scenario in which a user is located in the middle of its own beam (user 1) and another user is located on the beam border (user 2). We finally assume that the channel does not influence the phase of the users' signal but only the amplitude.

The channel matrix is thus manually composed of the following diagonal coefficients: $h_{1,1} = 1$ and $h_{2,2} = \sqrt{10^{(-3/10)}}$ since user 2 is perceived by the beam satellite with a receive gain inferior of 3 dB to what would be perceived in the middle of the beam (beam border at -3 dB).

As a summary the channel matrix $\boldsymbol{H}$ is:

$$\boldsymbol{H} = \begin{bmatrix} h_{1,1} & h_{1,2} \\ h_{2,1} & h_{2,2} \end{bmatrix} = \begin{bmatrix} 1 & 0 \\ 0 & 0.7079 \end{bmatrix}$$

The uncoded BER was evaluated for an energy per symbol over noise power spectral density E_s/N_0 ranging from -8 dB to 12 dB and with modulation BPSK. The results are shown in Fig. 2.5.

We can observe in Fig. 2.5 that the BER of user 1 is always lower than the one of user 2 which is perfectly normal. For high SNR, the shift between user 1 and user 2 becomes more clear. Actually user 2 needs 3 dB more E_s/N_0 in order to achieve the same BER as user 1. This result is perfectly logic because user 2 is at the beam border and thus the signal level received by its beam is 3 dB lower.

High Interference - "Bad Case"

Like in the previous case we consider the return-link of a 2×2 system, i.e. a system composed of two transmitters (users) and two receivers (beams). The channel matrix $\boldsymbol{H}$ is again of

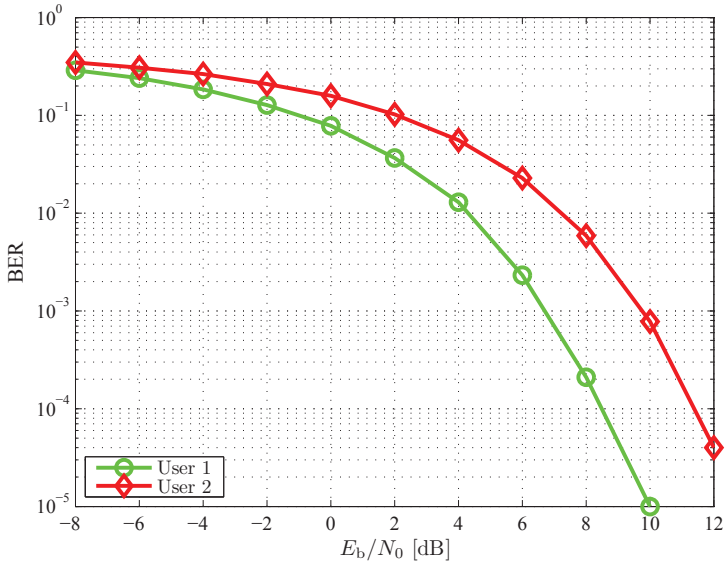


Figure 2.5. *BER of a simple* 2×2 *satellite system without interference and BPSK modulation.*

size 2×2. We still assume that user 1 is located in the middle of its own beam but user 2 is now located at a particular position which constitutes a so-called "bad case" for user 1 and therefore is seen as a "bad" user. Actually user 2 is located close to the border of its own beam but in such a way it interferes as much as possible with beam 1 and thus with user 1.

As example we consider as reference a beam covering the city of Munich (beam 1) and its top right surrounding beam (beam 2). The border of the beams and the location of the two users in each beam is depicted by Fig. 2.6.

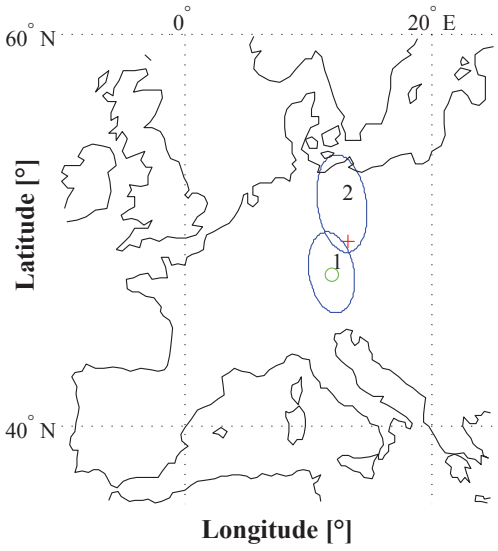


Figure 2.6. *Beam border and user location of a* 2×2 *system with high interference.*

The channel matrix of this system takes now into account two effects which are the difference in the receive gain of the satellite beams and the difference of free space loss with respect to the center of the beam as described in Section 1.2.4. In this particular case the channel matrix $\boldsymbol{H}$ is composed of the following coefficients:

$$\boldsymbol{H} = \begin{bmatrix} h_{1,1} & h_{1,2} \\ h_{2,1} & h_{2,2} \end{bmatrix} \simeq \begin{bmatrix} 1.00 & 0.63 \\ 0.33 & 0.83 \end{bmatrix}$$

When looking at the coefficients of the channel matrix $\boldsymbol{H}$ it can be seen that user 1 is located in the middle of its own beam ($h_{1,1} \simeq 1.0$) and that it interferes with beam 2 ($h_{2,1} \simeq 0.33$). In the same way user 2 is quite far from the center of the beam since the difference of gain is around -1.6 dB but that it interferes a lot with beam 1 ($h_{1,2} \simeq 0.63$). The carrier-to-interference ratio (CIR) perceived by the beams is around 4 dB and 8 dB for the first and the second beam, respectively. User 2 is therefore a strong interferer for beam 1. The purpose is to get an insight into the impact of the different receiver architectures on such very simple scenario.

No interference vs. no interference cancellation:

Fig. 2.7 shows the BER performance when having a simple receiver without interference and with interference, and linear filtering (ZF and MMSE). In the former case, i.e. without interference, the channel matrix $\boldsymbol{H}$ is forced to be strictly diagonal, i.e. $h_{1,2} = h_{2,1} = 0$ so that the interference between the users and the beams is removed. In the latter case the channel matrix is not modified and the received signal is either directly used to estimate the transmitted symbols, meaning there are no operations performed on the received vector $\boldsymbol{y}$ (simple receiver), or a linear filtering is applied. The uncoded BER is evaluated for an energy per bit over noise power spectral density E_b/N_0 ranging from -8 dB to 18 dB and with modulation BPSK.

The shift in the BER between user 1 and user 2 while having no interference (Fig. 2.7) corresponds to the difference of receive gain between both users (around 1.6 dB). One can see that user 1 performs better than user 2. However in the presence of interference and with a simple receiver the tendency is reversed as soon as we exit the noise-limited region, i.e. for $E_\mathrm{b}/N_0 > 0$ dB. Actually since user 1 is strongly interfered by user 2, its BER gets worse than the one of user 2. It has to be remarked that the best BER that can be reached in such a system while removing completely the interference is the one shown by the two “no

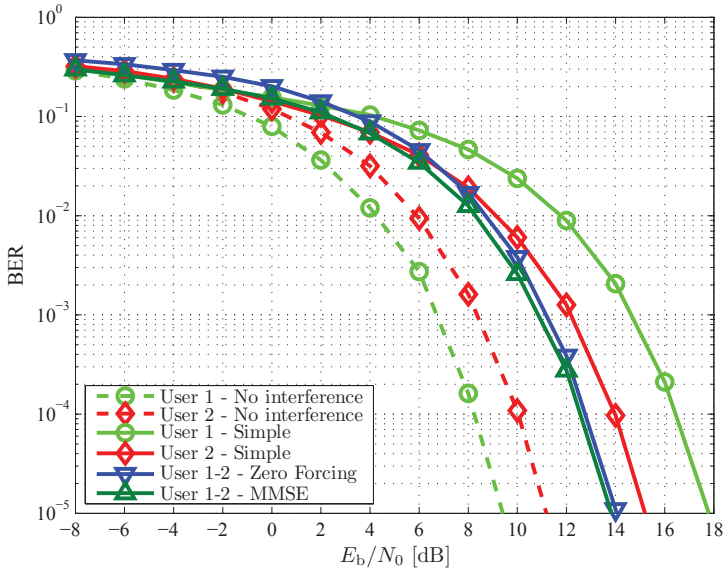


Figure 2.7. *BER performance in a* 2×2 *satellite system with high interference, no interference cancellation and BPSK modulation.*

interference" curves.

Zero Forcing:

The Zero Forcing (ZF) equalisation was implemented in order to better estimate the transmitted symbols in presence of interference (please refer to Section 2.1.2 for more details). To summarise this linear operation tries to null out the off-diagonal terms of the channel matrix, i.e. to remove interference. However Zero Forcing is not optimal since it amplifies the noise (please refer to Section C.2.3 for more information).

As expected Zero Forcing tries to remove interference since user 1 and user 2 now get the same BER (Fig. 2.7). However Zero Forcing does not operate correctly in the noise-limited region, it performs actually worse than the simple receiver. This is due to the amplification of the noise which is performed by the linear operation. Therefore Zero Forcing provides good results when the energy per bit over noise power spectral density is above 3 dB and 8 dB respectively for user 1 and user 2.

Minimum Mean Square Error:

The Minimum Mean Square Error (MMSE) operation requires the knowledge of the noise level in the system (please refer to Section 2.1.3 for more details). The expression of the filter is quite similar to the one of ZF but as mentioned before the noise power spectral density

is required. MMSE should perform better than ZF in theory and also by definition (please refer to Section C.2.3 for more information).

When compared to the results obtained with the ZF filter it is obvious that there is no more noise amplification (Fig. 2.7). Actually MMSE performs clearly better than ZF.

Zero Forcing with Successive Interference Cancellation:

The two receivers integrating Successive Interference Cancellation (SIC) presented in Section 2.1 are considered together with Zero Forcing as equaliser.

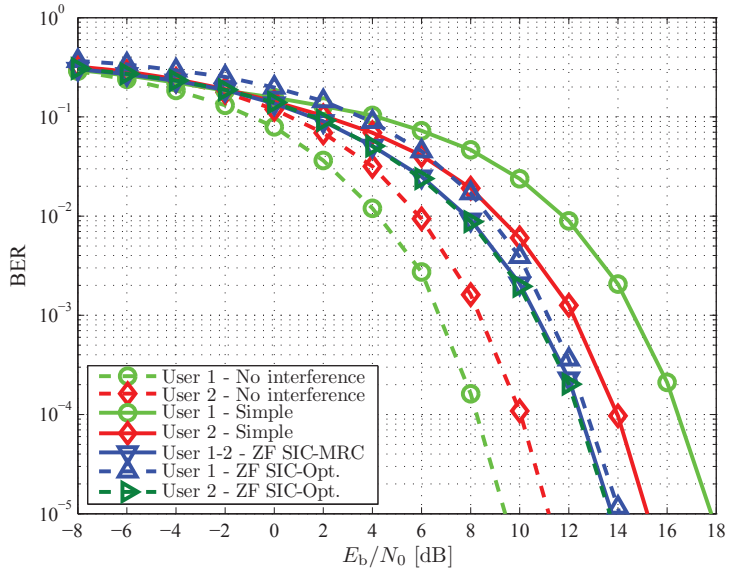


Figure 2.8. *BER performance in a* 2×2 *satellite system with high interference, Zero Forcing, Successive Interference Cancellation and BPSK modulation.*

The receivers performing SIC provides sightly better results than the one with Zero Forcing alone (Fig. 2.7). The SIC with Maximal Ratio Combining (MRC) architecture permits to offer perfectly identical performance to both users whereas the optimal architecture worsen the performance of the first user for low SNR. This behaviour is due to the amplification of the noise realised by Zero Forcing in the low SNR region, amplification which is actually removed using MRC.

Minimum Mean Square Error with Successive Interference Cancellation:

As before the two receivers capable of realising SIC are taken into account with the Minimum

Mean Square Error filter.

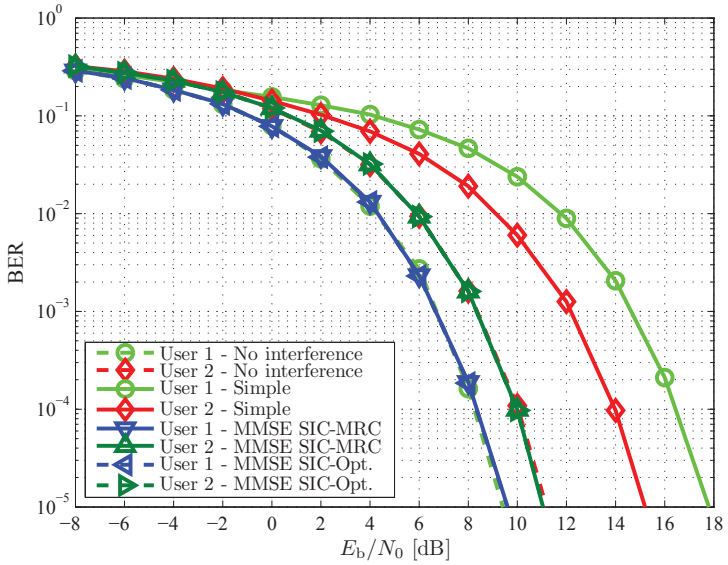


Figure 2.9. *BER performance in a* 2×2 *satellite system with high interference, Minimum Mean Square Error, Successive Interference Cancellation and BPSK modulation.*

The results shown by Fig. 2.9 indicate that both SIC architectures using MMSE are able to remove completely the interference from both users' signals. The SIC-MRC architecture gives promising results since it performs as well as the optimal SIC architecture but with lower complexity.

2.2.3 Satellite Channel with Full Frequency Reuse - 7×7 System

The purpose is now to evaluate the impact of the satellite channel on the performance of the different receivers when having seven beams ($B = 7$, therefore 7×7 system) and full frequency reuse ($K = 1$). The BER measured in this channel scenario is the one experienced by the user located in the middle of the system. We are actually interested in the ability of the receivers to deal with the interference caused by the six surrounding users (the BER seen by the surrounding users is actually in another magnitude). As reminder the good case corresponds to a low interference scenario and the bad case to a high interference scenario from the point of view of the seven users placed in the different beams (please refer to Fig. 1.9).

Low Interference - "Good Case"

In the good case, i.e. the scenario containing the so-called "good users", the channel matrix has strong diagonal coefficients. Even if we are in a low interference scenario, the utilisation

of a single colour restricts our system to be interference-limited. It has to be remarked that the so-called "good case" is actually a good case for the seven users when considered all together but not from the single point of view of the user located in the beam of interest.

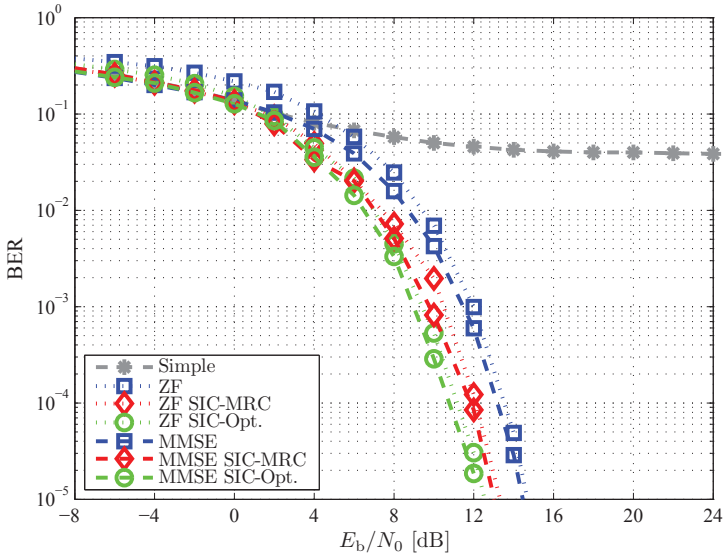


Figure 2.10. *BER performance of the receivers in a* 7×7 *satellite system, full frequency reuse* ($K = 1$)*, low interference scenario, BPSK modulation, and for the user located in beam 1.*

When analysing the results (Fig. 2.10) we see that the user of interest is interference-limited since with a simple receiver the BER decreases together with the noise level but remains constant for high SNR (about 4.10^{-2}). As before ZF tries to null out the interference but amplifies the noise and therefore provides worse results than a simple receiver for low SNR in this case. Both ZF and MMSE receivers tend to get the same performance as the SNR increases. This is due to the decrease of the noise and to the strong diagonal coefficients of the channel matrix. Like in the Rayleigh scenario the utilisation of SIC with MRC in the ZF receiver presents a compensation effect which acts on the amplified noise since it provides the same performance as MMSE alone in the range -8 dB - 0 dB. The two receivers with SIC and MRC outperform the ones without IC; the best results are obtained by the receivers using the optimal SIC architecture. In the Rayleigh channel scenario the filtering stage impacted radically the gains, here the architecture of the receiver is of utmost importance. Thereby when analysing the results at BER 10^{-4} the SIC with MRC receivers bring about 1.4 dB gain with respect to the architecture without IC and the receivers with the optimal SIC architecture 1 dB additional gain leading to a total gain of about 2.4 dB again with respect to the architecture without IC. It has to be remarked that at 12 dB the BER experienced by the surrounding users (not shown by Fig. 2.10) is about 6 times less than the BER of the user of interest when using the simple receiver.

High Interference - "Bad Case"

In the bad case, i.e. the scenario containing the so-called "bad users", the channel matrix is not strongly diagonal. In this particular scenario, the utilisation of one single colour makes our system highly interference-limited, more particularly for the user located in the beam of interest.

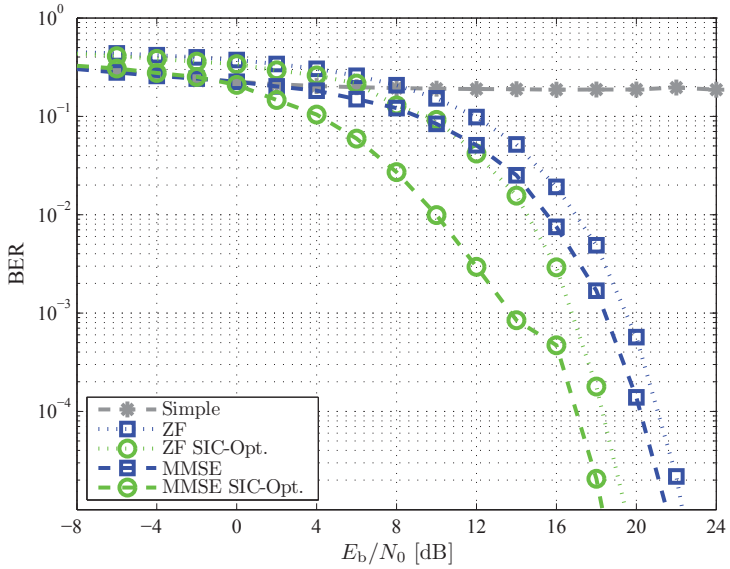


Figure 2.11. *BER performance of the receivers in a* 7×7 *satellite system, full frequency reuse* ($K = 1$)*, high interference scenario, BPSK modulation, and for the user located in beam 1.*

The results are radically different with this scenario (Fig. 2.11). On the one hand, when using a simple receiver the user is highly interference-limited since it reaches a BER no less than 2.10^{-1} for high SNR (5 times higher than the one obtained in the low interference scenario, Fig. 2.10). This was of course expected. On the other hand, even if the receivers integrating SIC with MRC (not shown in these results for the reasons mentioned hereafter) outperforms the optimal complex SIC architecture in the low SNR region, this sub-optimal receiver architecture does not perform well for high SNRs. Actually such receiver is not suited to this specific channel since it introduces additional errors which are spread during the estimation process. However the receivers with the optimal SIC architecture still provide the best results for the two types of filter. For a BER of 10^{-3} the gain offered by optimal SIC is about 2.7 and 4.7 dB respectively for ZF and MMSE without IC. It has to be remarked that the disruptions in the slope of the curves, particularly visible in Fig. 2.11, are related to a modification of the order in which the different users are decoded.

Average Case

In the average case the position of the user in the beam of interest is fixed (i.e. centre of the beam). The position of the users covered by the surrounding beams is generated randomly. By producing 100 000 different user locations in each beam, and therefore, 100 000 different channel realisations, the interference level seen by the user in the middle was computed. Using the corresponding Cumulative Density Function (CDF), the average level of interference was estimated and a channel matrix involving the same interference level was produced. The purpose is to evaluate the performance of the optimal SIC receiver architecture with MMSE and with both BPSK and Quadrature Phase-Shift Keying (QPSK) modulations in this average scenario, which is, again, from the point of view of the user located in the beam of interest.

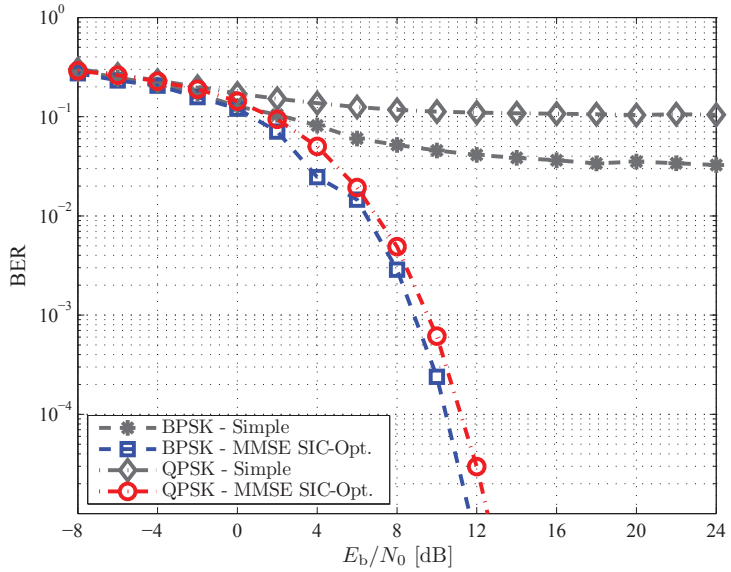


Figure 2.12. *BER performance of the receivers in a 7×7 satellite system, full frequency reuse ($K = 1$), average interference scenario, BPSK and QPSK modulations, and for the user located in beam 1.*

Like in the two previous cases, the uncoded BER obtained with the simple receiver is restricted by the level of interference (Fig. 2.12). With BPSK the lowest BER achieved is around $3.5\,10^{-2}$ for high SNR and around $1.1\,10^{-1}$ with QPSK. The utilisation of Successive Interference Cancellation (SIC), more particularly with the optimal architecture and MMSE, enables to decrease considerably the BER for high SNR. As seen both BPSK and QPSK are quite close from each other (difference of about 0.6 dB) which means that such receiver is capable of reducing interference even if a residual component remains (theoretically both BPSK BER and QPSK BER are matching and offer equivalent BER at lower E_b/N_0 than

what we obtain here). Finally in this scenario a BER lower than 10^{-3} requires a E_b/N_0 of at least 8.9 and 9.5 dB respectively for BPSK and QPSK.

In all cases Interference Cancellation (IC) is mandatory since for $K = 1$ the system is interference-limited. In order to reach a BER of 10^{-3}, considering the MMSE with optimal SIC architecture and BPSK, the required E_b/N_0 is about 8.9, 9, and 13.7 dB respectively for the average case, the good case and the bad case.

2.2.4 Satellite Channel with Three Colours - 7×7 System

When using higher number of colours than one in the multi-beam satellite system, beams using the same frequency are not directly adjacent. This reduces dramatically the level of interference and for this reason in conventional satellite systems IC is not mandatory and therefore not used. We focus here on the three colours system. The purpose is to investigate the impact of such satellite channel, which is even more diagonal than the low interference case with $K = 1$. The SNR was adjusted according to the parameter K such as the per-user power is kept constant.

Average Case

Like in the previous scenario, i.e. with $K = 1$, in the average case the position of the user in the beam of interest is fixed (i.e. centre of the beam) and the position of the users covered by the surrounding beams is generated randomly. Using the same principle as before, a channel matrix corresponding to the average interference level for the user in the middle was produced. The purpose is to evaluate the performance of the simple receiver, which is used in conventional systems, for different modulation orders: BPSK, QPSK, 8-PSK and 16-PSK. The uncoded BER curve obtained with this scenario (Fig. 2.13) confirms that for $K = 3$ the system has, on average, from the point of view of the user located in the centre of the beam of interest, nearly no interference. This is shown by both BPSK and QPSK curves which are almost matching on the considered BER range. A BER lower than 10^{-3} is reached with E_b/N_0 of at least 2.3, 6.4 and 15.5 dB respectively with BPSK and QPSK, 8-PSK, and 16-PSK.

2.2.5 Full Frequency Reuse versus Three Colours

In this case the BER is evaluated for higher modulation orders and for an energy per symbol over noise power spectral density, E_s/N_0, ranging from -8 to 24 dB. The bandwidth available

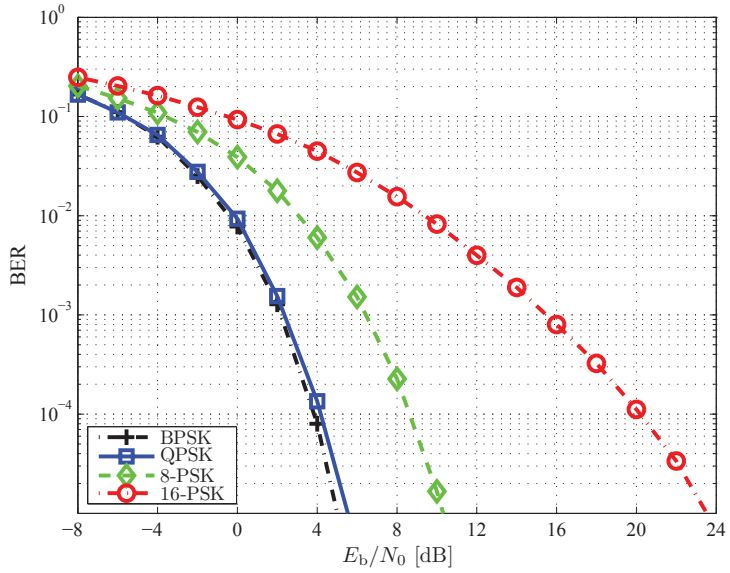


Figure 2.13. *BER performance of the receivers in a 7×7 satellite system, three colours ($K = 3$), average interference scenario, BPSK and QPSK modulations, and for the user located in beam 1.*

with $K = 1$ is three times the one with $K = 3$. For this reason the universal frequency reuse allows us to achieve higher rates but requires employing IC techniques. When comparing the performance of the receivers with $K = 3$ and $K = 1$ it is possible to estimate the possible achievable gains (Fig. 2.14). Over the whole Signal-to-Noise Ratio (SNR) range $K = 1$ with QPSK outperforms $K = 3$ with 16-PSK. Using the number of bits available per symbol and the bandwidth, $K = 1$ increases the rate by a factor of 1.5. Higher gains can be reached when considering other modulation orders. For instance while targeting a BER of 10^{-5}, $K = 1$ with QPSK modulation requires at least almost the same SNR as $K = 3$ with 8-PSK. In this case $K = 1$ increases the rate by a factor of 2. Moreover for even higher SNR it provides lower BER than $K = 3$. Another example is when targeting a BER of 10^{-2}: $K = 1$ with 8-PSK requires at least the same SNR as $K = 3$ with 16-PSK. The gain is here a factor of 2.25 between $K = 1$ and $K = 3$ knowing that for higher SNR $K = 1$ performs even better. The summary of these different gains is given in Table 2.1.

Table 2.1. *Summary of the uncoded bit error rate performance between universal frequency reuse and three colours.*

Comparison ID	Modulation $K = 1$ w/ IC	Modulation $K = 3$ w/o IC	Bit Error Rate	SNR [dB]	Gain [factor]
1	QPSK	16-PSK	-	whole	1.5
2	QPSK	8-PSK	10^{-5}	≥ 15	2.0
3	8-PSK	16-PSK	10^{-2}	≥ 15	2.25

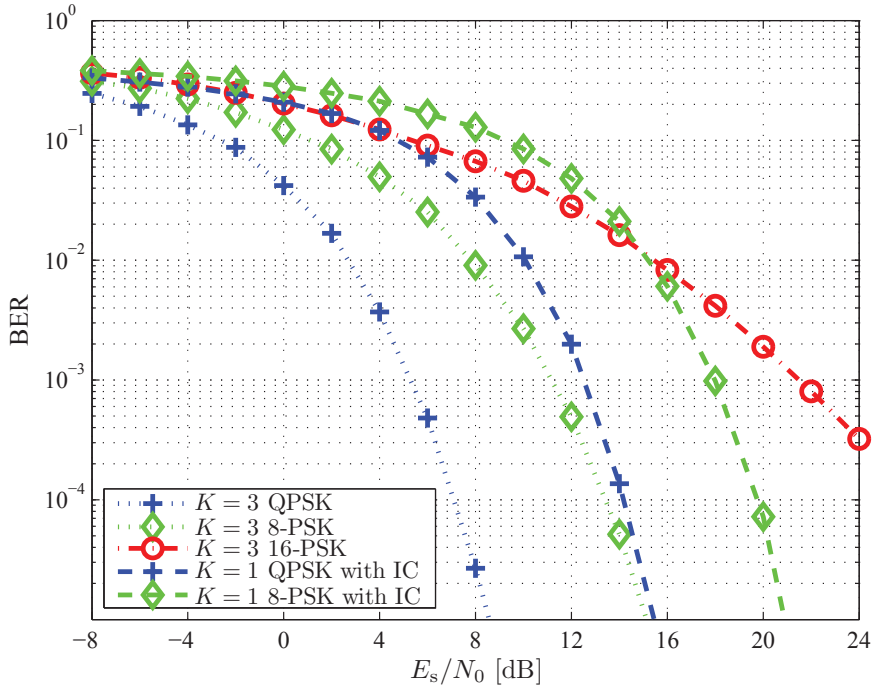


Figure 2.14. *BER performance of the receivers in a 7×7 satellite system, with one and three colours ($K = 1$ and $K = 3$), average interference scenario, different modulations, and for the user located in beam 1.*

2.3 Summary

Using state-of-the-art receivers, such as a simple conventional receiver which integrates only phase detection, linear filtering (Zero Forcing (ZF) and Minimum Mean Square Error (MMSE)), non-linear Successive Interference Cancellation (SIC) with Maximal Ratio Combining (MRC) and an optimal SIC architecture, it has been shown that the channel corresponding to the return-link of a multi-beam satellite system differs completely from a Rayleigh channel and because of the particular diagonal structure of the satellite channel matrix, the behaviour of classical SIC receiver is completely changed.

On the one hand, it has been shown that performing IC with $K = 1$ is mandatory since the system is interference-limited. On the other hand, the level of interference with $K = 3$ is rather low and this confirms why IC is not used in such systems. The optimal SIC MMSE receiver has been proved to give the best results, also with the satellite channel. This perfectly copes with information theory since MMSE together with SIC is capacity achieving. Moreover based on these simulations such receiver is almost able to remove completely the effect of interference. A system employing full frequency reuse permits to reach considerable

gain factors ranging from 1.5 to 2.25, in terms of uncoded throughput, with respect to a three colours scheme, depending on the modulations taken into account.

The aim is now to make use of information theory to better understand the gain brought by Multiple-Input and Multiple-Output (MIMO) in such system and to study the influence of Successive Interference Cancellation (SIC) on the users. Bit Error Rate (BER) analysis cannot be used to improve the resource management in the return-link, more particularly the user schedules, when considering different sets of satellite terminals within the beam footprints. It is therefore of interest to move towards information theory to also design later efficient algorithms aiming at optimising the resource management.

Chapter 3

Theoretical Analysis of the Satellite Channel: Achievable Rate

On the one hand, the theoretical capacity of Multiple-Input and Multiple-Output (MIMO) terrestrial channels has already been widely investigated (e.g., see [GJJV03]). On the other hand, there exists some recent work that studied the information theoretical capacity of the land mobile satellite channel [AlMaTu10]. The outage capacity while considering a satellite system as a MIMO system has been investigated in [LiPaAr09] and [LPCR09]. Anyway some fundamental insights are still missing, so in this chapter we address more particularly the achievable rate in the return-link of a multi-beam satellite system using tools provided by information theory, assuming clear sky and realistic beam pattern for the multi-beam satellite antenna.

The chapter first gives the different expressions used for computing the achievable sum rates of Single-Input and Single-Output (SISO), Single-Input and Multiple-Output (SIMO) and Multiple-Input and Multiple-Output (MIMO) systems, including the impact of the number of colours on those rates. The reachable gains offered by the Input-Output (IO) systems for different colours are then investigated, showing the benefit of using full frequency reuse. Finally, based on multi-user detection (MUD), the achievable per-user rates are derived and are investigated, through the concept of optimal Successive Interference Cancellation (SIC) ordering, to target a particular criterion which is the maximisation of the minimum user rate.

3.1 Achievable Sum Rate

The sum rate represents the overall rate present in the system for a given channel matrix and a given signal-to-noise ratio.

3.1.1 Single-Input - Single-Output (SISO)

In the Single-Input and Single-Output (SISO) system, all received signals are treated separately. For this reason the diagonal coefficients of the channel matrix $\boldsymbol{H}$ correspond to the "useful" signal whereas the off-diagonal elements (interference) are considered as "unexpected" and therefore are treated as noise (Fig. 3.1).

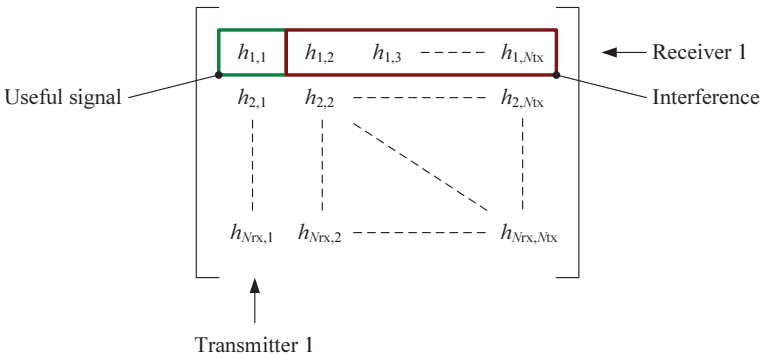


Figure 3.1. *Channel matrix seen by the first receiver in a SISO system.*

The average signal power perceived by receiver i is driven by the "useful" channel coefficient, the average interference power received is related to all unexpected transmitters and finally the noise level is directly issued from the noise power spectral density:

$$S_{\text{SISO},i} = |h_{i,i}|^2 \, E_\text{s} \, W \qquad I_{\text{SISO},i} = \sum_{j \neq i} |h_{i,j}|^2 \, E_\text{s} \, W \qquad N_{\text{SISO},i} = N_0 \, W$$

where W is the bandwidth.

The signal-to-interference plus noise ratio (SINR) seen by receiver i is thus:

$$\text{SINR}_{\text{SISO},i} = \frac{S_{\text{SISO},i}}{I_{\text{SISO},i} + N_{\text{SISO},i}} = \frac{|h_{i,i}|^2 \, E_\text{s}}{\sum_{j \neq i} |h_{i,j}|^2 \, E_\text{s} + N_0} = \frac{|h_{i,i}|^2}{\sum_{j \neq i} |h_{i,j}|^2 + N_0 / E_\text{s}}$$

The maximum achievable rate at receiver i in a SISO system can thus be written as [Sha49]:

$$R_{\text{SISO},i} = \log_2 \left(1 + \text{SINR}_{\text{SISO},i}\right) = \log_2 \left(1 + \frac{|h_{i,i}|^2}{\sum_{j \neq i} |h_{i,j}|^2 + (E_\text{s}/N_0)^{-1}}\right)$$

The resulting maximum achievable sum rate in a SISO system is finally:

$$R_{\text{SISO}} = \sum_{i=1}^{N_\text{Rx}} \log_2 \left(1 + \frac{|h_{i,i}|^2}{\sum_{j \neq i} |h_{i,j}|^2 + (E_\text{s}/N_0)^{-1}}\right) \tag{3.1}$$

3.1.2 Single-Input - Multiple-Output (SIMO)

In a Single-Input and Multiple-Output (SIMO) system, the transmitted signals are processed independently but since the system is composed of multiple receive antennas the signal of transmitter j may be perceived by other receivers (i.e. $i \neq j$). The receiver thus has the possibility to combine the signal issued from different antennas in order to increase the signal-to-noise ratio. Such receiver is therefore nothing else than a receiver performing Maximal Ratio Combining (MRC).

One Transmitter - Two Receivers (2×1)

Let's consider a system which is composed of one single transmitter and of two receivers (Fig. 3.2).

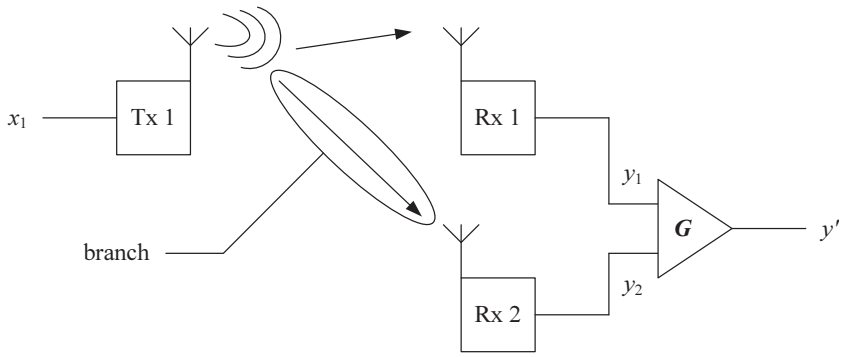


Figure 3.2. 2×1 *SIMO system.*

The received signals can be written as follows:

$$y_1 = h_{1,1}\, x_1 + \eta_1$$
$$y_2 = h_{2,1}\, x_1 + \eta_2$$

The statistical signal-to-noise ratio (SNR) of each branch is therefore $|h_{1,1}|^2/\sigma^2_{\eta_1}$ and $|h_{2,1}|^2/\sigma^2_{\eta_2}$, where $\sigma^2_{\eta_i}$ represents the variance of the noise perceived by the i-th receiver. Now if we combine the two signals y_1 and y_2 in a filter $\boldsymbol{G}$ such that $\boldsymbol{G}^{\mathrm{H}}\, \boldsymbol{y} = y'$ and $\boldsymbol{G}^{\mathrm{H}}\, \boldsymbol{G} = \boldsymbol{I}$, we obtain:

$$y' = g_1^*\, h_{1,1}\, x_1 + g_2^*\, h_{2,1}\, x_1 + g_1^*\, \eta_1 + g_2^*\, \eta_2$$

The purpose is to design $\boldsymbol{G}$ such that the SNR of the combined signals y' is maximized. When looking at the previous expression the SNR is:

$$\mathrm{SNR} = \frac{|g_1^*\, h_{1,1} + g_2^*\, h_{2,1}|^2}{\mathrm{E}\left[(g_1^*\, \eta_1 + g_2^*\, \eta_2)\,(g_1^*\, \eta_1 + g_2^*\, \eta_2)^*\right]}$$

Denominator:

The denominator can be written as:

$$\begin{aligned}\mathrm{E}\left[\left(g_1^*\,\eta_1 + g_2^*\,\eta_2\right)\left(g_1^*\,\eta_1 + g_2^*\,\eta_2\right)^*\right] &= \mathrm{E}\left[\left(g_1^*\,\eta_1 + g_2^*\,\eta_2\right)\left(g_1\,\eta_1^* + g_2\,\eta_2^*\right)\right] \\ &= |g_1|^2\,\sigma_{\eta_1}^2 + g_1^*\,g_2\,\mathrm{E}\left[\eta_1\,\eta_2^*\right] + g_2^*\,g_1\,\mathrm{E}\left[\eta_2\,\eta_1^*\right] + |g_2|^2\,\sigma_{\eta_2}^2\end{aligned}$$

since the noise is statistically independent we have $\mathrm{E}\left[\eta_1\,\eta_2^*\right] = \mathrm{E}\left[\eta_2\,\eta_1^*\right] = 0$, thus:

$$\mathrm{E}\left[\left(g_1^*\,\eta_1 + g_2^*\,\eta_2\right)\left(g_1^*\,\eta_1 + g_2^*\,\eta_2\right)^*\right] = |g_1|^2\,\sigma_{\eta_1}^2 + |g_2|^2\,\sigma_{\eta_2}^2$$

The noise is independent and identically distributed (i.i.d.), i.e. $\sigma_{\eta_1}^2 = \sigma_{\eta_2}^2 = \sigma_\eta^2$ and since $\boldsymbol{G}^{\mathrm{H}}\,\boldsymbol{G} = \boldsymbol{I}$ we have $|g_1|^2 + |g_2|^2 = 1$. It involves that:

$$\mathrm{E}\left[\left(g_1^*\,\eta_1 + g_2^*\,\eta_2\right)\left(g_1^*\,\eta_1 + g_2^*\,\eta_2\right)^*\right] = \sigma_\eta^2$$

Numerator:

When looking at the numerator we have an inner product of the terms within the norm:

$$|g_1^*\,h_{1,1} + g_2^*\,h_{2,1}|^2 = |\boldsymbol{G}^{\mathrm{H}}.\boldsymbol{h}|^2 = |<\boldsymbol{G}^{\mathrm{H}}, \boldsymbol{h}>|^2$$

The Cauchy-Schwarz inequality implies that:

$$|<x, y>|^2 \leq <x, x>\,.\,<y, y> \tag{3.2}$$

which is equivalent in our case to:

$$|<\boldsymbol{G}^{\mathrm{H}}, \boldsymbol{h}>|^2 \leq\ ||\boldsymbol{G}^{\mathrm{H}}||^2.||\boldsymbol{h}||^2 \tag{3.3}$$

where:

$$||\boldsymbol{x}||^2 = |x_1|^2 + |x_2|^2 + ... \qquad \text{with} \qquad |x_i|^2 = x_i\,x_i^*$$

Maximising the SNR is thus equivalent to satisfy:

$$|<\boldsymbol{G}^{\mathrm{H}}, \boldsymbol{h}>|^2 \leq\ ||\boldsymbol{G}^{\mathrm{H}}||^2.||\boldsymbol{h}||^2 = ||\boldsymbol{h}||^2 = |h_{1,1}|^2 + |h_{2,1}|^2$$

since $||\boldsymbol{h}||^2 = \boldsymbol{h}^{\mathrm{H}}\,\boldsymbol{h}$:

$$|<\boldsymbol{G}^{\mathrm{H}}, \boldsymbol{h}>| = \sqrt{\boldsymbol{h}^{\mathrm{H}}\,\boldsymbol{h}} \tag{3.4}$$

The previous equality exists if:

$$\boldsymbol{G}^{\mathrm{H}} = \left[\frac{h_{1,1}^*}{\sqrt{|h_{1,1}|^2 + |h_{2,1}|^2}} \quad \frac{h_{2,1}^*}{\sqrt{|h_{1,1}|^2 + |h_{2,1}|^2}}\right] = \frac{\boldsymbol{h}^{\mathrm{H}}}{\sqrt{\boldsymbol{h}^{\mathrm{H}}\,\boldsymbol{h}}}$$

The signal-to-noise ratio is thus finally:

$$\mathrm{SNR} = \frac{|g_1^*\,h_{1,1} + g_2^*\,h_{2,1}|^2}{\mathrm{E}\left[\left(g_1^*\,\eta_1 + g_2^*\,\eta_2\right)\left(g_1^*\,\eta_1 + g_2^*\,\eta_2\right)^*\right]} = \frac{|h_{1,1}|^2 + |h_{2,1}|^2}{\sigma_\eta^2} = \mathrm{SNR}_1 + \mathrm{SNR}_2$$

When performing MRC in a SIMO system, the SNR perceived at the receiver is thus the sum of the SNRs present in the different branches of the system.

One Transmitter - N Receivers ($N \times 1$)

As shown before the overall SNR is the sum of the SNR seen by the different receivers. Using the principle of the Signal-to-Interference-plus-Noise Ratio (SINR) computation for the SISO system (Section 3.1.1), the SINR perceived from transmitter j is (Fig. 3.3):

$$\mathrm{SINR}_{\mathrm{SIMO},j} = \sum_{l=1}^{N_{\mathrm{Rx}}} \left(\frac{|h_{l,j}|^2}{\sum_{k \neq j} |h_{l,k}|^2 + (E_\mathrm{s}/N_0)^{-1}} \right)$$

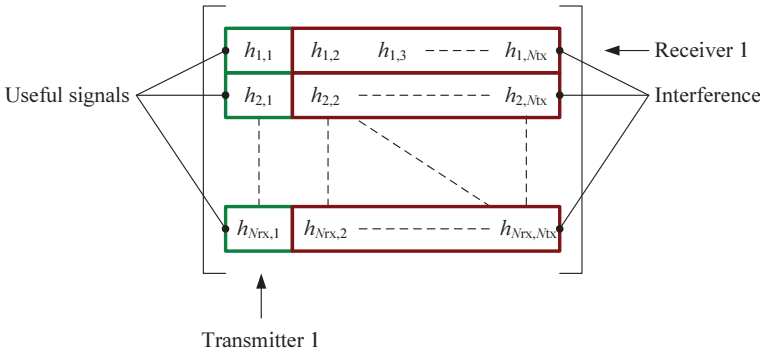


Figure 3.3. *Channel matrix of transmitter 1 seen by the receivers in a SIMO system.*

Final formulation

The maximum achievable rate of transmitter j in a SIMO system can thus be written as:

$$R_{\mathrm{SIMO},j} = \log_2 \left(1 + \sum_{l=1}^{N_{\mathrm{Rx}}} \left(\frac{|h_{l,j}|^2}{\sum_{k \neq j} |h_{l,k}|^2 + (E_\mathrm{s}/N_0)^{-1}} \right) \right)$$

The resulting maximum achievable sum rate in a SIMO system is finally:

$$R_{\mathrm{SIMO}} = \sum_{j=1}^{N_{\mathrm{Tx}}} \log_2 \left(1 + \sum_{l=1}^{N_{\mathrm{Rx}}} \left(\frac{|h_{l,j}|^2}{\sum_{k \neq j} |h_{l,k}|^2 + (E_\mathrm{s}/N_0)^{-1}} \right) \right) \tag{3.5}$$

3.1.3 Multiple-Input - Multiple-Output (MIMO)

Let's consider the system of Fig. 3.4. The maximum achievable rate of such system can be expressed using the mutual information (please refer to Section C.3.2 for more details).

A vector of symbols $\boldsymbol{x}$ is sent over a channel $\boldsymbol{H}$. A noise represented by the vector $\boldsymbol{\eta}$ is added during the transmission and the signal received is the vector $\boldsymbol{y}$. Therefore we have:

$$\boldsymbol{y} = \boldsymbol{H}\,\boldsymbol{x} + \boldsymbol{\eta}$$

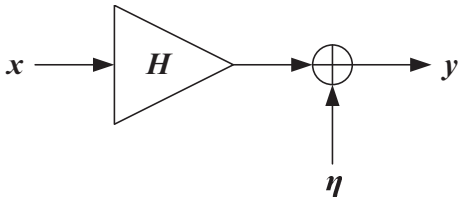


Figure 3.4. *Typical IO system.*

Mutual Information

The mutual information, which gives the maximum capacity of a channel, and therefore constitutes an upper-bound to the achievable rate, is a function of the entropy (please refer to Section C.3.2 for more details):

$$I(\boldsymbol{x};\boldsymbol{y}) = h(\boldsymbol{x}) - h(\boldsymbol{x}|\boldsymbol{y}) = h(\boldsymbol{y}) - h(\boldsymbol{y}|\boldsymbol{x})$$

The entropy of a random Gaussian variable x in N-dimensions is equal to:

$$h(\boldsymbol{x}) = \log_2 \det(\pi\, e\, \boldsymbol{C_x}) \tag{3.6}$$

where $\boldsymbol{C}$ represents the covariance matrix. Therefore we can write:

$$I(\boldsymbol{x};\boldsymbol{y}) = h(\boldsymbol{y}) - h(\boldsymbol{y}|\boldsymbol{x}) = \log_2 \det(\pi\, e\, \boldsymbol{C_y}) - \log_2 \det\left(\pi\, e\, \boldsymbol{C_{y|x}}\right)$$

Marginal Entropy

Let's express the marginal entropy $h(\boldsymbol{y})$, more particularly the covariance of the received signal $\boldsymbol{C_y}$. By definition:

$$\boldsymbol{C_y} = \mathrm{E}\left[(\boldsymbol{y} - \mathrm{E}[\boldsymbol{y}])\,(\boldsymbol{y} - \mathrm{E}[\boldsymbol{y}])^{\mathrm{H}}\right]$$

which we can also write:

$$\boldsymbol{C_y} = \boldsymbol{C_{H\,x+\eta}} = \mathrm{E}\left[((\boldsymbol{H}\,\boldsymbol{x} + \boldsymbol{\eta}) - \mathrm{E}[\boldsymbol{H}\,\boldsymbol{x} + \boldsymbol{\eta}])\,((\boldsymbol{H}\,\boldsymbol{x} + \boldsymbol{\eta}) - \mathrm{E}[\boldsymbol{H}\,\boldsymbol{x} + \boldsymbol{\eta}])^{\mathrm{H}}\right]$$

The expectation of the received signal is:

$$\mathrm{E}[\boldsymbol{y}] = \mathrm{E}[\boldsymbol{H}\,\boldsymbol{x} + \boldsymbol{\eta}] = \mathrm{E}[\boldsymbol{H}\,\boldsymbol{x}] + \mathrm{E}[\boldsymbol{\eta}] = \boldsymbol{H}\,\mathrm{E}[\boldsymbol{x}]$$

since $\boldsymbol{H}$ and $\boldsymbol{x}$ are independent and $\mathrm{E}[\boldsymbol{\eta}] = 0$.

This leads to:

$$\boldsymbol{C_y} = \mathrm{E}\left[((\boldsymbol{H}\,\boldsymbol{x} + \boldsymbol{\eta}) - \boldsymbol{H}\,\mathrm{E}[\boldsymbol{x}])\,((\boldsymbol{H}\,\boldsymbol{x} + \boldsymbol{\eta}) - \boldsymbol{H}\,\mathrm{E}[\boldsymbol{x}])^{\mathrm{H}}\right]$$

which is also:

$$\boldsymbol{C_y} = \mathrm{E}\left[\left(\boldsymbol{H}\left(\boldsymbol{x} - \mathrm{E}\left[\boldsymbol{x}\right]\right) + \boldsymbol{\eta}\right)\left(\boldsymbol{H}\left(\boldsymbol{x} - \mathrm{E}\left[\boldsymbol{x}\right]\right) + \boldsymbol{\eta}\right)^{\mathrm{H}}\right]$$

$$\boldsymbol{C_y} = \mathrm{E}\left[\boldsymbol{H}\left(\boldsymbol{x} - \mathrm{E}\left[\boldsymbol{x}\right]\right)\left(\boldsymbol{x} - \mathrm{E}\left[\boldsymbol{x}\right]\right)^{\mathrm{H}}\boldsymbol{H}^{\mathrm{H}}\right] + \mathrm{E}\left[\boldsymbol{H}\left(\boldsymbol{x} - \mathrm{E}\left[\boldsymbol{x}\right]\right)\boldsymbol{\eta}^{\mathrm{H}}\right] + \mathrm{E}\left[\boldsymbol{\eta}\left(\boldsymbol{x} - \mathrm{E}\left[\boldsymbol{x}\right]\right)^{\mathrm{H}}\boldsymbol{H}^{\mathrm{H}}\right] + \mathrm{E}\left[\boldsymbol{\eta}\,\boldsymbol{\eta}^{\mathrm{H}}\right]$$

since $\mathrm{E}\left[\boldsymbol{\eta}\right] = 0$ and $\mathrm{E}\left[\boldsymbol{\eta}\,\boldsymbol{\eta}^{\mathrm{H}}\right] = \boldsymbol{C_\eta}$ by definition, we finally have:

$$\boldsymbol{C_y} = \boldsymbol{H}\,\mathrm{E}\left[\left(\boldsymbol{x} - \mathrm{E}\left[\boldsymbol{x}\right]\right)\left(\boldsymbol{x} - \mathrm{E}\left[\boldsymbol{x}\right]\right)^{\mathrm{H}}\right]\boldsymbol{H}^{\mathrm{H}} + \boldsymbol{C_\eta} = \boldsymbol{H}\,\boldsymbol{C_x}\,\boldsymbol{H}^{\mathrm{H}} + \boldsymbol{C_\eta}$$

The marginal entropy $h\left(\boldsymbol{y}\right)$ can thus be written as follows:

$$h\left(\boldsymbol{y}\right) = \log_2\,\det\left(\pi\,e\,\boldsymbol{C_y}\right) = \log_2\,\det\left(\pi\,e\left(\boldsymbol{H}\,\boldsymbol{C_x}\,\boldsymbol{H}^{\mathrm{H}} + \boldsymbol{C_\eta}\right)\right) \tag{3.7}$$

Conditional Entropy

Let's now express the conditional entropy $h\left(\boldsymbol{y}|\boldsymbol{x}\right)$, more particularly the covariance of the received signal $\boldsymbol{C_{y|x}}$. By definition:

$$\boldsymbol{C_{y|x}} = \mathrm{E}\left[\left(\boldsymbol{y} - \mathrm{E}\left[\boldsymbol{y}|\boldsymbol{x}\right]\right)\left(\boldsymbol{y} - \mathrm{E}\left[\boldsymbol{y}|\boldsymbol{x}\right]\right)^{\mathrm{H}}\right]$$

The expectation of $\boldsymbol{y}$ knowing $\boldsymbol{x}$ is:

$$\mathrm{E}\left[\boldsymbol{y}|\boldsymbol{x}\right] = \mathrm{E}\left[\boldsymbol{H}\,\boldsymbol{x} + \boldsymbol{\eta}|\boldsymbol{x}\right] = \mathrm{E}\left[\boldsymbol{H}\,\boldsymbol{x}|\boldsymbol{x}\right] + \mathrm{E}\left[\boldsymbol{\eta}|\boldsymbol{x}\right] = \boldsymbol{H}\,\boldsymbol{x} + \mathrm{E}\left[\boldsymbol{\eta}\right] = \boldsymbol{H}\,\boldsymbol{x}$$

since $\boldsymbol{\eta}$ and $\boldsymbol{x}$ are independent and $\mathrm{E}\left[\boldsymbol{\eta}\right] = 0$.

This leads to:

$$\boldsymbol{C_{y|x}} = \mathrm{E}\left[\left(\boldsymbol{y} - \boldsymbol{H}\,\boldsymbol{x}\right)\left(\boldsymbol{y} - \boldsymbol{H}\,\boldsymbol{x}\right)^{\mathrm{H}}\right] = \mathrm{E}\left[\boldsymbol{\eta}\,\boldsymbol{\eta}^{\mathrm{H}}\right] = \boldsymbol{C_\eta}$$

The conditional entropy $h\left(\boldsymbol{y}|\boldsymbol{x}\right)$ can thus be written as follows:

$$h\left(\boldsymbol{y}|\boldsymbol{x}\right) = \log_2\,\det\left(\pi\,e\,\boldsymbol{C_{y|x}}\right) = \log_2\,\det\left(\pi\,e\,\boldsymbol{C_\eta}\right) \tag{3.8}$$

Final Expression

Having expressed both marginal and conditional entropies, it is now possible to give the final expression of the mutual information:

$$I\left(\boldsymbol{x};\boldsymbol{y}\right) = H\left(\boldsymbol{y}\right) - H\left(\boldsymbol{y}|\boldsymbol{x}\right) = \log_2\,\det\left(\pi\,e\,\boldsymbol{C_y}\right) - \log_2\,\det\left(\pi\,e\,\boldsymbol{C_{y|x}}\right)$$

$$I\left(\boldsymbol{x};\boldsymbol{y}\right) = \log_2\,\det\left(\pi\,e\left(\boldsymbol{H}\,\boldsymbol{C_x}\,\boldsymbol{H}^{\mathrm{H}} + \boldsymbol{C_\eta}\right)\right) - \log_2\,\det\left(\pi\,e\,\boldsymbol{C_\eta}\right)$$

which can also be written, using the properties of the logarithm, as:

$$I(\boldsymbol{x};\boldsymbol{y}) = \log_2 \det\left(\boldsymbol{C}_{\boldsymbol{\eta}}^{-1}\,\boldsymbol{H}\,\boldsymbol{C}_{\boldsymbol{x}}\,\boldsymbol{H}^{\mathrm{H}} + \boldsymbol{I}\right)$$

We finally obtain, using the properties of the determinant:

$$R_{\mathrm{MIMO}} = I(\boldsymbol{x};\boldsymbol{y}) = \log_2 \det\left(\boldsymbol{I} + \boldsymbol{C}_{\boldsymbol{\eta}}^{-1}\,\boldsymbol{H}\,\boldsymbol{C}_{\boldsymbol{x}}\,\boldsymbol{H}^{\mathrm{H}}\right) \tag{3.9}$$

As can be seen the previous expression (3.9) looks very close to the one of Shannon and actually corresponds to the one given by Telatar [Tel99]. It has to be remarked that if the energy per symbol E_{s} is normalised and equals 1, the covariance of the transmitted signal, namely $\boldsymbol{C}_{\boldsymbol{x}}$, also noted $\boldsymbol{Q}$, is such that:

$$\boldsymbol{C}_{\boldsymbol{x}} = \boldsymbol{Q} = \mathrm{E}\left[(\boldsymbol{x} - \mathrm{E}[\boldsymbol{x}])\,(\boldsymbol{x} - \mathrm{E}[\boldsymbol{x}])^{\mathrm{H}}\right] = \mathrm{E}\left[\boldsymbol{x}\,\boldsymbol{x}^{\mathrm{H}}\right] = \boldsymbol{I} \tag{3.10}$$

since $\mathrm{E}[\boldsymbol{x}] = 0$. Therefore (3.9) can be simplified in such a case in:

$$R_{\mathrm{MIMO}} = \log_2 \det\left(\boldsymbol{I} + \boldsymbol{C}_{\boldsymbol{\eta}}^{-1}\,\boldsymbol{H}\,\boldsymbol{H}^{\mathrm{H}}\right) \tag{3.11}$$

3.1.4 Impact of the Phase

As seen in previous expressions, more particularly for evaluating the SISO sum rate (3.1) and the SIMO sum rate (3.5), only the absolute values of the channel coefficients is involved. The phase has therefore no impact on these sum rates.

On the other hand when looking at the MIMO sum rate (3.11) it is no more the case. When considering a realistic phase applied to the channel matrix $\boldsymbol{H}$, i.e. both beam and user phases (please refer to Section 1.2.5 for more details), we will show in the following that such phase has actually no impact on the MIMO sum rate.

User Phase

With the so-called user phase we have:

$$R_{\boldsymbol{\phi}_{\mathrm{Tx}}} = \log_2 \det\left(\boldsymbol{I}_{N_{\mathrm{b}}} + \boldsymbol{C}_{\boldsymbol{\eta}}^{-1}\,\boldsymbol{H}_{\boldsymbol{\phi}_{\mathrm{Tx}}}\,\boldsymbol{H}_{\boldsymbol{\phi}_{\mathrm{Tx}}}^{\mathrm{H}}\right)$$

with:

$$\boldsymbol{H}_{\boldsymbol{\phi}_{\mathrm{Tx}}}\,\boldsymbol{H}_{\boldsymbol{\phi}_{\mathrm{Tx}}}^{\mathrm{H}} = \boldsymbol{H}\,\boldsymbol{\phi}_{\mathrm{Tx}}\,(\boldsymbol{H}\,\boldsymbol{\phi}_{\mathrm{Tx}})^{\mathrm{H}} = \boldsymbol{H}\,\boldsymbol{\phi}_{\mathrm{Tx}}\,\boldsymbol{\phi}_{\mathrm{Tx}}^{\mathrm{H}}\,\boldsymbol{H}^{\mathrm{H}}$$

We finally have:

$$R_{\boldsymbol{\phi}_{\mathrm{Tx}}} = \log_2 \det\left(\boldsymbol{I}_{N_{\mathrm{b}}} + \boldsymbol{C}_{\boldsymbol{\eta}}^{-1}\,\boldsymbol{H}\,\boldsymbol{H}^{\mathrm{H}}\right) = R_{\mathrm{MIMO}} \tag{3.12}$$

The phase applied on each column of the channel matrix $\boldsymbol{H}$ thus has no impact on the achievable rate.

Beam Phase

With the so-called beam phase we have:

$$R_{\boldsymbol{\phi}_{\mathrm{Rx}}} = \log_2 \det \left(\boldsymbol{I}_{N_\mathrm{b}} + \boldsymbol{C}_{\boldsymbol{\eta}}^{-1} \, \boldsymbol{H}_{\boldsymbol{\phi}_{\mathrm{Rx}}} \, \boldsymbol{H}_{\boldsymbol{\phi}_{\mathrm{Rx}}}^{\mathrm{H}} \right)$$

with:

$$\det \left(\boldsymbol{I}_{N_\mathrm{b}} + \boldsymbol{C}_{\boldsymbol{\eta}}^{-1} \, \boldsymbol{H}_{\boldsymbol{\phi}_{\mathrm{Rx}}} \, \boldsymbol{H}_{\boldsymbol{\phi}_{\mathrm{Rx}}}^{\mathrm{H}} \right) = \det \left(\boldsymbol{I}_{N_\mathrm{b}} + \boldsymbol{C}_{\boldsymbol{\eta}}^{-1} \, \boldsymbol{\phi}_{\mathrm{Rx}} \, \boldsymbol{H} \, \left(\boldsymbol{\phi}_{\mathrm{Rx}} \, \boldsymbol{H} \right)^{\mathrm{H}} \right)$$

The following property on determinants is particularly useful:

$$\det \left(\boldsymbol{I} + \boldsymbol{A} \, \boldsymbol{B} \right) = \det \left(\boldsymbol{I} + \boldsymbol{B} \, \boldsymbol{A} \right)$$

It permits to write:

$$\det \left(\boldsymbol{I}_{N_\mathrm{b}} + \boldsymbol{C}_{\boldsymbol{\eta}}^{-1} \, \boldsymbol{H}_{\boldsymbol{\phi}_{\mathrm{Rx}}} \, \boldsymbol{H}_{\boldsymbol{\phi}_{\mathrm{Rx}}}^{\mathrm{H}} \right) = \det \left(\boldsymbol{I}_{N_\mathrm{b}} + \boldsymbol{C}_{\boldsymbol{\eta}}^{-1} \, \boldsymbol{\phi}_{\mathrm{Rx}}^{\mathrm{H}} \, \boldsymbol{\phi}_{\mathrm{Rx}} \, \boldsymbol{H} \, \boldsymbol{H}^{\mathrm{H}} \right) \tag{3.13}$$

We finally have:

$$R_{\boldsymbol{\phi}_{\mathrm{Rx}}} = \log_2 \det \left(\boldsymbol{I}_{N_\mathrm{b}} + \boldsymbol{C}_{\boldsymbol{\eta}}^{-1} \, \boldsymbol{H} \, \boldsymbol{H}^{\mathrm{H}} \right) = R_{\mathrm{MIMO}} \tag{3.14}$$

The phase applied on each row of the channel matrix $\boldsymbol{H}$ has also no impact on the achievable rate.

When looking at the previous properties, if a realistic phase should be included in the channel matrix $\boldsymbol{H}$, then a particular phase for each user and the same phase shift between the beams should be added. However, because of the previous discussion, this does not have an influence on the achievable rate. For this reason the channel matrix in this scenario could contain only real numbers.

It has to be remarked that if the phases are fully independent and uniformly distributed between 0 and 2π, the MIMO sum rate would be higher and thus our computations constitute a lower bound for any system whose phase does not comply with the previous discussion, but the absolute value of the coefficients is the same as here.

3.1.5 Impact of the Cluster Size

The cluster size K, also referring to the number of colours (see Section 1.1.4), influences the bandwidth available in the system and therefore the link budget.

Since the bandwidth of $K = 1$ is three time the one of $K = 3$ for instance, we write, in order to enable fair comparison between different numbers of colours, that:

$$R_{K,\mathrm{IO}} = \frac{1}{K} R_{\mathrm{IO}} \tag{3.15}$$

where IO identifies the input-output system type, i.e. SISO, SIMO or MIMO.

Additionally the SNR for K colours and a channel gain $|h_{i,i}| = 1$ is denoted as $(E_\mathrm{s}/N_0)_K$. The symbol without bracket E_s/N_0 represents the SNR for $K = 1$. Since the per-user power is kept constant as K is changed, the following relationships hold:

$$\left(\frac{E_\mathrm{s}}{N_0}\right)_K = K \left(\frac{E_\mathrm{s}}{N_0}\right)_1 = K \frac{E_\mathrm{s}}{N_0} \tag{3.16}$$

We obtain, injecting the cluster size K in expressions (3.1), (3.5) and (3.9), the following new formulations:

$$R_{K,\mathrm{SISO}} = \frac{1}{K} \sum_{i=1}^{N_\mathrm{Rx}} \log_2 \left(1 + \frac{|h_{i,i}|^2}{\sum_{j \neq i} |h_{i,j}|^2 + (K\, E_\mathrm{s}/N_0)^{-1}}\right) \tag{3.17}$$

$$R_{K,\mathrm{SIMO}} = \frac{1}{K} \sum_{j=1}^{N_\mathrm{Tx}} \log_2 \left(1 + \sum_{l=1}^{N_\mathrm{Rx}} \left(\frac{|h_{l,j}|^2}{\sum_{k \neq j} |h_{l,k}|^2 + (K\, E_\mathrm{s}/N_0)^{-1}}\right)\right) \tag{3.18}$$

$$R_{K,\mathrm{MIMO}} = \frac{1}{K} \log_2 \det \left(\boldsymbol{I} + \boldsymbol{C}_{\boldsymbol{\eta}}^{-1}\, \boldsymbol{H}\, \boldsymbol{Q}\, \boldsymbol{H}^{\mathrm{H}}\right) \tag{3.19}$$

with:

$$\boldsymbol{C}_{\boldsymbol{\eta}} = \sigma^2\, \boldsymbol{I} = \frac{1}{K} \frac{N_0}{E_\mathrm{s}}\, \boldsymbol{I} \tag{3.20}$$

as mentioned in Section 3.1.3, the symbols are assumed to be independent and to have unit transmit power, therefore the covariance matrix $\boldsymbol{Q}$ is equal to $\boldsymbol{I}$.

3.1.6 Evaluations with Full Frequency Reuse and Three Colours

The maximum achievable sum rate is analysed for the full system size, i.e. ninety six beams ($B = 96$), two numbers of colours ($K = 1$ and $K = 3$) and the different IO systems previously defined [BBRJ11]. Even if the four colours system is part of the scenarios (Section 1.1.4), it is not considered in this analysis due to the invariance of the results with the different IO systems.

SISO can be seen as a conventional system in which the user information is decoded exclusively based on the signal received on the dedicated beam. Therefore one single output, out

of the N_{Rx} available, is used for a given user. All users signals are independently processed meaning that interference is not cancelled and is thus considered as noise. In the MIMO we take advantage of having the user signal actually received by multiple beams. When employing additionally SIC we can expect an increase of the achievable rate. In between the SIMO system takes into account the fact that a particular user signal is present in all beams. By performing MRC on the signals received by the beams the user's signal can be recovered.

The maximum achievable rate per user was evaluated for 10 000 channel realisations. A channel realisation actually refers to random user locations in each beam. This represents a total of about 1 million of users (satellite terminals) randomly placed in the ninety six beams. At a given time one single user is allocated in each beam. This abstraction actually complies with the Multi-Frequency Time-Division Multiple Access (MF-TDMA) transmission present in the Digital Video Broadcasting - Return Channel via Satellite (DVB-RCS) standard [DVB-RCS].

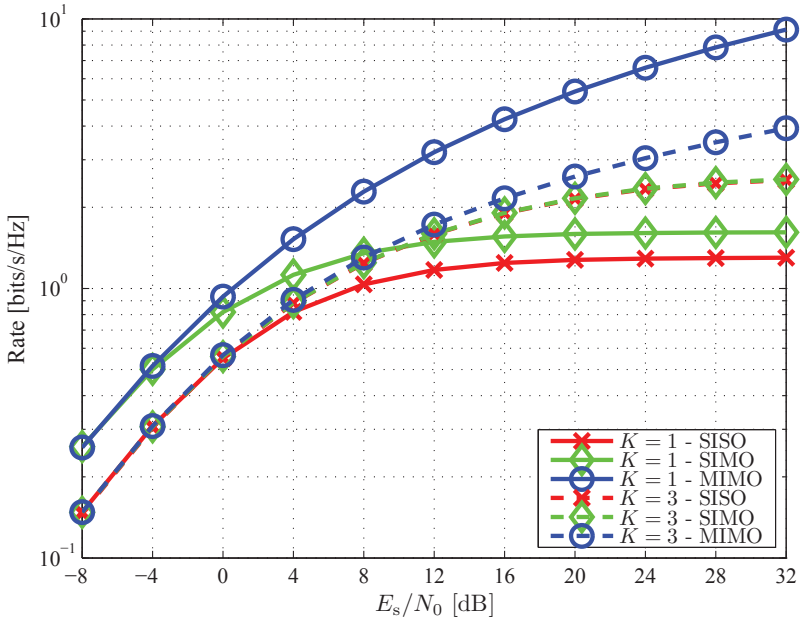


Figure 3.5. *Average user rates for ninety six beams ($B = 96$), with full frequency reuse ($K = 1$) and three colours ($K = 3$), and issued from 10 000 random sets.*

When analysing the results of Fig. 3.5 we can see that cluster size 1 ($K = 1$) with MIMO provides more capacity than cluster size 3 ($K = 3$) over the entire E_s/N_0 range. The improvement of SIC is thus clear for $K = 1$ but also for $K = 3$ above 8 dB. The level of interference with the latter cluster size is actually very low and this can be acknowledged by the difference between both SISO and SIMO systems. Actually the signal level received by other users in a given beam is almost negligible. The lowest rates are achieved for the SISO system and

cluster size 1. This is perfectly normal since this system is highly interference-limited. For this reason SIMO brings some gain since we can take advantage of the signal received in all beams. The gain is visible in the noise-limited region, i.e. for E_s/N_0 below 0 dB, afterwards the interference level becomes too high for SIMO. At this stage SIC makes sense since it tries to suppress interference.

When looking at the gains at 20 dB, the average user rate for a system with cluster size 3 with SISO and MIMO is about 2.1 and 2.7 bits/s/Hz, respectively, whereas for cluster size 1 with MIMO it is about 5.4 bits/s/Hz. This shows the capacity gain brought by SIC in a satellite system is about almost a factor of 3, compared to a conventional system (SISO $K = 3$ without IC) and about a factor of 2 with respect to a classic frequency reuse scheme but with IC. Moreover, the slope of the rate capacity curve at high SNR for MIMO $K = 1$ is larger than the slope of the corresponding curve for MIMO $K = 3$. The reason is that for stronger frequency reuse the signal of each user is received with higher energy. Indeed, since all beams employ the same frequency, also the beams close to the desired one contribute to the user detection and these beams have a quite strong gain that can improve the system capacity quite remarkably.

3.1.7 Analysis of the Sum Rate Results for one and three Colours

The purpose of this section is to give a more detailed analysis of the results presented in the previous section (Section 3.1.6), i.e. the rates achievable in the ninety six multi-beam satellite system while considering different Input-Output (IO) systems and two numbers of colours, more particularly $K = 1$ and $K = 3$.

The sum rate, i.e. the achievable system rate, was evaluated using the formulae given in Section 3.1. Knowing the size of the system, in particular the number of users, noted $N_{\text{users,total}}$, it is possible to derive easily the average per-user rate:

$$\overline{R}_{K,\text{IO,user}} = \frac{R_{K,\text{IO}}}{N_{\text{users,total}}} \tag{3.21}$$

where $\overline{R}_{K,\text{IO,user}}$ represents the average per-user rate for a given cluster size K and IO system (SISO, SIMO or MIMO), and $R_{K,\text{IO}}$ the corresponding system sum rate, as defined in Section 3.1.5.

Single-Input - Single-Output

Low signal-to-noise ratios:

When analysing the results of Fig. 3.5 one can see that the two SISO curves are matching for $K = 1$ and $K = 3$ at low SNRs. We remind that the value of the signal-to-interference plus noise ratio (SINR) perceived by a receiver in a SISO system is:

$$\mathrm{SINR}_{\mathrm{SISO},i} = \frac{|h_{i,i}|^2}{\sum_{j\neq i} |h_{i,j}|^2 + (E_\mathrm{s}/N_0)^{-1}}$$

where i designates the receiver index.

For low SNRs the term $(E_\mathrm{s}/N_0)^{-1}$ dominates and the term $\sum_{j\neq i} |h_{i,j}|^2$ can be neglected. Moreover using the properties of the logarithm, i.e.:

$$\ln(1+X) \simeq X \;\Rightarrow\; \log_2(1+X) \simeq \frac{1}{\ln(2)} X \qquad \text{for small values of } X$$

we obtain:

$$R_{\mathrm{SISO},i} \simeq \frac{1}{\ln(2)} \frac{|h_{i,i}|^2}{(E_\mathrm{s}/N_0)^{-1}} \qquad \text{for low SNRs}$$

We also remind that for comparing the cluster sizes both achievable rate and per-user power were adjusted. Since the bandwidth for three colours ($K = 3$) is three times smaller than the one of full frequency reuse (one colour, $K = 1$) the resulting rate is divided by three:

$$R_{K=3,\mathrm{SISO},i} = \frac{1}{3} R_{K=1,\mathrm{SISO},i}$$

and since three times more power is needed to reach the same signal-to-noise ratio for $K = 1$ it is assumed that:

$$\left(\frac{E_\mathrm{s}}{N_0}\right)_{K=1} = \frac{E_\mathrm{s}}{N_0} = \frac{1}{3}\left(\frac{E_\mathrm{s}}{N_0}\right)_{K=3}$$

The resulting SISO user rates are:

$$R_{K=3,\mathrm{SISO},i} \simeq \frac{1}{\ln(2)} \frac{1}{3} \frac{|h_{i,i}|^2}{(3\,E_\mathrm{s}/N_0)^{-1}} \qquad \text{and} \qquad R_{K=1,\mathrm{SISO},i} \simeq \frac{1}{\ln(2)} \frac{|h_{i,i}|^2}{(E_\mathrm{s}/N_0)^{-1}}$$

Since the beam coverage and the antenna pattern is the same for both cluster sizes, $|h_{i,i}|^2_{K=1} = |h_{i,i}|^2_{K=3}$. It finally gives:

$$R_{K=3,\mathrm{SISO},i} \simeq R_{K=1,\mathrm{SISO},i} \qquad \text{for low SNRs}$$

and this explains why the two curves for the Single-Input and Single-Output (SISO) system match when having $K = 1$ and $K = 3$.

High signal-to-noise ratios:

On the one hand, for high SNRs the term $(E_s/N_0)^{-1}$ becomes negligible but on the other hand, the term $\sum_{j\neq i}|h_{i,j}|^2$ is predominant. This means the rate is not affected by the noise level anymore and therefore will saturate. The user rate is thus:

$$R_{\mathrm{SISO},i} \simeq \log_2\left(1+\frac{|h_{i,i}|^2}{\sum_{j\neq i}|h_{i,j}|^2}\right) \qquad \text{for high SNRs}$$

When considering the system with full frequency reuse for instance, the mean value of $|h_{i,i}|$ is about 0.865 and the mean value of $\sum_{j\neq i}|h_{i,j}|$ is about 0.698 (mean values computed over the 10 000 random sets and over the $N_{\mathrm{users,total}}$ users). This results into $\overline{R}_{K=1,\mathrm{SISO,user}} \simeq$ 1.342 bits/s/Hz for high SNRs. In the same way when considering the system with three colours, i.e. $K=3$, it results into $\overline{R}_{K=3,\mathrm{SISO,user}} \simeq 2.424$ bits/s/Hz for high SNRs. These approximations are confirmed when looking at two curves in Fig. 3.5 saturating at high SNRs for both $K=1$ and $K=3$ systems.

Single-Input - Multiple-Output

For the Single-Input and Multiple-Output (SIMO) system we take benefit from the multiple received signals. The value of the SINR for a user in such a system is:

$$\mathrm{SINR}_{\mathrm{SIMO},j} = \sum_{l=1}^{N_{\mathrm{Rx}}}\left(\frac{|h_{l,j}|^2}{\sum_{k\neq j}|h_{l,k}|^2+(E_s/N_0)^{-1}}\right)$$

Low signal-to-noise ratios:

As before for low signal-to-noise ratios (SNRs), the interference can be neglected when compared to the noise level. This means the user rate can be approximated by:

$$R_{\mathrm{SIMO},j} \simeq \frac{1}{\ln(2)}\frac{E_s}{N_0}\sum_{l=1}^{N_{\mathrm{Rx}}}|h_{l,j}|^2$$

For the system using three colours ($K=3$), the level of signal received by the other beams, i.e. by the beams l with $l\neq j$, is very low meaning that there is almost no interference. For this reason the term $\sum_{l=1}^{N_{\mathrm{Rx}}}|h_{l,j}|^2$ is almost equal to $|h_{j,j}|^2$ and therefore both SISO and SIMO curves are matching for this number of colours. For universal frequency reuse, i.e. $K=1$, the term $\sum_{l=1}^{N_{\mathrm{Rx}}}|h_{l,j}|^2$ is almost equal to 1.237 and this leads to:

$$\overline{R}_{K=1,\mathrm{SIMO,user}} \simeq 1.653\,\overline{R}_{K=1,\mathrm{SISO,user}} \qquad \text{for low SNRs}$$

and this corresponds perfectly to the behaviour of the two curves related to the SIMO system.

High signal-to-noise ratios:

For high signal-to-noise ratios (SNRs), the SIMO user rate can be approximated by:

$$R_{\mathrm{SIMO},j} \simeq \log_2\left(1+\sum_{l=1}^{N_{\mathrm{Rx}}}\frac{|h_{l,j}|^2}{\sum_{k\neq j}|h_{l,k}|^2}\right)$$

In the case of universal frequency reuse ($K=1$), the mean value of $\sum_{l=1}^{N_{\mathrm{Rx}}}\frac{|h_{l,j}|^2}{\sum_{k\neq j}|h_{l,k}|^2}$ is about 2.089 which gives $\overline{R}_{K=1,\mathrm{SIMO,user}} \simeq 1.627$ bits/s/Hz for high SNRs and this approximates matches perfectly with the results shown by Fig. 3.5.

Multiple-Input - Multiple-Output

Low signal-to-noise ratios:

Concerning the Multiple-Input and Multiple-Output (MIMO) system curves, they match the ones obtained with the SIMO system for low signal-to-noise ratios (SNRs). Actually for low SNRs the noise is predominant and for this reason the interference cannot be removed.

High signal-to-noise ratios:

Due to its nature MIMO will always perform equally (for low SNRs) or better (for high SNRs) than SIMO. Moreover the achievable rates of MIMO systems do not saturate at high signal-to-noise ratios. The previously discussed properties can be observed on Fig. 3.5 directly.

3.2 Achievable Per-User Rate

In the previous part (Section 3.1), the maximum achievable sum rate was expressed for different Input-Output (IO) systems. On the one hand, the maximum achievable rate at the user level can be easily derived for both SISO and SIMO systems. On the other hand, the expression of the sum rate gives directly the achievable rate of the system for MIMO systems. The purpose is thus to evaluate the maximum achievable rate at the user level for MIMO systems.

3.2.1 Successive Interference Cancellation

In MIMO systems the receiver can take advantage of the receive diversity (multiple receive antennas, i.e. multiple output) and of the transmit diversity (multiple transmitters, i.e. multiple input). If we assume that all signals are received by one single entity, which is the case

for the return-link of a transparent multi-beam satellite systems, then it is possible to implement Successive Interference Cancellation (SIC) at the receiver side. With a star network topology, this means SIC is performed by the gateway on ground. Much recent research has shown the benefits of jointly decoding all beams at the gateway (e.g., see [ALBPCG11]). Successive Interference Cancellation (SIC) techniques for the return-link of satellite system have been analysed [MBBD07], [NISIM05] and [LeGr08].

The gateway thus receives the signals issued from different beams and can process them jointly, knowing the Channel State Information (CSI), in order to remove interference. The receiver can remove successively the interference caused by other transmitters in order to get a better estimate of the initial transmitted signal. If we look at the channel matrix, whose size is $N_{\mathrm{Rx}} \times N_{\mathrm{Tx}}$, then the first user to be decoded will "see" the whole channel matrix, i.e. all interferers. At the end of the process, since the interference of users are removed one by one, the last user to be decoded will therefore only "see" its own channel, more particularly its own column of the channel matrix.

Using this strategy can help us in finding an expression which aims at computing the maximum rate at the user level. We suppose, when looking at the channel matrix, that while employing SIC the user signals will be decoded from the left to the right. Therefore the last user to be decoded has index "N_{Tx}" and the first one, index "1". The channel matrix seen by the last user will contain one single column, i.e. $\boldsymbol{H}_{:,N_{\mathrm{Tx}}}$, which is a column vector and can be also noted $\boldsymbol{h}_{N_{\mathrm{Tx}}}$. The maximum achievable rate of this user can be computed using the formula (3.11) of Section 3.1.3:

$$R_{\mathrm{MIMO},N_{\mathrm{Tx}}} = \log_2 \det\left(\boldsymbol{I}_{N_{\mathrm{Rx}}} + \boldsymbol{C}_{\boldsymbol{\eta}}^{-1}\, \boldsymbol{H}_{:,N_{\mathrm{Tx}}}\, \boldsymbol{H}_{:,N_{\mathrm{Tx}}}^{\mathrm{H}}\right)$$

The penultimate user to be decoded, i.e. user with index "$N_{\mathrm{Tx}} - 1$", will see the last two columns of the channel matrix $\boldsymbol{H}$ since there is actually still one interferer present which is user "N_{Tx}", the last user to be decoded. The channel matrix will be composed of the last two columns of the initial channel matrix, i.e. $\boldsymbol{H}_{:,N_{\mathrm{Tx}}-1:N_{\mathrm{Tx}}}$ (Fig. 3.6). The maximum achievable rate of the system represented by this new channel matrix is:

$$R_{\mathrm{MIMO},N_{\mathrm{Tx}}-1:N_{\mathrm{Tx}}} = \log_2 \det\left(\boldsymbol{I}_{N_{\mathrm{Rx}}} + \boldsymbol{C}_{\boldsymbol{\eta}}^{-1}\, \boldsymbol{H}_{:,N_{\mathrm{Tx}}-1:N_{\mathrm{Tx}}}\, \boldsymbol{H}_{:,N_{\mathrm{Tx}}-1:N_{\mathrm{Tx}}}^{\mathrm{H}}\right)$$

Knowing the sum rate of this system and knowing the maximum rate of the last user to be decoded we thus obtain:

$$R_{\mathrm{MIMO},N_{\mathrm{Tx}}-1} = \log_2 \det\left(\boldsymbol{I}_{N_{\mathrm{Rx}}} + \boldsymbol{C}_{\boldsymbol{\eta}}^{-1}\, \boldsymbol{H}_{:,N_{\mathrm{Tx}}-1:N_{\mathrm{Tx}}}\, \boldsymbol{H}_{:,N_{\mathrm{Tx}}-1:N_{\mathrm{Tx}}}^{\mathrm{H}}\right) - R_{\mathrm{MIMO},N_{\mathrm{Tx}}}$$

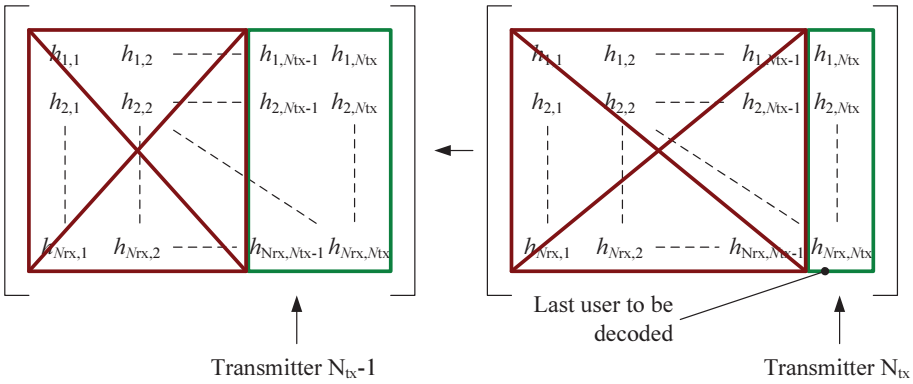


Figure 3.6. *MIMO SIC - Channel matrix seen by the last user (right) and the last but one user (left).*

By generalising this concept we can write that the maximum achievable rate of user j in a MIMO system employing SIC is:

$$R_{\mathrm{MIMO},j} = \log_2 \det\left(\boldsymbol{I}_{N_{\mathrm{Rx}}} + \boldsymbol{C}_{\boldsymbol{\eta}}^{-1}\, \boldsymbol{H}_{:,j:N_{\mathrm{Tx}}}\, \boldsymbol{H}_{:,j:N_{\mathrm{Tx}}}^{\mathrm{H}}\right) - \log_2 \det\left(\boldsymbol{I}_{N_{\mathrm{Rx}}} + \boldsymbol{C}_{\boldsymbol{\eta}}^{-1}\, \boldsymbol{H}_{:,j+1:N_{\mathrm{Tx}}}\, \boldsymbol{H}_{:,j+1:N_{\mathrm{Tx}}}^{\mathrm{H}}\right) \quad (3.22)$$

Another way of writing the previous expression is:

$$R_{\mathrm{MIMO},j} = \log_2 \det\left(\boldsymbol{I}_{N_{\mathrm{Rx}}} + \boldsymbol{C}_{\boldsymbol{\eta}}^{-1}\, \boldsymbol{H}^{(N_{\mathrm{Tx}}-j+1)}\, \left(\boldsymbol{H}^{(N_{\mathrm{Tx}}-j+1)}\right)^{\mathrm{H}}\right) - \log_2 \det\left(\boldsymbol{I}_{N_{\mathrm{Rx}}} + \boldsymbol{C}_{\boldsymbol{\eta}}^{-1}\, \boldsymbol{H}^{(N_{\mathrm{Tx}}-j)}\, \left(\boldsymbol{H}^{(N_{\mathrm{Tx}}-j)}\right)^{\mathrm{H}}\right) \quad (3.23)$$

where $\boldsymbol{H}^{(N_{\mathrm{Tx}}-j)}$ represents the matrix composed of the $N_{\mathrm{Tx}} - j$ rightmost columns of the initial channel matrix $\boldsymbol{H}$. By definition we have $\boldsymbol{H}^{(N_{\mathrm{Tx}})} = \boldsymbol{H}$ and $\boldsymbol{H}^{(0)}$ is assumed to be the empty matrix.

3.2.2 Impact of the Ordering in the Interference Cancellation Process

Introduction

As can be seen from the previous formulae (3.22) and (3.23), when evaluating the maximum achievable rate at the user level, the order in which the users are decoded will modify the rate perceived by each user. Therefore the ordering influences the single user rates also called per-user rates in this document.

As mentioned before the order in which the users will be decoded depends on their position in the channel matrix, more particularly it is assumed the interference cancellation process is performed from the first (left) column to the last (right) column of the channel matrix.

The position of the transmitters can actually be modified in the channel matrix (i.e. the column) but the pairs transmitters-receivers have to be kept identical. This can be achieved by permuting the channel matrix as follows:

$$\boldsymbol{H}' = \boldsymbol{\Pi}\,\boldsymbol{H}\,\boldsymbol{\Pi}^{\mathrm{T}} \tag{3.24}$$

where $\boldsymbol{H}'$ is the permuted version of $\boldsymbol{H}$ and $\boldsymbol{\Pi}$ is the so-called permutation matrix such that $\boldsymbol{\Pi} \in \{0,1\}^{N_{\mathrm{Rx}} \times N_{\mathrm{Rx}}}$.

Properties of the ordering on the MIMO sum rate:

The permutation matrix $\boldsymbol{\Pi}$ is an orthogonal matrix which means by definition that:

$$\boldsymbol{\Pi}^{\mathrm{T}} = \boldsymbol{\Pi}^{-1} \tag{3.25}$$

In the case all transmitters send with unit transmit power we have $\boldsymbol{C_x} = \boldsymbol{I}_{N_{\mathrm{Tx}}}$. The maximum achievable rate of the MIMO can therefore be written as:

$$R_{\mathrm{MIMO}} = \log_2 \det\left(\boldsymbol{I}_{N_{\mathrm{Rx}}} + \boldsymbol{C}_{\boldsymbol{\eta}}^{-1}\,\boldsymbol{H}\,\boldsymbol{H}^{\mathrm{H}}\right)$$

When computing the sum rate of a permuted version of the channel matrix, we get:

$$R_{\mathrm{MIMO}} = \log_2 \det\left(\boldsymbol{I}_{N_{\mathrm{Rx}}} + \boldsymbol{C}_{\boldsymbol{\eta}}^{-1}\,\boldsymbol{H}'\,\boldsymbol{H}'^{\mathrm{H}}\right) = \log_2 \det\left(\boldsymbol{I}_{N_{\mathrm{Rx}}} + \boldsymbol{C}_{\boldsymbol{\eta}}^{-1}\,\boldsymbol{\Pi}\,\boldsymbol{H}\,\boldsymbol{\Pi}^{\mathrm{T}}\,\left(\boldsymbol{\Pi}\,\boldsymbol{H}\,\boldsymbol{\Pi}^{\mathrm{T}}\right)^{\mathrm{H}}\right)$$

since $(\boldsymbol{A}\,\boldsymbol{B})^{\mathrm{H}} = \boldsymbol{B}^{\mathrm{H}}\,\boldsymbol{A}^{\mathrm{H}}$, we obtain:

$$R_{\mathrm{MIMO}} = \log_2 \det\left(\boldsymbol{I}_{N_{\mathrm{Rx}}} + \boldsymbol{C}_{\boldsymbol{\eta}}^{-1}\,\boldsymbol{\Pi}\,\boldsymbol{H}\,\boldsymbol{\Pi}^{\mathrm{T}}\,\boldsymbol{\Pi}\,\boldsymbol{H}^{\mathrm{H}}\,\boldsymbol{\Pi}^{\mathrm{T}}\right) = \log_2 \det\left(\boldsymbol{I}_{N_{\mathrm{Rx}}} + \boldsymbol{C}_{\boldsymbol{\eta}}^{-1}\,\boldsymbol{\Pi}\,\boldsymbol{H}\,\boldsymbol{H}^{\mathrm{H}}\,\boldsymbol{\Pi}^{\mathrm{T}}\right)$$

which is the same as writing:

$$R_{\mathrm{MIMO}} = \log_2 \det\left(\boldsymbol{I}_{N_{\mathrm{Rx}}} + \boldsymbol{C}_{\boldsymbol{\eta}}^{-1}\,\boldsymbol{\Pi}\,\boldsymbol{H}\,\left(\boldsymbol{\Pi}\,\boldsymbol{H}\right)^{\mathrm{H}}\right)$$

When looking at the previous expression the sum rate is thus equal to the one obtained when simply permuting the columns of the $\boldsymbol{H}$ matrix, i.e.:

$$\boldsymbol{H}' = \boldsymbol{\Pi}\,\boldsymbol{H} \tag{3.26}$$

This means that the order of the elements in each column of the channel matrix $\boldsymbol{H}$, i.e. the pairs transmitters-receivers, does not influence the maximum achievable sum rate of the system.

The covariance matrix of the noise $\boldsymbol{C_\eta}$ can also be written:

$$\boldsymbol{C_\eta} = \mathrm{E}\left[(\boldsymbol{\eta} - \mathrm{E}[\boldsymbol{\eta}])\,(\boldsymbol{\eta} - \mathrm{E}[\boldsymbol{\eta}])^{\mathrm{H}}\right] = \mathrm{E}\left[\boldsymbol{\eta}\,\boldsymbol{\eta}^{\mathrm{H}}\right] = N_0\,\boldsymbol{I}_{N_{\mathrm{Rx}}} \tag{3.27}$$

Using the properties of the determinant we can formulate the sum rate as:

$$R_{\mathrm{MIMO}} = \log_2 \det\left(\boldsymbol{I}_{N_{\mathrm{Rx}}} + N_0^{-1}\,\boldsymbol{I}_{N_{\mathrm{Rx}}}\,\boldsymbol{\Pi}\,\boldsymbol{H}\,\boldsymbol{H}^{\mathrm{H}}\,\boldsymbol{\Pi}^{\mathrm{T}}\right) = \log_2 \det\left(\boldsymbol{I}_{N_{\mathrm{Tx}}} + \boldsymbol{H}^{\mathrm{H}}\,\boldsymbol{\Pi}^{\mathrm{T}}\,\boldsymbol{\Pi}\,\boldsymbol{H}\,N_0^{-1}\,\boldsymbol{I}_{N_{\mathrm{Tx}}}\right)$$

as before, since $\boldsymbol{\Pi}^{\mathrm{T}}\,\boldsymbol{\Pi} = \boldsymbol{I}$, we obtain:

$$R_{\mathrm{MIMO}} = \log_2 \det\left(\boldsymbol{I}_{N_{\mathrm{Tx}}} + \boldsymbol{H}^{\mathrm{H}}\,\boldsymbol{H}\,N_0^{-1}\,\boldsymbol{I}_{N_{\mathrm{Tx}}}\right) = \log_2 \det\left(\boldsymbol{I}_{N_{\mathrm{Rx}}} + N_0^{-1}\,\boldsymbol{I}_{N_{\mathrm{Rx}}}\,\boldsymbol{H}\boldsymbol{H}^{\mathrm{H}}\right)$$

Performing a permutation of the channel matrix $\boldsymbol{H}$ does not change the maximum achievable sum rate of the system. Therefore when evaluating the maximum achievable rate of a MIMO system the order in which decoding is performed does not play a role. The columns of the channel matrix $\boldsymbol{H}$ can be permuted without having an impact on the sum rate.

Properties of the ordering on the MIMO single user rate:

As already mentioned the position of the columns in the channel matrix $\boldsymbol{H}$ plays a role on the single user rates when performing SIC. The number of possible permutations is directly driven by the number of columns present in the channel matrix $\boldsymbol{H}$, i.e. the number of transmitters N_{Tx}:

$$N_{\mathrm{perm}} = N_{\mathrm{Tx}}! \tag{3.28}$$

Since the sum rate does not change with permuted versions of the channel matrix, an increase of a given rate using a particular permutation matrix will necessarily involve the decrease of other user rate(s). One can understand that modifying the ordering of the IC process does not permit to act on the sum rate but allows influencing the single user rates.

Fig. 3.7 gives an example of a permutation applied on a channel matrix (7×7 system, bad case, permutation #1862). In this figure the difference of rate perceived by each user, w.r.t. to the initial ordering, is shown (i.e. the difference of rates between the original matrix and the permuted matrix). On the one hand, over the entire SNR range users 2, 4, 5 and 7 get an increase of their rates. On the other hand, users 1, 3 and 6 see a decrease of their rates. As can be seen at an energy per symbol over noise power spectral density ratio of 10 dB (highlighted points in red), the total increase of the single user rates (sum of the positive differences) is about 5.5 bits/s/Hz whereas the total decrease of the single user rates (sum

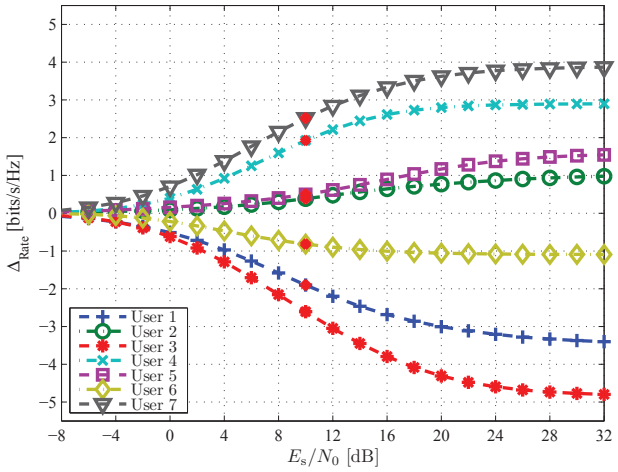


Figure 3.7. *Example of the impact of the permutation on the single user rates (difference).*

of the negative differences) is about -5.5 bits/s/Hz. The overall sum of the differences is therefore zero which confirms that the sum rate is kept constant whatever the permutation matrix applied.

3.2.3 Max-Min Criterion - Maximisation of the Minimum Rate

We have seen in the previous section (Section 3.2.2) that the order in which the interference cancellation process is performed does not have an impact on the achievable sum rate. However it has an impact on the achievable per-user rate and therefore permuting the columns of the channel matrix influences directly the rates perceived by the users. It is thus possible to take into account user requirements, i.e. Quality of Service (QoS), such that the ordering targets particular user rates. For instance the so-called "max-min" criterion, considered in the following, aims at maximising the lowest rates experienced by the users in the system. The optimal ordering for satisfying such criterion can be obtained in several ways.

Exhaustive Search

The exhaustive search consists into looking at all possible permutations of the channel matrix $\boldsymbol{H}$, i.e. among the $N_{\text{Tx}}!$ possibilities. By applying a particular permutation matrix $\boldsymbol{\Pi}$, the single user rates can be adjusted in order to target the max-min criterion, more particularly:

$$\boldsymbol{\Pi}' = \arg \max_{\boldsymbol{\Pi}} \left\{ \min_{j} R_{j,\text{MIMO}} (\boldsymbol{\Pi}) \right\} \tag{3.29}$$

where $\boldsymbol{\Pi}'$ represents the permutation matrix offering the optimal ordering (OO).

The previous criterion aims at finding over all possible permutation matrices the permutation which will maximise the minimum user rate. Since an increase of the minimum user rate will involve the decrease of other higher rate(s) such criterion also permits to provide more fairness to the users.

This method is clearly not optimal from the computational complexity point of view since the search space increases rapidly with the number of transmitters. Hence other methods need to be investigated.

Power from Transmitter to Receiver

The ordering for applying SIC can be decided according to the transmitter to receiver link. If we assume identical power for all transmitters, then the diagonal elements of the channel matrix permit to differentiate the links. Selecting first the link with the highest power from transmitter to receiver increases the probability of decoding correctly the transmitted signal and thus avoids propagating an error in the system. Therefore we can write:

$$j_n^* = \arg\max_j \left\{|h_{j,j}|^2\right\} \quad j \in \{1,...,N_{\mathrm{Tx}}\} \setminus \left\{j_1^*, j_2^*, ..., j_{n-1}^*\right\}, \; n = 1,...,N_{\mathrm{Tx}} \tag{3.30}$$

Doing so results in having $|h_{j_1^*,j_1^*}|^2 \geq |h_{j_2^*,j_2^*}|^2 \geq ... \geq |h_{j_{N_{\mathrm{Tx}}}^*,j_{N_{\mathrm{Tx}}}^*}|^2$, i.e. sorting the power from transmitter to receiver in descending order.

This method, which is quite straightforward, actually considers the system as a Single-Input and Single-Output (SISO) system since only the "useful" part of the channel matrix, i.e. its diagonal, is taken into account. Hence it is sub-optimal even if the computational complexity is very low.

Power from Transmitter to Receivers

Using the same principle as before the ordering of SIC can be driven by the power from transmitter to multiple receivers. In such a case the order is obtained as follows:

$$j_n^* = \arg\max_j \left\{\sum_{i=1}^{N_{\mathrm{Rx}}} |h_{i,j}|^2\right\} \quad j \in \{1,...,N_{\mathrm{Tx}}\} \setminus \left\{j_1^*, j_2^*, ..., j_{n-1}^*\right\}, \; n = 1,...,N_{\mathrm{Tx}} \tag{3.31}$$

Doing so results in having $||\boldsymbol{h}_{j_1^*}||^2 \geq ||\boldsymbol{h}_{j_2^*}||^2 \geq ... \geq ||\boldsymbol{h}_{j_{N_{\mathrm{Tx}}}^*}||^2$ ($\boldsymbol{h}_j$ is the j-th column vector of the channel matrix $\boldsymbol{H}$), i.e. sorting the power from transmitter to all receivers in descending order.

With this method the system is seen as a Single-Input and Multiple-Output (SIMO) system and once again even if it offers a low computational complexity it is sub-optimal since it still does not consider the multiple-input property.

Ordering based on the Signal-to-Interference plus Noise Ratio

The criterion previously defined consists into maximising of the minimum per-user rate. As mentioned before it is possible to realise an exhaustive search in order to determine the optimal ordering for this criterion. In the two previous sections only the signal levels were taken into account. Actually both interference and noise levels should also be considered, i.e. the Signal-to-Interference-plus-Noise Ratio (SINR).

Foschini has shown that maximising the minimum rate with SIC can be achieved by first selecting the stream with the highest SINR. The impact of this stream is then removed (IC), the SINR is evaluated on the remaining streams and once again the stream with the highest SINR is selected. The algorithms continues until all streams are processed [FGVW99].

The SINR evaluation for optimising the ordering depends on the receiver architecture, more particularly at which stage ordering is realised. Actually the Signal-to-Interference-plus-Noise Ratio (SINR) depends on the operations performed on the received signal.

Zero Forcing:
If the Zero Forcing equalisation is realised right before the ordering decision then the SINR has to be evaluated on the new estimate of the transmitted vector $\hat{\boldsymbol{x}}$. With ZF we have:

$$\hat{\boldsymbol{x}} = \boldsymbol{W}\,\boldsymbol{y} = \boldsymbol{H}^{+}\,\boldsymbol{y} = \left(\boldsymbol{H}^{\mathrm{H}}\,\boldsymbol{H}\right)^{-1}\,\boldsymbol{H}^{\mathrm{H}}\,\boldsymbol{y}$$

where $\boldsymbol{W}$ is the so-called Moore-Penrose pseudo-inverse matrix, also written $\boldsymbol{H}^{+}$ the pseudo-inverse of the channel matrix $\boldsymbol{H}$.

The vector $\hat{\boldsymbol{x}}$ can also be written:

$$\hat{\boldsymbol{x}} = \left(\boldsymbol{H}^{\mathrm{H}}\,\boldsymbol{H}\right)^{-1}\,\boldsymbol{H}^{\mathrm{H}}\,\boldsymbol{y} = \left(\boldsymbol{H}^{\mathrm{H}}\,\boldsymbol{H}\right)^{-1}\,\boldsymbol{H}^{\mathrm{H}}\,\left(\boldsymbol{H}\,\boldsymbol{x}+\boldsymbol{\eta}\right) = \boldsymbol{x} + \boldsymbol{H}^{+}\,\boldsymbol{\eta} = \boldsymbol{x} + \boldsymbol{\eta}'$$

as can be seen $\boldsymbol{x}$ represents the signal part and $\boldsymbol{\eta}'$ the noise part.

The covariance of the new noise $\boldsymbol{\eta}'$, which appears after the Zero Forcing linear operation, is:

$$\boldsymbol{C}_{\boldsymbol{\eta}'} = \mathrm{E}\left[\left(\boldsymbol{\eta}' - \mathrm{E}\left[\boldsymbol{\eta}'\right]\right)\,\left(\boldsymbol{\eta}' - \mathrm{E}\left[\boldsymbol{\eta}'\right]\right)^{\mathrm{H}}\right]$$

The expectation of the new noise $\boldsymbol{\eta}'$ is:

$$\mathrm{E}\left[\boldsymbol{\eta}'\right] = \mathrm{E}\left[\boldsymbol{H}^{+}\,\boldsymbol{\eta}\right] = \mathrm{E}\left[\boldsymbol{H}^{+}\right]\,\mathrm{E}\left[\boldsymbol{\eta}\right] = 0$$

since $\boldsymbol{H}$ and $\boldsymbol{\eta}$ are independent and $\mathrm{E}\left[\boldsymbol{\eta}\right] = 0$.

The covariance of $\boldsymbol{\eta}'$ can therefore be formulated as:

$$\boldsymbol{C}_{\boldsymbol{\eta}'} = \mathrm{E}\left[\boldsymbol{\eta}'\,\boldsymbol{\eta}'^{\mathrm{H}}\right] = \mathrm{E}\left[\left(\boldsymbol{H}^{\mathrm{H}}\,\boldsymbol{H}\right)^{-1}\,\boldsymbol{H}^{\mathrm{H}}\,\boldsymbol{\eta}\,\left(\left(\boldsymbol{H}^{\mathrm{H}}\,\boldsymbol{H}\right)^{-1}\,\boldsymbol{H}^{\mathrm{H}}\,\boldsymbol{\eta}\right)^{\mathrm{H}}\right]$$

since $\left(\boldsymbol{A}\,\boldsymbol{B}\right)^{\mathrm{H}} = \boldsymbol{B}^{\mathrm{H}}\,\boldsymbol{A}^{\mathrm{H}}$ and $\left(\boldsymbol{A}^{-1}\right)^{\mathrm{H}} = \left(\boldsymbol{A}^{\mathrm{H}}\right)^{-1}$ we obtain:

$$\boldsymbol{C}_{\boldsymbol{\eta}'} = \mathrm{E}\left[\left(\boldsymbol{H}^{\mathrm{H}}\,\boldsymbol{H}\right)^{-1}\,\boldsymbol{H}^{\mathrm{H}}\,\boldsymbol{\eta}\,\boldsymbol{\eta}^{\mathrm{H}}\,\boldsymbol{H}\,\left(\boldsymbol{H}^{\mathrm{H}}\,\boldsymbol{H}\right)^{-1^{\mathrm{H}}}\right] = \left(\boldsymbol{H}^{\mathrm{H}}\,\boldsymbol{H}\right)^{-1^{\mathrm{H}}} N_0 = \left(\boldsymbol{H}^{\mathrm{H}}\,\boldsymbol{H}\right)^{-1}\,N_0$$

This explain why Zero Forcing does not perform well in the noise-limited region because the noise power is increased by a factor $\left(\boldsymbol{H}^{\mathrm{H}}\,\boldsymbol{H}\right)^{-1}$. Since the covariance of the noise $\boldsymbol{C}_{\boldsymbol{\eta}}$ equals $N_0\,\boldsymbol{I}$, we can finally write:

$$\boldsymbol{C}_{\boldsymbol{\eta}'} = \left(\boldsymbol{H}^{\mathrm{H}}\,\boldsymbol{C}_{\boldsymbol{\eta}}^{-1}\,\boldsymbol{H}\right)^{-1}$$

this is thus equivalent to having a noise $\boldsymbol{\eta}'$ such that $\boldsymbol{\eta}' \sim \mathcal{N}_{\mathbb{C}}\left(0, \left(\boldsymbol{H}^{\mathrm{H}}\,\boldsymbol{C}_{\boldsymbol{\eta}}^{-1}\,\boldsymbol{H}\right)^{-1}\right)$.

The covariance of the signal part is simply $\boldsymbol{C}_{\boldsymbol{x}}$ and since the transmitted signals are i.i.d with expectation 0 and normalised transmit power, we can finally write that the SINR of the estimated signal $\hat{x}_j$ after Zero Forcing is [1]:

$$\mathrm{SINR}_{\mathrm{ZF},j} = \frac{1}{\left[\boldsymbol{C}_{\boldsymbol{\eta}'}\right]_{j,j}} = \frac{1}{\left[\left(\boldsymbol{H}^{\mathrm{H}}\,\boldsymbol{C}_{\boldsymbol{\eta}}^{-1}\,\boldsymbol{H}\right)^{-1}\right]_{j,j}} \tag{3.32}$$

where $\left[\boldsymbol{A}\right]_{j,j}$ represents the j-th diagonal element of the matrix $\boldsymbol{A}$.

The optimal ordering after Zero Forcing (ZF) equalisation is thus:

$$j^{*}_{\mathrm{ZF},n} = \arg\,\min_{j}\left\{\left[\left(\boldsymbol{H}^{\mathrm{H}}\,\boldsymbol{C}_{\boldsymbol{\eta}}^{-1}\,\boldsymbol{H}\right)^{-1}\right]_{j,j}\right\} \quad j \in \{1, ..., N_{\mathrm{Tx}}\} \setminus \left\{j^{*}_{\mathrm{ZF},1}, j^{*}_{\mathrm{ZF},2}, ..., j^{*}_{\mathrm{ZF},n-1}\right\} \tag{3.33}$$

with $n = 1, ..., N_{\mathrm{Tx}}$.

1. It has to be remarked that there is in principle no interference remaining after Zero-Forcing. The term SINR is used here for harmonising the notations.

When performing Successive Interference Cancellation (SIC) the impact of the streams is subtracted successively which means that the channel matrix $\boldsymbol{H}$ is different after each IC. The ordering when having ZF and SIC is thus:

$$\mathrm{SINR}_{\text{ZF-SIC},j}^{(r)} = \frac{1}{\left[\left(\boldsymbol{H}^{(r)\mathrm{H}}\,\boldsymbol{C}_{\boldsymbol{\eta}}^{-1}\,\boldsymbol{H}^{(r)}\right)^{-1}\right]_{j',j'}} \tag{3.34}$$

where $\boldsymbol{H}^{(r)}$ is the (r)-th realisation of the channel matrix $\boldsymbol{H}$ and which is composed of the columns vectors $\boldsymbol{h}_j$ such that j satisfies $j \in \{1, ..., N_{\mathrm{Tx}}\}$ and also $j \notin \left\{j_{\text{ZF-SIC},1}^{*}, j_{\text{ZF-SIC},2}^{*}, ..., j_{\text{ZF-SIC},r-1}^{*}\right\}$, j' represents the position, i.e. the column index, of $\boldsymbol{h}_j$ in $\boldsymbol{H}(r)$, knowing that:

$$j_{\text{ZF-SIC},r}^{*} = \arg\max_{j}\{\mathrm{SINR}_{\text{ZF-SIC},j}^{(r)}\},\ j \in \{1, ..., N_{\mathrm{Tx}}\}\backslash\{j_{\text{ZF-SIC},1}^{*}, j_{\text{ZF-SIC},2}^{*}, ..., j_{\text{ZF-SIC},r-1}^{*}\} \tag{3.35}$$

this operation is performed for $r = 1, ..., N_{\mathrm{Tx}} - 1$, the last optimal position $j_{\text{ZF-SIC},N_{\mathrm{Tx}}}^{*}$ being equal to the last index j remaining.

Minimum Mean Square Error:

In the presence of an MMSE linear receiver the new estimate of the transmitted vector $\hat{\boldsymbol{x}}$ is:

$$\hat{\boldsymbol{x}} = \boldsymbol{G}_{\mathrm{MMSE}}\,\boldsymbol{y} = \boldsymbol{H}^{\mathrm{H}}\left[\boldsymbol{H}\,\boldsymbol{H}^{\mathrm{H}} + N_0\,\boldsymbol{I}\right]\,\boldsymbol{y} = \left[\boldsymbol{H}^{\mathrm{H}}\,\boldsymbol{H} + N_0\,\boldsymbol{I}\right]\,\boldsymbol{H}^{\mathrm{H}}\,\boldsymbol{y}$$

When looking at each stream separately, one stream per transmitter, the received signal can be written [TsVi08]:

$$\boldsymbol{y} = \boldsymbol{h}_j\,x_j + \boldsymbol{z}_j \tag{3.36}$$

where $\boldsymbol{h}_j$ represents the j-th column of the channel matrix $\boldsymbol{H}$.

The vector $\boldsymbol{z}_j$ contains the noise and also the interference issued from other transmitters, i.e.:

$$\boldsymbol{z}_j = \boldsymbol{\eta} + \sum_{k\neq j}\boldsymbol{h}_k\,x_k \tag{3.37}$$

The covariance of the vector $\boldsymbol{z}_j$ is:

$$\boldsymbol{C}_{\boldsymbol{z}_j} = \mathrm{E}\left[\left(\boldsymbol{\eta} + \sum_{k\neq j}\boldsymbol{h}_k\,x_k\right)\,\left(\boldsymbol{\eta} + \sum_{k\neq j}\boldsymbol{h}_k\,x_k\right)^{\mathrm{H}}\right] = N_0\,\boldsymbol{I} + \sum_{k\neq j}\boldsymbol{h}_k\,\boldsymbol{h}_k^{\mathrm{H}} \tag{3.38}$$

When processing each stream independently, one stream per transmitter, the filter maximising the SINR is:

$$\left[\boldsymbol{g}_{j,\mathrm{MMSE}}\right]^{\mathrm{T}} = \boldsymbol{h}_j^{\mathrm{H}}\,\boldsymbol{C}_{\boldsymbol{z}_j}^{-1} = \boldsymbol{h}_j^{\mathrm{H}}\,\left(N_0\,\boldsymbol{I} + \sum_{k\neq j}\boldsymbol{h}_k\,\boldsymbol{h}_k^{\mathrm{H}}\right)^{-1}$$

When applying the filter on the received signal we get:

$$\hat{\boldsymbol{x}}_j = [\boldsymbol{g}_{j,\mathrm{MMSE}}]^{\mathrm{T}}\ \boldsymbol{y} = \boldsymbol{h}_j^{\mathrm{H}}\,\boldsymbol{C}_{\boldsymbol{z}_j}^{-1}\,(\boldsymbol{h}_j\,x_j + \boldsymbol{z}_j) = \boldsymbol{h}_j^{\mathrm{H}}\,\boldsymbol{C}_{\boldsymbol{z}_j}^{-1}\,\boldsymbol{h}_j\,x_j + \boldsymbol{h}_j^{\mathrm{H}}\,\boldsymbol{C}_{\boldsymbol{z}_j}^{-1}\,\boldsymbol{z}_j$$

The signal part is represented by $\boldsymbol{h}_j^{\mathrm{H}}\,\boldsymbol{C}_{\boldsymbol{z}_j}^{-1}\,\boldsymbol{h}_j\,x_j$ and the noise part by $\boldsymbol{h}_j^{\mathrm{H}}\,\boldsymbol{C}_{\boldsymbol{z}_j}^{-1}\,\boldsymbol{z}_j$.

The signal-to-interference plus noise ratio (SINR) experienced by the j-th stream after the MMSE filter is thus:

$$\mathrm{SINR}_{\mathrm{MMSE},j} = \boldsymbol{h}_j^{\mathrm{H}}\,\boldsymbol{C}_{\boldsymbol{z}_j}^{-1}\,\boldsymbol{h}_j = \boldsymbol{h}_j^{\mathrm{H}}\left(\boldsymbol{C}_{\boldsymbol{\eta}} + \sum_{i\neq j}\boldsymbol{h}_i\,\boldsymbol{h}_i^{\mathrm{H}}\right)^{-1}\boldsymbol{h}_j \tag{3.39}$$

The optimal ordering after Minimum Mean Square Error (MMSE) is thus:

$$j^*_{\mathrm{MMSE},n} = \arg\max_j\left\{\boldsymbol{h}_j^{\mathrm{H}}\left(\boldsymbol{C}_{\boldsymbol{\eta}} + \sum_{i\neq j}\boldsymbol{h}_i\,\boldsymbol{h}_i^{\mathrm{H}}\right)^{-1}\boldsymbol{h}_j\right\} \tag{3.40}$$

with $j \in \{1,...,N_{\mathrm{Tx}}\} \setminus \left\{j^*_{\mathrm{MMSE},1}, j^*_{\mathrm{MMSE},2}, ..., j^*_{\mathrm{MMSE},n-1}\right\}$ and $n = 1,...,N_{\mathrm{Tx}}$.

Once again when performing Successive Interference Cancellation (SIC) the impact of the streams is subtracted successively which means that the channel matrix $\boldsymbol{H}$ is different after each IC. The ordering when having MMSE and SIC is thus:

$$\mathrm{SINR}^{(r)}_{\text{MMSE-SIC},j} = \boldsymbol{h}_j^{\mathrm{H}}\left(\boldsymbol{C}_{\boldsymbol{\eta}}^{-1} + \sum_{i\neq j}\boldsymbol{h}_i\,\boldsymbol{h}_i^{\mathrm{H}}\right)^{-1}\boldsymbol{h}_j \tag{3.41}$$

where i also satisfies $i \notin \{j^*_{\text{MMSE-SIC},1}, ..., j^*_{\text{MMSE-SIC},j-1}\}$, knowing that:

$$j^*_{\text{MMSE-SIC},r} = \arg\max_j\{\mathrm{SINR}^{(r)}_{\text{MMSE-SIC},j}\},\ j \in \{1,...,N_{\mathrm{Tx}}\}\backslash\{j^*_{\text{MMSE-SIC},1}, ..., j^*_{\text{MMSE-SIC},r-1}\}$$

this operation is performed for $r = 1,...,N_{\mathrm{Tx}} - 1$. The term $\boldsymbol{h}_j$ designates the j-th column of the channel matrix $\boldsymbol{H}$.

It has to be remarked that the elements in each line of the MMSE filter represented by the matrix $\boldsymbol{G}_{\mathrm{MMSE}}$ are not directly identical but are proportional to the elements present in the vector previously defined, i.e. $[\boldsymbol{g}_{j,\mathrm{MMSE}}]^{\mathrm{T}}$. Since both signal and noise plus interference are multiplied by the filter coefficients, the resulting SINR remains the same.

Properties of MMSE with SIC:

We have seen previously that the SINR after the MMSE linear filter can be expressed using (3.39). As already mentioned performing SIC will remove the impact of the interferers one by one. Therefore we can also write:

$$\mathrm{SINR}_{\text{MMSE-SIC},j} = \boldsymbol{h}_j^{\mathrm{H}} \left(\boldsymbol{C}_{\boldsymbol{\eta}} + \sum_{i>j} \boldsymbol{h}_i \, \boldsymbol{h}_i^{\mathrm{H}} \right)^{-1} \boldsymbol{h}_j \quad j = 1, ..., N_{\mathrm{Tx}} \tag{3.42}$$

The achievable rate for each stream j can be simply evaluated as:

$$R_{\text{MMSE-SIC},j} = \log_2 \left(1 + \mathrm{SINR}_{\text{MMSE-SIC},j}\right)$$

and the resulting sum rate is therefore:

$$R_{\text{MMSE-SIC}} = \sum_{j=1}^{N_{\mathrm{Tx}}} \log_2 \left(1 + \boldsymbol{h}_j^{\mathrm{H}} \left(\boldsymbol{C}_{\boldsymbol{\eta}} + \sum_{i>j} \boldsymbol{h}_i \, \boldsymbol{h}_i^{\mathrm{H}} \right)^{-1} \boldsymbol{h}_j \right)$$

since the determinant of a scalar is a scalar, we can also write:

$$R_{\text{MMSE-SIC}} = \sum_{j=1}^{N_{\mathrm{Tx}}} \log_2 \det \left(1 + \boldsymbol{h}_j^{\mathrm{H}} \left(\boldsymbol{C}_{\boldsymbol{\eta}} + \sum_{i>j} \boldsymbol{h}_i \, \boldsymbol{h}_i^{\mathrm{H}} \right)^{-1} \boldsymbol{h}_j \right)$$

Using the properties of the determinant, more particularly $\det \boldsymbol{A} \det \boldsymbol{B} = \det(\boldsymbol{A}\,\boldsymbol{B})$ and $\det(\boldsymbol{I} + \boldsymbol{A}\,\boldsymbol{B}) = \det(\boldsymbol{I} + \boldsymbol{B}\,\boldsymbol{A})$, we can reformulate the sum rate as:

$$R_{\text{MMSE-SIC}} = \log_2 \det \left(\Pi_{j=1}^{N_{\mathrm{Tx}}} \left[\boldsymbol{I} + \boldsymbol{h}_j \, \boldsymbol{h}_j^{\mathrm{H}} \left(\boldsymbol{C}_{\boldsymbol{\eta}} + \sum_{i>j} \boldsymbol{h}_i \, \boldsymbol{h}_i^{\mathrm{H}} \right)^{-1} \right] \right) \tag{3.43}$$

It can easily be shown, after some matrix manipulations, that:

$$R_{\text{MMSE-SIC}} = \log_2 \det \left(\boldsymbol{I} + \boldsymbol{C}_{\boldsymbol{\eta}}^{-1} \, \boldsymbol{H} \, \boldsymbol{H}^{\mathrm{H}} \right) = R_{\mathrm{MIMO}} \tag{3.44}$$

This proves that performing SIC with a linear MMSE receiver permits to obtain the maximum achievable rate of a MIMO system [VaGu97]. It has also to be remarked that the different expressions match perfectly with the evaluation of the single user rate in a MIMO system (please refer to Section 3.2.1).

3.2.4 Performance Analysis of the Ordering

In this section we show the performance of the ordering for the return-link of a multi-beam satellite system which is composed of seven beams with one user per beam at a given time (7×7 MIMO system) [BBRJ11]. Such small scenario is taken into account because of the brute

force approach which is considered here (exhaustive search, $N_{\mathrm{Tx}}!$ possible permutations). The cluster size K is set to 1 which means that all beams are using the same frequency. In this scenario we thus have the reference beam and its six surrounding beams. For each channel realisation the position of the users is determined randomly in each beam. The purpose is to extract the minimum user rate of each channel realisation while modifying the ordering in the Interference Cancellation (IC) process. In such a system Successive Interference Cancellation (SIC) is thus performed at the gateway where all user signals are received.

The average of the minimum user rate over 1 000 channel realisations is shown for the average, the brute force approach, Foschini and worst case scenarios. The average corresponds to the minimum user rates obtained while considering all possible detection orders. This strategy actually represents the performance of a non-optimised detection order. The brute force aims at finding the optimal ordering for maximising the minimum user rate (exhaustive search among all possible permutations). The Foschini algorithm, as already mentioned, targets the criterion of interest, i.e. the maximisation of the minimum user rate. It is assumed here that the ordering with the Foschini algorithm is realised right after MMSE filtering since it is capacity achieving. Finally in the worst case we select, using a brute force approach, the ordering which minimises the minimum user rate in order to evaluate the performance if the worst ordering was performed.

Fig. 3.8 clearly shows that the minimum rate is improved compared to an "average" strategy (left graph). The results issued from the brute force method perfectly match, as expected, the average minimum user rates obtained with the Foschini algorithm. Compared to an exhaustive search the Foschini algorithm offers the optimal result with low computation complexity. In terms of performance the minimum per-user rate can be increased by 30% with respect to a randomly selected permutation (so-called "average") and more than 50% with respect to the worst permutation, i.e. the one minimising the minimum rate.

Providing fairness between the different users in the system consists in minimising the difference of rate perceived by the users. This is equivalent to satisfy the following criterion:

$$\mathbf{\Pi}' = \arg\min_{\mathbf{\Pi}} \left\{ \frac{1}{N_{\mathrm{Tx}}} \sum_{j=1}^{N_{\mathrm{Tx}}} \left(R_{j,\mathrm{MIMO}}\left(\mathbf{\Pi}\right) - \frac{R_{\mathrm{MIMO}}}{N_{\mathrm{Tx}}} \right)^2 \right\} \tag{3.45}$$

where $\mathbf{\Pi}'$ is the permutation matrix which minimises the dispersion from the average sum

rate.

The same approach as for the max-min criterion is considered, i.e. the average, the brute force, the Foschini algorithm and the worst ordering are taken into account. The corresponding results are shown in Fig. 3.8 (right graph).

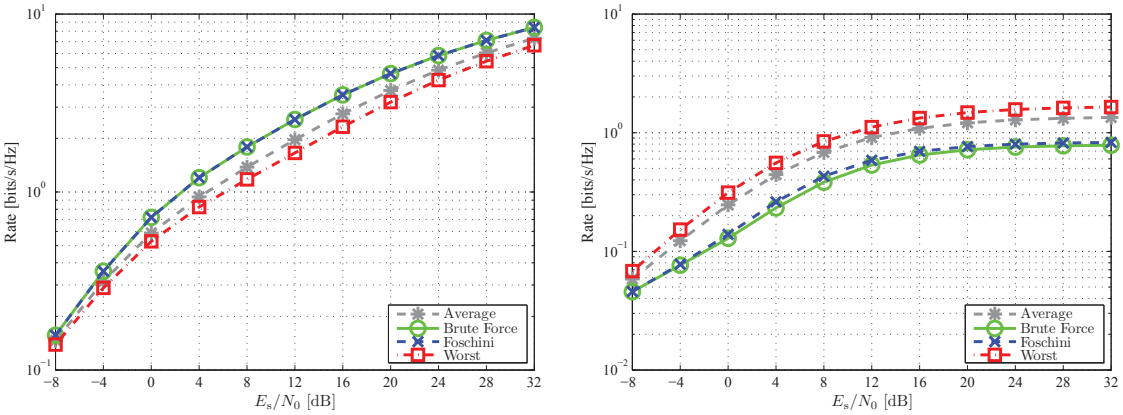


Figure 3.8. *Performance of the ordering on the minimum user rates (left) and on the dispersion from the average sum rates (right) for seven beams ($B = 7$) with full frequency reuse ($K = 1$) and issued from* 1 000 *channel realisations. The minimum per-user rates are compared for different methods: average, brute force approach, Foschini algorithm and worst case.*

In these results (Fig. 3.8, right) the brute force method and the Foschini algorithm permits to decrease the difference of rate between users by a factor of 2. However it has to be remarked that the exhaustive search offers slightly better performance than the Foschini algorithm.

3.2.5 Statistics on the Single User Rates

This section aims at providing some statistics which are directly related to the single user rates, also called achievable per-user rates in this document. The statistics concern the reduced multi-beam satellite system employing full frequency reuse ($K = 1$), which is therefore composed of seven beams ($B = 7$, please refer to Fig. 1.9), and are computed over ten thousand channel realisations ($N_{\text{ch}} = 10\,000$). The purpose is to better understand the impact of the Input-Output (IO) type but also of the Signal-to-Noise Ratio (SNR) on the user rates.

Impact of the Input - Output System

In order to investigate the impact of the Input-Output (IO) system type on the achievable per-user rates, the Signal-to-Noise Ratio (SNR) is fixed and set to 15 dB so that the communication system is mainly interference-limited. The achievable per-user rates are evaluated

for each IO system, more particularly Single-Input and Single-Output (SISO), Single-Input and Multiple-Output (SIMO) and Multiple-Input and Multiple-Output (MIMO), using the formulae provided in Section 3.1 for both SISO and SIMO systems, and in Section 3.2 for the MIMO system. For the latter, optimal ordering, i.e. a permutation of the channel matrix targeting the maximisation of the minimum per-user rate, is assumed. The single user rates are computed for each channel realisation together with the resulting Jain's fairness index, and for each system type.

The Jain's fairness index is commonly used in order to quantify the fairness between different rates achieved by users in a network [JaHaCh84]. It is defined as:

$$J = \frac{\left(\sum_{i=1}^{N} r_i\right)^2}{N \times \sum_{i=1}^{N} r_i^2} \tag{3.46}$$

where N is the number of users (i.e. N_{Tx}) and r_i the single user rate, i.e. the achievable rate for each user. On the one hand, when the index reaches 1 the maximum fairness is achieved, i.e. all users experience the same achievable rate (upper bound). On the other hand, when the index equals $1/N$ it means that one single user gets the total capacity available whereas the others get nothing.

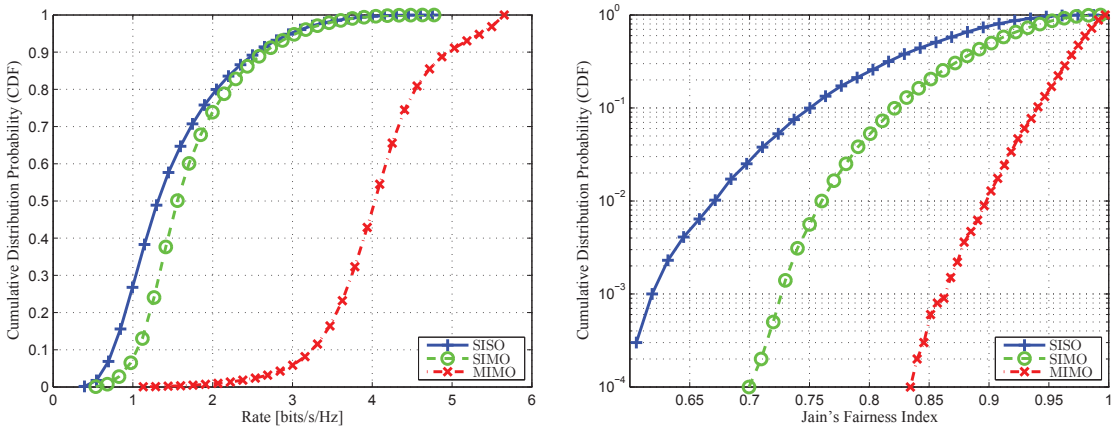


Figure 3.9. *Cumulative distribution functions of the achievable per-user rates (left) and of the Jain's fairness index (right) at SNR* 15 *dB and different input - output systems.*

As expected, and also as already known based on the different results obtained previously, the system type plays a role on the overall sum rate and consequently on the single user rates. SIMO outperforms SISO since the Cumulative Density Function (CDF) curve representing the achievable per-user rates is shifted on the right and therefore the probability of having higher per-user rates is more important (left graph in Fig. 3.9). However, the difference between the

two systems is not very important but when looking at the level of fairness between users, the improvement is more visible (right graph in Fig. 3.9)). The MIMO system offers clearly the best performance since the probability of having small per-user rates is very low when compared to both SISO and SIMO systems. Actually with SISO and SIMO, the CDF of the per-user rates starts around 0.5 bits/s/Hz whereas with MIMO the lowest achievable per-user rate is more than 1 bits/s/Hz. SISO and SIMO offers low rates with high probability (slope of the curves in the left graph of Fig. 3.9) and the CDF is also covering a wider range of rates. For this reason the Jain's fairness index, which measures the level of fairness between users, more particularly the difference of rates perceived by the users within the same channel realisation, is dramatically improved when using the MIMO system. The latter performance is actually achieved through the utilisation of SIC together with optimal ordering which aims at maximising the minimum per-user rate. Taking into account a probability of 10%, the gains with respect to the conventional SISO system are given by Table 3.1.

Table 3.1. *Gains on the achievable per-user rates with respect to the SISO system.*

Type	SIMO	MIMO
Rate [bits/s/Hz] (factor)	1.40	4.33
Jain's fairness index (percentage)	9.33 %	25.33%

Impact of the Signal-to-Noise Ratio

The purpose is to investigate the impact of the signal-to-noise ratio (SNR) on the achievable per-user rates while considering exclusively the Input-Output (IO) system offering the best performance, i.e. the Multiple-Input and Multiple-Output (MIMO) system. The same setup as in Section 3.2.5 is taken into account, more particularly the single user rates are evaluated considering optimal ordering in the Interference Cancellation (IC) process. For different SNR values, the statistics are computed over all channel realisations ($N_{\text{ch}} = 10\,000$).

As expected the Cumulative Density Function (CDF) of the achievable per-user rate shifts towards higher values when the signal-to-noise increases (left graph in Fig. 3.10). Interestingly the CDF of the Jain's fairness index has a totally different behaviour (right graph in Fig. 3.10). Clearly the Jain's fairness index gets improved when going from SNR -8 dB to 0 dB but surprisingly at SNR 8 dB the CDF matches almost perfectly the CDF obtained at -8 dB. Then, when looking at a probability of 10%, a gain appears for higher SNR values, more particularly here for SNR 15 dB. In other words the Jain's fairness index tends to get improved when the SNR increases and this between -8 dB and 0 dB, then it worsens from

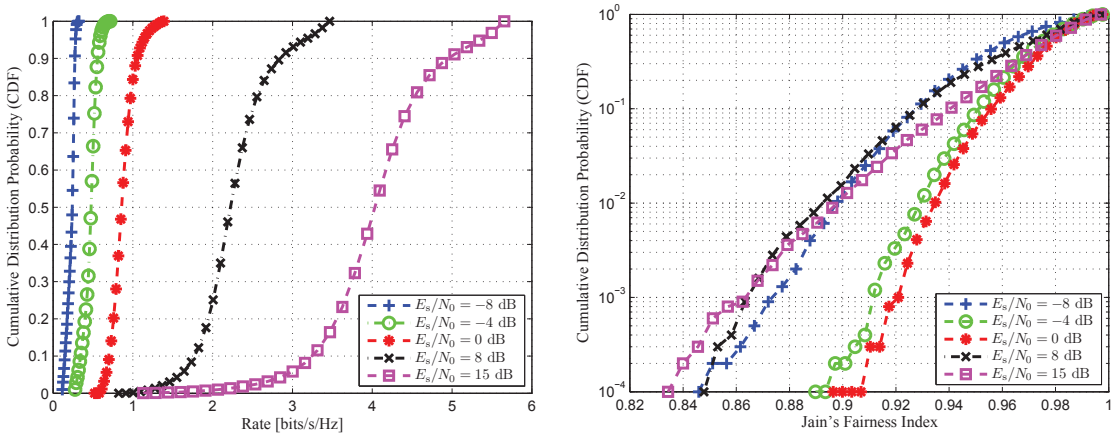


Figure 3.10. *Cumulative distribution function of the achievable per-user rates (left) and of the Jain's fairness index (right) for different SNRs and multiple-input - multiple-output system.*

0 dB to 8 dB, and finally gets better again for higher SNRs.

The interesting behaviour of the Jain's fairness index observed in the previous results leads to performing an analysis of the average value of this index with the different Input-Output (IO) systems. The aim is to better understand the causes of such tendency and also to evaluate the impact of the optimal ordering (OO) when considering the MIMO system.

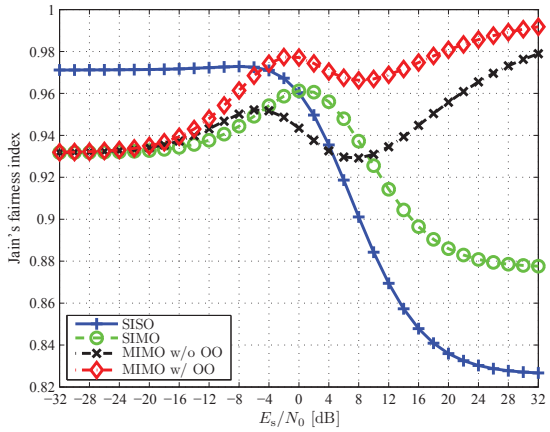


Figure 3.11. *Mean value of the Jain's fairness index for different SNRs and input - output systems.*

As seen in Fig. 3.11 the average value of the Jain's fairness index remains almost constant till -4 dB with the SISO system. Actually in such a case all users are noise-limited in this SNR range and therefore they all experience the same achievable per-user rates. Consequently the value of the Jain's fairness index is quite high (around 0.97) but then decreases dramatically when leaving the noise-limited region. More particularly as soon as the SNR becomes greater

than 0 dB, the system becomes interference-limited; the Jain's fairness index tends to saturate around 0.83 for high SNRs. When focusing on the Single-Input and Multiple-Output (SIMO) system, the Jain's fairness index is about 0.93 for low SNRs, i.e. below the one offered with the conventional SISO system. This is due to the fact such system performs the Maximal Ratio Combining (MRC) operation and is equivalent to a matched filter. The latter aims at maximising the SNR and therefore shows an improvement in the noise-limited region in terms of achievable per-user rates. Some users of the system will see their rates improved thanks to the matched filter, involving a difference in the achievable rates between the users, and therefore the level of fairness decreases. The Jain's fairness index increases up to 0.96 at SNR 0 dB and then decreases to saturate around 0.88 for high SNRs. Finally when looking at the Multiple-Input and Multiple-Output (MIMO) system without and with optimal ordering (OO), it acts like a matched filter for low SNRs and for this reason the same Jain's fairness index as the one obtained with the SIMO system is observed. On the one hand, without optimal ordering the Jain's fairness index worsens starting from -6 dB. On the other hand, with optimal ordering the benefit of performing Maximal Ratio Combining (MRC) together with Successive Interference Cancellation (SIC) permits to reach a Jain's fairness index almost equal to 0.98 at SNR 0 dB. Then since the system is no more noise-limited but rather interference-limited, the interference becomes predominant and the difference between users becomes more obvious. The Jain's fairness decreases, as with the SIMO system, till 8 dB for both cases to reach almost 0.93 and 0.96, without and with optimal ordering, respectively. Finally the system becomes exclusively interference-limited and the SIC process permits to remove properly the interference. Starting from this point, the Jain's fairness index increases and tends to reach 0.98 and 0.99 at SNR 32 dB respectively without performing any ordering operations and when realising optimal ordering. Through the latter, the minimum achievable per-user rate is maximised and consequently the level of fairness between users is increased, as shown by Fig. 3.11.

Ordering

We have seen in this section that the order in which the users are decoded while performing Successive Interference Cancellation (SIC) is of paramount importance and this fact has also been verified in the previous section. The ordering operation consists in our case into applying a permutation matrix to the channel matrix $\boldsymbol{H}$ so that the decoding order during the Interference Cancellation (IC) process is modified. It is actually assumed that the decoding of the users is performed from the left to the right, i.e. from the first column to the last column

of the channel matrix. The last column to be decoded corresponds to a column vector of size $N_{\mathrm{Rx}} \times 1$ in which all interferers have been removed.

The ordering taken into account is obtained using the Foschini algorithm [FGVW99] and permits to maximise the minimum achievable per-user rate in the system (please refer to Section 3.2.3 for more details). This ordering is considered as being the optimal one since it targets the criterion of interest with low complexity and similar performance as a pure exhaustive search (Section 3.2.4). The purpose of this section is to gather some statistics, still considering the same system scenario, i.e. $B = 7$ beams and $N_{\mathrm{ch}} = 10\,000$ channel realisations, about the order in which users are decoded.

Table 3.2. *Order in which the users are decoded in the multiple-input - multiple-output system.*

SNR\User ID	1	2	3	4	5	6	7
−8 dB	35.81%	11.34%	14.72%	10.57%	8.49%	10.67%	8.40%
−4 dB	16.87%	13.14%	16.01%	14.25%	13.82%	13.95%	11.96%
0 dB	6.37%	14.48%	16.43%	16.92%	16.73%	15.44%	13.63%
8 dB	1.56%	15.61%	15.81%	17.95%	18.58%	14.91%	15.58%
15 dB	1.09%	16.03%	15.60%	18.21%	18.80%	13.80%	16.47%

We remind that the principle of the Foschini algorithm is to sort the users to be decoded in ascending order, according to the Signal-to-Interference-plus-Noise Ratio (SINR) perceived by each user. The user with the strongest SINR is selected and the corresponding column is removed from the channel matrix $\boldsymbol{H}$. The process continues, i.e. with the new version of the channel matrix, and until one single column of the channel matrix remains. This column vector represents the last user to be decoded, i.e. the weakest user. The statistics given by Table 3.2 shows the percentage with which each user is decoded first. In the noise-limited region, i.e. below 0 dB, the first user, i.e. the user located in the middle, tends to be decoded first. For higher SNRs the system becomes interference-limited and since beam with ID 1 is located in the middle of the system, and is therefore surrounded by six other beams, the users covered by this beam suffer from interference much more than the others. This is confirmed at SNR 15 dB where user 1 is the first to be decoded with about 1% of probability, which is very low, the remaining percentage being distributed among the surrounding beams. The statistics shown by this table also confirm that the result of the ordering operation clearly depends on the SNR.

3.3 Summary

We have seen in this chapter that the phase present in the coefficients of the channel matrix has actually no impact on the achievable sum rate for SISO, SIMO and MIMO systems. On the one hand, the analysis of the sum rates which can be achieved in a system employing three colours has shown that interference cancellation does not bring sufficient gains in typical signal-to-noise ratio operating regions. The multi-beam satellite system considered as baseline scenario is actually designed so as to lower the level of co-channel interference when the cluster size is equal to or greater than three. For this reason a four colours scheme gives even lower gain, almost negligible, when considering maximal ratio combining (SIMO) or successive interference cancellation (MIMO). On the other hand, the gains reached when using full frequency reuse are considerable since the theoretical system capacity is multiplied by a factor 3 when compared with a conventional system (SISO) employing three colours, complying with [CCMO11]. However such gains are obtained under certain considerations which are listed hereafter.

First of all clear sky conditions are considered and also a perfect knowledge of the channel state information (CSI) at the gateway side is assumed. Then a gateway is responsible for a given number of beams within a multi-beam satellite system. We actually speak about cluster of beams. As an example in a 72 multi-beam satellite system there can be 5 gateways, each responsible of 14 or 15 beams [ESA-RM]. The gateways are mainly responsible for the air interface, i.e. for transmitting towards the satellite (forward up-link, also called feeder up-link) and receiving from the satellite (return down-link, also called feeder down-link).

Full frequency reuse imposes constraints on both space on ground segment. In the former segment more Travelling Wave Tube Amplifiers (TWTAs) are required, actually K times more where K refers to the nominal number of colours considered in the satellite system. This can be achieved by using more satellites or by increasing the size of the payload, therefore by designing larger satellites. In the latter segment the feeder link is impacted since more bandwidth is required. This can be realised through the utilisation of Q/V band/optical communications for instance, or by increasing the number of gateways. Recent work has been realised on hybrid architectures, mixing both on board and on ground processing, more particularly beamforming, so as to balance performance and payload complexity [ABCCGD11], [ADMN12].

Mechanisms are needed to estimate the current channel state of each satellite terminal, and also to predict future channel states, and second, it is required to have receivers (gateways) capable of performing Minimum Mean Square Error (MMSE) based on the CSI and on the noise level. The above mentioned requirements will permit to perform Multi-User Detection (MUD) via Successive Interference Cancellation (SIC) within the cluster of beams supported by the gateway of interest. This means the other surrounding beams, not belonging to this gateway, will generate interference but the latter will be considered as noise [DGMRV06]. In order to improve the performance and to treat correctly the interference, a full cooperation between the gateways is needed, using the terrestrial network in order to exchange information about the different CSI but also the users' data [ZCO11-2]. This implies an exchange of information between gateways and therefore the implementation of specific messages. The results presented in this section therefore correspond to the best ones that can be reached considering MIMO, clear sky conditions, perfect CSI and full cooperation between all gateways present in the multi-beam satellite system.

The different formulations and results have also shown that the order in which the users are decoded has no impact on the sum rate but plays a significant role at the user level since the achievable per-user rates change accordingly. Evaluating the single user rate with the proposed method enables to satisfy important Quality of Service (QoS) criteria, like the maximisation of the minimum rate. As expected the ordering issued from the Foschini algorithm achieves with low complexity the criterion previously defined. Since the sum rate is invariant, maximising the achievable per-user rate leads to an increase of the level of fairness between users. The contribution consisted here in evaluating the gains that can be reached with ordering in a satellite system.

It has to be remarked that the performance of the Interference Cancellation (IC) techniques widely depends on the level of interference among the users. By optimising the resources, when having more than one user per beam, it is possible to avoid differences in the achievable per-user rates. This will be shown in the next chapter.

Chapter 4

Scheduling

In previous chapters the number of users per beam was constrained to one, i.e. one single user in each spotbeam. We have seen that the single user rates can be optimised by taking advantage of the ordering used while performing Successive Interference Cancellation (SIC). When considering more than one user per beam and a uniform allocation of the resources, it is possible to modify the association of users which are transmitting at the same time and thus which are interfering to each other.

Scheduling for Multiple-Input and Multiple-Output (MIMO) cellular networks has been well investigated, more particularly for Rayleigh channels [AjHa05], [YoGo06], [YiLi02], [YFVG11]. In this chapter we present the overall concept of cross-layer scheduling [HSBAG06] applied to the return-link of multi-beam satellite MIMO systems and investigate an interesting property which is the invariance of the sum rate. Search algorithms are then described, first when looking at all possible number of schedules and then at all possible number of combinations of users in a slot. With the latter an approach based on multipartite graphs permits to better represent the generation of the final schedule and also to reduce the computational complexity. Scheduling algorithms are then derived in order to operate with large scale systems which are actually realistic in satellite communications. The performance of the different algorithms is assessed considering different system sizes, showing the improvements in both minimum achievable per-user rates and levels of fairness. Finally the impact of scheduling optimised using information theory is evaluated on the practical uncoded Bit Error Rate (BER).

4.1 Basics

4.1.1 Introduction

We consider a simple example the scenario depicted by Fig. 4.1 in which there are two beams and two users per beam. Since at a given time one user in each beam will transmit towards the satellite, the two slots are needed to serve all users (we assume a uniform allocation of the resources). As can be seen the users represented by a cross are close to the beam border whereas the users represented by a circle are closer to the beam centre.

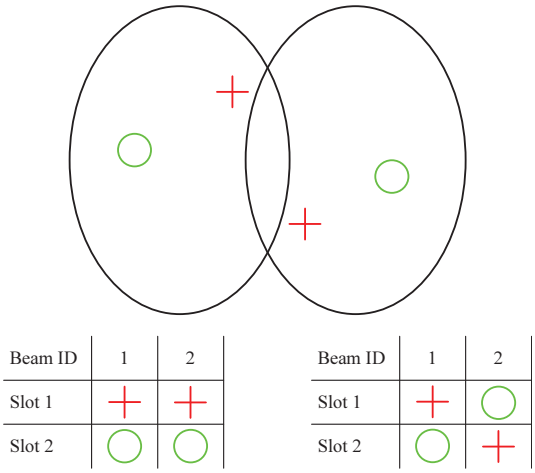


Figure 4.1. *Example of simple scheduling with 2 beams and 2 users per beam.*

On the one hand, if the two "cross" users are scheduled at the same time, then the level of interference will by high for both of them and therefore the achievable rate will be low. On the other hand, if the two "circle" users are scheduled at the same time we obtain the opposite, i.e. a rather high achievable rate. In such case the achievable rate in the first slot will be low and the achievable rate in the second slot two will be higher (left schedule in Fig. 4.1).

If we want to provide fairness to these four users we need to modify the schedule. To do so we can associate a "bad" user, i.e. a user close to the beam border, with a "good" user, i.e. close to the beam centre, in order to increase the minimum user rate. Actually since SIC is performed the user with the highest SINR will be decoded first (circle) and its impact (interference) will be removed before decoding the user with the lowest SINR (cross). Doing so will increase the achievable rate of the "bad" users (cross). In this example it is thus better to associate "bad" users with "good" users in order to provide an higher level of fairness (right schedule in Fig. 4.1).

When considering a multi-beam satellite system with a transparent payload, a star network topology, and both DVB-RCS (or its evolution DVB-RCS2) and DVB-S (or its evolution DVB-S2) for the return-link and the forward-link, respectively, the diagram depicted in Fig. 4.2 can be used to explain the scheduling process.

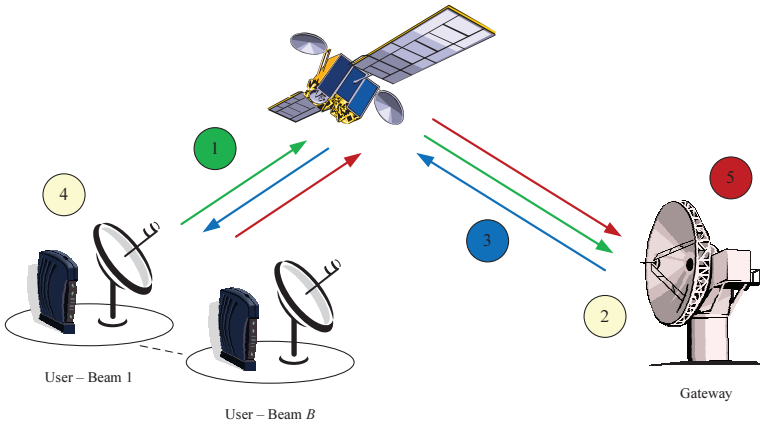


Figure 4.2. *Scheduling process in a multi-beam satellite system with transparent payload and star network topology.*

The scheduling process can be summarised in five steps as shown in Fig. 4.2. The user (satellite terminal) first sends a capacity request, which can be of different types, such as Rate-Based Dynamic Capacity (RBDC), Absolute Volume-Based Dynamic Capacity (AVBDC) or Volume-Based Dynamic Capacity (VBDC) (or even Constant Rate Assignment (CRA)) as in [DVB-RCS] and [DVB-RCS2], based on the incoming traffic which has to be transmitted (step 1). This capacity request is forwarded to the gateway using the return-link, more particularly using carriers dedicated to signalling. The gateway analyses the request, together with the requests received from all other terminals it is responsible for, and allocates the resources (so-called Radio Resource Management (RRM)). In our case the gateway optimises the allocation of the resources such that the level of interference between users is lowered (step 2). The resulting allocation (schedule) is transmitted to the terminals using the Terminal Burst Time Plan (TBTP) (step 3). It permits to indicate to the users on which carrier and in which time slot they have to transmit their data. The satellite terminal sends data, according to the resources it received, towards the gateway (step 4). The gateway processes the users' signals, performing, in theory, Minimum Mean Square Error (MMSE) combined with Successive Interference Cancellation (SIC) which is capacity achieving (step 5).

4.1.2 Number of Possible Allocations

The term "allocation" used in this document refers to a possible schedule for serving M users per beam covered by B different beams in the satellite system. In each of the B beams the

users are numbered from 1 to M. An example of allocation when having a system composed of three beams (therefore $B = 3$) and two users per beam (therefore $M = 2$) is given by Table 4.1.

Table 4.1. *Example of allocation with three beams ($B = 3$) and two users per beam ($M = 2$).*

Beam ID	1	2	3
Slot 1	2	1	2
Slot 2	1	2	1

As can be seen in Table 4.1, in the first slot users 2, 1 and 2 will transmit respectively in beam 1, 2 and 3. Since users can transmit only once the remaining users are scheduled at the same time in the next slot, more particularly in slot 2, users 1, 2 and 1 respectively in beam 1, 2 and 3.

We define with the term "combination" a possible association of users transmitting at the same time, i.e. scheduled in the same time slot. In the previous example (Table 4.1) the allocation is therefore composed of two combinations, i.e. one combination for the first slot and another one for the second slot.

In a system composed of B beams and with M users per beam (we assume the same amount of users per beam), the resulting number of possible allocations is:

$$(M!)^B \tag{4.1}$$

Hence in a slot the association of users located in B different beams corresponds to a combination. The set of M combinations of users defines the scheduling output, i.e. the allocation. The number of users to be taken into account in order to determine an allocation is noted $N_{\text{users,sched}}$ and represents the scheduling size:

$$N_{\text{users,sched}} = M\,B \tag{4.2}$$

The two parameters influence the scheduling, B defines the system size and M the scheduling depth.

When looking at the rates perceived by the users with a particular allocation we can understand that the order of the slot does not really play a role. This means that in the example given by Table 4.1 the first slot and the second slot can be swapped. Since the order does

not play a role in the scheduling, the number of possible allocations is reduced to:

$$N_{\text{alloc}} = \frac{(M!)^B}{M!} = (M!)^{B-1} \tag{4.3}$$

With the scenario considered in Table 4.1 we obtain four possible allocations, more particularly we obtain the allocations shown by Table 4.2. As already mentioned the content of the slots in Table 4.2 can be swapped since the order of the slot is considered as not relevant.

Table 4.2. *Possible allocations with three beams ($B = 3$) and two users per beam ($M = 2$).*

Beam ID	1	2	3
Slot 1	1	1	1
Slot 2	2	2	2

Beam ID	1	2	3
Slot 1	1	1	2
Slot 2	2	2	1

Beam ID	1	2	3
Slot 1	1	2	2
Slot 2	2	1	1

Beam ID	1	2	3
Slot 1	2	1	2
Slot 2	1	2	1

4.1.3 Scheduling and Channel Matrices

A given channel matrix corresponds to particular user locations. Modifying the scheduling consists into combining different users at the same time, in our case different transmitters. Therefore an allocation will result into the association of columns issued from different channel matrices.

With the example given by Table 4.1 we have two initial channel matrices of size 3×3 and noted $\boldsymbol{H}^{(1)}$ and $\boldsymbol{H}^{(2)}$. $\boldsymbol{H}^{(1)}$ corresponds to the channel matrix of the users with index "1" and $\boldsymbol{H}^{(2)}$ to the channel matrix of the users with index "2". With this particular allocation we have:

$$\boldsymbol{H}^{(1)'} = \left[\boldsymbol{h}_1^{(2)}\ \boldsymbol{h}_2^{(1)}\ \boldsymbol{h}_3^{(2)}\right] \qquad \boldsymbol{H}^{(2)'} = \left[\boldsymbol{h}_1^{(1)}\ \boldsymbol{h}_2^{(2)}\ \boldsymbol{h}_3^{(1)}\right]$$

where $\boldsymbol{h}_j^{(i)}$ represents the j-th column vector of the i-th channel matrix realisation. $\boldsymbol{H}^{(i)'}$ corresponds to the new channel matrix issued from the combination of users in the i-th slot. In other words scheduling consists into swapping one or more columns of different channel matrices.

The total number of channel matrices, also referred as channel realisations, is denoted as N_{ch} (please remind that M refers to the number of users per beam taken into account for a

schedule); the total number of users in the system is therefore:

$$N_{\text{users,total}} = N_{\text{ch}}\, B \tag{4.4}$$

and the number of schedules to be optimised is:

$$N_{\text{sched}} = \left\lceil \frac{N_{\text{users,total}}}{N_{\text{users,sched}}} \right\rceil = \left\lceil \frac{N_{\text{ch}}\, B}{M\, B} \right\rceil = \left\lceil \frac{N_{\text{ch}}}{M} \right\rceil \tag{4.5}$$

where $\lceil \cdot \rceil$ represents the ceiling operator, and $N_{\text{users,sched}}$ the number of users per schedule.

4.1.4 Impact of Scheduling on the Sum Rate

We consider a system composed of seven beams ($B = 7$, i.e. 7×7 MIMO system) with full frequency reuse ($K = 1$). More particularly we assume two users per beams ($M = 2$) which leads to a total of fourteen users ($N_{\text{users,total}} = N_{\text{users,sched}} = 14$). The users with index 1 are actually the "bad" users and the users with index 2 the "good" users (please refer to Fig. 1.9). We thus have two channel realisations, $\boldsymbol{H}^{(1)}$ and $\boldsymbol{H}^{(2)}$, where $\boldsymbol{H}^{(1)}$ represents the channel matrix of the bad case and $\boldsymbol{H}^{(2)}$ the channel matrix of the good case. In such scenario there are sixty four possible allocations ($N_{\text{alloc}} = 64$) and thus sixty four different sum rates over the two slots. Fig. 4.3 shows the following overall sum rates: the average, the maximum and the minimum values over the sixty four possible allocations (left axis) and the standard deviation of the sum rates (right axis).

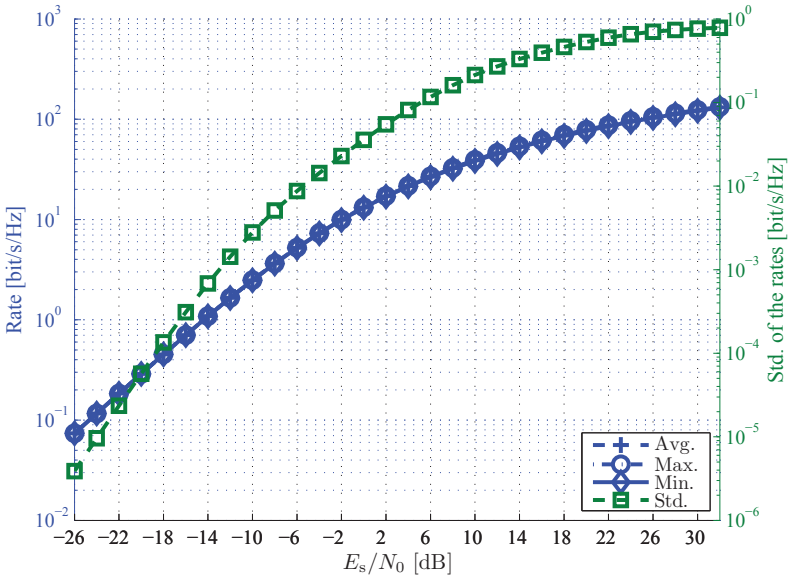


Figure 4.3. *Impact of scheduling on the sum rate with the bad / good users in a 7×7 system. The sum rate over the two slots (left axis) and the standard deviation (right axis) are shown.*

If we apply scheduling with this particular scenario, then the sum rate over the two slots remains almost the same, whatever the allocation applied (Fig. 4.3). Actually scheduling does not radically change the sum rate over the slots but permits to change the sum rate perceived per slot and therefore the single user rates.

4.2 Invariance of the Sum Rate to Scheduling

This section investigates the influence of scheduling on the sum rate while considering a satellite channel. Actually it has been observed, through several evaluations, that the sum rate computed over M slots does not radically change while performing scheduling. For instance with both "bad" and "good" cases the sum rate obtained over the two slots without re-organising the channel matrices (i.e. with both $\boldsymbol{H}^{(1)}$ and $\boldsymbol{H}^{(2)}$) is almost the same as the sum rate computed over the new optimal channel matrices (i.e. with both $\boldsymbol{H}^{(1)'}$ and $\boldsymbol{H}^{(2)'}$). Fig. 4.3 in Section 4.1.4 shows this particular behaviour. However, it has to be remarked that the sum rate evaluated on a slot basis is dramatically modified by the scheduling operation. It it clear that the sum rate computed with the channel matrix corresponding to the "bad" case is lower than the one computed with the channel matrix representing the "good" case. For this reason scheduling does not aim at improving the overall system rate but at adjusting the sum rates perceived on a slot basis and therefore at possibly increasing the level of fairness between users.

The purpose of this section is therefore to understand why the sum rate is not dramatically impacted by scheduling. To this aim we first consider scheduling with two users per beam, i.e. $M = 2$, then three users per beam and finally generalise for M users per beam.

4.2.1 Scheduling with two Users per Beam

As already mentioned performing scheduling consists into swapping one or more columns of the channel matrices (Section 4.1.3). We first consider a simple case in which scheduling is performed with $M = 2$. The channel matrix related to users with index 1 is noted $\boldsymbol{H}^{(1)}$ and the channel matrix related to users with index 2 $\boldsymbol{H}^{(2)}$. We denote the sum rate achieved in the first slot, which is composed exclusively of users with index 1, as $R^{(1)}_{\text{MIMO}}$. In the same way the sum rate achieved in the second slot is denoted $R^{(2)}_{\text{MIMO}}$. The overall sum rate, i.e. the sum rate achieved over the two slots, is:

$$R_{\text{MIMO,total},M=2} = R^{(1)}_{\text{MIMO}} + R^{(2)}_{\text{MIMO}} \tag{4.6}$$

For ease of notation, and since we always consider a MIMO system with SIC, the subscript "MIMO" is omitted. Using (3.9), the sum rate over the $M = 2$ slots is:

$$R_{\text{total},M=2} = \log_2 \det\left(\boldsymbol{I} + \boldsymbol{C}_\eta^{-1}\, \boldsymbol{H}^{(1)}\, \boldsymbol{H}^{(1)\,\mathrm{H}}\right) + \log_2 \det\left(\boldsymbol{I} + \boldsymbol{C}_\eta^{-1}\, \boldsymbol{H}^{(2)}\, \boldsymbol{H}^{(2)\,\mathrm{H}}\right) \tag{4.7}$$

which is also equal to:

$$R_{\text{total},M=2} = \log_2 \det\left(\left(\boldsymbol{I} + \boldsymbol{C}_\eta^{-1}\, \boldsymbol{H}^{(1)}\, \boldsymbol{H}^{(1)\,\mathrm{H}}\right)\, \left(\boldsymbol{I} + \boldsymbol{C}_\eta^{-1}\, \boldsymbol{H}^{(2)}\, \boldsymbol{H}^{(2)\,\mathrm{H}}\right)\right)$$

In our case the covariance of the noise $\boldsymbol{C}_\eta$ equals $N_0/E_\mathrm{s}\, \boldsymbol{I}$, therefore we can write:

$$R_{\text{total},M=2} = \log_2 \det\left(\boldsymbol{I} + \left(\frac{E_\mathrm{s}}{N_0}\right)\, \boldsymbol{I}\left(\boldsymbol{H}^{(1)}\, \boldsymbol{H}^{(1)\,\mathrm{H}} + \boldsymbol{H}^{(2)}\, \boldsymbol{H}^{(2)\,\mathrm{H}}\right) + \left(\frac{E_\mathrm{s}}{N_0}\right)^2\, \boldsymbol{I}\left(\boldsymbol{H}^{(1)}\, \boldsymbol{H}^{(1)\,\mathrm{H}}\, \boldsymbol{H}^{(2)}\, \boldsymbol{H}^{(2)\,\mathrm{H}}\right)\right) \tag{4.8}$$

In the previous expression the term $\left(\frac{E_\mathrm{s}}{N_0}\right)^2$ can be neglected for low SNRs, while it dominates for high SNRs.

Low Signal-to-Noise Ratios

By definition we have:

$$\boldsymbol{H}\, \boldsymbol{H}^{\mathrm{H}} = \sum_{j=1}^{N_\mathrm{Tx}} \boldsymbol{h}_j\, \boldsymbol{h}_j^{\mathrm{H}}$$

Therefore:

$$\boldsymbol{H}^{(1)}\, \boldsymbol{H}^{(1)\,\mathrm{H}} + \boldsymbol{H}^{(2)}\, \boldsymbol{H}^{(2)\,\mathrm{H}} = \sum_{j=1}^{N_\mathrm{Tx}} \boldsymbol{h}_j^{(1)}\, \boldsymbol{h}_j^{(1)\,\mathrm{H}} + \sum_{j=1}^{N_\mathrm{Tx}} \boldsymbol{h}_j^{(2)}\, \boldsymbol{h}_j^{(2)\,\mathrm{H}} \tag{4.9}$$

Since in this expression the columns of the channel matrices are multiplied between them and summed, swapping the columns does not play a role:

$$\boldsymbol{H}^{(1)}\, \boldsymbol{H}^{(1)\,\mathrm{H}} + \boldsymbol{H}^{(2)}\, \boldsymbol{H}^{(2)\,\mathrm{H}} = \boldsymbol{H}^{(1)'}\, \boldsymbol{H}^{(1)'\,\mathrm{H}} + \boldsymbol{H}^{(2)'}\, \boldsymbol{H}^{(2)'\,\mathrm{H}} \tag{4.10}$$

where $\boldsymbol{H}^{(1)'}$ and $\boldsymbol{H}^{(2)'}$ are the channel matrices issued from the scheduling, and defined for the first slot and the second slot, respectively.

An approximation of the overall sum rate for low SNRs is therefore:

$$R_{\text{total},M=2} \simeq R^{-}_{\text{total},M=2} = \log_2 \det\left(\boldsymbol{I} + \left(\frac{E_\mathrm{s}}{N_0}\right)\, \left(\boldsymbol{H}^{(1)}\, \boldsymbol{H}^{(1)\,\mathrm{H}} + \boldsymbol{H}^{(2)}\, \boldsymbol{H}^{(2)\,\mathrm{H}}\right)\right) \tag{4.11}$$

Scheduling does not affect the overall sum rate for low signal-to-noise ratios.

High Signal-to-Noise Ratios

For high signal-to-noise ratios (SNRs), an approximation of the overall sum rate is:

$$R_{\text{total},M=2} \simeq R^{+}_{\text{total},M=2} = \log_2 \det\left(\boldsymbol{I} + \left(\frac{E_\text{s}}{N_0}\right)^2 \left(\boldsymbol{H}^{(1)}\,\boldsymbol{H}^{(1)\,\text{H}}\,\boldsymbol{H}^{(2)}\,\boldsymbol{H}^{(2)\,\text{H}}\right)\right) \tag{4.12}$$

and for very high SNRs, the previous expression can be written as:

$$R_{\text{total},M=2} \simeq R^{++}_{\text{total},M=2} = \log_2 \det\left(\left(\frac{E_\text{s}}{N_0}\right)^2 \left(\boldsymbol{H}^{(1)}\,\boldsymbol{H}^{(1)\,\text{H}}\,\boldsymbol{H}^{(2)}\,\boldsymbol{H}^{(2)\,\text{H}}\right)\right) \tag{4.13}$$

since $\log_2(1+x) \approx \log_2 x$ for high values of x.

Using the properties of the determinant and of the logarithm, this can also be written as:

$$R^{++}_{\text{total},M=2} = \log_2 \det\left(\frac{E_\text{s}}{N_0}\right)^2 + \log_2 \det\left(\boldsymbol{H}^{(1)}\,\boldsymbol{H}^{(1)\,\text{H}}\,\boldsymbol{H}^{(2)}\,\boldsymbol{H}^{(2)\,\text{H}}\right) \tag{4.14}$$

Since $\det(\alpha\,\boldsymbol{A}) = \alpha^N \det(\boldsymbol{A})$, where $\boldsymbol{A}$ is an $N \times N$ matrix, we can write:

$$R^{++}_{\text{total},M=2} = 2\,N_\text{Rx}\,\log_2\left(\frac{E_\text{s}}{N_0}\right) + \log_2 \det\left(\boldsymbol{H}^{(1)}\,\boldsymbol{H}^{(1)\,\text{H}}\,\boldsymbol{H}^{(2)}\,\boldsymbol{H}^{(2)\,\text{H}}\right) \tag{4.15}$$

The left part of the previous equation does not depend on the channel matrices and therefore on the scheduling whereas the right part does.

Modification of the determinant with scheduling:

When focusing on the right part of the equation, we have:

$$\det\left(\boldsymbol{H}^{(1)}\,\boldsymbol{H}^{(1)\,\text{H}}\,\boldsymbol{H}^{(2)}\,\boldsymbol{H}^{(2)\,\text{H}}\right) = \det\left(\boldsymbol{H}^{(2)\,\text{H}}\,\boldsymbol{H}^{(1)}\,\boldsymbol{H}^{(1)\,\text{H}}\,\boldsymbol{H}^{(2)}\right) \tag{4.16}$$

since $\det(\boldsymbol{A}\,\boldsymbol{B}) = \det(\boldsymbol{B}\,\boldsymbol{A})$. Using once again the properties of the determinant, more particularly, $\det(\boldsymbol{A}\,\boldsymbol{B}) = \det(\boldsymbol{A})\det(\boldsymbol{B})$, we can also formulate the previous expression as follows:

$$\det\left(\boldsymbol{H}^{(2)\,\text{H}}\,\boldsymbol{H}^{(1)}\,\boldsymbol{H}^{(1)\,\text{H}}\,\boldsymbol{H}^{(2)}\right) = \det\left(\boldsymbol{H}^{(2)\,\text{H}}\,\boldsymbol{H}^{(1)}\right)\det\left(\boldsymbol{H}^{(1)\,\text{H}}\,\boldsymbol{H}^{(2)}\right) \tag{4.17}$$

which is also:

$$\det\left(\boldsymbol{H}^{(2)\,\text{H}}\,\boldsymbol{H}^{(1)}\right)\det\left(\boldsymbol{H}^{(1)\,\text{H}}\,\boldsymbol{H}^{(2)}\right) = \det\left(\boldsymbol{H}^{(1)}\,\boldsymbol{H}^{(2)\,\text{H}}\right)\det\left(\boldsymbol{H}^{(2)}\,\boldsymbol{H}^{(1)\,\text{H}}\right) \tag{4.18}$$

We know that:

$$\boldsymbol{A}\,\boldsymbol{B}^\text{H} = \sum_{j=1}^{N} \boldsymbol{a}_j\,\boldsymbol{b}_j^\text{H}$$

where $\boldsymbol{A}$ and $\boldsymbol{B}$ are both $M \times N$ matrices, $\boldsymbol{a}_j$ and $\boldsymbol{b}_j$ represents the j-th column vector of the matrices $\boldsymbol{A}$ and $\boldsymbol{B}$, respectively.

The previous expressions can therefore also be formulated as follows:

$$\det\left(\boldsymbol{H}^{(1)}\,\boldsymbol{H}^{(2)\,\mathrm{H}}\right)\det\left(\boldsymbol{H}^{(2)}\,\boldsymbol{H}^{(1)\,\mathrm{H}}\right)=\det\left(\sum_{j=1}^{N_{\mathrm{Tx}}}\boldsymbol{h}_j^{(1)}\,\boldsymbol{h}_j^{(2)\,\mathrm{H}}\right)\det\left(\sum_{j=1}^{N_{\mathrm{Tx}}}\boldsymbol{h}_j^{(2)}\,\boldsymbol{h}_j^{(1)\,\mathrm{H}}\right) \quad (4.19)$$

As can be seen from the previous expression, swapping the columns between $\boldsymbol{H}^{(1)}$ and $\boldsymbol{H}^{(2)}$ clearly modifies the value of the determinants. For instance if we swap the 2nd column of the two channel matrices, then we would have:

$$\begin{aligned}\det\left(\sum_{j=1}^{N_{\mathrm{Tx}}}\boldsymbol{h}_j^{(1)'}\,\boldsymbol{h}_j^{(2)'\,\mathrm{H}}\right)\det\left(\sum_{j=1}^{N_{\mathrm{Tx}}}\boldsymbol{h}_j^{(2)'}\,\boldsymbol{h}_j^{(1)'\,\mathrm{H}}\right) \;=\\ \det\left(\sum_{j\neq 2}\boldsymbol{h}_j^{(1)}\,\boldsymbol{h}_j^{(2)\,\mathrm{H}}+\boldsymbol{h}_2^{(2)}\,\boldsymbol{h}_2^{(1)\,\mathrm{H}}\right)\det\left(\sum_{j\neq 2}\boldsymbol{h}_j^{(2)}\,\boldsymbol{h}_j^{(1)\,\mathrm{H}}+\boldsymbol{h}_2^{(1)}\,\boldsymbol{h}_2^{(2)\,\mathrm{H}}\right)\end{aligned} \quad (4.20)$$

since $\boldsymbol{h}_2^{(2)}\,\boldsymbol{h}_2^{(1)\,\mathrm{H}} \neq \boldsymbol{h}_2^{(1)}\,\boldsymbol{h}_2^{(2)\,\mathrm{H}}$, the value of the determinant will change. More particularly in this case:

$$\boldsymbol{h}_j^{(1)}\,\boldsymbol{h}_j^{(2)\,\mathrm{H}}=\left(\boldsymbol{h}_j^{(2)}\,\boldsymbol{h}_j^{(1)\,\mathrm{H}}\right)^{\mathrm{H}} \quad (4.21)$$

Impact of the determinant on the sum rate:

The multi-beam satellite channel matrices have special behaviours. First they are strongly diagonal with diagonal coefficients having an absolute value comprised between around 0.707 and 1. Second the off-diagonal coefficients have absolute values smaller than 0.707. For these reasons we have:

$$\det\left(\boldsymbol{H}^{(1)}\right)\leq 1 \qquad \det\left(\boldsymbol{H}^{(2)\,\mathrm{H}}\right)\leq 1 \qquad \det\left(\boldsymbol{H}^{(2)}\right)\leq 1 \qquad \det\left(\boldsymbol{H}^{(1)\,\mathrm{H}}\right)\leq 1 \quad (4.22)$$

The product of the four determinants gives even a smaller value. It has to be remarked that the determinant equals one if the channel matrices is the identity matrix, i.e. with the highest receive antenna gain, i.e. the users are located in the center of each beam, and no co-channel interference, i.e. higher numbers of colours.

So far we have shown that for high signal-to-noise ratios the swapping of columns in the channel matrices has an impact on the value of the determinant, i.e. on the right part of equation (4.15). Since the value of the determinant is smaller than one, the value of the logarithm is negative and therefore will be subtracted to the value issued from the left term,

i.e. the result of $2\,N_{\mathrm{Rx}}\,\log_2\left(E_{\mathrm{s}}/N_0\right)$. The slope of the curve representing the logarithm is very steep for values smaller than one and for this reason the subtracted value can have a high variance.

The purpose is now to evaluate how the value of the determinant fluctuates when swapping the columns of the channel matrices, and therefore to estimate how fast we move on the negative part of $\log_2(x)$. To do so we consider both high and low interferences scenarios with seven beams ($B = 7$) as in Section 4.1.4 and compute for each possible allocations, i.e. $N_{\mathrm{alloc}} = (M!)^{B-1} = 2^6 = 64$, the value of the determinant, more particularly the value of $\det\left(\boldsymbol{H}^{(1)}\,\boldsymbol{H}^{(1)\,\mathrm{H}}\,\boldsymbol{H}^{(2)}\,\boldsymbol{H}^{(2)\,\mathrm{H}}\right)$. The corresponding results for the highest SNR, i.e. 32 dB, are given by Fig. 4.4.

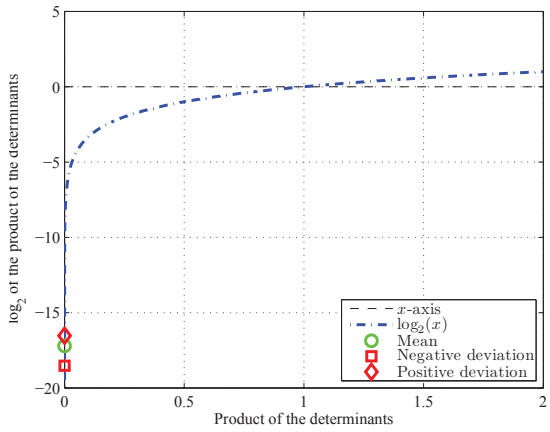


Figure 4.4. *Behaviour of the product of determinants for the highest SNR and for all possible allocations when considering both high and low interference scenarios with seven beams ($B = 7$).*

As can be seen the variation of the value of the product of the determinants is rather high, actually about 40% and 60% around the mean value for the negative and the positive dispersion, respectively. However such variation when compared to the value of $2\,N_{\mathrm{Rx}}\,\log_2\left(E_{\mathrm{s}}/N_0\right)$, which equals in this case about 150 bits/s/Hz, is very small and represents at the end a negative dispersion of 1% and a positive dispersion of 0.5% of the final sum rate. This means scheduling does not really impact the sum rate for high SNRs.

Validity of the Approximations

Fig. 4.5 finally shows the two approximations performed when having two users per beam, i.e. $M = 2$. The approximation for low signal-to-noise ratios is valid in the noise-limited region, as expected, whereas the approximation for very high SNRs is only valid for SNRs

above 14 dB. The latter is actually directly related to the omission of the term $\boldsymbol{I} + \cdot$ in (4.13) and this is confirmed by the curve showing the approximation for high SNRs.

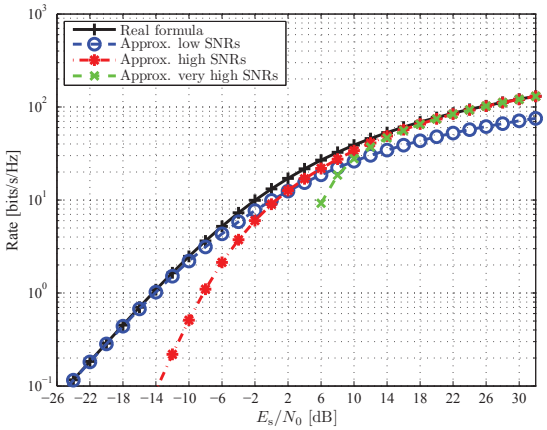


Figure 4.5. *Approximations realised when performing scheduling and having two users per beam ($M = 2$). These approximations are computed when considering both high and low interference scenarios with seven beams ($B = 7$).*

4.2.2 Scheduling with three Users per Beam

The same principle as in the previous section, i.e. when having two users per beam ($M = 2$) can be used. Therefore the channel matrix related to users with index 1 is noted $\boldsymbol{H}^{(1)}$, the channel matrix related to users with index 2 $\boldsymbol{H}^{(2)}$ and the channel matrix related to users with index 3 $\boldsymbol{H}^{(3)}$. We denote the sum rate achieved in each slot as $R^{(1)}$, $R^{(2)}$ and $R^{(3)}$, respectively for the first slot, the second slot and the third slot. The overall sum rate, i.e. the sum rate achieved over the three slots, is:

$$R_{\text{total},M=3} = R^{(1)} + R^{(2)} + R^{(3)} \tag{4.23}$$

As before, the sum rate over the $M = 3$ slots, using (3.9), is:

$$\begin{aligned} R_{\text{total},M=3} \quad = \quad & \log_2 \det\left(\boldsymbol{I} + \boldsymbol{C}_\eta^{-1}\, \boldsymbol{H}^{(1)}\, \boldsymbol{H}^{(1)\,\text{H}}\right) + \log_2 \det\left(\boldsymbol{I} + \boldsymbol{C}_\eta^{-1}\, \boldsymbol{H}^{(2)}\, \boldsymbol{H}^{(2)\,\text{H}}\right) \\ & + \log_2 \det\left(\boldsymbol{I} + \boldsymbol{C}_\eta^{-1}\, \boldsymbol{H}^{(3)}\, \boldsymbol{H}^{(3)\,\text{H}}\right) \end{aligned} \tag{4.24}$$

which is also equal to:

$$R_{\text{total},M=3} = \log_2 \det\left(\left(\boldsymbol{I} + \boldsymbol{C}_\eta^{-1}\, \boldsymbol{H}^{(1)}\, \boldsymbol{H}^{(1)\,\text{H}}\right)\left(\boldsymbol{I} + \boldsymbol{C}_\eta^{-1}\, \boldsymbol{H}^{(2)}\, \boldsymbol{H}^{(2)\,\text{H}}\right)\left(\boldsymbol{I} + \boldsymbol{C}_\eta^{-1}\, \boldsymbol{H}^{(3)}\, \boldsymbol{H}^{(3)\,\text{H}}\right)\right)$$

Using the same properties as before, when decomposing the multiplication of the terms in the previous expression, it is possible to derive an approximation for low signal-to-noise ratios (SNRs) and for high SNRs.

Low Signal-to-Noise Ratios

For low SNRs the sum rate can be approximated as follows:

$$R_{\text{total},M=3} \simeq R^{-}_{\text{total},M=3} = \log_2 \det\left(\boldsymbol{I} + \left(\frac{E_\text{s}}{N_0}\right)\left(\boldsymbol{H}^{(1)}\,\boldsymbol{H}^{(1)\,\text{H}} + \boldsymbol{H}^{(2)}\,\boldsymbol{H}^{(2)\,\text{H}} + \boldsymbol{H}^{(3)}\,\boldsymbol{H}^{(3)\,\text{H}}\right)\right) \tag{4.25}$$

which is invariant when performing scheduling.

High Signal-to-Noise Ratios

For very high SNRs the sum rate can be approximated as follows:

$$R_{\text{total},M=3} \simeq R^{++}_{\text{total},M=3} = 3\,N_\text{Rx}\,\log_2\left(\frac{E_\text{s}}{N_0}\right) + \log_2 \det\left(\boldsymbol{H}^{(1)}\,\boldsymbol{H}^{(1)\,\text{H}}\,\boldsymbol{H}^{(2)}\,\boldsymbol{H}^{(2)\,\text{H}}\,\boldsymbol{H}^{(3)}\,\boldsymbol{H}^{(3)\,\text{H}}\right) \tag{4.26}$$

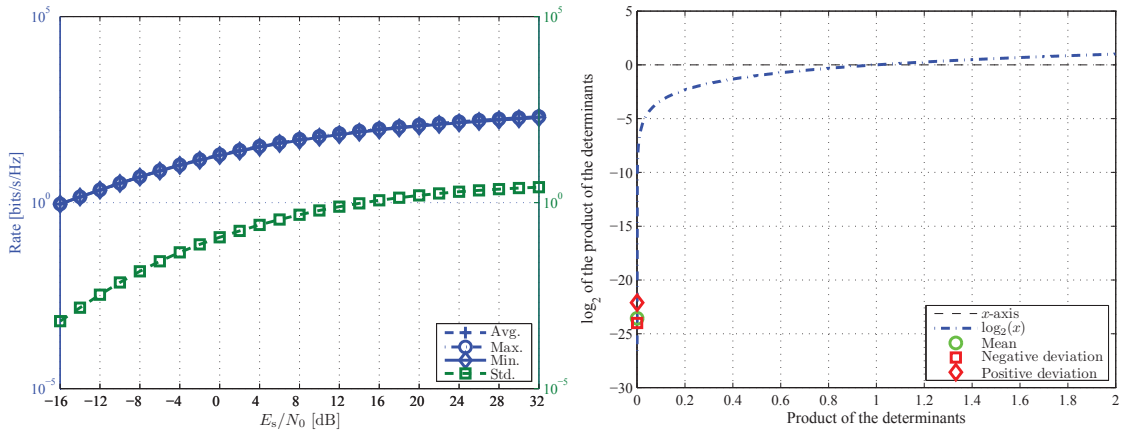


Figure 4.6. *Variation of the sum rate (left) and dispersion of the logarithm for the highest SNR (right) when considering three users per beam ($B = 3$) and random channel realisations with seven beams ($B = 7$).*

Fig. 4.6 shows the variation of the sum rate in the same signal-to-noise ratio range as before (left), and when considering three random channel realisations for optimising the schedules, and the dispersion of the logarithm for the highest SNR (right). When compared to the value of $3\,N_\text{Rx}\,\log_2\left(E_\text{s}/N_0\right)$, which equals in this case about 220 bits/s/Hz, the variation of the product of the determinant is very small and represents at the end a negative dispersion of 0.2% and a positive dispersion of 0.7% of the final sum rate. As before, scheduling has a negligible impact on the sum rate for high SNRs.

4.2.3 Scheduling with M Users per Beam

The overall sum rate, i.e. the sum rate achieved over the M slots, is:

$$R_{\text{total},M} = \sum_{m=1}^{M} R^{(m)} \tag{4.27}$$

Using the principle of the mathematical induction, we can generalise the formulae obtained with two users per beam ($M = 2$) and three users per beam ($M = 3$), and approximate the sum rate for low signal-to-noise ratios (SNRs) and high SNRs.

Low Signal-to-Noise Ratios

For low SNRs the sum rate can be approximated as follows:

$$R_{\text{total},M} \simeq R^{-}_{\text{total},M} = \log_2 \det\left(\boldsymbol{I} + \left(\frac{E_\text{s}}{N_0}\right)\left(\sum_{m=1}^{M} \boldsymbol{H}^{(m)}\,\boldsymbol{H}^{(m)\,\text{H}}\right)\right) \tag{4.28}$$

which is invariant when performing scheduling.

Very High Signal-to-Noise Ratios

For very high SNRs the sum rate can be approximated as follows:

$$R_{\text{total},M} \simeq R^{++}_{\text{total},M} = M\,N_\text{Rx}\,\log_2\left(\frac{E_\text{s}}{N_0}\right) + \log_2 \det\left(\prod_{m=1}^{M}\left(\boldsymbol{H}^{(m)}\,\boldsymbol{H}^{(m)\,\text{H}}\right)\right) \tag{4.29}$$

which is an expression varying with scheduling because of the right term.
Once the set of channel matrices $\left\{\boldsymbol{H}^{(i)}\right\}$ is defined, maximising the sum rate via scheduling remains into finding the schedule which maximises (4.29), or, on a slot basis, which maximises $R^{++}_{\text{total},M}/M$. When taking into account one random schedule for each set of given matrices, and then computing the expected value of $\frac{R^{++}_{\text{total},M}}{M}$ over all possible sets of matrices (i.e. over all possible users), considering that schedules and users are independent, we obtain:

$$\mathbb{E}\left[\frac{R^{++}_{\text{total},M}}{M}\right] = N_\text{Rx}\log_2\left(\frac{E_\text{s}}{N_0}\right) + \frac{1}{M}\sum_{m=1}^{M}\mathbb{E}\left[\log_2 \det\left(\boldsymbol{H}^{(m)}\,\boldsymbol{H}^{(m)\text{H}}\right)\right], \tag{4.30}$$

where $\boldsymbol{H}^{(m)}$ is a random set of users in a slot. So the average sum rate per slot is the arithmetic average of a set of independent random variables plus a constant. This, for the central limit theorem, implies that for M sufficiently large, this random variable is Gaussian distributed. In particular if we define $\Delta_{\boldsymbol{H}} = \mathbb{E}\left[\log_2 \det\left(\boldsymbol{H}\boldsymbol{H}^\text{H}\right)\right]$, and $\sigma^2_{\boldsymbol{H}} = \mathbb{E}\left[\left(\log_2 \det\left(\boldsymbol{H}\boldsymbol{H}^\text{H}\right)\right)^2\right] - \Delta^2_{\boldsymbol{H}}$, then we have that $\frac{R^{++}_{\text{total},M}}{M} \sim \mathcal{N}\left(N_\text{Rx}\log_2\left(\frac{E_\text{s}}{N_0}\right) + \Delta_{\boldsymbol{H}}, \frac{\sigma^2_{\boldsymbol{H}}}{M}\right)$.

Given the particular properties and structure of the multi-beam satellite channel matrices mentioned previously, in general $\Delta_{\boldsymbol{H}}$ and $\sigma^2_{\boldsymbol{H}}$ are well-defined values, function of N_{Rx} and of the SNR. The dependency of both $\Delta_{\boldsymbol{H}}$ and $\sigma^2_{\boldsymbol{H}}$ on N_{Rx} is linear (Fig. 4.7, simulations show that $\Delta_{\boldsymbol{H}} \leq -N_{\mathrm{Rx}}$ for $N_{\mathrm{Rx}} > 5$). So the ratio $\frac{\sigma^2_{\boldsymbol{H}}}{N_{\mathrm{Rx}} \log_2\left(\frac{E_{\mathrm{S}}}{N_0}\right) + \Delta_{\boldsymbol{H}}}$ does not evolve with N_{Rx} and it is in the order of a few percentage points. This means that at high SNRs and for a random schedule the sum rate can be modelled as a Gaussian distribution with a standard deviation $\frac{\sigma_{\boldsymbol{H}}}{\sqrt{M}}$ that decreases with the scheduling depth. So the probability of finding a good schedule that improves the sum rate of a small fraction of the average (a few percentage points) decreases as an error function of the relative improvement and it tends to zero for increasing M. Moreover this is true for any N_{Rx}. In conclusion trying to improve the sum rate by means of scheduling is not very beneficial.

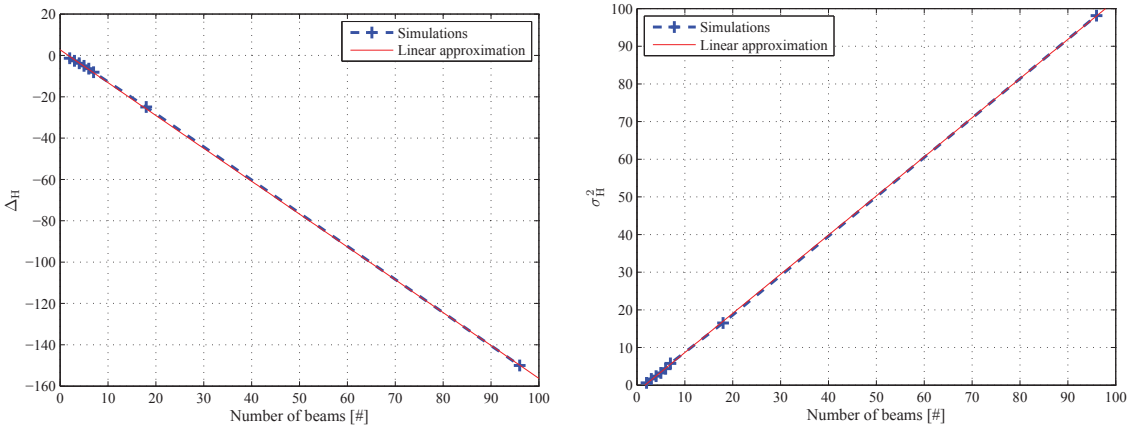


Figure 4.7. *Evolution of $\Delta_{\boldsymbol{H}}$ (left) and of $\sigma^2_{\boldsymbol{H}}$ (right) according to the number of beams.*

4.3 Search Algorithms

This section presents the so-called "search algorithms" which correspond to the pillars for optimising the user schedules. It explains the concept of performing a search over the different possible allocations, and presents a new approach, based on multipartite graphs, for realising a search over all possible combinations. Both aims at targeting the maximisation of the minimum per-user rate and the latter aims additionally at reducing considerably the computational complexity.

4.3.1 Search over All Possible Allocations

This first search consists into satisfying over all possible allocations the criterion of interest, and therefore can be seen as an exhaustive search (ES). One can understand that such

algorithm offers the best results but requires huge processing time. It has to be remarked that because of (4.3), for particular scheduling size this exhaustive search cannot be performed. Some examples of number of possible allocations according to the number of beams (B) and to the number of users per beam (M) are given in Table 4.3. It can be seen from the numbers present in this table that such exhaustive search becomes rapidly infeasible when the number of users per beam and/or the number of beams increases.

Table 4.3. *Example of number of possible allocations.*

Number of beams B	3	4	7
$M = 2$	4	8	64
$M = 3$	36	216	$4.67\,10^4$
$M = 4$	576	$1.38\,10^4$	$1.91\,10^8$

This exhaustive search is of course sub-optimal in terms of processing time since it has to go through all possible allocations. However redundancy can appear in the allocations, more particularly when looking at the user's combinations. An example is given in the next table with two possible allocations while having three beams ($B = 3$) and three users per beam ($M = 3$, Table 4.4). In this example the combination of users "3 3 3" is redundant since it appears in both possible, but different, allocations. Actually as soon as the number of users per beam becomes greater than two, i.e. $M > 2$, redundancy appears in the list of all possible allocations.

Table 4.4. *Example of possible allocations with three beams ($B = 3$) and three users per beam ($M = 3$).*

Beam ID	1	2	3
Slot 1	1	1	1
Slot 2	2	2	2
Slot 3	3	3	3

Beam ID	1	2	3
Slot 1	1	2	1
Slot 2	2	1	2
Slot 3	3	3	3

When the criterion taken into account refers to the single user rates, the evaluation of the rates has to be performed at the slot level. For this reason with this search the rates are analysed for each allocation and for each slot. This leads to the following number of evaluations:

$$N_{\text{eval,ES}} = M\ (M!)^{B-1} \tag{4.31}$$

4.3.2 Search over All Possible Combinations - B-partite Graph Approach

Instead of working at the allocations level, and having possibly redundancy as seen in the previous section (Section 4.3.1), the overall complexity can be reduced when focusing on the different combinations instead.

The combinations of users can be represented using an approach based on multipartite graphs [CoLeRi90]. The nodes (or vertices) correspond to the transmitters in our system, more particularly the index of the nodes refers to the index of the user in the covering beam. As reminder the system is composed of B beams where each beam consists of M users. An edge (or line) represents the scheduling of a user in a given beam with a user in another beam. An edge is thus a combination of two users. We additionally define the term "path" as a combination of users, i.e. scheduled at the same time, in all B beams. An allocation is therefore the association of M paths in this multipartite graph approach, referred in the following as B-partite graph approach (BG). Users which are already connected, i.e. users which belong to an edge, cannot be further scheduled and the edges are said to be "symmetric". Fig. 4.8 summarises the different terms introduced so far.

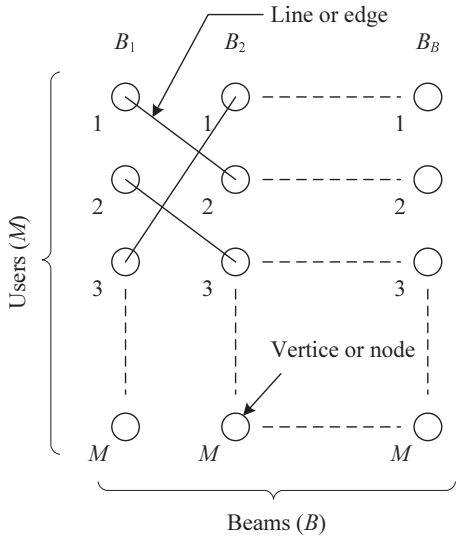


Figure 4.8. *Terms definition in the multipartite graph approach.*

The number of possible edges, i.e. the number of possible combinations of users between two beams (bipartite graph), is:

$$N_{\text{edges},B=2} = M \times M = M^2 \tag{4.32}$$

The number of possible paths, i.e. the number of possible combinations of users in all beams,

is:

$$N_{\text{paths}} = M^B \tag{4.33}$$

The principle for determining a schedule is to evaluate the achievable per-user rates for each path, and select a path, depending on the adopted strategy. Once the selection is done the nodes involved in the path have to be pruned since users cannot be scheduled more than once. Possible paths are thus removed from the multipartite graph and the number of remaining paths is therefore dramatically reduced. An example is given in Fig. 4.9 where $M = 3$ and $B = 3$. In the left graph (a) all possible edges are shown. In (b) a path is selected, more particularly user 2 in beam 1, user 1 in beam 2 and user 3 in beam 3 are scheduled at the same time. Finally in (c) the edges involving the nodes of the previous selected path are pruned, reducing the number of remaining combinations.

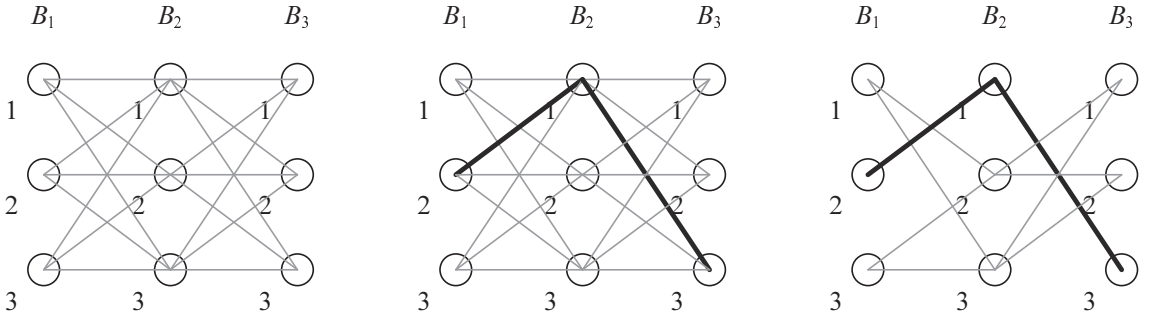


Figure 4.9. *Example of multipartite graph with three users per beam ($M = 3$) and three beams ($B = 3$).*

One can understand the reduction of complexity using this approach. Actually the redundancy present in the search realised over all possible allocations is avoided and also the number of rate evaluations to be performed at the slot level is lowered when compared to (4.31):

$$N_{\text{eval,BG}} = M^B \tag{4.34}$$

In Fig.4.10 the relation between an example of allocation (a), the corresponding multipartite graph (b) and the resulting channel matrices (c) is depicted with three beams ($B = 3$) and three users per beam ($M = 3$).

4.3.3 The Max-Min Criterion - Maximisation of the Minimum Rate

As defined in Section 3.2.2, more particularly with (3.29), this criterion aims at maximising the minimum rates experienced by the users in the system. This criterion also targets providing more fairness to users. On the one hand, when combined to the search performed over all possible allocations, the principle is simply to determine the allocation satisfying as best as

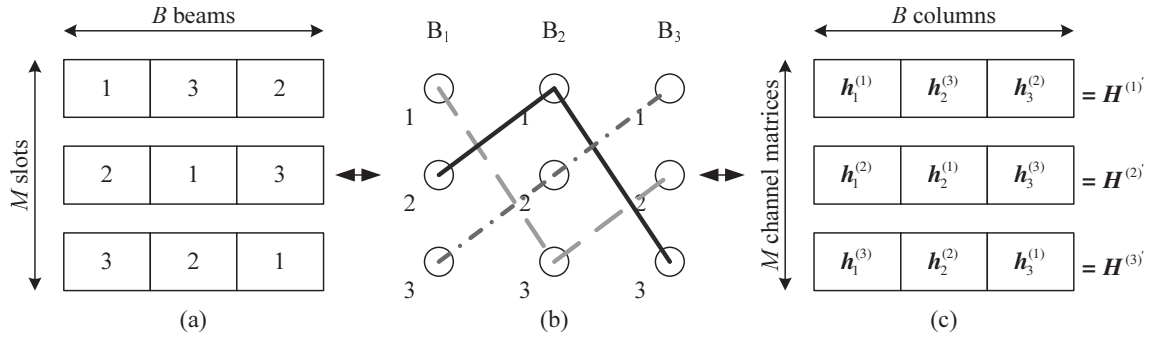


Figure 4.10. *Relation between allocation, multipartite graph and channel matrices with three users per beam ($M = 3$) and three beams ($B = 3$).*

possible this criterion. On the other hand, when combined to the B-partite graph approach there are two possibilities.

We consider that the single user rates were computed for a given list of edges or paths. From this single user rates the minimum rate can be extracted. This means that for each edge or path is associated a given minimum user rate. The minimum rates are sorted in descending order, i.e. the first minimum rate is the highest one and the last minimum rate the lowest one. Two different algorithms are presented hereafter and aim at maximising the minimum per-user rate. The first one is the most straightforward for satisfying this criterion. The second one, more complex, better reaches the criterion over all M slots.

Maximum Selection Algorithm

From the list of minimum user rates which are sorted, the maximum, i.e. the first one, is selected. To this selection corresponds a particular path. Since the path is taken into account as a solution to the scheduling problem, the nodes involved have to be removed from the list of remaining possibilities. Therefore the list of minimum rates is shortened. The next available path is selected and the process is repeated until all M paths are found. This algorithm is called "maximum selection algorithm" since it picks up the maximum of the possible minimum rates. An example of the maximum selection algorithm is given in Fig. 4.11 for three users per beam ($M = 3$) and two beams ($B = 2$).

In the example of Fig. 4.11 the minimum rates for each path (since we have two beams, a path is actually also an edge) are organised in descending order. The first column on the left shows the initial paths. The path giving the maximum of the minimum user rates is selected (first element) and the paths involving the corresponding nodes are removed (second column).

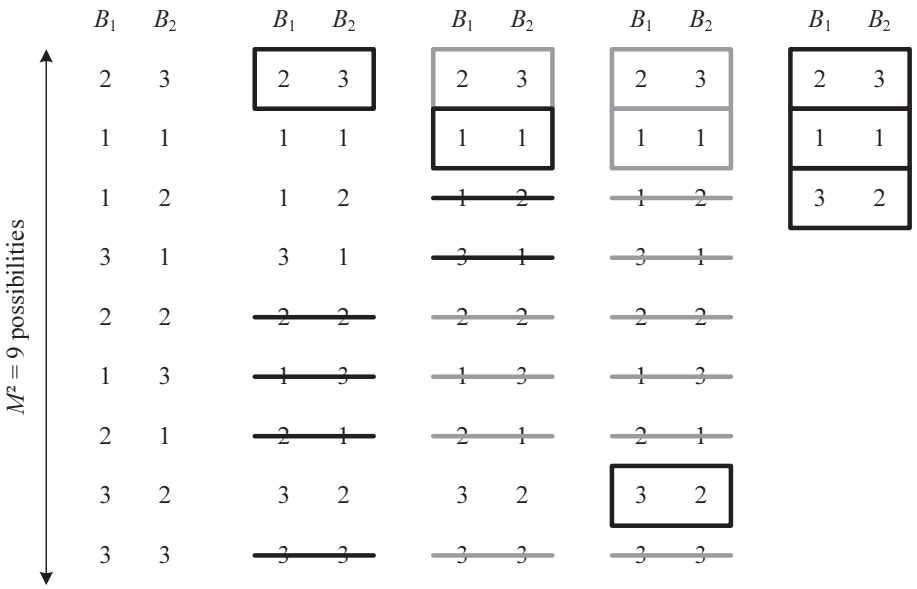


Figure 4.11. *Example of maximum selection algorithm. In this example three users per beam ($M = 3$) and two beams ($B = 2$) are taken into account.*

Then the second maximum rate is selected from the remaining list of paths. Again the nodes are pruned (third column). Finally the last possible path (fourth column) is inserted in the list of M final paths (fifth column). We obtain the final allocation which consists of three different paths. As can be seen this algorithm permits to obtain the maximum of the minimum single user rates for the first selection. However, the last path to be selected corresponds in this example to the last but one path, i.e. to one of the paths providing the minimum of the minimum user rates. For this reason this algorithm is not optimal when trying to optimise the minimum user rates over M slots. In this example the minimum user rate is maximised in the first two slots but is almost minimised in the last slot.

Minimum Deletion Algorithm

In the so-called "minimum deletion algorithm" the minimum of the minimum user rates are removed from the list of possible solutions. One by one the last path of the list is deleted by taking care there is still a remaining solution to the scheduling problem. If a deletion of a path involves no more solution then this path is part of the final solution. The corresponding nodes are pruned and the process continues until M paths are part of the solution. The principle of this algorithm is derived from [BaCaZo08]. An example of the minimum deletion algorithm is given in Fig. 4.12 for three users per beam ($M = 3$) and two beams ($B = 2$).
In the example of Fig. 4.12 the minimum rates for each path (again since the number of beams equals two, a path also corresponds to an edge) are organised in descending order

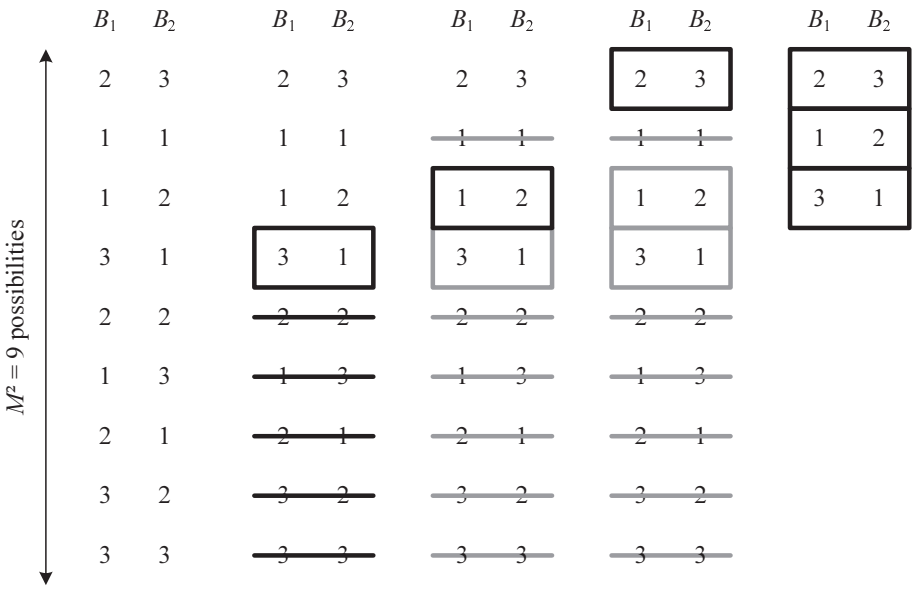


Figure 4.12. *Example of minimum deletion algorithm. In this example three users per beam ($M = 3$) and two beams ($B = 2$) are taken into account.*

(first column). The paths are removed one by one from the bottom to the top until the removal of a path avoid finding a solution for the scheduling. As can be seen in the second column the last five paths are removed until a path should be part of the final solution. The selection of this path will involve the deletion of solutions implying the nodes (third column). The process is repeated and the next solution available is selected (third column). Finally there is only one solution remaining (fourth column). The resulting allocation is given in the fifth column.

This algorithm is clearly more complex than the maximum selection algorithm but as seen in this example it permits to select paths in which the minimum user rates are higher over the M slots.

4.4 Scheduling Algorithms for Large Scale Systems

Because of the complexity in finding an optimal scheduling solution for large scale systems, ad-hoc scheduling algorithms have to be designed. In this section two scheduling algorithms, which make use of the search algorithms presented in the previous section (Section 4.3), are described.

4.4.1 "Viterbi-Like Algorithm"

The "Viterbi-like algorithm" is based on the B-partite graph approach. This algorithm starts with two beams and computes the minimum user rates for all possible edges. A weight is then given to the edges according to the associated value of the minimum user rate. M edges are selected for these two beams and a new beam is added. The process is repeated until all beams are considered. Instead of evaluating the minimum user rate of all possible paths (M^B) this algorithm performs at the edge level, and reduces to M^2 evaluations realised $B-1$ times:

$$N_{\text{eval,VL}} = (B-1)\,M^2 \tag{4.35}$$

Fig. 4.13 gives an example for a system composed of three beams ($B = 3$) and three users per beam ($M = 3$). In this example the evaluation of the minimum user rates is performed for all edges existing between beam 1 and beam 2 (left). Once the edges are selected a new beam is added and the process is repeated (middle). The results paths represent the final allocation (right).

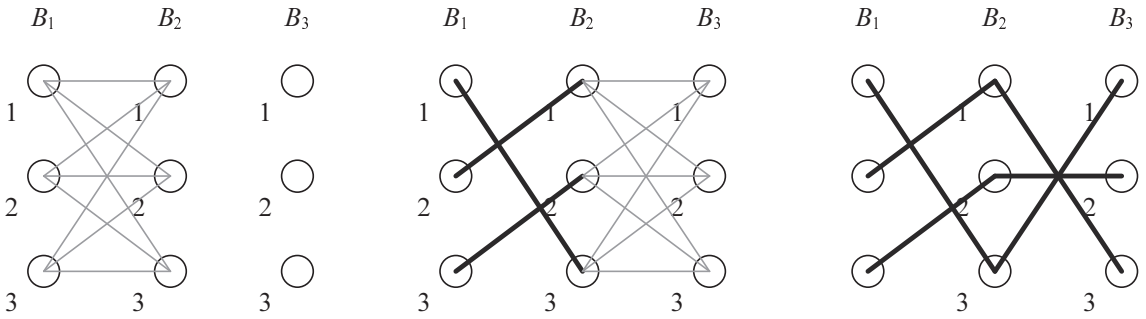


Figure 4.13. *Viterbi-like scheduling algorithm example with three users per beam ($M = 3$) and three beams ($B = 3$).*

The problem with this algorithm is to have the beams added one by one, one after the other, for finding the best scheduling. This means that a good combination of users in two beams may not necessarily involve, in the next step, still a good combination when adding a new beam to the system. Therefore the order in which the beams are processed in this algorithm

plays a role.

One could think of different possible optimisations to the aforementioned problem. First the algorithm could be run for different beam ordering and the best solution could be selected. However this increases the complexity since the number of possible beam ordering is $B!$. Another optimisation could be at the end of the algorithm to restart the algorithm by removing the edges between two beams. This actually offers the possibility to re-schedule users in two beams if the combinations were not optimal. Once again this increases the complexity of the algorithm. It has to be remarked that the Viterbi-like algorithm performs bad when using the maximum selection algorithm, thus from now on we only consider the minimum deletion algorithm.

The complexity of this algorithm scales directly with the complexity of finding the optimal edges of two beams. There are actually M^2 edges for which the rates have to be evaluated and also over which the minimum deletion algorithm needs to be performed. The complexity of the operations mentioned before is in the order of $O\left(M^4\right)$ and since they have to be performed $B-1$ times it results into a complexity of magnitude $O\left(M^4\ (B-1)\right)$.

4.4.2 "Geo-Like Algorithm"

The so-called "Geo-like algorithm" takes advantage of the particularities of the channel we are facing, i.e. a satellite channel. The level of interference is actually directly driven by the radiation pattern of the multi-beam antennas. With cluster size one, i.e. $K = 1$, the system is highly interference-limited whereas with cluster size three, i.e. $K = 3$, the level of interference is rather low since neighbouring beams employing the same frequency are far from each other. The algorithm uses this property in order to reduce the complexity of the scheduling problem.

The algorithm consists into associating each beam to a "virtual" colour. The "virtual" colour actually corresponds to the real colour of the beam in a system using more than one frequency band (i.e. more than one colour). We define C as the number of colours considered in the Geo-like algorithm and B_c as the number of beams belonging to the virtual colour c. Therefore the total number of beams in the system is simply:

$$B = \sum_{c=1}^{C} B_c \tag{4.36}$$

Beams of the same colour are more noise-limited than interference-limited when the number

of "virtual" colours is sufficiently large, therefore interference is almost negligible for SNRs of practical interest. For this reason the order in which users are scheduled in those beams impacts only marginally their performance.

The algorithm selects randomly an allocation for each group of beams, and of course for the users belonging to each group. The M users of each beam are still scheduled in different slots. The algorithm then associates the groups in order to get as much as possible low mutual interference. The final schedule is thus the merging of C partial schedules. The principle is explained by Fig. 4.14 where the number of users per beam is three ($M = 3$) and the number of "virtual" colours is also three ($C = 3$).

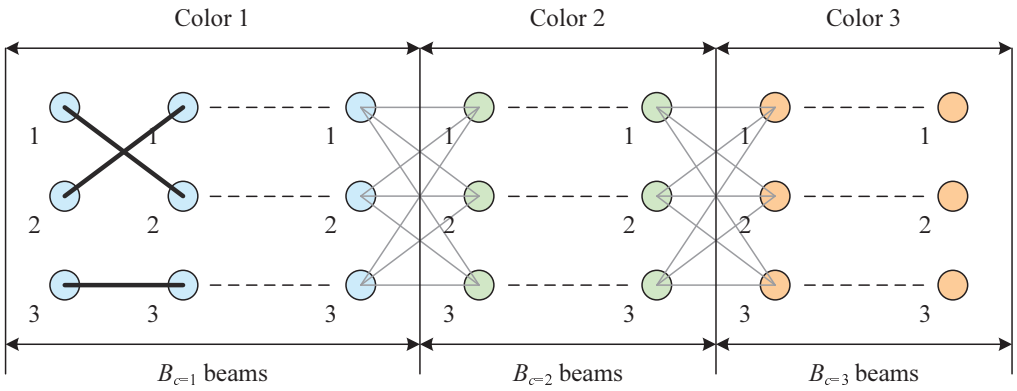


Figure 4.14. *Geo-like scheduling principle with three users per beam ($M = 3$) and three virtual colours ($C = 3$).*

In the next figure (Fig. 4.15) an example is given with the same configuration as before and with seven beams ($B = 7$). As can be seen the first colour is composed of three beams and the allocation for these three beams is selected randomly. It is the same for the second colour. The last colour consists in one single beam. The algorithm then combines the allocations of the three colours.

The association of the partial schedules was initially realised using a search over all possible allocations (exhaustive search). Compared to the initial complete exhaustive search, the Geo-like algorithm already reduces dramatically the complexity. The association was then optimised using the B-partite graph approach, more particularly using the minimum deletion algorithm. Two types of merging are supported. The first one consists into merging the partial schedules one after the other, i.e. $C - 1$ times (so-called "distinct" method). The second one consists into merging all partial schedules at the same time (so-called "common" method). In the previous example (Fig. 4.15) the number of possible edges is $9 + 9$ with the "distinct" method and with the "common" method the number of possible paths is $9 \times 9 = 81$.

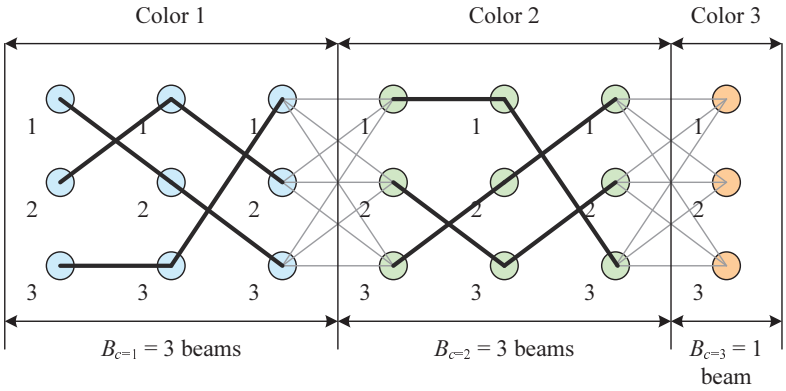


Figure 4.15. *Geo-like scheduling example with three users per beam ($M = 3$), three virtual colours ($C = 3$) and seven beams ($B = 7$).*

The number of rate evaluations to be performed at the slot level (combination of users) is therefore:

$$N_{\text{eval,GL,distinct}} = M^2\,(C-1) \qquad N_{\text{eval,GL,common}} = M^{2\,C} \tag{4.37}$$

The complexity to merge two partial schedules scales with $O\left(M^4\right)$ thus with the "distinct" method the algorithm scales with $O\left(M^4\,(C-1)\right)$ and with the "common" method with $O\left(M^{2\,C}\right)$. In both cases it is a massive reduction compared to the complexity related to the initial $(M!)^{B-1}$ possible number of allocations.

4.5 Performance Evaluation of the Different Algorithms

4.5.1 Introduction

The different algorithms described previously are all targeting the same criterion which is the maximisation of the minimum user rate. As already mentioned such criterion permits to increase the fairness among users, i.e. the difference of rates between users is reduced. In order to compare the performance of the scheduling algorithms the results have to be analysed either on a slot basis or on a block basis.

Slot Basis

The minimum user rates are compared for each slot, i.e. on a slot basis. This is useful when looking at the statistics of the minimum rates over several channel realisations. It permits for instance to compute the Cumulative Density Function (CDF) or to measure the fairness slot by slot.

Block Basis

We define a so-called "block" as M subsequent slots. When considering the results at the block level the minimum rate is the one perceived over the M slots and for each of the M slots. Doing analysis on a block basis is useful for comparing the performance of a scheduling algorithm with respect to the no-scheduling strategy, i.e. for $M = 1$.

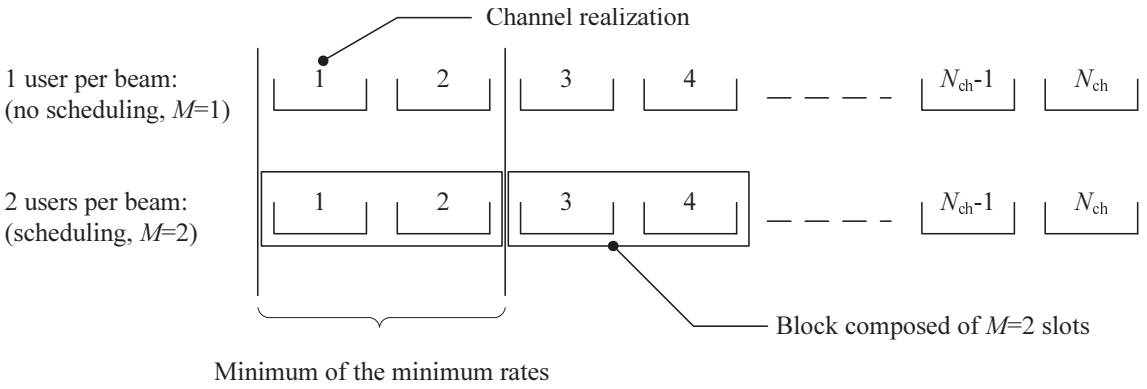


Figure 4.16. *Principle of the block basis evaluation. In this example there are two users per beam ($M = 2$) when performing scheduling.*

We consider the following example, already used in the previous sections, which consists of two users per beam in a 7×7 system. The first channel realisation is a bad case and the second channel realisation a good case. Without scheduling the bad users are scheduled in the first slot and the good users in the second slot. This will involve a low minimum rate for the first slot (high interference) and a high minimum rate for the second slot (low interference). When applying scheduling, i.e. fixing $M = 2$, the allocation will be optimised between the good and the bad cases in order to maximise the minimum user rate per slot. Hence to perform a fair comparison the minimum of the two minimum rates when having no scheduling has to be considered together with the minimum rate obtained over the two slots with scheduling. To summarise the block basis aims at doing comparison of the minimum rates obtained over M slots.

Channel Realisations

The higher the number of channel realisations, the better the results. The different scheduling algorithms can be run over many channel realisations in order to assess their performance. A channel realisation actually corresponds to the channel matrix $\boldsymbol{H}^{(i)}$ where i represents the channel realisation index. For each channel realisation users on ground are placed randomly in each beam. Hence 10 000 channel realisations with a ninety six multi-beam satellite system

represent almost 1 millions of satellite terminals. As already addressed in Section 4.1.3 a channel realisation corresponds to a specific user index for the scheduling process. The number of channel realisations, written N_{ch}, has to be a multiple of the number of users per beam M. We thus have $N_{\text{ch}} = N_{\text{blocks}}\, M$ where N_{blocks} represents the number of blocks. For instance when evaluating the performance of scheduling algorithms with three users per beam ($M = 3$) and one thousand channel realisations, the closest multiple is $N_{\text{ch}} = 999$. In such a case $N_{\text{blocks}} = 333$ and represents the number of allocations to be optimised. The channel realisation index i' for a scheduling is:

$$i' = i \,\%\, M$$

where % is the modulo operator and i ranges from 1 to N_{ch}.

Jain's Fairness Index

We remind the definition of the Jain's fairness index which is commonly used in order to quantify the fairness between different rates achieved by users in a network [JaHaCh84]:

$$J = \frac{\left(\sum_{i=1}^{N} r_i\right)^2}{N \times \sum_{i=1}^{N} r_i^2}$$

where N in this case corresponds to the number of users per slot (i.e. N_{Tx}) and r_i to the single user rate, i.e. the achievable rate for each user. By definition when all users experience the same achievable rate (upper bound), the index reaches 1 and the maximum level of fairness is achieved. When one single user gets the total capacity available whereas the others get nothing, the index equals $1/N$.

4.5.2 Results

All results shown in this section are based on the maximisation of the minimum rate criterion and are obtained in a scenario employing universal frequency reuse ($K = 1$).

Bad and Good Cases

The 7×7 scenario which consists of two users per beam with first channel realisation the bad case and second channel realisation the good case is considered. An optimisation of the scheduling aims at providing fairness between the $N_{\text{users,sched}} = 14$ users.

Fig. 4.17 shows the minimum rate on a block basis (a block is therefore composed of $M = 2$ slots) for this scenario (left graph). The average per-user rate corresponds to the maximum

rate achievable in the two slots divided by the total number of users. For this rate the Jain's fairness index equals 1 since all users experience the same rate; this rate can be seen as the upper bound. On the one hand, the Viterbi-like algorithm provides results which are close to the optimal ones, i.e. the ones issued from the search performed over all possible allocations. On the other hand, the Geo-like algorithm is able to give the same results as the exhaustive search with a computational complexity dramatically reduced. It has to be remarked that both the Exhaustive Search (ES) and the Geo-like algorithm provide a minimum per-user rate which is lower than the average per-user one. The upper bound cannot be reached because of the strong difference between the bad and the good cases. An optimisation of the schedule permits clearly to increase the minimum per-user rate in the system. For instance at $E_s/N_0 = 10$ dB the minimum rate is increased by around 55%.

Fig. 4.17 shows the Jain's fairness index on a block basis (right graph). In the noise-limited region the index is quite high since all users are perceived identically (same noise level). In the transient zone, i.e. when leaving the noise-limited region and entering the interference-limited region, the Jain's index decreases. For high SNRs the system becomes strictly interference-limited and IC permits to increase the fairness between users (this behaviour was already observed in Section 3.2.5). The scheduling algorithms provide the same performance as before, i.e. both exhaustive search and Geo-like algorithms give the same and best results.

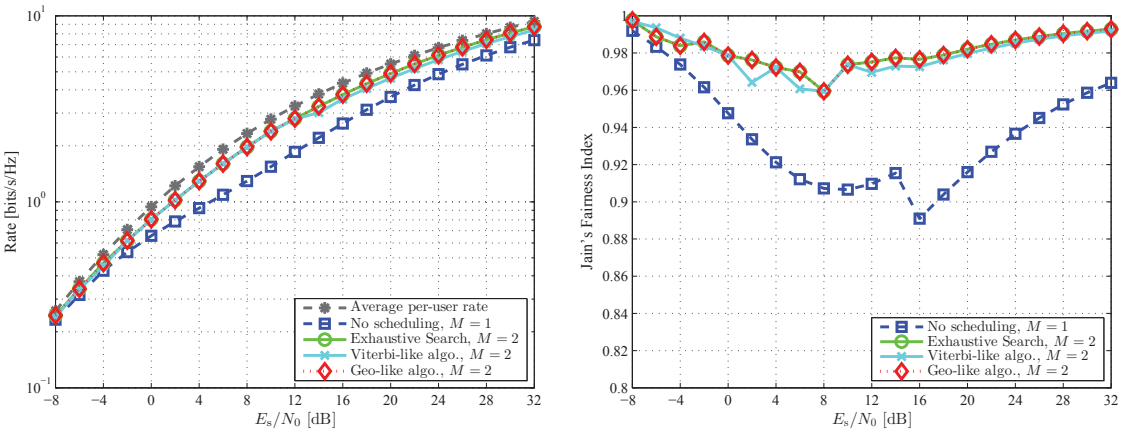


Figure 4.17. *Impact of the scheduling algorithms on the minimum per-user rate (left) and on the Jain's fairness index (right) for the bad and good cases with seven beams ($B = 7$).*

It has to be remarked that the different scheduling algorithms consider optimal ordering when trying to find out the best allocation. This means the achievable per-user rates are computed, based on modified versions of the channel matrices (swapping of columns between the initial

channel matrices) on which the Foschini algorithm is performed. This increases inevitably the overall complexity but offers better performance, as investigated in Section C.4.1. Therefore the different schedules issued from the algorithms are always obtained, unless stated, assuming optimal ordering at the reception.

Performance of the Scheduling Algorithms over Several Channel Realisations

The performance over several channel realisations is evaluated for the different scheduling algorithms described in the previous sections. They are all based on a max-min heuristic, i.e. they arrange the terminals so that the minimum user rate is maximised. The system is of size 7×7 and therefore consists of a beam and its six neighbouring beams. The number of users per beam M is set to three ($M = 3$) in order to be able to evaluate the performance of the exhaustive search. The number of channel realisations is $N_{\text{ch}} = 999$ and the SNR ranges from -8 to 32 dB.

Fig. 4.18 shows the average on a block basis (left graph) and the first percentile on a slot basis of the minimum per-user rate (right graph). The optimal scheduling performs on average 1.5 dB worse than the average per-user rate. The Geo-like algorithm and the Viterbi-like algorithm perform 1.9 dB worse which is thus very close to optimality. It has to be remarked that a system without scheduling performs 5.4 dB and 3 dB worse than the optimal scheduling and the Geo-like scheduling, respectively (Fig. 4.18, left). When analysing the first percentile the differences are even higher. For reaching a spectral efficiency of at least 2 bits/s/Hz the loss is about 4.1 and 12.4 dB, compared to the average per-user rate, for the exhaustive search and no-scheduling, respectively. Such improvement is related to the ability of the algorithms to avoid pairing users that are geographically close to each other, i.e. having low gains and high mutual interference. As before the Geo-like algorithm and the Viterbi-like optimised algorithm provide results which are very close to the ones of the exhaustive search (Fig. 4.18, right).

The benefits of the scheduling algorithms can also be observed when looking at the Jain's fairness index (Fig. 4.19). The Geo-like algorithm loses about 1% compared to the optimal value obtained with the exhaustive search. Having no scheduling can reduce the fairness among users by over 5%.

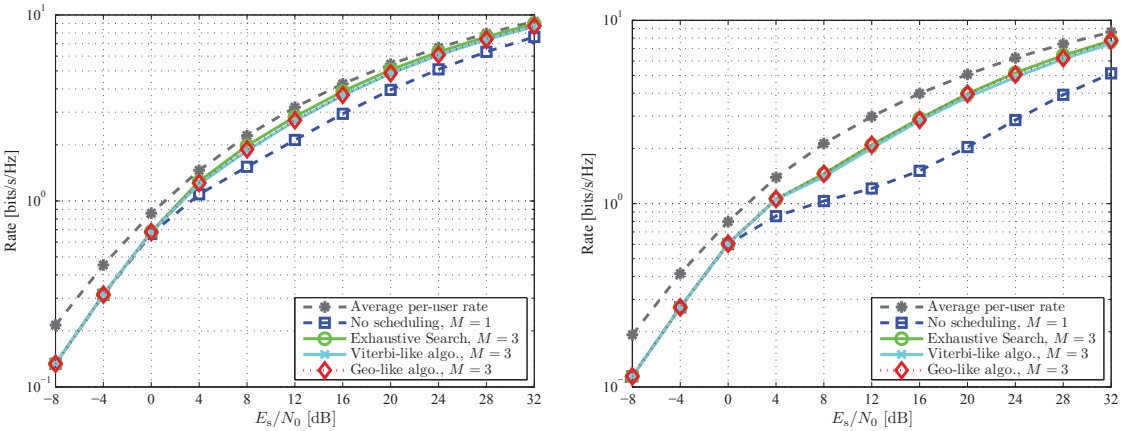


Figure 4.18. *Impact of the scheduling algorithms on the minimum per-user rate (left) and 1st percentile of the per-user rate (right) with seven beams ($B = 7$), three users per beam ($M = 3$) and $N_{ch} = 999$ channel realisations.*

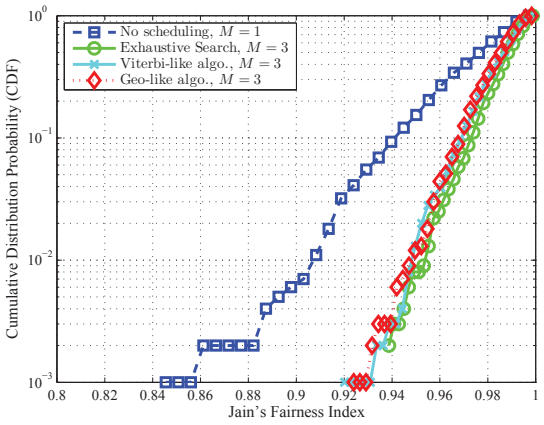


Figure 4.19. *CDF of the Jain's index. The number of beams B is 7, the number of users per beam is $M = 3$ and the number of channel realisation $N_{ch} = 999$.*

Performance of the Scheduling Algorithms with 96 Beams

In this scenario the entire multi-beam satellite system is considered, i.e. ninety six beams ($B = 96$). As before the number of users per beam is three ($M = 3$); the number of channel realisation is $N_{\text{ch}} = 24$. It has to be remarked that both exhaustive search and Viterbi-like algorithms are not considered due to their computational complexity for such system scale.

The evaluation of the minimum per-user rate (Fig. 4.20) shows that smart scheduling improves the performance between 20 and 25% at high SNR, which is a noteworthy gain. At low SNR the improvement is significantly smaller since the system is mainly noise-limited. It has to be remarked that the average per-user rate is about twice as large as the minimum per-user rate without scheduling. The Geo-like algorithm reaches about two thirds of this average

rate whereas in the previous plots it was quite close to the maximum attainable minimum rate.

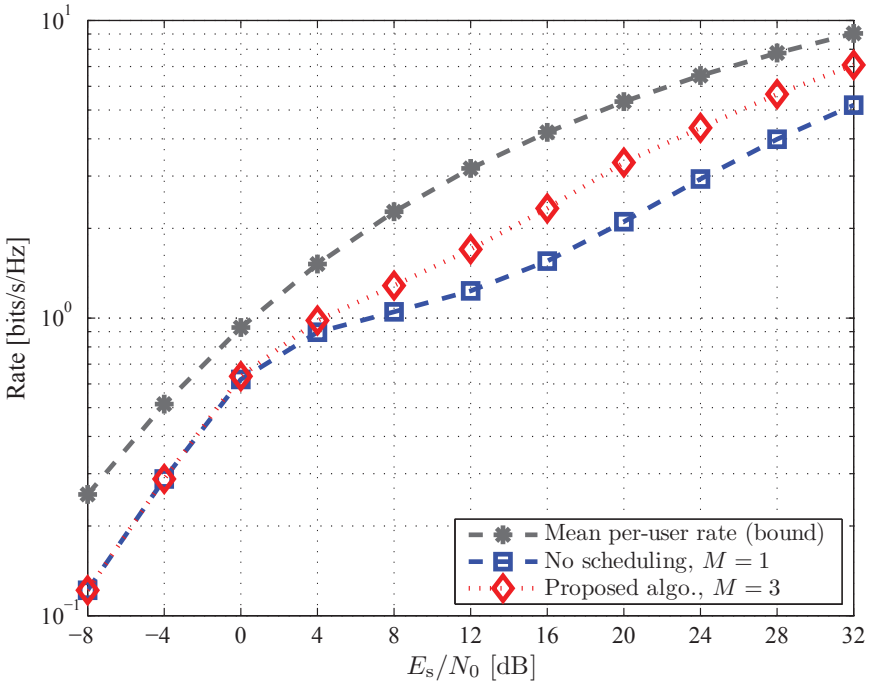


Figure 4.20. *Minimum per-user rate. The number of beams B is 96, the number of users per beam is $M = 3$ and the number of channel realisation $N_{ch} = 24$.*

This behaviour can be explained by the properties of the channel matrix. Hence we surmise that in contrast to a typical terrestrial Rayleigh fading environment, where for sufficiently large M the users can be scheduled so as to attain the single user rate [YoGo06], [YFVG11], this is not the case in satellite networks. This is due to the composition of the channel matrix which is driven by the antenna beam pattern. Actually the statistical distribution of the coefficients strongly deviates from the Rayleigh one since it is directly determined by the position of the user in the beam. More particularly the dynamic range of a Rayleigh channel is infinite in principle and this is not true for antenna gains which cannot be zero or greater than the maximum gain. For these reasons the gains which can be obtained through multi-user diversity are limited and the orthogonality of the users we can have in a terrestrial MIMO system cannot be ensured [YoGo06], [YiLi02], [YFVG11]. Anyhow the proposed algorithm offers performances which are rather close to the upper bound.

It has to be remarked that a performance comparison of both search algorithms, i.e. the search based on all possible allocations and the search based on all possible combinations

(B-partite graph approach), can be found in Section C.4.2.

4.6 Impact of Scheduling on the Uncoded Bit Error Rate

The optimisation of the schedules based on BER simulations is practically infeasible and for this reason investigations on the achievable rates were realised so that scheduling algorithms could be designed in an efficient way (Chapter 3 and this chapter, respectively). This section shows the impact of scheduling, realised using information theory, on the bit error rate performance [BoMaBe12-2]. To this aim we consider the scenario composed of seven beams ($B = 7$) and in which the so-called "good" and "bad" users are covered by the seven spotbeams. Therefore we have two different channels, one issued from the low interference scenario and another one issued from the high interference scenario. This leads to a total of $N_{\text{users,total}} = 14$ since there are two users per beam. Considering the bad and the good cases, we have seen in Section 2.2.3 that the BER experienced by the users was radically different. We expect with scheduling to improve the fairness between users, i.e. to offer the users almost the same BER. On the one hand using, information theory we maximised the minimum per-user rate but also increased the fairness between users. On the other hand, by performing BER simulations we should see a decrease of the maximum and therefore the worst BER and also, like with the achievable rates, an increase of the fairness.

4.6.1 Principle and Process

The fourteen users ($N_{\text{users,total}} = 14$) need to be scheduled so that they can transmit data towards the gateway (return-link). First the gateway decides which users, more particularly which combination of B users maximises the minimum per-user achievable rate and this over the $M = 2$ slots. Therefore the gateway optimises the schedule based on information theory. Once the schedule is decided, it is sent back to the satellite terminals so that they know when to transmit, i.e. in which slot. The users send their data accordingly and the signals are received by the gateway so that they can be processed. Scheduling can thus be seen as a kind of pre-processing realised by the gateway whereas the operations performed on the users' signals can be assimilated to a post-processing. The gateway handles all users' signals and performs Successive Interference Cancellation (SIC) in order to suppress interference. Therefore both scheduling and signal processing are two distinct operations realised by the gateway but are strictly correlated.

Scheduling is actually performed based on achievable per-user rates which are directly evaluated assuming a Multiple-Input and Multiple-Output (MIMO) system. When dealing with bit error rates, the return-link of this MIMO system is actually a multi-user MIMO multiple access channel (MU-MIMO MAC, Section 1.2.2). The receiver will perform Multi-User Detection (MUD) so that to extract the data originally sent by the different users. In our case scheduling is based on the assumption SIC will be realised once users' signals are received. As seen before the optimisation of the schedule can be done taking into account optimal ordering or not. Optimal ordering is part of the SIC operation realised once the users have transmitted their data and are received by the gateway.

For the above-mentioned reason the receiver selected for analysing the impact of scheduling on the bit error rate performance is the one with the optimal SIC architecture (please refer to Section 2.1.4 for more details). The optimisation through optimal ordering can be enabled or disabled either in the scheduler or in the receiver.

4.6.2 Optimal Allocation

Dynamic Allocation

With this particular scenario, the number of possible allocations is, according to (4.3):

$$N_{\text{alloc}} = (M!)^{B-1} = (2!)^{7-1} = 64$$

The different possible allocations are numbered from 1 to N_{alloc}.

As seen previously in this section, the optimal allocation depends on the signal-to-noise ratio (SNR). For this reason BER simulations with scheduling need to be realised with channel matrices which are optimised for given SNRs (please refer to Tables 4.5 and 4.6).

Table 4.5. *Optimal allocations between -8 and 8 dB (step of 2 dB) with seven beams ($B = 7$) and two users per beam ($M = 2$).*

SNR [dB]	-8	-6	-4	-2	0	2	4	6	8
Index [#]	10	6	26	10	15	14	14	14	15
Occurrence	2	1	1	2	5	3	3	3	5

In Table 4.5 and Table 4.6 the index represents the index of the allocation (comprised between 1 and N_{alloc}) and the occurrence the number of time the corresponding allocation was considered as optimal in the SNR range taken into account.

Table 4.6. *Optimal allocations between 10 and 24 dB (step of 2 dB) with seven beams ($B = 7$) and two users per beam ($M = 2$).*

SNR [dB]	10	12	14	16	18	20	22	24
Index [#]	15	15	50	51	50	15	50	50
Occurrence	5	5	4	1	4	5	4	4

Most Appearing Allocation

The most appearing allocation with respect to Tables 4.5 and 4.6 is shown in the next table (Table 4.7).

Table 4.7. *Most appearing allocation between -8 and 24 dB (step of 2 dB) with seven beams ($B = 7$) and two users per beam ($M = 2$), i.e. allocation index 15.*

Beam ID	1	2	3	4	5	6	7
Slot 1	1	1	1	2	2	2	1
Slot 2	2	2	2	1	1	1	2

4.6.3 Performance Analysis

The BER performance is evaluated considering the MMSE receiver integrating the optimal SIC architecture. The simulations are realised with the QPSK modulation, with an energy per symbol over noise power spectral density ranging from -8 dB to 24 dB; the resulting uncoded bit error rates are averaged over all users.

Fig. 4.21 shows clearly that the BER decreases when performing optimal ordering with SIC and also when optimising the schedules. Realising Interference Cancellation (IC) with optimal ordering (OO) and without scheduling offers a gain of 3 dB for high SNRs. Interestingly scheduling without optimal ordering gives almost identical results. This proves that both strategies need to be combined in order to reach the best performance. If scheduling is performed assuming optimal ordering but actually the latter is not applied at the receiver side, there is a mismatch and consequently the BER gets worse, i.e. increases. As expected the highest gains are obtained when the schedules are optimised considering optimal ordering and when the latter operation is realised at the reception. For a BER of 10^{-4}, the gain is about 7 dB which is quite a huge improvement. It has to be remarked that the disruption in the slope of the curves is related to a change of the order in which each user is decoded.

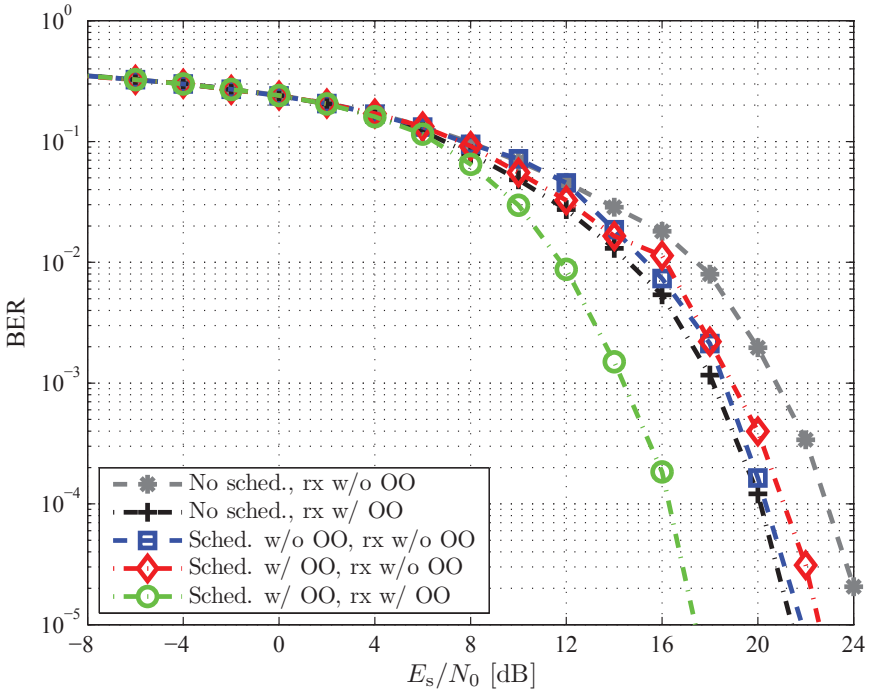


Figure 4.21. *Impact of ordering and scheduling on the average BER for the bad and good cases. "OO" stands for optimal ordering.*

In the previous results the uncoded bit error rates were averaged over all users. This kind of results does not give information about the fairness between users, more particularly about the difference of BER experienced between the fourteen users ($N_{\text{users,total}} = 14$). In order to measure the fairness we consider once again, as for the achievable rates, the so-called Jain's fairness index [JaHaCh84]. However the way of computing this index was modified since what is important for the users here is to operate in the same level of BER magnitude. As an example two users experiencing a bit error rate of $2 \cdot 10^{-1}$ and $5 \cdot 10^{-1}$ will give the same Jain's fairness index as if they were experiencing a BER of $2 \cdot 10^{-12}$ and $5 \cdot 10^{-12}$. Considering the logarithm allows focusing on the value of the exponent and for this reason the Jain's fairness index was modified such that:

$$J_{\text{BER}} = \frac{\left(\sum_{i=1}^{N} \log\left(\text{BER}_i\right)\right)^2}{N \times \sum_{i=1}^{N} \log\left(\text{BER}_i\right)^2} \tag{4.38}$$

where BER_i represents the bit error rate experienced by user i, subject to $\text{BER}_i > 0$, and N the total number of users, i.e. $N_{\text{users,total}}$.

When analysing the results of Fig. 4.22 [1] the modified Jain's fairness index is close to 1 in

1. The SNR range was adjusted because of the constraint $\text{BER}_i > 0 \ \forall i$ with $i \in \{1, ..., N\}$.

the noise-limited region. In such region the noise is dominant therefore all users get the same BER. Once the noise-limited region is left, the difference between the users' channels can be distinguished and consequently the fairness index decreases. The optimal ordering helps increasing the level of fairness (the curve representing no scheduling with optimal ordering at the receiver) but if the level of interference gets too high and almost identical for all users (this is the case for the high interference scenario, i.e. the one composed of the "bad" users), SIC is not efficient. Optimising the schedules permits to balance the level of interference between the two slots (this can be seen with the allocation shown by Table 4.7) and therefore SIC achieves better performance, increasing consequently the level of fairness (scheduling without optimal ordering offers a fairness index greater than 0.9 over the entire SNR range). On one side the mismatch between the scheduler and the receiver resulted in bad BER (Fig. 4.21), on the other side it increases the level of fairness since the errors are spread among all users. As before the best results are obtained when scheduling with optimal ordering is realised and when the latter is performed at the receiver. What is remarkable in Fig. 4.22 is the matching between the modified Jain's fairness index curve obtained via BER simulations and the Jain's fairness index curve computed with the achievable per-user rates, i.e. using Information Theory (IT). In the interference-limited region scheduling with SIC and optimal ordering maximises the minimum per-user rates and this permits to increase the level of fairness. For these reasons the users perceive almost the same level of BER magnitude when employing these strategies.

4.7 Summary

We have shown in this chapter that the sum rate cannot be increased through scheduling in the low SNR region, and only marginally in the high SNR region. Hence the analysis of the user combinations and their impact on the sum rate has shown that improvement can be done on the single user rates. We investigated a low complexity algorithm in order to derive close-to-optimum schedules for multi-beam satellite systems, more particularly for large scale systems. This work has permitted to evaluate the gains that a scheduler can reach in interference-limited satellite networks. Actually interesting performance improvements are achievable even if it is not possible to reach the single user bound in this context as in the case of Rayleigh fading channels. The characteristics of classic beam patterns limit the gains which seem here to be limited to 25% with respect to no-scheduling schemes.

It is possible using tools provided by Information Theory (IT) to optimise the users' schedules

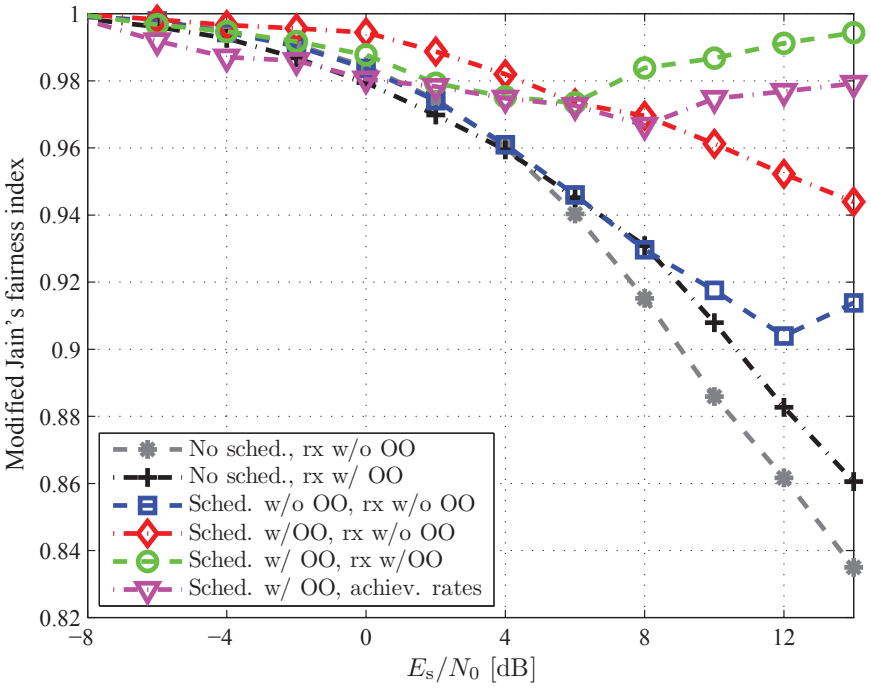


Figure 4.22. *Impact of ordering and scheduling on the modified Jain's fairness index for the bad and good cases. "OO" stands for optimal ordering.*

so as to maximise the minimum achievable per-user rates in the system and as an outcome the level of fairness between the users gets improved (see Section 4.5). Practical simulations have shown the same behaviour for the uncoded Bit Error Rate (BER). As expected the maximum BER is dramatically decreased and the users experience almost identical error rates, increasing consequently the level of fairness. The optimisations realised in the resource management all targeted the maximisation of the minimum per-user rate and practically the minimisation of the maximum bit error rate. It is possible, using the different tools and algorithms designed until now, to investigate more advanced mechanisms to take into account different Quality of Service (QoS) constraints.

Chapter 5

Scheduling with Quality of Service Constraints

This chapter uses the scheduling concept and the different algorithms described in the previous chapter (Chapter 4), in which the maximisation of the minimum single per-user rate was targeted, and now introduces Quality of Service (QoS) constraints.

In this chapter we first analyse the impact of the number of spot beams and of the number of users considered for scheduling. The results obtained with this study are exploited in order to design novel algorithms, each satisfying different QoS constraints. The first one, named Free Slot Assignment (FSA), is able to add unnecessary slots to the schedules in order to have a non-full slots/beams matrix and thus to reduce the mutual interference among the users; this can be exploited to guaranteed minimum QoS levels in terms of service rate. The second one, named Window algorithm, optimises the schedule selection in order to keep under control the delay between the time a user arrives in the system and the time it is scheduled. For each constraint, the performance is analysed together with the complexity of the proposed algorithm. Finally a combination of the two constraints, and therefore of the two algorithms, is realised and the improvements achieved with this new hybrid algorithm are shown.

5.1 Impact of the Number of Beams and Users per Beam

In this section we address the impact of the system size, which is driven by the number of beams B, but also of the scheduling depth driven by the number of users per beam M [BoBeRo11] [BoMaBe12-1]. These two factors play an important role in the complexity while optimising the schedules but also permits to understand their impact while designing scheduling algorithms taking into account specific Quality of Service (QoS) constraints.

The Signal-to-Noise Ratio (SNR) is set to 15 dB such that the communication between the transmitters and the receivers can be considered as mainly interference-limited. Adding more beams in the system consists into adding more users and therefore more interferers. For a given number of beams B, increasing the number of users per beam M, which is equivalent to increasing the so-called scheduling depth, permits to offer more possibilities for optimising the schedules. For evaluating the impact of the number of beams, the B-partite Graph (BG) approach is considered, whereas for seven beams ($B = 7$) the users which are weakly interfering each other can be grouped in fictitious colours and randomly scheduled so that the complexity is reduced [BoBeRo11] (Geo-like algorithm, please refer to Section 4.4.2 for more details).

The scenario taken into account and the numbering of the beam such that $B_i = i$ with $i = 1 \dots B$ is depicted by Fig 5.1. The Jain's fairness index [JaHaCh84], already introduced in Section 4.5.1, is considered and measured on a slot basis. In this section we define the outage probability, or non-availability, for a given minimum rate r as follows:

$$p_r = P\{r_{\min} \leqslant r\} \tag{5.1}$$

The Cumulative Density Function (CDF) of the minimum per-user rates will be interpreted using (5.1) while analysing the different results.

5.1.1 Impact of the System Size

As already specified the system size is considered to be driven by the number of beams B. The impact on the minimum per-user rates and on the Jain's fairness index are shown by Fig. 5.2 when having no scheduling, i.e. the number of users per beam for each schedule is such that $M = 1$.

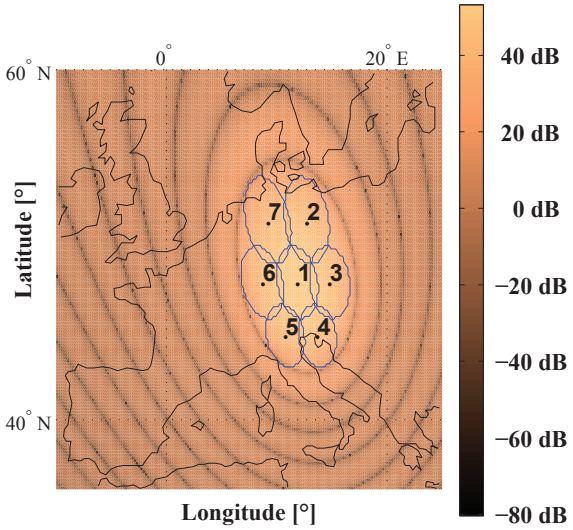


Figure 5.1. *Multi-beam scenario considered for evaluating the impact of the system size and of the scheduling depth. The radiation of the beam in the middle is shown, together with the beam centres and the corresponding beam numbering.*

As expected the increase of the number of beams B involves a decrease of performance (Fig. 5.2, left). In other words the minimum guaranteed rate r decreases as B gets higher for a given outage probability p_r. For instance when having two beams ($B = 2$) and seven beams ($B = 7$) the non-availability $p_{r=3}$ ranges from about 0.06 to 0.31 (i.e. factor 5), respectively. It has to be remarked that between two and three beams ($B = 2$ and $B = 3$) the decrease of performance is huge since disposition of the beams (5.1) increases dramatically the probability of having interferers. For higher values of B the diminution of the performance is quite moderate. This can be explained by the expected improvement considering the multi-beam satellite system as a MIMO system. Actually the increase of CCI due to the higher number of beams is balanced by the gain offered by the multiple receive antennas. What is remarkable is the lowest minimum per-user rate in the different CDFs which remains constant and close to 1.1 bits/s/Hz despite the fact that the probability to occur increases for bigger values of B. Finally Fig. 5.2 (left) shows an important curve which corresponds to the so-called per-user bound. The latter is obtained by dividing the sum rate with the number of users. This per-user bound is therefore the upper-bound for which all users experience identical rates.

The impact of the number of beams B on the Jain's fairness index is the opposite (Fig. 5.2, right). Actually the fairness increases together with B. The explanation is that for larger B the probability of having users experiencing different SINRs gets higher and this helps improving the performance of SIC when realising optimal ordering. The smallest fairness

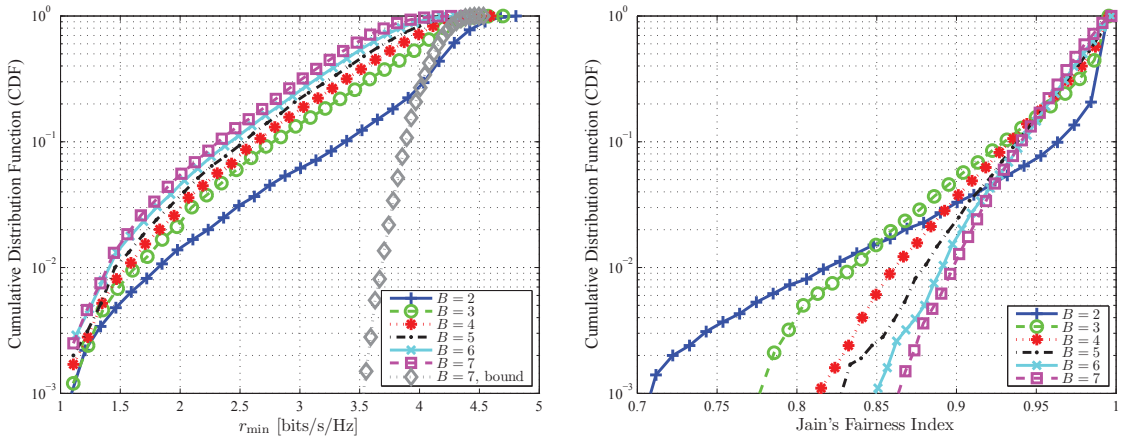


Figure 5.2. *Impact of the number of beams on the minimum per-user rates (left) and on the Jain's fairness index (right).*

index ranges from 71% to 86% respectively between $B = 2$ and $B = 7$.

5.1.2 Impact of the Scheduling Depth

The purpose is to evaluate the impact of the number of users per beam M while performing scheduling. To do so the number of beams is fixed to seven ($B = 7$). Increasing the number of users per beam M for optimising the schedules is equivalent to enlarge the degree of freedom for scheduling. A gain is expected with larger M since the probability of finding proper combinations of users, less interfered, gets higher. In this particular case the target is to reach the upper-bound. As mentioned previously the upper-bound corresponds to the ideal case in which all users experience the same rate and therefore the Jain's fairness index is unitary.

When considering a particular outage probability, the results of Fig. 5.3 (left) illustrates that, as foreseen, the minimum per-user rates are improved for higher scheduling depths. However a kind of saturation effect appears and the gain decreases with M. For instance for a non-availability $p_r = 0.01$, having $M > 5$ does not bring any additional gain. The upper-bound is almost impossible to reach since the number of interferers in the system is too high. For this reason Fig. 5.3 (left) shows that using a scheduling depth bigger than $M = 5$ for this particular scenario does not improve anymore the performance. As a summary, when considering $p_r = 0.1$, the minimum per-user rates evolves from 1.4 to 3.5 bits/s/Hz (factor 2.5) when having $M = 1$ without ordering and $M \geq 5$.

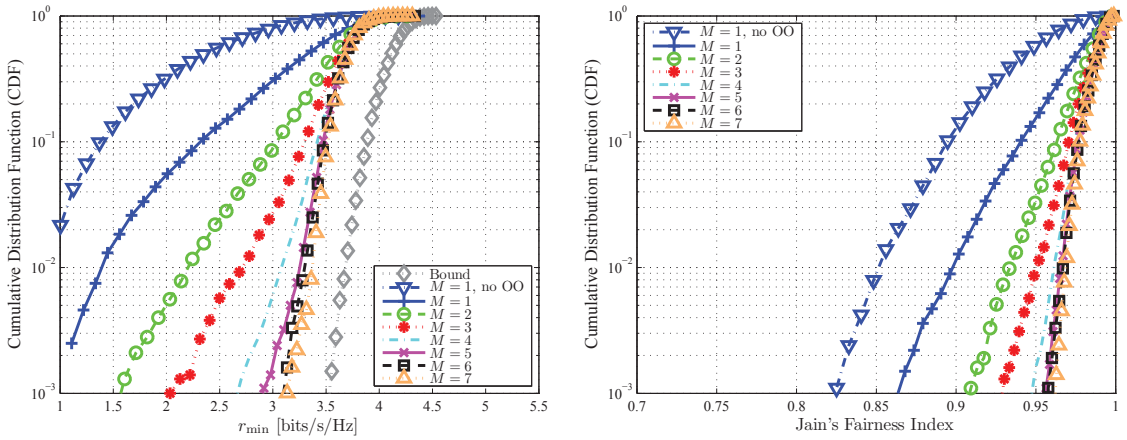


Figure 5.3. *Impact of the number of users per beam on the minimum per-user rates (left) and on the Jain's fairness index (right).*

Fig. 5.3 (right) indicates that the level of fairness between the users is increased once scheduling is realised. The same effect as before can be seen, i.e. the gain can be almost neglected as $M > 5$. It has to be noticed that with $M = 5$ the minimum level of fairness achieved is 95% which is a considerable improvement.

As expected increasing the scheduling depth permits to offer better performance in terms of minimum achievable per-user rates and consequently in terms of level of fairness. With this particular scenario, i.e. a 7×7 multi-beam satellite MIMO system, with users randomly placed within the footprints of the beams, the scheduling depth $M = 5$ permits to obtain close to optimal results. As specified previously having users uniformly distributed creates high SNRs unbalances and this can be taken as an advantage for optimising the schedules.

5.2 Rate Constraints

Performing scheduling with so-called "rate constraints" consists into trying to provide to the users present in the system a particular minimum per-user rate, defined as r_{th}. As seen in the previous section (Section 5.1) both system size and scheduling depth are of paramount importance and influence directly the probability of reaching a minimum per-user rate value. The satellite operator may be interested to offer in the return-link of the system an higher minimum per-user rate than the one reachable for a given B and M, keeping in mind that the complexity, while optimising the schedules, is directly dimensioned by those parameters. Fixing a minimum achievable per-user rate will impact, when considering the different layers present on top, the datarates perceived by the users at the application level.

5.2.1 Free Slot Assignment Concept

Introduction

When setting the system size, i.e. the number of beams B present in the system, we have seen in Section 5.1.2 that increasing the scheduling depth, driven by the number of users per beam considered for optimising the schedules (parameter M), improves the performance but the latter saturates at a given point. In other words playing with M will not help guaranteeing a minimum per-user rate target. Therefore optimising the schedules in such a way helps reducing the level of interference, more particularly the CCI, but another solution has to be found such that this level is even more reduced.

One straightforward solution is to avoid having necessarily B users scheduled in the same time slot and therefore transmitting at the same time. In the following we consider that instead of using M slots available for allocating resources to the users, we use one additional slot, i.e. $M+1$ slot. This slot can be seen as an empty slot, i.e. a free slot without any users, and this strategy is referred as Free Slot Assignment (FSA). For instance when performing scheduling with $M = 2$, i.e. two users per beam for optimising a schedule, one additional slot will lead to schedule the two users present in each beam by using three slots instead of two.

Number of Allocations

If it is allowed to have empty slots in the list of possible allocations, i.e. strictly no users transmitting in the B beams during one slot, then the number of possible allocations is:

$$N_{\text{alloc,FSA,with\_empty\_slots}} = ((M+1)!)^{(B-1)} \tag{5.2}$$

As mentioned previously having empty slot in the system consists into having the possibility to send no data during that slot (all transmitters are switched off). The probability to have an empty slot at a given time is:

$$p_{\text{empty\_slots,with\_order}} = \left(\frac{1}{M+1}\right)^{B} \tag{5.3}$$

Since the order of the slots does not play a role, this probability becomes:

$$p_{\text{empty\_slots,without\_order}} \left(\frac{1}{M+1}\right)^{(B-1)} \tag{5.4}$$

The number of allocations in which a slot has all transmitters off is:

$$N_{\text{alloc,empty\_slots}} = \left(\frac{1}{M+1}\right)^{(B-1)} ((M+1)!)^{(B-1)} = \left(\frac{(M+1)!}{M+1}\right)^{(B-1)} = M!^{(B-1)} \tag{5.5}$$

The number of possible allocations while performing scheduling with FSA in a multi-beam satellite system composed of B beams and M users per beam, and in which empty slots are not allowed, is therefore:

$$N_{\text{alloc,FSA}} = ((M+1)!)^{(B-1)} - M!^{(B-1)} \tag{5.6}$$

It is of course of interest to avoid having empty slots when considering FSA since it wastes resources and does not provide any gain when compared to the classical scheduling, i.e. scheduling realised with M slots and B users per slot. For this reason the utilisation of FSA is always done in such a way empty slots are forbidden.

Theoretical Gain

It is obvious that inserting one additional free slot for optimising the schedules involves a gain in the sum rate perceived over all slots, i.e. perceived on a block basic (please refer to Section 4.5.1 for more details about both block and slot basis concepts). Having $M+1$ slots available instead of M, and no empty slots among these $M+1$ slots, means that there will necessarily be in each of the $M+1$ slots less than B users transmitting at the same time. Since the system is interference-limited when having full frequency reuse, it means that the level of interference perceived in each of the $M+1$ slots is lower than the one perceived in each of the M slots when having no additional free slot. Let's define $R^{(m)}$ as the sum rate achievable in slot m without FSA, and $R^{(m)'}$ as the sum rate achievable in slot m with FSA. We have:

$$\sum_{m}^{M} R^{(m)} < \sum_{m}^{M+1} R^{(m)'} \tag{5.7}$$

Therefore on a block basis the overall sum rate with FSA is greater than the one obtained without FSA. However using FSA leads to the utilisation of one additional free slot, i.e. scheduling the users over $M+1$ slots instead of M, and involves a loss in terms of efficiency. In other words when looking at the sum rate on a slot basis we have:

$$\frac{1}{M}\sum_{m}^{M} R^{(m)} \geq \frac{1}{M+1}\sum_{m}^{M+1} R^{(m)'} \tag{5.8}$$

For instance if we consider two users per beam, i.e. $M = 2$, in order for the sum rate computed on a slot basis with FSA to be equal to the one without FSA, the improvement of the sum rate should be at least 50%. Such gain could be actually reached if there was no Interference Cancellation (IC) performed which is not the case here.

On the one hand, reducing the level of Co-Channel Interference (CCI) by introducing an additional slot will undoubtedly increase the performance but on the other hand, it will be done at the expense of using additional resources in the system, and therefore will result in loosing efficiency.

Practical Gains and Losses

This section aims at investigating the gains and the losses related to the utilisation of one additional free slot for performing scheduling, i.e. using the so-called Free Slot Assignment (FSA).

Impact on the sum rate:
As shown in the previous section, the overall sum rate computed on a block basis will increase since the insertion of one free slot permits to decrease the level of interference perceived in each of the $M+1$ slots (5.7). However the use of one additional slot, i.e. $M+1$ slots instead of M initial slots, involves a loss in terms of efficiency. Therefore when computing the sum rate on a slot basis we obtain (5.8).

The efficiency loss in terms of resources is simply computed as follows:

$$L_{\text{eff}} = \frac{1}{M} \tag{5.9}$$

since we use one additional free slot over M slots, i.e. $M+1$ slots instead of M.

Simulation results:
Simulations were realised in order to verify the different gains and losses achieved when using FSA. For this the signal-to-noise ratio (SNR) of the system was set to 15 dB such that interference plays the most important role. As usual thousands of channel realisations are taken into account with full frequency reuse and seven beams ($B = 7$). The purpose is to compare the performance of the sum rate on both block and slot basis when having no FSA and with FSA. The scheduling depth M varies between 1 and 7 and the FSA scheduling algorithm is set in a mode which "forces" the utilisation of one additional free slot and does not target any rate constraint.

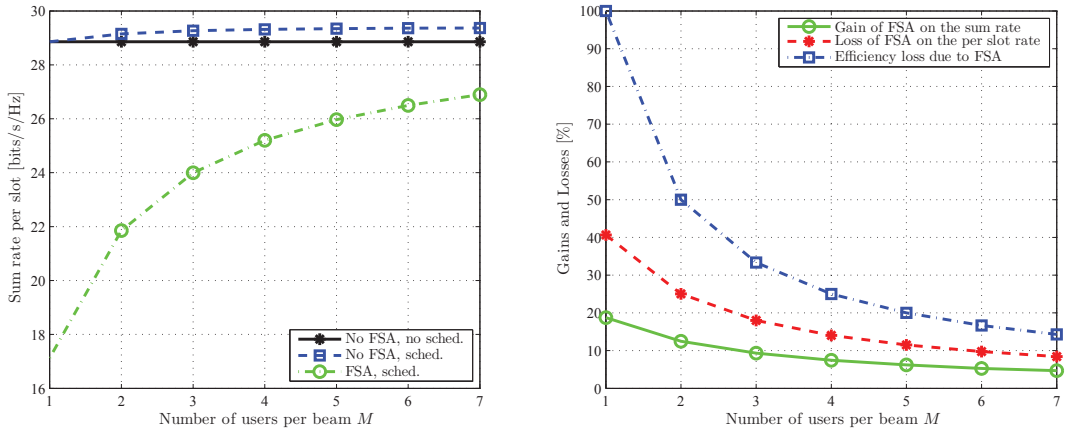


Figure 5.4. *Impact of the scheduling depth M on the FSA performance with SNR 15 dB in terms of sum rate per slot (left) and gains and losses (right).*

As shown by Fig. 5.4, the sum rate per slot (left) does not evolve with M when using no additional free slot and performing no scheduling and this is perfectly normal. Once scheduling is performed one can see an increase of the sum rate per slot which is actually quite small (around 1%) and saturates for scheduling depths greater than three. This again confirms the invariance of the sum rate when performing scheduling as mentioned in Section 4.1.4. When enabling Free Slot Assignment (FSA) the sum rate per slot is clearly smaller than the one obtained without FSA which corresponds to the expression (5.8). This curve increases rapidly with M and then seems to saturate. The gains and losses (right) summarises the impact of FSA together with M on the performance. The efficiency loss decreases with M, as expected, and also the loss due to FSA on the sum rate computed on a slot basis. The gain of FSA on the sum rate, i.e. calculated on a block basis, decreases with M since the total number of users in the system increases ($N_{\text{users,total}} = M\,B$) and therefore the number of users transmitting at the same time, even in the presence of one additional free slot, also. The loss of FSA on the per-slot rate and the gain of FSA on the sum rate tend to reach the same level, which is actually true when M goes to infinity.

5.2.2 "Smart Free Slot Assignment Scheduling Algorithm"

Motivation

The utilisation of one additional free slot involves unfortunately a loss in efficiency and increases also the scheduling complexity (please refer to (5.6)). In order to try providing the best trade off between guaranteeing the minimum per-user rate constraint r_{th}, avoiding loosing efficiency and also, not least, trying to reduce the complexity of scheduling as much

as possible, an algorithm has to be designed. This algorithm is named "Smart Free Slot Assignment Scheduling Algorithm" [1] and its principle is described hereafter.

Description

In the following we still consider $N_{\text{users,total}}$ as defined by (4.4) in Section 5.1 but the number of schedules to be determined is not anymore as in (4.5) since the scheduling depth M is not fixed. The purpose of this scheduling algorithm is still to schedule all $N_{\text{users,total}}$ users but using a different strategy. The algorithm starts with $M = 1$ which is equivalent to not performing scheduling. Actually when the scheduling depth is unitary the users are taken as they "arrive", i.e. as they are located in the B beams. The minimum achievable per-user rate $r_{\min}$ is computed and if the constraint is reached, i.e. $r_{\min} \geq r_{\text{th}}$, then the B users of this channel realisation are scheduled together. If the constraint is not reached then the scheduling depth is increased by one, i.e. $M = 2$. In such a case the schedule is optimised, using the algorithms described in Chapter 4, and the corresponding minimum per-user is calculated. In other words scheduling is realised taking into account the current channel and the next one available since $M = 2$. As before, if the minimum rate obtained is greater than r_{th} then the optimal schedule is saved and the next channels available are processed. If the constraint is not respected then the scheduling depth is increased. This last process continues until the scheduling depth exceeds the so-called "FSA threshold", noted M_{FSA}, i.e. until $M > M_{\text{FSA}}$. In the latter case scheduling is realised inserting one additional free slot, i.e. using FSA, more particularly $M_{\text{FSA}}+1$ slots. The result of this last try, i.e. of optimising the schedule in such a way $r_{\min} \geq r_{\text{th}}$, can be either positive or negative. In the first case the optimal schedule was found using FSA and the constraint is guaranteed. In the second case there are two possibilities. Either the complete schedule process of the current channel matrix is cancelled and the algorithm processes the next channel realisation available, or the optimal schedule performed using $M_{\text{FSA}} + 1$ slots is kept because anyhow it will provide a minimum per-user rate which is closer to the constraint. The latter solution is preferred of course, even if the constraint was not reached. The principle of the algorithm is shown by the diagram of Fig. 5.5.

1. A patent was submitted by the author in Germany for this algorithm, this patent will also be submitted at the European level.

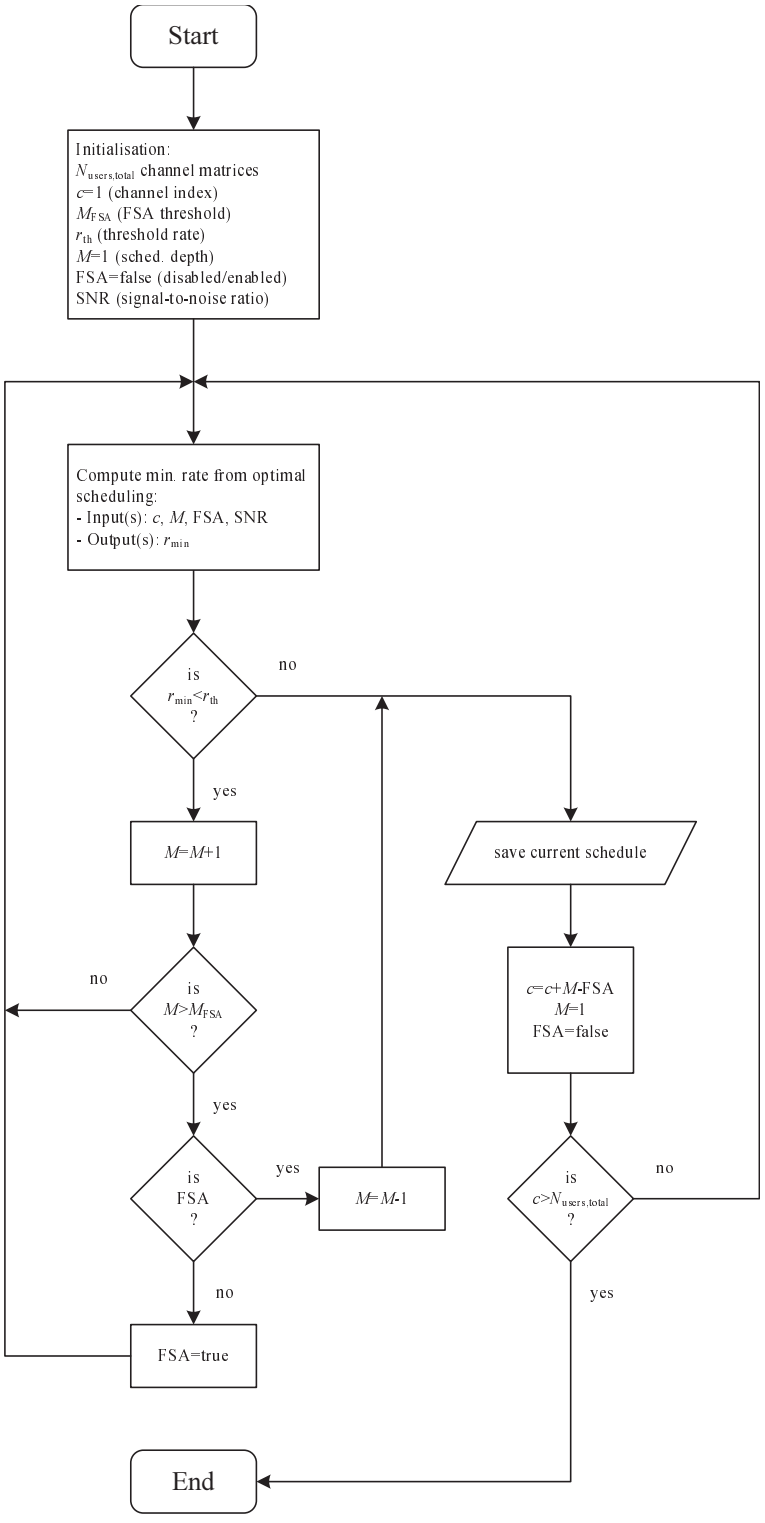


Figure 5.5. *Principle of the Smart Free Slot Assignment Scheduling Algorithm.*

5.2.3 Performance Analysis

As in Section 5.1 the signal-to-noise ratio (SNR) is fixed at 15 dB such that the communication remains mainly interference-limited; the results are obtained considering thousands of channel matrices. The algorithm needs two inputs parameters which are the rate constraint r_{th} and the FSA threshold M_{FSA}. The values of these two parameters are issued from the results obtained in Section 5.1, more particularly for an outage probability $p_{r_{\text{th}},M} \simeq 0.1$, with M varying between 2 and 4. For instance with $M = 3$ this probability is reached with $r_{\text{th}} \simeq 3.3$ bits/s/Hz (please refer to Fig. 5.3, left). The frequency at which a free slot has to be assigned to the users can be estimated as follows:

$$f_{\text{FSA}} = p_{r_{\text{th}},M} \times \frac{1}{M_{\text{FSA}}} \tag{5.10}$$

It has to be remarked that (5.10) assumes that the outage happens once per schedule (i.e. only over one slot) and this is not necessarily the case in reality. However it permits to give an idea about the FSA utilisation and therefore about the loss in efficiency.

Results

Table 5.1 and Table 5.2 show the performance without the proposed algorithm (benchmark) and with the proposed algorithm, respectively. "Slots without sched." gives the percentage of slots for which scheduling was not necessary (i.e. $M = 1$). "Slots with $M = x$" and "Slots availability" indicate respectively the percentage of slots for which the scheduling size is $M = x$ and the percentage of slots for which r_{th} could be guaranteed. Finally the "Efficiency" relates to the loss of resources due to FSA.

Table 5.1. *Scheduling performance without FSA.*

M [users per beam]	2	3	4
Service rate req. r_{th} [bits/s/Hz]	3	3.3	3.41
Slots with $M = 2$ [%]	100.0	-	-
Slots with $M = 3$ [%]	-	100.0	-
Slots with $M = 4$ [%]	-	-	100.0
Slots availability [%]	91.08	89.63	90.11
Efficiency [%]	100.0	100.0	100.0

Table 5.2. *Scheduling performance with FSA.*

M_{FSA} [users per beam]	2	3	4
Service rate req. r_{th} [bits/s/Hz]	3	3.3	3.41
Slots without sched. [%]	56.46	34.04	25.18
Slots with $M = 2$ [%]	30.44	29.24	23.80
Slots with $M = 3$ [%]	13.10[1]	20.85	21.18
Slots with $M = 4$ [%]	-	15.87[1]	14.92
Slots with $M = 5$ [%]	-	-	14.92[1]
Slots availability [%]	99.46	98.89	99.20
Efficiency [%]	93.85	94.98	96.40

[1] *also equivalent to the percentage of slots in which FSA is used.*

When analysing the different values provided by Table 5.2 one can immediately remark the aptitude of the algorithm to detect when lower scheduling depths are sufficient and even if no scheduling at all is enough. Consequently the complexity and the related computation time are dramatically reduced while optimising the user schedules and also trying to guarantee the rate constraint. What is also remarkable is the possibility to reach higher rate constraints by increasing the FSA threshold M_{FSA} keeping the loss in efficiency almost identical.

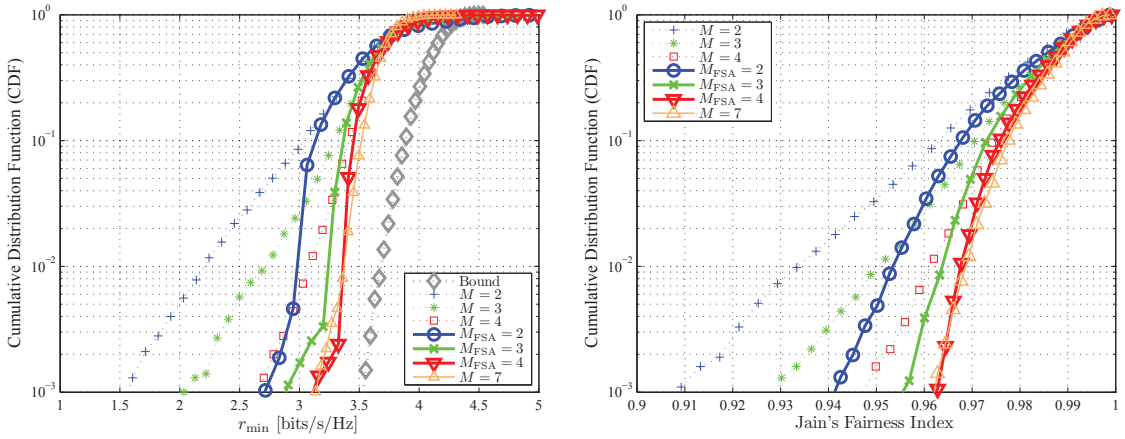


Figure 5.6. *Impact of FSA on the minimum per-user rates (left) and on the Jain's fairness index (right).*

Fig. 5.6 shows the corresponding CDFs of the minimum per-user rates (left) and of the fairness between users (right). The impact of the FSA algorithm is the expected one since it improves the minimum per-user rates and also, consequently, the fairness. It has to be noted that the proposed algorithm is even able to perform as well as scheduling without FSA and with larger scheduling depth ($M = 7$ shows almost identical performance than $M_{\mathrm{FSA}} = 4$).

Using the FSA algorithm allows to increase the fairness from about 82% without scheduling and optimal ordering (please refer to Fig. 5.3, right) to more than 96% with $M_{\mathrm{FSA}} = 4$.

Complexity Analysis

As specified previously the purpose while designing the FSA algorithm is to respect a given rate constraint, to minimise the efficiency loss, but also to reduce as much as possible the complexity of the scheduling optimisation. The complexity of the proposed FSA algorithm cannot be predicted easily since the scheduling depth M varies dynamically. Moreover the utilisation of one additional free slot is directly related to the rate constraint r_{th} and also to the level of CCI in the system.

We have seen in Section 4.4.2 that the complexity of a schedule, with the so-called "Geo-like" algorithm, and once scaled to a slot basis, is proportional to:

$$\alpha_M = M^4 \, (C-1) \, \frac{1}{M} = 2\, M^3 \tag{5.11}$$

since in this performance analysis the number of beams B equals 7 and the number of fictitious colours C equals 3. The average complexity of a schedule with the proposed FSA algorithm is proportional to:

$$\alpha_{M_{\mathrm{FSA}}} = \sum_{i=1}^{M_{\mathrm{FSA}}} \frac{f_i}{i} \sum_{j=1}^{i} 2\, j^4 + \frac{f_{M_{\mathrm{FSA}}+1}}{M_{\mathrm{FSA}}} \sum_{j=1}^{M_{\mathrm{FSA}}+1} 2\, j^4 \tag{5.12}$$

where f_i represents the frequency at which slots with $M = i$ are used, therefore $f_{M_{\mathrm{FSA}}+1} = f_{\mathrm{FSA}}$. The left term in (5.12) corresponds to the complexity without the presence of an additional free slot, the inner sum is related to the tries which are performed while increasing M. The right term relates to the complexity when FSA is enabled.

It is expected that the gain in complexity reduction improves together with M_{FSA} since the probability of finding an intermediate $M \leq M_{\mathrm{FSA}}$ fulfilling the requirement increases. This expectation is verified with Table 5.3.

The results of Table 5.3 show that with $M_{\mathrm{FSA}} = M = 2$ the FSA algorithm is more complex (around 20%) than conventional scheduling since the utilisation of additional free slots increases dramatically the computations. This is actually the price to pay in order to satisfy the rate constraint. When increasing M_{FSA} to three, the loss in complexity becomes lower

Table 5.3. *Complexity analysis: proposed FSA algorithm vs no FSA.*

M or M_{FSA} [users per beam]	2	3	4
Service rate req. r_{th} [bits/s/Hz]	3	3.3	3.41
Gain wrt. no FSA [%]	-19.54	-5.05	7.95[1]

[1] 82.82% *gain with respect to* $M = 7$.

(around 5%) because the algorithm has the possibility to select lower values of M for optimising the schedules, i.e. such that $M < 3$. Finally once the FSA threshold is set to four there is no loss but a gain in terms of complexity (around 8%). It has to be remarked that since $M_{\text{FSA}} = 4$ reaches almost the same performance as $M = 7$, the complexity can be compared for these two values and the gain in complexity in such a case is almost equal to 83%, which is a considerable improvement.

5.3 Time Constraints

The whole scheduling concept presented until now is hereinafter regarded as being constrained by time. We remind the reader that the notion of time in the different scheduling processes was let in background on purpose. For this reason the order of the slots had no importance for instance, reducing immediately the complexity when looking at the number of possible allocations. In the following, time is seen as a constraint.

5.3.1 Time Concept with Scheduling

In the return-link of a multi-beam satellite system employing the DVB-RCS standard [DVB-RCS], and also its evolution, referred as the DVB-RCS2 standard [DVB-RCS2], the satellite terminals on ground send requests to the gateway in order to get some resources allocated. The gateway processes the different requests and attributes the resources accordingly. The latter operation is actually performed by the so-called Radio Resource Management (RRM) module which produces a Terminal Burst Time Plan (TBTP) (Terminal Burst Time Plan version 2 (TBTP2) in the case of DVB-RCS2), indicating, in a simplified way, when the satellite terminals can transmit their data (please refer to Section 4.1, more particularly to Fig. 4.2). Therefore the RRM can be seen as a scheduler taking care of allocating users in the best way, in our case so as to minimise the level of interference.

Taking into account the general concept described previously, we consider from now on the

index of the channel matrix as being related to the arrival time of the request in the gateway. The channel realisation with index i, noted $\boldsymbol{H}^{(i)}$, corresponds to a group of B users requesting for resources at the gateway at time index i. The time scale, more particularly the granularity of the time, is abstracted and can be seen as slotted for instance, where the time scale is driven by the slot size, i.e. the slot duration. As an example if we consider the first ten channel realisations, i.e. $\boldsymbol{H}^{(i)}$ with $1 \leq i \leq 10$, for performing scheduling, then there are $B \times 10$ requests for resources. The scheduler allocates the resources, trying to maximise the minimum per-user rate, as before, and can also take care of attributing slots to users so that their original position, i.e. defined by the index (i), does not differ too much from the new position, indicated by the new index $(i)'$. Actually, a user initially represented by a column vector of the channel matrix $\boldsymbol{H}^{(i)}$, is, after having optimised the schedules, a column vector of the channel matrix noted $\boldsymbol{H}^{(i)'}$. In our example if a user was initially in the channel realisation $\boldsymbol{H}^{(1)}$ and gets finally scheduled in $\boldsymbol{H}^{(10)'}$ (remind that scheduling consists into swapping the columns of different channel realisations), then this user will experience additional delay since it is scheduled in the "future". The contrary can happen, i.e. a user represented by a column vector in the channel matrix $\boldsymbol{H}^{(10)}$ may be scheduled in the new channel realisation $\boldsymbol{H}^{(1)'}$. In the latter case the user is somehow schedule in the "past". Scheduling can therefore be performed taking into account this criterion, which will impact the delay experienced by the users at higher layers.

We have seen in Section 5.1.2 that the scheduling depth, characterised by the parameter M, which is the number of users per beam considered for optimising the schedules, is of paramount importance in the scheduling performance. The higher M, the better the performance, knowing that for an increasing scheduling depth the gains tend to decrease and to saturate. Instead of selecting the next channel realisations available for optimising the schedule, for a given value M, we propose in the following algorithms to add more flexibility to the scheduler. On the one hand the first algorithm is briefly described since it is based on well-known mechanisms. It permits to understand the insight behind the notion of the so-called "window scheduling". On the other hand the focus is brought on the second algorithm, which is based on a novel approach and therefore is described more in details.

5.3.2 "Normal Window Scheduling Algorithm"

The "normal window scheduling algorithm" is based on the principle of the well-known sliding window algorithm which can be found in Transmission Control Protocol (TCP) for instance.

We apply the principle of the sliding window algorithm in order to optimise the schedules among the different channel realisations available.

Principle

We introduce the so-called "window size" which is represented by W_s. The window size influences the research depth, or search space, while trying to optimise the schedules. The parameter M is still considered and represents, as before, the scheduling depth, which is actually the number of users per beam considered by the scheduler for finding out the optimal (or sub-optimal) allocation. The purpose of the scheduler remains the same, i.e. maximising the minimum per-user rate and consequently improving the overall level of fairness between the users present in the multi-beam satellite system.

The "normal" window scheduling algorithm performs as follows. The scheduler points the first channel matrix available. The corresponding channel realisation is constrained by the algorithm to be part of the final schedule solution (allocation). According to the size of the window, driven by the parameter W_s, the scheduler computes all possible combinations of channel matrices, taking into account all channel realisations present in the current window and also the scheduling depth M, i.e. the number of channel matrices to be associated. The scheduler optimises the schedules for all channel combinations and selects the association of channels maximising the minimum per-user rate. The channel combination, i.e. the set of channel matrices, is saved and the index of the channel realisations is re-organised accordingly. The algorithm then slides the window towards the next channel realisation available and performs the same operations. The different steps described previously are repeated until all channel realisations are processed. Depending on the number of channel realisations available, the algorithm adapts automatically both window size and scheduling depth. The latter steps are actually necessary when reaching the total number of channel realisations N_ch.

Example

An example with $W_\mathrm{s} = 5$ and $M = 2$ is shown by Fig. 5.7. The algorithm points the first channel matrix available, i.e. $\boldsymbol{H}^{(1)}$, and computes all possible association of channels knowing the parameter M. The combination $\boldsymbol{H}^{(1)}$ with $\boldsymbol{H}^{(4)}$ maximises the minimum per-user rate and is selected. The indexes are re-organised and the window slides towards the next channel matrix available, more particularly $\boldsymbol{H}^{(2)}$. The window still contains W_s channel matrices

and the combination $\boldsymbol{H}^{(2)}$ with $\boldsymbol{H}^{(6)}$ is the best one satisfying the criterion. The process continues until all the channels available are processed. The result of the schedules is shown at the bottom of Fig. 5.7 for better understanding. As can be seen the principle of this algorithm is quite straightforward.

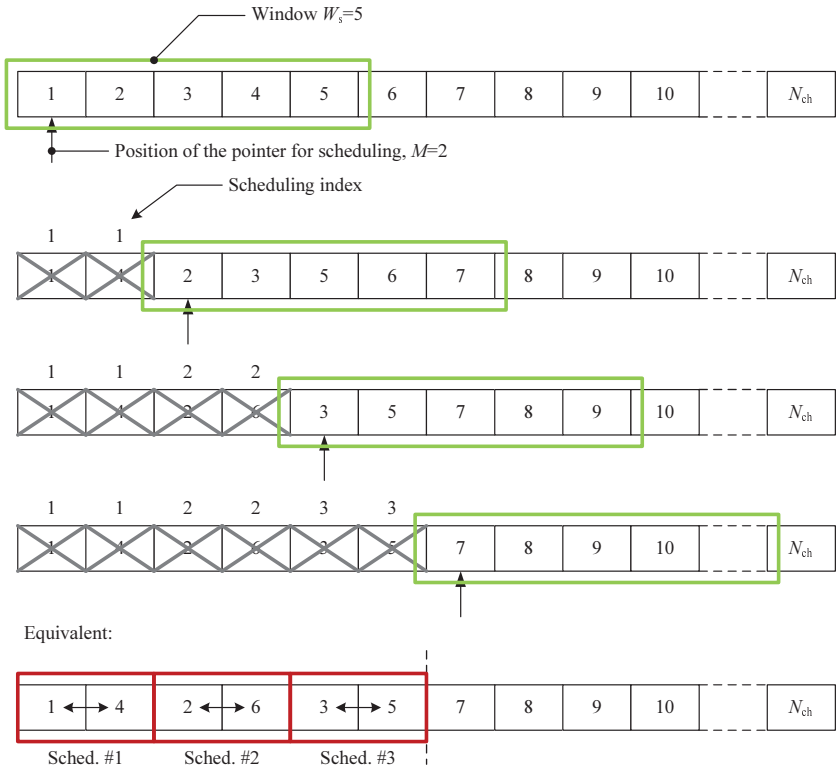


Figure 5.7. *Example with the "Normal Window Scheduling Algorithm".*

Impact of the Window Size

As seen previously, the scheduling depth M is relevant but the parameter of paramount importance in such algorithm is the window size, i.e. W_s. The window size needs to be at least equal or greater than the scheduling depth, i.e.:

$$W_s \geq M \tag{5.13}$$

If the window size equals the scheduling depth it is obvious that the window scheduling algorithm reduces to a "simple" scheduling algorithm, driven exclusively by the parameter M. It is also clear that the scheduling complexity scales with both parameters M and W_s. The window size actually influences the number of possible associations of channel realisations while optimising the schedules, as seen in the previous example (Fig. 5.7). The window size plays also an important role on the delay experienced by the users, as an outcome of the

schedule optimisation process.

A user initially present in the channel realisation $\boldsymbol{H}^{(i)}$ is scheduled, according to both scheduling depth M and window size W_s, in a new channel realisation $\boldsymbol{H}^{(i)'}$. As seen previously the new channel realisation, which index is related to time, is composed of B column vectors, representing the users, and which can be scheduled in advance or later, according to their initial position. For ease of notation we assume that a user arriving at time i is in fact scheduled at time i'. As mentioned previously users can be either in advance or later, depending wether $i' < i$ or $i' > i$ respectively. It is obvious that negative values of the expression $i' - i$ are not feasible in practice, but this gives information on the buffering needed to employ this scheduling algorithm. The new position i', is actually such that:

$$1 - W_\mathrm{s} \leq i' - i \leq (W_\mathrm{s} + 1 - M)\ (M - 1) \tag{5.14}$$

On the one hand the left extreme comes directly from a normal sliding window concept. On the other hand the right extreme is derived from the worst possible delay a user arriving at time i could experience. The latter corresponds to the fact the scheduling of that user is delayed as much as possible. This can actually happen $W_\mathrm{s} - M$ times, because after that the user becomes the first user in the window and is therefore forced to be scheduled. The original position of such user is $i = W_\mathrm{s} - M + 1$ and the algorithm has performed $W_\mathrm{s} - M$ steps since the beginning. Now, at the $(W_\mathrm{s} - M + 1)$-th step this user is scheduled and the worst that can happen is that this user is scheduled as last one, i.e. at the M-th position of the schedule. All together it means that $i' = (W_\mathrm{s} - M)\, M + M$, since M users have been scheduled in each of the previous $W_\mathrm{s} - M$ steps. This results in the worst-case $i' - i$ given by (5.14).

5.3.3 "Advanced Window Scheduling Algorithm"

As mentioned previously the window scheduling algorithm is introduced so that to add more flexibility to the scheduler while trying to optimise the allocations. The algorithm described in this section is referred as "Advanced Window Scheduling Algorithm" [2] and is a refinement of the algorithm described in the previous section (Section 5.3.2). The principle of the algorithm is presented hereafter.

2. A patent was submitted by the author in Germany for this algorithm, this patent will also be submitted at the European level.

Example

To better understand the principle of the advanced window scheduling algorithm, we first consider an example in which the window size is set to $W_s = 5$ and the scheduling depth to $M = 2$. The algorithm starts with the first channel realisation available, i.e. $\boldsymbol{H}^{(1)}$, and tries the different schedules taking into account the scheduling depth but also the window size. Therefore the algorithm finds the optimal schedules for all possible channel realisations present in the window, i.e. $\boldsymbol{H}^{(1)}$ with $\boldsymbol{H}^{(2)}$, $\boldsymbol{H}^{(1)}$ with $\boldsymbol{H}^{(3)}$, $\boldsymbol{H}^{(1)}$ with $\boldsymbol{H}^{(4)}$ and finally $\boldsymbol{H}^{(1)}$ with $\boldsymbol{H}^{(5)}$. $\boldsymbol{H}^{(6)}$ is not taken into account since it is not part of the current window (this channel realisation is on the outside of the window). Among the possible combinations of channel realisations, the association $\boldsymbol{H}^{(1)}$ with $\boldsymbol{H}^{(4)}$ gives the best result for instance. These two matrices are thus combined and marked as belonging to the scheduling index 1. The algorithm selects the next channel realisation available, i.e. points to $\boldsymbol{H}^{(2)}$ since the latter was not selected in the previous operation. Therefore the window "slides" of one channel index on the right. The same principle is applied, still taking into account the two parameters $W_s = 5$ and $M = 2$, and going through the remaining channel realisations available. Therefore the algorithm optimises the schedules for $\boldsymbol{H}^{(2)}$ with $\boldsymbol{H}^{(3)}$, $\boldsymbol{H}^{(2)}$ with $\boldsymbol{H}^{(5)}$ and $\boldsymbol{H}^{(2)}$ with $\boldsymbol{H}^{(6)}$. This time the association $\boldsymbol{H}^{(2)}$ with $\boldsymbol{H}^{(6)}$ offers the best results and these two channel realisations are marked with scheduling index 2. As before the algorithm slides the window until the next channel realisation available and continues. The different possibilities are $\boldsymbol{H}^{(3)}$ with $\boldsymbol{H}^{(5)}$ and $\boldsymbol{H}^{(3)}$ with $\boldsymbol{H}^{(7)}$. $\boldsymbol{H}^{(3)}$ with $\boldsymbol{H}^{(5)}$ is selected, are marked as scheduling index 3 and the window now slides on the right to channel realisation $\boldsymbol{H}^{(7)}$. The algorithm continues until all channel realisations, i.e. all N_{ch} channel matrices, are processed. This example is depicted by Fig. 5.8 for better understanding.

As can be seen in Fig. 5.8, the output of the algorithm for the first six channel matrices is given at the bottom and is equivalent to having $\boldsymbol{H}^{(1)}$ associated with $\boldsymbol{H}^{(4)}$, $\boldsymbol{H}^{(2)}$ associated with $\boldsymbol{H}^{(6)}$ and $\boldsymbol{H}^{(3)}$ associated with $\boldsymbol{H}^{(5)}$. Each channel realisation contains B column vectors which represent the users initially requesting for resources at index (i). We still consider that the order of the slot within a schedule, and therefore for a given scheduling index, does not play a role in order to reduce the overall complexity. Anyway this consideration makes sense since the scheduling depth M is constrained for computational reasons. On the one hand, in this example one can see $\boldsymbol{H}^{(1)}$ associated with $\boldsymbol{H}^{(4)}$, therefore users initially positioned at channel realisation (1) can either stay at position $(1)'$ or be scheduled at position $(2)'$ instead. For these users the difference in terms of time constraint is not relevant. On the other hand,

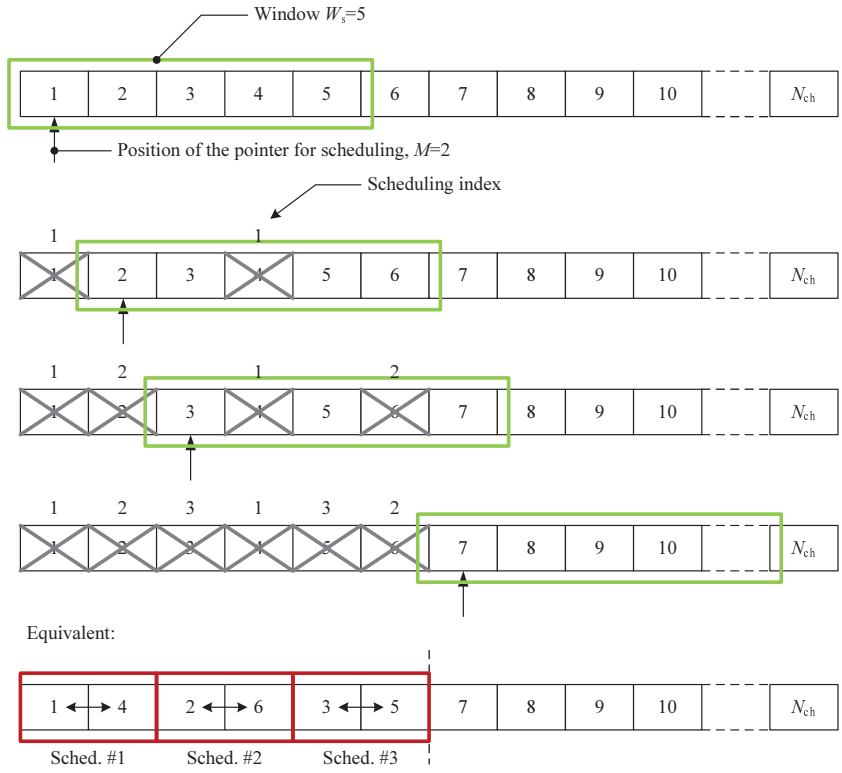


Figure 5.8. *Example with the "Advanced Window Scheduling Algorithm".*

the users belonging to channel realisation $\boldsymbol{H}^{(4)}$ are either scheduled at position $(1)'$ or $(2)'$ and experience therefore less delay since they are scheduled somehow in the "past".

Impact of the Window Size

Due to the modification of both window size and scheduling depth, directly related to the number of channels available, the new position, represented by i', is now such that:

$$1 - W_\mathrm{s} \leq i' - i \leq W_\mathrm{s} - 1 \tag{5.15}$$

As can be seen, when comparing (5.14) with (5.15), this algorithm is designed in such a way it tries to minimise the delay experienced by the users once they get scheduled. The principle resides in the way the channel realisations are associated and the way the window slides towards the next channel realisation available. We remind that the scheduling depth is adapted automatically by the advanced window scheduling algorithm since the amount of channels available in the window may be smaller than M.

Principle

Fig. 5.9 summarises the principle of the algorithm. The channel index to which the left side of the window points is noted c and is such that $1 \leq c \leq N_\mathrm{ch}$. As seen the scheduling depth

adapts dynamically according to the number of channel matrices available in the window and is referred as M'. This scheduling depth is such that:

$$1 \leq M' \leq M \tag{5.16}$$

The number of possible channel combinations also evolves, as seen in the example of Section 5.3.3, while the algorithm operates and this number, noted $N_{\text{ch,comb}}$, is such that:

$$1 \leq N_{\text{ch,comb}} \leq N_{\text{ch,comb,max}} \tag{5.17}$$

where $N_{\text{ch,comb,max}}$ represents the maximum number of channel combinations and which depends directly on both the scheduling depth M and the window size W_{s}:

$$N_{\text{ch,comb,max}} = \frac{(W_{\text{s}}-1)!}{((W_{\text{s}}-1)-(M-1))!}\frac{1}{(M-1)!} = \begin{pmatrix} W_{\text{s}}-1 \\ M-1 \end{pmatrix} \tag{5.18}$$

The two terms "-1" in (5.18) accounts for the fact the algorithm points a given channel matrix when sliding the window and this channel matrix is part of the final combination of channels. Expression (5.18) is the well-known number of possible combinations of n number of elements to select from and in which k elements are chosen, therefore $n = W_{\text{s}} - 1$ and $k = M - 1$.

The number of possible channel combinations $N_{\text{ch,comb}}$ depends on both the number of channel available in the window, noted $N_{\text{ch,avail}}$, and of the scheduling depth M':

$$N_{\text{ch,comb}} = \begin{pmatrix} N_{\text{ch,avail}}-1 \\ M'-1 \end{pmatrix} \tag{5.19}$$

knowing that the number of channels available $N_{\text{ch,avail}}$ influences directly the scheduling depth M'. More particularly as long as $N_{\text{ch,avail}}$ is smaller than M', the scheduling depth has to be reduced, i.e. $M' = M' - 1$.

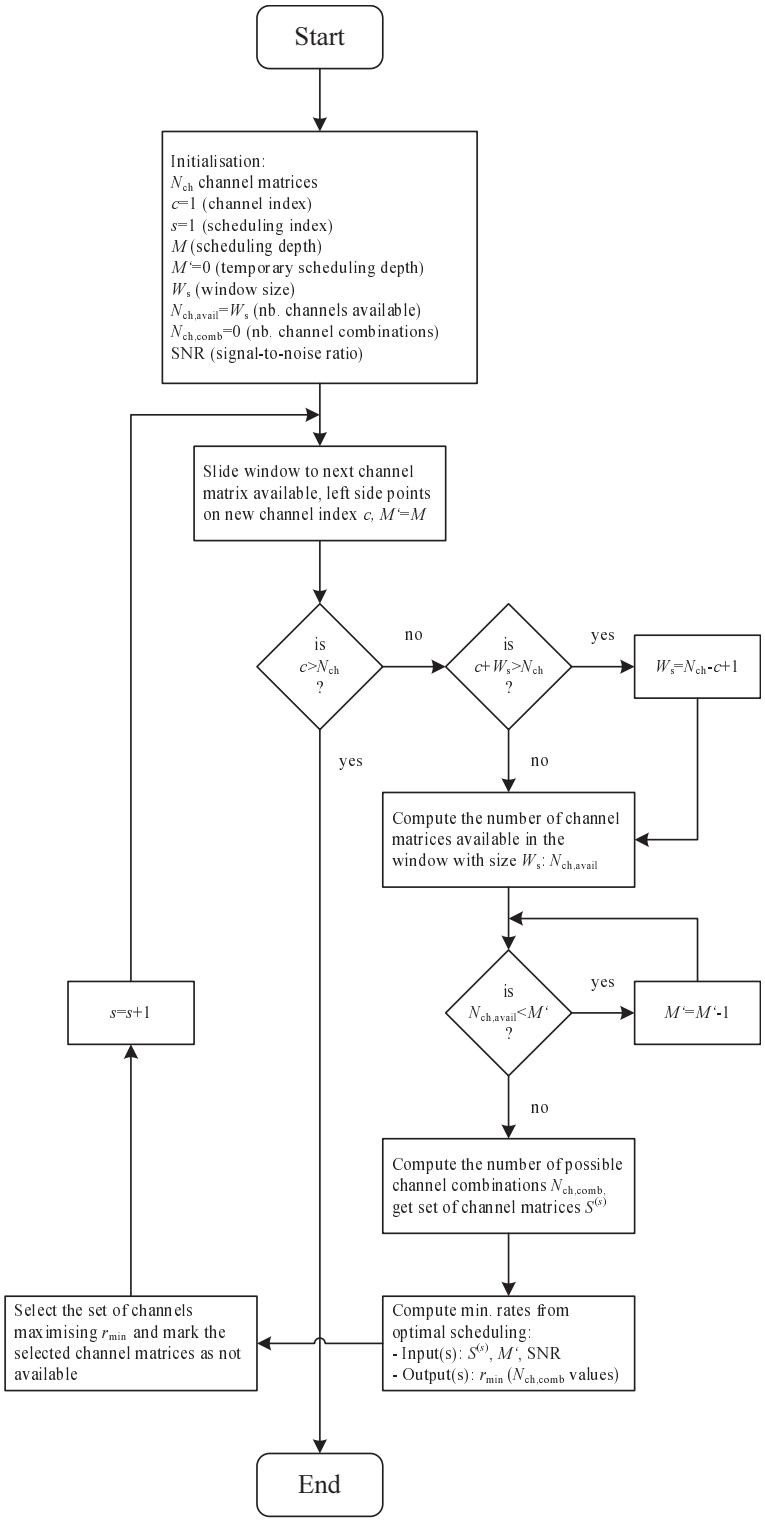


Figure 5.9. *Principle of the "Advanced" Window Scheduling Algorithm.*

Finally the scheduling index is defined by s and permits to differentiate the sets of channel matrices, noted $S^{(s)}$, and which contain the possible combinations of channels. With the

previous example (Fig. 5.8) it means that:

$$S^{(1)} = \left\{ < \boldsymbol{H}^{(1)}, \boldsymbol{H}^{(2)} >, < \boldsymbol{H}^{(1)}, \boldsymbol{H}^{(3)} >, < \boldsymbol{H}^{(1)}, \boldsymbol{H}^{(4)} >, < \boldsymbol{H}^{(1)}, \boldsymbol{H}^{(5)} > \right\}$$

where $< \boldsymbol{H}^{(1)}, \boldsymbol{H}^{(2)} >$ corresponds, in this chapter, to the association of the channel matrices $\boldsymbol{H}^{(1)}$ and $\boldsymbol{H}^{(2)}$ for optimising the schedule. Once the schedule is optimised for each possible association of channel matrices, i.e. for each possible combinations of matrices, we obtain $N_{\text{ch,comb}}$ different minimum per-user rates. The principle is to select the combination maximising the minimum per-user rates and to mark the selected channel matrices as not available for the next scheduling rounds. We note $S^{(s)'}$ the final set of channel matrices corresponding to the scheduling index s. As before with the previous example (Fig. 5.8), we obtain:

$$S^{(1)'} = \left\{ < \boldsymbol{H}^{(1)}, \boldsymbol{H}^{(4)} > \right\}$$

One can understand the complexity of the advanced window scheduling algorithm cannot be foreseen since the scheduling depth and also the number of channel matrices available for optimising the schedules change dynamically. The complexity therefore depends on the parameter M' and on the number of channel combinations $N_{\text{ch,comb}}$. We have seen in Section 4.4.2 and Section 5.2.3 that the complexity of a schedule, with the so-called "Geo-like" algorithm and scaled to a slot basis, is proportional to:

$$\alpha_M = M^4 \, (C-1) \, \frac{1}{M} = 2\, M^3$$

since we have seven beams ($B = 7$) and three fictitious colours ($C = 3$) in the next performance analysis. The complexity of the proposed algorithm is therefore proportional to:

$$\alpha_{M,W_s} = \sum_{i=1}^{M} \sum_{j=1}^{N_{\text{ch,comb,max}}} \frac{f_{i,j}}{i} \, j \, 2 \, i^4 = \sum_{i=1}^{M} \sum_{j=1}^{N_{\text{ch,comb,max}}} f_{i,j} \, j \, 2 \, i^3 \tag{5.20}$$

where the left sum accounts for the variation of the scheduling depth M', the second sum to the number of possible combinations of channels $N_{\text{ch,comb}}$, j for the number of times the scheduling algorithm is run and $f_{i,j}$ represents the frequency at which slots with $M' = i$ and $N_{\text{ch,comb}} = j$ are used. It has to be remarked that with the design of the algorithm the scheduling depth M' adapts itself according to the number of channels available, more particularly it is designed such that $M' = N_{\text{ch,avail}}$ as soon as $M' < M$. Therefore the number of possible channel combinations for smaller scheduling depths than the one initially defined is such that:

$$N_{\text{ch,comb}} = \begin{pmatrix} N_{\text{ch,avail}} - 1 \\ M' - 1 \end{pmatrix} = \begin{pmatrix} M' - 1 \\ M' - 1 \end{pmatrix} = 1 \qquad \text{s.t. } M' < M \tag{5.21}$$

5.3.4 Performance Analysis

Still using the same principle as in Section 5.1 and Section 5.2, the SNR is fixed at 15 dB such that the communication is mainly interference-limited, and the results are issued from thousands of channel matrices. The window scheduling algorithms require two inputs parameters which are the scheduling depth M and the window size W_{s}.

Results

The purpose is to compare the performance of the normal scheduler, i.e. the one not implementing the window scheduling concept, with the two window scheduling algorithms. To this aim we set the scheduling depth to $M = 3$ for realising normal scheduling, and then the combinations $M = 2$ / $W_{\mathrm{s}} = 4$ and $M = 3$ / $W_{\mathrm{s}} = 6$ for both normal and advanced window scheduling algorithms (as seen the window size is such that $W_{\mathrm{s}} = 2\,M$). The performance is measured based on the Cumulative Density Function (CDF) of the minimum achievable per-user rates and of the Jain's fairness index, as introduced in Section 5.2.3.

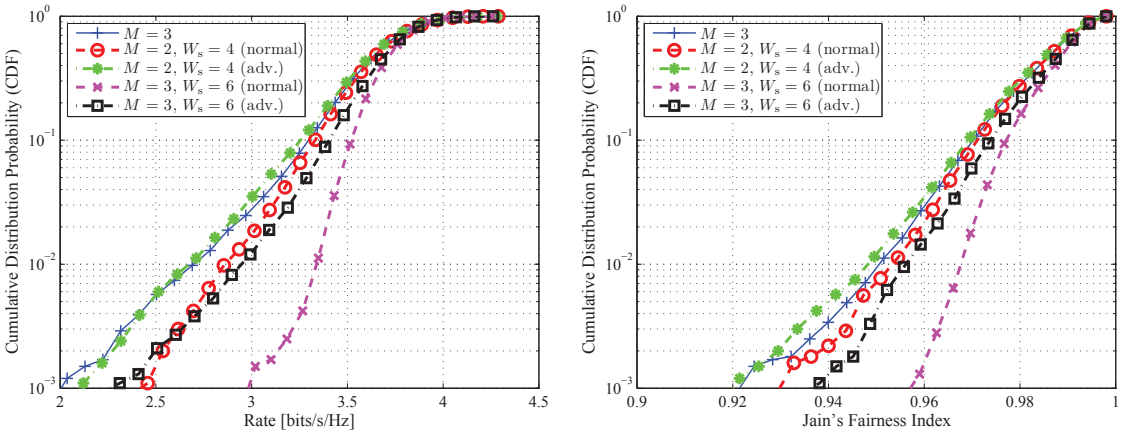


Figure 5.10. *Impact of the window scheduling algorithms on the minimum per-user rates (left) and on the Jain's fairness index (right).*

Both CDFs show that the window scheduling algorithms improve the performance (Fig. 5.10). As expected the normal window scheduling algorithm performs better since the window size W_{s} does not evolve over time (actually only when the number of channel realisations available N_{ch} is reached), therefore the scheduler has more freedom for combining different channel matrices. The advanced window scheduling algorithm with the parameters $M = 2$ / $W_{\mathrm{s}} = 4$ offers almost identical results as the normal scheduler with $M = 3$. Finally using the advanced scheduling algorithm with $M = 3$ and $W_{\mathrm{s}} = 6$ permits to obtain some gain when comparing

the normal window scheduling algorithm with lower scheduling depth and window size.

What is more interesting when using such algorithms is to look at the maximum time drift a user can experience. For the normal scheduling algorithm the maximum time drift is given by (5.14). The advanced window scheduling algorithm was designed in such a way the maximum time drift gets reduced (5.15).

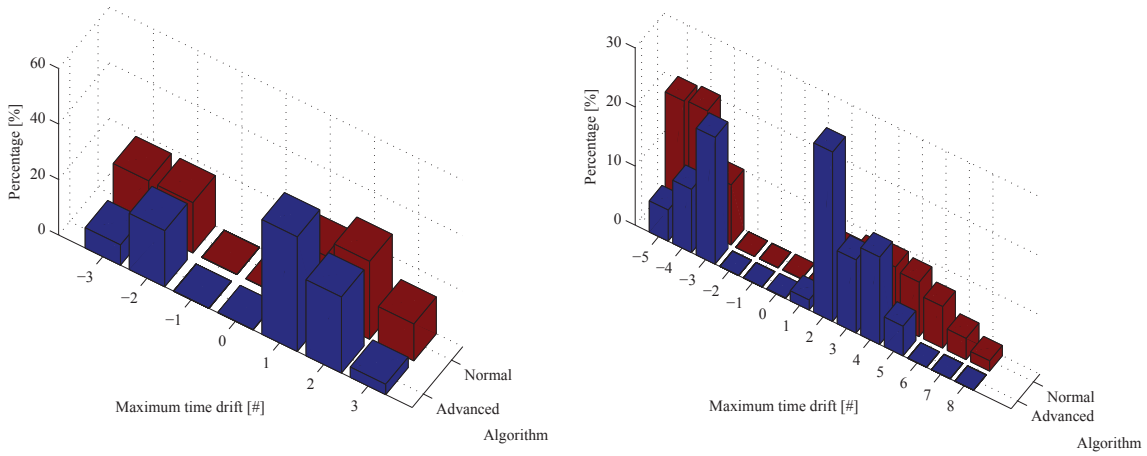


Figure 5.11. *Impact of the window scheduling algorithms on the maximum time drifts for* $M = 2$ *and* $W_s = 4$ *(left) and* $M = 3$ *and* $W_s = 6$ *(right).*

The two graphs shown by Fig. 5.11 give the percentage reached for each possible maximum time drift which are in the "past" (negative values) or in the "future" (positive values). The advanced window scheduling algorithm reduces the range of the maximum time drift, depending on both scheduling depth and window size values (on the right for instance) in the future and also permits to concentrate the maximum time drift around zero, i.e. the initial position.

Complexity Analysis

The complexity of the different algorithms is analysed using expression (5.20). On the one hand, using the normal window scheduling algorithm with $M = 2$ and $W_\mathrm{s} = 4$ permits to reduce the complexity of about 11% when compared to the conventional scheduling algorithm with $M = 3$. Providing almost identical performance (Fig. 5.10), the advanced window scheduling algorithm, with the same values, permits to reduce this complexity of about 30%. On the other hand, for higher values of scheduling depth and window size, more particularly $M = 3$ and $W_\mathrm{s} = 6$, the complexity is undoubtedly increased when compared to the normal scheduling algorithm with the same scheduling depth. Therefore the complexity becomes ten

times higher with these latter values and using the normal window scheduling algorithm and five times higher using the advanced window scheduling algorithm. In this case the advanced window scheduling algorithm reduces the complexity by two when compared to the normal window scheduling algorithm.

5.4 Rate and Time Constraints

In Section 5.2 was introduced the so-called "Smart Free Slot Assignment Scheduling Algorithm" which permits to fix a rate constraint to the scheduler and to optimise the resources in such a way the minimum achievable per-user rates are improved, the level of fairness is increased between the users and also the complexity of the scheduling is lowered. In Section 5.3 an algorithm based on a sliding window and named "Advanced Window Scheduling Algorithm" was described. This algorithm helps again at improving the minimum achievable per-user rates, the fairness and the complexity, taking into account constraints based on time. The purpose in this section is to combine the two algorithms, and to create an hybrid algorithm called "Window FSA Scheduling Algorithm".

5.4.1 Principle of the Hybrid Algorithm

The principle is actually the combination of each algorithm described respectively in Section 5.2.2 and in Section 5.3.3. Therefore the overall principle remains the same, the algorithm is now driven by the rate constraint r_{th}, by the Free Slot Assignment (FSA) threshold M_{FSA} and by the window size W_{s}. It is expected, combining the two algorithms, to increase the overall scheduling performance.

5.4.2 Performance Analysis

As in the two previous sections, the SNR is fixed at 15 dB such that the communication remains mainly interference-limited and the different results are issued from thousands of channel matrices. The window FSA scheduling algorithms require three inputs parameters which are the FSA threshold M_{FSA}, the window size W_{s}, and the rate constraint r_{th}. The values selected for evaluating the performance are issued from Section 5.2, directly, and the window size is set so that $W_{\mathrm{s}} = 2\,M$.

When comparing the results given by Table 5.4 with the ones of Table 5.2, the percentage of free slot assignment is dramatically reduced and therefore the overall efficiency is improved.

Table 5.4. *Scheduling performance with window FSA.*

M_{FSA} [users per beam]	2	3	4
Window size W_{s} [#]	4	6	8
Service rate req. r_{th} [bits/s/Hz]	3	3.3	3.41
Slots without sched. [%]	52.50	29.53	20.22
Slots with $M = 2$ [%]	44.28	59.94	63.86
Slots with $M = 3$ [%]	3.22[1]	7.47	11.88
Slots with $M = 4$ [%]	-	3.06[1]	1.60
Slots with $M = 5$ [%]	-	-	2.44[1]
Slots availability [%]	99.98	99.97	99.89
Efficiency [%]	98.42	98.99	99.39

[1] *also equivalent to the percentage of slots in which FSA is used.*

Moreover the slot availability gets higher, meaning that the rate constraint can be more easily satisfied. Finally the percentage of slots using a scheduling depth $M = 2$ is much more important and therefore, as seen in Section 5.3.4, the overall complexity should be reduced.

Without considering the complexity added by the window mechanism, the gains in terms of complexity are given by Table 5.5 for the different values taken into account. It has to be remarked that the analysis of the complexity when involving the operations realised by the window scheduling algorithm itself, cannot be realised practically.

Table 5.5. *Complexity analysis of the proposed window FSA scheduling algorithm versus conventional scheduling without FSA.*

M or M_{FSA} [users per beam]	2	3	4
Service rate req. r_{th} [bits/s/Hz]	3	3.3	3.41
Gain wrt. no FSA [%]	26.67	57.63	73.60[1]

[1] 95.07% *gain with respect to* $M = 7$.

Fig. 5.12 shows the improvement of the minimum achievable per-user rates (left) and the Jain's fairness index (right) when mixing both rate and time constraints algorithms. The increase of the slot availability can be observed in both curves which present a stronger water fall effect than the ones of Fig. 5.6.

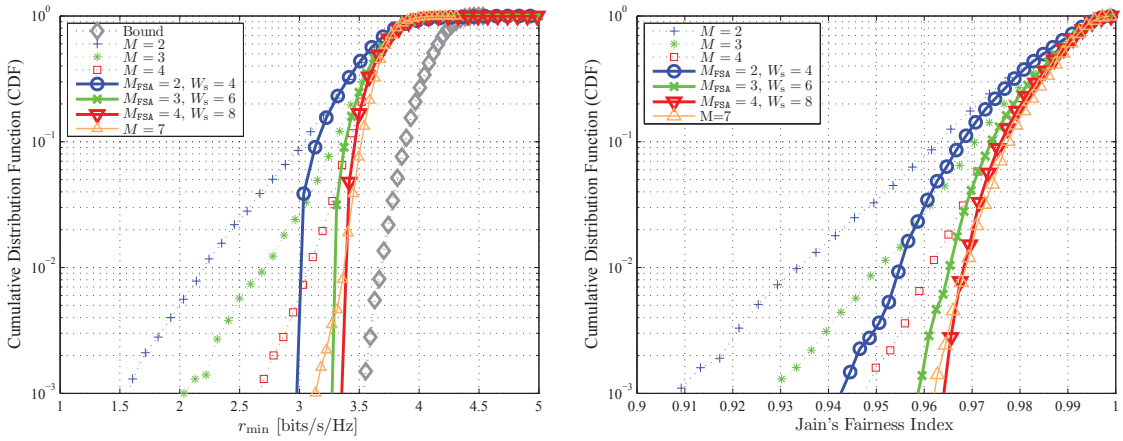


Figure 5.12. *Impact of the window FSA scheduling algorithm on the minimum per-user rates (left) and on the Jain's fairness index (right).*

Finally Fig. 5.13 illustrates the maximum time drifts obtained with the mixture of the two algorithms. The scenario corresponds to the configuration parameters taken into account for performing the simulations, i.e. the set M_{FSA} - W_{s} - r_{th}. The same behaviour as in Section 5.3 can be observed, i.e. the advanced window scheduling algorithm permits to concentrate the maximum time drifts around the initial position.

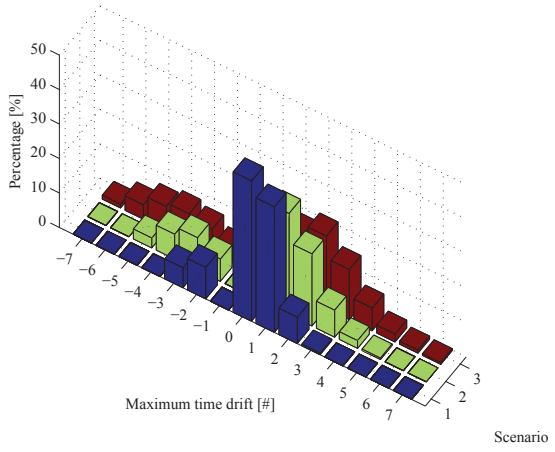


Figure 5.13. *Impact of the window FSA scheduling algorithm on the maximum time drift.*

5.5 Summary

The MIMO capacity achieving architecture, with optimal Successive Interference Cancellation (SIC) ordering, has been assumed to quantify the impact of the scheduling size while maximising the minimum per-user rate. On the one hand, the level of co-channel interference increased with the system size, as expected, and the gain of multiple receiving antennas balanced the decrease of performance. On the other hand, while increasing the number of

users per schedule, a convergence to the upper-bound and a saturation of the performance have been observed. With the users population uniformly distributed into the spot beams, a reduced scheduling depth permits to reach close to optimal performance in terms of minimum per-user rates but also in terms of fairness.

The different simulations have shown that the Free Slot Assignment (FSA) algorithm proposed for satisfying rate constraints, and consisting in allocating one additional free slot as a last solution for reducing the overall level of interference, permits to achieve good performance at different levels. First of all it is designed to improve the minimum achievable per-user rates and therefore increases the level of fairness between users. The value of the threshold activating the utilisation of an additional free slot plays a role on the complexity of the algorithm and even permits to outperform conventional scheduling algorithms. The gains in performance are achieved at the cost of a small waste of system capacity, which the algorithm tries in any case to minimise.

A Window scheduling algorithm permits to offer to the scheduler more freedom for selecting the channel matrices and therefore helps improving the minimum achievable per-user rates and also the fairness between users. Depending on the time constraints fixed at higher layers the scheduler can adapt the so-called window size W_{s} and also the scheduling depth M. A state-of-the-art Window scheduling algorithm has shown an improvement in both performance and complexity when compared to a conventional scheduling algorithm. A novel algorithm based on this approach and named "Advanced Window Scheduling Algorithm" permits to reduce even more the complexity and also to better control the maximum time drift a user can experience at higher layers.

As expected, the merging of the two algorithms helps providing huge improvements when considering both rate and time constraints. On the one hand, the so-called "Smart FSA Scheduling Algorithm" permits guaranteing requirements in terms of minimum per-user rates by trying reducing the scheduling depth and consequently the scheduling complexity. Moreover, as already mentioned, this algorithm also limits the loss of efficiency when the insertion of additional resources is needed. On the other hand, the so-called "Advanced Window Scheduling Algorithm" allows increasing the search space when optimising the schedules, taking into account the time drift involved by this mechanism and trying to keep it as small as possible. The hybrid algorithm takes benefits of each algorithm and is able to satisfy in most cases the required QoS constraints.

Chapter 6

Conclusions

This Ph.D. thesis investigated the improvements which can be realised in the return-link of interference-limited multi-beam satellite systems, by means of some cross-layer optimisations, going from the physical layer to higher layers. The overall concept is based on the fact that multi-beam satellite systems can be seen as virtual Multiple-Input and Multiple-Output (MIMO) systems, more particularly the return-link can be seen as a MIMO Multiple Access Channel (MAC). Hence, joint processing techniques at the reception side, i.e. the gateway, can be implemented so as to suppress the interference.

The work presented in this thesis is based on a specific and realistic satellite system scenario. More particularly it focuses on a multi-beam satellite system with transparent payload and star network topology covering Europe with ninety six spotbeams, but it can be extended to any other scenarios. It is known from information theory that the capacity available in the satellite system increases as the number of colours, also called frequency reuse factor or cluster size, decreases, and this because of the bandwidth available per beam. For this reason employing full frequency reuse permits in principle to enhance the throughput. However in practice the Co-Channel Interference (CCI) limits the system and turns it into a highly interference-limited network. The purpose was thus to assess the gains reachable with a full frequency reuse scheme when compared to schemes employing higher number of colours.

The impact of the satellite channel on state-of-the art receivers, including Multi-User Detection (MUD) receivers performing Successive Interference Cancellation (SIC), is addressed by analysing the uncoded Bit Error Rate (BER). As expected the satellite channel differs completely from the well-known Rayleigh channel which is commonly used to describe trans-

missions in a multi-path environment such as terrestrial networks. A receiver, based on a novel proposal for realising Interference Cancellation (IC), shows promising results with the Rayleigh channel but unfortunately turns out to be not suited for satellite channels with high interference levels. Receivers integrating an optimal SIC architecture, more particularly performing Minimum Mean Square Error (MMSE) with optimal ordering, allow reaching in theory the best results: this is verified and confirmed through simulations, also with the satellite channel. The gain factors in terms of uncoded throughput range from 1.5 to 2.25 for different modulation orders when comparing full frequency reuse with a three colours satellite beam pattern, when assuming perfect Channel State Information (CSI) at the receiver.

Based on the outcome issued from the previous practical analysis, the gain in terms of system capacity is investigated by moving towards information theory. More particularly the achievable sum rates are expressed for Single-Input and Single-Output (SISO), Single-Input and Multiple-Output (SIMO) and Multiple-Input and Multiple-Output (MIMO) systems, taking into consideration the number of colours. In such a case universal frequency reuse multiplies the ergodic capacity by a factor 3 when confronted to a three colours scheme. The principle of Successive Interference Cancellation (SIC) is then used in order to derive the achievable per-user rates and the impact of the ordering present in the Interference Cancellation (IC) process is studied. In this thesis the maximisation of the minimum (max-min) achievable per-user rates is especially considered, leading, due to the MIMO sum rate invariance to the ordering, to an improvement of the level of fairness between users. The best ordering for reaching this max-min criterion can be found using the Foschini algorithm and in the satellite scenario gains are in the order of 30% w.r.t. unordered SIC.

Considering a Multi-Frequency Time-Division Multiple Access (MF-TDMA) scheme, the resource management is optimised so as to improve the per-user rates. This is achieved by modifying the scheduling plans so that users interfering more significantly to each other do not transmit data on the same frequency at the same time. It is shown that scheduling does not impact on the sum rate obtained over the whole schedule but allows modifying the per-user rates in each slot. Search algorithms are proposed and implemented in this thesis. A first proposal considers all possible number of user schedules, which constitutes a pure Exhaustive Search (ES). A second proposal identifies all possible number of user combinations in each slot. For the latter search, graph theory is used, more particularly, a B-partite Graph (BG) approach is adopted in order to better represent the user schedules and also to reduce the

overall computational complexity, still targeting the so-called max-min criterion previously defined. Scheduling algorithms are then designed to deal with very large MIMO systems such as in multi-beam satellite communications. A particular algorithm, taking advantage of the multi-beam satellite pattern, performs as well as a pure exhaustive search but with a dramatically reduced complexity. When considering the full multi-beam satellite system, which consists of ninety six beams, this algorithm improves the minimum single user rates by 25% with respect to schemes without scheduling. The impact of the optimised scheduling plans, obtained using information theory, is then analysed for uncoded BERs. At BER 10^{-4} scheduling offered between 4 and 7 dB gain when compared to no scheduling and depending on the ordering operation realised by the SIC receivers.

Using all results obtained so far, scheduling taking into account different Quality of Service (QoS) constraints, in terms of service rate, fairness and delay, is investigated. First the impact of the number of spot beams and the number of users on the scheduling performance is studied, representing the system size and the scheduling depth, respectively. Interestingly, but logically, the minimum achievable per-user rates get worse as the system size increases but the tendency diminishes while reaching a given number of spot beams, mainly due to the gains offered by the multiple receive antennas. Also increasing the number of users per beam considered for optimising the schedules allows to improve the minimum user rates but the gain saturates at some point, due to the sufficient number of users available to find appropriate scheduling plans. Guided by the previous observations, a novel scheduling algorithm aiming at guaranteeing a max-min rate requirement to the users is designed. This algorithm exploits the resources available in the satellite and permits, through a Free Slot Assignment (FSA) strategy, to achieve the same performance as the previous algorithm, but with reduced scheduling depth. More particularly it allows fulfilling some rate requirement at the price of a small loss in efficiency. Another novel algorithm, based on the window sliding concept, is proposed in order to take into account time constraints, more particularly the delay introduced by the scheduling process. It permits to increase the search space of the scheduler for achieving the optimisations while avoiding important time drifts between the requests for resources and the allocation of resources. This algorithm results in an improvement of the max-min criterion for smaller scheduler depth but at the expense of higher computational complexity. Finally a combination of the two novel algorithms is presented. This hybrid algorithm contributes in better meeting the max-min rate requirement, keeping the efficiency loss and the scheduling depth under control, and achieving close to optimal performance.

The different investigations carried out in the framework of this Ph.D. thesis are based on strong hypotheses since the aim was to evaluate what are the maximum theoretical gains achievable in the return-link while considering multi-beam satellite systems as MIMO systems and while optimising the allocation of resources. We have shown that it is worth the effort using universal frequency reuse and complex scheduling for large scale systems. We first considered clear-sky conditions, perfect line-of-sight and static terminals with identical properties. We then assumed that all satellite terminals are perfectly synchronised so that MIMO receivers can be taken into account. Finally a perfect knowledge of the channel state information and one single virtual gateway were presumed. In reality the gains will be clearly lower due to practical implementation issues, all related to these different assumptions. The channel matrix will not reflect the real channel states even if it was shown that only the absolute values of the coefficients need to be retrieved for optimising the schedules. A multi-beam satellite system is generally composed of several gateways which implies in practice an exchange of information, especially of both channel state information and user data, so that to enable cooperation. This cooperation is in fact mandatory to first schedule efficiently the different users and second to suppress correctly the interference. These ideal assumptions were needed to derive a deep understanding of such a virtual MIMO satellite system and insights on the gains achievable through scheduling.

As previously mentioned, a perfect knowledge of the Channel State Information (CSI), more particularly of the absolute values of the channel coefficients at the receiver side was assumed. This implies in practice the implementation of mechanisms to estimate the current channel state, which can be done for example through the transmission of known training sequences. In reality the CSI will be imperfect, leading to an error while computing the achievable per-user rates and therefore first while trying to optimise the schedules and second while cancelling interference. Imperfect CSI can actually be seen in different ways; for instance it can be related to the channel conditions which are influenced by the atmosphere (rain, clouds, etc.). This imperfect knowledge can also be turned into an advantage, as future work, in order to refine the scheduling algorithms presented in this thesis and design new scheduling algorithms which are based on areas of uncertainties. The area covered by a beam can be subdivided into sub-areas in which the same channel state information is assumed and in which users can be therefore grouped since they are considered as having the same channel. This strategy involves an error in the channel state information and taking this error into account, a scheduling algorithm, based on set of users, can be designed and should reduce even more the computational complexity.

Bibliography

[ABCCGD11] J. Arnau, M. Bergmann, E. .A. Candevra, G. E. Corazza, R. de Gaudenzi, B. Devillers, W. Gappmair, F. Lombardo, C. Mosquera, A. Pérez-Neira, I. Thibault, and A. Vanelli-Coralli, "Hybrid Space-Ground Processing for High-Capacity Multi-beam Satellite Systems", in *GLOBECOM*, Houston (Texas, USA), Dec. 2011.

[ADMN12] J. Arnau, B. Devillers, C. Mosquera, and A. Pérez-Neira, "Performance study of multiuser interference mitigation schemes for hybrid broadband mulibeam satellite architectures", in *EURASIP Journal on Wireless Communications and Networking*, 132, 2012.

[AjHa05] W. Ajib, and D. Haccoun, "An overview of scheduling algorithms in MIMO-based fourth-generation wireless systems", in *IEEE Network*, vol. 19, no. 5, pp. 43-48, Sep. 2005.

[AlMaTu10] G. Alfano, A. De Maio, and A. M. Tulino, "A Theoretical Framework for LMS MIMO Communication Systems Performance Analysis", in *IEEE Transactions on Information Theory*, vol. 56, no. 11, pp. 5614-5630, Nov. 2010.

[ALBPCG11] P.-D. Arapoglou, K. Liolis, M. Bertinelli, A. Panagopoulos, P. Cottis, and R. De Gaudenzi, "MIMO over Satellite: A Review", in *IEEE Communications Surveys and Tutorials*, vol. 13, no. 1, pp. 27-51, 2011.

[Bab52] W. C. Babock, "Intermodulation Interference in Radio Systems", in *The Bell System Technical Journal*, pp. 63-73, Aug. 1952.

[BaCaZo08] N. Baldo, P. Casari, and M. Zorzi, "Cognitive spectrum access for underwater acoustic communications", in *IEEE ICC*, Beijing (China), May 2008.

[BaMeLe03] J. R. Barry, D. G. Messerschmitt, and E. A. Lee, "Digital Communication", *Third Edition*, Springer, 2003.

[BBKNL07] H. Brandt, V. Boussemart, C. Kissling, C. Parraga Niebla, O. L ucke, R. Vilalta, E. Dupont, R. Schweikert, and T. W orz, "Resources Management using Adaptive Fade

Mitigation Techniques in DVB-S2/RCS Multi-Beam Systems", in *ICSSC*, Seoul (South Korea), Apr. 2007.

[BBRJ11] V. Boussemart, M. Berioli, F. Rossetto, and M. Joham, "On the Achievable Rates for the Return-Link of Multi-Beam Satellite Systems Using Successive Interference Cancellation", in *IEEE MILCOM*, Baltimore (MD, USA), Nov. 2011.

[BeCh02] N. Benvenuto, and G. Cherubini, "Algorithms for Communications Systems and their Applications", *First Edition*, Wiley, 2002.

[BeGaKa02] B. F. Beidas, H. El Gamal, and S. Kay, "Iterative Interference Cancellation for High Spectral Efficiency Satellite Communications", in *IEEE Transactions on Communications*, vol. 50, no. 1, pp. 31-36, Jan. 2002.

[BoBeRo11] V. Boussemart, M. Berioli, and F. Rossetto, "User Scheduling for Large Multibeam Satellite MIMO Systems", in *ASILOMAR*, Pacific Grove (CA, USA), Nov. 2011.

[BoBr08] V. Boussemart, and H. Brandt, "A Tool for Satellite Communications", in *IWSPSC*, Rhodes Island (Greece), Oct. 2008.

[BoBr09-1] V. Boussemart, and H. Brandt, "Performance Assessment using ACM in DVB-S2/Advanced DVB-RCS Satellite Systems", in *ICSSC*, Edinburgh (UK), June 2009.

[BoBr09-2] V. Boussemart, and H. Brandt, "A System Simulator for Advanced DVB-S2/RCS Multibeam Systems", in *DLRK*, Aachen (Germany), Sep. 2009.

[BoGr05] V. Boussemart, and O. Grémillet, "Investigation on the Self-Similarity of Web Traffic Generated by Aggregated Individual Browsers", in *ICSSC*, Rome (Italy), Sep. 2005.

[BoMaBe12-1] V. Boussemart, L. Marini, and M. Berioli, "Impact of Scheduling in the Return-Link of Multi-Beam Satellite MIMO Systems", in *GLOBECOM*, Anaheim (CA, USA), Dec. 2012.

[BoMaBe12-2] V. Boussemart, L. Marini, and M. Berioli, "Multi-Beam Satellite MIMO Systems: BER Analysis of Interference Cancellation and Scheduling", in *ASMS*, Baiona (Spain), Sep. 2012.

[Bou05] V. Boussemart, "Investigations on Internet Traffic", *Technological Research Diplom Report* for the Diplôme de Recherche Technologique (D.R.T.), DLR Munich (Germany) and University of Valenciennes (France) - Ecole National Supérieure d'Ingénieurs en Informatique Automatique Mécanique énergétique Electronique (ENSIAME), Dec. 2005.

[CCFRV92] C. Caini, G. E. Corazza, G. Falciasecca, M. Ruggieri and F. Vatalaro: "A Spectrum- and Power-Efficient EHF Mobile Satellite System to be integrated with Ter-

restrial Cellular Systems", in *IEEE Journal on Selected Areas in Communications*, vol. 10, no. 8, pp. 1315-1325, 1992.

[CCMO11] D. Christopoulos, S. Chatzinotas, M. Matthaiou, and B. Ottersten, "Capacity Analysis of Multibeam Joint Decoding over Composite Satellite Channels", in *ASILOMAR*, Pacific Grove (CA, USA), Nov. 2011.

[CeGa10] F. Di Cecca, and G. Gallinaro, "Cross-Polar Interference Cancellation for Earth Observation Data Downlink", in *Ka and Broadband Communications, Navigation and Earth Observation Conference*, Ka-band conf., Milan (Italy), Oct. 2010.

[ChChOt11] S. Chatzinotas, D. Christopoulos, and B. Ottersten, "Coordinated Multi-Point Decoding with Dual-polarized Antennas", in the proceedings of *IEEE IWCMC*, pp. 157-161, 2011.

[Clar45] A. C. Clarke, "Extraterrestrial Relays", in *Wireless World* magazine, 1945.

[Col85] R. E. Collin, "Antennas and Radiowave Propagation", *International Student Edition*, 1985.

[CoLeRi90] T. H. Cormen, C. E. Leiserson, and R. L. Rivest, "Introduction to Algorithms", *MIT Press*, Cambridge (MA, USA), 1990.

[Cou06] N. Courville, "Critical Issues of Resource Management in Geostationnary Satellite Systems with On-Board Switching", *Ph.D. Report*, DLR Munich (Germany) and SUPAERO Toulouse (France), Oct. 2006.

[DCMLC07] M. À. Díaz, N. Courville, C. Mosquera, G. Liva, and G. E. Corazza, "Non-Linear Interference Mitigation for Broadband Multimedia Satellite Systems", in *IWSSC*, Salzburg (Austria), pp. 61-65, Sep. 2007.

[DGMRV06] M. Debbah, G. Gallinaro, R. M uller, R. Rinaldo, and A. Vernucci, "Interference Mitigation for the Reverse-Link of Interactive Satellite Networks", in *IWSPSC*, Noordwjik (Netherlands), Sep. 2006.

[DVB-RCS] Digital Video Broadcasting (DVB): "Interaction channel for satellite distribution systems", in *ETSI EN 301 790 V1.5.1*, European Standard (Telecommunication series), Jan. 2009.

[DVB-RCS2] Digital Video Broadcasting (DVB): "Second Generation DVB Interactive Satellite System; Part Lower Layers for Satellite standard", in *DVB Document A155-2*, European Standard (Telecommunication series), Mar. 2011.

[DVB-RCS2-P1] Digital Video Broadcasting (DVB): "Second Generation DVB Interactive Satellite System (RCS2); Part 1: Overview and System Level specification", in *DVB Document A155-1*, European Standard (Telecommunication series), Mar. 2011.

[DVB-S] Digital Video Broadcasting (DVB), "Framing structure, channel coding and modulation for 11/12 GHz satellite services", in *ETSI EN 300 421 V1.1.2*, European Standard (Telecommunication series), Aug. 1997.

[DVB-S2] Digital Video Broadcasting (DVB): "Second generation framing structure, channel coding and modulation systems for broadcasting, interactive services, new gathering and other broadband satellite applications", in *ETSI EN 302 307 V1.1.2*, European Standard (Telecommunications series), June 2006.

[ESA-RM] ESA Project: "Resources Management using Adaptive Fade Mitigation Techniques (FMT) in DVB-RCS Multi-Beam Systems", *Contract 18826/05/NL/US*, Jan. 2005 to Dec. 2008.

[FGVW99] G. J. Foschini, G. D. Golden, R. A. Valenzuela, and P. W. Wolniansky, "Simplified Processing for High Spectral Efficiency Wireless Communication Employing Multi-Element Arrays", in *IEEE Journal on Selected Areas in Communications*, vol. 17, no. 11, pp. 1841-1852, Nov. 1999.

[GaVeRi07] G. Gallinaro, A. Vernucci, and R. Rinaldo, "Increasing Throughput of Wideband Satellite Systems Reverse-Link through Adjacent Channel Interference Mitigation", in *ICSSC*, Seoul (Korea), Apr. 2007.

[Gay09] J.-D. Gayrard, "Terabit Satellite: Myth or Reality", in *SPACOMM*, Colmar (France), July 2009.

[GJJV03] A. Goldsmith, S. A. Jafar, N. Jindal, and S. Vishwanath, "Capacity limits of MIMO channels, in *IEEE Journal on Selected Areas in Communications*, vol. 21, no. 5, pp. 684-702, June 2003.

[HeJoUt10] C. Hellings, M. Joham, and W. Utschick, "Power Minimization in Parallel Vector Broadcast Channels with Zero-Forcing Beamforming", in *GLOBECOM*, Miami (USA), Dec. 2010.

[HSBAG06] C. Antón-Haro, P. Svedman, M. Bengtsson, A. Alexiou, and A. Gameiro, "Cross-Layer Scheduling for Multi-User MIMO Systems", in *IEEE Communications Magazine*, pp. 39-45, Sep. 2006.

[JaHaCh84] R. Jain, W. Hawe, and D. Chiu, "A quantitative measure of fairness and discrimination for resource allocation in shared computer systems", *Digital Equipment Corporation*, Tech. Rep. DEC-TR-301, Sep. 1984.

[JiVaLi05] Y. Jiang, M. K. Varanasi, and J. Li, "Performance Analysis of ZF and MMSE Equalizers for MIMO Systems: An In-Depth Study of the High SNR Regime", in *GLOBECOM*, St. Louis (MO, USA), Nov. 2005.

[KaViHa05] T. Kailath, H. Vikalo, and B. Hassibi, "MIMO Receive Algorithms", in *Space-Time Wireless Systems: From Array Processing to MIMO Communications*, Cambridge University Press, 2005.

[LeGr08] N. Letzepis, and A. Grant, "Capacity of the multiple spot beam satellite channel with rician fading", in *IEEE Transactions on Information Theory*, vol. 54, no. 11, pp. 5210-5222, Nov. 2008.

[LiPaAr09] K. P. Liolis, A. D. Panagopoulos, and P.-D. M. Arapoglou, "An analytical unifying approach for outage capacity achieved in SIMO and MISO broadband satellite channel configurations", in the proceedings of *EuCAP*, pp. 2911-2915, Mar. 2009.

[LPCR09] K. P. Liolis, A. D. Panagopoulos, P. G. Cottis and B. D. Rao, "On the applicability of MIMO principle to 10-66 GHz BFWA networks: capacity enhancement through spatial multiplexing and interference reduction through selection diversity", in *IEEE Transactions on Communications*, vol. 57, no. 2, pp. 530-541, Feb. 2009.

[LuWeJa00] E. Lutz, M. Werner, and A. Jahn, "Satellite Systems for Personal and Broadband Communications", *First Edition*, Springer-Verlag, 2000.

[MaBo02] G. Maral, and M. Bousquet, "Satellite Communications Systems", *Fourth Edition*, Wiley, 2002.

[Mar12] L. Marini, "Investigations on the Return-Link of Interference-Limited Multi-Beam Satellite Systems", *Master Thesis Report*, DLR Munich (Germany) and University of Rome (Italy) Tor Vergata, Apr. 2012.

[MBBD07] J. P. Millerioux, M. L. Boucheret, C. Bazile and A. Ducasse, "Iterative interference cancellation and channel estimation in multibeam satellite systems", in *International Journal of Satellite Communications and Networking*, Wiley, vol. 25, no. 3, pp. 263-283, Mar. 2007.

[MEGAAH11] D. Mignolo, R. Emiliano, A. Ginesi, A. B. Alamanac, P. Angeletti, and M. Harverson, "Approaching Terabit/s Satellite Capacity: A System Analysis", in *Ka Broadband Conference*, Oct. 2011.

[NISIM05] "Novel Intra-System Interference Mitigation Techniques & Technologies for Next Generations Broadband Satellite Systems", *Final report*, ESTEC Contract No. 18070/04/NL/US, 2005.

[Ogu83] T. Oguchi, "Electromagnetic Wave Propagation and Scattering in Rain and Other Hydrometeors", in the proceedings of the *IEEE*, vol. 71, no. 9, pp. 1029-1079, Sep. 1983.

[PoBeBa09] M. Poggioni, M. Berioli and P. Banelli, "BER Performance of Multibeam Satellite Systems with Tomlinson Harashima Precoding", in *ICC*, Dresden (Germany), June 2009.

[Pro00] J. Proakis, "Digital Communications", *Fourth Edition*, McGraw-Hill Science, 2000.

[RaLiTa98] F. Rashid-Farrokhi, K. J. R. Liu, and L. Tassiulas, "Transmit beamforming and power control for cellular wireless systems", in *IEEE Journal on Selected Areas in Communications*, vol. 16, no. 8, pp. 1437-1449, Oct. 1998.

[RyLi09] W. E. Ryan, and S. Lin, "Channel Codes - Classical and Modern", *First Edition*, Cambridge University Press, 2009.

[Sha49] C. E. Shannon, "Communication in the Presence of Noise", in the proceedings of the *Institute of Radio Engineers*, vol. 37, pp. 10-21, Jan. 1949.

[SSBHU09] D. A. Schmidt, C. Shi, R. A. Berry, M. L. Honig, and W. Utschick, "Distributed Resource Allocation Schemes", in *IEEE Signal Processing Magazine*, vol. 26, no. 5, pp. 53-63, Sep. 2009.

[Tel99] E. Telatar, "Capacity of multi-antenna gaussian channels", in *European Transactions on Telecommunications*, vol. 10, no. 6, pp. 585-596, 1999.

[TsVi08] D. Tse, and P. Viswanath, "Fundamentals of Wireless Communication", *Fourth printing edition*, University Press, Cambridge, 2008.

[VaGu97] M. K. Varanasi, and T. Guess, "Optimal decision feedback multiuser equalization with successive decoding achieves the total capacity of the gaussian multiple-access channel", in the proceedings of *ASILOMAR*, pp. 1405-1409, Nov. 1997.

[Vas00] H. Vasseur, "Degradation of Availability Performance in Dual-Polarized Satellite Communications Systems", in *IEEE Transactions on Communications*, vol. 48, no. 3, pp. 465-472, Mar. 2000.

[WuMi06] G. Wunder, and T. Michel, "Minimum Rates Scheduling for MIMO OFDM Broadcast Channels", in the proceedings of *IEEE International Symposium on Spread Spectrum Techniques and Applications*, Manaus (Brazil), Aug. 2006.

[YFVG11] T. Yoo, G. Foschini, R. Valenzuela, and A. Goldsmith, "Common rate support in multi-antenna downlink channels using semi-orthogonal user selection", in *IEEE Transactions on Information Theory*, vol. 57, no. 6, pp. 3449-3461, June 2011.

[YiLi02] H. Yin, and H. Liu, "Performance of Space-Division Multiple-Access (SDMA) with Scheduling", in *IEEE Transactions on Wireless Communincations*, vol. 3, no. 4, pp. 611-618, Oct. 2002.

[YoGo06] T. Yoo, and A. Goldsmith, "On the optimality of multiantenna broadcast scheduling using zero-forcing beamforming", in *IEEE Journal on Selected Areas in Communications*, vol. 24, no. 3, pp. 528-541, Mar. 2006.

[ZCO11-1] G. Zheng, S. Chatzinotas, and B. Ottersten, "Generic Optimization of Linear Precoding in Multibeam Satellite Systems", *CoRR*, vol. abs/1109.0681, 2011.

[ZCO11-2] G. Zheng, S. Chatzinotas, and B. Ottersten, "Multi-Gateway Cooperation in Multibeam Satellite Systems", *CoRR*, vol. abs/1111.7094, 2011.

List of Figures

1.1 Example of transparent star network topology in a satellite system. 3
1.2 Definition of the satellite links considered in this scenario. 3
1.3 Principle of frequency allocation in beams with cluster size three ($K = 3$, left) and cluster size four ($K = 4$, right). 4
1.4 Example of carrier organisation involving adjacent-channel interference. . . . 8
1.5 Principle of co-channel interference in the return-link. 9
1.6 Example of carrier organisation involving co-channel interference. 9
1.7 Principle of cross-polarisation interference when using linear polarisations. . . 10
1.8 Example of carrier organisation involving cross-polarisation interference. . . . 11
1.9 Small system scale for full frequency reuse ($K = 1$) and three colours ($K = 3$). For each colour the system is composed of seven beams ($B = 7$) which are directly adjacent when all beams use the same frequency (thin beam contours) and which are farther for three colours (thicker beam contours). Two users per beam are shown for universal frequency reuse: "bad users" (crosses) and "good users" (circles). 16
1.10 Full system size for three colours ($K = 3$, left) and four colours ($K = 4$, right). The system is composed of ninety six beams ($B = 96$) using three or four different frequencies. 17
1.11 Satellite system and example of beam radiation pattern. The footprints of the ninety six beams considered in the multi-beam satellite scenario are shown. The beam radiation pattern of one single beam is illustrated with the gain in decibels (dB). In this example the highlighted beam has the following centre coordinates: latitude 48.75° North and longitude 11.9° East (beam ID 33). . . 18
1.12 Basic transmission block diagram. 23

1.13 Basic input - output system with multiple transmitters and multiple receivers. 24
1.14 Input - output system with multiple transmitters and multiple receivers equipped with several antennas. 25
1.15 MIMO broadcast channel in a terrestrial system (left) and analogy with a satellite system (right). 26
1.16 MIMO multiple access channel in a terrestrial system (left) and analogy with a satellite system (right). 26
1.17 Multi-beam transmission block diagram. It is composed (from the left to the right) of the inter-beam interference block, satellite antenna feeds, satellite spotbeams, the noise block and the gateway. The number of satellite antenna feeds is generally equal or bigger to / than the number of spotbeams. 28

2.1 Typical input-output system for bit error rate simulations. 33
2.2 Receiver architecture with optimal SIC. 37
2.3 Receiver architecture integrating SIC with MRC. 40
2.4 Average BER performance of the receivers with a 7×7 Rayleigh channel and BPSK modulation. 41
2.5 BER of a simple 2×2 satellite system without interference and BPSK modulation. 43
2.6 Beam border and user location of a 2×2 system with high interference. . . . 43
2.7 BER performance in a 2×2 satellite system with high interference, no interference cancellation and BPSK modulation. 45
2.8 BER performance in a 2×2 satellite system with high interference, Zero Forcing, Successive Interference Cancellation and BPSK modulation. 46
2.9 BER performance in a 2×2 satellite system with high interference, Minimum Mean Square Error, Successive Interference Cancellation and BPSK modulation. 47
2.10 BER performance of the receivers in a 7×7 satellite system, full frequency reuse ($K = 1$), low interference scenario, BPSK modulation, and for the user located in beam 1. 48
2.11 BER performance of the receivers in a 7×7 satellite system, full frequency reuse ($K = 1$), high interference scenario, BPSK modulation, and for the user located in beam 1. 49
2.12 BER performance of the receivers in a 7×7 satellite system, full frequency reuse ($K = 1$), average interference scenario, BPSK and QPSK modulations, and for the user located in beam 1. 50

2.13 BER performance of the receivers in a 7×7 satellite system, three colours ($K = 3$), average interference scenario, BPSK and QPSK modulations, and for the user located in beam 1. 52

2.14 BER performance of the receivers in a 7×7 satellite system, with one and three colours ($K = 1$ and $K = 3$), average interference scenario, different modulations, and for the user located in beam 1. 53

3.1 Channel matrix seen by the first receiver in a SISO system. 56

3.2 2×1 SIMO system. 57

3.3 Channel matrix of transmitter 1 seen by the receivers in a SIMO system. . . 59

3.4 Typical IO system. 60

3.5 Average user rates for ninety six beams ($B = 96$), with full frequency reuse ($K = 1$) and three colours ($K = 3$), and issued from 10 000 random sets. . . . 65

3.6 MIMO SIC - Channel matrix seen by the last user (right) and the last but one user (left). 71

3.7 Example of the impact of the permutation on the single user rates (difference). 74

3.8 Performance of the ordering on the minimum user rates (left) and on the dispersion from the average sum rates (right) for seven beams ($B = 7$) with full frequency reuse ($K = 1$) and issued from 1 000 channel realisations. The minimum per-user rates are compared for different methods: average, brute force approach, Foschini algorithm and worst case. 82

3.9 Cumulative distribution functions of the achievable per-user rates (left) and of the Jain's fairness index (right) at SNR 15 dB and different input - output systems. 83

3.10 Cumulative distribution function of the achievable per-user rates (left) and of the Jain's fairness index (right) for different SNRs and multiple-input - multiple-output system. 85

3.11 Mean value of the Jain's fairness index for different SNRs and input - output systems. 85

4.1 Example of simple scheduling with 2 beams and 2 users per beam. 92

4.2 Scheduling process in a multi-beam satellite system with transparent payload and star network topology. 93

4.3 Impact of scheduling on the sum rate with the bad / good users in a 7×7 system. The sum rate over the two slots (left axis) and the standard deviation (right axis) are shown. 96

4.4 Behaviour of the product of determinants for the highest SNR and for all possible allocations when considering both high and low interference scenarios with seven beams ($B = 7$). 101

4.5 Approximations realised when performing scheduling and having two users per beam ($M = 2$). These approximations are computed when considering both high and low interference scenarios with seven beams ($B = 7$). 102

4.6 Variation of the sum rate (left) and dispersion of the logarithm for the highest SNR (right) when considering three users per beam ($B = 3$) and random channel realisations with seven beams ($B = 7$). 103

4.7 Evolution of $\Delta_{\boldsymbol{H}}$ (left) and of $\sigma^2_{\boldsymbol{H}}$ (right) according to the number of beams. 105

4.8 Terms definition in the multipartite graph approach. 107

4.9 Example of multipartite graph with three users per beam ($M = 3$) and three beams ($B = 3$). 108

4.10 Relation between allocation, multipartite graph and channel matrices with three users per beam ($M = 3$) and three beams ($B = 3$). 109

4.11 Example of maximum selection algorithm. In this example three users per beam ($M = 3$) and two beams ($B = 2$) are taken into account. 110

4.12 Example of minimum deletion algorithm. In this example three users per beam ($M = 3$) and two beams ($B = 2$) are taken into account. 111

4.13 Viterbi-like scheduling algorithm example with three users per beam ($M = 3$) and three beams ($B = 3$). 112

4.14 Geo-like scheduling principle with three users per beam ($M = 3$) and three virtual colours ($C = 3$). 114

4.15 Geo-like scheduling example with three users per beam ($M = 3$), three virtual colours ($C = 3$) and seven beams ($B = 7$). 115

4.16 Principle of the block basis evaluation. In this example there are two users per beam ($M = 2$) when performing scheduling. 116

4.17 Impact of the scheduling algorithms on the minimum per-user rate (left) and on the Jain's fairness index (right) for the bad and good cases with seven beams ($B = 7$). 118

4.18 Impact of the scheduling algorithms on the minimum per-user rate (left) and 1st percentile of the per-user rate (right) with seven beams ($B = 7$), three users per beam ($M = 3$) and $N_{\text{ch}} = 999$ channel realisations. 120
4.19 CDF of the Jain's index. The number of beams B is 7, the number of users per beam is $M = 3$ and the number of channel realisation $N_{\text{ch}} = 999$. 120
4.20 Minimum per-user rate. The number of beams B is 96, the number of users per beam is $M = 3$ and the number of channel realisation $N_{\text{ch}} = 24$. 121
4.21 Impact of ordering and scheduling on the average BER for the bad and good cases. "OO" stands for optimal ordering. 125
4.22 Impact of ordering and scheduling on the modified Jain's fairness index for the bad and good cases. "OO" stands for optimal ordering. 127

5.1 Multi-beam scenario considered for evaluating the impact of the system size and of the scheduling depth. The radiation of the beam in the middle is shown, together with the beam centres and the corresponding beam numbering. . . . 131
5.2 Impact of the number of beams on the minimum per-user rates (left) and on the Jain's fairness index (right). 132
5.3 Impact of the number of users per beam on the minimum per-user rates (left) and on the Jain's fairness index (right). 133
5.4 Impact of the scheduling depth M on the FSA performance with SNR 15 dB in terms of sum rate per slot (left) and gains and losses (right). 137
5.5 Principle of the Smart Free Slot Assignment Scheduling Algorithm. 139
5.6 Impact of FSA on the minimum per-user rates (left) and on the Jain's fairness index (right). 141
5.7 Example with the "Normal Window Scheduling Algorithm". 146
5.8 Example with the "Advanced Window Scheduling Algorithm". 149
5.9 Principle of the "Advanced" Window Scheduling Algorithm. 151
5.10 Impact of the window scheduling algorithms on the minimum per-user rates (left) and on the Jain's fairness index (right). 153
5.11 Impact of the window scheduling algorithms on the maximum time drifts for $M = 2$ and $W_{\text{s}} = 4$ (left) and $M = 3$ and $W_{\text{s}} = 6$ (right). 154
5.12 Impact of the window FSA scheduling algorithm on the minimum per-user rates (left) and on the Jain's fairness index (right). 157
5.13 Impact of the window FSA scheduling algorithm on the maximum time drift. 157

C.1 Representation of a point in the Cartesian coordinates system. 203
C.2 Value of z in the OZP plane. 203
C.3 Value of x and y in the OXY plane. 204
C.4 Position of the satellite in the geocentric coordinates system. 205
C.5 Rotation of the axis to point the satellite. 206
C.6 Position of the satellite in the coordinates system pointing the satellite. . . . 208
C.7 Satellite-centred coordinates system. 209
C.8 Satellite true view angles. 211
C.9 Coordinates of point P according to the satellite view angles. 211
C.10 Beam width. 216
C.11 Building a cone to determine the beam border (1). 217
C.12 Building a cone to determine the beam border (2). 218
C.13 Beam border example - building a cone. 219
C.14 Beam border example - final beam border. 219
C.15 Example of antenna pattern. 232
C.16 BPSK modulation. 235
C.17 QPSK modulation. 235
C.18 8-PSK modulation. 235
C.19 16-PSK modulation. 235
C.20 Example of noise generation for two different signal-to-noise ratios. 237
C.21 Example of noise PDFs for BPSK modulation. 239
C.22 Example of noise PDFs for QPSK modulation. 241
C.23 Example of symbol detection for 8-PSK modulation. 242
C.24 BER validation for both BPSK and QPSK modulations. 244
C.25 BER (left) and SER (right) validations for both 8-PSK and 16-PSK modulations. 244
C.26 System considered for filter design. 245
C.27 BER simulator. 250
C.28 Theoretical evaluations versus practical evaluations of the SER (left) and BER (right) for seven beams ($B = 7$), the high interference scenario (”bad” case) and QPSK modulation. 253
C.29 Theoretical evaluations versus practical evaluations of the SER (left) and BER (right) for seven beams ($B = 7$), the average interference scenario and QPSK modulation. 254

C.30 Theoretical evaluations versus practical evaluations of the BER for seven beams ($B = 7$), the high interference scenario ("bad" case), QPSK modulation, and when considering SIC. 255
C.31 Representation of the mutual information (example). 257
C.32 Constrained-capacity with a simple channel as a function of the energy per symbol (left) and energy per bit (right). 265
C.33 Constrained-capacity with a satellite channel consisting of seven beams ($B = 7$), with full frequency reuse ($K = 1$), average interference level and for the first user. 266
C.34 Minimum per-user rates (left) and Jain's fairness index (right) for the bad and good cases, with and without ordering in the scheduling process, and with seven beams ($B = 7$). 268
C.35 Summary of the different scheduling algorithms, including their dependencies. 273

List of Tables

1.1 Satellite terminal configurations for the return up-link budgets. 19
1.2 Satellite terminal bandwidths and rates for the return up-link budgets. 19
1.3 Satellite terminal return up-link budget values. 20
1.4 Satellite terminal return down-link budget values. 21
1.5 Satellite terminal total return link budget values. 21

2.1 Summary of the uncoded bit error rate performance between universal frequency reuse and three colours. 52

3.1 Gains on the achievable per-user rates with respect to the SISO system. . . . 84
3.2 Order in which the users are decoded in the multiple-input - multiple-output system. 87

4.1 Example of allocation with three beams ($B = 3$) and two users per beam ($M = 2$). 94
4.2 Possible allocations with three beams ($B = 3$) and two users per beam ($M = 2$). 95
4.3 Example of number of possible allocations. 106
4.4 Example of possible allocations with three beams ($B = 3$) and three users per beam ($M = 3$). 106
4.5 Optimal allocations between -8 and 8 dB (step of 2 dB) with seven beams ($B = 7$) and two users per beam ($M = 2$). 123
4.6 Optimal allocations between 10 and 24 dB (step of 2 dB) with seven beams ($B = 7$) and two users per beam ($M = 2$). 124
4.7 Most appearing allocation between -8 and 24 dB (step of 2 dB) with seven beams ($B = 7$) and two users per beam ($M = 2$), i.e. allocation index 15. . . 124

5.1 Scheduling performance without FSA. 140
5.2 Scheduling performance with FSA. 141
5.3 Complexity analysis: proposed FSA algorithm vs no FSA. 143
5.4 Scheduling performance with window FSA. 156
5.5 Complexity analysis of the proposed window FSA scheduling algorithm versus conventional scheduling without FSA. 156

C.1 Beam centre coordinates and frequency allocation for the 96 multi-beam satellite system (1 of 3). 221
C.2 Beam centre coordinates and frequency allocation for the 96 multi-beam satellite system (2 of 3). 222
C.3 Beam centre coordinates and frequency allocation for the 96 multi-beam satellite system (3 of 3). 223
C.4 Beam centre coordinates and frequency allocation for the seven multi-beam satellite system ($B = 7$) and full frequency reuse ($K = 1$). 224
C.5 Beam centre coordinates and frequency allocation for the seven multi-beam satellite system ($B = 7$) and three colours ($K = 3$). 224
C.6 Satellite terminal coordinates for the seven multi-beam satellite system ($B = 7$) and corresponding to the "bad" case. 225
C.7 Satellite terminal coordinates for the seven multi-beam satellite system ($B = 7$) and corresponding to the "good" case. 225
C.8 Allocation obtained with the "pure" exhaustive search with three beams ($B = 3$) and two users per beam ($M = 2$). 271
C.9 Allocation obtained with the multipartite graph approach with three beams ($B = 3$) and two users per beam ($M = 2$). 271
C.10 Sorted list of edges for the multipartite graph approach with three beams ($B = 3$) and two users per beam ($M = 2$). 272

Appendix A

Acronyms and Notations

A.1 Acronyms

ACI Adjacent-Channel Interference

ACM Adaptive Coding and Modulation

AVBDC Absolute Volume-Based Dynamic Capacity

AWGN Additive White Gaussian Noise

BC Broadcast Channel

BCH Bose, Chaudhuri, and Hocquenghem

BER Bit Error Rate

BG B-partite Graph

BPSK Binary Phase-Shift Keying

BS Base Station

CCI Co-Channel Interference

CCM Constant Coding and Modulation

CDF Cumulative Density Function

CIR Carrier-to-Interference Ratio

CNR Carrier-to-Noise Ratio

COIN Communications in Interference-Limited Networks

CPCI Cross-Polarisation Channel Interference

CRA Constant Rate Assignment

CSI Channel State Information

DL Down-Link

DLR Deutsches Zentrum für Luft- und Raumfahrt

DPC Dirty Paper Coding

DRA Dynamic Rate Assignment

DSL Digital Subscriber Line

DVB-RCS Digital Video Broadcasting - Return Channel via Satellite

DVB-RCS2 Digital Video Broadcasting - Return Channel via Satellite version 2

DVB-S Digital Video Broadcasting via Satellite

DVB-S2 Digital Video Broadcasting via Satellite version 2

D.R.T. Diplôme de Recherche Technologique

EIRP Effective Isotropic Radiated Power

ENSIAME Ecole National Supérieure d'Ingénieurs en Informatique Automatique Mécanique énergétique Electronique

ER Error Rate

ES Exhaustive Search

ETSI European Telecommunications Standards Institute

FDL Forward Down-Link

FDM Frequency-Division Multiplexing

FL Forward-Link

FMT Fade Mitigation Technique

FSA Free Slot Assignment

FSL Free Space Loss

FUL Forward Up-Link

GEO Geostationary

GL Geo-Like algorithm

HPA High-Power Amplifier

I In-phase

IBO Input Back-Off

IC Interference Cancellation

ID Identifier

IEEE Institute of Electrical and Electronics Engineers

IMI Inter-Modulation Interference

IO Input-Output

IQ In-phase and Quadrature

ISAE Institut Supérieur de l'Aéronautique et de l'Espace

ISI Inter-Symbol Interference

IT Information Theory

i.i.d. independent and identically distributed

LDPC Low Density Parity Check Code

LEO Low Earth Orbit

LNA Low-Noise Amplifier

LoS Line-of-Sight

MAC Multiple Access Channel

MEO Medium Earth Orbit

MF-TDMA Multi-Frequency Time-Division Multiple Access

MIMO Multiple-Input and Multiple-Output

MIMO BC MIMO Broadcast Channel

MIMO MAC MIMO Multiple Access Channel

MISO Multiple-Input and Single-Output

MMSE Minimum Mean Square Error

ModCod Modulation and Coding

MRC Maximal Ratio Combining

MUD Multi-User Detection

MUT Mobile User Terminal

NCC Network Control Centre

NF Noise Figure

OBO Output Back-Off

OO Optimal Ordering

PAM Pulse Amplitude Modulation

PDF Probability Density Function

PER Packet Error Rate

Ph.D. Philosophiae Doctor

PSK Phase-Shift Keying

Q Quadrature

QoS Quality of Service

QPSK Quadrature Phase-Shift Keying

RBDC Rate-Based Dynamic Capacity

RDL Return Down-Link

RL Return-Link

RRM Radio Resource Management

RTT Round-Trip-Time

RUL Return Up-Link

SER Symbol Error Rate

SIC Successive Interference Cancellation

SIMO Single-Input and Multiple-Output

SINR Signal-to-Interference-plus-Noise Ratio

SISO Single-Input and Single-Output

SNIR Signal-to-Noise plus Interference Ratio

SNR Signal-to-Noise Ratio

ST Satellite Terminal

SUPAERO école nationale SUPérieure de l'AEROnautique et de l'espace

TBTP Terminal Burst Time Plan

TBTP2 Terminal Burst Time Plan version 2

TCP Transmission Control Protocol

TDM Time-Division Multiplexing

THP Tomlinson-Harashima Precoding

TUM Technische Universität München

TWTA Travelling Wave Tube Amplifier

UPC Up-link Power Control

UL Up-Link

UT User Terminal

VBDC Volume-Based Dynamic Capacity

VL Viterbi-Like algorithm

XPI Cross-Polarisation Interference

ZF Zero Forcing

A.2 Notations

A.2.1 Scalars, Vectors and Matrices

- $\mathcal{N}\left(\mu, \sigma^2\right)$: Real Gaussian variable with mean value μ and variance σ^2
- $\mathcal{CN}\left(0, \sigma^2\right)$: Circularly symmetric complex Gaussian random variable with real and imaginary parts $\mathcal{N}\left(0, \sigma^2/2\right)$ (i.i.d.)
- Vectors and matrices are denoted by boldface lowercase and uppercase respectively (e.g. $\boldsymbol{a}$ and $\boldsymbol{A}$)
- Element i of vector $\boldsymbol{a}$: a_i
- Element at row i - column j of matrix $\boldsymbol{A}$: $a_{i,j}$
- i-th column vector of matrix $\boldsymbol{A}$: $\boldsymbol{a}_i$
- All rows, columns i to j of $\boldsymbol{A}$: $\boldsymbol{A}_{:,i:j}$

A.2.2 Operators

- $|a_{i,j}|$: Norm of $a_{i,j}$
- $\text{diag}\{a_1, a_2, \cdots, a_N\}$: Diagonal matrix with elements a_1, a_2, ..., a_N
- $\boldsymbol{A}^{\text{T}}$: Transpose of the matrix $\boldsymbol{A}$
- $\boldsymbol{A}^*$: Conjugate of the matrix $\boldsymbol{A}$
- $\boldsymbol{A}^{\text{H}}$: Hermitian of the matrix $\boldsymbol{A}$ (conjugate transpose)

A.2.3 List of Variables

- a: Amplitude of the wave in the vertical polarisation at the transmission
- $\boldsymbol{a}$: Vector of signal received by the satellite antenna feeds
- a_c: Amplitude of the wave in the vertical polarisation at the reception

– a_x: Amplitude of the wave in the unwanted vertical polarisation at the reception
– A_b: coverage area of a beam $\left[\mathrm{m}^2\right]$
– b: Amplitude of the wave in the horizontal polarisation at the transmission
– b_c: Amplitude of the wave in the horizontal polarisation at the reception
– b_x: Amplitude of the wave in the unwanted horizontal polarisation at the reception
– B: Number of beams [#]
– $\boldsymbol{B}$: Inter-beam interference matrix
– B_c: Number of beams belonging to colour c [#]
– B_i: Beam index i
– BER_i: Bit error rate experienced by user i
– c: Celerity - speed of light, $3\,10^8$ [m/s] or channel index [#]
– C: Carrier power [W] or number of colours [#]
– $\boldsymbol{C}$: Covariance matrix
– $c_{i,j}$: Carrier in beam i and with sub-carrier index j
– $c_{i,\mathrm{P},j}$: Carrier in beam i, with polarisation P and with sub-carrier index j
– D: Distance between beams using the same frequency [km]
– d_a: Diameter of the antenna [m]
– D_ant: Diameter of the antenna [m]
– E_b: Energy per bit [joules]
– $\boldsymbol{e}_j$: Standard basis vector with the j-th column of the identity matrix
– E_s: Energy per symbol [joules]
– f: Frequency [Hz]
– $\boldsymbol{F}$: Beamformer matrix
– f_D: Frequency used in the down-link [Hz]
– f_FSA: Frequency at which FSA is used
– f_i: Frequency index i or frequency at which slots with $M = i$ are used
– f_U: Frequency used in the up-link [Hz]
– G: Gain
– $\boldsymbol{G}$: Filter matrix
– $G_{i,j}$: Gain of beam i with respect to transmitter j
– G_max: Maximum gain
– $G_\mathrm{max,dB}$: Maximum gain [dB]
– $\boldsymbol{G}_\mathrm{MMSE}$: MMSE filter matrix
– $G_\mathrm{Rx,gtw}$: Receive gain at the gateway

– G_{sat}: Receive gain at the satellite
– $G_{\text{Tx,sat}}$: Antenna transmit gain of the satellite
– $G_{\text{Tx,t}}$: Antenna transmit gain of the terminal
– $\boldsymbol{G}_{\text{ZF}}$: ZF filter matrix
– $\boldsymbol{H}$: Channel matrix
– $\boldsymbol{I}$: Identity matrix
– J: Jain's fairness index
– J_{BER}: Modified Jain's fairness index for operating on the bit error rate
– J_i: Bessel function of the first kind and of order i
– K: Cluster size - number of colours - frequency reuse factor [#]
– $L_{\text{ant,gtw}}$: Losses at the gateway antenna
– $L_{\text{ant,sat}}$: Losses at the satellite antenna
– $L_{\text{ant,sat,lna}}$: Pre-low-noise amplifier input loss at the satellite
– L_{eff}: Loss of efficiency [%]
– L_{FS}: Free space losses
– L_{FS_j}: Free space losses of transmitter j
– $L_{\text{FS,min}}$: Minimum free space loss
– $L_{\text{OBO,sat}}$: Output back-off loss of the satellite
– $L_{\text{OBO,t}}$: Output back-off loss of the terminal
– $L_{\text{out,sat}}$: Output loss of the satellite
– $L_{\text{out,t}}$: Output loss of the terminal
– $L_{\text{pointing,sat}}$: Pointing loss of the satellite
– $L_{\text{pointing,t}}$: Pointing loss of the terminal
– M: Modulation order [#] or number of users per beam per schedule [#]
– M_{FSA}: FSA threshold in terms of number of users per beam per schedule [#]
– N: Total number of users [#] or noise power [W]
– N_0: Power spectral density of the Additive White Gaussian Noise
– N_{a}: Number of satellite antenna feeds [#]
– N_{alloc}: Number of allocations (schedules) [#]
– $N_{\text{alloc,empty\_slots}}$: Number of allocations (schedules) with empty slots [#]
– $N_{\text{alloc,FSA}}$: Number of allocations (schedules) with FSA [#]
– $N_{\text{alloc,FSA,with\_empty\_slots}}$: Number of allocations (schedules) with FSA and empty slots [#]
– N_{b}: Number of beams [#]
– N_{bits}: Number of bits per symbol [#]

- N_{blocks}: Number of blocks [#]
- N_{ch}: Number of channel realisations / channel matrices [#]
- $N_{\text{ch,avail}}$: Number of channels available [#]
- $N_{\text{ch,comb}}$: Number of channel combinations [#]
- $N_{\text{ch,comb,max}}$: Maximum number of channel combinations [#]
- N_{edges}: Number of edges [#]
- $N_{\text{eval,BG}}$: Number of evaluations with the B-partite graph approach [#]
- $N_{\text{eval,ES}}$: Number of evaluations with the exhaustive search [#]
- N_{paths}: Number of paths [#]
- N_{perm}: Number of permutations [#]
- N_{Rx}: Number of receive antenna [#]
- N_{sched}: Number of schedules [#]
- N_{Tx}: Number of transmit antenna [#]
- $N_{\text{users,sched}}$: Number of users per schedule [#]
- $N_{\text{users,total}}$: Total number of users [#]
- $\text{NF}_{\text{Rx,sat}}$: Noise figure at the reception of the satellite
- $\text{NF}_{\text{Tx,gtw}}$: Noise figure at the transmission of the gateway
- $O()$: Complexity
- p: Coefficient managing the rate at which the aperture field decreases
- P: Transmit power [W]
- $\boldsymbol{P}$: Transmit power matrix
- P_{b}: Probability to have a bit in error, i.e. bit error rate
- $P_{\text{b,BPSK}}$: Bit error rate for BPSK modulation
- $P_{\text{b,QPSK}}$: Bit error rate for QPSK modulation
- $P_{\text{b,M-PSK}}$: Bit error rate for M-PSK modulation
- $p_{\text{empty\_slots,with\_order}}$: Probability to have an empty slot at a given time when the order plays a role
- $p_{\text{empty\_slots,without\_order}}$: Probability to have an empty slot at a given time when the order does not play a role
- p_j: Transmit power of transmitter j [W]
- p_r: Outage probability or non-availability for a given rate r
- $P_{\text{Rx,sat}}$: Power received by the gateway [W]
- $P_{\text{Rx,sat}}$: Power received by the satellite [W]
- P_{s}: Probability to have a symbol in error, i.e. symbol error rate

- $P_{\mathrm{s,QPSK}}$: Symbol error rate for QPSK modulation
- $P_{\mathrm{s,M\text{-}PSK}}$: Symbol error rate for M-PSK modulation
- $P_{\mathrm{Tx,sat}}$: Power transmitted by the satellite [W]
- $P_{\mathrm{Tx,t}}$: Power transmitted by the terminal [W]
- $\boldsymbol{Q}$: Covariance of the transmitted signal
- r: Distance from the centre of the earth to the satellite [km] or rate [bit/s/Hz]
- R: Rate [bit/s/Hz]
- r': Slant range, i.e. distance between the satellite and the beam centre [km]
- R_{c}: Radius of the circle for projecting the beam border [km]
- R_{e}: Radius of the earth [km]
- r_{grid}: Resolution of the grid [°]
- r_i: Rate of user i [bit/s/Hz]
- r_{min}: Minimum rate [bit/s/Hz]
- R_{o}: Altitude of the satellite [km]
- R_{s}: Transmission rate [bauds] or symbols per second [sps]
- r_{th}: Threshold rate [bit/s/Hz]
- $\boldsymbol{s}$: Symbol vector
- S: Slant range, i.e. distance between the satellite and the beam centre [km] or signal power [W] or set
- S_j: Slant range of transmitter j [km]
- SNR_i: SNR perceived by the i-th receiver
- T: Aperture edge taper or system noise temperature [K]
- $T_{\mathrm{ant,sat}}$: Antenna noise temperature at the satellite [K]
- T_{D}: Temperature of the down-link [K]
- T_{F}: Temperature of the feeder [K]
- T_{ground}: Temperature of the ground [K]
- T_{s}: Symbol duration [s]
- T_{sky}: Temperature of the sky [K]
- W: Bandwidth [Hz]
- $\boldsymbol{W}$: Moore-Penrose pseudo-inverse matrix
- W_{N}: Bandwidth of the noise [Hz]
- W_{s}: Window size [#]
- $\boldsymbol{x}$: Transmitted signal vector
- $\hat{\boldsymbol{x}}$: Estimates of the transmitted signal vector

- XPI_{H}: Cross-polarisation isolation for the horizontal polarisation
- XPI_{V}: Cross-polarisation isolation for the vertical polarisation
- $\boldsymbol{y}$: Received signal vector
- α_{cs}: Channel spacing [%]
- α_i: Complexity related to the parameter i
- β: Roll-off factor [%]
- η: Antenna efficient or noise
- $\boldsymbol{\eta}$: Additive Gaussian noise vector
- φ_{beam}: Latitude of the beam centre [°]
- $\boldsymbol{\Phi}_{\mathrm{Rx}}$: Phase shift matrix of the receivers
- φ_{sat}: Latitude of the satellite [°]
- $\boldsymbol{\Phi}_{\mathrm{Tx}}$: Phase shift matrix of the transmitters
- λ: Wavelength [m]
- λ_{beam}: Longitude of the beam centre [°]
- λ_{D}: Wavelength of the down-link [m]
- λ_{sat}: Longitude of the satellite [°]
- λ_{U}: Wavelength of the up-link [m]
- μ: Mean value
- $\boldsymbol{\Pi}$: Permutation matrix
- σ^2: Variance
- θ: Open angle [°]
- $\theta_{i,j}$: Phase between receiver i and transmitter j [°]
- θ_{R}: Maximum pointing error [°]
- θ_{3dB}: Half-side beam width [°]

Appendix B

Useful Mathematical Background

B.1 Mathematical Properties

B.1.1 Logarithm

The logarithm is commonly written "log" but can also be written "ln".

Typical values:

$$\log(1) = 0 \tag{B.1}$$

Operations:

$$\log(a\,b) = \log(a) + \log(b) \tag{B.2}$$

$$\log\left(\frac{a}{b}\right) = \log(a) - \log(b) \tag{B.3}$$

$$\log\left(\frac{1}{a}\right) = -\log(a) \tag{B.4}$$

Approximations:

$$\log_2(1+x) \approx x\,\log_2 \mathrm{e} \qquad \text{when } x \approx 0 \tag{B.5}$$

$$\log_2(1+x) \approx \log_2 x \qquad \text{when } x \gg 1 \tag{B.6}$$

Base:

The base of the logarithm is indicated as a subindex, for instance $\log_2$ for the base 2 logarithm. The logarithm base N is computed as follows:

$$\log_N(a) = \frac{\log(a)}{\log(N)} \tag{B.7}$$

In information theory the base of the logarithm gives directly the unit of the mutual information. The base 2 logarithm permits to measure the mutual information in terms of bits

(binary digit), the base e in terms of nats and the base 10 in terms of bans (or dits, decimal digit).

B.1.2 Error Function

The error function, also named Gauss error function, is denoted "erf" and is defined as:

$$\operatorname{erf}(x) = \frac{2}{\sqrt{\pi}} \int_0^x e^{-t^2} dt \tag{B.8}$$

The complementary error function is denoted "erfc" and is therefore defined as:

$$\operatorname{erfc}(x) = 1 - \operatorname{erf}(x) = \frac{2}{\sqrt{\pi}} \int_x^\infty e^{-t^2} dt \tag{B.9}$$

B.1.3 Determinant

The determinant is commonly written "det" but can also be written "|.|".

Operations:

$$\frac{1}{\det(\boldsymbol{A})} = \det\left(\boldsymbol{A}^{-1}\right) \tag{B.10}$$

$$\det(\boldsymbol{A}) \det(\boldsymbol{B}) = \det(\boldsymbol{A}\,\boldsymbol{B}) \tag{B.11}$$

$$\det\left(\boldsymbol{I} + \boldsymbol{A}^{-1}\,\boldsymbol{B}\right) = \det\left(\boldsymbol{A}^{-1}\,(\boldsymbol{A} + \boldsymbol{B})\right) = \det\left(\boldsymbol{A}^{-1}\right) \det(\boldsymbol{A} + \boldsymbol{B}) \tag{B.12}$$

$$\det(\boldsymbol{I}_M + \boldsymbol{A}\,\boldsymbol{B}) = \det(\boldsymbol{I}_N + \boldsymbol{B}\,\boldsymbol{A}) \tag{B.13}$$

where $\boldsymbol{A}$ is a $M \times N$ matrix and $\boldsymbol{B}$ is a $N \times M$ matrix.

$$\det(\alpha\,\boldsymbol{A}) = \alpha^N \det(\boldsymbol{A}) \tag{B.14}$$

where $\boldsymbol{A}$ is a $N \times N$ matrix.

Derivatives:

$$\frac{\partial}{\partial \boldsymbol{A}} \det(\boldsymbol{A}) = (\det(\boldsymbol{A})\ \boldsymbol{A})^{\mathrm{T}} \tag{B.15}$$

$$\frac{\partial}{\partial \boldsymbol{A}^{\mathrm{T}}} \det(\boldsymbol{A}) = \det(\boldsymbol{A})\ \boldsymbol{A}^{-1} \tag{B.16}$$

Other properties:

If we decompose $\boldsymbol{I} + \boldsymbol{A}$ such that $\boldsymbol{I} + \boldsymbol{A} = \boldsymbol{L}\boldsymbol{L}^{\mathrm{H}}$ (Cholesky decomposition) then:

$$\det(\boldsymbol{I} + \boldsymbol{A}) = \det\left(\boldsymbol{L}\,\boldsymbol{L}^{\mathrm{H}}\right) = |\det(\boldsymbol{L})|^2 \tag{B.17}$$

B.1.4 Trace

The trace is usually written "tr" and corresponds to the sum of the diagonal elements of a square matrix:

$$\mathrm{tr}\{\boldsymbol{A}\} = a_{1,1} + a_{2,2} + \ldots + a_{N,N} = \sum_{i=1}^{N} a_{i,i} \tag{B.18}$$

where $\boldsymbol{A}$ is a matrix of size $N \times N$.

Properties:

$$\mathrm{tr}\{\boldsymbol{A} + \boldsymbol{B}\} = \mathrm{tr}\{\boldsymbol{A}\} + \mathrm{tr}\{\boldsymbol{B}\} \tag{B.19}$$

$$\mathrm{tr}\{\alpha\} = \alpha \tag{B.20}$$

$$\mathrm{tr}\{\alpha\, \boldsymbol{A}\} = \alpha\, \mathrm{tr}\{\boldsymbol{A}\} \tag{B.21}$$

$$\mathrm{tr}\{\boldsymbol{A}\, \boldsymbol{B}\} = \mathrm{tr}\{\boldsymbol{B}\, \boldsymbol{A}\} \tag{B.22}$$

$$\mathrm{tr}\{\boldsymbol{A}\, \boldsymbol{B}\, \boldsymbol{C}\} = \mathrm{tr}\{\boldsymbol{C}\, \boldsymbol{B}\, \boldsymbol{A}\} \neq \mathrm{tr}\{\boldsymbol{A}\, \boldsymbol{C}\, \boldsymbol{B}\} \tag{B.23}$$

$$\mathrm{tr}\{\boldsymbol{I}\} = N \tag{B.24}$$

where $\boldsymbol{I}$ is the identify matrix of size $N \times N$.

Derivatives:

We consider two matrices $\boldsymbol{X}$ and $\boldsymbol{A}$ such that $\boldsymbol{X} \in \mathbb{R}^{M \times N}$ and $\boldsymbol{A} \in \mathbb{R}^{N \times M}$. The derivative of the different traces are:

$$\frac{\partial \mathrm{tr}\left\{\boldsymbol{X}\right\}}{\partial \boldsymbol{X}} = \frac{\partial \mathrm{tr}\left\{\boldsymbol{X}^{\mathrm{T}}\right\}}{\partial \boldsymbol{X}} = \boldsymbol{I} \tag{B.25}$$

$$\frac{\partial \mathrm{tr}\left\{\boldsymbol{X}\, \boldsymbol{A}\right\}}{\partial \boldsymbol{X}} = \boldsymbol{A}^{\mathrm{T}} \tag{B.26}$$

$$\frac{\partial \mathrm{tr}\left\{\boldsymbol{X}^{\mathrm{T}}\, \boldsymbol{A}\right\}}{\partial \boldsymbol{X}} = \frac{\partial \mathrm{tr}\left\{\boldsymbol{A}\, \boldsymbol{X}^{\mathrm{T}}\right\}}{\partial \boldsymbol{X}} = \boldsymbol{A} \tag{B.27}$$

$$\frac{\partial \mathrm{tr}\left\{\boldsymbol{X}\, \boldsymbol{A}\, \boldsymbol{X}^{\mathrm{T}}\right\}}{\partial \boldsymbol{X}} = \boldsymbol{X}\, \boldsymbol{A}^{\mathrm{T}} + \boldsymbol{X}\, \boldsymbol{A} \tag{B.28}$$

Complex derivatives:

We take into account two matrices $\boldsymbol{A}$ and $\boldsymbol{X}$ such that $\boldsymbol{A} \in \mathbb{C}^{M \times N}$ and $\boldsymbol{X} \in \mathbb{C}^{M \times N}$.

$$\frac{\partial \mathrm{tr}\left\{\boldsymbol{A}\, \boldsymbol{X}^{\mathrm{H}}\right\}}{\partial \Re(\boldsymbol{X})} = \boldsymbol{A} \tag{B.29}$$

$$\mathrm{j}\frac{\partial \mathrm{tr}\left\{\boldsymbol{A}\,\boldsymbol{X}^{\mathrm{H}}\right\}}{\partial \Im(\boldsymbol{X})} = \boldsymbol{A} \tag{B.30}$$

$$\frac{\partial \mathrm{tr}\left\{\boldsymbol{X}\,\boldsymbol{A}^{\mathrm{H}}\right\}}{\partial \Re(\boldsymbol{X})} = \boldsymbol{A}^{*} \tag{B.31}$$

$$\mathrm{j}\frac{\partial \mathrm{tr}\left\{\boldsymbol{X}\,\boldsymbol{A}^{\mathrm{H}}\right\}}{\partial \Im(\boldsymbol{X})} = -\boldsymbol{A}^{*} \tag{B.32}$$

$$\frac{\partial \mathrm{tr}\left\{\boldsymbol{X}\,\boldsymbol{A}\,\boldsymbol{X}^{\mathrm{H}}\right\}}{\partial \Re(\boldsymbol{X})} = \boldsymbol{X}\,\boldsymbol{A} + \boldsymbol{X}^{*}\boldsymbol{A}^{\mathrm{T}} \tag{B.33}$$

$$\mathrm{j}\frac{\partial \mathrm{tr}\left\{\boldsymbol{X}\,\boldsymbol{A}\,\boldsymbol{X}^{\mathrm{H}}\right\}}{\partial \Im(\boldsymbol{X})} = \boldsymbol{X}\,\boldsymbol{A} - \boldsymbol{X}^{*}\boldsymbol{A}^{\mathrm{T}} \tag{B.34}$$

Generalised and conjugate complex derivatives:

The generalised complex derivative of the expression $f(\boldsymbol{X})$ with respect to the complex matrix $\boldsymbol{X}$ is:

$$\frac{\partial f(\boldsymbol{X})}{\partial \boldsymbol{X}} = \frac{1}{2}\left(\frac{\partial f(\boldsymbol{X})}{\partial \Re(\boldsymbol{X})} - \mathrm{j}\frac{\partial f(\boldsymbol{X})}{\partial \Im(\boldsymbol{X})}\right) \tag{B.35}$$

The conjugate complex derivative of the expression $f(\boldsymbol{X})$ with respect to the conjugate of the complex matrix $\boldsymbol{X}$ is:

$$\frac{\partial f(\boldsymbol{X})}{\partial \boldsymbol{X}^{*}} = \frac{1}{2}\left(\frac{\partial f(\boldsymbol{X})}{\partial \Re(\boldsymbol{X})} + \mathrm{j}\frac{\partial f(\boldsymbol{X})}{\partial \Im(\boldsymbol{X})}\right) \tag{B.36}$$

Therefore we have:

$$\frac{\partial \mathrm{tr}\left\{\boldsymbol{A}\,\boldsymbol{X}^{\mathrm{H}}\right\}}{\partial \boldsymbol{X}^{*}} = \boldsymbol{A} \tag{B.37}$$

$$\frac{\partial \mathrm{tr}\left\{\boldsymbol{X}\,\boldsymbol{A}^{\mathrm{H}}\right\}}{\partial \boldsymbol{X}} = \boldsymbol{A}^{*} \tag{B.38}$$

$$\frac{\partial \mathrm{tr}\left\{\boldsymbol{X}\,\boldsymbol{A}\,\boldsymbol{X}^{\mathrm{H}}\right\}}{\partial \boldsymbol{X}} = \boldsymbol{X}^{*}\boldsymbol{A}^{\mathrm{T}} \tag{B.39}$$

B.1.5 Expectation

The expectation is also named expected value or mean value and is written "$\mathrm{E}[.]$". The expectation of a discrete random variable "X" is:

$$\mathrm{E}[X] = \sum_{i=1}^{\infty} x_i\, p_i \tag{B.40}$$

where x_i is the value taken by X and p_i the corresponding probability.

The expectation of a continuous random variable "X" is:

$$\mathrm{E}\left[X\right] = \int_{-\infty}^{+\infty} x\, f\left(x\right)\, dx \tag{B.41}$$

where $f\left(x\right)$ is the probability density function of X.

Properties:

$$\mathrm{E}\left[X + Y\right] = \mathrm{E}\left[X\right] + \mathrm{E}\left[Y\right] \tag{B.42}$$

$$\mathrm{E}\left[\alpha\, X\right] = \alpha\, \mathrm{E}\left[X\right] \tag{B.43}$$

$$\mathrm{E}\left[X\, Y\right] = \mathrm{E}\left[X\right]\, \mathrm{E}\left[Y\right] \tag{B.44}$$

if X and Y are two independent random variables.

B.1.6 Conditional Expectation

The conditional expectation used to compute the expectation of a random variable knowing another random variable. It is generally written ""$\mathrm{E}\left[.|.\right]$".

Properties:

$$\mathrm{E}\left[X + Y|Z\right] = \mathrm{E}\left[X|Z\right] + \mathrm{E}\left[Y|Z\right] \tag{B.45}$$

$$\mathrm{E}\left[\alpha\, X|Y\right] = \alpha\, \mathrm{E}\left[X|Y\right] \tag{B.46}$$

$$\mathrm{E}\left[X|X\right] = X \tag{B.47}$$

B.1.7 Hermitian

The Hermitian of a matrix is the conjugate transpose of this matrix. It is generally written using the superscript "H".

Properties:

$$\left(\boldsymbol{A} + \boldsymbol{B}\right)^{\mathrm{H}} = \boldsymbol{A}^{\mathrm{H}} + \boldsymbol{B}^{\mathrm{H}} \tag{B.48}$$

$$\left(\boldsymbol{A}\, \boldsymbol{B}\right)^{\mathrm{H}} = \boldsymbol{B}^{\mathrm{H}}\, \boldsymbol{A}^{\mathrm{H}} \tag{B.49}$$

B.2 Mathematical Proofs

This section gathers some mathematical proofs that are used within these notes.

B.2.1 Trace Derivatives of Real Matrices

We consider two matrices $\boldsymbol{X}$ and $\boldsymbol{A}$ such that $\boldsymbol{X} \in \mathbb{R}^{M \times N}$ and $\boldsymbol{A} \in \mathbb{R}^{N \times M}$. The trace of the product of these two matrices is:

$$\mathrm{tr}\{\boldsymbol{X}\,\boldsymbol{A}\} = \mathrm{tr}\left\{\begin{bmatrix} \sum_{i=1}^{N} x_{1,i}\,a_{i,1} & \sum_{i=1}^{N} x_{1,i}\,a_{i,2} & \cdots & \sum_{i=1}^{N} x_{1,i}\,a_{i,M} \\ \sum_{i=1}^{N} x_{2,i}\,a_{i,1} & \sum_{i=1}^{N} x_{2,i}\,a_{i,2} & \cdots & \sum_{i=1}^{N} x_{2,i}\,a_{i,M} \\ \vdots & \vdots & \ddots & \vdots \\ \sum_{i=1}^{N} x_{M,i}\,a_{i,1} & \sum_{i=1}^{N} x_{M,i}\,a_{i,2} & \cdots & \sum_{i=1}^{N} x_{M,i}\,a_{i,M} \end{bmatrix}\right\}$$

which leads to:

$$\mathrm{tr}\{\boldsymbol{X}\,\boldsymbol{A}\} = \sum_{i=1}^{N} x_{1,i}\,a_{i,1} + \sum_{i=1}^{N} x_{2,i}\,a_{i,2} + \cdots + \sum_{i=1}^{N} x_{M,i}\,a_{i,M}$$

The derivative of this product with respect to $x_{1,i}$ is:

$$\frac{\partial \mathrm{tr}\,\{\boldsymbol{X}\,\boldsymbol{A}\}}{\partial x_{1,i}} = a_{i,1}$$

The generalised form is thus:

$$\frac{\partial \mathrm{tr}\,\{\boldsymbol{X}\,\boldsymbol{A}\}}{\partial x_{j,i}} = a_{i,j}$$

which finally gives:

$$\left[\frac{\partial \mathrm{tr}\,\{\boldsymbol{X}\,\boldsymbol{A}\}}{\partial \boldsymbol{X}}\right]_{i,j} = a_{j,i} \qquad \Rightarrow \qquad \frac{\partial \mathrm{tr}\,\{\boldsymbol{X}\,\boldsymbol{A}\}}{\partial \boldsymbol{X}} = A^{\mathrm{T}}$$

B.2.2 Trace Derivatives of Complex Matrices

The same principle can be applied when considering complex matrices. We now take into account two matrices $\boldsymbol{A}$ and $\boldsymbol{X}$ such that $\boldsymbol{A} \in \mathbb{C}^{M \times N}$ and $\boldsymbol{X} \in \mathbb{C}^{M \times N}$. The purpose is to evaluate the derivative of $\mathrm{tr}\left\{\boldsymbol{A}\,\boldsymbol{X}^{\mathrm{H}}\right\}$ with respect to $\boldsymbol{X}$.

The matrices $\boldsymbol{A}$ and $\boldsymbol{X}^{\mathrm{H}}$ can be written in their usual forms, i.e.:

$$\boldsymbol{A} = \begin{bmatrix} a_{1,1} & a_{1,2} & \cdots & a_{1,N} \\ a_{2,1} & a_{2,2} & \cdots & a_{2,N} \\ \vdots & \vdots & \ddots & \vdots \\ a_{M,1} & a_{M,2} & \cdots & a_{M,N} \end{bmatrix} \qquad \boldsymbol{X}^{\mathrm{H}} = \begin{bmatrix} x_{1,1}^{*} & x_{2,1}^{*} & \cdots & x_{M,1}^{*} \\ x_{1,2}^{*} & x_{2,2}^{*} & \cdots & x_{M,2}^{*} \\ \vdots & \vdots & \ddots & \vdots \\ x_{1,N}^{*} & x_{2,N}^{*} & \cdots & x_{M,N}^{*} \end{bmatrix}$$

The trace of the product of the two matrices gives:

$$\mathrm{tr}\left\{\boldsymbol{A}\,\boldsymbol{X}^{\mathrm{H}}\right\} = \sum_{i=1}^{N} a_{1,i}\,x_{1,i}^{*} + \sum_{i=1}^{N} a_{2,i}\,x_{2,i}^{*} + \cdots + \sum_{i=1}^{N} a_{M,i}\,x_{M,i}^{*}$$

Since both matrices $\boldsymbol{A}$ and $\boldsymbol{X}$ are complex, we can write:

$$a_{i,j} = \Re\left(a_{i,j}\right) + \mathrm{j}\Im\left(a_{i,j}\right) \qquad x_{i,j}^{*} = \Re\left(x_{i,j}\right) - \mathrm{j}\Im\left(x_{i,j}\right)$$

The derivative of the trace of the product of the two matrices with respect to the real part of $x_{1,i}$ is:

$$\frac{\partial \mathrm{tr}\left\{\boldsymbol{A}\,\boldsymbol{X}^{\mathrm{H}}\right\}}{\partial \Re(x_{1,i})} = \frac{\partial\left(\sum_{i=1}^{N}\, a_{1,i}\,x_{1,i}^{*}\right)}{\partial \Re(x_{1,i})}$$

This leads to:

$$\frac{\partial \mathrm{tr}\left\{\boldsymbol{A}\,\boldsymbol{X}^{\mathrm{H}}\right\}}{\partial \Re(x_{1,i})} = a_{1,i}$$

which finally gives:

$$\left[\frac{\partial \mathrm{tr}\left\{\boldsymbol{A}\,\boldsymbol{X}^{\mathrm{H}}\right\}}{\partial \Re(\boldsymbol{X})}\right]_{i,j} = a_{i,j} \qquad \Rightarrow \qquad \frac{\partial \mathrm{tr}\left\{\boldsymbol{A}\,\boldsymbol{X}^{\mathrm{H}}\right\}}{\partial \Re(\boldsymbol{X})} = \boldsymbol{A} \tag{B.50}$$

In the same way we can show that:

$$\left[\mathrm{j}\frac{\partial \mathrm{tr}\left\{\boldsymbol{A}\,\boldsymbol{X}^{\mathrm{H}}\right\}}{\partial \Im(\boldsymbol{X})}\right]_{i,j} = a_{i,j} \qquad \Rightarrow \qquad \mathrm{j}\frac{\partial \mathrm{tr}\left\{\boldsymbol{A}\,\boldsymbol{X}^{\mathrm{H}}\right\}}{\partial \Im(\boldsymbol{X})} = \boldsymbol{A} \tag{B.51}$$

We consider two matrices $\boldsymbol{X}$ and $\boldsymbol{A}$ such that $\boldsymbol{X} \in \mathbb{C}^{M\times N}$ and $\boldsymbol{A} \in \mathbb{C}^{M\times N}$. The purpose is to evaluate the derivative of $\mathrm{tr}\left\{\boldsymbol{X}\,\boldsymbol{A}^{\mathrm{H}}\right\}$ with respect to $\boldsymbol{X}$.

The matrices $\boldsymbol{X}$ and $\boldsymbol{A}^{\mathrm{H}}$ can be written in their usual forms, i.e.:

$$\boldsymbol{X} = \begin{bmatrix} x_{1,1} & x_{1,2} & \cdots & x_{1,N} \\ x_{2,1} & x_{2,2} & \cdots & x_{2,N} \\ \vdots & \vdots & \ddots & \vdots \\ x_{M,1} & x_{M,2} & \cdots & x_{M,N} \end{bmatrix} \qquad \boldsymbol{A}^{\mathrm{H}} = \begin{bmatrix} a_{1,1}^{*} & a_{2,1}^{*} & \cdots & a_{M,1}^{*} \\ a_{1,2}^{*} & a_{2,2}^{*} & \cdots & a_{M,2}^{*} \\ \vdots & \vdots & \ddots & \vdots \\ a_{1,N}^{*} & a_{2,N}^{*} & \cdots & a_{M,N}^{*} \end{bmatrix}$$

The trace of the product of the two matrices gives:

$$\mathrm{tr}\left\{\boldsymbol{X}\,\boldsymbol{A}^{\mathrm{H}}\right\} = \sum_{i=1}^{N} x_{1,i}\,a_{1,i}^{*} + \sum_{i=1}^{N} x_{2,i}\,a_{2,i}^{*} + \cdots + \sum_{i=1}^{N} x_{M,i}\,a_{M,i}^{*}$$

The derivative of the trace of the product of the two matrices with respect to the real part of $x_{1,i}$ is:

$$\frac{\partial \mathrm{tr}\left\{\boldsymbol{X}\,\boldsymbol{A}^{\mathrm{H}}\right\}}{\partial \Re(x_{1,i})} = \frac{\partial\left(\sum_{i=1}^{N}\, x_{1,i}\,a_{1,i}^{*}\right)}{\partial \Re(x_{1,i})}$$

This leads to:

$$\frac{\partial \mathrm{tr}\left\{\boldsymbol{X}\,\boldsymbol{A}^{\mathrm{H}}\right\}}{\partial \Re(x_{1,i})} = a_{1,i}^{*}$$

which finally gives:

$$\left[\frac{\partial \mathrm{tr}\left\{\boldsymbol{X}\,\boldsymbol{A}^{\mathrm{H}}\right\}}{\partial \Re(\boldsymbol{X})}\right]_{i,j} = a_{i,j}^{*} \qquad \Rightarrow \qquad \frac{\partial \mathrm{tr}\left\{\boldsymbol{X}\,\boldsymbol{A}^{\mathrm{H}}\right\}}{\partial \Re(\boldsymbol{X})} = \boldsymbol{A}^{*} \tag{B.52}$$

In the same way we can show that:

$$\left[\mathrm{j}\frac{\partial \mathrm{tr}\left\{\boldsymbol{X}\,\boldsymbol{A}^{\mathrm{H}}\right\}}{\partial \Im(\boldsymbol{X})}\right]_{i,j} = -a_{i,j}^{*} \qquad \Rightarrow \qquad \mathrm{j}\frac{\partial \mathrm{tr}\left\{\boldsymbol{X}\,\boldsymbol{A}^{\mathrm{H}}\right\}}{\partial \Im(\boldsymbol{X})} = -\boldsymbol{A}^{*} \tag{B.53}$$

Let's now find the expression of the following derivatives:

$$\frac{\partial \mathrm{tr}\left\{\boldsymbol{X}\,\boldsymbol{A}\,\boldsymbol{X}^{\mathrm{H}}\right\}}{\partial \Re(\boldsymbol{X})} \qquad \text{and} \qquad \mathrm{j}\frac{\partial \mathrm{tr}\left\{\boldsymbol{X}\,\boldsymbol{A}\,\boldsymbol{X}^{\mathrm{H}}\right\}}{\partial \Im(\boldsymbol{X})}$$

To do so we use exactly the same principle as for (B.50), (B.51), (B.52) and (B.53), and start with matrices composed exclusively of real numbers only, i.e.:

$$\frac{\partial \mathrm{tr}\left\{\boldsymbol{X}\,\boldsymbol{A}\,\boldsymbol{X}^{\mathrm{T}}\right\}}{\partial \boldsymbol{X}}$$

We note $\boldsymbol{B} = \boldsymbol{X}\,\boldsymbol{A}$, therefore the elements of $\boldsymbol{B}$ are such that:

$$b_{i,j} = \sum_{k=1}^{N} x_{i,k}\,a_{k,j}$$

We also note $\boldsymbol{C} = \boldsymbol{B}\,\boldsymbol{X}^{\mathrm{T}}$ such that we obtain:

$$c_{i,j} = \sum_{l=1}^{N} b_{i,l}\,x_{j,l}$$

Since $\boldsymbol{C} = \boldsymbol{B}\,\boldsymbol{X}^{\mathrm{T}} = \boldsymbol{X}\,\boldsymbol{A}\,\boldsymbol{X}^{\mathrm{T}}$, we have:

$$c_{i,j} = \sum_{l=1}^{N}\left(\sum_{k=1}^{N} x_{i,k}\,a_{k,l}\right) x_{j,l} = \sum_{l=1}^{N}\sum_{k=1}^{N} x_{i,k}\,a_{k,l}\,x_{j,l}$$

The trace of the matrix $\boldsymbol{C}$ is thus:

$$\mathrm{tr}\left\{\boldsymbol{C}\right\} = \sum_{i=1}^{N} c_{i,i} = \sum_{i=1}^{N}\sum_{l=1}^{N}\sum_{k=1}^{N} x_{i,k}\,a_{k,l}\,x_{i,l}$$

The derivative of this trace according to the element $x_{1,1}$ is:

$$\frac{\partial \mathrm{tr}\left\{\boldsymbol{C}\right\}}{\partial x_{1,1}} = \frac{\partial\left(\sum_{l=1}^{N} x_{1,1}\,a_{1,l}\,x_{1,l}\right)}{\partial x_{1,1}} + \frac{\partial\left(\sum_{k=1}^{N} x_{1,k}\,a_{k,1}\,x_{1,1}\right)}{\partial x_{1,1}} = \sum_{l=1}^{N} a_{1,l}\,x_{1,l} + \sum_{k=1}^{N} x_{1,k}\,a_{k,1}$$

In the same way, the derivative of this trace according to the element $x_{1,2}$ is:

$$\frac{\partial \mathrm{tr}\left\{\boldsymbol{C}\right\}}{\partial x_{1,2}} = \frac{\partial\left(\sum_{l=1}^{N} x_{1,2}\, a_{2,l}\, x_{1,l}\right)}{\partial x_{1,2}} + \frac{\partial\left(\sum_{k=1}^{N} x_{1,k}\, a_{k,2}\, x_{1,2}\right)}{\partial x_{1,2}} = \sum_{l=1}^{N} a_{2,l}\, x_{1,l} + \sum_{k=1}^{N} x_{1,k}\, a_{k,2}$$

Generalising the different expressions obtained previously, we finally have:

$$\frac{\partial \mathrm{tr}\left\{\boldsymbol{X}\,\boldsymbol{A}\,\boldsymbol{X}^{\mathrm{T}}\right\}}{\partial \boldsymbol{X}} = \boldsymbol{X}\,\boldsymbol{A}^{\mathrm{T}} + \boldsymbol{X}\,\boldsymbol{A} \tag{B.54}$$

Using the same methodology let's derive the derivative of this trace but with complex matrices. As before we note $\boldsymbol{B} = \boldsymbol{X}\,\boldsymbol{A}$, therefore the elements of $\boldsymbol{B}$ are such that:

$$b_{i,j} = \sum_{k=1}^{N} x_{i,k}\, a_{k,j}$$

We also note $\boldsymbol{C} = \boldsymbol{B}\,\boldsymbol{X}^{\mathrm{H}}$ such that we obtain:

$$c_{i,j} = \sum_{l=1}^{N} b_{i,l}\, x_{j,l}^{*}$$

Since $\boldsymbol{C} = \boldsymbol{B}\,\boldsymbol{X}^{\mathrm{H}} = \boldsymbol{X}\,\boldsymbol{A}\,\boldsymbol{X}^{\mathrm{H}}$, we have:

$$c_{i,j} = \sum_{l=1}^{N}\left(\sum_{k=1}^{N} x_{i,k}\, a_{k,l}\right) x_{j,l}^{*} = \sum_{l=1}^{N}\sum_{k=1}^{N} x_{i,k}\, a_{k,l}\, x_{j,l}^{*}$$

The trace of the matrix $\boldsymbol{C}$ is thus:

$$\mathrm{tr}\left\{\boldsymbol{C}\right\} = \sum_{i=1}^{N} c_{i,i} = \sum_{i=1}^{N}\sum_{l=1}^{N}\sum_{k=1}^{N} x_{i,k}\, a_{k,l}\, x_{i,l}^{*}$$

The derivative of this trace according to the real part of the element $x_{1,1}$ is:

$$\frac{\partial \mathrm{tr}\left\{\boldsymbol{C}\right\}}{\partial \Re(x_{1,1})} = \frac{\partial\left(\sum_{l=1}^{N} x_{1,1}\, a_{1,l}\, x_{1,l}^{*}\right)}{\partial \Re(x_{1,1})} + \frac{\partial\left(\sum_{k=1}^{N} x_{1,k}\, a_{k,1}\, x_{1,1}^{*}\right)}{\partial \Re(x_{1,1})} = \sum_{l=1}^{N} a_{1,l}\, x_{1,l}^{*} + \sum_{k=1}^{N} x_{1,k}\, a_{k,1}$$

Therefore we obtain:

$$\frac{\partial \mathrm{tr}\left\{\boldsymbol{X}\,\boldsymbol{A}\,\boldsymbol{X}^{\mathrm{H}}\right\}}{\partial \Re(\boldsymbol{X})} = \boldsymbol{X}^{*}\,\boldsymbol{A}^{\mathrm{T}} + \boldsymbol{X}\,\boldsymbol{A} \tag{B.55}$$

In the same way, the derivative of this trace according to the imaginary part of the element $x_{1,1}$ is:

$$j\,\frac{\partial \mathrm{tr}\left\{\boldsymbol{C}\right\}}{\partial \Im(x_{1,1})} = j\,\frac{\partial\left(\sum_{l=1}^{N} x_{1,1}\, a_{1,l}\, x_{1,l}^{*}\right)}{\partial \Im(x_{1,1})} + j\,\frac{\partial\left(\sum_{k=1}^{N} x_{1,k}\, a_{k,1}\, x_{1,1}^{*}\right)}{\partial \Im(x_{1,1})} = -\sum_{l=1}^{N} a_{1,l}\, x_{1,l}^{*} + \sum_{k=1}^{N} x_{1,k}\, a_{k,1}$$

Therefore we obtain:

$$\frac{\partial \mathrm{tr}\left\{\boldsymbol{X}\,\boldsymbol{A}\,\boldsymbol{X}^{\mathrm{H}}\right\}}{\partial \Im(\boldsymbol{X})} = \boldsymbol{X}\,\boldsymbol{A} - \boldsymbol{X}^{*}\,\boldsymbol{A}^{\mathrm{T}} \tag{B.56}$$

Appendix C

Useful Satellite and Communications Background

This chapter aims at providing additional content to the Ph.D. thesis and is organised according to the main structure of the document.

C.1 Satellite

C.1.1 Beam Border

Introduction

This section shows how the beam border is computed for a multi-beam satellite system. It comprises the basics for computing coordinates, the method for determining the beam border, etc.

In this section the following is considered:
– Altitude of the satellite: $R_o = 35\,786$ km,
– Radius of the earth: $R_e \simeq 6\,378.137$ km,
– Latitude of the satellite: φ_{sat},
– Longitude of the satellite: λ_{sat}.
The distance from the centre of the earth to the satellite is noted r and is equal to:

$$r = R_e + R_o \tag{C.1}$$

When considering a geostationary satellite (the type of the satellite is determined by its altitude), the latitude φ_{sat} is usually equal to 0°: a GEO satellite is generally located in the equatorial plane. If φ_{sat} is different from 0° then the satellite will have a so-called orbit inclination: viewed from the earth the satellite will draw an "eight" in the sky.

Geocentric Coordinates System

The geocentric coordinates system is also known as inertial spherical coordinates system with earth-centred origin. The relation between Cartesian coordinates system and spherical coordinates system is:

$$\begin{pmatrix} x \\ y \\ z \end{pmatrix} = \begin{pmatrix} r\,\cos\varphi\,\cos\lambda \\ r\,\cos\varphi\,\sin\lambda \\ r\,\sin\varphi \end{pmatrix} \tag{C.2}$$

where r is the distance from the origin, φ the latitude and λ the longitude.

The Cartesian coordinates system is represented by Fig. C.1 where a point P is located at a distance r from the origin. The angle λ defines the angle between the x-axis towards the

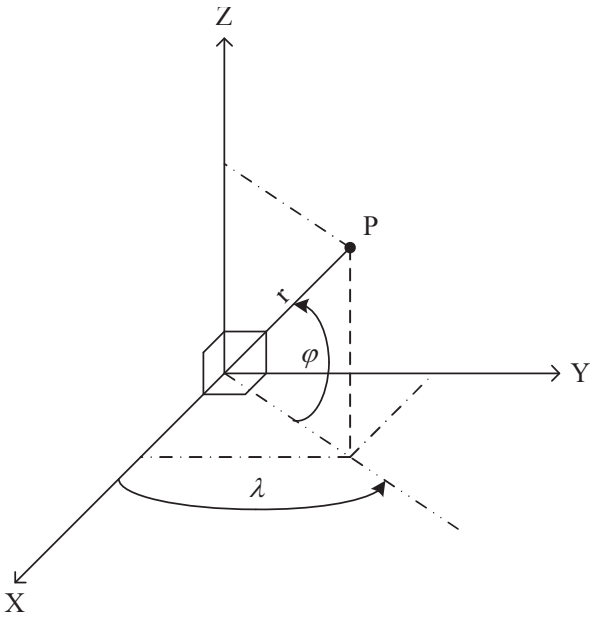


Figure C.1. *Representation of a point in the Cartesian coordinates system.*

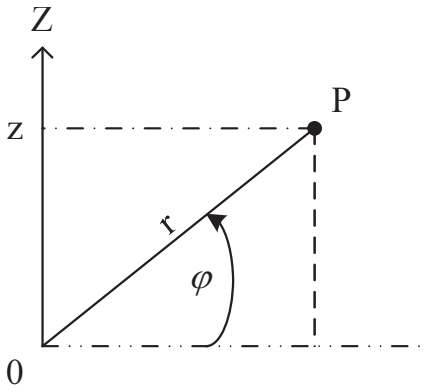


Figure C.2. *Value of z in the OZP plane.*

y-axis (angle within the OXY plane and which corresponds to the longitude). The angle φ defines the angle between the OXY plane and the segment [OP] towards the z-axis (latitude).

The value of z is simply obtained by considering the OZP plane (Fig. C.2):

$$\sin\varphi = \frac{z}{r} \Leftrightarrow z = r\,\sin\varphi$$

When looking at the OXY plane from the top (Fig. C.2) we can easily determine the value of x and y. The projection of the point P in the OXY plane is noted P'. The distance between 0 and P' is:

$$\cos\varphi = \frac{r'}{r} \Leftrightarrow r' = r\,\cos\varphi$$

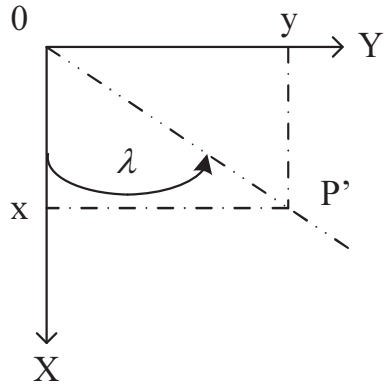


Figure C.3. *Value of x and y in the OXY plane.*

The value of x is thus:

$$\cos\lambda = \frac{x}{r'} \Leftrightarrow x = r\ \cos\varphi\ \cos\lambda$$

The value of y is obtained using the angle $\frac{\pi}{2} - \lambda$:

$$\cos\left(\frac{\pi}{2} - \lambda\right) = \frac{y}{r'} \Leftrightarrow y = r'\ \cos\left(\frac{\pi}{2} - \lambda\right) = r\ \cos\varphi\ \cos\left(\frac{\pi}{2} - \lambda\right)$$

We known that:

$$\cos\left(a + b\right) = \cos a\ \cos b - \sin a\ \sin b \tag{C.3}$$

therefore:

$$\cos\left(\frac{\pi}{2} - \lambda\right) = \cos\frac{\pi}{2}\ \cos\lambda + \sin\frac{\pi}{2}\ \sin\lambda = 0\ \cos\lambda + 1\ \sin\lambda = \sin\lambda$$

which finally gives:

$$y = r\ \cos\varphi\cos\left(\frac{\pi}{2} - \lambda\right) = r\ \cos\varphi\ \sin\lambda \tag{C.4}$$

The previous equations verify the relation between the Cartesian coordinates system and the spherical coordinates system:

$$\begin{pmatrix} x_{\mathrm{P}} \\ y_{\mathrm{P}} \\ z_{\mathrm{P}} \end{pmatrix} = \begin{pmatrix} r\ \cos\varphi\ \cos\lambda \\ r\ \cos\varphi\ \sin\lambda \\ r\ \sin\varphi \end{pmatrix} \tag{C.5}$$

If we consider the satellite then the coordinates can be expressed as follows:

$$\begin{pmatrix} x_{\mathrm{S}} \\ y_{\mathrm{S}} \\ z_{\mathrm{S}} \end{pmatrix} = \begin{pmatrix} r\ \cos\varphi_{\mathrm{sat}}\ \cos\lambda_{\mathrm{sat}} \\ r\ \cos\varphi_{\mathrm{sat}}\ \sin\lambda_{\mathrm{sat}} \\ r\ \sin\varphi_{\mathrm{sat}} \end{pmatrix} \tag{C.6}$$

here $r = R_{\mathrm{e}} + R_{\mathrm{o}}$.

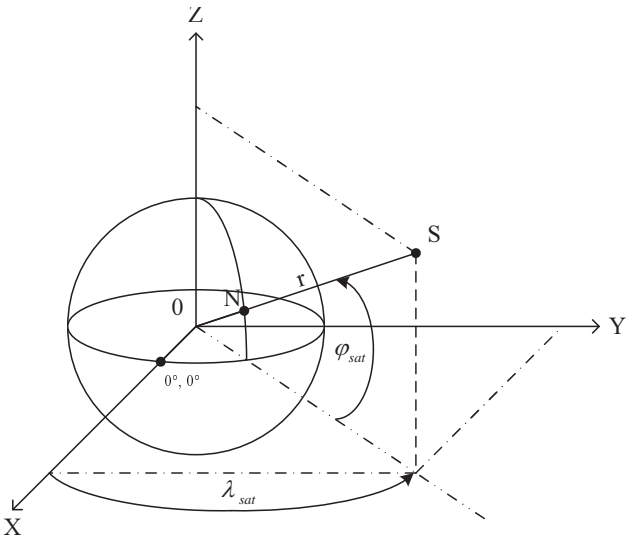


Figure C.4. *Position of the satellite in the geocentric coordinates system.*

Fig. C.4 shows the position of the satellite (point S) in the geocentric coordinates system. The z-axis points towards the North and the x-axis the latitude and longitude 0°, 0°. The point N represents the sub-satellite point on the earth surface and is also called the Nadir point.

In order to be able to work on the satellite coverage it is recommended to centre the coordinates system on the satellite itself. To do so a transformation has to be applied on the geocentric coordinates system obtained previously.

Satellite-Centred Coordinates System

Let's suppose we have a 2D Cartesian coordinates system with two axis x_i and y_i. When performing a rotation of angle θ_{i+1} on both axis we obtain the new axis x_{i+1} and y_{i+1}. The relation between the two coordinates systems is:

$$\begin{pmatrix} x_{i+1} \\ y_{i+1} \end{pmatrix} = \begin{pmatrix} \cos\theta_{i+1} & -\sin\theta_{i+1} \\ \sin\theta_{i+1} & \cos\theta_{i+1} \end{pmatrix} \times \begin{pmatrix} x_i \\ y_i \end{pmatrix} \tag{C.7}$$

Within a 3D Cartesian coordinates system the rotation of an angle θ around the different axis is expressed by the following formulas:

$$\text{Around the } x\text{-axis: } \boldsymbol{A} = \begin{pmatrix} 1 & 0 & 0 \\ 0 & \cos\theta & -\sin\theta \\ 0 & \sin\theta & cos\theta \end{pmatrix} \tag{C.8}$$

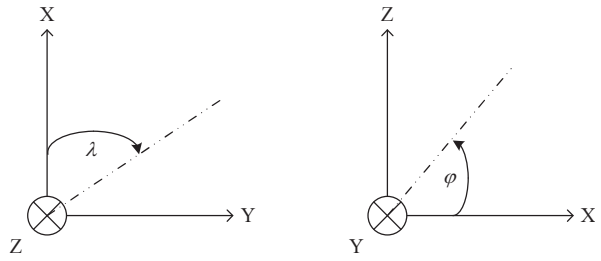


Figure C.5. *Rotation of the axis to point the satellite.*

$$\text{Around the } y\text{-axis: } \boldsymbol{B} = \begin{pmatrix} \cos\theta & 0 & \sin\theta \\ 0 & 1 & 0 \\ -\sin\theta & 0 & \cos\theta \end{pmatrix} \tag{C.9}$$

$$\text{Around the } z\text{-axis: } \boldsymbol{C} = \begin{pmatrix} \cos\theta & -\sin\theta & 0 \\ \sin\theta & \cos\theta & 0 \\ 0 & 0 & 1 \end{pmatrix} \tag{C.10}$$

In our case we need first to rotate the geocentric Cartesian coordinates system of an angle $-\lambda$ around the z-axis and then of an angle φ around the y-axis. The sign of the angles is determined by looking carefully at the axis of the coordinates system (Fig. C.5).
This leads to:

$$\begin{pmatrix} x' \\ y' \\ z' \end{pmatrix} = \boldsymbol{A} \begin{pmatrix} x \\ y \\ z \end{pmatrix} \tag{C.11}$$

with $\boldsymbol{A} = \boldsymbol{C}\,\boldsymbol{B}$, $\boldsymbol{B}$ being the rotation matrix around the z-axis and $\boldsymbol{C}$ the rotation matrix around the y-axis.

The matrix $\boldsymbol{B}$ can be expressed using the previous formulae where $\theta = -\lambda$ and knowing that:

$$\cos(-\lambda) = \cos(0-\lambda) = \cos 0\,\cos\lambda + \sin 0\,\sin\lambda = 1\,\cos\lambda + 0\,\sin\lambda = \cos\lambda$$

and:

$$\sin(-\lambda) = \sin(0-\lambda) = \sin 0\,\cos\lambda - \sin\lambda\,\cos 0 = 0\,\cos\lambda - \sin\lambda\,1 = -\sin\lambda$$

We obtain:

$$\boldsymbol{B} = \begin{pmatrix} \cos\theta & -\sin\theta & 0 \\ \sin\theta & \cos\theta & 0 \\ 0 & 0 & 1 \end{pmatrix} = \begin{pmatrix} \cos(-\lambda) & -\sin(-\lambda) & 0 \\ \sin(-\lambda) & \cos(-\lambda) & 0 \\ 0 & 0 & 1 \end{pmatrix} = \begin{pmatrix} \cos\lambda & \sin\lambda & 0 \\ -\sin\lambda & \cos\lambda & 0 \\ 0 & 0 & 1 \end{pmatrix} \tag{C.12}$$

The matrix $\boldsymbol{C}$ is:

$$\boldsymbol{C} = \begin{pmatrix} \cos\varphi & 0 & \sin\varphi \\ 0 & 1 & 0 \\ -\sin\varphi & 0 & \cos\varphi \end{pmatrix} \tag{C.13}$$

The multiplication of the two matrices $\boldsymbol{C}$ and $\boldsymbol{B}$ gives:

$$\boldsymbol{A} = \boldsymbol{C}\,\boldsymbol{B} = \begin{pmatrix} \cos\varphi & 0 & \sin\varphi \\ 0 & 1 & 0 \\ -\sin\varphi & 0 & \cos\varphi \end{pmatrix} \begin{pmatrix} \cos\lambda & \sin\lambda & 0 \\ -\sin\lambda & \cos\lambda & 0 \\ 0 & 0 & 1 \end{pmatrix}$$

which results in:

$$\boldsymbol{A} = \begin{pmatrix} \cos\varphi\,\cos\lambda & \cos\varphi\,\sin\lambda & \sin\varphi \\ -\sin\lambda & \cos\lambda & 0 \\ -\sin\varphi\,\cos\lambda & -\sin\varphi\,\sin\lambda & \cos\varphi \end{pmatrix} \tag{C.14}$$

The new coordinates of the satellite according to the coordinates system which is still centered on the earth but is now pointing the satellite are:

$$\boldsymbol{A} \begin{pmatrix} x_\mathrm{S} \\ y_\mathrm{S} \\ z_\mathrm{S} \end{pmatrix} = \begin{pmatrix} \cos\varphi\,\cos\lambda & \cos\varphi\,\sin\lambda & \sin\varphi \\ -\sin\lambda & \cos\lambda & 0 \\ -\sin\varphi\,\cos\lambda & -\sin\varphi\,\sin\lambda & \cos\varphi \end{pmatrix} \begin{pmatrix} x_\mathrm{S} \\ y_\mathrm{S} \\ z_\mathrm{S} \end{pmatrix}$$

$$\boldsymbol{A} \begin{pmatrix} x_\mathrm{S} \\ y_\mathrm{S} \\ z_\mathrm{S} \end{pmatrix} = \begin{pmatrix} \cos\varphi_\mathrm{sat}\,\cos\lambda_\mathrm{sat} & \cos\varphi_\mathrm{sat}\,\sin\lambda_\mathrm{sat} & \sin\varphi_\mathrm{sat} \\ -\sin\lambda_\mathrm{sat} & \cos\lambda_\mathrm{sat} & 0 \\ -\sin\varphi_\mathrm{sat}\,\cos\lambda_\mathrm{sat} & -\sin\varphi_\mathrm{sat}\,\sin\lambda_\mathrm{sat} & \cos\varphi_\mathrm{sat} \end{pmatrix} \begin{pmatrix} r\,\cos\varphi_\mathrm{sat}\,\cos\lambda_\mathrm{sat} \\ r\,\cos\varphi_\mathrm{sat}\,\sin\lambda_\mathrm{sat} \\ r\,\sin\varphi_\mathrm{sat} \end{pmatrix}$$

$$\boldsymbol{A} \begin{pmatrix} x_\mathrm{S} \\ y_\mathrm{S} \\ z_\mathrm{S} \end{pmatrix} = \begin{pmatrix} r\,\cos^2\varphi_\mathrm{sat}\,\cos^2\lambda_\mathrm{sat} + r\,\cos^2\varphi_\mathrm{sat}\,\sin^2\lambda_\mathrm{sat} + r\,\sin^2\varphi_\mathrm{sat} \\ -r\,\sin\lambda_\mathrm{sat}\,\cos\varphi_\mathrm{sat}\,\cos\lambda_\mathrm{sat} + r\,\cos\lambda_\mathrm{sat}\,\cos\varphi_\mathrm{sat}\,\sin\lambda_\mathrm{sat} \\ -r\,\sin\varphi_\mathrm{sat}\,\cos^2\lambda_\mathrm{sat}\,\cos\varphi_\mathrm{sat} - r\,\sin\varphi_\mathrm{sat}\,\sin^2\lambda_\mathrm{sat}\,\cos\varphi_\mathrm{sat} + r\,\cos\varphi_\mathrm{sat}\,\sin\varphi_\mathrm{sat} \end{pmatrix}$$

$$\boldsymbol{A} \begin{pmatrix} x_\mathrm{S} \\ y_\mathrm{S} \\ z_\mathrm{S} \end{pmatrix} = \begin{pmatrix} r\,\cos^2\varphi_\mathrm{sat}\,\left(\cos^2\lambda_\mathrm{sat} + \sin^2\lambda_\mathrm{sat}\right) + r\,\sin^2\varphi_\mathrm{sat} \\ 0 \\ -r\,\sin\varphi_\mathrm{sat}\,\cos\varphi_\mathrm{sat}\,\left(\cos^2\lambda_\mathrm{sat} + \sin^2\lambda_\mathrm{sat}\right) + r\,\cos\varphi_\mathrm{sat}\,\sin\varphi_\mathrm{sat} \end{pmatrix}$$

Knowing that:

$$\cos^2\theta + \sin^2\theta = \cos\theta\,\cos\theta + \sin\theta\,\sin\theta = \cos\left(\theta - \theta\right) = \cos 0 = 1$$

we obtain:

$$\boldsymbol{A} \begin{pmatrix} x_\mathrm{S} \\ y_\mathrm{S} \\ z_\mathrm{S} \end{pmatrix} = \begin{pmatrix} r\,\cos^2\varphi_\mathrm{sat} + r\,\sin^2\varphi_\mathrm{sat} \\ 0 \\ -r\,\sin\varphi_\mathrm{sat}\,\cos\varphi_\mathrm{sat} + r\,\cos\varphi_\mathrm{sat}\,\sin\varphi_\mathrm{sat} \end{pmatrix} = \begin{pmatrix} r \\ 0 \\ 0 \end{pmatrix} \tag{C.15}$$

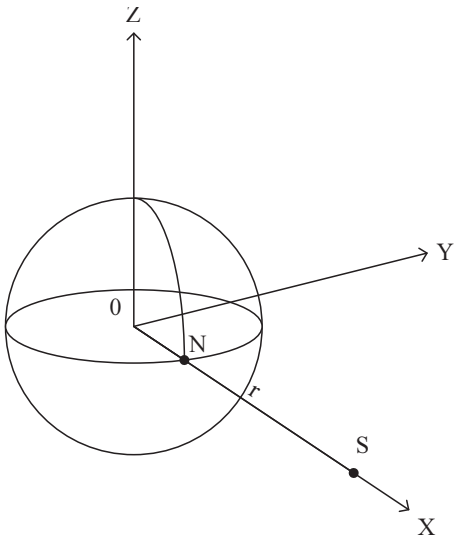


Figure C.6. *Position of the satellite in the coordinates system pointing the satellite.*

The position of the satellite in the new coordinates system can be represented by the next figure (Fig. C.6), the x-axis points towards the satellite.

In order to centre the coordinates system on the satellite itself, we just need to shift the origin of the new coordinates system (which points the satellite) of a value r over the x-axis. To centre the coordinates system on the satellite the value $-r$ is added so that:

$$\begin{pmatrix} x'_{\mathrm{S}} \\ y'_{\mathrm{S}} \\ z'_{\mathrm{S}} \end{pmatrix} = \boldsymbol{A} \begin{pmatrix} x_{\mathrm{S}} \\ y_{\mathrm{S}} \\ z_{\mathrm{S}} \end{pmatrix} - \begin{pmatrix} r \\ 0 \\ 0 \end{pmatrix} = \begin{pmatrix} r \\ 0 \\ 0 \end{pmatrix} - \begin{pmatrix} r \\ 0 \\ 0 \end{pmatrix} = \begin{pmatrix} 0 \\ 0 \\ 0 \end{pmatrix} \tag{C.16}$$

The satellite-centred coordinates system can be represented by the next figure (Fig. C.7).
If we consider a point P which belongs to the earth surface with the following coordinates in the geocentric coordinates system:

$$\begin{pmatrix} x_{\mathrm{P}} \\ y_{\mathrm{P}} \\ z_{\mathrm{P}} \end{pmatrix} = \begin{pmatrix} r_{\mathrm{P}} \cos\varphi_{\mathrm{P}} \cos\lambda_{\mathrm{P}} \\ r_{\mathrm{P}} \cos\varphi_{\mathrm{P}} \sin\lambda_{\mathrm{P}} \\ r_{\mathrm{P}} \sin\varphi_{\mathrm{P}} \end{pmatrix} \tag{C.17}$$

with $r_{\mathrm{P}} = R_{\mathrm{e}}$.

The coordinates of this point P in the coordinates system centred on the satellite are noted:

$$\begin{pmatrix} x'_{\mathrm{P}} \\ y'_{\mathrm{P}} \\ z'_{\mathrm{P}} \end{pmatrix} \tag{C.18}$$

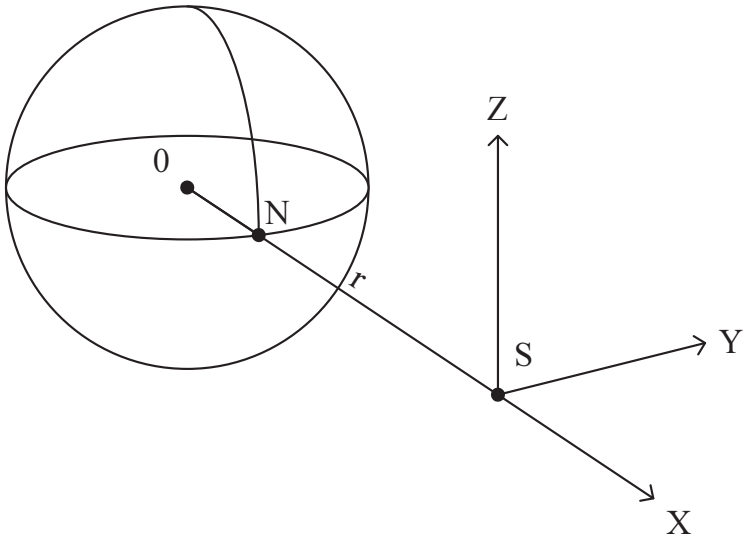


Figure C.7. *Satellite-centred coordinates system.*

To compute the coordinates we need first to apply two rotations as described previously: angle $-\lambda$ around the z-axis and angle φ around the y-axis.

$$\boldsymbol{A} = \begin{pmatrix} \cos\varphi_{\text{sat}}\,\cos\lambda_{\text{sat}} & \cos\varphi_{\text{sat}}\,\sin\lambda_{\text{sat}} & \sin\varphi_{\text{sat}} \\ -\sin\lambda_{\text{sat}} & \cos\lambda_{\text{sat}} & 0 \\ -\sin\varphi_{\text{sat}}\,\cos\lambda_{\text{sat}} & -\sin\varphi_{\text{sat}}\,\sin\lambda_{\text{sat}} & \cos\varphi_{\text{sat}} \end{pmatrix} \tag{C.19}$$

This gives:

$$\boldsymbol{A}\begin{pmatrix} x_{\text{P}} \\ y_{\text{P}} \\ z_{\text{P}} \end{pmatrix} = \begin{pmatrix} \cos\varphi_{\text{sat}}\,\cos\lambda_{\text{sat}} & \cos\varphi_{\text{sat}}\,\sin\lambda_{\text{sat}} & \sin\varphi_{\text{sat}} \\ -\sin\lambda_{\text{sat}} & \cos\lambda_{\text{sat}} & 0 \\ -\sin\varphi_{\text{sat}}\,\cos\lambda_{\text{sat}} & -\sin\varphi_{\text{sat}}\,\sin\lambda_{\text{sat}} & \cos\varphi_{\text{sat}} \end{pmatrix} \begin{pmatrix} R_{\text{e}}\,\cos\varphi_{\text{P}}\,\cos\lambda_{\text{P}} \\ R_{\text{e}}\,\cos\varphi_{\text{P}}\,\sin\lambda_{\text{P}} \\ R_{\text{e}}\,\sin\varphi_{\text{P}} \end{pmatrix} \tag{C.20}$$

$$\boldsymbol{A}\begin{pmatrix} x_{\text{P}} \\ y_{\text{P}} \\ z_{\text{P}} \end{pmatrix} = \begin{pmatrix} R_{\text{e}}\,[\cos\varphi_{\text{P}}\,\cos\varphi_{\text{sat}}\,\cos(\lambda_{\text{P}}-\lambda_{\text{sat}}) + \sin\varphi_{\text{P}}\,\sin\varphi_{\text{sat}}] \\ R_{\text{e}}\,\cos\varphi_{\text{P}}\,\sin(\lambda_{\text{P}}-\lambda_{\text{sat}}) \\ R_{\text{e}}\,[\sin\varphi_{\text{P}}\,\cos\varphi_{\text{sat}} - \cos\varphi_{\text{P}}\,\sin\varphi_{\text{sat}}\,\cos(\lambda_{\text{P}}-\lambda_{\text{sat}})] \end{pmatrix} \tag{C.21}$$

We can write that $\lambda_{\Delta} = \lambda_{\text{P}} - \lambda_{\text{sat}}$, which gives:

$$\boldsymbol{A}\begin{pmatrix} x_{\text{P}} \\ y_{\text{P}} \\ z_{\text{P}} \end{pmatrix} = \begin{pmatrix} R_{\text{e}}\,[\cos\varphi_{\text{P}}\,\cos\varphi_{\text{sat}}\,\cos\lambda_{\Delta} + \sin\varphi_{\text{P}}\,\sin\varphi_{\text{sat}}] \\ R_{\text{e}}\,\cos\varphi_{\text{P}}\,\sin\lambda_{\Delta} \\ R_{\text{e}}\,[\sin\varphi_{\text{P}}\,\cos\varphi_{\text{sat}} - \cos\varphi_{\text{P}}\,\sin\varphi_{\text{sat}}\,\cos\lambda_{\Delta}] \end{pmatrix} \tag{C.22}$$

The coordinates of P in the satellite-centred coordinates system are finally:

$$\begin{pmatrix} x'_{\mathrm{P}} \\ y'_{\mathrm{P}} \\ z'_{\mathrm{P}} \end{pmatrix} = \boldsymbol{A} \begin{pmatrix} x_{\mathrm{P}} \\ y_{\mathrm{P}} \\ z_{\mathrm{P}} \end{pmatrix} - \begin{pmatrix} r \\ 0 \\ 0 \end{pmatrix} = \begin{pmatrix} R_{\mathrm{e}} \left[\cos\varphi_{\mathrm{P}} \cos\varphi_{\mathrm{sat}} \cos\lambda_{\Delta} + \sin\varphi_{\mathrm{P}} \sin\varphi_{\mathrm{sat}}\right] - r \\ R_{\mathrm{e}} \cos\varphi_{\mathrm{P}} \sin\lambda_{\Delta} \\ R_{\mathrm{e}} \left[\sin\varphi_{\mathrm{P}} \cos\varphi_{\mathrm{sat}} - \cos\varphi_{\mathrm{P}} \sin\varphi_{\mathrm{sat}} \cos\lambda_{\Delta}\right] \end{pmatrix} \tag{C.23}$$

$$\begin{pmatrix} x'_{\mathrm{P}} \\ y'_{\mathrm{P}} \\ z'_{\mathrm{P}} \end{pmatrix} = \begin{pmatrix} R_{\mathrm{e}} \left[\cos\varphi_{\mathrm{P}} \cos\varphi_{\mathrm{sat}} \cos\lambda_{\Delta} + \sin\varphi_{\mathrm{P}} \sin\varphi_{\mathrm{sat}}\right] - (R_{\mathrm{e}} + R_{\mathrm{o}}) \\ R_{\mathrm{e}} \cos\varphi_{\mathrm{P}} \sin\lambda_{\Delta} \\ R_{\mathrm{e}} \left[\sin\varphi_{\mathrm{P}} \cos\varphi_{\mathrm{sat}} - \cos\varphi_{\mathrm{P}} \sin\varphi_{\mathrm{sat}} \cos\lambda_{\Delta}\right] \end{pmatrix} \tag{C.24}$$

If the latitude of the satellite φ_{sat} is equal to 0° then:

$$\boldsymbol{A} \begin{pmatrix} x_{\mathrm{P}} \\ y_{\mathrm{P}} \\ z_{\mathrm{P}} \end{pmatrix} = \begin{pmatrix} R_{\mathrm{e}} \cos\varphi_{\mathrm{P}} \cos\lambda_{\Delta} \\ R_{\mathrm{e}} \cos\varphi_{\mathrm{P}} \sin\lambda_{\Delta} \\ R_{\mathrm{e}} \sin\varphi_{\mathrm{P}} \end{pmatrix} \tag{C.25}$$

which finally gives:

$$\begin{pmatrix} x'_{\mathrm{P}} \\ y'_{\mathrm{P}} \\ z'_{\mathrm{P}} \end{pmatrix} = \begin{pmatrix} R_{\mathrm{e}} \cos\varphi_{\mathrm{P}} \cos\lambda_{\Delta} - (R_{\mathrm{e}} + R_{\mathrm{o}}) \\ R_{\mathrm{e}} \cos\varphi_{\mathrm{P}} \sin\lambda_{\Delta} \\ R_{\mathrm{e}} \sin\varphi_{\mathrm{P}} \end{pmatrix} \tag{C.26}$$

Satellite View Angles

As written previously the coordinates of the point P which is located on the surface of the earth can be expressed viewed from the satellite, i.e. considering a satellite-centred coordinates system.

The coordinates of the point P can also be expressed according to the view angles of the satellite antenna. Let's define the angle υ as the off-axis angle and σ as the orientation in the vertical and the horizontal directions ([LuWeJa00]). These two angles are also called the true view angles of the satellite.

The angle υ thus describes the angle between the semi-segment [SX) and the segment [SP'] where S is the satellite, X the x-axis and P the point located on the surface of the earth. Knowing this angle permits to draw a circle around the point N. The angle σ identifies the position of the point P on the circle (Fig. C.8) according to the XSY plane.
The point P' in Fig. C.8 corresponds to the position of the point in the SXZ plane according to the off-axis angle υ. A rotation of angle σ around the x-axis gives the final position of the

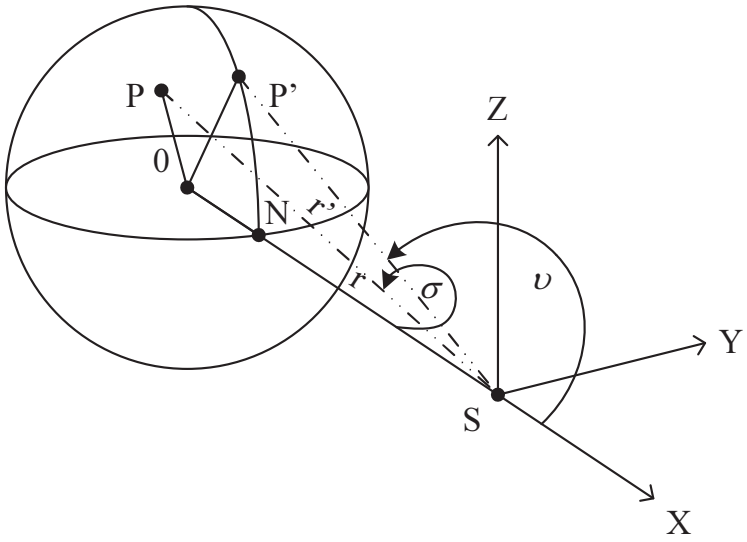


Figure C.8. *Satellite true view angles.*

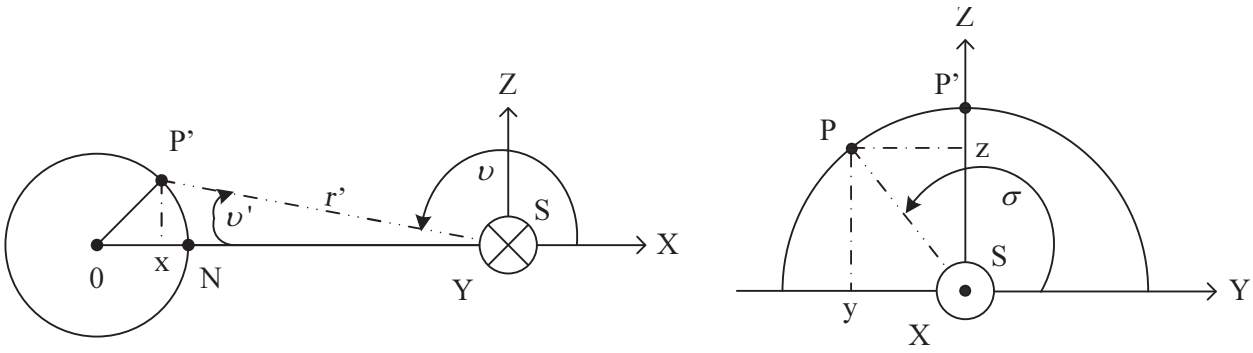


Figure C.9. *Coordinates of point P according to the satellite view angles.*

point P on the earth surface.

The coordinates of the point P while considering the satellite true view angles and a satellite-centred coordinates system are computed as follows (Fig. C.9).

The coordinates of P according to the x-axis is:

$$\cos \upsilon' = \frac{x'_{\mathrm{P}}}{r'} \Leftrightarrow x'_{\mathrm{P}} = r' \cos \upsilon' = r' \cos \pi - \upsilon \tag{C.27}$$

therefore:

$$x'_{\mathrm{P}} = r' \left(\cos \pi \cos \upsilon + \sin \pi \sin \upsilon\right) = -r' \cos \upsilon \tag{C.28}$$

The coordinates of P according to the y-axis is:

$$\sin \upsilon' = \frac{\mathrm{OP'}}{r'} \Leftrightarrow \mathrm{OP'} = r' \sin \upsilon' = r' \sin \pi - \upsilon \tag{C.29}$$

therefore:

$$\text{OP'} = r' \ (\sin\pi \, cos\upsilon - \sin\upsilon \ \cos\pi) = r' \ \sin\upsilon \tag{C.30}$$

since:

$$\cos\sigma = \frac{y'_{\mathrm{P}}}{\mathrm{OP}} = \frac{y'_{\mathrm{P}}}{\mathrm{OP'}} \Leftrightarrow y'_{\mathrm{P}} = r' \ \sin\upsilon \ \cos\sigma \tag{C.31}$$

Finally the coordinates of P according to the z-axis is:

$$\sin\sigma = \frac{z'_{\mathrm{P}}}{\mathrm{OP}} = \frac{z'_{\mathrm{P}}}{\mathrm{OP'}} \Leftrightarrow z'_{\mathrm{P}} = r' \ \sin\upsilon \ \sin\sigma \tag{C.32}$$

The coordinates of the point P according to the true view angles of the satellite are:

$$\begin{pmatrix} x'_{\mathrm{P}} \\ y'_{\mathrm{P}} \\ z'_{\mathrm{P}} \end{pmatrix} = \begin{pmatrix} -r' \ \cos\upsilon \\ r' \ \sin\upsilon \ \cos\sigma \\ r' \ \sin\upsilon \ \sin\sigma \end{pmatrix} \tag{C.33}$$

Knowing the coordinates of the point P in the satellite-centred coordinates system, it is possible to determine the satellite view angles and the distance between the satellite and the point P, also called slant-range:

$$x'_{\mathrm{P}} = -r' \ \cos\upsilon \Leftrightarrow cos\upsilon = -\frac{x'_{\mathrm{P}}}{r'} \Leftrightarrow \upsilon = \arccos\left(-\frac{x'_{\mathrm{P}}}{r'}\right) \tag{C.34}$$

In the same way:

$$\frac{z'_{\mathrm{P}}}{y'_{\mathrm{P}}} = \frac{r' \ \sin\upsilon \ \sin\sigma}{r' \ \sin\upsilon \ \cos\sigma} = \frac{\sin\sigma}{\cos\sigma} = \tan\sigma \Leftrightarrow \sigma = \arctan\left(\frac{z'_{\mathrm{P}}}{y'_{\mathrm{P}}}\right) \tag{C.35}$$

$$r' = \sqrt{x'^2_{\mathrm{P}} + y'^2_{\mathrm{P}} + z'^2_{\mathrm{P}}} \tag{C.36}$$

Knowing the satellite view angles υ and σ but not the distance r' it is also possible to find back the coordinates of the point P located on the surface of the earth. Actually the principle is to solve the equation which corresponds to the intersection of the semi-segment [SP) with the earth. There will be two solutions: one located at one side of the earth and one located at the other side of the earth.

We know:

– The position of the satellite, i.e. φ_{sat}, λ_{sat} and R_{o}

– The satellite view angles υ and σ

The coordinates of the earth surface viewed from the satellite are:

$$\begin{pmatrix} x'_{\mathrm{E}} \\ y'_{\mathrm{E}} \\ z'_{\mathrm{E}} \end{pmatrix} = \begin{pmatrix} R_{\mathrm{e}} \ [\cos\varphi_{\mathrm{E}} \ \cos\varphi_{\mathrm{sat}} \ \cos\lambda_{\Delta} + \sin\varphi_{\mathrm{E}} \ \sin\varphi_{\mathrm{sat}}] - (R_{\mathrm{e}} + R_{\mathrm{o}}) \\ R_{\mathrm{e}} \ \cos\varphi_{\mathrm{E}} \ \sin\lambda_{\Delta} \\ R_{\mathrm{e}} \ [\sin\varphi_{\mathrm{E}} \ \cos\varphi_{\mathrm{sat}} - \cos\varphi_{\mathrm{E}} \ \sin\varphi_{\mathrm{sat}} \ \cos\lambda_{\Delta}] \end{pmatrix} \tag{C.37}$$

with $\lambda_\Delta = \lambda_E - \lambda_{sat}$.

The distance from the satellite to a point located on the surface of the earth is:

$$d = \sqrt{x'^2_E + y'^2_E + z'^2_E} \tag{C.38}$$

therefore:

$$\begin{aligned} d^2 &= [R_e\ [\cos\varphi_E\ \cos\varphi_{sat}\ \cos\lambda_\Delta + \sin\varphi_E\ \sin\varphi_{sat}]]^2 + \\ &\quad (R_e\ \cos\varphi_E\ \sin\lambda_\Delta)^2 + [R_e\ [\sin\varphi_E\ \cos\varphi_{sat} - \cos\varphi_E\ \sin\varphi_{sat}\ \cos\lambda_\Delta]]^2 \end{aligned}$$

which leads to:

$$\begin{aligned} d^2 &= R_e^2\ (\cos\varphi_E\ \cos\varphi_{sat}\ \cos\lambda_\Delta + \sin\varphi_E\ \sin\varphi_{sat})^2 + r^2 - 2\,R_e\,r \\ &\quad (\cos\varphi_E\ \cos\varphi_{sat}\ \cos\lambda_\Delta + \sin\varphi_E\ \sin\varphi_{sat}) + R_e^2\ \cos^2\varphi_E\ \sin^2\lambda_\Delta + \\ &\quad R_e^2\ \sin^2\varphi_E\ \cos^2\varphi_{sat} + R_e^2\ \cos^2\varphi_E\ \sin^2\varphi_{sat}\ \cos^2\lambda_\Delta - \\ &\quad 2\,R_e^2\ \sin\varphi_E\ \cos\varphi_{sat}\ \cos\varphi_E\ \sin\varphi_{sat}\ \cos\lambda_\Delta \end{aligned}$$

then to:

$$\begin{aligned} d^2 &= R_e^2\ \cos^2\varphi_E\ \cos^2\varphi_{sat}\ + \cos^2\lambda_\Delta + R_e^2\ \sin^2\varphi_E\ \sin^2\varphi_{sat} + \\ &\quad 2\,R_e^2\ \cos\varphi_E\ \cos\varphi_{sat}\ \cos\lambda_\Delta\ \sin\varphi_E\ \sin\varphi_{sat} + r^2 - 2\,R_e\,r \\ &\quad \cos\varphi_E\ \cos\varphi_{sat}\ \cos\lambda_\Delta - 2\,R_e\,r\,\sin\varphi_E\ \sin\varphi_{sat} + R_e^2\ \cos^2\varphi_E\ \sin^2\lambda_\Delta + \\ &\quad R_e^2\ \sin^2\varphi_E\ \cos^2\varphi_{sat} + R_e^2\ \cos^2\varphi_E\ \sin^2\varphi_{sat}\ \cos^2\lambda_\Delta - \\ &\quad 2\,R_e^2\ \sin\varphi_E\ \cos\varphi_{sat}\ \cos\varphi_E\ \sin\varphi_{sat}\ \cos\lambda_\Delta \end{aligned}$$

which reduces to:

$$\begin{aligned} d^2 &= R_e^2\ \cos^2\varphi_E\ \cos^2\lambda_\Delta\ \left(\cos^2\varphi_{sat} + \sin^2\varphi_{sat}\right) + R_e^2\ \sin^2\varphi_E\ \left(\sin^2\varphi_{sat} + \cos^2\varphi_{sat}\right) + \\ &\quad r^2 - 2\,R_e\,r\ (\cos\varphi_E\ \cos\varphi_{sat}\ \cos\lambda_\Delta + \sin\varphi_E\ \sin\varphi_{sat}) + R_e^2\ \cos^2\varphi_E\ \sin^2\lambda_\Delta \end{aligned}$$

and to:

$$\begin{aligned} d^2 &= R_e^2\ \cos^2\varphi_E\ \left(\cos^2\lambda_\Delta + \sin^2\lambda_\Delta\right) + R_e^2\ \sin^2\varphi_E + r^2 - \\ &\quad 2\,R_e\,r\ (\cos\varphi_E\ \cos\varphi_{sat}\ \cos\lambda_\Delta + \sin\varphi_E\ \sin\varphi_{sat}) \end{aligned}$$

The previous expression simplifies into:

$$d^2 = R_e^2\ \left(\cos^2\varphi_E + \sin^2\varphi_E\right) + r^2 - 2\,R_e\,r\ (\cos\varphi_E\ \cos\varphi_{sat}\ \cos\lambda_\Delta + \sin\varphi_E\ \sin\varphi_{sat})$$

which finally gives:

$$d^2 = R_e^2 + r^2 - 2\,R_e\,r\,(\cos\varphi_E\,\cos\varphi_{sat}\,\cos\lambda_\Delta + \sin\varphi_E\,\sin\varphi_{sat}) \tag{C.39}$$

Finding the coordinates of the point P knowing the satellite view angle υ and σ remains in solving the equation:

$$d^2 = R_e^2 + r^2 - 2\,R_e\,r\,(\cos\varphi_E\,\cos\varphi_{sat}\,\cos\lambda_\Delta + \sin\varphi_E\,\sin\varphi_{sat}) = r'^2 \tag{C.40}$$

with $\lambda_\Delta = \lambda_P - \lambda_{sat}$, i.e.:

$$R_e^2 + r^2 - 2\,R_e\,r\,(\cos\varphi_E\,\cos\varphi_{sat}\,\cos\lambda_\Delta + \sin\varphi_E\,\sin\varphi_{sat}) - r'^2 = 0 \tag{C.41}$$

We expressed previously the coordinate x'_P according to the satellite-centred coordinates system:

$$x'_P = R_e\,[\cos\varphi_P\,\cos\varphi_{sat}\,\cos\lambda_\Delta + \sin\varphi_P\,\sin\varphi_{sat}] - (R_e + R_o) \tag{C.42}$$

which is equivalent as writing:

$$\frac{x'_P + (R_e + R_o)}{R_e} = [\cos\varphi_P\,\cos\varphi_{sat}\,\cos\lambda_\Delta + \sin\varphi_P\,\sin\varphi_{sat}] \tag{C.43}$$

The coordinate x'_P according to the satellite true view angles is equal to:

$$x'_P = -r'\,\cos\upsilon \tag{C.44}$$

We can thus write:

$$[\cos\varphi_P\,\cos\varphi_{sat}\,\cos\lambda_\Delta + \sin\varphi_P\,\sin\varphi_{sat}] = \frac{x'_P + (R_e + R_o)}{R_e} = \frac{-r'\,\cos\upsilon + (R_e + R_o)}{R_e} \tag{C.45}$$

The previous equation becomes:

$$R_e^2 + r^2 - 2\,R_e\,r\,\frac{-r'\,\cos\upsilon + (R_e + R_o)}{R_e} - r'^2 = 0 \tag{C.46}$$

which is also:

$$-r'^2 + 2\,r\,\cos\upsilon\,r' + R_e^2 + r^2 - 2\,r\,(R_e + R_o) = 0 \tag{C.47}$$

which finally gives:

$$r'^2 - 2\,r\,\cos\upsilon\,r' + r^2 - R_e^2 = 0 \tag{C.48}$$

Knowing the off-axis angle υ we can thus solve the previous polynomial:

$$a\,r'^2 + b\,r' + c = 0 \tag{C.49}$$

with $a = 1$, $b = -2\,r\,cos\upsilon$ and $c = r^2 - R_e^2$ (please remind that $r = R_e + R_o$).

Among the two solutions available the smallest value will correspond to the point located at the correct side of the earth, i.e. the point seen by the satellite. The smallest value will thus give the value of r'.

Using the previous relations and considering the latitude of the satellite φ_{sat} is equal to 0°:

$$z'_P = R_e \sin\varphi_P = r' \sin\upsilon \sin\sigma \Leftrightarrow \sin\varphi_P = \frac{r' \sin\upsilon \sin\sigma}{R_e} \tag{C.50}$$

which leads to:

$$\varphi_P = \arcsin \frac{r' \sin\upsilon \sin\sigma}{R_e} \tag{C.51}$$

In the same way:

$$\frac{z'_P}{y'_P} = \tan\sigma = \frac{R_e \sin\varphi_P}{R_e \cos\varphi_P \sin\lambda_\Delta} = \tan\varphi_P \frac{1}{\sin\lambda_\Delta} \Leftrightarrow \sin\lambda_\Delta = \frac{\tan\varphi_P}{\tan\sigma} \tag{C.52}$$

which gives:

$$\lambda_\Delta = \arcsin\left(\frac{\tan\varphi_P}{\tan\sigma}\right) \tag{C.53}$$

with $\lambda_P = \lambda_\Delta + \lambda_{sat}$. or:

$$y'_P = R_e \cos\varphi_P \sin\lambda_\Delta = r' \sin\upsilon \cos\sigma \Leftrightarrow \sin\lambda_\Delta = \frac{r' \sin\upsilon \cos\sigma}{R_e \cos\varphi_P} \tag{C.54}$$

which finally leads to:

$$\lambda_\Delta = \arcsin\left(\frac{r' \sin\upsilon \cos\sigma}{R_e \cos\varphi_P}\right) \tag{C.55}$$

with $\lambda_P = \lambda_\Delta + \lambda_{sat}$.

Beam Border Computation

The beam border of a satellite designates the border at which the satellite antenna transmission gain reaches a given threshold. One can consider for instance the border of a beam at -3 dB. The beam border is directly related to the radiation pattern of the satellite antenna. The antenna points towards a given direction, i.e. to a point located on the surface of the earth. This point is called beam centre. The radiation pattern of the antenna contains one main lobe and several side lobes. The gain of the transmit antenna decreases when moving out of the pointing direction. At a given angle the gain will be two times lower than the maximum one. The full angle (both sides) is called beam width and is usually noted θ_{3dB} (Fig. C.10).

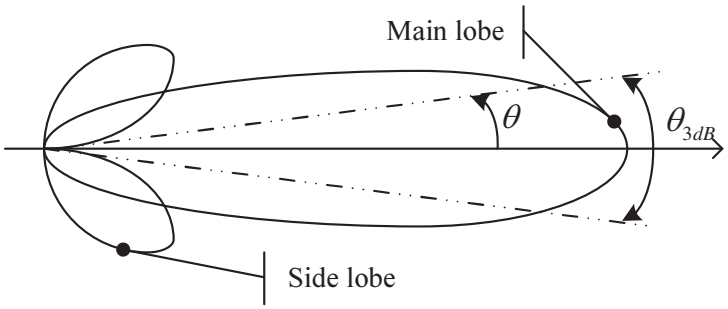


Figure C.10. *Beam width.*

Knowing the direction to which a given beam (belonging to a satellite: multi-beam satellite) is pointing to, we would like to determine the corresponding beam border. The beam targets a point located on the surface of the earth which is the beam centre. The coordinates of the beam centre are as follows.

In the geocentric coordinates system:

$$\begin{pmatrix} x_{\mathrm{B}} \\ y_{\mathrm{B}} \\ z_{\mathrm{B}} \end{pmatrix} = \begin{pmatrix} R_{\mathrm{e}} \cos\varphi_{\mathrm{B}} \cos\lambda_{\mathrm{B}} \\ R_{\mathrm{e}} \cos\varphi_{\mathrm{B}} \sin\lambda_{\mathrm{B}} \\ R_{\mathrm{e}} \sin\varphi_{\mathrm{B}} \end{pmatrix} \tag{C.56}$$

where φ_{B} and λ_{B} are respectively the latitude and the longitude of the beam centre.

In the satellite-centred coordinates system (we suppose that the latitude of the satellite φ_{sat} is equal to 0°):

$$\begin{pmatrix} x'_{\mathrm{B}} \\ y'_{\mathrm{B}} \\ z'_{\mathrm{B}} \end{pmatrix} = \begin{pmatrix} R_{\mathrm{e}} \cos\varphi_{\mathrm{B}} \cos\lambda_{\Delta} - (R_{\mathrm{e}} + R_{\mathrm{o}}) \\ R_{\mathrm{e}} \cos\varphi_{\mathrm{B}} \sin\lambda_{\Delta} \\ R_{\mathrm{e}} \sin\varphi_{\mathrm{B}} \end{pmatrix} \tag{C.57}$$

Determining the beam border consists into computing the intersection between the cone drawn by the satellite antenna and the surface of the earth. The slant-range, i.e. the distance between the satellite and the beam centre is obtained using the following formula:

$$r' = \sqrt{x'^2_{\mathrm{B}} + y'^2_{\mathrm{B}} + z'^2_{\mathrm{B}}} \tag{C.58}$$

A cone is drawn viewed from the satellite towards the centre of the earth. Actually a circle is built at a distance r' from the satellite with centre pointing the centre of the earth (Fig. C.11).

The radius of the circle is:

$$\tan\theta = \frac{R_{\mathrm{c}}}{r'} \Leftrightarrow R_{\mathrm{c}} = r' \tan\theta \tag{C.59}$$

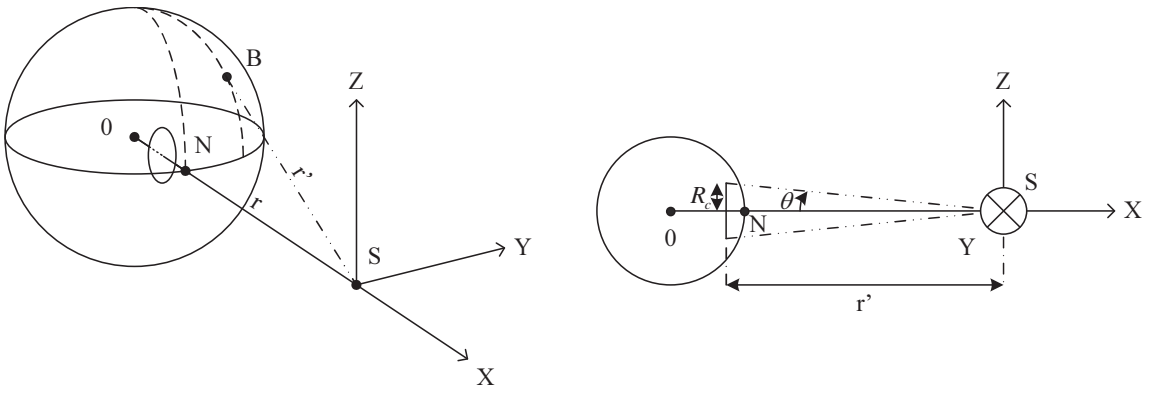


Figure C.11. *Building a cone to determine the beam border (1).*

with $\theta = \theta_{3\mathrm{dB}}/2$.

The coordinates of this circle viewed from the satellite are by definition:

$$\begin{pmatrix} x'_{\mathrm{C}} \\ y'_{\mathrm{C}} \\ z'_{\mathrm{C}} \end{pmatrix} = \begin{pmatrix} -r' \\ R_{\mathrm{c}} \cos\alpha \\ R_{\mathrm{c}} \sin\alpha \end{pmatrix} \tag{C.60}$$

with $0 \leq \alpha \leq 2\pi$.

We then perform two rotations according to the satellite view angles i.e. the view angles while pointing the centre of the beam: rotation of an angle υ around the y-axis and rotation of an angle σ around the x-axis:

$$\begin{pmatrix} x''_{\mathrm{C}} \\ y''_{\mathrm{C}} \\ z''_{\mathrm{C}} \end{pmatrix} = \begin{pmatrix} 1 & 0 & 0 \\ 0 & \cos\sigma & -\sin\sigma \\ 0 & \sin\sigma & \cos\sigma \end{pmatrix} \begin{pmatrix} \cos\upsilon & 0 & \sin\upsilon \\ 0 & 1 & 0 \\ -\sin\upsilon & 0 & \cos\upsilon \end{pmatrix} \begin{pmatrix} x'_{\mathrm{C}} \\ y'_{\mathrm{C}} \\ z'_{\mathrm{C}} \end{pmatrix} \tag{C.61}$$

The centre of the circle is now located in the beam centre (Fig. C.12).

The purpose is to compute for each point of the circle ($0 \leq \alpha \leq 2\pi$) the two angles υ and σ and to find the corresponding r' which belongs to the surface of the earth.

To do so we solve (refer to the previous demonstration):

$$r'^2 - 2\,r\,cos\upsilon\,r' + r^2 - R_{\mathrm{e}}^2 = 0 \tag{C.62}$$

and we compute:

$$\varphi_{\mathrm{P}} = \arcsin\left(\frac{r'\,\sin\upsilon\,\sin\sigma}{R_{\mathrm{e}}}\right) \tag{C.63}$$

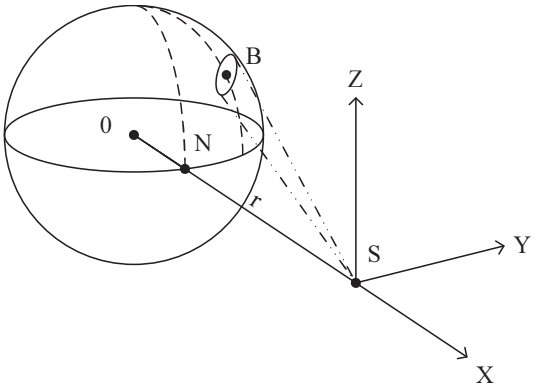


Figure C.12. *Building a cone to determine the beam border (2).*

$$\lambda_\Delta = \arcsin\left(\frac{\tan\varphi_\mathrm{P}}{\tan\sigma}\right) \tag{C.64}$$

with $\lambda_\mathrm{P} = \lambda_\Delta + \lambda_\mathrm{sat}$ and where P is a point belonging to the beam border.

As an example we consider the following:
– Altitude R_o is 35 786 km (geostationary satellite),
– Radius of the earth R_e is about 6 378.137 km,
– Latitude of the satellite φ_sat is 0°,
– Longitude of the satellite λ_sat is 19.2°,
– Latitude of the beam centre φ_B is 50° North,
– Longitude of the beam centre λ_B is 5° West,
– Half-side beam width θ is 0.6°.
Fig. C.13 shows the cone that was built according to the previous formulae (green shape).

Fig. C.14 illustrates the beam border after having solved the intersection of the cone with the surface of the earth (shape with the blue contour).

Beam Centre Coordinates

The next tables (Table C.1, Table C.2 and Table C.3) indicate the beam center coordinates and the corresponding frequency allocation for the ninety six multi-beam satellite system ($B = 96$).

Table C.4 gives the same information but for the seven multi-beam satellite system ($B = 7$) and universal frequency reuse ($K = 1$). It has to be remarked that the identifiers of beam (beam IDs) indicated in this table are the ones considered in all scenarios in which those

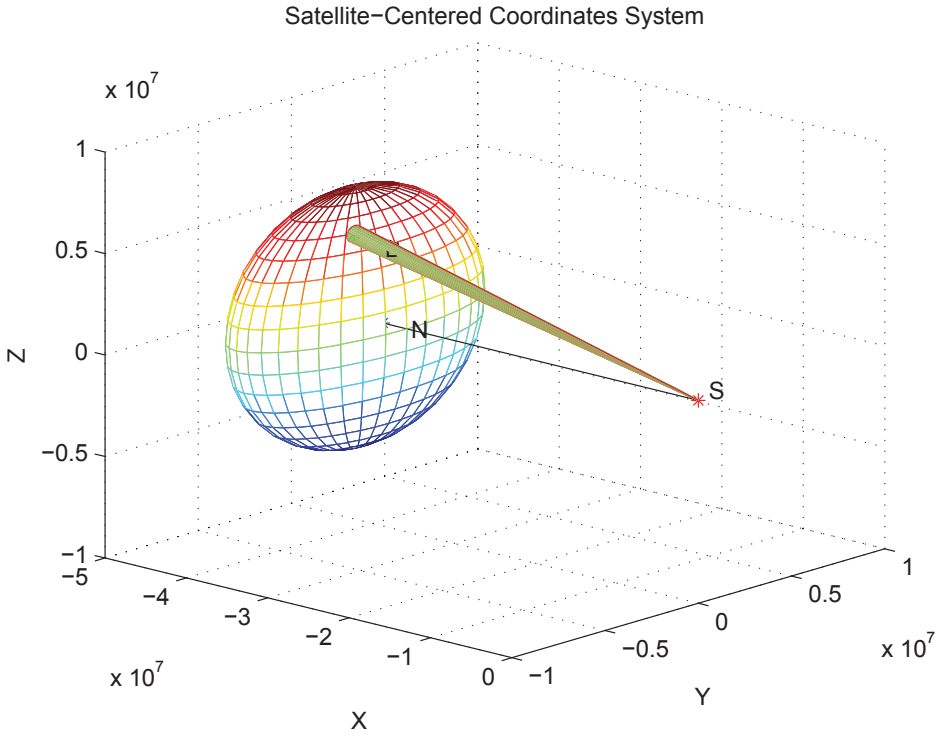


Figure C.13. *Beam border example - building a cone.*

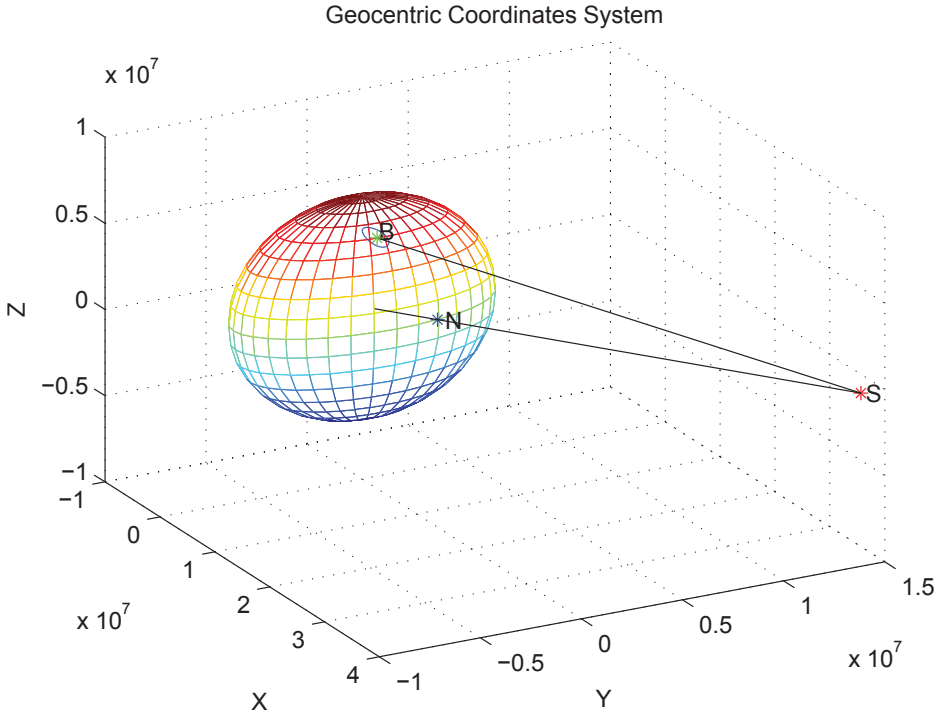


Figure C.14. *Beam border example - final beam border.*

seven beams are considered. Therefore the beam IDs indicated in this table and their order do not match the ones of the ninety six beams system. Table C.5 presents exactly the same information but for three colours ($K = 3$).

Table C.1. *Beam centre coordinates and frequency allocation for the 96 multi-beam satellite system (1 of 3).*

Beam ID [#]	Latitude [°]	Longitude [°]	Freq. ID $K = 1$	Freq. ID $K = 3$	Freq. ID $K = 4$
01	67.00	11.00	1	1	1
02	67.00	16.25	1	2	2
03	67.00	21.75	1	3	1
04	67.00	27.50	1	1	2
05	61.00	6.50	1	1	3
06	61.00	10.75	1	2	4
07	61.00	15.00	1	3	3
08	61.00	19.25	1	1	4
09	61.00	23.50	1	2	3
10	61.00	27.75	1	3	4
11	56.20	−6.25	1	2	1
12	56.20	−2.00	1	3	2
13	56.20	10.00	1	3	1
14	56.20	13.75	1	1	2
15	56.20	17.50	1	2	1
16	56.20	21.25	1	3	2
17	56.20	25.00	1	1	1
18	52.25	−8.90	1	2	3
19	52.25	−5.65	1	3	4
20	52.25	−1.85	1	1	3
21	52.00	2.20	1	2	4
22	52.25	5.75	1	3	3
23	52.25	9.25	1	1	4
24	52.25	12.75	1	2	3
25	52.25	16.00	1	3	4
26	52.25	19.25	1	1	3
27	52.25	22.50	1	2	4
28	48.75	−4.00	1	1	1
29	48.75	−1.25	1	2	2
30	48.75	2.00	1	3	1
31	48.75	5.40	1	1	2
32	48.75	8.75	1	2	1

Table C.2. *Beam centre coordinates and frequency allocation for the 96 multi-beam satellite system (2 of 3).*

Beam ID [#]	Latitude [°]	Longitude [°]	Freq. ID $K = 1$	Freq. ID $K = 3$	Freq. ID $K = 4$
33	48.75	11.90	1	3	2
34	48.75	14.80	1	1	1
35	48.75	17.80	1	2	2
36	48.75	21.00	1	3	1
37	45.50	−0.90	1	3	3
38	45.50	2.00	1	1	4
39	45.50	4.80	1	2	3
40	45.50	7.80	1	3	4
41	45.50	10.80	1	1	3
42	45.50	13.70	1	2	4
43	45.50	16.50	1	3	3
44	45.50	19.30	1	1	4
45	45.50	22.10	1	2	3
46	42.25	−7.25	1	2	2
47	42.50	−4.25	1	3	1
48	42.50	−1.25	1	1	2
49	42.50	1.50	1	2	1
50	42.50	4.25	1	3	2
51	42.50	7.25	1	1	1
52	42.50	10.00	1	2	2
53	42.50	12.75	1	3	1
54	42.50	15.50	1	1	2
55	42.50	18.25	1	2	1
56	42.50	20.75	1	3	2
57	42.50	23.25	1	1	1
58	42.50	25.75	1	2	2
59	42.50	28.50	1	3	1
60	42.50	31.25	1	1	2
61	42.50	34.25	1	2	1
62	42.50	37.00	1	3	2
63	39.90	−7.50	1	3	3
64	39.75	−4.25	1	1	4

Table C.3. *Beam centre coordinates and frequency allocation for the 96 multi-beam satellite system (3 of 3).*

Beam ID [#]	Latitude [°]	Longitude [°]	Freq. ID $K = 1$	Freq. ID $K = 3$	Freq. ID $K = 4$
65	39.75	−1.50	1	2	3
66	39.75	0.75	1	3	4
67	39.75	3.50	1	1	3
68	39.75	9.25	1	3	3
69	39.75	14.50	1	2	3
70	39.75	17.00	1	3	4
71	39.75	19.50	1	1	3
72	39.75	21.75	1	2	4
73	39.75	24.00	1	3	3
74	39.75	26.50	1	1	4
75	39.75	29.25	1	2	3
76	39.75	32.00	1	3	4
77	39.75	34.75	1	1	3
78	39.75	37.50	1	2	4
79	39.75	40.25	1	3	3
80	39.75	43.20	1	1	4
81	37.75	−7.75	1	1	2
82	37.25	−5.00	1	2	1
83	37.25	−2.00	1	3	2
84	37.25	13.50	1	3	2
85	37.25	16.00	1	1	1
86	37.25	22.75	1	1	2
87	37.25	25.00	1	2	1
88	37.25	27.50	1	3	2
89	37.25	30.25	1	1	1
90	37.25	32.75	1	2	2
91	37.25	35.50	1	3	1
92	37.25	38.00	1	1	2
93	37.25	40.75	1	2	1
94	37.25	43.50	1	3	2
95	35.00	25.00	1	1	3
96	35.00	33.50	1	1	4

Table C.4. *Beam centre coordinates and frequency allocation for the seven multi-beam satellite system ($B = 7$) and full frequency reuse ($K = 1$).*

Beam ID [#]	Beam ID [#] (full)	Latitude [°]	Longitude [°]	Freq. ID $K = 1$	Freq. ID $K = 3$	Freq. ID $K = 4$
01	33	48.75	11.90	1	3	2
02	24	52.25	12.75	1	2	3
03	34	48.75	14.80	1	1	1
04	42	45.50	13.70	1	2	4
05	41	45.50	10.80	1	1	3
06	32	48.75	8.75	1	2	1
07	23	52.25	9.25	1	1	4

Table C.5. *Beam centre coordinates and frequency allocation for the seven multi-beam satellite system ($B = 7$) and three colours ($K = 3$).*

Beam ID [#]	Beam ID [#] (full)	Latitude [°]	Longitude [°]	Freq. ID $K = 1$	Freq. ID $K = 3$	Freq. ID $K = 4$
01	33	48.75	11.90	1	3	2
02	13	56.20	10.00	1	3	1
03	25	52.25	16.00	1	3	4
04	43	45.50	16.50	1	3	3
05	53	42.50	12.75	1	3	1
06	40	45.50	7.80	1	3	4
07	22	52.25	5.75	1	3	3

Satellite Terminal Coordinates

The coordinates of the satellite terminals corresponding to the so-called “bad” case of the seven beams ($B = 7$) are given in Table C.6.

Table C.6. *Satellite terminal coordinates for the seven multi-beam satellite system ($B = 7$) and corresponding to the "bad" case.*

Beam ID [#]	Latitude [°]	Longitude [°]
01	48.75	11.90
02	50.50	13.20
03	47.50	14.00
04	47.00	13.40
05	47.20	10.50
06	49.50	9.80
07	50.50	10.00

The coordinates of the satellite terminals corresponding to the so-called "good" case of the seven beams ($B = 7$) are given in Table C.7. In that case the coordinates of the satellite terminals are identical to the beam center coordinates (Table C.4).

Table C.7. *Satellite terminal coordinates for the seven multi-beam satellite system ($B = 7$) and corresponding to the "good" case.*

Beam ID [#]	Latitude [°]	Longitude [°]
01	48.75	11.90
02	52.25	12.75
03	48.75	14.80
04	45.50	13.70
05	45.50	10.80
06	48.75	8.75
07	52.25	9.25

Important Coordinates

The following important coordinates are used in this document:

– Munich: Latitude 48.14° North, Longitude 11.58° East

– London: Latitude 51.51° North, Longitude 0.13° West

– Beam covering Munich: beam ID 33 as referred in Table C.2

C.1.2 Radiation Pattern

Introduction

Using the satellite view angles defined in the previous section (Section C.1.1), it is possible to determine the receive gain of the satellite antenna (link from the user terminal on ground to the satellite, i.e. return- up-link) for a given position on earth. The receive gain depends directly on the antenna characteristics and generally satellite antennas can be seen as paraboloidal reflectors antennas.

The maximum gain is proportional to the antenna area [MaBo02]:

$$G_{\max} = \eta \left(\frac{\pi \, d_{\mathrm{a}}}{\lambda} \right)^2 \tag{C.65}$$

where η is the antenna efficiency (generally comprised between 0.55 and 0.65), d_{a} is the diameter of the antenna in meters and λ is the wavelength in meters per second. The wavelength is obtained as follows:

$$\lambda = c/f \tag{C.66}$$

where c is the speed light ($2.998\,10^8$ m/s, generally assumed at $3\,10^8$ m/s) and f is the frequency in Hertz.

The half-side beam width $\theta_{3\mathrm{dB}}$ is defined as the antenna span in which the gain is larger than $G_{\max} - 3$ dB and is approximated as follows [MaBo02]:

$$2\,\theta_{3\mathrm{dB}} \simeq 70^\circ \, \lambda/d_{\mathrm{a}} \qquad \text{for non-uniform illumination} \tag{C.67}$$

$$2\,\theta_{3\mathrm{dB}} \simeq 58^\circ \, \lambda/d_{\mathrm{a}} \qquad \text{for a uniform illumination} \tag{C.68}$$

An highly focused satellite antenna beam, i.e. with a rather small $\theta_{3\mathrm{dB}}$ (few degrees), is called spot beam. The purpose is now to determine what is really the receive gain according to the satellite view angles and also to the satellite antenna characteristics.

Paraboloidal Reflector Antennas

According to [Col85] (section 4.6), the expression of the aperture-field along the y-axis is:

$$f_y = 2\,\pi \, E_0 \int_0^a J_0 \left(k_0 \, \rho \, \sin\theta \right) \left[(1 - T) + T \left(1 - \frac{\rho^2}{a^2} \right)^n \right] \rho \, d\rho \tag{C.69}$$

where a is the radius of the antenna (i.e. $d_{\mathrm{a}}/2$), T is the value of the field at the edge of aperture, $k_0 = 2\pi/\lambda$, and J_0 is the Bessel function knowing that first order Bessel function

of order n is defined by:

$$J_n(x) = \left(\frac{x}{2}\right)^n \sum_{p=0}^{\infty} \frac{(-1)^p}{2^{2p}\, p!\, (n+p)!}\, x^{2p} \tag{C.70}$$

First part of the integral:

Let's solve the first part of the integral, i.e.:

$$A = (1-T) \int_0^a J_0(k_0\, \rho\, \sin\theta)\; \rho\, d\rho$$

To do so we set $u = k_0\, a\, \sin\theta$ and $x = \rho/a$ such that we can write:

$$A = (1-T) \int_0^1 J_0(u\, x)\; a^2\, x\, dx \tag{C.71}$$

which is also:

$$A = (1-T)\; a^2 \int_0^1 \sum_{p=0}^{\infty} \frac{(-1)^p}{2^{2p}\, p!\, p!}\; (ux)^{2p}\; x\, dx \tag{C.72}$$

which can also be written as:

$$\sum_{p=0}^{\infty} \frac{(1-T)\; a^2}{2^{2p}}\, \frac{(-1)^p}{(p!)^2}\, u^{2p} \int_0^1 x^{2p+1}\, dx \tag{C.73}$$

Solving the integral leads to:

$$\int_0^1 x^{2p+1}\, dx = \left[\frac{x^{2p+2}}{2p+2}\right]_0^1 = \frac{1}{2p+2} \tag{C.74}$$

A becomes:

$$A = \sum_{p=0}^{\infty} (1-T)\; a^2\, \frac{(-1)^p}{2^{2p}\; (p!)^2}\, u^{2p}\, \frac{1}{2p+2} \tag{C.75}$$

which can also be written as follows:

$$A = (1-T)\; a^2\, \frac{1}{u}\, \frac{u}{2} \sum_{p=0}^{\infty} \frac{(-1)^p\; u^{2p}}{2^{2p}\, p!\; p!\; (p+1)} \tag{C.76}$$

the right part of the previous equation corresponds to $J_1(u)$ such that:

$$A = (1-T)\; a^2\, \frac{1}{u}\, J_1(u) \tag{C.77}$$

Second part of the integral:

Let's solve now the right part of (C.69), i.e.:

$$B = T \int_0^a J_0(k_0\, \rho\, \sin\theta) \left(1 - \frac{\rho^2}{a^2}\right)^n \rho\, d\rho \tag{C.78}$$

By setting as before $u = k_0\, a\, \sin\theta$ and $x = \rho/a$ we obtain:

$$B = T\, a^2 \int_0^1 J_0(ux)\; \left(1 - x^2\right)^n\; x\, dx \tag{C.79}$$

By definition of the Bessel function, this is equivalent to:

$$B = T\,a^2 \sum_{p=0}^{\infty} \frac{(-1)^p}{2^{2p}\,p!\,p!}\,u^{2p} \int_0^1 x^{2p+1}\,\left(1-x^2\right)^n\,dx \tag{C.80}$$

Let's denote the integral of the previous equation as C_1 and solve it:

$$C_1 = \int_0^1 x^{2p+1}\,\left(1-x^2\right)^n\,dx \tag{C.81}$$

$$C_1 = \left[\left(1-x^2\right)^n\,\frac{x^{2p+2}}{2p+2}\right]_0^1 - \int_0^1 \frac{x^{2p+2}}{2p+2}\,(-2x)\,n\,\left(1-x^2\right)^{n-1}\,dx \tag{C.82}$$

which gives:

$$C_1 = \int_0^1 2n\,\frac{1}{2p+2}\,x^{2p+3}\,\left(1-x^2\right)^{n-1}\,dx \tag{C.83}$$

Let's solve this new integral that we now denote as C_2:

$$C_2 = \frac{2n}{2\,(p+1)}\int_0^1 x^{2p+3}\,\left(1-x^2\right)^{n-1}\,dx = \frac{2^2(n)(n-1)}{2^2\,(p+1)\,(p+2)}\int_0^1 x^{2p+5}\,\left(1-x^2\right)^{n-2}\,dx \tag{C.84}$$

and we denote the previous expression as C_3. Solving C_3 gives the following:

$$C_3 = \frac{2^3(n)(n-1)(n-2)}{2^3\,(p+1)\,(p+1)\,(p+2)\,(p+3)}\int_0^1 x^{2p+7}\,\left(1-x^2\right)^{n-3}\,dx \tag{C.85}$$

By generalising to the k-th step, we obtain:

$$C_k = \frac{2^k(n)(n-1)(n-2)\cdots(n-k+1)}{2^k\,(p+1)\,(p+2)\cdots(p+k)}\int_0^1 x^{2p+2k+1}\,\left(1-x^2\right)^{n-k}\,dx \tag{C.86}$$

Setting $k = n$ leads to:

$$C_n = \frac{2^n\,n!}{2^n\,(p+1)\,(p+2)\cdots(p+n)}\int_0^1 x^{2p+2n+1}\,\left(1-x^2\right)^0\,dx \tag{C.87}$$

In the previous expression the integral leads to:

$$\int_0^1 x^{2p+2n+1}\,dx = \left[\frac{x^{2p+2p+2}}{2p+2p+2}\right]_0^1 = \frac{1}{2p+2n+2} \tag{C.88}$$

Therefore we have:

$$\begin{aligned}
B &= T\,a^2 \sum_{p=0}^{\infty} \frac{(-1)^p}{2^{2p}\,p!\,p!}\,u^{2p} \int_0^1 x^{2p+1}\,\left(1-x^2\right)^n\,dx \\
&= T\,a^2 \sum_{p=0}^{\infty} \frac{(-1)^p}{2^{2p}\,p!\,p!}\,u^{2p}\,\frac{2^n\,n!}{2^{n+1}\,\frac{(p+n+1)!}{p!}} \\
&= T\,a^2\,\frac{2^n\,n!}{2^{n+1}\,u^{n+1}}\,u^{n+1} \sum_{p=0}^{\infty} \frac{(-1)^p\;u^{2p}}{2^{2p}\,p!\;(p+n+1)!} \\
&= T\,a^2\,\frac{2^n\,n!}{u^{n+1}}\,\frac{u^{n+1}}{2^{n+1}} \sum_{p=0}^{\infty} \frac{(-1)^p\;u^{2p}}{2^{2p}\,p!\;(p+n+1)!} \\
&= T\,a^2\,\frac{2^{n+1}}{2}\,n!\,\frac{J_{n+1}\,(u)}{u^{n+1}}
\end{aligned} \tag{C.89}$$

which finally gives:

$$B = T\,\frac{a^2}{2}\,2^{n+1}\,n!\,\frac{J_{n+1}\,(u)}{u^{n+1}} \tag{C.90}$$

The expression (C.69) can finally be written as:

$$f_y = 2\,\pi\,E_0\int_0^a J_0\,(k_0\,\rho\,\sin\theta)\,\left[(1-T)+T\left(1-\frac{\rho^2}{a^2}\right)^n\right]\,\rho\,d\rho = 2\,\pi\,E_0\,\,(A+B)$$

which can finally be written as:

$$f_y = \pi\,E_0\,a^2\,\left[2\,(1-T)\,\frac{J_1\,(u)}{u}+T\,2^{n+1}\,n!\,\frac{J_{n+1}\,(u)}{u^{n+1}}\right] \tag{C.91}$$

As can be seen (C.91) does not exactly correspond to the expression present in [Col85] (page 211, (4.84)). There is actually an error in [Col85] as reported in Section D.2.

Aperture Field Variation

(C.91) can also be written as follows:

$$f_y(u) = \pi\,E_0\,a^2\,\,(1-T)\,\left[2\,\frac{J_1\,(u)}{u}+\frac{T}{1-T}\,2^{n+1}\,n!\,\frac{J_{n+1}\,(u)}{u^{n+1}}\right] \tag{C.92}$$

We denote with $F\,(u)$ the ratio between the aperture field for a given value of θ with the maximum aperture field obtained, i.e. when $\theta = 0$:

$$u = k_0\,a\,\sin\theta = \frac{2\pi}{\lambda}\,\frac{d_{\mathrm{a}}}{2}\,\sin\theta = \frac{\pi\,d_{\mathrm{a}}}{\lambda}\,\sin\theta \Rightarrow u = 0 \text{ when } \theta = 0$$

$$F\,(u) = \frac{f_y(u)}{f_y(u=0)} \tag{C.93}$$

The purpose is now to determine the expression of $f_y(u=0)$.

Bessel function of order 1:

Let's evaluate the expression $J_1(u)/u$:

$$\frac{J_1(u)}{u} = \frac{1}{u}\,\frac{u}{2}\,\sum_{p=0}^{\infty}\frac{(-1)^p}{2^{2p}\,p!\,\,(p+1)!}\,u^{2p}$$

which can also be written when $u = 0$ as follows:

$$\frac{1}{2}\,\lim_{u\to 0}\,\frac{1\,u^0}{1\,1\,1}+\frac{1}{2}\,\sum_{p=1}^{\infty}\frac{(-1)^p}{2^{2p}\,p!\,\,(p+1)!}\,0^{2p} = \frac{1}{2}\,1+0 = \frac{1}{2}$$

Bessel function of order $n+1$***:***

Let's in that case evaluate the expression $2^{n+1}\,n!\,J_{n+1}(u)/u^{n+1}$:

$$2^{n+1}\,n!\,\frac{J_{n+1}(u)}{u^{n+1}} = n!\sum_{p=0}^{\infty}\frac{(-1)^p}{2^{2p}\,p!\;(n+1+p)!}\,u^{2p}$$

using the same method as for the Bessel function of order 1, we get:

$$n!\lim_{u\to 0}\frac{1\,u^0}{1\,1\;(n+1)!} + n!\sum_{p=1}^{\infty}\frac{(-1)^p}{2^{2p}\,p!\;(n+1+p)!}\,0^{2p} = \frac{1}{n+1}$$

Therefore the ratio $F(u)$ can be written as follows:

$$F(u) = \frac{f_y(u)}{f_y(u=0)} = \frac{\pi\,E_0\,a^2\;(1-T)\left[2\,\frac{J_1(u)}{u} + \frac{T}{1-T}\,2^{n+1}\,n!\,\frac{J_{n+1}(u)}{u^{n+1}}\right]}{\pi\,E_0\,a^2\;(1-T)\left[2\,\frac{1}{2} + \frac{T}{1-T}\,\frac{1}{n+1}\right]}$$

which is also:

$$F(u) = \frac{(n+1)\;(1-T)}{(n+1)\;(1-T)+T}\left[2\,\frac{J_1\,(u)}{u} + \frac{T}{1-T}\,2^{n+1}\,n!\,\frac{J_{n+1}\,(u)}{u^{n+1}}\right]$$

The parameter n is generally denoted as p and is a coefficient managing the rate at which the aperture field decreases, therefore the following formula is more commonly found in literature like in [CCFRV92]:

$$F(u) = \frac{(p+1)\;(1-T)}{(p+1)\;(1-T)+T}\left[2\,\frac{J_1\,(u)}{u} + \frac{T}{1-T}\,2^{p+1}\,p!\,\frac{J_{p+1}\,(u)}{u^{p+1}}\right] \tag{C.94}$$

Gain Variation

As mentioned previously the function $F(u)$ corresponds to the ratio between the aperture field for a given value of θ with the maximum aperture field obtained. Therefore the value of the gain can be computed as follows:

$$G(u) = G_{\max}\;[F(u)]^2 = G_{\max}\left[\frac{(p+1)\;(1-T)}{(p+1)\;(1-T)+T}\left(2\,\frac{J_1\,(u)}{u} + \frac{T}{1-T}\,2^{p+1}\,p!\,\frac{J_{p+1}\,(u)}{u^{p+1}}\right)\right]^2 \tag{C.95}$$

where $u = \frac{\pi\,d_{\mathrm{a}}}{\lambda}\,\sin\theta$. θ represents here the open-angle between the satellite antenna and a point located on earth. $G_{\max}$ represents the maximum gain of the satellite antenna.

Example

When applying typical values for paraboloidal reflector antennas of a satellite it is not possible to obtain immediately the final expression for computing the gain. In our case we consider the following typical values: an antenna efficiency $\eta = 0.6$, a frequency $f = 30$ GHz, an aperture

edge taper $T_{\mathrm{dB}} = 20$ dB, and the rate at which the aperture field decreases is managed by the coefficient p ($p = 2$). The half-sided beam width is $\theta_{3\mathrm{dB}} = 0.2°$.

Simplification of the expression:

The linear value of the aperture edge taper T is obtained as follows [Col85]:

$$T_{\mathrm{dB}} = -10 \log (1-T)^2 \Leftrightarrow T = 1 - 10^{-T_{\mathrm{dB}}/20} \tag{C.96}$$

Such values of T and p lead to:

$$\frac{(p+1)\ (1-T)}{(p+1)\ (1-T)+T} = \frac{1}{4}$$

and:

$$\frac{T}{1-T}\, 2^{p+1}\, p! = 144$$

Therefore (C.95) can be written as [DCMLC07]:

$$G(u) = G_{\max} \left(\frac{J_1(u)}{2u} + 36\, \frac{J_3(u)}{u^3} \right)^2 \tag{C.97}$$

In order to find the expression of u we solve:

$$\left(\frac{J_1(u)}{2u} + 36\, \frac{J_3(u)}{u^3} \right)^2 \simeq \frac{1}{2} \tag{C.98}$$

since at -3 dB the gain should be almost reduced by a factor 2.

From the value of u obtained, and which is denoted as $u_{3\mathrm{dB}}$, we compute the maximum gain of the antenna:

$$G_{\max} = \eta \left(\frac{u_{3\mathrm{dB}}}{\sin \theta_{3\mathrm{dB}}} \right)^2 \tag{C.99}$$

in our case the maximum gain is $G_{\max} \simeq 53.23$ dB (remind that $\theta_{3\mathrm{dB}} = 0.2°$).

The corresponding diameter of the antenna can also be computed:

$$d_{\mathrm{a}} = \frac{\lambda\, u_{3\mathrm{dB}}}{\pi\, \sin \theta_{3\mathrm{dB}}} \tag{C.100}$$

the resulting value of the antenna diameter is $d_{\mathrm{a}} \simeq 1.89$ m.

Once $G_{\max}$ and d_{a} are determined the value of the gain for different satellite view angles can be computed.

Since:

$$u = \frac{\pi\, d_{\mathrm{a}}}{\lambda}\, \sin\theta \quad \text{and} \quad d_{\mathrm{a}} = \frac{\lambda\, u_{3\mathrm{dB}}}{\pi\, \sin\theta_{3\mathrm{dB}}}$$

we can also write:

$$u = u_{3\mathrm{dB}}\, \frac{\sin\theta}{\sin\theta_{3\mathrm{dB}}} \tag{C.101}$$

which results in our case to the following expression of u, like in [LuWeJa00] and [DCMLC07]:

$$u \simeq 2.0713\, \frac{\sin\theta}{\sin\theta_{3\mathrm{dB}}}$$

As a summary:

$$G(u) = G_{\max} \left(\frac{J_1(u)}{2u} + 36\, \frac{J_3(u)}{u^3} \right)^2$$

with:

$$u \simeq 2.0713\, \frac{\sin\theta}{\sin\theta_{3\mathrm{dB}}} \quad \text{and} \quad G_{\max} \simeq 53.23 \text{ dB}$$

Resulting pattern:

The antenna pattern for the parameters previously mentioned is computed for different satellite view angles comprised between 0° and 5°. The approximation for small angles and issued from [MaBo02] is also shown. The results are displayed in Fig. C.15.

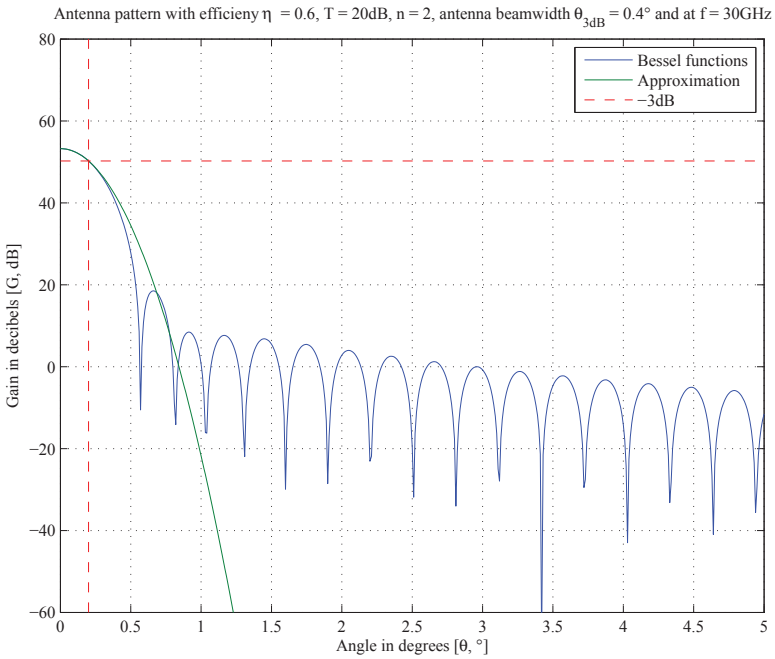


Figure C.15. *Example of antenna pattern.*

C.1.3 Link Budget

Satellite Temperature

The satellite temperature, or more particularly the thermodynamic temperature of the satellite antenna, is quite high and generally comprised between 600 K and 1 000 K. This can be explained by the Noise Figure (NF) which can range from 2.8 dB (H2Sat for instance) to about 4 dB.

As an example we can consider a satellite with a transparent payload and having the following properties: the pre- low-noise amplifier input loss $L_{\text{ant,sat,lna}} = 1$ dB, the antenna noise temperature $T_{\text{ant,sat}} = 290$ K and the noise figure $\text{NF}_{\text{Rx,sat}} = 3$ dB. The resulting system temperature is [MaBo02]:

$$T = T_{\text{ant,sat}} + 290\left(10^{L_{\text{ant,sat,lna}}/10} - 1\right) + 290\left(10^{L_{\text{ant,sat,lna}}/10}\right)\left(10^{\text{NF}_{\text{Rx,sat}}/10} - 1\right) \quad \text{(C.102)}$$

In this example we obtain $T \simeq 728.5$ K (28.6 dBK).

If we now consider another example, more detailed, of a satellite equipped with a transparent payload. The reception chain at the satellite is now equipped with three distinct components: the feed, the so-called repeater mismatch, and the repeater itself. The antenna receive temperature of the satellite is as before, i.e. $T_{\text{ant,sat}} = 290$ K. The antenna feed loss is such that $L_{\text{F,Rx}} = 1.5$ dB, and the antenna feed physical temperature to be $T_{\text{F,phy}} = 355$ K. The antenna repeater mismatch loss is considered to be $L_{\text{RM,Rx}} = 0.05$ dB and the repeater noise figure is $\text{NF}_{\text{R,Rx}} = 3.4$ dB.

Using the different values listed previously, we can derive the different thermodynamic temperature of the reception chain. The antenna feed noise temperature is:

$$T_{\text{F,Rx}} = T_{\text{F,phy}}\left(10^{L_{\text{F,Rx}}/10} - 1\right) = 355\left(10^{1.5/10} - 1\right) \simeq 146.5 \text{ K}$$

Using the antenna repeater mismatch loss at T_0 (i.e. $T_0 = 290$ K), the resulting antenna repeater mismatch noise temperature is:

$$T_{\text{RM,Rx}} = T_0\left(10^{L_{\text{Rm,Rx}}/10} - 1\right) = 290\left(10^{0.05/10} - 1\right) \simeq 3.4 \text{ K}$$

In the same way the repeater noise temperature can be computed, using the repeater noise figure value at T_0:

$$T_{\text{R,Rx}} = T_0\left(10^{\text{NF}_{\text{R,Rx}}/10} - 1\right) = 290\left(10^{3.4/10} - 1\right) \simeq 344.5 \text{ K}$$

The system noise temperature is obtained considering all the components present in the reception chain [MaBo02]:

$$T_1 = T_{\text{ant,sat}} + T_{\text{F,Rx}} + T_{\text{RM,Rx}}\, L_{\text{F,Rx}} + T_{\text{R,Rx}}\, L_{\text{F,Rx}}\, \text{NF}_{\text{R,Rx}} \simeq 933.6 \text{ K}$$

Such system noise temperature leads to $(T_1)_{\text{dB}} \simeq 29.7$ dB.

C.2 Uncoded Bit Error Rate

C.2.1 Generation of Vectors and Matrices

The signal generated by the so-called transmitters is represented by the vector $\boldsymbol{x}$. The transmitter signals are modified by the transmission medium which is described by the channel matrix $\boldsymbol{H}$. Noise is added and is represented by the vector $\boldsymbol{\eta}$. The signals finally perceived by the receivers is the vector $\boldsymbol{y}$. The following well-known relation can be written:

$$\boldsymbol{y} = \boldsymbol{H}\,\boldsymbol{x} + \boldsymbol{\eta} \tag{C.103}$$

Transmitted Signal

The signal generated by the transmitters is represented by the column vector $\boldsymbol{x}$. The vector $\boldsymbol{x}$ contains the symbols which are mapped in the constellation according to their in-phase and quadrature components (I and Q).

A sequence of bits is thus generated and groups of bits are created according to the modulation order M. The number of bits which can be represented by a symbol is:

$$N_{\text{bits}} = log_2\,(M) \tag{C.104}$$

According to the value of the bits and to the modulation order the symbol will have different In-phase and Quadrature (IQ) components.

The amplitude of the symbols, i.e. their norm with respect to the centre of the constellation, gives the energy per symbol which is noted E_{s}. E_{s} directly depends on the modulation type, for instance with constant amplitude modulations, like Phase-Shift Keying (PSK) modulations, it is identical among all symbols. Therefore by using a normalised PSK modulation the energy per symbol is $E_{\text{s}} = 1$.

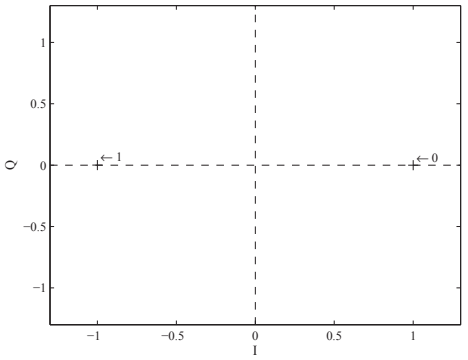


Figure C.16. *BPSK modulation.*

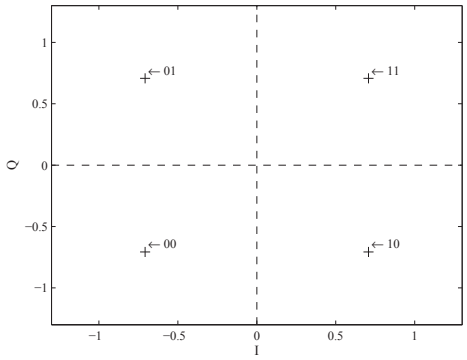


Figure C.17. *QPSK modulation.*

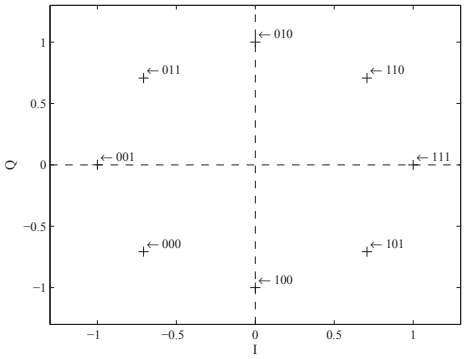


Figure C.18. *8-PSK modulation.*

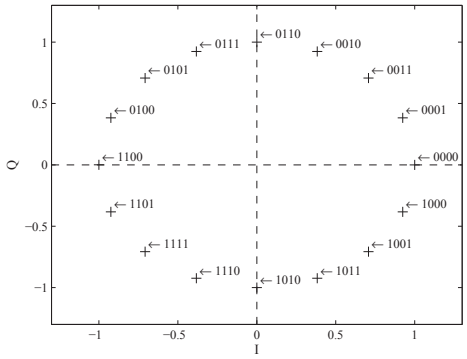


Figure C.19. *16-PSK modulation.*

Fig. C.16 represents the constellation considered for the BPSK modulation in which $M = 2$ and the number of bits per symbol is 1. Fig. C.17 shows the constellation of the QPSK modulation considered in this document. With such modulation $M = 4$ and the number of bits per symbol is 2. Fig. C.18 and Fig. C.19 represent the constellations for the 8-PSK modulation ($M = 8$, the number of bits per symbol is 3) and the 16-PSK modulation ($M = 16$, the number of bits per symbol is 4), respectively. For QPSK, 8-PSK and 16-PSK the Gray coded modulation mapping is considered meaning that only one bit differs in adjacent symbols.

The signal vector $\boldsymbol{x}$ is thus composed of complex numbers which are uniformly distributed and which is such that $\boldsymbol{x} \in \mathbb{C}^{N_{\mathrm{Tx}} \times 1}$, where N_{Tx} is the number of transmitters. Since the constellations are symmetric, the expectation of the vector of transmitted symbols $\boldsymbol{x}$ is:

$$\mathrm{E}\left[\boldsymbol{x}\right] = 0 \tag{C.105}$$

Channel Matrix

Uncoded Error Rate (ER) simulations were realised based on two different channel types: the so-called Rayleigh channel and our particular channel which represents the return-link of a multi-beam satellite system.

Rayleigh channel:
The so-called Rayleigh channel is widely used in communication to model a channel which consists of multiple taps. This is the case for instance with cellular networks in urban areas where the signal reflects on walls. The particularity of the Rayleigh channel is that the different paths are statistically independent and therefore the coefficients of the channel matrix can be generated using circularly symmetric complex Gaussian random variable [TsVi08].

The channel coefficient between transmitter j and receiver i is thus such that $h_{i,j} \sim \mathcal{CN}(0,1)$, i.e. both real and imaginary parts are i.i.d $\mathcal{N}(0,1/2)$. The channel coefficients are thus composed of random phases comprised between 0 and 2π and with expected value 1. This type of channel is considered in this study in order to validate the simulator implementation and to assess the performance of the receivers.

Satellite channel:
The satellite channel actually refers to the return-link of a multi-beam satellite system. The channel coefficients are generated according to the properties of the channel between the satellite terminals and the satellite.

On the one hand the norm of the channel coefficients is obtained considering the method described in Section 1.2.4. On the other hand the phase can be applied in different ways:

- No phase: the channel matrix is thus exclusively composed of real numbers,
- Random phase: a random phase is added independently on each coefficient,
- User phase: the so-called "user phase" (transmitter) is added to the channel matrix,
- Beam phase: the so-called "beam phase" (receiver) is added to the channel matrix,
- Beam and user phase: both "beam" and "user" phases are added to the channel matrix, this is the most realistic phase.

More details about "beam" and "user" phases (respectively transmitter and receiver phases) are provided in Section 1.2.5.

Additive Noise

The noise is represented by the vector $\boldsymbol{\eta}$. The elements of $\boldsymbol{\eta}$ are complex numbers, actually $\boldsymbol{\eta} \in \mathbb{C}^{N_{\mathrm{Rx}} \times 1}$ where N_{Rx} is the number of receivers. The noise is thus a column vector and is generally assumed to be white Gaussian. Therefore we speak about an Additive White Gaussian Noise (AWGN) since the noise is actually "added" at the receiver and has the following properties: a mean value which equals zero and a Gaussian distribution for each I, Q component. The terms "white" means that the spectrum is flat for all frequencies.

We can write: $\boldsymbol{\eta} \sim \mathcal{CN}\left(0, \sigma^2 \boldsymbol{I}\right)$ which means that $\boldsymbol{\eta}$ is composed of circularly symmetric complex Gaussian random variables with real and imaginary parts $\mathcal{N}\left(0, \sigma^2/2\right)$ (i.i.d.). If the energy per symbol E_{s} is normalised (i.e. equals 1) for different modulation orders, then $E_{\mathrm{s}}/N_0 = 1/N_0$. For this reason evaluating the BER for different signal-to-noise ratios or different E_{s}/N_0 remains into modifying the variance of the Gaussian distribution of the noise.

More particularly:

$$\eta_i = \Re\left(\eta_i\right) + j\,\Im\left(\eta_i\right) \qquad \text{with: } \Re\left(\eta_i\right) \sim \mathcal{N}\left(0, N_0/2\right) \text{ and } \Im\left(\eta_i\right) \sim \mathcal{N}\left(0, N_0/2\right) \tag{C.106}$$

where η_i represents the i-th element of the column vector $\boldsymbol{\eta}$. Doing so is equivalent to generate an additive noise such that $\boldsymbol{\eta} \sim \mathcal{CN}\left(0, N_0\,\boldsymbol{I}\right)$, i.e. a noise with expectation $\mathrm{E}\left[\boldsymbol{\eta}\right] = 0$ and covariance $\boldsymbol{C}_{\boldsymbol{\eta}} = \sigma^2\,\boldsymbol{I} = N_0\,\boldsymbol{I}$.

Fig. C.20 shows an example of noise generation when considering 10 000 samples and energy per symbol over noise power spectral density $E_{\mathrm{s}}/N_0 = 5$ dB and $E_{\mathrm{s}}/N_0 = 15$ dB.

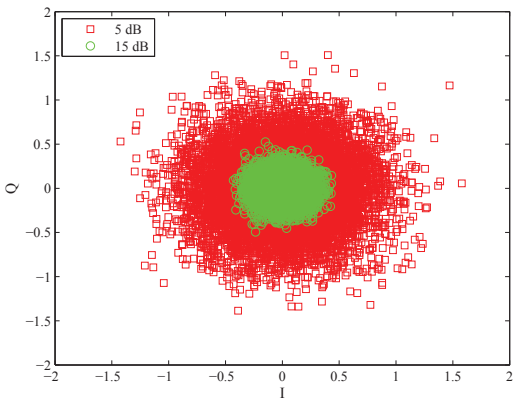


Figure C.20. *Example of noise generation for two different signal-to-noise ratios.*

In the example of Fig. C.20 the samples are generated using a normal distribution with mean

value $\mu = 0$ and standard deviation:

$$\sigma_{\Re(\eta_i)} = \sigma_{\Im(\eta_i)} = \sqrt{\frac{N_0}{2}} = \frac{10^{\frac{(-E_s/N_0)_{\mathrm{dB}}}{20}}}{\sqrt{2}} \tag{C.107}$$

since both real and imaginary parts are independent and identically distributed (i.i.d.).

C.2.2 Theoretical Evaluation of the Error Rate for Phase Shift Modulations

The bit error rate (BER) and the symbol error rate (SER) of each modulation and for different signal-to-noise ratios can be first evaluated analytically using probabilities [Pro00].

Binary Phase Shift Keying

With the BPSK modulation the symbols are mapped on the Q-axis, i.e. such that the quadrature component is null. Depending on the value of the bit the symbol is either on the left or on the right of the I-axis. In Fig. C.16 the modulation is normalised and the symbol is either -1 or +1. When generalising the symbol generated is either $-\sqrt{E_\mathrm{b}}$ or $+\sqrt{E_\mathrm{b}}$ and therefore in the presence of AWGN we have:

$$y = \pm\sqrt{E_\mathrm{b}} + \eta$$

where η is a complex random variable representing the white Gaussian noise, i.e. such that $\eta \sim \mathcal{CN}\left(0, \sigma^2\right)$. Therefore the real part of the noise is $\Re(\eta) \sim \mathcal{N}(0, N_0/2)$ since $\sigma^2 = N_0$.

A hard-decision demodulator will thus simply only rely on the sign of the real part of the received signal y. In the example of Fig. C.16 we thus have: $\Re(y) > 0$ means that bit "0" (b_0) was sent and $\Re(y) \leq 0$ means that bit "1" (b_1) was sent. The probability of having $\Re(y)$ knowing that b_0 was sent is:

$$p\left(\Re(y)\,|b_0\right) = \frac{1}{\sqrt{2\pi\,\sigma^2}}\, e^{-\frac{\left(\Re(y)-\sqrt{E_\mathrm{b}}\right)^2}{2\sigma^2}} = \frac{1}{\sqrt{\pi\,N_0}}\, e^{-\frac{\left(\Re(y)-\sqrt{E_\mathrm{b}}\right)^2}{N_0}}$$

since the variance of the real part of the received signal $\Re(y)$ is directly issued from the one of the noise, i.e. $\sigma^2 = N_0/2$. In the same way the probability of having $\Re(y)$ knowing that b_1 was sent is:

$$p\left(\Re(y)\,|b_1\right) = \frac{1}{\sqrt{\pi\,N_0}}\, e^{-\frac{\left(\Re(y)+\sqrt{E_\mathrm{b}}\right)^2}{N_0}}$$

The probability of having an error knowing that we have transmitted the bit "0" is the sum of the probabilities $p\left(\Re(y)\,|b_0\right)$ which are on the left of the I-axis, i.e. all probabilities that

the received signal is negative, and thus detected as bit "1" whereas bit "0" was sent:

$$p\left(\mathrm{e}|b_0\right) = \int_{-\infty}^{0} p\left(\Re\left(y\right)|b_0\right) = \frac{1}{\sqrt{\pi\, N_0}} \int_{-\infty}^{0} e^{-\frac{\left(\Re(y)-\sqrt{E_\mathrm{b}}\right)^2}{N_0}}\, d\Re\left(y\right)$$

We set x such that:

$$x = \frac{\left(\Re\left(y\right) - \sqrt{E_\mathrm{b}}\right)}{\sqrt{N_0}} \qquad \Rightarrow \qquad dx = \frac{1}{\sqrt{N_0}}\, d\Re\left(y\right)$$

we now have:

$$p\left(\mathrm{e}|b_0\right) = \frac{1}{\sqrt{\pi}} \int_{-\infty}^{-\sqrt{E_\mathrm{b}/N_0}} e^{-x^2} dx = \frac{1}{\sqrt{\pi}} \int_{\sqrt{E_\mathrm{b}/N_0}}^{+\infty} e^{-x^2} dx$$

since the function e^{-x^2} is symmetric. This probability can be written using the complementary error function "erfc":

$$p\left(\mathrm{e}|b_0\right) = \frac{1}{2}\,\mathrm{erfc}\left(\sqrt{\frac{E_\mathrm{b}}{N_0}}\right)$$

In the same way the probability of having an error knowing that we have transmitted the bit "1" is also:

$$p\left(\mathrm{e}|b_1\right) = \frac{1}{2}\,\mathrm{erfc}\left(\sqrt{\frac{E_\mathrm{b}}{N_0}}\right)$$

The principle of the previous operations can be represented by Fig. C.21. In this example the Probability Density Function (PDF)s of the real part of the noise is shown with variance $N_0 = 0.2$ dB.

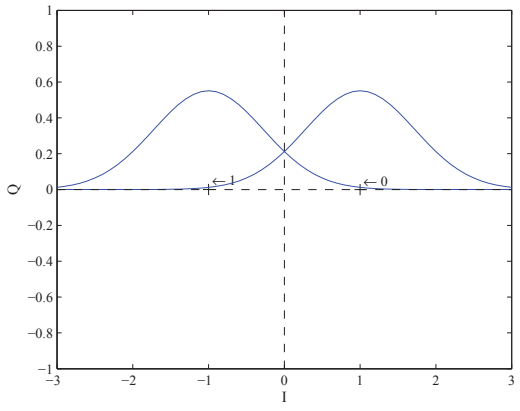


Figure C.21. *Example of noise PDFs for BPSK modulation.*

Knowing that the bits are equiprobable, the bit error rate with modulation BPSK and AWGN is:

$$P_\mathrm{b} = p\left(b_0\right)\, p\left(\mathrm{e}|b_0\right) + p\left(b_1\right)\, p\left(\mathrm{e}|b_1\right) = \frac{1}{2}\left(2 \times \frac{1}{2}\,\mathrm{erfc}\left(\sqrt{\frac{E_\mathrm{b}}{N_0}}\right)\right)$$

which finally gives:

$$P_{\mathrm{b,BPSK}} = \frac{1}{2}\,\mathrm{erfc}\left(\sqrt{\frac{E_\mathrm{b}}{N_0}}\right) \tag{C.108}$$

Since for BPSK there is one bit per symbol the symbol error rate is equal to the bit error rate, i.e. $P_\mathrm{s} = P_\mathrm{b}$. Also the energy per symbol equals the energy per bit, i.e. $E_\mathrm{s} = E_\mathrm{b}$.

Quadrature Phase Shift Keying

Using the same principle as before we can derive the probability of having a symbol error. The difference is that with QPSK both real and imaginary parts play a role.

Let's consider the symbol s_3 which is mapped in the upper right quadrant (refer to the example of Fig. C.17). We can write:

$$s_3 = |s_3|\, e^{j\theta_{s_3}} = \sqrt{E_\mathrm{s}}\, e^{j\frac{\pi}{4}}$$

The real part and the imaginary part of s_3 are:

$$\Re\left(s_3\right) = \sqrt{E_\mathrm{s}}\,\cos\left(\frac{\pi}{4}\right) = \sqrt{E_\mathrm{s}}\,\sin\left(\frac{\pi}{4}\right) \qquad\qquad \Im\left(s_3\right) = \sqrt{E_\mathrm{s}}\,\sin\left(\frac{\pi}{4}\right)$$

The probability of having a given real part of the receive signal y knowing the real part of the transmitted symbol s_3 is:

$$p\left(\Re\left(y\right)|\Re\left(s_3\right)\right) = \frac{1}{\sqrt{\pi\, N_0}}\, e^{\frac{-\left(\Re(y)-\sqrt{E_\mathrm{s}}\,\sin\left(\frac{\pi}{4}\right)\right)^2}{N_0}}$$

since the real part of the received signal y is influenced by the real part of the noise η which has variance $N_0/2$.

The probability of having an error on the real part is therefore:

$$p\left(e_\Re|\Re\left(s_3\right)\right) = \frac{1}{\sqrt{\pi\, N_0}} \int_{-\infty}^{0} e^{\frac{-\left(\Re(y)-\sqrt{E_\mathrm{s}}\,\sin\left(\frac{\pi}{4}\right)\right)^2}{N_0}}\, d\Re\left(y\right)$$

We set x such that:

$$x = \frac{\Re\left(y\right) - \sqrt{E_\mathrm{s}}\,\sin\left(\frac{\pi}{4}\right)}{\sqrt{N_0}} \qquad \Rightarrow \qquad dx = \frac{1}{\sqrt{N_0}}\, d\Re\left(y\right)$$

We obtain:

$$p\left(e_\Re|\Re\left(s_3\right)\right) = \frac{1}{\sqrt{\pi}} \int_{-\infty}^{-\sqrt{\frac{E_\mathrm{s}}{N_0}}\,\sin\left(\frac{\pi}{4}\right)} e^{-x^2} dx = \frac{1}{2}\,\mathrm{erfc}\left(\sqrt{\frac{E_\mathrm{s}}{N_0}}\,\sin\left(\frac{\pi}{4}\right)\right)$$

In the same way the probability of having an error on the imaginary part is:

$$p\left(e_{\Im}|\Im\left(s_3\right)\right) = \frac{1}{2}\operatorname{erfc}\left(\sqrt{\frac{E_\mathrm{s}}{N_0}}\sin\left(\frac{\pi}{4}\right)\right)$$

The probability of having a symbol error knowing that s_3 was sent is:

$$p\left(e|s_3\right) = p\left(e_{\Re}|\Re\left(s_3\right)\right) + p\left(e_{\Im}|\Im\left(s_3\right)\right) = \operatorname{erfc}\left(\sqrt{\frac{E_\mathrm{s}}{N_0}}\sin\left(\frac{\pi}{4}\right)\right)$$

The principle of the previous operations can be represented by Fig. C.22 in which the PDFs of the real and imaginary parts of the noise is shown with variance $N_0 = 0.1$ dB.

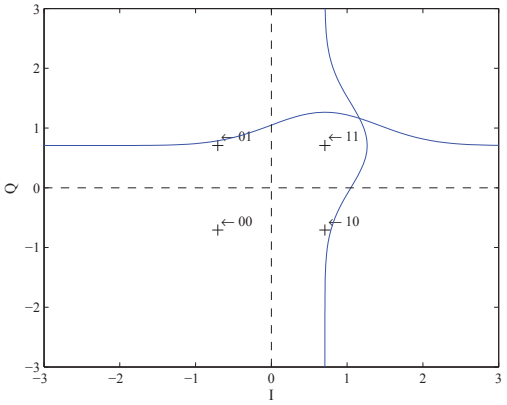


Figure C.22. *Example of noise PDFs for QPSK modulation.*

Since all symbols are generated with equiprobability and are symmetric we can finally write that the symbol error rate with modulation QPSK and AWGN is:

$$P_{\mathrm{s,QPSK}} = \operatorname{erfc}\left(\sqrt{\frac{E_\mathrm{s}}{N_0}}\sin\left(\frac{\pi}{4}\right)\right) \tag{C.109}$$

With this modulation one symbol represents two bits, therefore $E_\mathrm{s} = 2 \times E_\mathrm{b}$. Moreover when the level of the noise is limited and since we are using Gray coded modulation [1] the following approximation holds $P_\mathrm{s} \approx 2 \times P_\mathrm{b}$ (this approximation is valid for $E_\mathrm{s}/N_0 \gg 1$). The bit error rate with modulation QPSK and AWGN is thus:

$$P_{\mathrm{b,QPSK}} = \frac{1}{2}\operatorname{erfc}\left(\sqrt{\frac{2 \times E_\mathrm{b}}{N_0}}\sin\left(\frac{\pi}{4}\right)\right) = \frac{1}{2}\operatorname{erfc}\left(\sqrt{\frac{2 \times E_\mathrm{b}}{N_0}}\frac{\sqrt{2}}{2}\right)$$

we finally obtain:

$$P_{\mathrm{b,QPSK}} = \frac{1}{2}\operatorname{erfc}\left(\sqrt{\frac{E_\mathrm{b}}{N_0}}\right) \tag{C.110}$$

As can be seen the bit error rate of QPSK and AWGN is identical to the one of BPSK.

1. Only one bit differs between adjacent symbols.

M - Phase Shift Keying

For both BPSK and QPSK the symbol error probability was directly related to the fact the symbol was mapped in another quadrant than the one in which the transmitted symbol was originally mapped. When considering higher modulation orders, i.e. $M > 4$, the problem is not simply the quadrant in which the symbol is located but more particularly its phase.

Let's consider the mapping of the symbols of Fig. C.18 (8-PSK). We consider the symbol s_7 which is mapped on the Q-axis of the right quadrant. We can write:

$$s_7 = |s_7|\, e^{j\theta_{s_7}} = \sqrt{E_\mathrm{s}}\, e^{j\,0}$$

The real part and the imaginary part of s_7 are:

$$\Re\left(s_7\right) = \sqrt{E_\mathrm{s}} \qquad\qquad \Im\left(s_7\right) = 0$$

If the received signal y has a phase between $-\pi/8$ and $\pi/8$ then it will be correctly detected, otherwise the symbol will be different and an error will occur (Fig. C.23).

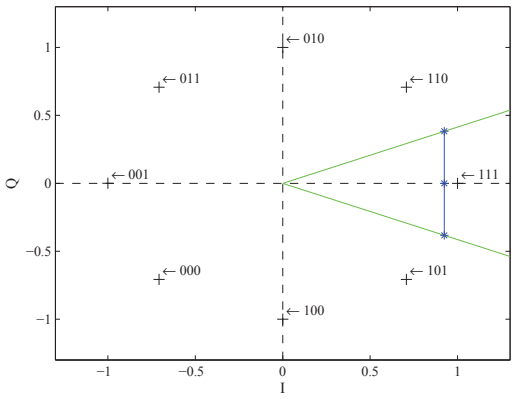


Figure C.23. *Example of symbol detection for 8-PSK modulation.*

When looking at Fig. C.23 we can see that for a given noise variance what is more subject to involve an error in detecting s_7 is not a modification of the real part but a modification of the imaginary part. We can approximate the value of the imaginary part from the symbol s_7 to the detection line driven by the phase $\pi/8$ as $\sqrt{E_\mathrm{s}}\,\sin\left(\pi/8\right)$. In the same way the value of the imaginary part from the symbol s_7 to the detection line driven by the phase $-\pi/8$ is $-\sqrt{E_\mathrm{s}}\,\sin\left(\pi/8\right)$.

The probability of having a symbol error while s_7 was transmitted is thus when the received

symbol is outside the area delimited by these two lines:

$$p\left(e|s_7\right) \approx p\left(e_{\Im}|s_7\right) = \frac{1}{\sqrt{\pi\, N_0}} \left(\int_{-\infty}^{-\sqrt{E_\mathrm{s}}\,\sin(\pi/8)} e^{\frac{-(\Im(y))^2}{N_0}} + \int_{\sqrt{E_\mathrm{s}}\,\sin(\pi/8)}^{+\infty} e^{\frac{-(\Im(y))^2}{N_0}} \right)$$

which is actually, as seen in the previous sections:

$$p\left(e|s_7\right) \approx \frac{1}{2}\,\mathrm{erfc}\left(\sqrt{\frac{E_s}{N_0}}\,\sin\left(\frac{\pi}{8}\right)\right) + \frac{1}{2}\,\mathrm{erfc}\left(\sqrt{\frac{E_s}{N_0}}\,\sin\left(\frac{\pi}{8}\right)\right) \approx \mathrm{erfc}\left(\sqrt{\frac{E_s}{N_0}}\,\sin\left(\frac{\pi}{8}\right)\right)$$

Since the symbols are generated with equiprobability and since the error probability on a symbol is the same for all symbols, the symbol error rate for 8-PSK and AWGN is:

$$P_{\mathrm{s,8\text{-}PSK}} \approx \mathrm{erfc}\left(\sqrt{\frac{E_\mathrm{s}}{N_0}}\,\sin\left(\frac{\pi}{8}\right)\right) \tag{C.111}$$

With such modulation one symbol represents three bits, therefore:

$$P_{\mathrm{b,8\text{-}PSK}} \approx \frac{1}{3}\mathrm{erfc}\left(\sqrt{\frac{3\times E_\mathrm{b}}{N_0}}\,\sin\left(\frac{\pi}{8}\right)\right) \tag{C.112}$$

By generalising the previous expressions for higher modulation orders, we can write that the symbol error rate and the bit error rate for M-PSK modulations and AWGN are:

$$P_\mathrm{s} \approx \mathrm{erfc}\left(\sqrt{\frac{E_\mathrm{s}}{N_0}}\,\sin\left(\frac{\pi}{M}\right)\right) \tag{C.113}$$

and:

$$P_\mathrm{b} \approx \frac{1}{N_\mathrm{bits}}\,\mathrm{erfc}\left(\sqrt{\frac{N_\mathrm{bits}\times E_\mathrm{b}}{N_0}}\,\sin\left(\frac{\pi}{M}\right)\right) \tag{C.114}$$

where M is the modulation order and N_bits is the number of bits per symbol, i.e. $N_\mathrm{bits} = \log_2\left(M\right)$. It has to be remarked that the two previous expressions are actually valid for both BPSK and QPSK modulations but in these two cases there are not approximations but exact expressions.

Preliminary Validation of the Simulator

Simulations were performed in order to evaluate the bit error rate of BPSK and QPSK for an energy per bit over noise power spectral density ratio ranging from -16 dB to 10 dB. The results are compared with the bit error rate provided by previous formulas (Fig. C.24).
The four curves of Fig. C.24 are all perfectly superimposed which means that both simulation and theory provide the same results and that $P_{\mathrm{b,BPSK}} = P_{\mathrm{b,QPSK}}$, as expected.

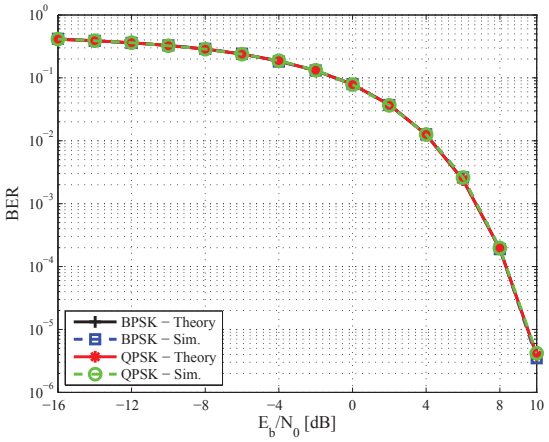


Figure C.24. *BER validation for both BPSK and QPSK modulations.*

Same kind of simulations were performed in order to evaluate the error rate of 8-PSK and 16-PSK for an energy per bit over noise power spectral density ratio ranging this time from -16 dB to 12 dB. The BER and the Symbol Error Rate (SER) results are compared with the ones provided by previous formulas (Fig. C.25).

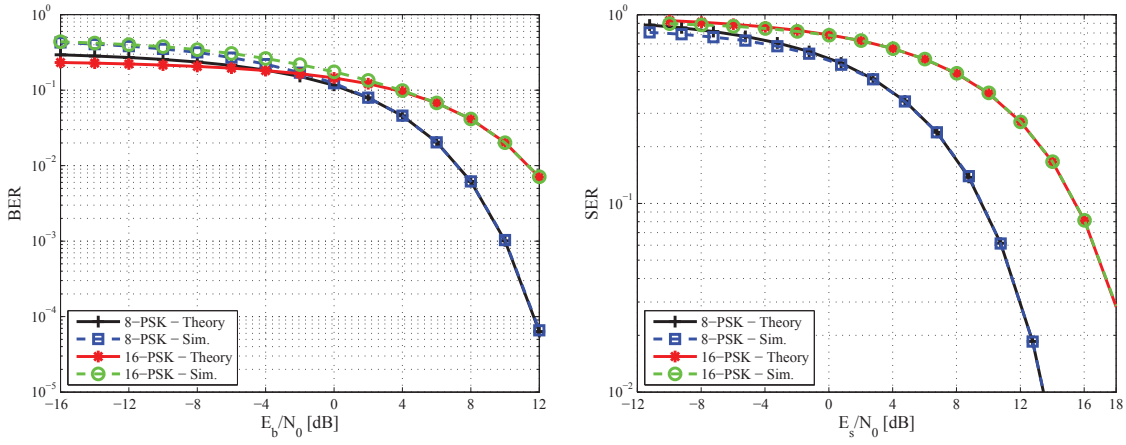


Figure C.25. *BER (left) and SER (right) validations for both 8-PSK and 16-PSK modulations.*

The BER curves in Fig. C.25 show that in the noise-limited region both theoretical and simulated results do not match anymore. This is actually related to the approximation on the SER computation but also to the approximation on the Gray coded modulation ($P_\mathrm{s} \approx N_\mathrm{bits} \times P_\mathrm{b}$). Actually the theory lowers the real BER since it assumes the level of noise is such that it changes the mapping of the transmitted symbol to a neighbour symbol, i.e. having only one bit different. Hence when having three bits per symbol in the case of 8-PSK, it is assumed an error on the symbol will involve one single bit error. This is of course not true in reality

as can be seen with these results.

Fig. C.25 shows the SER results using as x-axis the energy per symbol over noise power spectral density ratio issued from the energy per bit range. The SER on the y-axis was deliberately lowered in order to observe the difference between the theory and the simulations. Starting from 0 dB the curves are perfectly matching whereas in the noise-limited region a small difference can be observed. This is due to the approximation done while evaluating the error probability on a given symbol. The error of this approximation reduces of course as the modulation order increases. As a summary this validates both simulations and analytical expressions, more particularly outside the noise-limited region.

C.2.3 Filter Design

Introduction

Let's suppose we have the system depicted by Fig. C.26 and which is composed of the input signal vector $\boldsymbol{x}$, of the channel matrix $\boldsymbol{H}$, of an additional noise vector $\boldsymbol{\eta}$ and of a filter characterised by the matrix $\boldsymbol{G}$. The output signal vector $\boldsymbol{y}$ enters the filter and is modified in order to output the estimate vector of the input signal $\boldsymbol{x}$: $\hat{\boldsymbol{x}}$.

In other words we can write the following relations:

$$\boldsymbol{y} = \boldsymbol{H}\,\boldsymbol{x} + \boldsymbol{\eta} \tag{C.115}$$

and,

$$\hat{\boldsymbol{x}} = \boldsymbol{G}\,\boldsymbol{y} \tag{C.116}$$

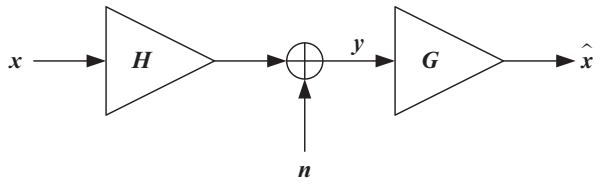


Figure C.26. *System considered for filter design.*

Zero Forcing Filter

The Problem:

When neglecting the presence of the noise in the system, i.e. when the level of the noise is low, we can write:

$$\boldsymbol{y} = \boldsymbol{H}\,\boldsymbol{x} \tag{C.117}$$

and this remains into having:

$$\hat{\boldsymbol{x}} = \boldsymbol{G}\,\boldsymbol{y} = \boldsymbol{G}\,\boldsymbol{H}\,\boldsymbol{x} \tag{C.118}$$

The best way of estimating the transmitted signal $\boldsymbol{x}$ is thus to simply solve:

$$\boldsymbol{G}\,\boldsymbol{H} = \boldsymbol{I} \tag{C.119}$$

Finding the solution:

On the one hand if the channel matrix $\boldsymbol{H}$ is square, i.e. when the number of transmitters equals the number of receivers, and has full rank then the system is solved by using:

$$\boldsymbol{G} = \boldsymbol{H}^{-1} \tag{C.120}$$

On the other hand if the channel matrix $\boldsymbol{H}$ is not square and has full column rank then we need to use a generalisation of the inverse which is called pseudo-inverse. The pseudo-inverse of a matrix $\boldsymbol{A}$, where $\boldsymbol{A} \in \mathbb{R}^{M \times N}$, is written $\boldsymbol{A}^{+}$ and is defined as:

$$\boldsymbol{A}^{+} = \left(\boldsymbol{A}^{\mathrm{T}}\,\boldsymbol{A}\right)^{-1}\boldsymbol{A}^{\mathrm{T}} \tag{C.121}$$

$\boldsymbol{A}^{+}$ is also-called Moore-Penrose pseudo-inverse. In the case of a matrix composed of complex numbers like our channel matrix $\boldsymbol{H}$ we have:

$$\boldsymbol{H}^{+} = \left(\boldsymbol{H}^{\mathrm{H}}\,\boldsymbol{H}\right)^{-1}\boldsymbol{H}^{\mathrm{H}} = \boldsymbol{W} \tag{C.122}$$

The Moore-Penrose pseudo-inverse of the channel matrix is generally denoted as $\boldsymbol{W}$.

Therefore if we know perfectly the channel matrix $\boldsymbol{H}$ at the receiver side then having a filter which is the pseudo-inverse of the channel matrix permits to find back an estimate the transmitted signal $\boldsymbol{x}$. Zero Forcing performs linear operations and consists into nulling the off diagonal elements of the channel matrix, i.e. to remove the interference (this explains the name "Zero Forcing"). However if we write down again the equation of the system, we obtain:

$$\boldsymbol{G}\,\boldsymbol{y} = \boldsymbol{W}\,\boldsymbol{y} = \boldsymbol{W}\left(\boldsymbol{H}\,\boldsymbol{x} + \boldsymbol{\eta}\right) = \boldsymbol{x} + \boldsymbol{W}\boldsymbol{\eta} \tag{C.123}$$

As can be seen from the previous equation, the drawback of the Zero Forcing equalisation is to amplify the noise (term $\boldsymbol{W}\boldsymbol{\eta}$).

Minimum Mean Square Error Filter

The Problem:

If we consider the Minimum Mean Square Error (MMSE) criteria to design the filter, i.e.

finding the filter which minimises the error between the input signal vector $\boldsymbol{x}$ and the estimate vector $\hat{\boldsymbol{x}}$, then we can write:

$$\arg\min_{\boldsymbol{G}} \left\{ \mathrm{E}\left[||\boldsymbol{x} - \hat{\boldsymbol{x}}||_2^2 \right] \right\} = \arg\min_{\boldsymbol{G}} \left\{ \mathrm{E}\left[||\boldsymbol{x} - \boldsymbol{G}\,\boldsymbol{y}||_2^2 \right] \right\} \tag{C.124}$$

The filter we are trying to design is the so-called "MMSE filter" and is represented by the matrix $\boldsymbol{G}_{\mathrm{MMSE}}$.

We know that:

$$||\boldsymbol{x}||_2^2 = \sum_i |x_i|^2 = \boldsymbol{x}^{\mathrm{H}}\,\boldsymbol{x} = \mathrm{tr}\left\{ \boldsymbol{x}^{\mathrm{H}}\,\boldsymbol{x} \right\} = \mathrm{tr}\left\{ \boldsymbol{x}\,\boldsymbol{x}^{\mathrm{H}} \right\} \tag{C.125}$$

therefore we can write:

$$\begin{aligned}
\mathrm{E}\left[||\boldsymbol{x} - \boldsymbol{G}\,\boldsymbol{y}||_2^2 \right] &= \mathrm{E}\left[\mathrm{tr}\left\{ (\boldsymbol{x} - \boldsymbol{G}\,\boldsymbol{y})\ (\boldsymbol{x} - \boldsymbol{G}\,\boldsymbol{y})^{\mathrm{H}} \right\} \right] \\
&= \mathrm{E}\left[\mathrm{tr}\left\{ \boldsymbol{x}\,\boldsymbol{x}^{\mathrm{H}} \right\} - \mathrm{tr}\left\{ \boldsymbol{x}\ (\boldsymbol{G}\,\boldsymbol{y})^{\mathrm{H}} \right\} - \mathrm{tr}\left\{ (\boldsymbol{G}\,\boldsymbol{y})\ \boldsymbol{x}^{\mathrm{H}} \right\} + \mathrm{tr}\left\{ (\boldsymbol{G}\,\boldsymbol{y})\ (\boldsymbol{G}\,\boldsymbol{y})^{\mathrm{H}} \right\} \right] \\
&= \mathrm{tr}\left\{ \mathrm{E}\left[\boldsymbol{x}\,\boldsymbol{x}^{\mathrm{H}} \right] \right\} - \mathrm{tr}\left\{ \mathrm{E}\left[\boldsymbol{x}\,\boldsymbol{y}^{\mathrm{H}} \right]\ \boldsymbol{G}^{\mathrm{H}} \right\} - \mathrm{tr}\left\{ \boldsymbol{G}\,\mathrm{E}\left[\boldsymbol{y}\,\boldsymbol{x}^{\mathrm{H}} \right] \right\} + \mathrm{tr}\left\{ \boldsymbol{G}\,\mathrm{E}\left[\boldsymbol{y}\,\boldsymbol{y}^{\mathrm{H}} \right]\ \boldsymbol{G}^{\mathrm{H}} \right\} \\
&= \mathrm{tr}\left\{ \boldsymbol{C}_{\boldsymbol{x}} \right\} - \mathrm{tr}\left\{ \boldsymbol{C}_{\boldsymbol{x},\boldsymbol{y}}\,\boldsymbol{G}^{\mathrm{H}} \right\} - \mathrm{tr}\left\{ \boldsymbol{G}\,\boldsymbol{C}_{\boldsymbol{y},\boldsymbol{x}} \right\} + \mathrm{tr}\left\{ \boldsymbol{G}\,\boldsymbol{C}_{\boldsymbol{y}}\,\boldsymbol{G}^{\mathrm{H}} \right\}
\end{aligned}$$

This gives since $\boldsymbol{C}_{\boldsymbol{y},\boldsymbol{x}} = \boldsymbol{C}_{\boldsymbol{x},\boldsymbol{y}}^{\mathrm{H}}$:

$$\boldsymbol{G}_{\mathrm{MMSE}} = \arg\min_{\boldsymbol{G}} \left\{ \mathrm{tr}\left\{ \boldsymbol{C}_{\boldsymbol{x}} \right\} - \mathrm{tr}\left\{ \boldsymbol{C}_{\boldsymbol{x},\boldsymbol{y}}\,\boldsymbol{G}^{\mathrm{H}} \right\} - \mathrm{tr}\left\{ \boldsymbol{G}\,\boldsymbol{C}_{\boldsymbol{x},\boldsymbol{y}}^{\mathrm{H}} \right\} + \mathrm{tr}\left\{ \boldsymbol{G}\,\boldsymbol{C}_{\boldsymbol{y}}\,\boldsymbol{G}^{\mathrm{H}} \right\} \right\} \tag{C.126}$$

Finding the solution:

Finding the filter $\boldsymbol{G}_{\mathrm{MMSE}}$ which satisfies (C.126) remains into solving the following equation:

$$-\frac{\partial \mathrm{tr}\left\{ \boldsymbol{C}_{\boldsymbol{x},\boldsymbol{y}}\,\boldsymbol{G}^{\mathrm{H}} \right\}}{\partial \boldsymbol{G}} - \frac{\partial \mathrm{tr}\left\{ \boldsymbol{G}\,\boldsymbol{C}_{\boldsymbol{x},\boldsymbol{y}}^{\mathrm{H}} \right\}}{\partial \boldsymbol{G}} + \frac{\partial \mathrm{tr}\left\{ \boldsymbol{G}\,\boldsymbol{C}_{\boldsymbol{y}}\,\boldsymbol{G}^{\mathrm{H}} \right\}}{\partial \boldsymbol{G}} = 0$$

Using the different properties shown in Section B.1.4, we know that:

$$\frac{\partial \mathrm{tr}\left\{ \boldsymbol{C}_{\boldsymbol{x},\boldsymbol{y}}\,\boldsymbol{G}^{\mathrm{H}} \right\}}{\partial \boldsymbol{G}} = 0$$

$$\frac{\partial \mathrm{tr}\left\{ \boldsymbol{G}\,\boldsymbol{C}_{\boldsymbol{x},\boldsymbol{y}}^{\mathrm{H}} \right\}}{\partial \boldsymbol{G}} = \boldsymbol{C}_{\boldsymbol{x},\boldsymbol{y}}^{*}$$

and:

$$\frac{\partial \mathrm{tr}\left\{ \boldsymbol{G}\,\boldsymbol{C}_{\boldsymbol{y}}\,\boldsymbol{G}^{\mathrm{H}} \right\}}{\partial \boldsymbol{G}} = \boldsymbol{G}^{*}\boldsymbol{C}_{\boldsymbol{y}}^{\mathrm{T}}$$

Therefore we have:

$$-\frac{\partial \mathrm{tr}\left\{ \boldsymbol{C}_{\boldsymbol{x},\boldsymbol{y}}\,\boldsymbol{G}^{\mathrm{H}} \right\}}{\partial \boldsymbol{G}} - \frac{\partial \mathrm{tr}\left\{ \boldsymbol{G}\,\boldsymbol{C}_{\boldsymbol{x},\boldsymbol{y}}^{\mathrm{H}} \right\}}{\partial \boldsymbol{G}} + \frac{\partial \mathrm{tr}\left\{ \boldsymbol{G}\,\boldsymbol{C}_{\boldsymbol{y}}\,\boldsymbol{G}^{\mathrm{H}} \right\}}{\partial \boldsymbol{G}} = -\boldsymbol{C}_{\boldsymbol{x},\boldsymbol{y}}^{*} + \boldsymbol{G}^{*}\boldsymbol{C}_{\boldsymbol{y}}^{\mathrm{T}} = 0$$

we can write:

$$\boldsymbol{G}^{*}\boldsymbol{C}_{\boldsymbol{y}}^{\mathrm{T}} = \boldsymbol{C}_{\boldsymbol{x},\boldsymbol{y}}^{*} \qquad \Rightarrow \qquad \left(\boldsymbol{G}^{*}\boldsymbol{C}_{\boldsymbol{y}}^{\mathrm{T}} \right)^{*} = \boldsymbol{C}_{\boldsymbol{x},\boldsymbol{y}}$$

which is also:

$$\boldsymbol{G}\left(\boldsymbol{C}_{\boldsymbol{y}}^{\mathrm{T}}\right)^{*}=\boldsymbol{C}_{\boldsymbol{x},\boldsymbol{y}}$$

Since $\left(\boldsymbol{A}^{\mathrm{T}}\right)^{*}=\boldsymbol{A}^{\mathrm{H}}$ by definition the previous relation becomes:

$$\boldsymbol{G}\,\boldsymbol{C}_{\boldsymbol{y}}^{\mathrm{H}}=\boldsymbol{C}_{\boldsymbol{x},\boldsymbol{y}}$$

The Hermitian of the covariance of the received signal vector $\boldsymbol{y}$ is:

$$\boldsymbol{C}_{\boldsymbol{y}}^{\mathrm{H}}=\mathrm{E}\left[\left(\boldsymbol{y}-\mathrm{E}\left[\boldsymbol{y}\right]\right)\left(\boldsymbol{y}-\mathrm{E}\left[\boldsymbol{y}\right]\right)^{\mathrm{H}}\right]^{\mathrm{H}}=\mathrm{E}\left[\left(\left(\boldsymbol{y}-\mathrm{E}\left[\boldsymbol{y}\right]\right)\left(\boldsymbol{y}-\mathrm{E}\left[\boldsymbol{y}\right]\right)^{\mathrm{H}}\right)^{\mathrm{H}}\right]$$

since $\left(\boldsymbol{A}\,\boldsymbol{B}\right)^{\mathrm{H}}=\boldsymbol{B}^{\mathrm{H}}\boldsymbol{A}^{\mathrm{H}}$ it is actually:

$$\boldsymbol{C}_{\boldsymbol{y}}^{\mathrm{H}}=\mathrm{E}\left[\left(\boldsymbol{y}-\mathrm{E}\left[\boldsymbol{y}\right]\right)\left(\boldsymbol{y}-\mathrm{E}\left[\boldsymbol{y}\right]\right)^{\mathrm{H}}\right]=\boldsymbol{C}_{\boldsymbol{y}}$$

We finally have:

$$\boldsymbol{G}\,\boldsymbol{C}_{\boldsymbol{y}}=\boldsymbol{C}_{\boldsymbol{x},\boldsymbol{y}}\qquad\Rightarrow\qquad\boldsymbol{G}\,\boldsymbol{C}_{\boldsymbol{y}}\,\boldsymbol{C}_{\boldsymbol{y}}^{-1}=\boldsymbol{C}_{\boldsymbol{x},\boldsymbol{y}}\,\boldsymbol{C}_{\boldsymbol{y}}^{-1}\qquad\Rightarrow\qquad\boldsymbol{G}=\boldsymbol{C}_{\boldsymbol{x},\boldsymbol{y}}\,\boldsymbol{C}_{\boldsymbol{y}}^{-1}$$

The final result is thus:

$$\boldsymbol{G}_{\mathrm{MMSE}}=\boldsymbol{C}_{\boldsymbol{x},\boldsymbol{y}}\,\boldsymbol{C}_{\boldsymbol{y}}^{-1}\tag{C.127}$$

Exploiting the solution:

In the previous paragraph the generic formula of the MMSE filter was given (C.127). Exploiting the properties of the transmitted signal vector $\boldsymbol{x}$, of the channel matrix $\boldsymbol{H}$ and of the noise vector $\boldsymbol{\eta}$ it is possible to reformulate $\boldsymbol{G}_{\mathrm{MMSE}}$.

We consider that all symbols are generate with equiprobability and transmitted with equal nominal power, that is:

$$\boldsymbol{C}_{\boldsymbol{x}}=\mathrm{E}\left[\left(\boldsymbol{x}-\mathrm{E}\left[\boldsymbol{x}\right]\right)\left(\boldsymbol{x}-\mathrm{E}\left[\boldsymbol{x}\right]\right)^{\mathrm{H}}\right]=\mathrm{E}\left[\boldsymbol{x}\,\boldsymbol{x}^{\mathrm{H}}\right]=\boldsymbol{I}\tag{C.128}$$

The noise is AWGN with mean value 0, i.e. $\mathrm{E}\left[\boldsymbol{\eta}\right]=0$.

According to the proof in Section 3.1.3 we know that:

$$\boldsymbol{C}_{\boldsymbol{y}}=\boldsymbol{H}\,\boldsymbol{C}_{\boldsymbol{x}}\,\boldsymbol{H}^{\mathrm{H}}+\boldsymbol{C}_{\boldsymbol{\eta}}=\boldsymbol{H}\,\boldsymbol{H}^{\mathrm{H}}+\boldsymbol{C}_{\boldsymbol{\eta}}$$

and we can also write $\boldsymbol{C}_{\boldsymbol{x},\boldsymbol{y}}$ as:

$$\boldsymbol{C}_{\boldsymbol{x},\boldsymbol{y}}=\mathrm{E}\left[\left(\boldsymbol{x}-\mathrm{E}\left[\boldsymbol{x}\right]\right)\left(\boldsymbol{y}-\mathrm{E}\left[\boldsymbol{y}\right]\right)^{\mathrm{H}}\right]=\mathrm{E}\left[\boldsymbol{x}\left(\boldsymbol{H}\,\boldsymbol{x}+\boldsymbol{\eta}-\mathrm{E}\left[\boldsymbol{H}\,\boldsymbol{x}+\boldsymbol{\eta}\right]\right)^{\mathrm{H}}\right]$$

which is also:

$$\boldsymbol{C}_{\boldsymbol{x},\boldsymbol{y}} = \mathrm{E}\left[\boldsymbol{x}\left(\boldsymbol{H}\,\boldsymbol{x} + \boldsymbol{\eta} - \boldsymbol{H}\mathrm{E}\left[\boldsymbol{x}\right] - \mathrm{E}\left[\boldsymbol{\eta}\right]\right)^{\mathrm{H}}\right] = \mathrm{E}\left[\boldsymbol{x}\left(\boldsymbol{H}\,\boldsymbol{x} + \boldsymbol{\eta}\right)^{\mathrm{H}}\right]$$

using the properties of the Hermitian operator, we obtain:

$$\boldsymbol{C}_{\boldsymbol{x},\boldsymbol{y}} = \mathrm{E}\left[\boldsymbol{x}\,\boldsymbol{x}^{\mathrm{H}}\boldsymbol{H}^{\mathrm{H}}\right] + \mathrm{E}\left[\boldsymbol{x}\,\boldsymbol{\eta}^{\mathrm{H}}\right] = \boldsymbol{C}_{\boldsymbol{x}}\,\boldsymbol{H}^{\mathrm{H}} + \mathrm{E}\left[\boldsymbol{x}\right]\,\mathrm{E}\left[\boldsymbol{\eta}^{\mathrm{H}}\right] = \boldsymbol{H}^{\mathrm{H}}$$

This finally gives:

$$\boldsymbol{G}_{\mathrm{MMSE}} = \boldsymbol{C}_{\boldsymbol{x},\boldsymbol{y}}\,\boldsymbol{C}_{\boldsymbol{y}}^{-1} = \boldsymbol{H}^{\mathrm{H}}\,\left[\boldsymbol{H}\,\boldsymbol{H}^{\mathrm{H}} + \boldsymbol{C}_{\boldsymbol{\eta}}\right]^{-1}$$

and since $\boldsymbol{C}_{\boldsymbol{\eta}} = N_0\,\boldsymbol{I}$ we have:

$$\boldsymbol{G}_{\mathrm{MMSE}} = \boldsymbol{H}^{\mathrm{H}}\left[\boldsymbol{H}\,\boldsymbol{H}^{\mathrm{H}} + N_0\,\boldsymbol{I}\right]^{-1} \tag{C.129}$$

where N_0 is the noise power spectral density.

Other formulation:

Using some basic properties of matrices, formula (C.129) can be written differently. If we consider the previous expression, omitting the inverse operator, then:

$$\boldsymbol{H}^{\mathrm{H}}\left[\boldsymbol{H}\,\boldsymbol{H}^{\mathrm{H}} + N_0\,\boldsymbol{I}\right] = \boldsymbol{H}^{\mathrm{H}}\boldsymbol{H}\,\boldsymbol{H}^{\mathrm{H}} + \boldsymbol{H}^{\mathrm{H}}\,N_0\,\boldsymbol{I} = \boldsymbol{H}^{\mathrm{H}}\boldsymbol{H}\,\boldsymbol{H}^{\mathrm{H}} + N_0\,\boldsymbol{I}\,\boldsymbol{H}^{\mathrm{H}}$$

because of the properties of the identity matrix $\boldsymbol{I}$. Therefore we have:

$$\boldsymbol{H}^{\mathrm{H}}\left[\boldsymbol{H}\,\boldsymbol{H}^{\mathrm{H}} + N_0\,\boldsymbol{I}\right] = \left[\boldsymbol{H}^{\mathrm{H}}\,\boldsymbol{H} + N_0\,\boldsymbol{I}\right]\boldsymbol{H}^{\mathrm{H}}$$

If we now compute the inverse of the previous expression, we get:

$$\left(\boldsymbol{H}^{\mathrm{H}}\left[\boldsymbol{H}\,\boldsymbol{H}^{\mathrm{H}} + N_0\,\boldsymbol{I}\right]\right)^{-1} = \left[\boldsymbol{H}\,\boldsymbol{H}^{\mathrm{H}} + N_0\,\boldsymbol{I}\right]^{-1}\left(\boldsymbol{H}^{\mathrm{H}}\right)^{-1} = \left(\boldsymbol{H}^{\mathrm{H}}\right)^{-1}\left[\boldsymbol{H}^{\mathrm{H}}\boldsymbol{H} + N_0\,\boldsymbol{I}\right]^{-1}$$

since $(\boldsymbol{A}\,\boldsymbol{B})^{-1} = \boldsymbol{B}^{-1}\boldsymbol{A}^{-1}$. By multiplying on the left and on the right by $\boldsymbol{H}^{\mathrm{H}}$ we obtain:

$$\boldsymbol{H}^{\mathrm{H}}\left[\boldsymbol{H}\,\boldsymbol{H}^{\mathrm{H}} + N_0\,\boldsymbol{I}\right]^{-1}\left(\boldsymbol{H}^{\mathrm{H}}\right)^{-1}\boldsymbol{H}^{\mathrm{H}} = \boldsymbol{H}^{\mathrm{H}}\left(\boldsymbol{H}^{\mathrm{H}}\right)^{-1}\left[\boldsymbol{H}^{\mathrm{H}}\boldsymbol{H} + N_0\,\boldsymbol{I}\right]^{-1}\boldsymbol{H}^{\mathrm{H}}$$

which finally gives:

$$\boldsymbol{H}^{\mathrm{H}}\left[\boldsymbol{H}\,\boldsymbol{H}^{\mathrm{H}} + N_0\,\boldsymbol{I}\right]^{-1} = \left[\boldsymbol{H}^{\mathrm{H}}\boldsymbol{H} + N_0\,\boldsymbol{I}\right]^{-1}\boldsymbol{H}^{\mathrm{H}} \tag{C.130}$$

Therefore another formulation of the MMSE filter is:

$$\boldsymbol{G}_{\mathrm{MMSE}} = \left[\boldsymbol{H}^{\mathrm{H}}\boldsymbol{H} + N_0\,\boldsymbol{I}\right]^{-1}\boldsymbol{H}^{\mathrm{H}} \tag{C.131}$$

C.2.4 Simulator Overview and Summary

This section summarises the so-called Bit Error Rate (BER) simulator implemented [2] to assess the performance of state-of-the-art receivers, including receivers capable of realising Multi-User Detection (MUD), and also, more interestingly, the impact of the satellite channel on those receivers.

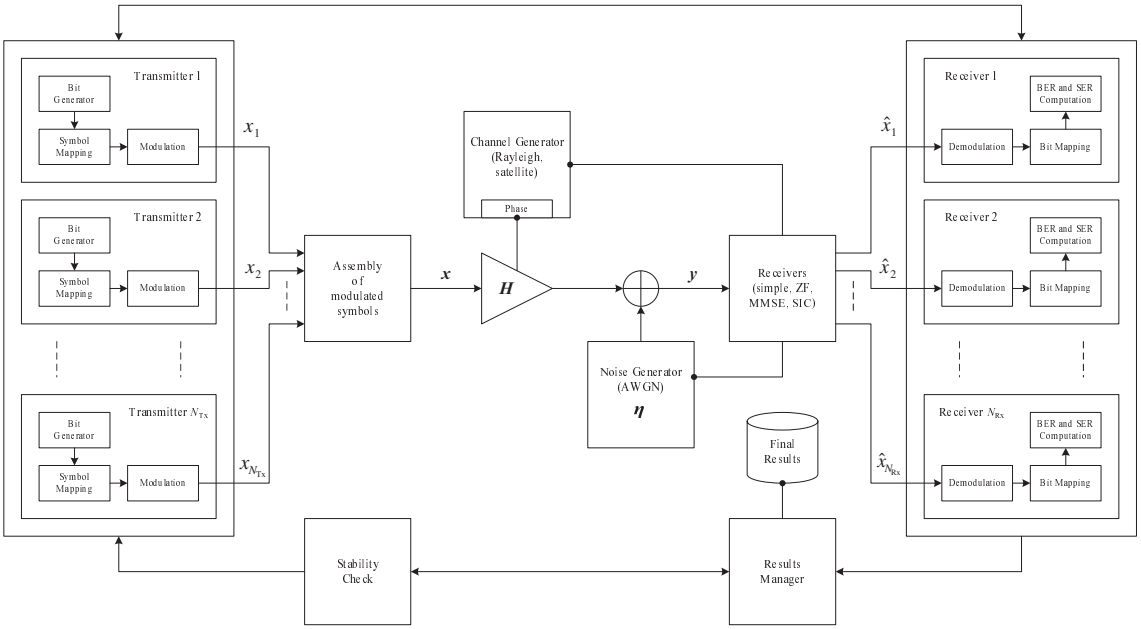


Figure C.27. *BER simulator.*

The BER simulator is depicted by the diagram of Fig. C.27. Each of the N_{Tx} transmitters is composed of a bit generator which produces binary sequences of variable lengths, of a module mapping the bits into symbols according to the modulation order selected, and of the modulation module which maps the symbol into the constellation. The x_j complex number, with $j = 1, 2, ..., N_{\mathrm{Tx}}$ are assembled in order to build the vector $\boldsymbol{x}$ to be transmitted.

The so-called "channel generator" is capable of managing channel matrices of different types. The channel matrices can be issued from different scenarios like the ones defined for the satellite system; phase can be added to the coefficients of the channel matrix as described in Section C.2.1. The channel matrix $\boldsymbol{H}$ produced by this module is multiplied with the vector $\boldsymbol{x}$ so that to obtain the part $\boldsymbol{H}\,\boldsymbol{x}$ of the final vector $\boldsymbol{y}$. The noise generator produces the column vector $\boldsymbol{\eta}$ according to the required signal-to-noise ratio. Noise is added to the current column vector issued from the product $\boldsymbol{H}\,\boldsymbol{x}$ and it results into the final column vector $\boldsymbol{y}$

2. The BER simulator was implemented in Matlab and in an object-oriented way, i.e. using Matlab classes.

which is of size $N_{\mathrm{Rx}} \times 1$. This vector is used by the different receivers implemented in the simulator ("simple" receiver, Zero Forcing, etc.) together with the channel matrix and the noise power spectral density, if they are required.

The outputs of the receivers correspond to the final estimates of the transmitted symbols which are forwarded to the single receivers. Each of the N_{Rx} receiver entities demodulates the estimates, maps the corresponding symbols into bits and finally performs both Symbol Error Rate (SER) and Bit Error Rate (BER) computations by comparing what was initially transmitted with what is finally received (connection between the single transmitters and the single receivers).

A results manager takes care of saving the simulations when needed, but also of offering the possibility to load results if simulations were already performed for given SNRs and to aggregate results with existing ones, if required. The last module performs some stability check of all SERs and BERs to decide wether the current simulation can be stopped (stability reached) or if additional blocks of symbols need to be simulated. Via this control loop the BER simulator is therefore capable of performing simulations in an autonomous way, adjusting the size of the blocks to be simulated automatically according to the evolution of both SERs and BERs, and deciding when the results are stable enough to be considered as valid.

C.2.5 Theoretical Evaluation with Signal Processing

Since performing Bit Error Rate (BER) simulations is really time consuming, it is also possible, to some extends, to move towards a theoretical approach in order to get more rapidly an estimation of both symbol error rate and bit error rate, SER and BER, respectively.

Introduction

The theoretical error rate can be evaluated based on probabilities and the probability of having an error directly depends on the noise level. We remind that the symbol error rate and the bit error rate for M-PSK modulations and AWGN are (please refer to Section C.2.2):

$$P_{\mathrm{s}} \approx \mathrm{erfc}\left(\sqrt{\frac{E_{\mathrm{s}}}{N_0}}\,\sin\left(\frac{\pi}{M}\right)\right)$$

and:

$$P_{\mathrm{b}} \approx \frac{1}{N_{\mathrm{bits}}}\,\mathrm{erfc}\left(\sqrt{\frac{N_{\mathrm{bits}} \times E_{\mathrm{b}}}{N_0}}\,\sin\left(\frac{\pi}{M}\right)\right)$$

where M is the modulation order and N_{bits} is the number of bits per symbol, i.e. $N_{\text{bits}} = \log_2(M)$. The ratio E_s/N_0 is equivalent to the signal-to-noise ratio in our case, i.e. the so-called SNR. If ¡interference is considered as noise, then we can also write:

$$P_s \approx \text{erfc}\left(\sqrt{\text{SINR}}\,\sin\left(\frac{\pi}{M}\right)\right) \tag{C.132}$$

or equivalently:

$$P_s \approx \text{erfc}\left(10^{\frac{\text{SINR}_{\text{dB}}}{20}}\,\sin\left(\frac{\pi}{M}\right)\right) \tag{C.133}$$

The bit error rate can be simply approximated, when considering Gray coded modulations, as follows:

$$P_b \approx \frac{P_s}{\log_2(M)}$$

"Simple" Filtering

In order to estimate the symbol error rate (SER) and the bit error rate (BER) when realising "simple" filtering operations, i.e. no Interference Cancellation (IC), the Signal-to-Interference-plus-Noise Ratio (SINR) at the output of these filters has to be first evaluated.

Zero Forcing:

At the output of the Zero Forcing (ZF) equaliser, the SINR perceived by the j-th stream is (please refer to Section 3.2.3 for more details):

$$\text{SINR}_{j,\text{ZF}} = \frac{1}{\left[\left(\boldsymbol{H}^{\text{H}}\,\boldsymbol{C}_{\boldsymbol{\eta}}^{-1}\,\boldsymbol{H}\right)^{-1}\right]_{j,j}}$$

where $[\boldsymbol{A}]_{j,j}$ represents the j-th diagonal element of the matrix $\boldsymbol{A}$, $\boldsymbol{H}$ is the channel matrix and $\boldsymbol{C}_{\boldsymbol{\eta}}$ corresponds the covariance of the noise.

Minimum Mean Square Error:

When considering a receiver performing Minimum Mean Square Error (MMSE) filtering, the SINR of the j-th stream is (again, please refer to Section 3.2.3 for more details):

$$\text{SINR}_{j,\text{MMSE}} = \boldsymbol{h}_j^{\text{H}}\left(\boldsymbol{C}_{\boldsymbol{\eta}} + \sum_{i\neq j}\boldsymbol{h}_i\,\boldsymbol{h}_i^{\text{H}}\right)^{-1}\boldsymbol{h}_j$$

where $\boldsymbol{h}_j$ represents the j-th column vector of the channel matrix $\boldsymbol{H}$ and $\boldsymbol{C}_{\boldsymbol{\eta}}$ the covariance of the noise, as before.

Theoretical evaluations versus practical evaluations:

Using $\text{SINR}_{j,\text{ZF}}$ and $\text{SINR}_{j,\text{MMSE}}$, respectively for ZF and MMSE filtering, it is thus possible to compute the theoretical uncoded SER and BER perceived by stream j. We focus on the reduced multi-beam satellite system due to the computational complexity in performing BER simulations. More particularly we consider seven beams ($B = 7$) with full frequency reuse ($K = 1$) as depicted in Fig. 1.9. The purpose is to realise simulations and to compare both SER and BER issued from practical evaluations with the theoretical ones obtained with the previous formulae.

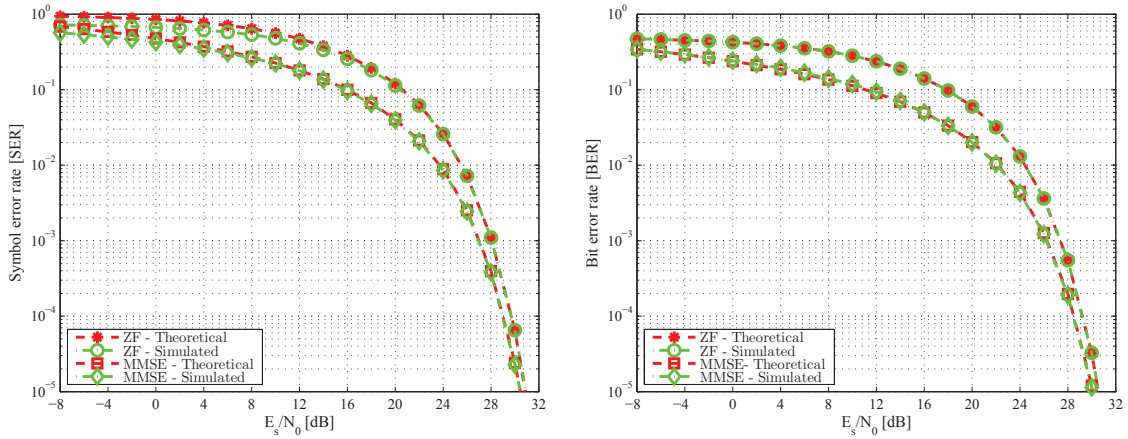


Figure C.28. *Theoretical evaluations versus practical evaluations of the SER (left) and BER (right) for seven beams ($B = 7$), the high interference scenario ("bad" case) and QPSK modulation.*

The graphs shown by Fig. C.28 validate both practical and theoretical evaluations for the high interference, i.e. the so-called "bad" case, and QPSK modulation since the curves almost perfectly match for the two filters (ZF and MMSE). It has to be remarked that both SER and BER are averaged among the users, i.e. over the $B = 7$ users.

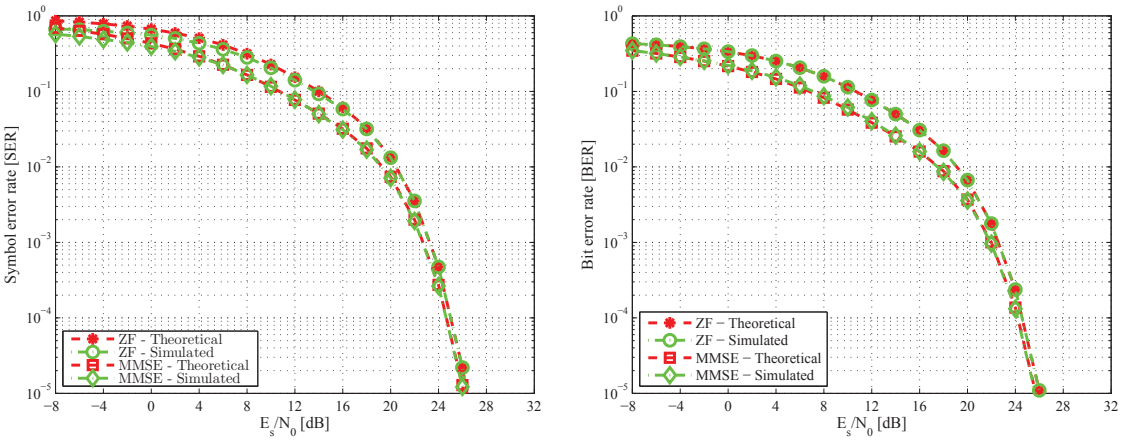


Figure C.29. *Theoretical evaluations versus practical evaluations of the SER (left) and BER (right) for seven beams ($B = 7$), the average interference scenario and QPSK modulation.*

The graphs shown by Fig. C.29 also validate both practical and theoretical evaluations for the average interference case and QPSK modulation since the curves almost perfectly match for the two filters (ZF and MMSE). As before, both SER and BER are averaged among the users, i.e. over the $B = 7$ users.

Interference Cancellation

Once Interference Cancellation (IC) is performed, the Symbol Error Rate (SER), and consequently the Bit Error Rate (BER), cannot be evaluated using the previous formulae. We consider in the following the Minimum Mean Square Error (MMSE) filter when doing no IC and the optimal architecture together with MMSE when realising Successive Interference Cancellation (SIC).

The order in which the IC process is realised plays a role. Actually the first user to be decoded in the process, i.e. the one with the strongest signal-to-interference plus noise ratio (SINR), gets its symbols decoded as if it was directly at the output of the MMSE filter. For this reason the theoretical approach used previously is still valid for this user. This can be verified using the "bad" case scenario and the QPSK modulation. We remind that the order in which the users are decoded depends on the signal-to-noise ratio. In the "bad" case the user to be first decoded for high SINRs, more particularly the user having the highest probability to be decoded first in the interference-limited region, is the second user, i.e. the user located in beam 2. In the same way the last user to be decoded in the interference-limited region is the third user.

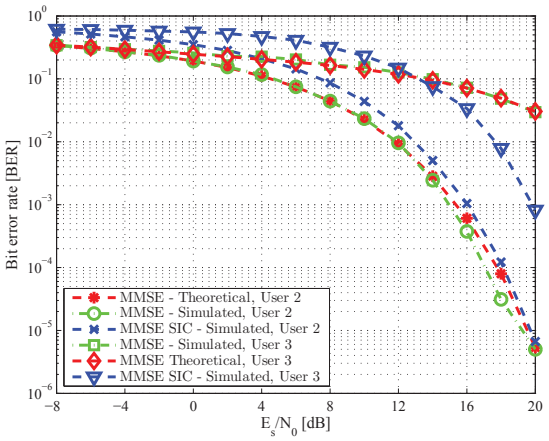


Figure C.30. *Theoretical evaluations versus practical evaluations of the BER for seven beams ($B = 7$), the high interference scenario ("bad" case), QPSK modulation, and when considering SIC.*

Fig. C.30 illustrates on the one hand that the BER of the second user can be theoretically evaluated for high SINRs (the curves almost match) whereas in the noise-limited region the difference is due to the fact this user is no more the first one to be decoded while performing SIC. On the other hand the BER of the third user completely differs from the ones issued from theoretical evaluations and simulations with MMSE filtering. This is actually clearly expected since the third user is at the end of the decoding chain and is explained in the following.

When the first user is decoded, the estimation of the transmitted symbols is used in order to cancel the interference, more particularly in order to remove its contribution from the received vector $\boldsymbol{y}$. If the estimation is correct then the contribution of this user is perfectly removed and therefore the interference created by this user disappears. However some errors may appear with a given probability (actually it is directly the symbol error rate) and the estimation may be incorrect. In such a case the interference created by this user is not removed correctly and therefore may remain or may even be additionally created. Moreover when performing optimal SIC the MMSE filter matrix $\boldsymbol{G}_{\text{MMSE}}$ needs to be recomputed after each interference cancellation, based on the new version of the channel matrix.

C.3 Achievable Rate

C.3.1 Considerations

The purpose of this short section is to describe how the maximum achievable rate of a system can be evaluated using information theory.

The capacity of an Additive White Gaussian Noise (AWGN) channel can be written, using the well-known formula derived by Shannon [Sha49], as:

$$C = W \log_2 (1 + \text{SNR}) \tag{C.134}$$

where W is the bandwidth of the channel (Hz) and SNR is the so-called signal-to-noise ratio. The unit of the capacity in (C.134) is in bits per second (bits/s).

The Shannon limit (upper-bound) is achieved when the bandwidth of the system is perfectly used:

$$R_{\max} = \frac{C}{W} = \log_2 (1 + \text{SNR}) \tag{C.135}$$

the maximum achievable rate $R_{\max}$ is expressed in bits per second per Hertz (bits/s/Hz).

The Signal-to-Noise Ratio (SNR) represents the average signal power in watts (W) S over the total noise power N also in watts (W). The average signal power is actually the ratio between the energy per symbol and the transmission duration of a symbol:

$$S = \frac{E_\text{s}}{T_\text{s}} = \frac{N_\text{bits} \times E_\text{b}}{T_\text{s}} \tag{C.136}$$

where E_s is the energy per symbol, T_s the symbol duration, N_bits the number of bits per symbol and E_b the energy per bit. The total noise power is:

$$N = W \times N_0 \tag{C.137}$$

where N_0 is the noise power spectral density.

The duration of a symbol is directly related to the bandwidth available. Assuming perfect bandwidth filtering at the receiver, the effective bandwidth available is W and therefore $1/T_\text{s} = W$. The SNR can thus also be expressed as:

$$\frac{S}{N} = \frac{E_\text{s}/T_\text{s}}{W \times N_0} = \frac{E_\text{s} \times W}{W \times N_0} = \frac{E_\text{s}}{N_0} \tag{C.138}$$

Therefore using information theory it is possible to evaluate the maximum achievable rate of a system, represented by its channel matrix $\boldsymbol{H}$, as a function of the energy per symbol over noise power spectral density.

C.3.2 Mutual Information

Introduction

The mutual information, also called transinformation, corresponds in information theory to the mutual dependence of two variables and is measured in terms of bits when using the base 2 logarithm.

Let's define two random variables X and Y which represent respectively the transmitted and the received signal. Using entropies the mutual information $I(X;Y)$ can be expressed as follows for discrete random variables:

$$I(X;Y) = H(X) - H(X|Y) = H(Y) - H(Y|X) \tag{C.139}$$

where $H(X)$ is the marginal (or differential) entropy of X and $H(X|Y)$ the conditional entropy, i.e. the entropy of X knowing Y. Reciprocally $H(Y)$ is the marginal entropy of Y and $H(Y|X)$ the conditional entropy, i.e. the entropy of Y knowing X.

For continuous random variables the entropy is written in lower case:

$$I(X;Y) = h(X) - h(X|Y) = h(Y) - h(Y|X) \tag{C.140}$$

The next figure (Fig. C.31) shows a representation of the mutual information of the related entropies.

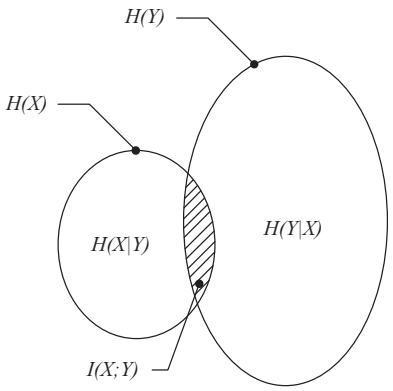


Figure C.31. *Representation of the mutual information (example).*

The mutual information $I(X;Y)$ permits to evaluate the capacity in terms of bits per channel use (when considering the base 2 logarithm). In the case where the received signal is represented by the vector $\boldsymbol{y}$ and the transmitted signal by the vector $\boldsymbol{x}$ the mutual information can be formulated as follows:

$$I(\boldsymbol{x};\boldsymbol{y}) = h(\boldsymbol{x}) - h(\boldsymbol{x}|\boldsymbol{y}) = h(\boldsymbol{y}) - h(\boldsymbol{y}|\boldsymbol{x}) \tag{C.141}$$

Entropy

For a discrete random variable X, with probability density function $p(x)$, the differential entropy (or marginal entropy) is:

$$H(X) = -\sum_{x \in \mathcal{X}} p(x) \log(p(x)) \tag{C.142}$$

where $\mathcal{X}$ is the discrete set of the random variable, i.e. $\mathcal{X} = \{x | p(x) > 0\}$.

For a continuous random variable X, with probability density function $f(x)$, the differential entropy (or marginal entropy) is:

$$h(X) = -\int_S f(x) \log(f(x)) \, dx \tag{C.143}$$

where S is the support set of the random variable, i.e. $S = \{x | f(x) > 0\}$.

Entropy of a random Gaussian Variable in one Dimension

The entropy of a random Gaussian variable in one dimension, i.e. a scalar can be computed from (C.143) considering:

$$f(x) = \frac{1}{\sqrt{2\pi}\,\sigma} \mathrm{e}^{-\frac{(x-\mu)^2}{2\sigma^2}} \tag{C.144}$$

where σ^2 and μ are respectively the variance and the mean value of the random variable.

The differential entropy of a Gaussian is then:

$$h(X) = -\int_{-\infty}^{+\infty} f(x) \log(f(x)) \, dx = -\int_{-\infty}^{+\infty} \frac{1}{\sqrt{2\pi}\,\sigma} \mathrm{e}^{-\frac{(x-\mu)^2}{2\sigma^2}} \log\left(\frac{1}{\sqrt{2\pi}\,\sigma} \mathrm{e}^{-\frac{(x-\mu)^2}{2\sigma^2}}\right) dx$$

$$h(X) = -\log\left(\frac{1}{\sqrt{2\pi}\,\sigma}\right) \int_{-\infty}^{+\infty} f(x) \, dx + \frac{1}{2\sigma^2} \int_{-\infty}^{+\infty} (x-\mu)^2 \, f(x) \, dx$$

Since $\int_{-\infty}^{+\infty} f(x) \, dx = 1$ by definition, and:

$$\int_{-\infty}^{+\infty} (x-\mu)^2 \, f(x) \, dx = \int_{-\infty}^{+\infty} x^2 f(x) \, dx - 2\mu \int_{-\infty}^{+\infty} x \, f(x) \, dx + \mu^2 \int_{-\infty}^{+\infty} f(x) \, dx$$

with $\int_{-\infty}^{+\infty} x \, f(x) \, dx$ being the mean value μ:

$$\int_{-\infty}^{+\infty} (x-\mu)^2 \, f(x) \, dx = \int_{-\infty}^{+\infty} x^2 f(x) \, dx - 2\mu^2 + \mu^2 = \int_{-\infty}^{+\infty} x^2 f(x) \, dx - \mu^2$$

The variance is actually computed as follows:

$$\sigma^2 = \int_{-\infty}^{+\infty} x^2 f(x) \, dx - \left(\int_{-\infty}^{+\infty} x \, f(x) \, dx\right)^2$$

which leads to:

$$\int_{-\infty}^{+\infty} (x-\mu)^2 \; f(x) \; dx = \sigma^2$$

We thus obtain:

$$h(X) = \log\left(\sqrt{2\pi}\,\sigma\right) + \frac{1}{2\sigma^2}\,\sigma^2 = \log\left(\sqrt{2\pi\sigma^2}\right) + \frac{1}{2} = \frac{1}{2}\,\log\left(2\pi\,\sigma^2\right) + \frac{1}{2}\,\log \mathrm{e}$$

which gives finally:

$$h(X) = \frac{1}{2}\,\log\left(2\pi\,e\,\sigma^2\right) \qquad \text{[nats]} \tag{C.145}$$

and:

$$h(X) = \frac{1}{2}\,\log_2\left(2\pi\,e\,\sigma^2\right) \qquad \text{[bits]} \tag{C.146}$$

As can be seen the differential entropy of a real Gaussian random variable does not depend on the mean value μ but only on the variance σ^2.

If the random Gaussian variable is complex the differential entropy is that of a real random vector $(\Re(x), \Im(x))$, thus $x \sim \mathcal{CN}\left(\mu, \sigma^2\right)$. The real part and the complex part of the random variable are independent and have variance $\sigma^2/2$, therefore:

$$h(X) = h(\Re(X)) + h(\Im(X)) = \frac{1}{2}\,\log\left(2\pi\,e\,\frac{\sigma^2}{2}\right) + \frac{1}{2}\,\log\left(2\pi\,e\,\frac{\sigma^2}{2}\right)$$

which leads to:

$$h(X) = \log\left(\pi\,e\,\sigma^2\right) \qquad \text{[nats]} \tag{C.147}$$

and:

$$h(X) = \log_2\left(\pi\,e\,\sigma^2\right) \qquad \text{[bits]} \tag{C.148}$$

Entropy of a random Gaussian Variable in N Dimensions

As for the scalar case, the entropy of a random Gaussian variable in N-dimension can be computed from (C.143) considering:

$$f(\boldsymbol{x}) = \frac{1}{\sqrt{(2\pi)^N \,\det(\boldsymbol{C_x})}}\,\mathrm{e}^{-\frac{1}{2}(\boldsymbol{x}-\mu)'\,\boldsymbol{C_x}^{-1}(\boldsymbol{x}-\mu)} \tag{C.149}$$

where $\boldsymbol{C_x}$ is the covariance matrix of the vector $\boldsymbol{x}$.

Using the same principle as for the scalar case we have:

$$h(X) = -\int_{-\infty}^{+\infty} f(\boldsymbol{x}) \log\left(f(\boldsymbol{x})\right)\, d\boldsymbol{x}$$

$$h(X) = \frac{1}{2} \log\left((2\pi)^N \det(\boldsymbol{C_x})\right) + \frac{1}{2} \int_{-\infty}^{+\infty} (\boldsymbol{x}-\mu)' \boldsymbol{C_x}^{-1} (\boldsymbol{x}-\mu) f(x) dx$$

From the law of the unconscious statistician, when knowing the probability density function $f(x)$ we can write:

$$\int_{-\infty}^{+\infty} g(x) f(x) = \mathrm{E}[g(x)]$$

which means:

$$\int_{-\infty}^{+\infty} (\boldsymbol{x}-\mu)' \boldsymbol{C_x}^{-1} (\boldsymbol{x}-\mu) f(x) dx = \mathrm{E}\left[(\boldsymbol{x}-\mu)' \boldsymbol{C_x}^{-1} (\boldsymbol{x}-\mu)\right]$$

Since $(\boldsymbol{x}-\mu)' \boldsymbol{C_x}^{-1} (\boldsymbol{x}-\mu)$ is a scalar we can write:

$$\mathrm{E}\left[(\boldsymbol{x}-\mu)' \boldsymbol{C_x}^{-1} (\boldsymbol{x}-\mu)\right] = \mathrm{E}\left[\mathrm{tr}\{(\boldsymbol{x}-\mu)' \boldsymbol{C_x}^{-1} (\boldsymbol{x}-\mu)\}\right]$$

and using the properties of the trace operator, we have:

$$\mathrm{E}\left[\mathrm{tr}\{(\boldsymbol{x}-\mu)' \boldsymbol{C_x}^{-1} (\boldsymbol{x}-\mu)\}\right] = \mathrm{E}\left[\mathrm{tr}\{(\boldsymbol{x}-\mu) (\boldsymbol{x}-\mu)' \boldsymbol{C_x}^{-1}\}\right]$$

which remains into writing:

$$\mathrm{E}\left[\mathrm{tr}\{(\boldsymbol{x}-\mu) (\boldsymbol{x}-\mu)' \boldsymbol{C_x}^{-1}\}\right] = \mathrm{tr}\{\mathrm{E}\left[(\boldsymbol{x}-\mu) (\boldsymbol{x}-\mu)'\right] \boldsymbol{C_x}^{-1}\} = \mathrm{tr}\{\boldsymbol{C_x} \boldsymbol{C_x}^{-1}\} = \mathrm{tr}\{\boldsymbol{I}\} = N$$

We thus have:

$$h(X) = \frac{1}{2} \log\left((2\pi)^N \det(\boldsymbol{C_x})\right) + \frac{N}{2} = \frac{1}{2} \log\left((2\pi\,\mathrm{e})^N \det(\boldsymbol{C_x})\right)$$

which leads to:

$$h(X) = \frac{1}{2} \log \det(2\pi\,\mathrm{e}\,\boldsymbol{C_x}) \qquad \text{[nats]} \tag{C.150}$$

and:

$$h(X) = \frac{1}{2} \log_2 \det(2\pi\,\mathrm{e}\,\boldsymbol{C_x}) \qquad \text{[bits]} \tag{C.151}$$

As for the scalar case if the Gaussian random variable is complex then we have:

$$h(X) = h(\Re(X)) + h(\Im(X)) = \frac{1}{2} \log \det\left(2\pi\,\mathrm{e}\,\frac{\boldsymbol{C_x}}{2}\right) + \frac{1}{2} \log \det\left(2\pi\,\mathrm{e}\,\frac{\boldsymbol{C_x}}{2}\right)$$

which leads to:

$$h(X) = \log \det(\pi\, e\, \boldsymbol{C_x}) \qquad \text{[nats]} \tag{C.152}$$

and:

$$h(X) = \log_2 \det(\pi\, e\, \boldsymbol{C_x}) \qquad \text{[bits]} \tag{C.153}$$

C.3.3 Constrained-Capacity

The so-called constrained-capacity, which relates to capacity obtained with a given discrete constellation, permits to estimate the achievable rate for different modulations. Its allows getting a better idea of the spectral efficiency, expressed in bits/s/Hz, obtained in a Input-Output (IO) system with a given modulation order, specially in our case with phase-shift modulations.

Principle

There are two possible methods to evaluate the capacity for discrete constellations. The first one consists into doing numerical evaluations and the second one into performing Monte Carlo simulations. Both methods are based on the formulation of the channel capacity, more particularly the mutual information (please refer to Section C.3.2). We remind that:

$$I\left(X;Y\right) = H\left(X\right) - H\left(X|Y\right)$$

The marginal (or differential) entropy of X, namely $H\left(X\right)$, can be computed easily when considering M-ary complex modulations like BPSK, QPSK, 8-PSK and 16-PSK. More particularly we have:

$$H\left(X\right) = \mathrm{E}\left[h\left(X\right)\right] \tag{C.154}$$

where $h\left(X\right) = \log\left(1/p\left(X\right)\right) = -\log\left(p\left(X\right)\right)$. Since the symbols are equiprobable, i.e. $p\left(X\right) = 1/M$, it gives:

$$H\left(X\right) = \mathrm{E}\left[h\left(X\right)\right] = \mathrm{E}\left[-\log\left(p\left(X\right)\right)\right] = \log\left(M\right) \tag{C.155}$$

and expressed in bits:

$$H\left(X\right) = \log_2\left(M\right) \tag{C.156}$$

The mutual information gives the ergodic capacity and therefore corresponds to the upper bound of the achievable rate. For this reason we consider that $R = I\left(X;Y\right)$, where R corresponds to the achievable rate in terms of bits/s/Hz (thus the mutual information has to be evaluated the base 2 logarithm). For a rate obtained with a particular energy per symbol over noise power spectral density E_s/N_0, the corresponding energy per bit over power spectral density, namely E_b/N_0, can be computed. More particularly:

$$\frac{E_\mathrm{s}}{N_0} = R\,\frac{E_\mathrm{b}}{N_0} \tag{C.157}$$

The energy per bit over power spectral density can thus be obtained as follows:

$$\left(\frac{E_\mathrm{b}}{N_0}\right)_\mathrm{dB} = \left(\frac{E_\mathrm{s}}{N_0}\right)_\mathrm{dB} - 10\,\log_{10}\left(R\right) \tag{C.158}$$

Monte Carlo Simulations:

The Monte Carlo method consists into evaluating an expression with sufficient number of random samples in order to compute the final result. Specially the aim is to generate N symbols, each symbol being represented by x_k, taking into account the alphabet of the modulation, to generate a Gaussian noise η, and to finally compute the simple relation $y = x_k + \eta$ [RyLi09].

The symbol x_k is chosen from the set S which depends on the modulation order, especially $S = \{x_1, x_2, ..., x_M\}$, and represents $\log_2(M)$ bits. As written previously the marginal entropy of X is such that $H(X) = \log(M)$. The purpose is to formulate the conditional entropy $H(X|Y)$ so as to compute the mutual information.

We denote with $p(y|x_k)$ the probability that the signal y was received knowing that the (complex) symbol x_k was transmitted. Since we consider an AWGN channel, this probability is:

$$p(y|x_k) = \frac{1}{2\pi\,\sigma^2}\,\exp\left(\frac{-|y - x_k|^2}{2\,\sigma^2}\right) \tag{C.159}$$

The conditional entropy of X given Y is:

$$H(X|Y) = \mathrm{E}\left[h(X|Y)\right] \tag{C.160}$$

where $h(x|y) = -\log\left(p(x|y)\right)$. Knowing that:

$$\sum_{x' \in S} p\left(x'|y\right) = 1 \tag{C.161}$$

we can formulate the probability of that a symbol x was transmitted given that the signal y was received as follows:

$$p(x|y) = \frac{p(x|y)}{\sum_{x' \in S}\, p(x'|y)} \tag{C.162}$$

Using the Bayes' theorem, the previous expression becomes:

$$\frac{p(x|y)}{\sum_{x' \in S}\, p(x'|y)} = \frac{\frac{p(y|x)\,p(x)}{p(y)}}{\sum_{x' \in S}\, \frac{p(y|x')\,p(x')}{p(y)}} = \frac{\frac{1}{M\,p(y)}\,p(y|x)}{\frac{1}{M\,p(y)}\,\sum_{x' \in S}\, p(y|x')} = \frac{p(y|x)}{\sum_{x' \in S}\, p(y|x')} \tag{C.163}$$

which can also be written as:

$$p(y|x_k) = \frac{\frac{1}{2\pi\,\sigma^2}\,f(y|x)}{\frac{1}{2\pi\,\sigma^2}\,f(y|x')} = \frac{f(y|x)}{f(y|x')} \tag{C.164}$$

with:

$$f(y|x) = \exp\left(\frac{-|y - x|^2}{2\,\sigma^2}\right) \tag{C.165}$$

Since the noise is composed of circularly symmetric complex Gaussian random variables with real and imaginary parts $\mathcal{N}\left(0, \sigma^2/2\right)$ (i.i.d.), more particularly such that $\mathcal{N}\left(0, N_0/2\right)$, and also since the average energy per symbol is $\mathrm{E}\left[|x|^2\right] = E_\mathrm{s}$, we have:

$$\log\left(f\left(y|x\right)\right) = \frac{-|y-x|^2}{2\,\sigma^2} = -\frac{E_\mathrm{s}}{N_0}\,|y-x|^2 \tag{C.166}$$

Considering the number of random samples N, which are actually the different symbols generated, the conditional entropy $H\left(X|Y\right)$ is computed as follows:

$$H\left(X|Y\right) = \lim_{N\to\infty}\,\frac{1}{N}\,\sum_{n=1}^{N} h\left(X^{(n)}|Y^{(n)}\right) \tag{C.167}$$

where $\left(X^{(n)}, Y^{(n)}\right)$ is the n-th realisation of the random pair (X, Y), and:

$$h\left(X^{(n)}|Y^{(n)}\right) = -\log\,f\left(y^{(n)}|x^{(n)}\right) + \log\sum_{x'\in S} f\left(y^{(n)}|x'\right) \tag{C.168}$$

The conditional entropy is therefore:

$$h\left(X^{(n)}|Y^{(n)}\right) = \lim_{N\to\infty}\,\frac{1}{N}\,\sum_{n=1}^{N}\left(\frac{E_\mathrm{s}}{N_0}\,|y^{(n)}-x^{(n)}|^2 + \log\sum_{x'\in S}\exp\left(-\frac{E_\mathrm{s}}{N_0}\,|y^{(n)}-x'|^2\right)\right) \tag{C.169}$$

and the mutual information can finally be expressed as:

$$I\left(X;Y\right) = \log\left(M\right) - \lim_{N\to\infty}\,\frac{1}{N}\,\sum_{n=1}^{N}\left(\frac{E_\mathrm{s}}{N_0}\,|y^{(n)}-x^{(n)}|^2 + \log\sum_{x'\in S}\exp\left(-\frac{E_\mathrm{s}}{N_0}\,|y^{(n)}-x'|^2\right)\right) \tag{C.170}$$

and in terms of bits:

$$I\left(X;Y\right) = \log_2\left(M\right) - \lim_{N\to\infty}\,\frac{1}{N}\,\sum_{n=1}^{N}\left(\frac{E_\mathrm{s}}{N_0}\,|y^{(n)}-x^{(n)}|^2 + \log_2\sum_{x'\in S}\exp\left(-\frac{E_\mathrm{s}}{N_0}\,|y^{(n)}-x'|^2\right)\right) \tag{C.171}$$

Numerical Evaluations:

Using a closed-form formula, still issued from the mutual information, the channel capacity of a system using Pulse Amplitude Modulation (PAM) can be computed as follows [BeCh02]:

$$C = log_2\left(M\right) - \frac{1}{M}\,\sum_{n=1}^{M}\int_{-\infty}^{+\infty}\frac{1}{\sqrt{2\pi\,\sigma^2}}\,\exp\left(-\frac{\xi^2}{2\,\sigma^2}\right)\,\log_2\left[\sum_{i=1}^{M}\exp\left(-\frac{\left(\alpha_n+\xi-\alpha_i\right)^2-\xi^2}{2\,\sigma^2}\right)\right]\,d\xi \tag{C.172}$$

where M represents the order of the amplitude modulation, and α represents a symbol belonging to the modulation.

The previous expression is valid for real-valued AWGN channel where the input signal is issued from a M-PAM modulation. Therefore the capacity is expressed in terms of bits/dimension. It has to be remarked that the capacity of the Binary Phase-Shift Keying (BPSK) modulation in a AWGN channel can also be obtained using (C.172) since the constellation of this modulation is mapped in one single dimension. However, it is no more valid for M-PSK modulations with order $M > 2$ because with these modulations we work in the complex dimension.

We now try to derive a closed-form formula for evaluating the channel capacity of a system using Phase-Shift Keying (PSK) modulations. We assume the energy per symbol is normalised to one and we will make use of an important property of PSK modulations which is their symmetry. The mutual information can be written as follows [RyLi09]:

$$I\left(X;Y\right) = \log_2\left(M\right) - \sum_{x\in S}\int_y p\left(y|x\right)\, p\left(x\right)\, \log_2\left(\frac{1}{p\left(x|y\right)}\right)\, dy \tag{C.173}$$

since x is discrete and y continuous. As before, S is the set of symbols which depends on the modulation order, especially $S = \{x_1, x_2, ..., x_M\}$.

Using the Bayes' theorem the previous expression can also be written as follows:

$$I\left(X;Y\right) = \log_2\left(M\right) - \frac{1}{M}\sum_{x\in S}\int_y p\left(y|x\right)\, \log_2\left(\frac{\frac{1}{M}\,\sum_{x'}\, p\left(y|x'\right)}{p\left(x|y\right)\, p\left(x\right)}\right)\, dy \tag{C.174}$$

which simplifies into:

$$I\left(X;Y\right) = \log_2\left(M\right) - \int_y p\left(y|x\right)\, \log_2\left(\frac{\sum_{x'}\, p\left(y|x'\right)}{p\left(x|y\right)}\right)\, dy \tag{C.175}$$

since $\sum_{x\in S}$ represents M symbols which are symmetric and occur with the same probability.

Developing the different probabilities we obtain:

$$I\left(X;Y\right) = \log_2\left(M\right) - \int_y \frac{1}{2\pi\,\sigma^2}\,\mathrm{e}^{-\frac{1}{2\sigma^2}\,|y-x|^2}\, \log_2\left(\frac{\sum_{x'}\,\mathrm{e}^{-\frac{1}{2\sigma^2}\,|y-x'|^2}}{\mathrm{e}^{-\frac{1}{2\sigma^2}\,|y-x|^2}}\right)\, dy \tag{C.176}$$

Let's consider a point of the constellation which we denote as x_1. Using the symmetric property of M-PSK modulations we can write:

$$I\left(X;Y\right) = \log_2\left(M\right) - \int_y \frac{1}{2\pi\,\sigma^2}\,\mathrm{e}^{-\frac{1}{2\sigma^2}\,|y-x_1|^2}\, \log_2\left(1 + \sum_{x'\neq x_1}\,\mathrm{e}^{-\frac{1}{2\sigma^2}\,\left[|y-x'|^2 - |y-x_1|^2\right]}\right)\, dy \tag{C.177}$$

From the previous expression we know that:

$$|y-x'|^2 = \left(y-x'\right)\,\left(y^*-x'^*\right) = |y|^2 - |x'|^2 - 2\,\Re\left[x'\,y^*\right] \tag{C.178}$$

and:

$$|y - x_1|^2 = |y|^2 - |x_1|^2 - 2\,\Re[x_1\,y^*] \tag{C.179}$$

This simplifies the expression into:

$$I\left(X;Y\right) = \log_2\left(M\right) - \int_y \frac{1}{2\pi\,\sigma^2}\,\mathrm{e}^{-\frac{1}{2\sigma^2}\,|y-x_1|^2}\,\log_2\left(1 + \sum_{x'\neq x_1}\mathrm{e}^{-\frac{1}{\sigma^2}\,\Re[(x'-x_1)\,y^*]}\right)dy \tag{C.180}$$

We now assume that x_1 is exclusively real and equal to 1 (remind that the energy per symbol is one), this finally gives: This simplifies the expression into:

$$I\left(X;Y\right) = \log_2\left(M\right) - \int_y \frac{1}{2\pi\,\sigma^2}\,\mathrm{e}^{-\frac{1}{2\sigma^2}\,|y-1|^2}\,\log_2\left(1 + \sum_{x'\neq 1}\mathrm{e}^{-\frac{1}{\sigma^2}\,\Re[(x'-1)\,y^*]}\right)dy \tag{C.181}$$

Validation with a Simple Channel

Both methods for evaluating the constrained capacity, i.e. through Monte Carlo simulations (C.171) and numerical evaluations (C.172) (C.181), are verified using a simple channel. More particularly the system is such that $y = x + \eta$, where x is the transmitted symbol, η the additive white Gaussian noise, and y the received signal. For the Monte Carlo method 100 000 samples are considered.

We remind that the Shannon capacity is such that [Sha49]:

$$C = \log_2\left(1 + \frac{E_\mathrm{s}}{N_0}\right)$$

where C is expressed in terms of bit/complex dimension or bit/s/Hz.

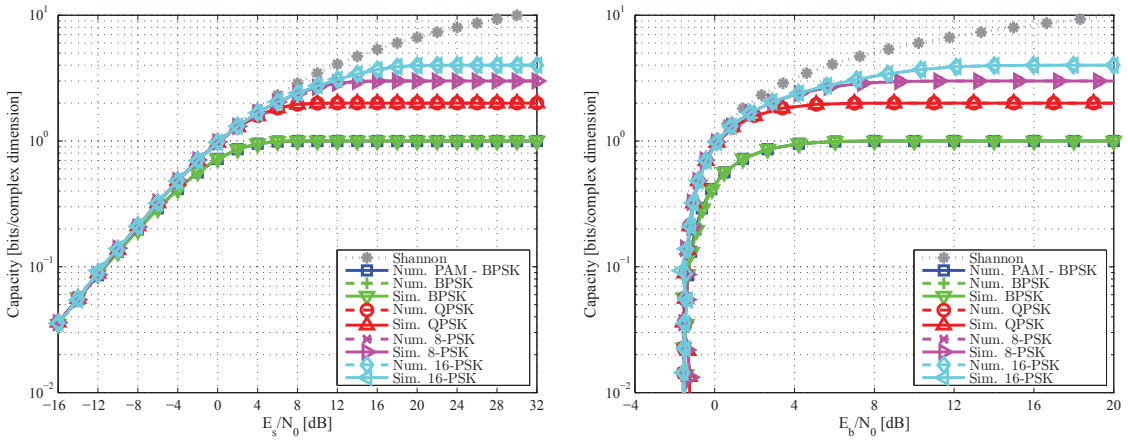


Figure C.32. *Constrained-capacity with a simple channel as a function of the energy per symbol (left) and energy per bit (right).*

Fig. C.32 shows the constrained-capacity for M-PSK modulation, including the Shannon capacity. As expected all curves match for low energy per symbol (left) and bit (right) over noise power spectral density. Also for all M-PSK modulations the Monte Carlo simulations, more time consuming, provide the same results as the numerical evaluations. For the different modulation orders the capacity saturates at $\log_2(M)$ bit/s/Hz, which actually corresponds to the number of bits per symbol supported by the modulation.

Satellite Channel

The purpose is to compute the constrained-capacity when taking into account the satellite channel. More particularly we consider the reduced scale system with seven beams ($B = 7$), full frequency reuse ($K = 1$) and the average interference level (so-called "average case", please refer to Section 2.2.3 for more details about this scenario). We focus on the user located in the beam of interest, i.e. the beam present in the centre of the system and surrounded by six adjacent beams using the same frequency; the achievable rate of this user considering MIMO is noted $R_{\text{MIMO},1}$. Using the Shannon capacity formula, it is possible to evaluate the equivalent signal-to-interference plus noise ratio (SINR) of this user at the output of the MMSE SIC receiver (remind that an MMSE receiver with the optimal SIC architecture is capacity-achieving). More particularly:

$$R_{\text{MIMO},j} = \log_2\left(1 + \text{SINR}_{\text{MIMO},j}\right) \quad \Leftrightarrow \quad \text{SINR}_{\text{MIMO},j} = 10\,\log_{10}\left(\mathrm{e}^{R_{\text{MIMO},j}\,\ln 2} - 1\right) \tag{C.182}$$

where $\text{SINR}_{\text{MIMO},j}$ is in linear in the left part of the expression and in decibels in the right part. The numerical evaluation for M-PSK modulations is taken into account since it is less time consuming.

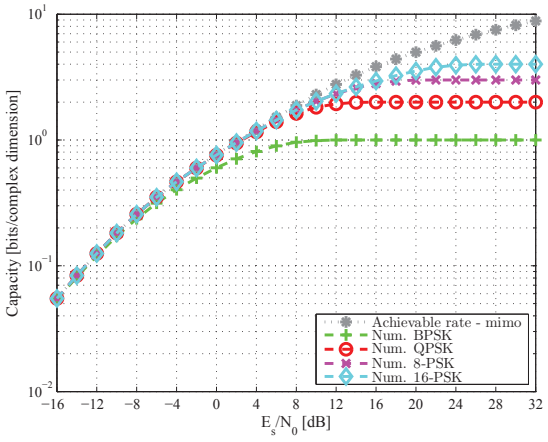


Figure C.33. *Constrained-capacity with a satellite channel consisting of seven beams ($B = 7$), with full frequency reuse ($K = 1$), average interference level and for the first user.*

Fig. C.33 shows the corresponding constrained capacity for M-PSK modulations, together with the initial achievable capacity ("achievable rate"). The energy per symbol over noise power spectral density on the x-axis relates to the SNR at the input of the system, more particularly the energy per transmitted symbol over the power spectral density of the noise added into the system. In this case the channel impacts the overall performance since we have $\boldsymbol{y} = \boldsymbol{H}\,\boldsymbol{x} + \boldsymbol{\eta}$, where $\boldsymbol{H}$ corresponds to the satellite channel. As expected the constrained capacities match the achievable rate curve in the noise-limited region and then reach the maximum number of bits per complex dimension, depending on the modulation order M.

C.4 Scheduling

C.4.1 Performance of Scheduling with and without Ordering

Introduction

We have seen that the ordering, i.e. the permutation applied to the channel matrix, directly impacts the achievable single user rates. The ordering determines in which sequence the user's signals will be decoded when employing Successive Interference Cancellation (SIC). User constraints can be taken into account and the optimal ordering can be determined based on Quality of Service (QoS). When performing the scheduling process, i.e. when optimising the combination of users in the multi-beam satellite system which is considered as interference-limited, the ordering will play a role.

On the one hand the ordering can be seen as a post-process which is executed by the Gateway when receiving the combination of the user's signal. On the other hand the scheduling process can be seen as a pre-process which has to be realised by the Gateway in order to optimise the allocation. The scheduling process can therefore be done by assuming optimal ordering. This permits to get an idea of what can be achieved at the end of the reception chain, once IC is performed. The scheduling algorithms presented in this document all determine the minimum per-user rate in order to select the optimal allocation through a pure exhaustive search or using a multipartite graph approach.

When computing the minimum per-user rate there are two possibilities: assume ordering and therefore determine the optimal one or assume no ordering, this process being realised at the very end of the scheduling process, i.e. once the optimal scheduling was found. In the first case ordering has to realised when evaluating each combination of users whereas in

the second case ordering is performed only once the optimal scheduling was found. What is the difference in terms of scheduling performance knowing that the processing time will be dramatically modified?

Bad and Good Cases

Both bad and good cases were considered in order to evaluate the impact of the ordering on the scheduling process. As usual the users issued from the bad case, i.e. the so-called "bad" users are the users with index 1 whereas the users issued from the good case, i.e. the so-called "good" users are the users with index 2 in the system. We therefore have $M = 2$ users per beam and $B = 7$ beams. This leads to 64 possible allocations when finding the optimal scheduling with the exhaustive search.

The minimum per-user rates and the Jain's fairness index were evaluated for SNRs ranging from -32 to 32 dB. As usual the minimum per-user rate is computed on a block basis (here a block is composed of $M = 2$ slots) and also the Jain's fairness index. Simulations have shown that scheduling without ordering in the process performs about 3.3 times faster than scheduling with ordering. This is of course a huge improvement but when looking at both minimum per-user rates (Fig. C.34, left) and Jain's fairness index (Fig. C.34, right) we observe a decrease of performance.

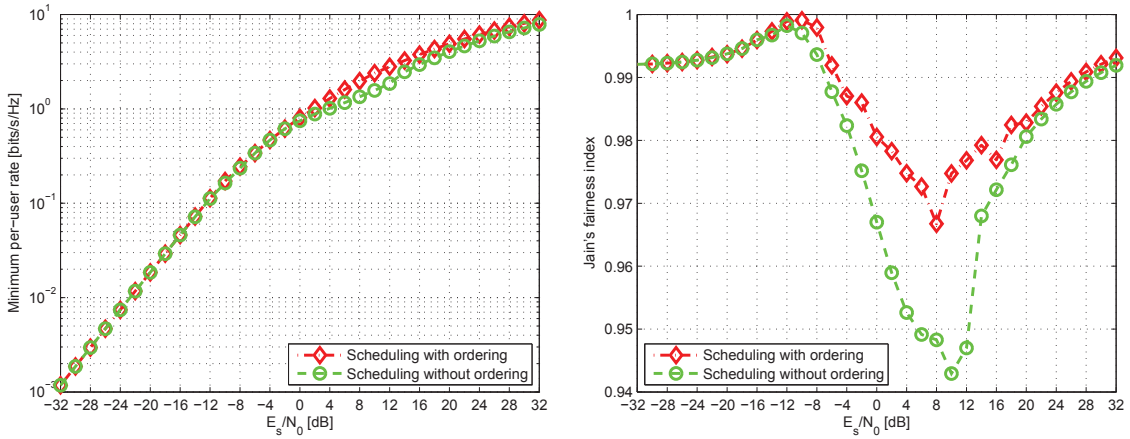


Figure C.34. *Minimum per-user rates (left) and Jain's fairness index (right) for the bad and good cases, with and without ordering in the scheduling process, and with seven beams ($B = 7$).*

Summary

From the results provided in the previous section (Section C.4.1) there is clearly a decrease of performance for both maximising the minimum achievable per-user rate but also for providing

fairness to users. On the one hand performing scheduling without taking optimal ordering reduces considerably the complexity and therefore permits to obtain optimised schedules more rapidly. On the other hand, as seen, it decreases the performance. For this reason in the different simulations involving the optimisation of the user schedules optimal ordering is always assumed, if not stated.

C.4.2 Search Algorithms - Allocations versus Combinations

The aim of this section is to compare the performance of both Exhaustive Search (ES) algorithms, more particularly the exhaustive search based on the allocations (please refer to Section 4.3.1), and referred as "pure" exhaustive search, with the exhaustive search based on the combinations (please refer to Section 4.3.2).

Introduction

The principle of the first exhaustive search is to produce all possible allocations for a given number of users per beam M and of beams B in the system. The algorithm go through all allocations and compute the minimum per-user rate for each of the M slots present in the allocation. Finally the algorithm selects the allocation maximising the minimum per-user rate over the M slots. The selection of the optimal allocation is thus performed on a block basis (please refer to Section 4.5.1 for a better understanding of both slot basis and block basis). Since there are $(M!)^{(B-1)}$ possible allocations one can understand that for some values of M and B this kind of exhaustive search cannot be performed.

The second exhaustive search performs at lower level, more particularly at the level in which users are associated in one particular slot. The association of B users in one slot is named combination in this document. A way of working at this level is to use a so-called multipartite graph approach. This type of exhaustive search permits to reduce dramatically the complexity of the scheduling algorithm. We remind that the principle is to produce all possible edges for a given number of users per beam M and of beams B in the system. An edge actually corresponds to a possible combination of users at a given time in B beams. The number of possible edges is M^B which considerably reduce the complexity when compared to the exhaustive search based on the allocations. The algorithm computes the minimum per-user rate for each edge and sort the results. A minimum deletion strategy is then applied in order to optimally select M edges in the list. The resulting M edges give the final allocation for which the minimum per-user rate is maximised. Contrary to the exhaustive search working

on all possible allocations, the B-partite graph approach tries to maximise the minimum per-user rate on a slot basis.

The multipartite graph approach should therefore select an optimal allocation faster than the pure exhaustive search since the number of possible edges is smaller than the number of possible allocations. It has to be remarked that this is true as soon as the number of users per beam M is greater than 2:

$$(M!)^{(B-1)} = M^{(B-1)} \qquad \text{when} \qquad M = 2$$

However the two algorithms should provide the same results, more particularly the minimum per-user rate obtained on a block basis, i.e. over M slots, should be identical. It was remarked, during several simulations, that the optimal allocation selected by the "pure" exhaustive search does not necessarily match the optimal allocation resulting from the multipartite graph approach algorithm, and therefore from the exhaustive search performing at the combination level.

In order to understand this behaviour a script was implemented in order to detect, among a given number of channel realisations, when the two algorithms provide different results. The script indicates, when this happens, if the minimum per-user rate obtained over a block basis is not the same (and actually this should never happen). If the two algorithms have the same minimum per-user rate then the script detects which of the two algorithms perform better (it compares the remaining $M - 1$ minimum per-user rates). Several simulations over large numbers of channel realisations have revealed that the two algorithms offer the same performance when looking at the minimum per-user rate on a block basis. This simply permit to validate the B-partite graph approach algorithm since it should provide the same result and therefore this consider this algorithm as an optimal one also. However for some channel realisations the remaining $M - 1$ minimum per-user rates differ. Most of the time the BG algorithm performs better than the "pure" ES but sometimes the contrary is observed. The purpose is to understand why this can happen.

Example

Let's consider the first ten thousand channel realisations of the channel matrices ($N_{\text{ch}} = 10\,000$) produced for universal frequency reuse ($K = 1$) and seven beams ($B = 7$). We select of part of the channel matrices such that we actually have a reduced number of beams,

more particularly three beams ($B = 3$). A difference of allocation is detected for channel realisations with index 7 and 8 for instance when considering two users per beam ($M = 2$) and having a SNR of 15 dB. In this case it is actually detected that the "pure" ES performs better than the BG algorithm. The allocation issued from the "pure" exhaustive search in given in Table C.8. The allocation given by the B-partite graph approach algorithm is given in Table C.9. One can clearly see that the two allocations differ but the minimum per-user rate obtained on a block basis is the same and equals 4.09 bits/s/Hz.

Table C.8. *Allocation obtained with the "pure" exhaustive search with three beams ($B = 3$) and two users per beam ($M = 2$).*

Beam ID	1	2	3
Slot 1	1	1	1
Slot 2	2	2	2

Table C.9. *Allocation obtained with the multipartite graph approach with three beams ($B = 3$) and two users per beam ($M = 2$).*

Beam ID	1	2	3
Slot 1	1	2	2
Slot 2	2	1	1

On the one hand, as already mentioned, the "pure" exhaustive search produces all possible allocations. When selecting the allocation achieving the highest minimum per-user rate it may happen that several allocations provide the same result. In such a case the "pure" ES picks up the first allocation appearing in the list, i.e. the allocation which is shown by Table C.8 (when generating all allocations the first possibility is straightforward and is the one of Table C.8). On the other hand the allocation coming out of the multipartite graph algorithm directly depends on the minimum deletion algorithm (please refer to Section 4.3.3 for more details). The sorted list of edges is given in Table C.10.

As can be seen in the list of sorted edges (Table C.10) some edges present the same minimum per-user rate. The minimum deletion algorithm will start from the edge with ID 1. It will remove the edges with IDs 1 and 2 since there are still solutions available if they are deleted from the list. The edge with ID 3 will also be deleted since the condition of having a solution is still satisfied. The algorithm will then select the edge with ID 4 and the corresponding edge with ID 7 as the final edges. For comparison the exhaustive search has selected the

Table C.10. *Sorted list of edges for the multipartite graph approach with three beams ($B = 3$) and two users per beam ($M = 2$).*

ID	B_1	B_2	B_3	Rate (bits/s/Hz)
1	1	1	2	3.76
2	2	1	2	3.76
3	1	1	1	4.09
4	2	1	1	4.09
5	1	2	1	4.32
6	2	2	1	4.44
7	1	2	2	4.44
8	2	2	2	4.50

edges with ID 3 and 8. Of course the edge with ID 8 provide an higher rate than the edge with ID 7. The difference of performance is thus related to the fact some combinations of users can provide the same minimum per-user rate. Then depending on the algorithms, more particularly how the allocations are produced and how they are selected, and how the edges are produced, how they are sorted and how they are finally selected, the two algorithms may output different optimal allocations. Anyway it was observed that when this happens most of the time the multipartite graph approach outperforms the "pure" exhaustive search in terms of minimum per-user rate.

Summary

On the one hand the so-called "pure" exhaustive search, i.e. the exhaustive search operating on all possible allocations, selects the allocation maximising the minimum achievable per-user rate on a block basis. On the other hand the other exhaustive search, based on all possible combinations of users within one slot, and using a multipartite graph approach, produces the final allocation while trying to maximise the minimum achievable per-user rate on a slot basis. This results into having identical minimum rates on a block basis, but not necessarily on a slot basis. Therefore for a given block of size M, the minimum of the minimum per-user rate is the same for the two algorithms, but the remaining $M - 1$ minimum per-user rates in this block may not be identical. It has been verified through several simulations, and also it can be verified using the results providing in Section 4.5, that on average both algorithms provide the same performance. Even if it is quite difficult, even impossible to be proved due to the utilisation of the so-called "minimum deletion algorithm", the exhaustive search based

on all possible combinations, and therefore the B-partite graph approach, can be considered, through this analysis and the different results obtained, as being an "optimal" algorithm.

C.4.3 Summary and Dependencies of the Scheduling Algorithms

The purpose of this section is to summarise the different scheduling algorithms implemented, more particularly to give an idea about their dependencies. To this aim the diagram shown by Fig. C.35 can be considered.

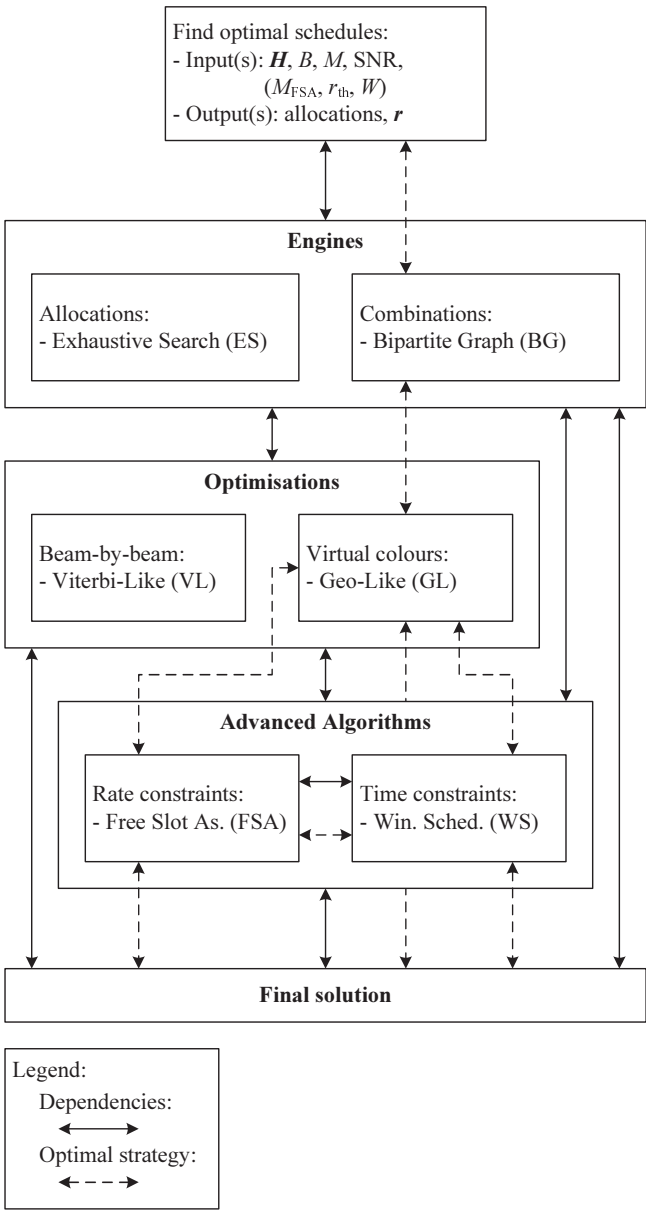


Figure C.35. *Summary of the different scheduling algorithms, including their dependencies.*

The purpose of the scheduling algorithms is to find optimal schedules that target the max-

min criterion, i.e. that maximise the minimum per-user rate (Fig. C.35). To do so the algorithms need as input the channel realisations, represented by the 3D matrix $\boldsymbol{H}$ which size is $N_{\mathrm{Rx}} \times N_{\mathrm{Tx}} \times N_{\mathrm{ch}}$, the number of beams B to be considered, the scheduling depth M and the signal-to-noise ratio (SNR). Optionally, depending if one or more advanced algorithms are taken into account, the Free Slot Assignment (FSA) threshold M_{FSA} together with the rate threshold r_{th}, and the window size W can be also used as inputs.

The two main algorithms for optimising the schedules are based on a search (please refer to Section 4.3) which is either performed on the different allocations (Section 4.3.1) or on the different combinations (B-partite Graph (BG) approach, Section 4.3.2). As indicated in Fig. C.35 the schedules can be optimised only based on these two algorithms which are referred as "engines". In order to reduce the complexity and work with large-scale systems, scheduling algorithms can be used (please refer to Section 4.4), especially either the "Viterbi-like algorithm" (Section 4.4.1) or the "Geo-like algorithm" (Section 4.4.2). These two algorithms are referred as "Optimisations" and make use of one of the two search algorithms. Again the final solution can be directly issued from these two sub-optimal algorithms. Finally the "advanced algorithms", especially the "smart Free Slot Assignment (FSA) scheduling algorithm" (Section 5.2) and the "window scheduling algorithms" (both "normal" and "advanced" versions, Section 5.3), can either compute the schedules based on the search algorithms or on the scheduling algorithms. The link between the rate constraints algorithm and the time constraints algorithm depicts the so-called "hybrid algorithm" (Section 5.4).

The optimal strategy for finding the best schedules is represented by dashed arrows in Fig. C.35. For instance without any rate and/or time constraints, the optimal strategy consists into using the Geo-like algorithm which in turn uses the algorithm based on the BG approach. This combination has shown close to optimal performance with highly reduced computational complexity (please refer to Section 4.5). When considering constraints, the best strategy resides into making use of the hybrid algorithm, together with the previously-mentioned algorithms combinations.

The output of the scheduling algorithms contains the list of optimised allocations and the corresponding per-user rates. From this statistics can be derived like the Cumulative Density Function (CDF) of the lowest user rates computed either on a slot or on a block basis, or the Jain's fairness index which measures the level of fairness between users.

Appendix D

Additional Side Information

D.1 List of Publications, Patents, and Other(s)

This section summarises the outcome of the Ph.D. thesis, more particularly the different conference and journal papers submitted, the attendance to workshops and summer school, and the patents registered.

D.1.1 Conference and Journal Paper(s)

[BBRJ11]: V. Boussemart, M. Berioli, F. Rossetto, and M. Joham, "On the Achievable Rates for the Return-Link of Multi-Beam Satellite Systems Using Successive Interference Cancellation", in *IEEE MILCOM*, Baltimore (MD, USA), Nov. 2011.
Status: *submitted, accepted and presented.*

[BoBeRo11]: V. Boussemart, M. Berioli, and F. Rossetto, "User Scheduling for Large Multi-beam Satellite MIMO Systems", in *ASILOMAR*, Pacific Grove (CA, USA), Nov. 2011.
Status: *submitted, accepted and presented.*

[BoMaBe12-1]: V. Boussemart, L. Marini, and M. Berioli, "Impact of Scheduling in the Return-Link of Multi-Beam Satellite MIMO Systems", in *GLOBECOM*, Anaheim (CA, USA), Dec. 2012.
Status: *submitted, accepted and presented.*

[BoMaBe12-2]: V. Boussemart, L. Marini, and M. Berioli, "Multi-Beam Satellite MIMO Systems: BER Analysis of Interference Cancellation and Scheduling", in *ASMS*, Baiona (Spain),

Sep. 2012.
Status: *submitted, accepted and presented.*

[BoBe12]: V. Boussemart, and M. Berioli, "Scheduling in Virtual MIMO Multi-Beam Satellite Systems", in *IEEE Journal on Selected Areas in Communications - Virtual MIMO (IEEE JSAC SI on Virtual MIMO)*, submitted on 15th of October 2012.
Status: *submitted.*

D.1.2 Workshops, Summer School and Other(s)

The author gave the following presentations in the framework of different workshops, summer school and others events, and in which he had the opportunity to describe his work and to receive useful feedbacks:

- Presentation of the Ph.D. topic and status at the department workshop in Munich (Germany), 11th to 12th of October 2010,
- Communications in Interference-Limited Networks (COIN) Workshop in Munich (Germany), 12th to 13th of October 2010,
- Presentation aiming at introducing broadband satellite communications at Technische Universität München (TUM), 18th of December 2010,
- COIN Workshop in Dresden (Germany), 31st of May to 1st of of June 2011,
- 2012 European School of Information Theory, IEEE Information Theory Society, in Antalya (Turkey), 16th to 20th of April 2012.

D.1.3 Patent(s)

The author registered the following patents in the framework of this Ph.D. thesis:

- "Smart Free Slot Assignment Scheduling Algorithm for Interference-Limited Networks", Deutsche Patentanmeldung DE 10 2012 213 755.6, May 2012,
- "Advanced Window Scheduling Algorithm for Interference-Limited Networks", Deutsche Patentanmeldung DE 10 2013 206 847.6, October 2012.

D.2 Erratum

In [Col85], page 211, expression (4.84):

$$f_y = \pi\, a^2\, E_0 \left[2\,(1-A)\, \frac{J_1\,(u)}{u} + A\, 2^n\, n!\, \frac{J_{n+1}\,(u)}{u^{n+1}} \right] \tag{D.1}$$

should actually be:

$$f_y = \pi\, a^2\, E_0 \left[2\,(1 - A)\, \frac{J_1\,(u)}{u} + A\, 2^{n+1}\, n!\, \frac{J_{n+1}\,(u)}{u^{n+1}} \right] \tag{D.2}$$

In [LuWeJa00], page 321, expression (12.7):

$$A\,(i) = \sum_u N_u\,(i)\; A_u \tag{D.3}$$

should actually be:

$$A\,(i) = \sum_u^{N_u(i)} A_u \tag{D.4}$$

In [MaBo02], page 333, Figure 7.2:
The two values of $\theta_{3\mathrm{dB}}$ should be reversed in the graph. An higher satellite antenna gain is actually achieved for smaller beamwidth which is not the case in this figure.

Université de Toulouse

THÈSE

En vue de l'obtention du

DOCTORAT DE L'UNIVERSITÉ DE TOULOUSE

Délivré par :

Institut Supérieur de l'Aéronautique et de l'Espace (ISAE)

Présentée et soutenue par :
Vincent BOUSSEMART

le lundi 22 avril 2013

Titre :

Bénéfices de la communication inter-protocoles au niveau applicatif et des ressources pour contrôler les interférences dans les communications satellites

-

On the Benefits of Cross-Layer - Assisted Interference, Resource and Application Management in Satellite-Based Communications

---

École doctorale et discipline ou spécialité :

ED MITT : Réseaux, télécom, système et architecture

Unité de recherche :

Équipe d'accueil ISAE-ONERA SCANR et DLR

Directeur(s) de Thèse :

M. José RADZIK (directeur de thèse)
M. Erich LUTZ (co-directeur de thèse)

Jury :

M. Emmanuel BOUTILLON -Rapporteur
Mme. Maryline HELARD -Examinateur
Mme. Marie-Laure BOUCHERET -Examinateur
M. Matteo BERIOLI -Examinateur
M. Michel BOUSQUET -Examinateur
M. José RADZIK -Directeur de thèse

Remarques concernant ce document :
Ce rapport correspond à la version française du mémoire de thèse de doctorat rédigé par l'auteur et intitulé, en anglais, *"On the Benefits of Cross-Layer - Assisted Interference, Resource and Application Management in Satellite-Based Communications"*. Ce document est une synthèse du rapport anglais, daté du 13 juin 2013, et est à utiliser en complément de ce dernier.

Les parties suivantes ont été entièrement traduites :
- Abstract (Résumé),
- Acknowledgment (Remerciements),
- Introduction (Introduction),
- Chapter 6 : Conclusions (Chapitre 6 : Conclusions),
- Bibliography (Bibliographie),
- Appendix A.1 : Acronyms (Annexe A.1 : Acronymes).

Les sections suivantes ont été en partie traduites :
- Appendix A.2 : Notations (Annexe A.2 : Notations),
- Appendix D : Additional Side Information (Annexe D : Informations Additionnelles).

Les chapitres 1 à 5 ont été traduits de la manière suivante :
- Introduction et résumé : traduction complète,
- Contenu : chaque chapitre est synthétisé en français et contient figures et tableaux principaux,
- Références : des références à la version anglaise sont indiquées de façon régulière.

Résumé

Cette thèse de doctorat vise à étudier les optimisations pouvant être mises en place au niveau de l'allocation des ressources dans le lien retour de systèmes satellites à faisceaux multiples qui sont limités par les interférences. Comme les systèmes satellites à faisceaux multiples peuvent être considérés comme des systèmes à entrées multiples et à sorties multiples (Multiple-Input - Multiple Output, MIMO), différentes techniques de traitement du signal peuvent être prises en compte de façon à améliorer le débit du système. Cette thèse se focalise sur les interférences générées par les utilisateurs qui sont positionnés dans différents faisceaux lorsque ceux-ci transmettent des données en même temps et avec la même fréquence. Ce type de dégradation du signal est aussi connu sous le nom d'interférences dites de co-canal (Co-Channel Interference, CCI). Le nombre de fréquences (*couleurs*) présentes dans le système satellite modifie directement la bande passante et de ce fait la capacité du système. D'un coté quand le nombre de couleurs est réduit, par exemple en considérant le cas particulier d'une seule couleur pour une ré-utilisation universelle/complète de la fréquence, le niveau des interférences entre utilisateurs augmente considérablement mais d'un autre coté la bande passante disponible dans chaque faisceau est plus importante. Pour cette raison il existe un compromis entre le nombre de couleurs et le niveau d'interférences co-canal. En utilisant ceci en tant que scénario de référence, l'influence du canal satellite est tout d'abord évalué de façon pratique en analysant le taux d'erreur non codé au niveau bit (uncoded Bit Error Rate, BER) qui est obtenu grace aux dernières techniques de suppression des interférences (Interference Cancellation, IC). En outre, en utilisant les gains obtenus avec une ré-utilisation complète de la fréquence, combinés avec la suppression successive des interférences (Successive Interference Cancellation, SIC), la thèse s'oriente vers la théorie de l'information et étudie l'impact du nombre de couleurs sur les débits totaux pouvant être atteints. Les mêmes thèmes de détection multi-utilisateurs (Multi-User Detection, MUD), inspirés des systèmes MIMO, sont ensuite pris en compte pour dériver les débits par utilisateur et en particulier le critère max-min est appliqué aux débits des utilisateurs montrant qu'une amélioration du niveau d'équité peut être envisagée. Les différents résultats de ces recherches sont utilisés pour optimiser l'allocation des ressources où les plans d'ordonnancement sont mis en forme de façon à améliorer les débits les plus bas des utilisateurs. Cependant, l'ordonnancement pour

des systèmes MIMO à grande échelle, tels que les liens retours de communications satellites, représente une tâche difficile puisque le domaine de recherche est d'une grandeur prohibitive. Pour cette raison cette thèse étudie également des algorithmes heuristiques à complexité réduite qui sont basés sur la théorie des graphes et qui visent à trouver des ordonnancements sous-optimaux offrant un meilleur équilibre en terme de débits utilisateurs. Finalement le nombre de faisceaux et le nombre d'utilisateurs pris en compte pour l'ordonnancement sont étudiés de manière à proposer de nouveaux algorithmes visant à satisfaire des contraintes de qualité de service (Quality of Service, QoS).

Table des matières

Résumé **iii**

Remerciements **vii**

Introduction **ix**

1 Scénario Satellite et Modèle de Canal **1**

1.1 Satellite 2

1.2 Modèle de Canal 6

1.3 Résumé 9

2 Analyse Pratique du Canal Satellite : Taux d'Erreurs Niveau Bit non Codé **11**

2.1 Traitement du Signal à la Réception 12

2.2 Analyse des Performances 13

2.3 Résumé 16

3 Analyse Théorique du Canal Satellite : Débit Atteignable **19**

3.1 Débit Total Atteignable 20

3.2 Débit Atteignable par Utilisateur 22

3.3 Résumé 24

4 Ordonnancement **27**

4.1 Bases 28

4.2 Invariance du Débit Total à l'Ordonnancement 29

4.3 Algorithmes de Recherche 30

4.4 Algorithmes d'Ordonnancement pour Systèmes à Grande Échelle 31

4.5 Évaluations des Performances des Différents Algorithmes 33
4.6 Impact de l'Ordonnancement sur le Taux d'Erreurs Non Codé au Niveau Bit 36
4.7 Résumé 38

5 Ordonnancement avec Contraintes de Qualité de Service 39
5.1 Impact du Nombre de Faisceaux et du Nombre d'Utilisateurs par Faisceau . . 40
5.2 Contraintes en Terme de Débit 41
5.3 Contraintes de Temps 46
5.4 Contraintes de Débit et de Temps 50
5.5 Résumé 51

6 Conclusions 53

Bibliography 59

A Acronymes and Notations 67
A.1 Acronymes 67
A.2 Notations 71
A.2.1 Scalaires, Vecteurs et Matrices 71
A.2.2 Opérateurs 71
A.2.3 Liste des Variables 71

B Bases Mathématiques Utiles 73

C Bases Utiles sur les Communications et les Satellites 75
C.1 Satellite 76
C.2 Taux d'Erreurs Niveau Bit non Codé 76
C.3 Débit Atteignable 76
C.4 Ordonnancement 76

D Informations Additionnelles 77
D.1 Liste des Publications, Brevets, et Autre(s) 77
D.1.1 Article(s) de Conférences et Journal 77
D.1.2 Workshops, École d'Été et Autre(s) 78
D.1.3 Brevet(s) 78

Remerciements

L'auteur aimerait remercier tout particulièrement ses **collègues** du **Deutsches Zentrum für Luft- und Raumfahrt (DLR, Centre Aérospatial Allemand)** :

- Prof.-Dr. Erich Lutz pour son implication et son support pendant la thèse,
- Dr. Matteo Berioli pour la supervision de cette thèse, toute l'aide, la motivation, et les idées qu'il a pu donner,
- Dr. Francesco Rosetto pour toutes les astuces, les explications, et sa disponibilité,
- Dr. Tomaso de Cola pour son incroyable expertise en mathématiques, plus particulièrement pour résoudre des intégrales (et apprécier cela),
- Hartmut Brandt pour ses connaissances dans beaucoup de domaines et son support personnel,
- Francisco Lazaro Blasco pour ses connaissances en théorie de l'information et toutes les discussions utiles que nous avons eues,
- Zoltan Katona pour son expertise dans les températures thermodynamiques des satellites,
- Federico Clazzer pour son aide sur les interférences de polarisations croisées,
- Dr. Gianluigi Liva pour son expertise en codage et en théorie de l'information,
- Dr. Andrea Munari pour son aide à fournir et à utiliser ce format LaTeX,
- et tous les autres collègues qui ont contribué à rendre tous ces jours de travail au DLR plus plaisants...

L'auteur aimerait aussi remercier les **personnes** suivantes qui travaillent à l'**Institut Supérieur de l'Aéronautique et de l'Espace (ISAE)** :

- Dr. José Radzik pour avoir accepté l'encadrement de cette thèse,
- Prof. Michel Bousquet pour tous les efforts mis en oeuvre pour que cette thèse entre l'ISAE et le DLR puisse avoir lieu,
- et toutes les autres personnes très gentilles comme Maryse Herbillon qui a simplifié toutes les procédures administratives entre la France et l'Allemagne.

L'auteur remercie l'étudiant **Loris Marini**, de l'Université de Rome "Tor Vergata", pour l'aide précieuse, son implication, son temps et les efforts qu'il a investis dans ce sujet. L'auteur a supervisé la thèse de Master de cet étudiant entre mi-Août 2011 et mi-Avril 2012 [Mar12].

Dernier remerciement, mais non des moindres : un remerciement tout particulier au Dr.-Ing. **Nicolas Courville** et à sa femme **Jessica**, qui ont grandement motivé l'auteur à démarrer cette thèse de doctorat.

Introduction

Les communications large bande par satellite permettent de couvrir de grandes étendues à la surface de la terre et de ce fait, d'englober des densités de population conséquentes. Ce type de communications offre l'accès à de nombreux services aux endroits où les infrastructures terrestres sont manquantes par exemple, puisque pas encore déployées, ou simplement parce de telles infrastructures ne peuvent pas être installées à cause de certaines contraintes géographiques. Dans le passé, l'utilisation des communications par satellite n'était pas vraiment abordable pour les consommateurs grand public, principalement à cause des frais trop élevés liés au contrat, à l'équipement, la bande passante et le rapport prix/quantité de données disponible qui était relativement conséquent par exemple. De nos jours les évolutions technologiques et les nouvelles techniques disponibles dans les standards pour communications satellites résultent en des terminaux satellites moins chers et plus petits, des débits de données plus élevés et une qualité de service (Quality of Service (QoS)) améliorée. De ce fait les communications satellites deviennent de plus en plus compétitives lorsque celles-ci sont comparées aux systèmes conventionnels terrestres. Par exemple l'Internet est désormais accessible par satellite pour ainsi dire le même prix et les mêmes conditions que le renommé et bien déployé Digital Subscriber Line (DSL) terrestre. Pour toutes ces différentes raisons les communications satellites large bande sont actuellement de plus en plus attractives et compétitives.

Les communications satellites sont en fait limitées par la puissance disponible à bord du satellite et la bande passante totale disponible [MaBo02]. Les tous premiers systèmes satellites étaient technologiquement simples et équipés d'une seule antenne, appelée communément faisceau, conçu pour couvrir tous les utilisateurs. Cependant de tels systèmes avaient un débit très bas dû au gain réduit du multiplexage utilisateur mais aussi de l'antenne. Les systèmes satellites modernes utilise la technique appelée multi-faisceaux, où la zone de couverture est divisée en cellules radio, de façon à servir de manière efficace un nombre important d'utilisateurs [LuWeJa00]. Pour cette raison les empreintes des faisceaux satellites, et aussi le concept complet du système, sont souvent comparés aux réseaux cellulaires terrestres conven-

tionnels. Les bandes à haute fréquence permettent d'atteindre des débits de données élevés dans les systèmes satellites multi-faisceaux, de l'ordre du mégabit/gigabit par seconde, mais les courtes longueurs d'onde souffrent de nombreuses détériorations, principalement liées aux effets atmosphériques et aussi aux différentes sources d'interférences. A l'horizon 2020 les satellites large bande à très haute capacité sont attendus et devraient atteindre des débits plus importants ("satellites terabit" [Gay09], [MEGAAH11]). L'évolution vers de tels systèmes constitue un gros challenge pour les concepteurs de satellites, les opérateurs et aussi en ce qui concerne le développement de nouveaux standards de communication par satellite. Le but est d'offrir toujours plus de bande passante, un rendement système plus important et aussi, et non des moindres, de garantir des niveaux de qualité de service QoS aux utilisateurs.

Cette thèse de doctorat se focalise sur les systèmes satellites géostationnaires (GEO, [Clar45]) à faisceaux multiples avec une charge transparente et une topologie de réseau en étoile, largement utilisés pour offrir des services Internet interactifs. Avec de tels satellites à faisceaux multiples, le domaine des ressources est souvent organisé de façon discrète en créneaux fréquentiels et temporels. La structure dite en créneaux des ressources en fréquence mène au fait que le système offre des canaux parallèles dans lesquels les signaux des utilisateurs doivent être distribués. La ré-utilisation des fréquences dans différents faisceaux crée cependant des interferences telles que les interférences dites de co-canal (Co-Channel Interference (CCI)).

Les systèmes satellites à faisceaux multiples actuels sont altérés par les conditions atmosphériques. Les évènements d'affaiblissement du signal sont liés aux perturbations atmosphériques telles que les nuages et la pluie, et peuvent être contrés en utilisant les techniques de réduction d'affaiblissement du signal (Fade Mitigation Techniques, FMTs). La puissance de transmission peut être adaptée (contrôle de puissance liaison ascendante, UPC), un débit de transmission différent du débit nominal peut être sélectionné (débit de transfert dynamique, DRA) et/ou la modulation et le codage (ModCod) peuvent être modifiés en conséquence (modulation et codage adaptifs, ACM). Ces techniques peuvent être implémentées dans le lien avant, càd le lien allant des gateways vers les terminaux satellites, et qui est spécifié par le standard digital video broadcasting version 2 (DVB-S2) [DVB-S2]. De telles techniques sont aussi disponibles dans le lien retour, càd le lien allant des terminaux satellites vers les gateways, comme spécifié par le standard DVB du lien retour par satellite version 2 (DVB-RCS2) [DVB-RCS2]. Le travail réalisé dans le cadre de cette thèse de doctorat considère les deux standards cités précédemment comme références.

Le but de cette thèse est d'étudier les limitations du système dues aux interférences, plus particulièrement aux interférences co-canal (Co-Channel Interference (CCI)) qui sont une

conséquence directe du facteur de ré-utilisation de la fréquence employé dans les systèmes satellites à faisceaux multiples. En réduisant le facteur de ré-utilisation de la fréquence, il est possible d'augmenter la bande passante totale du système et de ce fait la capacité théorique du système, qui est d'un intérêt capital, mais au détriment de niveaux d'interférences plus élevés. Les systèmes satellites à faisceaux multiples sont en fait des systèmes équipés avec plusieurs antennes de transmission et de réception et de ce fait peuvent effectuer un traitement du signal en collaboration et être vus comme des systèmes à entrées et sorties multiples (MIMO) virtuels. D'un coté, dans le lien avant, qui est équivalent au lien descendant des systèmes terrestres, les interférences co-canal peuvent être observées lorsque les données sont transmises à la même fréquence à des utilisateurs qui sont situés dans différents faisceaux. En utilisant le concept MIMO, la suppression de telles interférences au niveau du récepteur, plus particulièrement en utilisant une approche d'annulation itérative, n'est pas possible puisque chaque utilisateur agit comme un récepteur seul et donc le décodage en collaboration des sorties multiples du système MIMO n'est pas possible. Pour cette raison beaucoup d'efforts ont été investis de façon à annuler les interférence co-canal au niveau du transmetteur, qui n'est pas sensible aux coûts, par exemple en employant le codage dit de "dirty paper" (Dirty Paper Coding (DPC)) ou le précodage de Tomlinson-Harashima (THP) [DCMLC07], [PoBeBa09]. Cependant ce type de techniques est difficile à mettre en oeuvre en pratique à cause de leur très haut niveau de complexité pour des systèmes à large échelle, tels que les systèmes satellites à faisceaux multiples, et d'autres solutions de précodage doivent être envisagées [ZCO11-1]. D'un autre coté dans le lien retour, qui équivaut au lien ascendant des réseaux terrestres, les interférences peuvent être annulées par l'entité recevant les signaux des utilisateurs, càd la gateway, pour laquelle un décodage en commun est possible et la complexité n'est pas réellement un facteur limitant. Le travail présenté dans ce document est entièrement consacré à ce dernier point, càd au lien retour de systèmes satellite MIMO à faisceaux multiples. A noter que le trafic Internet [Bou05], qui est caractérisé par son auto-similarité (ensemble de bursts) [BoGr05], augmente considérablement. Plus particulièrement l'asymétrie en terme de données entre l'upload et le download, respectivement le lien retour et le lien avant dans un système satellite à faisceaux multiples transparent, tend à disparaître, principalement à cause de nouveaux services interactifs émergeants et consommant de la bande passante. De ce fait il est prévu que le lien retour soit de plus en plus sollicité et des solutions pour optimiser les ressources de manière efficace, càd rapidement et avec une complexité faible, doivent être étudiées.

L'allocation des ressources pour le lien retour est organisée, par exemple, sur un accès multiple

à plusieurs fréquences et divisé dans le temps (Multi-Frequency Time-Division Multiple Access (MF-TDMA)). Avec un tel schéma d'allocation, un utilisateur (terminal satellite) reçoit dans chaque laps de temps des ressources correspondant à une bande fréquence (porteuse) et un créneau temporel. Les solutions actuelles pour l'ordonnancement des utilisateurs en fréquence et en temps sont basées sur des approches heuristiques puisque la recherche de l'ordonnancement optimal est irréalisable. Dans cette thèse un concept basé sur l'optimisation de manière collaborée entre la couche physique et l'ordonnanceur est mis en oeuvre, où l'ordonnanceur alloue les créneaux temps-fréquence aux différents utilisateurs situés dans différents faisceaux de manière à réduire le niveau des interférences. Qui plus est, des techniques au niveau de la couche physique, et qui peuvent être implémentées en pratique, et de nouvelles solutions sous-optimales, capables de fonctionner avec un nombre important d'utilisateurs et de faisceaux, sont développées. Le but de ce travail est donc d'optimiser l'organisation des ressources dans le lien retour de systèmes satellites MIMO à faisceaux multiples, et limités par les interférences, de façon a réduire le niveau des interférences co-canal et d'améliorer la performance du processus de suppression des interférences au niveau du récepteur.

Ce document est organisé de la façon suivante. Le scénario satellite considéré dans cette étude et le modèle de canal correspondant sont détaillés dans le chapitre 1. Dans le chapitre 2, l'impact du canal satellite sur des récepteurs dernier cri, y compris avec détection d'utilisateurs multiples (Multi-User Detection (MUD)), et aussi un récepteur basé sur une nouvelle heuristique d'annulation des interférences (Interference Cancellation (IC)), est étudié de manière pratique en utilisant un simulateur à taux d'erreurs au niveau bit. Les outils mis à disposition par la théorie de l'information sont ensuite utilisés dans le chapitre 3, toujours en considérant le système satellite à faisceaux multiples comme étant un système MIMO virtuel. Dans ce chapitre la capacité ergodique totale, càd le débit total pouvant être atteint, est dérivé pour différents systèmes à entrées/sorties (Input-Output (IO)), et la suppression successive des interférences (Successive Interference Cancellation (SIC)) est utilisée afin d'obtenir les débits utilisateurs. Dans le chapitre 4, la notion d'ordonnancement est introduite, des algorithmes de recherche et d'ordonnancement, y compris de nouvelles approches, visant à maximiser les débits minimums des utilisateurs et à augmenter le niveau d'équité entre utilisateurs, sont décrits et leurs performances sont évaluées. En utilisant les résultats obtenus, de nouveaux algorithmes prenant en charge des contraintes de qualité de service (Quality of Service (QoS)) sont présentés dans le chapitre 5, incluant l'analyse des résultats de simulations et la complexité de calcul. Finalement les conclusions sont dressées dans le chapitre 6, résumant les principales contributions apportées par cette thèse de doctorat.

Chapitre 1

Scénario Satellite et Modèle de Canal

Ce chapitre est consacré à la description du scénario satellite et du modèle de canal.

La première section présente les bases nécessaires qui sont liées aux communications satellites large bande et détaille également les différents sous-scénarios pris en compte dans ce travail. Les sous-scénarios sont sélectionnés de sorte qu'ils soient très proches de la réalité et sont assez raisonnables pour constituer une fondation solide aux thèmes abordés. Bien entendu le travail présenté dans ce document ne se limite pas seulement à ces scénarios particuliers et peut être généralisé à beaucoup d'autres cas. Le but de cette section est principalement de décrire étape par étape le scénario complet du système considéré, les dégradations du signal et les sources d'interférences. Un exemple de bilan de liaison est également donné afin de mieux comprendre les différentes hypothèses prises en compte dans cette thèse.

La deuxième section introduit les bases fondamentales des différents systèmes à entrées/sorties (Input-Output (IO)) et explique pourquoi les systèmes satellites à faisceaux multiples peuvent être considérés comme des systèmes en entrées et sorties multiples (Multiple-Input and Multiple-Output (MIMO)). Plus particulièrement la corrélation entre le lien retour des systèmes satellites à faisceaux multiples et les systèmes MIMO à canal d'accès multiple (Multiple Access Channel (MAC)) est présenté. Cette section décrit le modèle du canal satellite, qui est basé sur un diagramme de transmission à blocs, et aussi comment la valeur absolue et la phase des coefficients du canal sont calculées. Cette section explique donc comment la matrice de canal $\boldsymbol{H}$ est générée, le tout basé sur un motif réaliste de faisceaux, et est de la plus haute importance puisque toutes les différentes études réalisées par la suite découlent directement du modèle de canal décrit dans ce chapitre.

1.1 Satellite

Les communications basées sur les satellites offrent une couverture efficace de zones à faible et haute densité de population mais sont limitées par plusieurs critères. Un satellite est avant tout limité en terme de ressources, principalement en terme de puissance et de bande passante disponibles [MaBo02]. Pour cette raison un satellite est limité en débit. Une autre contrainte est le temps aller-retour (Round-Trip-Time (RTT)) qui influence les délais bout à bout perçus pendant les transmissions. Le temps aller-retour est de l'ordre d'une demie seconde ($\sim$ 500 ms) pour les satellites géostationnaires (Geostationary (GEO)) par exemple. Enfin les communications satellites souffrent de coûts de service élevés même si aujourd'hui ceux-ci deviennent de moins en moins cher et donc plus attractifs.

Le scénario système pris en compte dans cette thèse de doctorat se base sur le concept de faisceaux multiples (Section 1.1.1 : Multi-Beam Concept) qui constitue le scénario de base. Ce dernier prend en compte les satellites géostationnaires (altitude de 35 786 km) avec une topologie réseau dite en étoile et transparente [MaBo02] dont un exemple est donné par la figure 1.1 (Section 1.1.1 : Orbit and Topology).

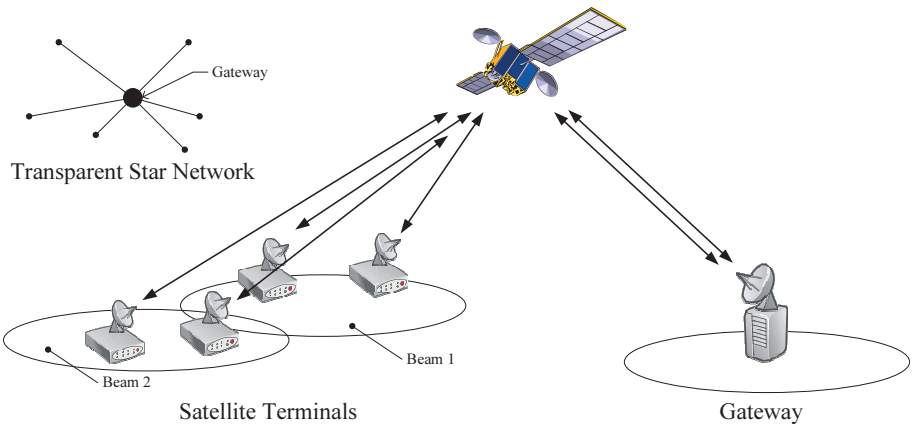


Figure 1.1. *Exemple de topologie réseau en étoile et transparente dans un système satellite.*

Les liens suivants caractérisent une telle topologie (Section 1.1.1 : Links) :

- De la gateway au terminal satellite (Satellite Terminal (ST)), le lien dit "avant" est constitué :
  - Du lien avant ascendant (Forward Up-Link (FUL)) de la gateway au satellite,
  - Du lien avant descendant (Forward Down-Link (FDL)) du satellite au terminal satellite.
- Du terminal satellite à la gateway, le lien dit "retour" est constitué :
  - Du lien retour ascendant (Return Up-Link (RUL)) du terminal satellite au satellite,

– Du lien retour descendant (Return Down-Link (RDL)) du satellite à la gateway.

Ces différents termes sont résumés par la figure 1.2 et seront utilisés à partir de maintenant dans ce document.

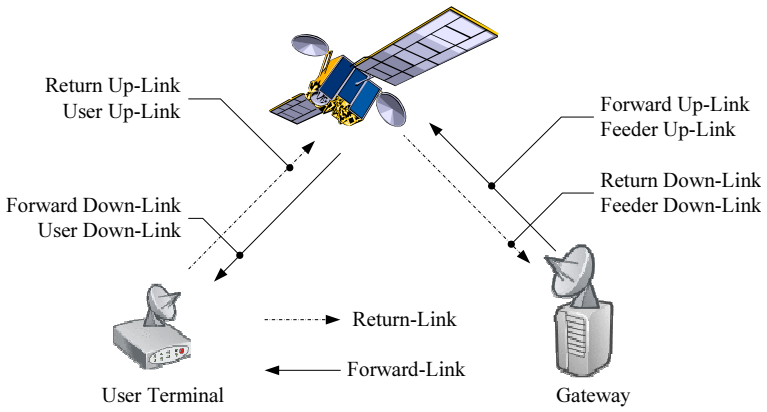


Figure 1.2. *Définition des liens satellites considérés dans ce scénario.*

Les fréquences considérées dans ces liens sont situées dans la gamme 20 - 30 GHz (bande Ka, Ka-band). Cette thèse de doctorat se focalise avant tout sur le lien retour, même si dans certaines sections le terme “lien avant” est considéré/mentionné pour une meilleure compréhension. De ce fait, à moins que cela soit indiqué explicitement, le lien retour (Return-Link (RL)) est le lien qui nous intéresse dans le reste de ce document.

La bande passante disponible dans les systèmes satellites à faisceaux multiples peut être divisée en plusieurs bandes de sorte que tous les faisceaux n'utilisent pas forcément la même fréquence. Le nombre de bandes de fréquence différentes, défini par K, correspond à la taille de cluster [LuWeJa00] (Section 1.1.1 : Cluster Size). La taille de cluster K représente aussi le nombre de couleurs utilisé dans le système satellite à faisceaux multiples et est aussi appelé dans ce document “facteur de ré-utilisation de fréquence” (frequency reuse factor).

Différentes sources vont contribuer à la dégradation du signal dans les liens (Section 1.1.2 : Main Impairments). D'un coté les mauvaises conditions météorologiques telles que la pluie vont avoir un impact important lorsque la band Ka est utilisée. De tels événements créent une fluctuation du niveau de signal (événements d'atténuation, fade events) à une large échelle de temps tandis que la scintillation, liée à l'atmosphère, crée des événements à des échelles de temps beaucoup plus réduites (fluctuations dites rapides). Enfin les pertes en espace libre (Free Space Loss (FSL)), qui correspondent à l'atténuation du signal due à la distance entre le satellite et la terre, est la composante de pertes la plus importante dans un bilan de liaison

pour un système satellite.

Des techniques de compensation à l'atténuation (Fade Mitigation Technique (FMT)) peuvent être utilisées pour remédier à la dégradation du niveau de signal. Nous pouvons citer par exemple le contrôle de la puissance de transmission pour le lien ascendant (Up-link Power Control (UPC)), l'adaptation dynamique du débit de transmission (Dynamic Rate Assignment (DRA)) ou encore l'adaptation de la modulation et du codage (Adaptive Coding and Modulation (ACM)). Ces techniques peuvent être utilisées afin de garantir une disponibilité du système.

Dans un système satellite à faisceaux multiples, les différentes sources d'interférences suivantes sont à prendre en compte [MaBo02] :

- Les interférences de canaux adjacents (Adjacent-Channel Interference (ACI)),
- Les interférences co-canal (Co-Channel Interference (CCI)),
- Les interférences de polarisations croisées (Cross-Polarisation Channel Interference (CPCI) ou Cross-Polarisation Interference (XPI)),
- Les interférences inter-modulations (Inter-Modulation Interference (IMI)),
- Les interférences inter-symboles (Inter-Symbol Interference (ISI)).

Ces différentes sources d'interférences sont décrites en détails dans la Section 1.1.3 : Sources of Interference du rapport anglais. Dans cette thèse nous nous concentrons sur la réduction du nombre de couleurs dans le système satellite à faisceaux multiples, jusqu'à une ré-utilisation complète de la fréquence, aussi appelée ré-utilisation de fréquence universelle, et de ce fait sur le niveau d'interférences co-canal en résultant, en considérant des bandes de garde suffisamment larges et une polarisation unique de sorte que les interférences de canaux adjacents et les interférences de polarisations croisées puissent être négligées. A noter que des contre-mesures existent pour les interférences inter-symboles et les interférences inter-modulations peuvent être également négligées si le nombre de porteuses par faisceau est bas et aussi si des filtres particuliers sont pris en compte.

Le nombre de couleurs présent dans le système satellite à faisceaux multiples influence directement le niveau des interférences co-canal mais permet aussi d'influencer la capacité théorique du système. Nous considérons trois sous-scénarios : quatre couleurs, trois couleurs et une seule couleur. Pour le premier scénario le niveau d'interférences co-canal sera le plus bas, pour le deuxième celui-ci sera plus élevé et enfin pour le dernier le niveau d'interférences pourra

être considéré comme étant critique mais en principe le gain théorique en terme de capacité sera non négligeable. La couverture des faisceaux au sol dépend de la position orbitale du satellite. Nous considérons ici un satellite dont la longitude est 19.2° Est. Ce satellite couvre l'Europe à l'aide de 96 faisceaux, ce qui est un nombre réaliste pour les systèmes satellites modernes. Les utilisateurs (terminaux satellites) sont distribués dans la zone de couverture de chaque faisceau. Enfin deux tailles de systèmes sont considérées : un système constitué de sept faisceaux ($B = 7$) et un système constitué de l'ensemble complet des faisceaux, càd quatre-vingt-seize faisceaux ($B = 96$). Ces sous-scénarios sont décrits plus en détails dans la Section 1.1.4 : Sub-Scenarios du rapport anglais.

Le niveau des interférences co-canal est lié aux caractéristiques de l'antenne située à bord du satellite. Le diagramme de rayonnement de l'antenna influence directement la quantité d'interférences créée par les faisceaux transmettant vers les terminaux satellites (lien avant descendant) et reçue par les faisceaux à partir des terminaux satellites (lien retour ascendant). Le diagramme de rayonnement des faisceaux est calculé à l'aide d'équations dérivées de [Col85] and [DCMLC07] puisque les faisceaux du satellite peuvent être considérés comme des antennes paraboliques (réflecteurs). Les formules suivantes permettent de calculer le gain pour différents angles d'ouverture du satellite (pour plus de détails, veuillez consulter la section C.1.2 du rapport anglais) :

$$G(u) = G_{\max}\,\alpha\,\left(2\,\frac{J_1(u)}{u} + \frac{T}{1-T}\,2^{p+1}\,p!\,\frac{J_{p+1}(u)}{u^{p+1}}\right)^2 \tag{1.1}$$

où J_i est la fonction de Bessel de premier type et d'ordre i, et :

$$G_{\max,\mathrm{dB}} = 53.23 \text{ dB}, \quad \alpha = \frac{(1-T)\,(p+1)}{(1-T)\,(p+1)+T} \quad \text{and} \quad u = \left(\frac{\pi\,d_{\mathrm{a}}}{\lambda}\right)\sin\theta$$

d_{a} est le diamètre de l'antenne (réflecteur), λ la longueur d'onde et θ représente l'angle d'ouverture qui nous intéresse ici. Dans cette étude nous avons considéré les valeurs types suivantes : une efficacité d'antenne $\eta = 0.6$, une fréquence $f = 30$ GHz (lien retour ascendant), un cône d'ouverture de bord $T = 20$ dB, et la vitesse à laquelle le champ d'ouverture décroît est régie par le coefficient p ($p = 2$). Un exemple est donné par la figure 1.3 dans laquelle le diagramme de rayonnement d'un seul faisceau est montré.

Un exemple de bilan de liaison pour le lien retour est donné dans la section 1.1.6 du rapport anglais, montrant principalement que le bilan de liaison total du lien retour est avant tout influencé par le lien retour ascendant.

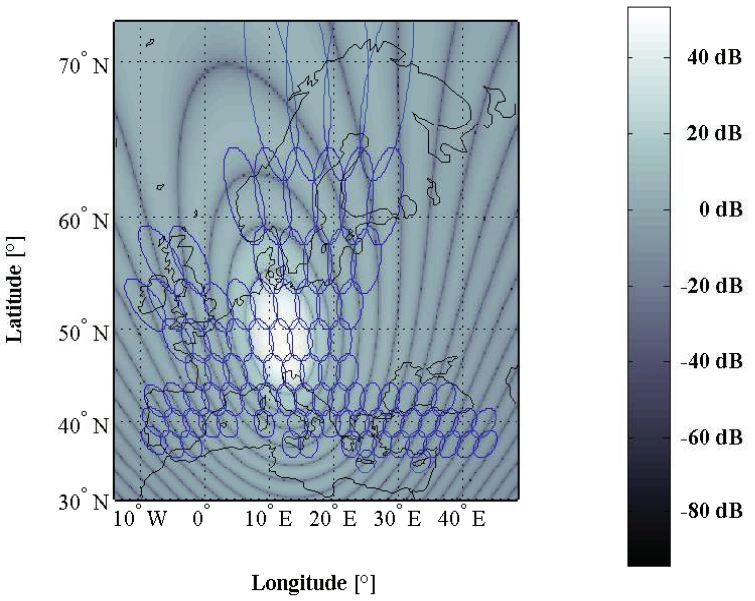


Figure 1.3. *Système satellite et exemple de diagramme de rayonnement pour un faisceau. L'empreinte des 96 faisceaux considérés dans le scénario satellite à faisceaux multiples est montrée. Le diagramme de rayonnement est présenté pour un seul faisceau et est illustré par le gain en décibels (dB). Dans cet exemple le faisceau pris en compte a son centre situé aux coordonnées suivantes : latitude 48.75° Nord et longitude 11.9° Est (faisceau numéro 33).*

1.2 Modèle de Canal

Cette section décrit le modèle de canal, plus particulièrement la génération de la matrice de canal. Dans cette section nous montrerons que les systèmes satellites à faisceaux multiples peuvent être considérés comme des systèmes à entrées et sorties multiples (Multiple-Input and Multiple-Output (MIMO)).

Dans des systèmes de transmission à entrées et sorties simples, le signal d'entrée $\boldsymbol{x}$ entre dans le système et il en résulte un signal de sortie $\boldsymbol{y}$. Le système peut être représenté par une matrice de canal $\boldsymbol{H}$ and un bruit $\boldsymbol{\eta}$ peut également être ajouté pendant la transmission (figure 1.4). L'expression suivante est communément utilisée pour modéliser un tel système :

$$\boldsymbol{y} = \boldsymbol{H}\boldsymbol{x} + \boldsymbol{\eta} \tag{1.2}$$

L'entrée $\boldsymbol{x}$ est un vecteur colonne de taille N_{Tx}, càd $\boldsymbol{x} = [x_1, x_2, \cdots, x_{N_{\mathrm{Tx}}}]^T$, $\boldsymbol{H}$ est la matrice de canal, $\boldsymbol{\eta}$ et $\boldsymbol{y}$ sont des vecteurs colonnes de taille N_{Rx}, càd $\boldsymbol{\eta} = [\eta_1, \eta_2, \cdots, \eta_{N_{\mathrm{Rx}}}]^T$ et $\boldsymbol{y} = [y_1, y_2, \cdots, y_{N_{\mathrm{Rx}}}]^T$ (veuillez consulter la Section 1.2.1 : Introduction to Simple Input-

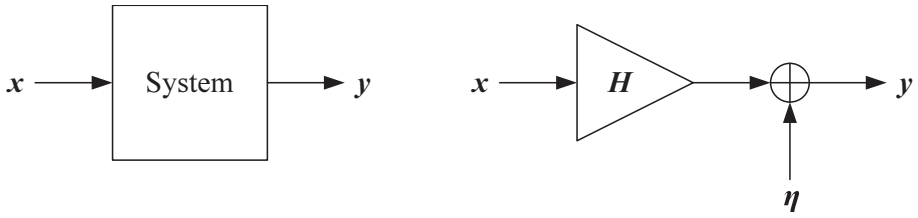


Figure 1.4. *Diagramme de transmission à blocs basique.*

Output Systems pour plus de détails).

La matrice de canal $\boldsymbol{H}$ définie précédemment peut être utilisée pour caractériser un canal radio par exemple. Ce canal radio peut être composé de plusieurs entrées (les transmetteurs) et de plusieurs sorties (les récepteurs). Le nombre d'entrées/sorties dépend du nombre d'entités, càd du nombre de transmetteurs et de récepteurs physiques, et/ou du nombre d'antennes à la transmission et à la réception. Le nombre d'entrées et sorties pris en compte détermine le type de système :

– Une seule entrée et une seule sortie (Single-Input and Single-Output (SISO)),
– Une seule entrée et plusieurs sorties (Single-Input and Multiple-Output (SIMO)),
– Plusieurs entrées et une seule sortie (Multiple-Input and Single-Output (MISO)),
– Plusieurs entrées et plusieurs sorties (Multiple-Input and Multiple-Output (MIMO)).

Dans un système satellite l'information transmise dans le lien avant descendant est un canal de transmission dit broadcast et de ce fait peut être vu comme un système MIMO Broadcast Channel (BC). Le lien retour ascendant est un canal à accès multiple et peut être à son tour vu comme un système MIMO Multiple Access Channel (MAC). Pour plus de détails, veuillez consulter la Section 1.2.2 : Multiple-Input and Multiple-Output Concept du rapport anglais.

Le diagramme de transmission à blocs pris en compte (figure 1.5) et les différentes considérations permettent d'écrire la relation suivante :

$$\boldsymbol{y} = \boldsymbol{F}\boldsymbol{a} + \boldsymbol{\eta} = \boldsymbol{F}(\boldsymbol{B}\boldsymbol{x}) + \boldsymbol{\eta} \tag{1.3}$$

Comme la distance entre le satellite et la gateway est constante, nous assumons que le signal reçu à la gateway est proportionnel à celui reçu par le satellite (en fait le lien retour descendant dans un système satellite transparent est conçu de sorte que le lien ascendant n'est que très peu modifié). Nous assumons également que le produit $\boldsymbol{F}\boldsymbol{B}$ est équivalent à la matrice de canal $\boldsymbol{H}$ de sorte que nous pouvons écrire :

$$\boldsymbol{y} = \boldsymbol{H}\boldsymbol{x} + \boldsymbol{\eta} \tag{1.4}$$

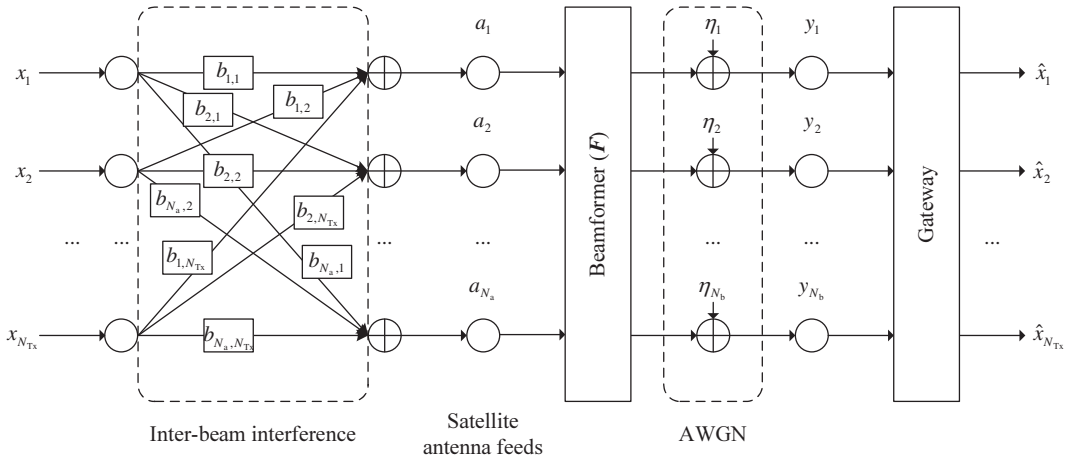


Figure 1.5. *Diagramme de transmission à blocs pour faisceaux multiples. Celui-ci est constitué (de gauche à droite) du bloc d'interférences inter-faisceaux, des feeds de l'antenne satellite, des faisceaux satellite, du bloc de bruit et de la gateway. Le nombre de feeds au niveau de l'antenne satellite est généralement égal ou plus grand que le nombre de faisceaux.*

où $\boldsymbol{y}$ est donc un vecteur constitué de N_b éléments. La gateway réalise différentes opérations de façon à estimer les symboles initialement transmis. Ces estimations sont notées $\hat{\boldsymbol{x}}$.

La valeur absolue des coefficients du canal, notés $|h_{i,j}|$, détermine la modification de l'amplitude du signal transmis entre le récepteur i et le transmetteur j. Ce coefficient est calculé de la façon suivante (Section 1.2.4 : Absolute Value of the Channel Coefficients) :

$$|h_{i,j}| = \sqrt{\frac{G_{i,j}}{L_{\mathrm{FS},j}} \cdot \frac{L_{\mathrm{FS,min}}}{G_{\max}}} \tag{1.5}$$

La matrice de canal $\boldsymbol{H}$ est en général constituée de nombres complexes. Le coefficient de canal $h_{i,j}$ peut aussi être noté sous la forme $|h_{i,j}|\,\mathrm{e}^{j\theta_{i,j}}$. Afin de calculer la phase $\theta_{i,j}$ nous prenons en compte deux effets. Le premier est lié aux transmetteurs : un décalage de phase sera introduit dans le signal transmit entre le terminal satellite et le satellite. Ceci peut être modélisé par un décalage de phase appliqué sur une colonne j de la matrice de canal $\boldsymbol{H}$ et qui sera le même quelque soit l'indice de la ligne i (tous les récepteurs sont situés au niveau du satellite). Le deuxième effet est lié aux récepteurs. Désormais la distance entre les feeds est prise en compte et un décalage de phase existe entre deux récepteurs. Pour modéliser une telle phase le même décalage de phase est appliqué entre les récepteurs, càd entre chaque ligne de la matrice de canal $\boldsymbol{H}$, quelque soit la colonne.

1.3 Résumé

Dans cette thèse de doctorat nous considérons des satellites géostationnaires (Geostationary (GEO)) avec une topologie de réseau en étoile et transparente. Nous nous focalisons tout particulièrement sur le lien retour (Return-Link (RL)) qui fonctionne à une fréquence située dans la bande Ka et nous assumons des conditions de ciel dégagé (clear-sky) avec une ligne de mire parfaite (perfect Line-of-Sight (LoS)). Pour les simulations nous prenons en compte un satellite géostationnaire dont la position orbitale est de longitude 19.2° Est. Ce satellite couvre l'Europe à l'aide de 96 faisceaux, ce qui est un nombre réaliste pour des systèmes satellites modernes. Notre attention est tout particulièrement portée sur la réduction du nombre de couleurs qui permet d'augmenter la bande passante dans chaque faisceau et en conséquence la capacité théorique.

Trois nombre de couleurs sont pris en charge dans ce travail. La ré-utilisation universelle de fréquence ($K = 1$) qui est hautement limitée par les interférences, trois couleurs ($K = 3$), ce qui augmente la distance entre les faisceaux utilisant la même fréquence, et quatre couleurs ($K = 4$) où le niveau d'interférences co-canal est le plus bas de ces trois scénarios (distance la plus élevée entre les faisceaux utilisant les mêmes fréquences). Deux tailles de systèmes sont considérées de façon à réaliser les différentes études. Un système à taille réduite qui est constitué d'un nombre limité de sept faisceaux ($B = 7$) et à taille complète qui correspond au système satellite à faisceaux multiples dit "complet", càd constitué des quatre-vingt-seize faisceaux ($B = 96$). Les utilisateurs, qui sont aussi appelés terminaux satellites, sont générés aléatoirement de sorte qu'ils sont situés dans la zone de couverture des faisceaux ou bien placés manuellement.

Les systèmes satellites à faisceaux multiples peut être considéré comme des systèmes MIMO virtuels. Plus particulièrement le lien retour (Return-Link (RL)) peut être vu comme un système MIMO avec un canal à multiples accès (Multiple Access Channel (MAC)) et nous considérons que dans ce lien tous les transmetteurs, càd tous les terminaux satellites, ont des caractéristiques identiques (en terme de puissance de transmission, propriétés d'antenne, etc.). Afin de modéliser le canal satellite, les seuls termes changeant les valeurs absolues des coefficients sont le gain de réception de l'antenne satellite et les pertes en espace libre entre le terminal et le satellite, tous deux dépendants de la position de l'utilisateur au sol. La phase des coefficients du canal est modélisée en prenant en compte deux effets : la phase à la transmission, càd un décalage de phase modifiant le signal transmis par le terminal satellite

vers le satellite, et la phase à la réception, càd un décalage de phase introduit par le formateur de faisceau (beamformer).

Chapitre 2

Analyse Pratique du Canal Satellite : Taux d'Erreurs Niveau Bit non Codé

Dans ce Chapitre le but est d'évaluer le taux d'erreurs non codé au niveau bit (uncoded Bit Error Rate (BER)) qui résulte d'un système pouvant être représenté par la figure 2.1.

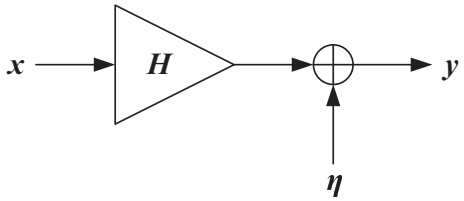


Figure 2.1. *Système à entrées et sorties typique pour simulations de taux d'erreurs au niveau bit.*

La mesure du taux d'erreurs non codé au niveau bit est très répandue lorsque la détection multi-utilisateurs (Multi-User Detection (MUD)) est réalisée et lorsque la suppression des interférences (Interference Cancellation (IC)) est considérée. Cela permet d'être entièrement indépendant de n'importe quel type de codage et décodage tel que Bose, Chaudhuri, and Hocquenghem (BCH), Low Density Parity Check Code (LDPC), etc.

Ce chapitre présente les différents récepteurs pris en compte dans cette étude, y compris des récepteurs visant à supprimer les interférences. Le simulateur de BER et les récepteurs sont validés en utilisant le canal de Rayleigh et enfin l'impact du canal satellite et les différents gains obtenus lors de la réduction du nombre de couleurs sont analysés. Un nouveau type de récepteur est également introduit.

2.1 Traitement du Signal à la Réception

Le récepteur dit "simple" est un récepteur conventionnel qui évalue directement le signal transmis $\boldsymbol{x}$ à partir du signal reçu $\boldsymbol{y}$, sans aucune opération particulière, hormis une détection de phase au niveau du signal transmis par les utilisateurs (Section 2.1.1 : Conventional Receiver).

L'égaliseur dit "Zero Forcing" est un filtre appliqué sur le signal $\boldsymbol{y}$ et visant à forcer à zéro la composante liée aux interférences (Section 2.1.2 : Zero Forcing Equalizer). Cet égaliseur est obtenu de la manière suivante :

$$\boldsymbol{H}^{+} = \left(\boldsymbol{H}^{\mathrm{H}}\,\boldsymbol{H}\right)^{-1}\boldsymbol{H}^{\mathrm{H}} = \boldsymbol{W} = \boldsymbol{G}_{\mathrm{ZF}} \tag{2.1}$$

La pseudo-inverse dite de Moore-Penrose de la matrice de canal, $\boldsymbol{H}^{+}$, est généralement notée $\boldsymbol{W}$. Un récepteur équipé d'un tel filtre nécessite la connaissance du canal de transmission qui est représenté par la matrice $\boldsymbol{H}$. L'inconvénient de ce filtre est d'amplifier la composante liée au bruit (voir la section 2.1.2 du rapport anglais pour plus de détails).

Le filtre dit "MMSE" (Minimum Mean Square Error (MMSE)) est obtenu en minimisant, comme son nom l'indique, l'erreur entre l'entrée et la sortie en utilisant la méthode des moindres carrés. L'expression du filtre est la suivante :

$$\boldsymbol{G}_{\mathrm{MMSE}} = \boldsymbol{H}^{\mathrm{H}}\left[\boldsymbol{H}\,\boldsymbol{H}^{\mathrm{H}} + N_0\,\boldsymbol{I}\right]^{-1} = \left[\boldsymbol{H}^{\mathrm{H}}\boldsymbol{H} + N_0\,\boldsymbol{I}\right]^{-1}\boldsymbol{H}^{\mathrm{H}} \tag{2.2}$$

où N_0 correspond à la densité spectrale de l'énergie liée au bruit.

La suppression optimale des interférences en utilisant une méthode successive (Successive Interference Cancellation (SIC)) est obtenue en étant insérée juste après les filtres définis précédemment. Le principe est d'estimer consécutivement les symboles transmis de façon à réduire les interférences pour lesquelles ils sont impliqués dans le vecteur du signal reçu $\boldsymbol{y}$ [TsVi08]. Cela revient à effectuer une détection multi-utilisateurs (Multi-User Detection (MUD)) dans le lien retour d'un système satellite à faisceaux multiples qui peut être considéré comme un système MIMO à accès multiples (MU-MIMO MAC). Comme représenté dans la figure 2.2 les transmetteurs sont détectés un par un et les interférences sont supprimées à chaque fois. La complexité d'un tel récepteur croit rapidement avec le nombre de transmetteur et un récepteur sous-optimal, avec une architecture différente, peut de ce fait être conçu de manière à réduire la complexité de l'opération de suppression des interférences (IC). Veuillez

consulter la Section 2.1.4 : Optimal Successive Interference Cancellation pour plus de détails.

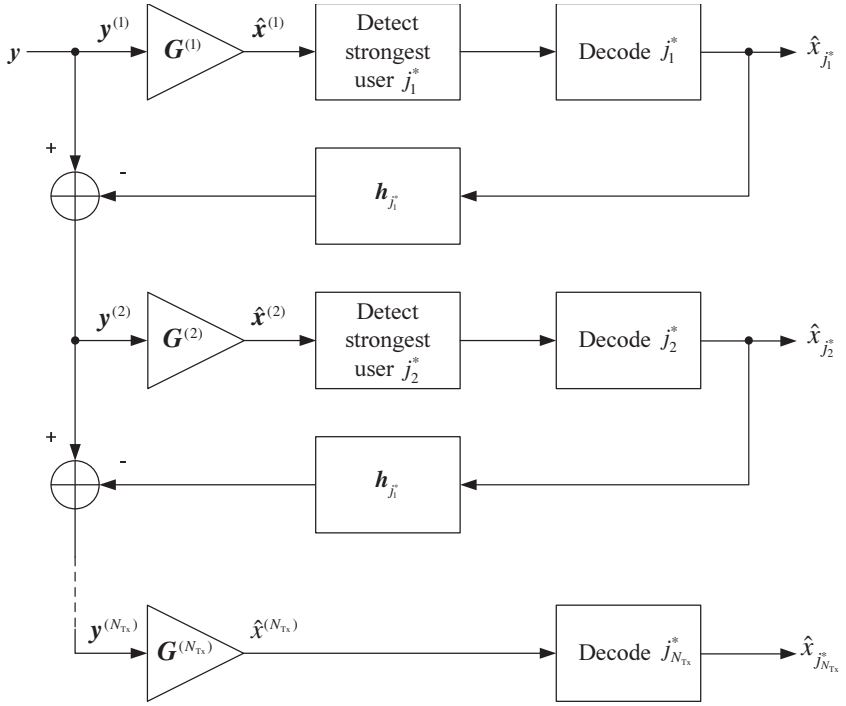


Figure 2.2. *Architecture de récepteur avec une suppression successive et optimale des interférences.*

Le récepteur précédent réalise pour chaque flux les opérations de filtrage et de classement. Il est possible de limiter la complexité du récepteur en prenant en compte la structure diagonale de la matrice du canal satellite, principalement due à la composante dominante liée à la ligne de mire (Line-of-Sight (LoS)). Pour cela nous nous basons sur un algorithme de suppression d'interférences connu sous le nom de Maximal Ratio Combining (MRC). Le but est de prendre avantage de la présence du signal au sein des multiples récepteurs de façon à maximiser le rapport signal sur bruit (Signal-to-Noise Ratio (SNR)). L'architecture de ce nouveau récepteur est représenté par la figure 2.3. Veuillez consulter la Section 2.1.5 : Successive Interference Cancellation with Maximal Ratio Combining pour de plus amples informations.

2.2 Analyse des Performances

Cette section présente la performance des différents récepteurs en terme de taux d'erreurs au niveau bit qui est tout d'abord évaluée et vérifiée avec le canal de Rayleigh et ensuite avec le canal satellite.

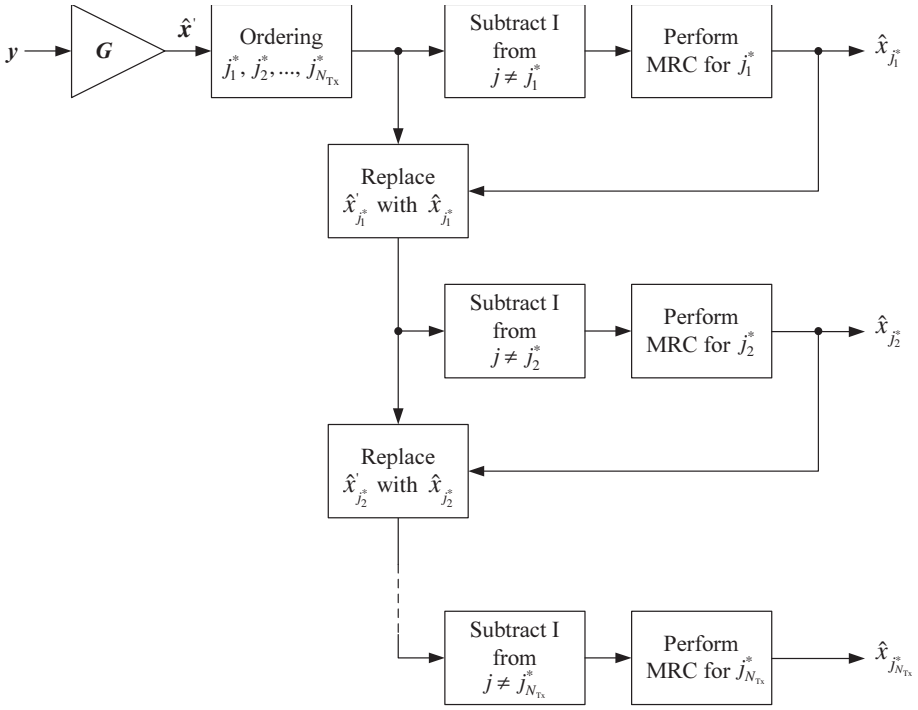


Figure 2.3. *Architecture de récepteur avec une suppression successive des interférences basée sur le Maximal Ratio Combining (MRC).*

Le canal de Rayleigh considéré ici est variant dans le temps ce qui signifie que pour chaque séquence de symbols transmise, il y a une réalisation particulière du canal. Le système est composé de sept transmetteurs et sept récepteurs et est donc équivalent à un système MIMO 7×7. Le taux d'erreurs au niveau bit et non codé est simulé en utilisant la modulation Binary Phase-Shift Keying (BPSK) et les résultats sont moyennés en prenant en compte tous les transmetteurs. L'analyse des performances (figure 2.4) indique un taux d'erreur de 50% pour un récepteur conventionnel. Ceci est directement lié à la nature multi-trajets de l'environnement et était attendu. Un récepteur intégrant une égalisation dite "Zero Forcing" permet déjà d'améliorer les performances. Cependant lorsque l'on compare avec le récepteur équipé d'un filtre MMSE, il est clair que l'inconvénient du ZF est l'amplification du bruit. MRC offre de bonnes performances dans la région limitée par le bruit puisqu'il agit comme un filtre adapté. En quittant la région limitée par le bruit, la suppression successive des interférences montre clairement un avantage. Le récepteur intégrant l'architecture optimale montre les meilleurs résultats. Les performances obtenues avec le canal de Rayleigh correspondent à ce qu'avance la théorie de l'information et valide de ce fait l'environnement de simulation. Plus de détails quant à l'analyse des résultats sont disponibles dans la Section 2.2.1 : Rayleigh Channel - Validation of the Receivers du rapport anglais.

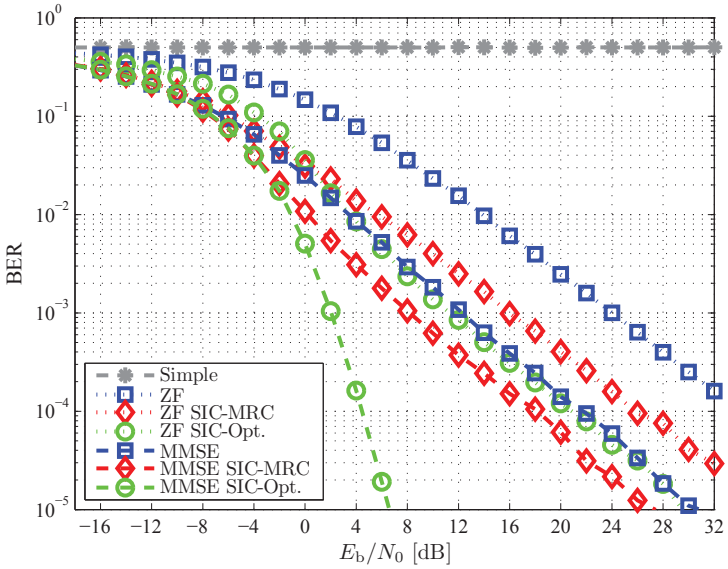


Figure 2.4. *Performance moyenne des récepteurs en terme de taux d'erreur niveau bit avec un canal de Rayleigh* 7×7 *et une modulation BPSK.*

Les effets des interférences et les performances sont étudiés étape par étape et en détails dans la Section 2.2.2 : Satellite Channel - 2×2 System du rapport rédigé en anglais. La méthode de suppression successive des interférences permet d'éliminer entièrement les interférences et d'obtenir des résultats optimaux que ce soit avec l'architecture optimale ou bien avec l'architecture nouvelle et moins complexe.

Pour un canal satellite constitué de sept faisceaux ($B = 7$) et avec un terminal satellite dans chaque faisceau, nous obtenons un système 7×7. Lorsque le niveau d'interférences est relativement "bas" dans un système employant une ré-utilisation complète de la fréquence, les performances des deux types de filtres (ZF et MMSE) sont quasi identiques et la suppression des interférences par MRC permet d'obtenir des résultats très proches de ceux obtenus avec l'architecture optimale. Avec un placement différent des utilisateurs et un niveau d'interférences correspondant relativement élevé, les résultats sont tout autre. Cette fois l'utilisation du filtre MMSE montre de meilleurs performances. Dans un scénario avec un niveau d'interférences moyen l'architecture optimale appuyée par le filtre MMSE permet d'éliminer toutes les interférences et ceci avec une modulation BPSK mais aussi une modulation Quadrature Phase-Shift Keying (QPSK). Un canal satellite de même taille mais basé sur trois couleurs montre clairement que le niveau d'interférences est très bas comparé à celui obtenu avec une seule couleur.

Lorsque l'on compare les performances obtenues entre des récepteurs conventionnels dans un système à trois couleurs avec celles obtenues avec des récepteurs éliminant de façon optimale les interférences dans un système à une seule couleur (figure 2.5), les constatations suivantes peuvent être faites. Sur la plage entière du rapport signal sur bruit, allant de $-8\ dB$ à $24\ dB$, $K = 1$ avec une modulation QPSK surpasse $K = 3$ avec une modulation 16-PSK. En utilisant le nombre de bits disponible par symboles ainsi que la bande passante, trois fois plus importante avec une seule couleur, le gain est de 1.5. Des gains plus importants peuvent être obtenus en considérant des ordres de modulations plus élevés. Par exemple en visant un taux d'erreurs niveau bit de 10^{-5}, $K = 1$ avec une modulation QPSK requiert à peu près le même rapport signal sur bruit que $K = 3$ avec 8-PSK. Dans ce cas $K = 1$ offre un facteur de gain égal à 2. Un autre exemple concerne un taux d'erreurs à 10^{-2} : $K = 1$ avec une modulation 8-PSK requiert à peu près le même SNR que $K = 3$ avec une modulation 16-PSK. Le facteur de gain est ici de 2.25 sachant qu'à des rapports signal sur bruit plus élevés, $K = 1$ offre même de meilleurs résultats. Le résumé de ces différents gains est donné par le tableau 2.1.

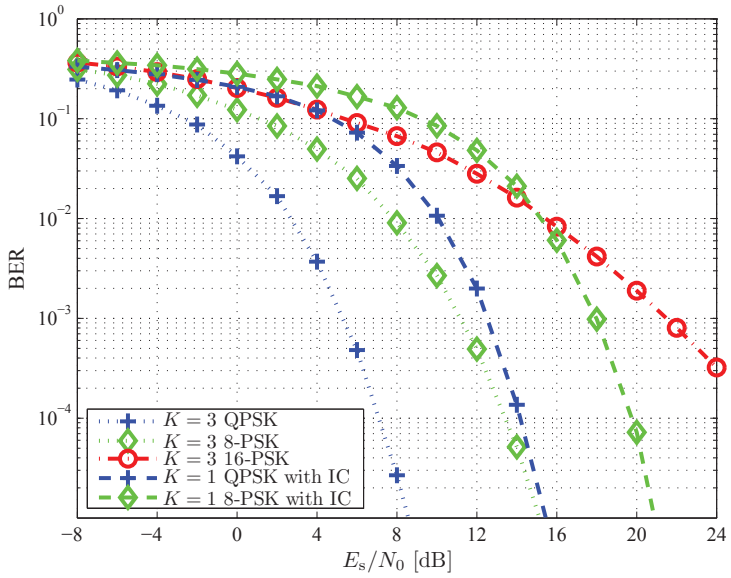


Figure 2.5. *Performance des récepteurs en terme de taux d'erreurs niveau bit dans un système satellite 7×7, avec une et trois couleurs ($K = 1$ and $K = 3$), un scénario à niveau d'interférences moyen, différentes modulations, et pour l'utilisateur situé dans le faisceau central.*

2.3 Résumé

En considérant des récepteurs actuels, tel qu'un récepteur simple conventionnel qui intègre uniquement la détection de phase, un filtrage linéaire (Zero Forcing (ZF) et Minimum Mean

Table 2.1. *Résumé des performances de taux d'erreurs niveau bit et non codé entre une ré-utilisation universelle de la fréquence et trois couleurs.*

Comparaison ID	Modulation $K = 1$ avec IC	Modulation $K = 3$ sans IC	Bit Taux d'erreur	SNR [dB]	Gain [facteur]
1	QPSK	16-PSK	-	plage entière	1.5
2	QPSK	8-PSK	10^{-5}	≥ 15	2.0
3	8-PSK	16-PSK	10^{-2}	≥ 15	2.25

Square Error (MMSE)), une suppression successive non linéaire des interférences (Successive Interference Cancellation (SIC)) avec Maximal Ratio Combining (MRC) et une architecture SIC optimale, nous avons montré que le canal correspondant au lien retour d'un système satellite à faisceaux multiples diffère complètement du canal de Rayleigh. Cela est principalement lié à la structure diagonale particulière de la matrice de canal satellite et de ce fait, le comportement des récepteurs à suppression successive des interférences dits "classiques" est entièrement modifié.

D'un coté nous avons montré que la suppression des interférences (Interference Cancellation (IC)) est nécessaire avec $K = 1$ puisque le système est limité par les interférences. D'un autre coté le niveau des interférences avec $K = 3$ est plutôt bas et cela explique pourquoi la suppression d'interférences n'est pas réalisée dans de tels systèmes. Le récepteur à suppression successive des interférences optimal a montré les meilleurs résultats, aussi avec le canal satellite. Cela correspond parfaitement à ce qui est avancé par la théorie de l'information puisque le filtre MMSE avec le système SIC permet d'atteindre la capacité du canal. De plus, basé sur ces simulations, un tel récepteur est quasiment capable de retirer entièrement les effets des interférences. Un système employant une ré-utilisation complète de la fréquence permet d'atteindre des facteurs de gain allant de 1.5 à 2.25 en terme de débit non codé, comparé à un système employant trois couleurs et ceci en fonction des différentes modulations considérées.

Le but est désormais d'utiliser la théorie de l'information afin de mieux comprendre les gains obtenus par les entrées et sorties multiples (MIMO) dans un tel système et d'étudier l'impact de la suppression successives des interférences sur les utilisateurs. L'analyse du taux d'erreurs au niveau bit ne peut pas être utilisée afin d'améliorer l'allocation des ressources dans le lien retour, en particulier l'ordonnancement des utilisateurs, en considérant différents

sets de terminaux satellites dans les zones de couverture des faisceaux. Il est donc important de se diriger vers la théorie de l'information afin de pouvoir aussi concevoir des algorithmes efficaces visant à optimiser l'organisation des ressources.

Chapitre 3

Analyse Théorique du Canal Satellite : Débit Atteignable

D'un coté la capacité théorique des canaux terrestres à multiples entrées et multiples sorties (Multiple-Input and Multiple-Output (MIMO)) a déjà été largement étudiée (voir par ex. [GJJV03]). D'un autre coté il existe quelques travaux récents dans lesquels la capacité théorique du canal satellite vers un terminal mobile a été analysée [AlMaTu10]. La capacité en cas de coupure de liaison en considérant un système satellite en tant que système MIMO a été étudiée dans [LiPaAr09] et [LPCR09]. Dans tous les cas, des connaissances fondamentales sont toujours manquantes donc dans ce chapitre, nous abordons le débit pouvant être atteint dans le lien retour d'un système satellite à faisceaux multiples en utilisant les outils qui sont mis à disposition par la théorie de l'information, en assumant des conditions de ciel dégagé (clear sky) et un motif réaliste d'antenne satellite à faisceaux multiples.

Ce chapitre donne tout d'abord les différentes expressions qui sont utilisées pour calculer les débits pouvant être atteints dans des systèmes à entrée et sortie unique (Single-Input and Single-Output (SISO)), à entrée unique et sorties multiples (Single-Input and Multiple-Output (SIMO)) et à entrées multiples et sorties multiples (Multiple-Input and Multiple-Output (MIMO)), en incluant l'impact du nombre de couleurs sur ces débits. Les gains atteignables par les systèmes à entrées et sorties (Input-Output (IO)) sont ensuite analysés, montrant le bénéfice de la ré-utilisation complète de la fréquence. Enfin, en se basant sur la détection d'utilisateurs multiples (Multi-User Detection (MUD)), les débits atteignables au niveau utilisateur sont dérivés et étudiés, par le concept du classement de la suppression successive optimal des interférences (optimal Successive Interference Cancellation (SIC)), afin de cibler un critère particulier qui est ici la maximisation du débit minimum utilisateur.

3.1 Débit Total Atteignable

Le débit total représente le débit complet présent dans le système pour une matrice de canal particulière et pour un rapport signal sur bruit spécifique.

Dans un système dit à une seule entrée et une seule sortie (Single-Input and Single-Output (SISO)), tous les signaux reçus sont traités séparément. Pour cette raison les coefficients diagonaux de la matrice de canal $\boldsymbol{H}$ correspondent au signal "utile" tandis que les coefficients en dehors de la diagonale sont considérés comme étant "non désirables" et sont donc perçus comme du bruit. Le débit total maximum pouvant être atteint dans un système SISO est calculé de la façon suivante (Section 3.1.1 : Single-Input - Single-Output) :

$$R_{\mathrm{SISO}} = \sum_{i=1}^{N_{\mathrm{Rx}}} \log_2 \left(1 + \frac{|h_{i,i}|^2}{\sum_{j \neq i} |h_{i,j}|^2 + (E_{\mathrm{s}}/N_0)^{-1}} \right) \tag{3.1}$$

Dans un système à une seule entrée et de multiples sorties (Single-Input and Multiple-Output (SIMO)), les signaux transmis sont traités indépendamment mais comme le système est constitué de plusieurs antennes de réception, le signal du transmetteur j peut être reçu par les autres récepteurs (càd $i \neq j$). Le système a donc la possibilité de combiner le signal provenant de plusieurs antennes afin d'augmenter le rapport signal sur bruit. Un tel récepteur n'est rien d'autre qu'un récepteur effectuant un combinaison maximale des ratios (Maximal Ratio Combining (MRC)). Dans ce cas le débit total maximum dans un système SIMO est formulé ainsi (Section 3.1.2 : Single-Input - Multiple-Output) :

$$R_{\mathrm{SIMO}} = \sum_{j=1}^{N_{\mathrm{Tx}}} \log_2 \left(1 + \sum_{l=1}^{N_{\mathrm{Rx}}} \left(\frac{|h_{l,j}|^2}{\sum_{k \neq j} |h_{l,k}|^2 + (E_{\mathrm{s}}/N_0)^{-1}} \right) \right) \tag{3.2}$$

Enfin dans un système composé de multiples entrées et de multiples sorties (Multiple-Input and Multiple-Output (MIMO)), chaque signal transmis est reçu par plusieurs antennes mais est également traité avec les autres signaux. Le débit total maximum est obtenu en utilisant l'information mutuelle et correspond à la formule donnée par Telatar [Tel99] (Section 3.1.3 : Multiple-Input - Multiple-Output) :

$$R_{\mathrm{MIMO}} = \log_2 \det \left(\boldsymbol{I} + \boldsymbol{C}_{\boldsymbol{\eta}}^{-1} \boldsymbol{H} \boldsymbol{H}^{\mathrm{H}} \right) \tag{3.3}$$

La phase présente dans la matrice de canal n'a aucun impact sur les expressions SISO et SIMO puisque ces dernières n'impliquent que la valeur absolue des coefficients. Dans le lien retour d'un système MIMO satellite, la phase liée aux transmetteurs et la phase liée aux récepteurs (cf. Section 1.2) n'a aussi aucun impact (voir Section 3.1.4 : Impact of the Phase).

La taille du cluster K, ou nombre de couleurs, influence directement la bande passante disponible dans le système et de ce fait le bilan de liaison. Dans un système à une seule couleur la bande passante disponible par faisceau est trois fois celle disponible dans un système à trois couleurs. Aussi, en prenant en compte une puissance par utilisateur identique lorsque K est modifié, nous obtenons les relations suivantes :

$$R_{K,\mathrm{SISO}} = \frac{1}{K} \sum_{i=1}^{N_{\mathrm{Rx}}} \log_2 \left(1 + \frac{|h_{i,i}|^2}{\sum_{j \neq i} |h_{i,j}|^2 + (K\, E_\mathrm{s}/N_0)^{-1}} \right) \tag{3.4}$$

$$R_{K,\mathrm{SIMO}} = \frac{1}{K} \sum_{j=1}^{N_{\mathrm{Tx}}} \log_2 \left(1 + \sum_{l=1}^{N_{\mathrm{Rx}}} \left(\frac{|h_{l,j}|^2}{\sum_{k \neq j} |h_{l,k}|^2 + (K\, E_\mathrm{s}/N_0)^{-1}} \right) \right) \tag{3.5}$$

$$R_{K,\mathrm{MIMO}} = \frac{1}{K} \log_2 \det \left(\boldsymbol{I} + \boldsymbol{C}_{\boldsymbol{\eta}}^{-1}\, \boldsymbol{H}\, \boldsymbol{Q}\, \boldsymbol{H}^{\mathrm{H}} \right) \tag{3.6}$$

avec :

$$\boldsymbol{C}_{\boldsymbol{\eta}} = \sigma^2\, \boldsymbol{I} = \frac{1}{K} \frac{N_0}{E_\mathrm{s}}\, \boldsymbol{I} \tag{3.7}$$

Le débit total maximum pouvant être atteint dans un système composé de quatre-vingt-seize faisceaux ($B = 96$), deux nombres de couleurs ($K = 1$ et $K = 3$) et les différents systèmes d'entrées/sorties décrits précédemment sont analysés [BBRJ11].

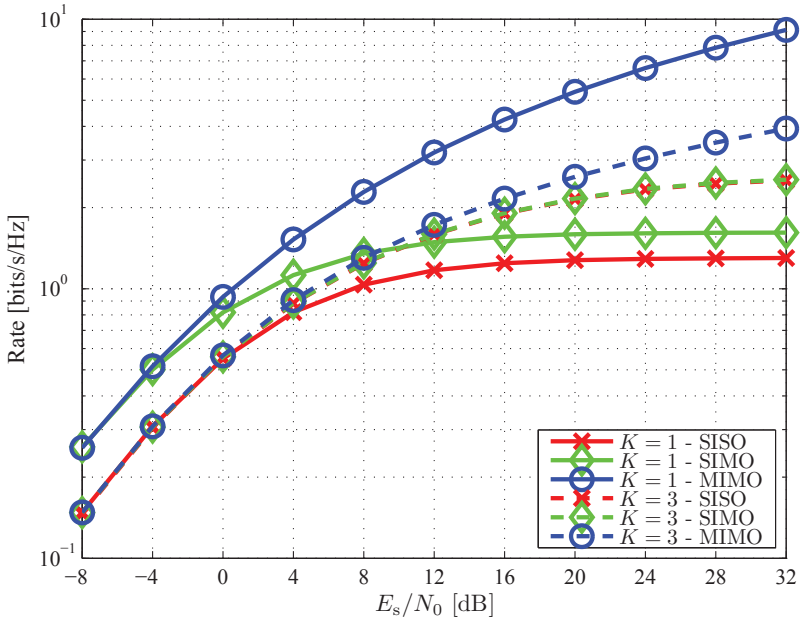


Figure 3.1. *Débit utilisateur moyen pour quatre-vingt-seize faisceaux ($B = 96$), avec ré-utilisation complète de la fréquence ($K = 1$) et trois couleurs ($K = 3$), et issu de 10 000 générations aléatoires.*

En regardant les résultats illustrés par la figure 3.1, nous pouvons voir que la taille de cluster 1 ($K = 1$) avec MIMO apporte plus de capacité que la taille de cluster 3 ($K = 3$) et ceci sur

la plage E_s/N_0 toute entière. Les améliorations apportées par la suppression successive des interférences sont donc claires pour $K = 1$ mais aussi pour $K = 3$ au dessus de 8 dB. Le niveau des interférences avec cette dernière taille de cluster est en fait assez bas et ceci est confirmé par la différence entre les systèmes SISO et SIMO. En fait le niveau de signal reçu par les autres utilisateurs dans un faisceau particulier est quasiment négligeable. Les débits les plus bas sont obtenus avec le système SISO et la taille de cluster 1. Ceci est parfaitement normal puisque le système est très fortement limité par les interférences. A 20 dB, le débit utilisateur moyen est multiplié par trois avec MIMO lorsque comparé à un système conventionnel SISO à trois couleurs (un analyse plus détaillée des résultats est disponible dans la Section 3.1.6 du rapport anglais, une analyse plus approfondie du comportement des courbes est faite dans la Section 3.1.7 du rapport anglais).

3.2 Débit Atteignable par Utilisateur

Dans la partie précédente (Section 3.1), le débit maximal total a été formulé pour différents systèmes à entrées/sorties (Input-Output (IO)). D'un coté le débit maximal pouvant être atteint au niveau utilisateur peut être obtenu facilement pour les systèmes à entrée et sortie unique (Single-Input and Single-Output (SISO)) et à entrée unique et sorties multiples (Single-Input and Multiple-Output (SIMO)). D'un autre coté l'expression du débit total pour des systèmes à entrées multiples et sorties multiples (Multiple-Input and Multiple-Output (MIMO)) donne directement le débit atteignable par le système. Le but ici est donc d'évaluer le débit maximum pour être atteint au niveau utilisateur pour des systèmes MIMO.

En utilisant le principe de la suppression successive des interférences (SIC) dans un système MIMO, il est possible de dériver l'expression du débit maximal pouvant être atteint par l'utilisateur j (principe expliqué dans la Section 3.2.1 du rapport anglais) :

$$R_{\mathrm{MIMO},j} = \log_2 \det\left(\boldsymbol{I}_{N_{\mathrm{Rx}}} + \boldsymbol{C}_{\boldsymbol{\eta}}^{-1}\, \boldsymbol{H}^{(N_{\mathrm{Tx}}-j+1)}\, \left(\boldsymbol{H}^{(N_{\mathrm{Tx}}-j+1)}\right)^{\mathrm{H}}\right) - \log_2 \det\left(\boldsymbol{I}_{N_{\mathrm{Rx}}} + \boldsymbol{C}_{\boldsymbol{\eta}}^{-1}\, \boldsymbol{H}^{(N_{\mathrm{Tx}}-j)}\, \left(\boldsymbol{H}^{(N_{\mathrm{Tx}}-j)}\right)^{\mathrm{H}}\right) \quad (3.8)$$

où $\boldsymbol{H}^{(N_{\mathrm{Tx}}-j)}$ représente la matrice composée des $N_{\mathrm{Tx}} - j$ colonnes les plus à droite de la matrice de canal initiale $\boldsymbol{H}$. Par définition nous avons $\boldsymbol{H}^{(N_{\mathrm{Tx}})} = \boldsymbol{H}$ et $\boldsymbol{H}^{(0)}$ est considérée comme étant une matrice vide.

Il peut être montré que l'ordre avec lequel le processus de suppression successive des in-

terférences, càd l'ordre avec lequel les colonnes de la matrice de canal sont décodées, n'a pas d'impact sur le débit total pouvant être atteint dans le système (Section 3.2.2 du rapport anglais). Cependant les débits utilisateurs vont quant à eux être directement impactés par l'ordre du processus. L'ordre du processus peut être modifié, en se référant à l'expression (3.8), en permutant la matrice de canal à l'aide de la matrice $\mathbf{\Pi}$ ($N_{\mathrm{Tx}}!$ permutations possibles). En appliquant une matrice de permutation particulière il est donc possible de cibler des critères particuliers, comme par exemple la maximisation du débit minimum utilisateur :

$$\mathbf{\Pi}' = \arg \max_{\mathbf{\Pi}} \left\{ \min_{j} R_{j,\mathrm{MIMO}} (\mathbf{\Pi}) \right\} \tag{3.9}$$

où $\mathbf{\Pi}'$ représente la matrice de permutation offrant le classement optimal (Optimal Ordering (OO)).

Le classement optimal est obtenu en utilisant l'algorithme de Foschini, càd en sélectionnant le flux avec le ratio signal sur interférences et bruit le plus élevé. L'impact de ce flux est retiré (suppression des interférences, IC), les rapports signal sur interférences et bruit restants sont évalués et comme précédemment le flux avec le SINR le plus élevé est sélectionné. L'algorithme continue ainsi jusqu'à ce que tous les flux soient traités [FGVW99]. L'évaluation du SINR dépend de l'architecture du récepteur prise en compte. Lorsqu'un récepteur MMSE avec SIC est considéré, le classement optimal est obtenu de la façon suivante :

$$\mathrm{SINR}^{(r)}_{\text{MMSE-SIC},j} = \boldsymbol{h}_j^{\mathrm{H}} \left(\boldsymbol{C}_{\boldsymbol{\eta}}^{-1} + \sum_{i \neq j} \boldsymbol{h}_i \, \boldsymbol{h}_i^{\mathrm{H}} \right)^{-1} \boldsymbol{h}_j \tag{3.10}$$

où i satisfait aussi $i \notin \{j^*_{\text{MMSE-SIC},1}, ..., j^*_{\text{MMSE-SIC},j-1}\}$, sachant que :

$$j^*_{\text{MMSE-SIC},r} = \arg \max_{j} \{\mathrm{SINR}^{(r)}_{\text{MMSE-SIC},j}\},\ j \in \{1, ..., N_{\mathrm{Tx}}\} \backslash \{j^*_{\text{MMSE-SIC},1}, ..., j^*_{\text{MMSE-SIC},r-1}\}$$

cette opération est réalisé pour $r = 1, ..., N_{\mathrm{Tx}} - 1$. Le terme $\boldsymbol{h}_j$ désigne la colonne j de la matrice de canal $\boldsymbol{H}$.

Les performances du classement dans le lien retour d'un système satellite à faisceaux multiples sont analysées avec sept faisceaux et un utilisateur dans chaque faisceau à chaque instant (système MIMO 7×7) [BBRJ11]. Une telle taille de système est considérée à cause du nombre de permutations possibles et la taille du cluster est fixée à 1 ($K = 1$). Le débit minimum utilisateur est ici analysé pour chaque réalisation du canal tout en modifiant l'ordre avec lequel le processus de suppression des interférences est réalisé (classement). La valeur

moyenne obtenue avec toutes les permutations possibles, l'approche dite de force brute, Foschini et le pire scénario sont pris en compte. La figure 3.2 montre clairement que le débit minimum est amélioré lorsque comparé à la stratégie "moyenne" (graphe de gauche). Les résultats obtenus avec l'approche de force brute correspondent, comme prévu, à ceux obtenus avec l'algorithme de Foschini, ce dernier offrant une complexité de calcul très réduite. En terme de performances, l'amélioration est de 30% par rapport au classement obtenu de façon aléatoire ("moyenne") et de plus de 50% lorsque comparée au pire scénario, càd celui minimisant le débit minimum.

Si nous tentons d'améliorer le niveau d'équité entre utilisateurs, cela revient à satisfaire le critère suivant :

$$\mathbf{\Pi}' = \arg\min_{\mathbf{\Pi}} \left\{ \frac{1}{N_{\mathrm{Tx}}} \sum_{j=1}^{N_{\mathrm{Tx}}} \left(R_{j,\mathrm{MIMO}}\left(\mathbf{\Pi}\right) - \frac{R_{\mathrm{MIMO}}}{N_{\mathrm{Tx}}} \right)^2 \right\} \tag{3.11}$$

où $\mathbf{\Pi}'$ est la matrice de permutation qui minimise la dispersion autour de la valeur moyenne. Les résultats obtenus sont montrés par le graphe de droite dans la figure 3.2, plus de détails sont donnés dans la Section 3.2.4 du rapport anglais.

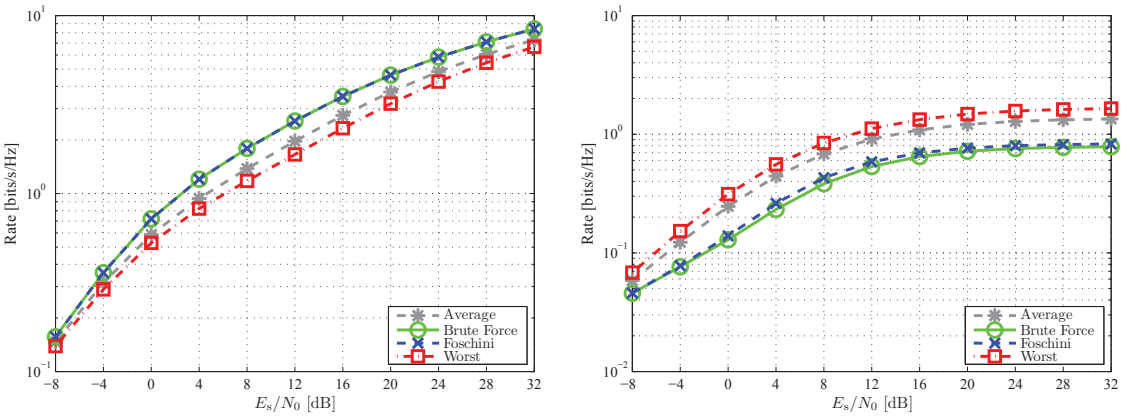


Figure 3.2. *Performances du classement sur les débits minimums utilisateurs (à gauche) et sur la dispersion autour de la valeur moyenne (à droite) pour sept beams ($B = 7$) avec ré-utilisation complète de la fréquence ($K = 1$) et issues de* 10000 *réalisations de canal. Les débits minimums par utilisateur sont comparés à l'aide de différentes méthodes : moyenne, approche par force brute, l'algorithme de Foschini et le pire scénario.*

3.3 Résumé

Nous avons vu dans ce chapitre que la phase présente dans les coefficients de la matrice de canal n'a actuellement aucun impact sur le débit total pouvant être atteint dans des systèmes

SISO, SIMO et MIMO. D'un coté l'analyse des débits totaux pouvant être obtenus dans un système employant trois couleurs a montré que la suppression des interférences n'apporte pas un gain suffisant dans les régions typiques de rapport signal sur bruit. Le système satellite à faisceaux multiples considéré en scénario de base est en fait conçu de façon à limiter les interférences co-canal lorsque la taille du cluster est égale ou supérieure à trois. Pour cette raison un système à quatre couleurs donne des gains encore plus réduits, quasiment négligeables, en considérant le maximal ratio combining (SIMO) ou la suppression successive des interférences (MIMO). D'un autre coté les gains atteints lorsqu'une ré-utilisation complète de la fréquence est considérée sont bien plus importants puisque la capacité théorique du système est multipliée par un facteur 3 quand celle-ci est comparée avec un système conventionnel (SISO) à trois couleurs, ce qui est conforme avec [CCMO11]. Cependant de tels gains sont obtenus dans certaines conditions qui sont mentionnées ci-dessous.

Tout d'abord les conditions de ciel dégagé considérées, ainsi que la connaissance parfaite de l'information quant à l'état du canal de transmission (perfect Channel State Information (CSI)), au niveau de la gateway sont supposées. Une gateway est en général responsable d'un certain nombre de faisceaux dans un système satellite à faisceaux multiples. Nous parlons en fait de cluster de faisceaux. Comme exemple, dans un système constitué de 72 faisceaux et dans lequel il y a 5 gateways, chacune d'elle sera responsable de 14 à 15 faisceaux [ESA-RM]. Les gateways sont généralement responsables de l'interface radio, càd de la transmission vers le satellite (lien avant ascendant, appelé aussi feeder up-link) et de la réception provenant du satellite (lien retour descendant, appelé aussi feeder down-link).

Une ré-utilisation complète de la fréquence impose des contraintes au niveau des segments spatiaux et terrestres. Dans le premier segment plus d'amplificateurs (Travelling Wave Tube Amplifiers, TWTAs) sont requis, en fait K fois plus où K représente le nombre nominal de couleurs considérées dans le système satellite. Ceci peut être réalisé en utilisant plus de satellites ou en augmentant la taille de la charge (payload), impliquant de ce fait la conception de satellites plus volumineux. Dans le dernier segment, le lien de la gateway est directement impacté puisque plus de bande passante est nécessaire. Ceci peut être obtenu en utilisant la bande Q/V ou des communications optiques par exemple, ou bien en augmentant le nombre de gateways. Des travaux récents ont été effectués sur les architectures dites hybrides, mélangeant le traitement à bord et au sol, plus particulièrement la formation de faisceaux (beamforming), de façon à équilibrer les performances et la complexité de la charge [ABCCGD11], [ADMN12].

Des mécanismes sont nécessaires afin d'estimer l'état actuel du canal pour chaque terminal

satellite, et aussi afin de prédire les états futurs, et il est également nécessaire d'avoir des récepteurs (gateways) capables de réaliser le filtrage Minimum Mean Square Error (MMSE) basé sur les informations quant à l'état du canal (CSI) et le niveau de bruit. Les conditions précédentes permettront de faire une détecteur multi-utilisateurs (Multi-User Detection (MUD)) grace à la suppression successive des interférences (Successive Interference Cancellation (SIC)) au sein du cluster de faisceaux pris en charge par la gateway. Ceci signifie que les autres faisceaux environnants, n'appartenant pas à cette gateway, généreront des interférences mais celles-ci seront considérées comme du bruit [DGMRV06]. De manière à améliorer les performance et à traiter correctement les interférences, une coopération complète entre gateways est nécessaire, utilisant le réseau terrestre de façon à échanger des informations quant aux différents états de canal mais aussi les données utilisateurs [ZCO11-2]. Cela implique un échange d'information entre les gateways et donc une implémentation de messages spécifiques. Les résultats présentés dans cette section correspondent donc au maximum pouvant être atteint en utilisant un système MIMO, des conditions de ciel dégagé, une connaissance parfaite du canal et une coopération complète entre les gateways présentes dans le système satellite à faisceaux multiples.

Les différentes formules et résultats ont aussi montré que l'ordre dans lequel les utilisateurs sont décodés n'a aucun impact sur le débit total mais joue un role significatif au niveau utilisateur puisque les débits pouvant être atteints par chaque utilisateur changent en conséquence. L'évaluation des débits utilisateurs avec la méthode proposée permet de satisfaire des critères de qualité de service (Quality of Service (QoS)), comme la maximisation du débit minimum. Comme prévu le classement obtenu via l'algorithme de Foschini satisfait le critère précédent et ceci avec une complexité réduite. Comme le débit total est invariant, la maximisation du débit atteignable par utilisateur implique une augmentation du niveau d'équité entre utilisateurs. La contribution consistait ici à évaluer les gains pouvant être atteints dans un système satellite en modifiant le classement.

A remarquer que les performances des techniques de suppression des interférences (Interference Cancellation (IC)) dépendent du niveau d'interférences entre les utilisateurs. En optimisant les ressources, lorsque plusieurs utilisateurs sont disponibles dans chaque faisceau, il est possible d'éviter les différences dans les débits pouvant être atteints au niveau utilisateur. Ceci va être illustré dans le prochain chapitre.

Chapitre 4

Ordonnancement

Dans les chapitres précédents le nombre d'utilisateurs par faisceau était fixé à un, càd un seul utilisateur dans chaque empreinte de faisceau. Nous avons vu que les débits peuvent être optimisés en prenant en compte l'ordre dans lequel l'opération de suppression successive des interférences (SIC) est réalisée. En considérant plus d'un utilisateur par faisceau et une allocation uniforme des ressources, il est possible de modifier l'association des utilisateurs transmettant en même temps et qui interfèrent donc les uns avec les autres.

L'ordonnancement pour les réseaux cellulaires MIMO ont déjà été bien étudiés, plus particulièrement pour les canaux de Rayleigh [AjHa05], [YoGo06], [YiLi02], [YFVG11]. Dans ce chapitre nous présentons le concept global de l'ordonnancement avec communications intercouches [HSBAG06] appliqué au lien retour de systèmes satellite MIMO à faisceaux multiples et nous étudions une propriété intéressante qui est l'invariance du débit total. Des algorithmes de recherche sont ensuite décrits, tout d'abord en identifiant tous les possibilités d'ordonnancement et ensuite toutes les combinaisons possibles d'utilisateurs dans un créneau (slot). Avec cette dernière, une approche basée sur les graphes multipartites permet de mieux représenter la génération de l'ordonnancement final et aussi de réduire la complexité de calcul. Des algorithmes d'ordonnancement sont ensuite dérivés afin de fonctionner avec des systèmes à grande échelle tels que dans les communications satellites. Les performances des différents algorithmes sont vérifiées en prenant en compte différentes tailles de systèmes, montrant une amélioration du débit minimum pouvant être atteint par utilisateur mais aussi du niveau d'équité. Enfin l'impact de l'ordonnancement, qui a été optimisé à l'aide de la théorie de l'information, est évalué sur un approche pratique du taux d'erreurs non codé au niveau bit.

4.1 Bases

Le principe de l'optimisation de l'ordonnancement des utilisateurs est d'associer des utilisateurs qui sont situés dans des faisceaux différents de façon à ce qu'ils génèrent le moins possible d'interférences dites mutuelles. Un exemple est donné par la figure 4.1 : avec l'ordonnancement initial (tableau de gauche) les utilisateurs représentés par des croix créent l'un envers l'autre un niveau élevé d'interférences, contrairement aux utilisateurs représentés par les cercles. Les débits pouvant être atteints par les utilisateurs seront de ce fait très différents. Il convient donc de changer l'association des utilisateurs, et donc l'ordonnancement, de façon à réduire le niveau d'interférences (tableau de droite). Pour plus de détails, veuillez consulter la section 4.1.1 du rapport anglais.

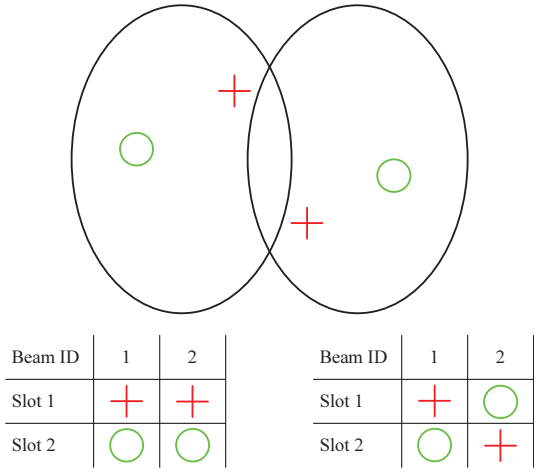


Figure 4.1. *Exemple d'ordonnancement simple avec deux faisceaux et deux utilisateurs par faisceau.*

Le terme "allocation" réfère dans ce document à un ordonnancement possible pour servir M utilisateurs par faisceau et qui sont couverts par B faisceaux différents dans le système satellite. Dans chacun des B faisceaux, les utilisateurs sont numérotés de 1 à M. Le terme combinaison définit une association possible d'utilisateurs transmettant en même temps et qui sont donc prévus dans le même créneau. Le nombre d'allocations possibles, en considérant que l'ordre des créneaux n'a pas d'importance, est (Section 4.1.2 : Number of Possible Allocations) :

$$N_{\text{alloc}} = \frac{(M!)^B}{M!} = (M!)^{B-1} \tag{4.1}$$

Les deux paramètres B et M influencent donc l'ordonnancement, B régit la taille du système et M la profondeur de l'ordonnancement.

Chaque matrice de canal (réalisation) correspond à un placement particulier d'utilisateurs

au sein des faisceaux. Modifier l'ordonnancement consiste à combiner différents utilisateurs en même temps, dans notre cas différents transmetteurs. De ce fait une allocation sera le résultat de l'association de colonnes issues de différentes matrices de canal (Section 4.1.3 : Scheduling and Channel Matrices).

4.2 Invariance du Débit Total à l'Ordonnancement

Le but de cette section est de comprendre pourquoi le débit total n'est pas impacté de façon significative par l'ordonnancement. Nous pouvons montrer que dans un système avec M utilisateurs par faisceau, une approximation du débit total pour un rapport signal sur bruit faible peut être formulée de la manière suivante (voir la démarche détaillée en Section 4.2.1, Section 4.2.2 et Section 4.2.3) :

$$R_{\text{total},M} \simeq R^{-}_{\text{total},M} = \log_2 \det\left(\boldsymbol{I} + \left(\frac{E_\text{s}}{N_0}\right)\left(\sum_{m=1}^{M} \boldsymbol{H}^{(m)}\,\boldsymbol{H}^{(m)\,\text{H}}\right)\right) \tag{4.2}$$

Dans ce cas l'ordonnancement n'a aucun impact sur le débit total. Pour des rapports signal sur bruit élevés, une approximation du débit total est :

$$R_{\text{total},M} \simeq R^{++}_{\text{total},M} = M\,N_\text{Rx}\,\log_2\left(\frac{E_\text{s}}{N_0}\right) + \log_2 \det\left(\prod_{m=1}^{M}\left(\boldsymbol{H}^{(m)}\,\boldsymbol{H}^{(m)\,\text{H}}\right)\right) \tag{4.3}$$

dont la valeur varie avec l'ordonnancement à cause du terme de droite.

En considérant un ordonnancement aléatoire pour chaque set de matrices et en calculant ensuite l'espérance mathématique de $\frac{R^{++}_{\text{total},M}}{M}$ parmi tous les sets possibles de matrices (càd parmi tous les utilisateurs possibles), en considérant également que les ordonnancements et les utilisateurs sont indépendants, nous obtenons :

$$\mathbb{E}\left[\frac{R^{++}_{\text{total},M}}{M}\right] = N_\text{Rx}\log_2\left(\frac{E_\text{s}}{N_0}\right) + \frac{1}{M}\sum_{m=1}^{M}\mathbb{E}\left[\log_2\det\left(\boldsymbol{H}^{(m)}\,\boldsymbol{H}^{(m)\text{H}}\right)\right], \tag{4.4}$$

où $\boldsymbol{H}^{(m)}$ est un set aléatoire d'utilisateurs dans un créneau. En utilisant le théorème de la limite centrale, la partie droite de l'expression précédente implique que pour de larges valeurs de M la variable aléatoire est distribuée de façon Gaussienne. A cause des propriétés particulières et de la structure des matrices de canal des satellites à faisceaux multiples, la déviation standard de la distribution Gaussienne diminue avec la profondeur de l'ordonnancement. En conclusion essayer d'améliorer le débit total en optimisant l'ordonnancement n'apporte pas grand chose.

4.3 Algorithmes de Recherche

Cette section présente les algorithmes dits de “recherche” qui correspondent aux fondations de l'édifice permettant d'améliorer l'ordonnancement des utilisateurs. Le concept de la recherche parmi toutes les allocations possibles, et une nouvelle approche, basée sur les graphes multipartites, permettant de faire une recherche parmi toutes les combinaisons possibles, sont expliqués. Ces deux recherches visent à maximiser le débit minimum par utilisateur et la deuxième approche vise particulièrement à réduire de façon considérable la complexité de calcul.

La première recherche représente une approche de force brute pour trouver l'allocation optimale. Lorsque le critère pris en compte est directement lié aux débits au niveau des utilisateurs, l'évaluation des débits doit être réalisée au niveau des créneaux. Pour cette raison, le nombre d'évaluations devant être faites est :

$$N_{\text{eval,ES}} = M\ (M!)^{B-1} \tag{4.5}$$

Plutôt que de travailler au niveau des allocations, la complexité globale peut être réduite en se focalisant sur les différentes combinaisons. Les combinaisons d'utilisateurs peuvent être représentées en utilisant une approche basés sur les graphes multipartites [CoLeRi90]. Les termes sont expliqués en détail dans la Section 4.3.2 du rapport anglais et sont résumés dans la figure 4.2.

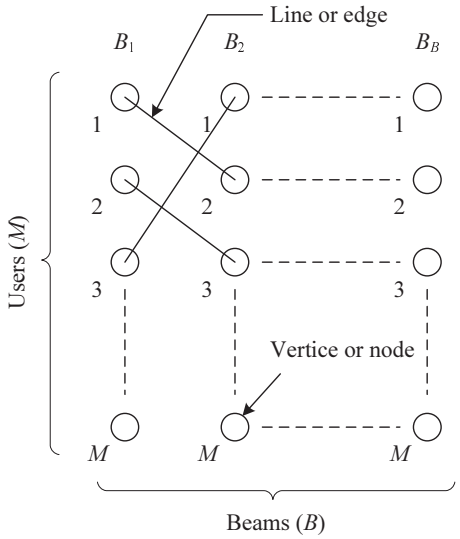


Figure 4.2. *Définition des termes dans une approche de graphe multipartite.*

Le nombre d'évaluations devant être effectuées avec cette approche est bien plus réduit qu'avec

l'approche de force brute :

$$N_{\text{eval,BG}} = M^B \tag{4.6}$$

Il existe plusieurs possibilités en travaillant au niveau des combinaisons d'utilisateurs afin de satisfaire le critère maximisant le débit minimum par utilisateurs. L'algorithme retenu ici est l'algorithme dit de suppression des minimums. Son principe est dérivé de [BaCaZo08] et est adapté à des scénarios à grande échelle. Pour chaque combinaison possible d'utilisateur, le débit minimum par utilisateur est calculé. Les combinaisons sont classées de celle offrant le débit minimum le plus bas à celle offrant le débit minimum le plus élevé. L'algorithme sélectionne les combinaisons fournissant les débits minimum les moins élevés et les supprime de la liste de combinaisons possibles tant qu'il reste une solution au problème d'ordonnancement. Si la suppression d'une combinaison entraîne l'impossibilité de trouver un ordonnancement final, cette combinaison est insérée dans la liste des combinaisons finales. L'algorithme s'arrête lorsque les M combinaisons ont été sélectionnées. L'algorithme est décrit en détail dans la Section 4.3.3 du rapport anglais.

4.4 Algorithmes d'Ordonnancement pour Systèmes à Grande Échelle

A cause de la complexité à trouver une solution optimale d'ordonnancement pour des systèmes à grande échelle, de nouveaux algorithmes d'ordonnancement doivent être conçus. Dans cette section deux algorithmes d'ordonnancement, qui utilisent les algorithmes de recherche présentés dans la section précédente (Section 4.3), sont décrits.

L'algorithme dit de "Viterbi" se base sur l'approche de graphe multipartites (ou B-partites). Cet algorithme démarre avec deux faisceaux et calcule tous les débits minimums utilisateurs pour chaque combinaison. Un poids est donné aux combinaisons en fonction de la valeur du débit utilisateur minimum. M combinaisons sont sélectionnées pour ces deux faisceaux et un nouveau faisceau est ajouté. Le processus est répété jusqu'à ce que tous les faisceaux soient considérés. Plutôt que d'évaluer le débit utilisateur minimum pour toutes les combinaisons possibles (M^B), cet algorithme réduit à M^2 évaluations réalisées $B-1$ fois :

$$N_{\text{eval,VL}} = (B-1)\,M^2 \tag{4.7}$$

Cet algorithme présente un problème puisque les faisceaux sont ajoutés les uns après les autres afin de trouver le meilleur ordonnancement. Une bonne combinaison d'utilisateurs

dans deux faisceaux ne signifie pas nécessairement qu'il s'agisse toujours d'une bonne combinaison lorsqu'un nouveau faisceau est ajouté au système. Pour plus de plus amples détails, veuillez consulter la section 4.4.1 du rapport en anglais.

L'algorithme dit "géographique" prend pour avantage les particularités du canal satellite. Le niveau d'interférences est en fait directement régi par le diagramme de rayonnement des multiples faisceaux. L'algorithme consiste à associer une couleur virtuelle à chaque faisceau. La couleur virtuelle correspond à la véritable couleur du faisceau dans un système utilisant plus d'une couleur. Les faisceaux de la même couleur sont plus limités par le bruit que par les interférences lorsque le nombre de couleurs virtuelles est suffisamment grand et donc le niveau d'interférences est quasi négligeable pour les rapports signal sur bruit qui nous intéressent. Pour cette raison l'ordre avec lequel les utilisateurs sont ordonnancés dans de tels faisceaux n'impacte que très faiblement leurs performances. L'algorithme sélectionne de façon aléatoire l'allocation pour chaque groupe de faisceaux et, bien entendu, pour les utilisateurs appartenant à chaque groupe. Les M utilisateurs de chaque faisceau sont toujours positionnés dans différents créneaux. L'algorithme associe ensuite les groupes de façon à obtenir le niveau le plus bas d'interférences mutuelles. L'ordonnancement final est donc l'association d'ordonnancements partiels. Un exemple est donné par la figure 4.3) avec trois utilisateurs par faisceau ($M = 3$) et sept faisceaux ($B = 7$). Plus de détails quant au fonctionnement de cet algorithme sont disponibles dans la section 4.4.2 du rapport anglais.

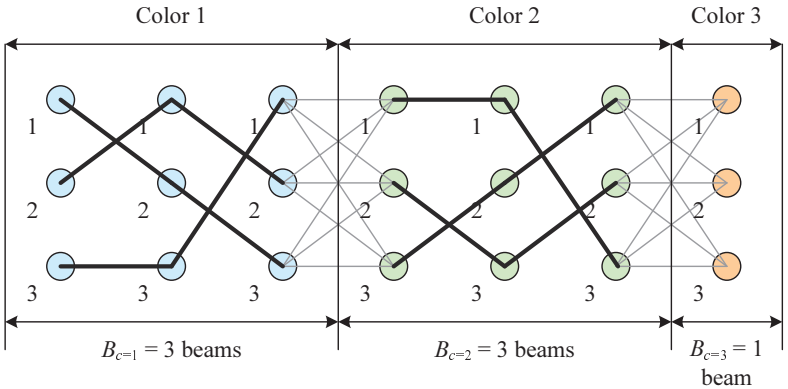


Figure 4.3. *Exemple d'ordonnancement géographique avec trois utilisateurs par faisceau ($M = 3$), trois couleurs virtuelles et sept faisceaux ($B = 7$).*

La complexité pour associer deux ordonnancements partiels est proportionnel à $O\left(M^4\right)$ et donc avec C couleurs virtuelles, la complexité est proportionnelle à $O\left(M^4\ (C-1)\right)$. Ceci représente une réduction considérable lorsqu'on la compare avec la complexité liée au nombre initial possible de $(M!)^{B-1}$ ordonnancements (allocations).

4.5 Évaluations des Performances des Différents Algorithmes

La section 4.5.1 du rapport rédigé en anglais explique le principe de l'analyse des résultats au niveau des créneaux et au niveau des blocs. La notion de "réalisation" de matrice de canal est également détaillée. Enfin l'index d'équité de Jain est formulé. Ce dernier est souvent utilisé pour quantifier le niveau d'équité entre les débits atteints par différents utilisateurs au sein d'un réseau [JaHaCh84] :

$$J = \frac{\left(\sum_{i=1}^{N} r_i\right)^2}{N \times \sum_{i=1}^{N} r_i^2}$$

où N représente dans ce cas le nombre d'utilisateurs par créneau, càd le nombre de transmetteurs, et r_i le débit utilisateur, càd le débit pouvant être atteint par chaque utilisateur. Par définition lorsque tous les utilisateurs perçoivent le même débit, l'index est égal à 1 et correspond donc au niveau maximum d'équité. Lorsqu'un seul utilisateur obtient la capacité totale disponible alors que les autres n'ont rien, cet index vaux $1/N$.

Nous considérons tout d'abord un système de taille 7×7 et avec une seule couleur de sorte qu'il est constitué d'un faisceau et de six faisceaux directement adjacents. Le nombre d'utilisateurs par faisceau est fixé à trois ($M = 3$) de façon à pouvoir réaliser l'évaluation des performances avec la recherche exhaustive. Le nombre de réalisation du canal est $N_{\text{ch}} = 999$ et le rapport signal à bruit est situé entre -8 et 32 dB. La figure 4.4 montre la valeur moyenne au niveau bloc (graphe de gauche) et le premier centile au niveau créneau (graphe de droite) du débit minimum par utilisateur. L'ordonnancement optimal est en retrait de 1.5 dB par rapport au débit moyen par utilisateur. L'algorithme de Viterbi et l'algorithme géographique sont à 1.9 dB en retrait ce qui est donc très proche du résultat optimal. A remarquer que le système sans ordonnancement fait 5.4 dB et 3 dB moins bien que l'ordonnancement optimal et l'ordannancement géographique, respectivement (graphe de gauche). Ces différences deviennent d'autant plus grandes lorsqu'on analyse le premier centile (graphe de droite). De telles améliorations sont liées au fait que les algorithmes évitent d'associer des utilisateurs qui sont géographiquement proches les uns des autres, càd ayant des gains bas et des niveaux d'interférences mutuelles élevés. L'algorithme géographique offre des résultats qui sont très proches de ceux obtenus avec la recherche exhaustive.

Les bénéfices des algorithmes d'ordonnancement peuvent aussi être observés en analysant l'index d'équité de Jain (figure 4.5). L'algorithme géographique perd environ 1% lorsque comparé à la valeur optimale obtenue avec la recherche exhaustive. N'avoir aucune optimisation de

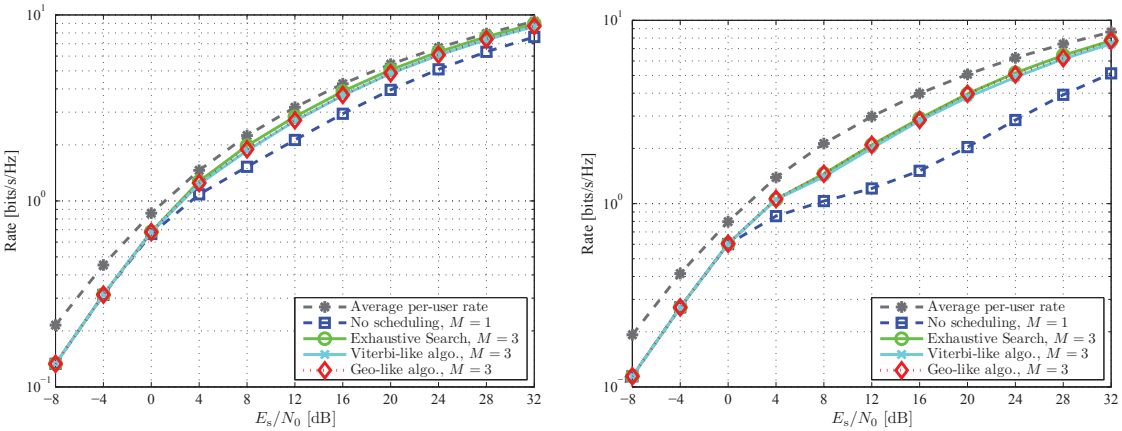


Figure 4.4. *Impact des algorithms d'ordonnancement sur les débits minimums par utilisateur (à gauche) et sur le premier centile (à droite) avec sept faisceaux ($B = 7$), trois utilisateurs par faisceau ($M = 3$) et $N_{ch} = 999$ réalisations de canal.*

l'ordonnancement peut réduire le niveau d'équité entre utilisateurs de plus de 5%.

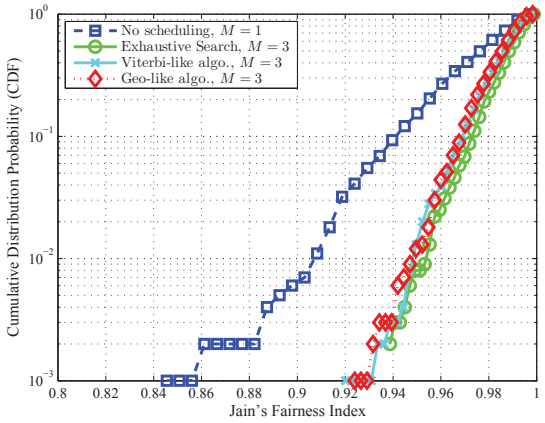


Figure 4.5. *Function de répartition de l'index de Jain. Le nombre de faisceaux B est 7, le nombre d'utilisateurs par faisceau $M = 3$ et le nombre de réalisation de canal $N_{ch} = 999$.*

En prenant en compte le système satellite à faisceaux multiples complet, càd quatre-vingt-seize faisceaux, le système devient un système à grande échelle. Comme précédemment le nombre d'utilisateurs par faisceau est égal à trois et désormais le nombre de réalisation de canal est $N_{\text{ch}} = 24$. Les deux recherches exhaustives ainsi que l'algorithme de Viterbi ne sont pas considérés car trop complexes pour un système de cette taille. L'évaluation du débit minimum par utilisateur (figure 4.6) montre qu'un ordonnancement intelligent améliore les performances entre 20 et 25% pour des rapports signal sur bruit élevés, ce qui est un gain considérable. Pour des rapports SNR plus bas, l'amélioration est réduite puisque le système est avant tout limité par le bruit. A remarquer que le débit utilisateur moyen est deux fois

plus élevé que le débit minimum utilisateur sans ordonnancement. L'algorithme géographique atteint environ deux tiers de ce débit moyen alors que dans les graphes précédents il était relativement proche du débit maximum pouvant être atteint.

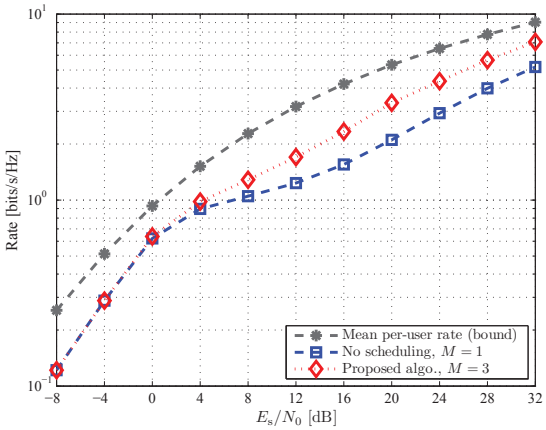


Figure 4.6. *Débit minimum par utilisateur. Le nombre de faisceaux B est 96, le nombre d'utilisateur par faisceau $M = 3$ et le nombre de réalisation de canal $N_{ch} = 24$.*

Ce comportement peut être expliqué par les propriétés de la matrice de canal. En fait nous présumons que, contrairement à un environnement d'altération de signal terrestre typique de Rayleigh, où pour de grandes valeurs M les utilisateurs peuvent être ordonnancés de façon à obtenir le débit d'un seul utilisateur [YoGo06], [YFVG11], ceci n'est pas le cas dans des systèmes satellites. Ceci est dû à la composition de la matrice de canal qui est régie essentiellement par le diagramme de rayonnement de l'antenne. En fait la distribution statistique des coefficients dévie fortement de celle de Rayleigh puisque celle-ci est directement déterminée par la position des utilisateurs dans le faisceau. Plus particulièrement, la plage dynamique du canal de Rayleigh est infinie en principe et ceci n'est pas vrai pour des gains d'antenne qui ne peuvent pas être nuls ou plus élevés que le gain maximum. Pour ces raisons les gains pouvant être atteints grace à la diversité multi-utilisateurs sont limités et l'orthogonalité des utilisateurs qui peut exister dans un système terrestre MIMO ne peut pas être assurée [YoGo06], [YiLi02], [YFVG11]. Dans tous les cas l'algorithme proposé offre des performances qui sont plutôt proche de la limite supérieure.

4.6 Impact de l'Ordonnancement sur le Taux d'Erreurs Non Codé au Niveau Bit

L'optimisation des ordonnancement via des simulations basées sur le taux d'erreurs au niveau bit n'est pas réalisable en pratique et pour cette raison des études ont été faites sur les débits pouvant être atteints de façon à ce que des algorithmes d'ordonnancement puissent être conçus de manière efficace (chapitre 3 et dans ce chapitre, respectivement). Cette section montre l'impact de l'ordonnancement, réalisé en utilisant la théorie de l'information, sur la performance du taux d'erreurs au niveau bit [BoMaBe12-2]. Pour cela nous considérons le scénario composé de sept beams ($B = 7$) et dans lequel les utilisateurs dits "bons" et "mauvais" sont couverts par les sept faisceaux. Nous avons donc deux matrices de canal différentes, l'une issue du scénario à niveau d'interférences bas et l'autre issue du scénario d'interférences élevées. Ceci mène à un total de $N_{\text{users,total}} = 14$ puisque nous avons deux utilisateurs par faisceau. Avec de tels scénarios les taux d'erreurs au niveau bit sont totalement différents. Nous nous attendons donc à ce que l'ordonnancement améliore le niveau d'équité entre utilisateurs, càd à offrir aux utilisateurs un taux d'erreurs niveau bit quasiment identique. D'un coté en utilisant la théorie de l'information nous avons maximisé le débit minimum par utilisateur et aussi augmenté le niveau d'équité entre utilisateurs. D'un autre coté en réalisant des simulations du taux d'erreurs au niveau bit, nous devrions observer une baisse du maximum et donc du taux d'erreurs niveau bit le plus élevé, et aussi, comme pour les débits pouvant être atteints, une amélioration de l'équité.

Les performances en terme de taux d'erreurs au niveau bit sont évaluées en considérant le récepteur MMSE intégrant l'architecture optimale de suppression successive des interférences (SIC). Les simulations sont réalisées avec la modulation QPSK, avec un rapport du niveau d'énergie par symbol sur densité spectrale du bruit allant de -8 dB à 24 dB. Les taux d'erreurs au niveau bit non codés sont moyennés parmi tous les utilisateurs. Le principe et le processus sont détaillés dans la section 4.6.1 du rapport anglais, l'allocation optimale est décrite dans la section 4.6.2.

La figure 4.7 montre clairement que le taux d'erreurs niveau bit diminue lorsque le classement optimal est réalisé au sein du processus de suppression successive d'interférences et également lorsque les ordonnancements sont optimisés. La suppression des interférences (IC) avec le classement optimal (OO) et sans ordonnancement offre un gain de 3 dB pour des rapports signal à bruit élevés. Il est intéressant de noter que l'ordonnancement sans classement optimal donne

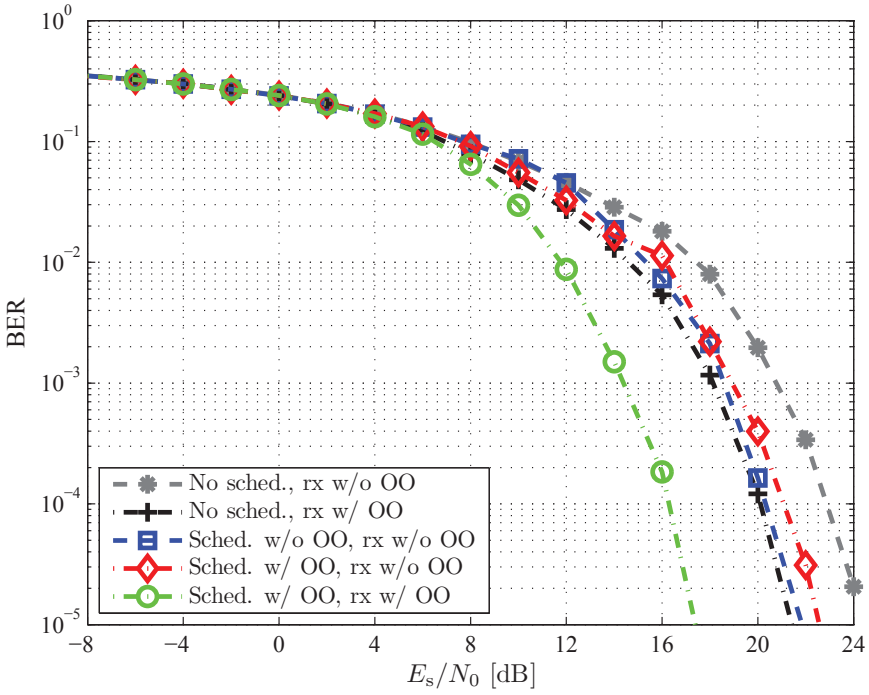


Figure 4.7. *Impact du classement et de l'ordonnancement sur le taux d'erreurs niveau bit moyenné pour le mauvais et le bon scénario. "OO" signifie optimal ordering (classement optimal).*

quasiment des résultats identiques. Ceci prouve que les deux stratégies ont besoin d'être combinées de manière à obtenir les meilleures performances. Si l'ordonnancement est réalisé en considérant le classement optimal mais qu'en fait ce dernier n'est pas appliqué au niveau du récepteur, il y a incompatibilité et en conséquence le taux d'erreurs niveau bit se dégrade, càd augmente. Comme prévu les gains les plus élevés sont obtenus lorsque les ordonnancements sont optimisés en considérant le classement optimal et lorsque cette dernière opération est réalisée à la réception. Pour un taux d'erreurs niveau bit de 10^{-4}, le gain est d'environ 7 dB, ce qui est une amélioration assez remarquable. A noter que les interruptions dans l'inclinaison des courbes sont liées à la modification de l'ordre avec lequel chaque utilisateur est décodé.

Enfin le niveau d'équité, non illustré ici (voir la section 4.6.3 du rapport anglais), est aussi amélioré lorsque les ordonnancements sont optimisés et aussi lorsque le classement optimal est pris en compte.

4.7 Résumé

Nous avons montré dans ce chapitre que le débit total ne peut pas être optimisé grace à l'ordonnancement dans la région basse du rapport sinal à bruit, et seulement légèrement dans la région haute. De ce fait l'analyse des combinaisons d'utilisateurs et leurs impacts sur le débit total a montré qu'une amélioration peut être faite au niveau des débits utilisateurs. Nous avons étudié un algorithme à faible complexité de façon à dériver des ordonnancements proches de l'ordonnancement optimal pour des systèmes satellites à faisceaux multiples, plus particulièrement pour des systèmes à grande échelle. Ce travail a permis d'évaluer les gains qu'un ordonnanceur peut atteindre dans des réseaux satellites qui sont limités par les interférences. En fait des améliorations intéressantes peuvent être obtenues au niveau des performances, même s'il n'est pas possible d'atteindre la limite de l'utilisateur seul dans ce contexte, comme cela serait le cas dans des canaux dégradés de Rayleigh. Les caractéristiques des rayonnements classiques des faisceaux limitent les gains qui semblent être ici restreints à 25% comparé à des scénarios sans ordonnancement.

Il est possible d'utiliser les outils mis à disposition par la théorie de l'information de façon à optimiser l'ordonnancement des utilisateurs pour maximiser les débits minimums pouvant être atteints au niveau des utilisateurs. En conséquence le niveau d'équité entre utilisateurs se retrouve amélioré. Des simulations dites "pratiques" ont montré le même comportement sur le taux d'erreurs niveau bit non codé. Comme prévu le taux d'erreurs maximum est réduit de manière considérable et les utilisateurs perçoivent quasiment des taux identiques, ce qui augmente le niveau d'équité. Les optimisations réalisées au niveau de l'allocation des ressources visent toutes à maximiser le débit minimum au niveau utilisateur et en pratique la minimisation du taux d'erreurs maximum. Il est possible, en utilisant les différents outils et algorithmes conçus jusqu'ici, d'étudier des algorithmes plus avancés de manière à prendre en compte des contraintes de qualité de service (Quality of Service (QoS).

Chapitre 5

Ordonnancement avec Contraintes de Qualité de Service

Ce chapitre utilise le concept d'ordonnancement et les différents algorithmes décrits dans le chapitre précédent (chapitre 4) dans lequel la maximisation du débit minimum de chaque utilisateur était visée et introduit maintenant les contraintes de qualité de service (Quality of Service (QoS)).

Dans ce chapitre nous analysons tout d'abord l'impact du nombre de faisceaux et du nombre d'utilisateurs qui sont pris en compte pour l'optimisation de l'ordonnancement. Les résultats obtenus avec cette étude sont exploités afin de concevoir des algorithmes innovants satisfaisant différentes contraintes de qualité de service. Le premier, dit d'"affectation de créneau libre" (Free Slot Assignment (FSA)), est capable d'ajouter des créneaux non-nécessaires aux ordonnancements de manière à avoir une matrice non pleine en créneaux/faisceaux et donc de réduire les interférences mutuelles parmi les utilisateurs. Ceci peut être exploité pour garantir des niveaux minimums de qualité de service (QoS) en terme de débits de service. Le deuxième, appelé "algorithme de fenêtrage", optimise la sélection de l'ordonnancement de façon à garder sous contrôle le délai entre l'arrivée de l'utilisateur dans le système et le moment auquel celui-ci sera planifié. Pour chaque contrainte les performances sont analysées ainsi que la complexité de l'algorithme proposé. Enfin une combinaison des deux contraintes, et de ce fait de deux algorithmes, est mise en place et les améliorations obtenues avec ce nouvel algorithme hybride sont montrées.

5.1 Impact du Nombre de Faisceaux et du Nombre d'Utilisateurs par Faisceau

Dans cette section nous nous focalisons sur l'impact de la taille du système, qui est régie par le nombre de faisceaux B, mais aussi de la profondeur de l'ordonnancement, qui est, elle, régie par le nombre d'utilisateurs par faisceau M [BoBeRo11] [BoMaBe12-1]. Ces deux facteurs jouent un rôle important dans la complexité de calcul pendant l'optimisation des ordonnancements mais permet également de comprendre leurs impacts dans la conception d'algorithmes d'ordonnancement qui prennent en compte des contraintes de qualité de service spécifiques.

Le rapport signal sur bruit est fixé à 15 dB de sorte que la communication entre transmetteurs et récepteurs soit essentiellement limitée par les interférences. Ajouter des faisceaux supplémentaires dans le système consiste à ajouter plus d'utilisateurs et de ce fait plus d'interférences. Pour un nombre donné de faisceaux B, augmenter le nombre d'utilisateurs par faisceau M, ce qui est équivalent à augmenter la dite profondeur d'ordonnancement, permet d'offrir plus de possibilités pour l'optimisation des ordonnancements. Afin d'évaluer l'impact du nombre de faisceaux, l'approche des graphes multipartites est considérée, alors que pour sept faisceaux ($B = 7$) les utilisateurs qui s'interfèrent faiblement les uns les autres peuvent être groupés dans des couleurs fictives et être planifiés aléatoirement de sorte que la complexité soit réduite [BoBeRo11] (algorithme géographique, veuillez consulter la section 4.4 pour plus de détails).

Le scénario pris en compte et la numérotation des faisceaux est telle que $B_i = i$ avec $i = 1 \dots B$ comme illustré par la figure 5.1 du rapport anglais. Dans cette section nous définissons la probabilité d'interruption de service, ou non-disponibilité, pour un débit minimum donné r comme suit :

$$p_r = P\{r_{\min} \leqslant r\} \tag{5.1}$$

La fonction de répartition des débits minimums par utilisateur sera interprétée en utilisant (5.1) pendant l'analyses des différents résultats.

L'impact du nombre de faisceaux B sur les débits minimums par utilisateur et sur l'index d'équité de Jain est montré dans la figure 5.1 lorsque l'ordonnancement n'est pas optimisé, càd lorsque le nombre d'utilisateurs par faisceau est tel que $M = 1$. Comme prévu l'augmentation du nombre de faisceaux implique une diminution des performances (graphe de gauche).

En d'autres termes le débit minimum garanti r décroît pour une probabilité particulière de non-disponibilité p_r lorsque B augmente. La diminution des performances devient modérée car l'augmentation des interférences co-canal est balancée par les gains offerts par les multiples antennes de réception. Pour ce qui est du niveau d'équité, celle-ci augmente avec B car la probabilité d'avoir des utilisateurs avec des rapports signal à bruit différents augmente et ceci aide à améliorer les performances de la suppression successive des interférences en réalisant le classement optimal. Une analyse plus détaillée des résultats est disponible dans la section 5.1.1 du rapport anglais.

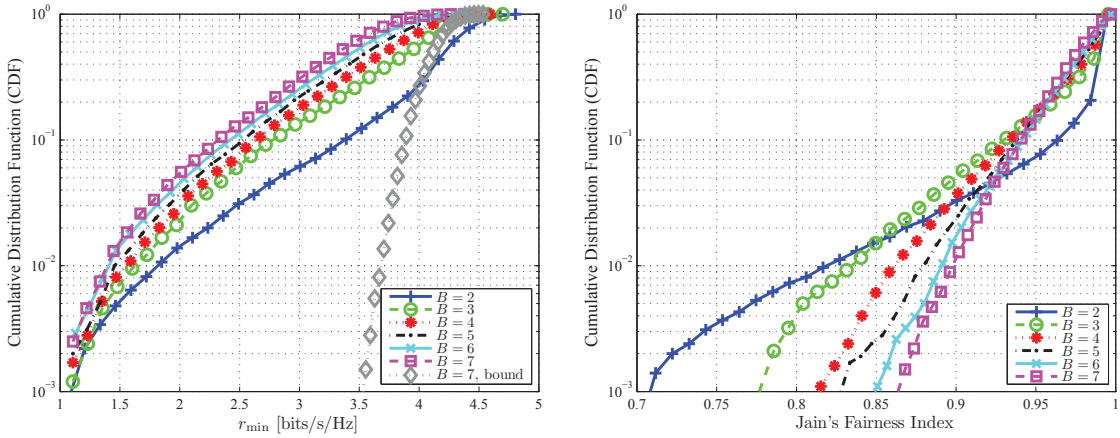


Figure 5.1. *Impact du nombre de faisceaux sur les débits minimums utilisateurs (à gauche) et sur l'index d'équité de Jain (à droite).*

L'impact de la profondeur de l'ordonnancement est évalué en fixant la taille du système à sept beams ($B = 7$). Augmenter le nombre d'utilisateurs par faisceau M revient à augmenter le degré de liberté (degree of freedom) pour l'ordonnancement. En considérant une probabilité particulière de non-disponibilité les débits minimums par utilisateur sont améliorés pour des profondeurs d'ordonnancement plus élevées (figure 5.2, à droite) et un effet de saturation est observé. Le niveau d'équité entre utilisateurs est également amélioré par la profondeur de l'ordonnancement (figure 5.2, à gauche). Lorsque $M > 5$, les gains deviennent négligeables pour les deux mesures. Plus de détails sont présents dans la section 5.1.2 du rapport anglais.

5.2 Contraintes en Terme de Débit

Réaliser des ordonnancements avec des contraintes en terme de débit consiste à tenter de fournir aux utilisateurs présents dans le système un débit minimum particulier par utilisateur, défini par r_{th}. Le but est de garantir, pour une taille de système donnée B et un nombre

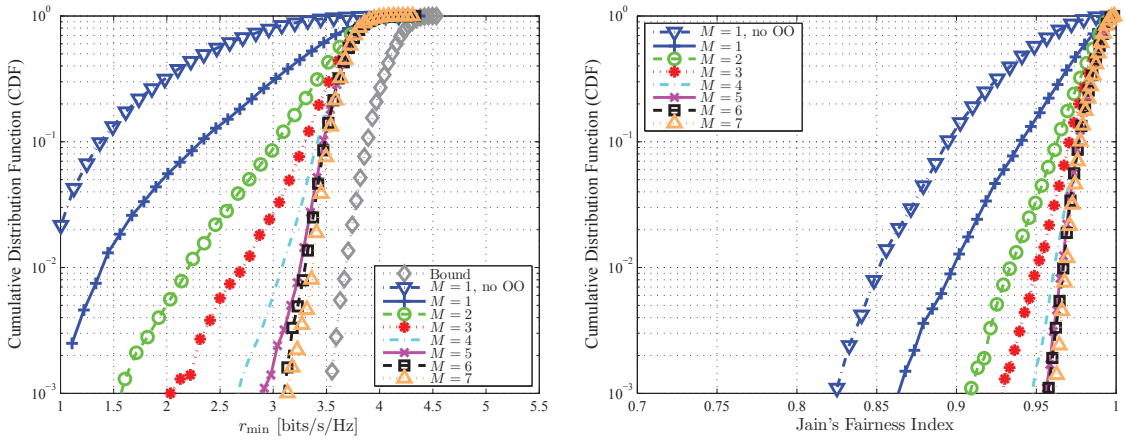


Figure 5.2. *Impact du nombre d'utilisateurs par faisceau sur les débits minimums par utilisateur (à droite) et sur l'index d'équité de Jain (à droite).*

d'utilisateurs par faisceau M, tout en gardant à l'esprit la complexité, un débit pré-défini qui aura un impact direct sur les couches supérieures, càd sur les débits de donnée perçu par les utilisateurs au niveau applicatif. Augmenter la profondeur de l'ordonnancement permet d'améliorer les débits minimums mais ces derniers saturent à partir d'une certaine valeur de M. Une autre solution doit être trouvée pour diminuer le niveau d'interférences mutuelles et ceci peut être obtenu en introduisant un créneau vide. Au lieu que l'ordonnancement soit optimisé en utilisant M créneaux, nous introduisons un créneau supplémentaire de sorte que l'ordonnancement puisse être réalisé avec $M + 1$ créneaux. Cette stratégie est appelée "affectation de créneau libre" (Free Slot Assignment (FSA)). Le nombre d'allocations possibles dans lesquelles des créneaux vides ne sont pas permis est :

$$N_{\text{alloc,FSA}} = ((M+1)!)^{(B-1)} - M!^{(B-1)} \tag{5.2}$$

Les gains théoriques, les gains pratiques et les pertes d'efficacité sont détaillés dans la section 5.2.1 du rapport rédigé en anglais.

Un algorithme intelligent basé sur cette stratégie d'utilisation de créneau supplémentaire a été conçu. En effet cette stratégie entraîne une perte d'efficacité (utilisation de ressources supplémentaires) et augmente également la complexité de l'ordonnancement. L'algorithme vise à donner un compromis entre la garantie d'une contrainte de débit minimum au niveau utilisateur, r_{th}, en évitant une perte d'efficacité et aussi, et non des moindres, en réduisant le plus possible la complexité de l'opération. Cet algorithme est appelé "Smart Free Slot Assignment Scheduling Algorithm" [1] et son principe est décrit dans ce qui suit. La profon-

1. Un brevet a été déposé par l'auteur au niveau de l'Allemagne pour cet algorithme, ce brevet sera

deur de l'ordonnancement M n'est désormais plus fixe et l'algorithme débute avec $M = 1$ de sorte que l'ordonnancement ne soit pas optimisé (les utilisateurs sont alloués comme ils "arrivent", càd de la façon avec laquelle ils sont placés dans les faisceaux). Le débit minimum pouvant être atteint par utilisateur $r_{\min}$ est calculé et si la contrainte est atteinte, càd $r_{\min} \geq r_{\text{th}}$, les B utilisateurs sont alloués ensemble pour cette réalisation du canal. Par contre si la contrainte n'est pas respectée, la profondeur de l'ordonnancement est incrémentée d'une unité, càd $M = 2$, et l'ordonnancement est optimisé. Comme précédemment si le débit minimum obtenu est plus grand que r_{th} l'ordonnancement optimal est enregistré et les matrices de canal suivantes sont prises en compte. Sinon la profondeur de l'ordonnancement est à nouveau augmentée jusqu'à ce que celle-ci soit plus grande que le seuil FSA, noté M_{FSA}, càd jusqu'à ce que $M > M_{\text{FSA}}$. Dans ce dernier cas l'optimisation de l'ordonnancement est effectuée en insérant un créneau supplémentaire vide, càd en utilisant la stratégie FSA, plus particulièrement $M_{\text{FSA}} + 1$ créneaux. Ce dernier essai peut être se révéler concluant ou pas. Dans le premier cas l'ordonnancement optimal a été trouvé et la contrainte est garantie. Dans le second cas deux possibilités s'offrent à nous : soit l'ordonnancement est annulé, soit il est enregistré. La dernière solution est préférable bien entendu puisque même si la contrainte n'est pas respectée, l'ordonnancement trouvé permettra d'obtenir un débit minimum par utilisateur qui est plus proche de la contrainte. Le principe de l'algorithme est illustré par le diagramme de la figure 5.5 présent dans la section 5.2.2 du rapport anglais.

Afin d'évaluer les performances de cet algorithme, le rapport signal à bruit est fixé à 15 dB, la probabilité de coupure $p_{r_{\text{th}},M} \simeq 0.1$, et M variant entre 2 et 4. Les valeurs de ces deux paramètres proviennent des résultats obtenus dans la section précédente (section 5.1). Les tableaux 5.1 et 5.2 montre les performances sans l'algorithme (benchmark) et avec l'algorithme proposé, respectivement.

En analysant les différentes valeurs fournies par le tableau 5.2, nous pouvons remarquer de suite l'aptitude de l'algorithme à détecter quand les profondeurs d'ordonnancement réduites sont suffisantes et également quand l'ordonnancement n'est pas nécessaire. En conséquence la complexité et le temps de calcul sont grandement réduits en optimisant les ordonnancements et également en tentant de garantir la contrainte de débit. Ce qui est aussi remarquable est la possibilité d'atteindre des contraintes de débit plus élevées en augmentant le seuil M_{FSA} tout en gardant une perte en efficacité quasiment constante.

également soumis au niveau européen.

Table 5.1. *Performance de l'ordonnancement sans FSA.*

M [utilisateurs par faisceau]	2	3	4
Contrainte de débit de service r_{th} [bits/s/Hz]	3	3.3	3.41
Créneaux avec $M = 2$ [%]	100.0	-	-
Créneaux avec $M = 3$ [%]	-	100.0	-
Créneaux avec $M = 4$ [%]	-	-	100.0
Disponibilité des créneaux [%]	91.08	89.63	90.11
Efficacité [%]	100.0	100.0	100.0

Table 5.2. *Performance de l'ordonnancement avec FSA.*

M_{FSA} [utilisateurs par faisceau]	2	3	4
Contrainte de débit de service r_{th} [bits/s/Hz]	3	3.3	3.41
Créneaux sans ord. [%]	56.46	34.04	25.18
Créneaux avec $M = 2$ [%]	30.44	29.24	23.80
Créneaux avec $M = 3$ [%]	13.10[1]	20.85	21.18
Créneaux avec $M = 4$ [%]	-	15.87[1]	14.92
Créneaux avec $M = 5$ [%]	-	-	14.92[1]
Disponibilité des créneaux [%]	99.46	98.89	99.20
Efficacité [%]	93.85	94.98	96.40

[1] *aussi équivalent au pourcentage de créneaux dans lesquels la stratégie FSA est utilisée.*

Les fonctions de répartition des débits minimums par utilisateur et de l'index d'équité sont illustrées dans la figure 5.3 respectivement sur le graphe de gauche et le graphe de droite. L'impact de l'algorithme FSA est celui attendu puisqu'il améliore les débits minimums par utilisateur et aussi, par conséquent, le niveau d'équité. A noter que l'algorithme proposé est même capable de faire aussi bien que l'ordonnancement sans FSA mais avec une profondeur d'ordonnancement plus élevée ($M = 7$ montre des performances quasi identiques que celles obtenues avec $M_{\text{FSA}} = 4$). L'utilisation de cet algorithme permet d'augmenter le niveau d'équité de 82% environ sans ordonnancement et avec un classement optimal (figure 5.2, à droite) à plus de 96% avec $M_{\text{FSA}} = 4$.

En ce qui concerne la complexité de cet algorithme, la complexité moyenne d'un ordonnan-

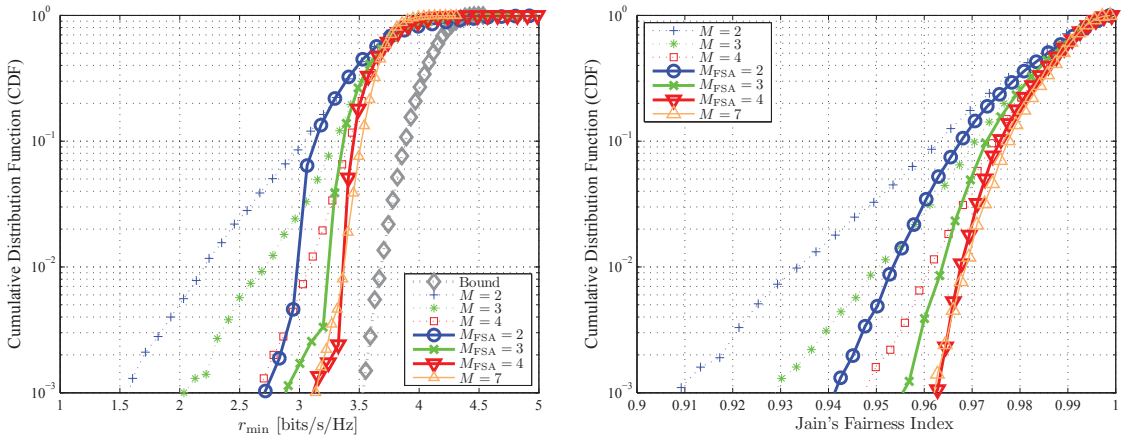


Figure 5.3. *Impact de la stratégie FSA sur les débits minimums par utilisateur (à gauche) et sur l'index d'équité de Jain (à droite).*

cement est proportionnel à (voir la section 5.2.3 du rapport anglais pour plus de détails) :

$$\alpha_{M_{\text{FSA}}} = \sum_{i=1}^{M_{\text{FSA}}} \frac{f_i}{i} \sum_{j=1}^{i} 2\,j^4 + \frac{f_{M_{\text{FSA}}+1}}{M_{\text{FSA}}} \sum_{j=1}^{M_{\text{FSA}}+1} 2\,j^4 \tag{5.3}$$

où f_i représente la fréquence avec laquelle les créneaux avec $M = i$ sont utilisés, de ce fait $f_{M_{\text{FSA}}+1} = f_{\text{FSA}}$. Le terme de gauche dans (5.3) correspond à la complexité en présence de créneaux additionnels, la somme intérieure est liée aux essais qui sont réalisés tout en augmentant M. Le terme de droite se réfère à la complexité lorsque la stratégie FSA est activée. Comme prévu le gain en réduction de complexité s'améliore avec M_{FSA} puisque la probabilité de trouver un $M \leq M_{\text{FSA}}$ intermédiaire respectant la contrainte augmente (tableau 5.3).

Table 5.3. *Analyse de complexité : algorithme FSA proposé vs. sans FSA.*

M or M_{FSA} [utilisateurs par faisceau]	2	3	4
Contrainte de débit de service r_{th} [bits/s/Hz]	3	3.3	3.41
Gain par rapport à sans FSA [%]	−19.54	−5.05	7.95[1]

[1] 82.82% *de gain par rapport à* $M = 7$.

Le détail quant à l'analyse des résultats figurants dans le tableau 5.3 est donné dans la section 5.2.3 du rapport en anglais. A remarque que comme $M_{\text{FSA}} = 4$ atteint quasiment les mêmes performances que $M = 7$, la complexité peut être comparée pour ces deux valeurs et dans ce cas le gain s'élève à 83%, ce qui est une amélioration remarquable.

5.3 Contraintes de Temps

Le concept tout entier de l'ordonnancement présenté jusqu'à maintenant est désormais considéré comme étant contraint par le temps. Nous rappelons au lecteur que la notion de temps dans les différents processus d'ordonnancement avait consciemment été laissée en retrait. Pour cette raison l'ordre des créneaux n'avait pas d'importance par exemple, réduisant immédiatement la complexité liée au nombre possible d'allocations. Dans ce qui suit le temps est vu comme étant une contrainte.

Nous assumons à partir de maintenant que l'index de la matrice de canal est lié au temps d'arrivée de la requête de ressources dans la gateway (plus de détails sur le concept de temps avec l'ordonnancement sont donnés en section 5.3.1 du rapport anglais). La réalisation du canal avec index i, notée $\boldsymbol{H}^{(i)}$, correspond à un groupe d'utilisateurs demandant des ressources à la gateway au même indice de temps i. L'échelle des temps, plus particulièrement la granularité du temps, est abstraite et peut être vue comme basée sur des créneaux par exemple où l'échelle du temps sera donc régie par la durée des créneaux. Par exemple si nous considérons les dix premières réalisations du canal, càd $\boldsymbol{H}^{(i)}$ avec $1 \leq i \leq 10$, pour réaliser l'ordonnancement, alors il y a $B \times 10$ requêtes. L'ordonnanceur alloue les ressources en essayant de maximiser le débit minimum par utilisateur, comme précédemment, et prend aussi soin d'attribuer les créneaux aux utilisateurs de sorte que leur position originale, càd définie par l'index i, ne diffère pas trop de la nouvelle position, définie par le nouvel index i'. En fait un utilisateur initialement représenté par un vecteur colonne de la matrice de canal $\boldsymbol{H}^{(i)}$, se retrouve, après avoir optimisé les ordonnancements, dans la matrice de canal notée $\boldsymbol{H}^{(i)'}$. Dans notre exemple si un utilisateur était initialement dans la réalisation de canal $\boldsymbol{H}^{(1)}$ et se retrouve finalement alloué dans $\boldsymbol{H}^{(10)'}$ (nous rappelons que l'ordonnancement consiste à échanger les colonnes des différentes matrices du canal), alors cet utilisateur perçoit un délai additionnel puisqu'il se retrouve alloué dans le "futur". Le contraire se passe si un utilisateur est représenté par un vecteur colonne de la matrice $\boldsymbol{H}^{(10)}$ et qu'il se retrouve alloué dans la matrice $\boldsymbol{H}^{(1)'}$. Dans ce cas l'utilisateur est en quelque sorte alloué dans le "passé". L'ordonnancement peut donc être réalisé en prenant ce critère en compte, ce qui impactera le délai perçu par les utilisateurs au niveau des couches supérieures.

Plutôt que de sélectionner les prochaines réalisations de canal disponibles pour optimiser les ordonnancements avec une valeur donnée M, nous offrons plus de flexibilité à l'ordonnanceur. Le premier algorithme est décrit brièvement puisqu'il correspond à des mécanismes bien

connus. Cela permet de mieux comprendre les principes se cachant derrière la notion d'ordonnancement à fenêtrage. Nous nous focalisons particulièrement sur le second algorithme qui est basé sur une approche innovante.

L'algorithme dit d'"ordonnancement à fenêtrage normal" se base sur le principe bien connu de l'algorithme à fenêtrage glissant qui peut être trouvé dans TCP par exemple. Nous appliquons ce principe de manière à optimiser les ordonnancements parmi les différentes réalisations de canal disponibles. Pour cela nous introduisons la taille de fenêtre, représentée par W_s, qui influencera la profondeur de la recherche, ou espace de recherche. L'ordonnanceur pointe la première réalisation de matrice disponible qui est contrainte par l'algorithme à faire partie de la solution finale d'ordonnancement (allocation). En fonction de la taille de la fenêtre l'ordonnanceur calcule toutes les combinaisons possibles de matrices de canal, en prenant en compte la profondeur d'ordonnancement M, càd le nombre de matrices de canal devant être associées. L'ordonnanceur optimise les ordonnancements pour toutes les combinaisons de canal et sélectionne l'association qui maximise le débit minimum par utilisateur. La combinaison de canaux, càd le set de matrices de canal, est enregistrée et l'index des réalisations de canal est ré-organisé en conséquence. L'algorithme fait ensuite glisser la fenêtre vers la réalisation de canal suivante et réalise les mêmes opérations. Les différentes étapes décrites précédemment sont répétées jusqu'à ce que toutes les réalisations de canal soient traitées. Un exemple est donné dans la section 5.3.2 du rapport anglais dans laquelle il est également expliqué que la nouvelle position i' est en fait telle que :

$$1 - W_\mathrm{s} \leq i' - i \leq (W_\mathrm{s} + 1 - M)\ (M - 1) \tag{5.4}$$

où un utilisateur arrivant au temps i est en fait alloué au temps i'.

L'algorithme dit d'"ordonnancement à fenêtrage avancé" [2] correspond à une amélioration de l'algorithme précédent. Cette fois, les indexes des réalisations de canal ne sont pas ré-organisées et les matrices sélectionnées pour des ordonnancements optimisés sont marquées comme indisponibles. Cela signifie que dans une fenêtre de taille W_s le nombre de matrices disponibles n'est plus forcément égal à W_s. De ce fait le nombre de combinaisons possibles et également la profondeur de l'ordonnancement change de façon dynamique en fonction des associations réalisées plus tôt (un exemple est donné dans la section 5.3.3 du rapport anglais).

2. Un brevet a été déposé par l'auteur au niveau de l'Allemagne pour cet algorithme, ce brevet sera également soumis au niveau européen.

La nouvelle position i' est désormais telle que :

$$1 - W_{\mathrm{s}} \leq i' - i \leq W_{\mathrm{s}} - 1 \tag{5.5}$$

En comparant les expressions (5.4) et (5.5), il est clair que cet algorithme est conçu de sorte à minimiser les délais perçus par les utilisateurs une fois qu'ils ont été alloués. Le principe complet ainsi que le diagramme expliquant le fonctionnement de cet algorithme sont présents dans la section 5.3.3 du rapport écrit en anglais.

En utilisant le même principe que dans les sections précédentes, càd section 5.1 et section 5.2, le rapport signal à bruit est fixé à 15 dB de sorte que les communications soient principalement limitées par les interférences et les résultats sont obtenus à partir de plusieurs milliers de matrices de canal. Les algorithmes de fenêtrage requièrent deux paramètres d'entrée qui sont la profondeur de l'ordonnancement M et la taille de fenêtre W_{s}. Le but est de comparer les performances de l'ordonnanceur dit normal, càd celui n'intégrant pas le concept de fenêtrage, avec les deux algorithmes de fenêtrage. Pour cela nous fixons la profondeur d'ordonnancement à $M = 3$ pour réaliser l'ordonnancement normal, et les combinaisons $M = 2$ / $W_{\mathrm{s}} = 4$ et $M = 3$ / $W_{\mathrm{s}} = 6$ pour les algorithmes de fenêtrage (la taille de la fenêtre est donc telle que $W_{\mathrm{s}} = 2\,M$). Les performances sont évaluées en se basant sur la fonction de répartition des débits minimums par utilisateur et l'index d'équité de Jain.

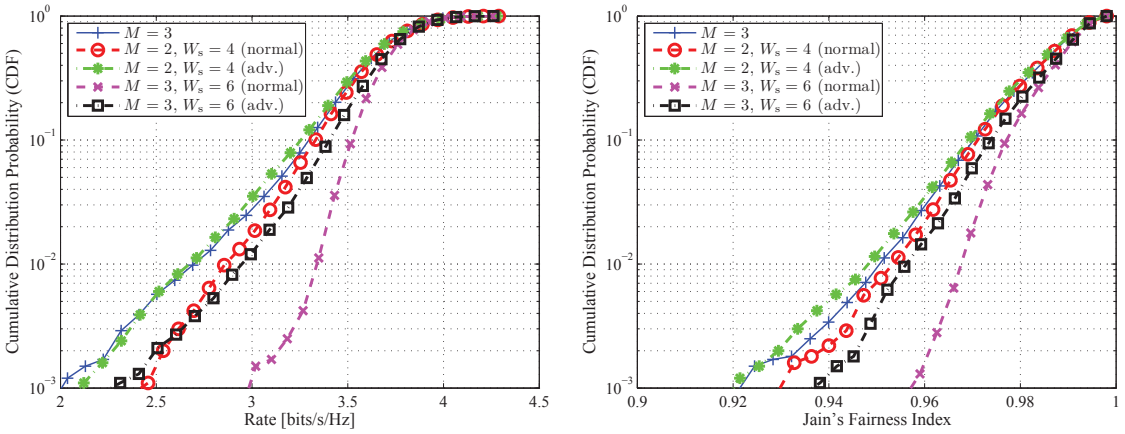


Figure 5.4. *Impact des algorithmes de fenêtrage sur les débits minimums par utilisateur (à gauche) et sur l'index d'équité de Jain (à droite).*

Les deux fonctions de répartition montrent que les algorithmes de fenêtrage améliorent les performances (figure 5.4). Comme prévu l'algorithme de fenêtrage normal fait mieux puisque la taille de la fenêtre n'évolue pas dans le temps et donc l'ordonnanceur a plus de liberté

pour combiner des matrices de canal différentes. L'algorithme de fenêtrage avancé avec les paramètres $M = 2$ / $W_s = 4$ offre des résultats quasi identiques à ceux de l'ordonnanceur normal avec $M = 3$. Enfin l'utilisation de l'algorithme de fenêtrage avancé avec $M = 3$ et $W_s = 6$ permet d'obtenir quelques gains lorsque comparé à l'algorithme de fenêtrage normal fonctionnant avec une profondeur d'ordonnancement et une taille de fenêtre plus faibles. Ce qui est plus intéressant concerne l'analyse de la dérive maximale dans le temps qu'un utilisateur peut percevoir. Les deux graphes montrés par la figure 5.5 indiquent les pourcentages atteints pour chaque valeur possible de la dérive maximale dans le temps qui sont dans le "passé" (valeurs positives) ou dans le "futur" (valeurs positives). L'algorithme de fenêtrage avancé réduit la plage de la dérive maximale dans le temps et permet également de concentrer cette dérive autour de zéro, càd autour de la position initiale.

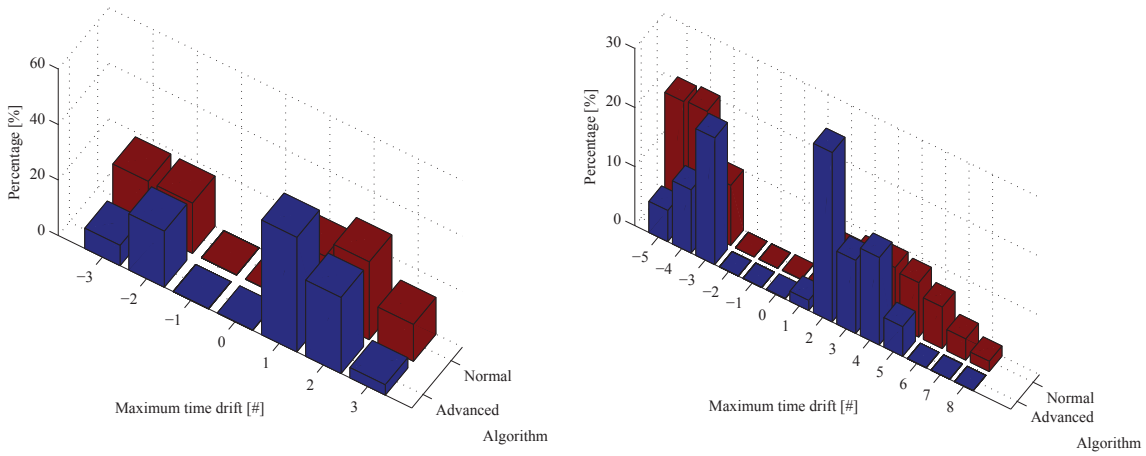


Figure 5.5. *Impact des algorithmes à fenêtre sur les dérives de temps maximales pour $M = 2$ et $W_s = 4$ (à gauche) et $M = 3$ et $W_s = 6$ (à droite).*

L'analyse de la complexité des différentes algorithmes (expressions données dans le rapport écrit en anglais) montre d'un coté que l'algorithme de fenêtrage normal permet avec $M = 2$ et $W_s = 4$ de réduire la complexité d'environ 11% lorsque comparé à l'algorithme d'ordonnancement conventionnel avec $M = 3$. En offrant des performances quasiment identiques (figure. 5.4), l'algorithme de fenêtrage avancé, avec les mêmes valeurs, permet de réduire la complexité de 30% environ. D'un autre coté, pour des valeurs plus élevées de profondeur d'ordonnancement et de taille de fenêtre, plus particulièrement $M = 3$ et $W_s = 6$, la complexité est indubitablement plus élevée que l'algorithme normal avec la même profondeur d'ordonnancement. En effet la complexité devient dix fois plus élevée avec ces valeurs et en utilisant l'algorithme de fenêtrage normal et cinq fois plus élevé en utilisant l'algorithme de fenêtrage avancé. Dans ce cas l'algorithme de fenêtrage avancé réduit la complexité de

l'ordonnancement par fenêtrage par deux.

5.4 Contraintes de Débit et de Temps

Dans la section 5.2 nous avons introduit l'algorithme dit "Smart Free Slot Assignment Scheduling Algorithm" qui permet de fixer une contrainte de débit à l'ordonnanceur et d'optimiser les ressources de sorte que les débits minimums pouvant être atteints au niveau utilisateur soient améliorés, le niveau d'équité entre utilisateurs soit augmenté, et aussi que la complexité de l'ordonnancement soit réduite. Dans la section 5.3 un algorithme basé sur une fenêtre glissante et nommé "Advanced Window Scheduling Algorithm" était décrit. Cet algorithme aide une fois de plus à améliorer les débits minimums par utilisateur, l'équité et la complexité en prenant en compte des contraintes liées au temps. Le but de cette section est de combiner ces deux algorithmes et de créer un algorithme hybride appelé "Window FSA Scheduling Algorithm".

Le principe global reste le même, l'algorithme est désormais régi par la contrainte de débit r_{th}, par le seuil FSA M_{FSA} et par la taille de fenêtre W_{s}. Il est attendu, en combinant ces deux algorithmes, d'augmenter les performances globales de l'ordonnancement. Les valeurs utilisés pour évaluer les performances sont directement issues de la section 5.2 et la taille de fenêtre est telle que $W_{\mathrm{s}} = 2\,M$.

Table 5.4. *Performances de l'ordonnancement avec l'algorithme window FSA.*

M_{FSA} [utilisateurs par faisceau]	2	3	4
Taille de fenêtre W_{s} [#]	4	6	8
Contrainte de débit de service r_{th} [bits/s/Hz]	3	3.3	3.41
Créneaux sans ord. [%]	52.50	29.53	20.22
Créneaux avec $M = 2$ [%]	44.28	59.94	63.86
Créneaux avec $M = 3$ [%]	3.22[1]	7.47	11.88
Créneaux avec $M = 4$ [%]	-	3.06[1]	1.60
Créneaux avec $M = 5$ [%]	-	-	2.44[1]
Disponibilité des créneaux [%]	99.98	99.97	99.89
Efficacité [%]	98.42	98.99	99.39

[1] *aussi équivalent au pourcentage de créneaux dans lesquels la stratégie FSA est utilisée.*

En comparant les résultats donnés par le tableau 5.4 avec ceux du tableau 5.2, le pourcentage de créneaux vides ajoutés est radicalement réduit et de ce fait l'efficacité est améliorée. De plus la disponibilité augmente ce qui signifie que la contrainte de débit est encore mieux respectée. Enfin le pourcentage de créneaux utilisant une profondeur d'ordonnancement $M = 2$ est encore plus important et donc la complexité devrait se retrouver diminuée. Les gains en terme de complexité ainsi que l'impact de l'algorithme hybride sur la dérive maximale de temps sont donnés dans la partie 5.4.2 du rapport anglais. La figure 5.6 montre les améliorations des débits minimums par utilisateur (à gauche) et de l'index d'équité de Jain (à droite). L'augmentation de la disponibilité des créneaux peut être observée sur les courbes qui présentent des effets de chute plus prononcés que ceux de la figure 5.3.

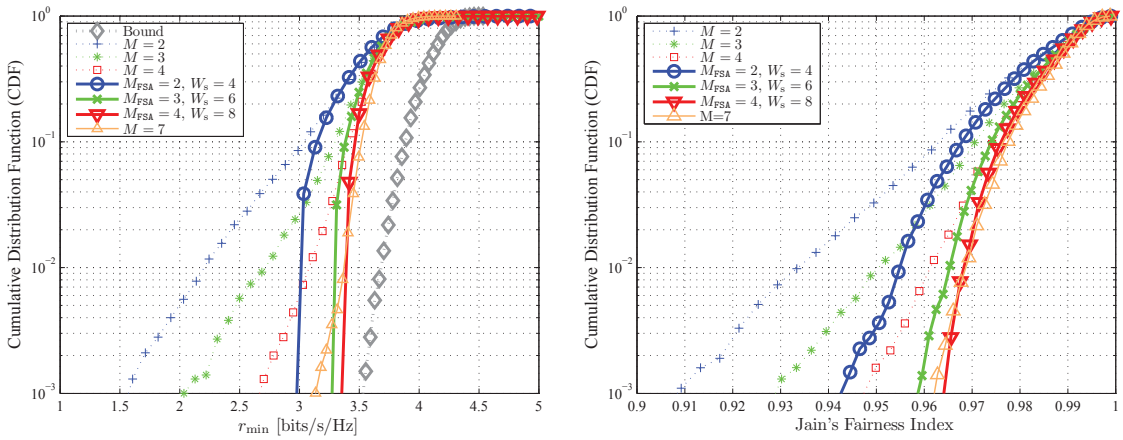


Figure 5.6. *Impact de l'algorithme hybride sur les débits minimums par utilisateur (à gauche) et sur l'index d'équité de Jain (à droite).*

5.5 Résumé

L'architecture MIMO permettant d'atteindre la capacité avec le classement optimal de suppression successive des interférences a été considéré de façon à quantifier l'impact de la taille de l'ordonnancement sur la maximisation du débit minimum par utilisateur. D'un coté le niveau d'interférences co-canal augmente avec la taille du système, comme prévu, et le gain offert par les multiples antennes à la réception balance la diminution des performances. D'un autre coté en augmentant le nombre d'utilisateurs par ordonnancement, une convergence vers la limite haute et un phénomène de saturation des performances ont été observés. Avec une population d'utilisateurs distribuée de façon aléatoire dans les faisceaux, une profondeur d'ordonnancement réduite permet d'obtenir des performances proches des performances op-

timales en terme de débits minimums par utilisateur et également en terme d'équité.

Les différentes simulations ont montré que l'algorithm FSA proposé et visant à satisfaire des contraintes de débits, qui consiste à allouer un créneau additionnel vide comme dernière solution pour réduire le niveau global des interférences, permet d'atteindre de bons résultats à différents niveaux. Tout d'abord il est conçu de façon à améliorer les débits minimums par utilisateur et donc à augmenter le niveau d'équité entre utilisateurs. La valeur du seuil activant l'utilisation du créneau additionnel joue un rôle sur la complexité de l'algorithme et permet même de surpasser les algorithmes d'ordonnancement conventionnels. Les gains en performances sont obtenus au détriment d'une petite perte en capacité système, que l'algorithme s'efforce à minimiser dans tous les cas.

L'algorithme de fenêtrage permet d'offrir à l'ordonnanceur plus de liberté pour sélectionner les matrices de canal et aide donc à améliorer les débits minimums par utilisateurs et aussi l'équité entre utilisateurs. En fonction de la contrainte de temps fixée aux couches supérieures, l'ordonnanceur peut adapter la taille de fenêtre W_{s} et également la profondeur d'ordonnancement M. Un algorithme conventionnel à fenêtre a montré une amélioration des performances et aussi une réduction de la complexité lorsque comparé à un algorithme d'ordonnancement normal. Un algorithme innovant basé sur cette approche et appelé "Advanced Window Scheduling Algorithm" permet de réduire encore plus la complexité et aussi de mieux contrôler la dérive maximale de temps qui peut être perçue aux couches supérieures par un utilisateur.

Comme prévu la combinaison des deux algorithmes aide à obtenir des améliorations importantes en considérant contraintes de débit et de temps. D'un coté le "Smart FSA Scheduling Algorithm" permet de garantir des exigences en terme de débits minimums par utilisateur en réduisant la profondeur de l'ordonnancement et en conséquence la complexité. De plus, comme déjà indiqué, cet algorithme limite également la perte en efficacité lorsque l'insertion de ressources additionnelles est nécessaire. D'un autre coté le "Advanced Window Scheduling Algorithm" permet d'augmenter l'espace de recherche pour optimiser les ordonnancements, en prenant en compte la dérive de temps issue par ce mécanisme et en essayant de la maintenir la plus basse possible. L'algorithme hybride prend les avantages de chacun des algorithmes et est capable de satisfaire dans la plupart des cas les contraintes de qualité de service demandées.

Chapitre 6

Conclusions

Dans cette thèse de doctorat, les différentes améliorations pouvant être réalisées dans le lien retour de systèmes satellites à faisceaux multiples, et limités par les interférences, ont été étudiées. Ces améliorations sont tout particulièrement obtenues en mettant en oeuvre des échanges inter-protocoles, allant de la couche physique aux couches supérieures. Le concept global est basé sur le fait que les systèmes satellites à faisceaux multiples peuvent être considérés comme des systèmes virtuels avec de multiples entrées et de multiples sorties (Multiple-Input Multiple-Output), et plus particulièrement le lien retour peut être vu comme un système MIMO avec un canal à accès multiples (Multiple-Access Channel, MAC). De cette manière des techniques de traitement du signal commun peuvent être mises en place au niveau du récepteur, càd de la passerelle (gateway), de façon à supprimer les interférences.

Le travail présenté dans cette thèse est basé sur un scénario de système satellite particulier et réaliste. Plus particulièrement un système satellite à faisceaux multiples, avec une charge transparente et une architecture de réseau en étoile (star network topology), et couvrant l'Europe avec 96 faisceaux, est pris en compte. Toutefois ce travail peut être étendu à d'autres scénarios. Il est connu par la théorie de l'information que la capacité disponible dans le système satellite augmente lorsque le nombre de couleurs, aussi appelé facteur de ré-utilisation de la fréquence ou taille du groupe (cluster), diminue et ceci à cause de la bande passante disponible dans chaque faisceau. Pour cette raison, employer une ré-utilisation de fréquence complète, càd une seule couleur, permet en principe d'augmenter le débit. En pratique, cependant, l'interférence co-canal (Co-Channel Interference, CCI) limite le système et le transforme en un réseau grandement limité par les interférences. Le but était donc d'évaluer quels gains peuvent être obtenus avec un système à ré-utilisation de fréquence complète com-

paré à un système basé sur un nombre de couleurs plus élevé.

L'impact du canal satellite sur des récepteurs modernes, incluant des récepteurs capables de faire de la détection de multiples utilisateurs (Multi-User Detection, MUD) avec de la suppression successive des interférences (Successive Interference Cancellation, SIC), est étudié en analysant le taux d'erreurs au niveau bits non codés (uncoded Bit Error Rate BER). Sans surprise, le canal satellite diffère complètement du canal de Rayleigh, bien connu et utilisé pour décrire les transmissions dans un environnement à trajets multiples tel que dans les réseaux de télécommunications terrestres. Un récepteur, basé sur une nouvelle approche pour supprimer les interférences (Interference Cancellation, IC), montre des résultats prometteurs avec le canal de Rayleigh mais n'est malheureusement pas aussi performant avec les canaux satellites soumis à des niveaux d'interférences élevés. Les récepteurs intégrant l'architecture optimale pour supprimer les interférences de façon successive, plus particulièrement ceux réalisant le calcul d'erreur par la méthode des moindres carrés (Minimum-Mean Square Error, MMSE) avec un classement optimal (optimal ordering, OO), permettent d'atteindre en théorie les meilleurs résultats. Ceci a été vérifié et confirmé à l'aide de simulations, également avec le canal satellite. Les gains en terme de débit non codé varie entre 1.5 et 2.25 pour différents ordres de modulation lorsque l'on compare le système à réutilisation de fréquence complète avec un système à trois couleurs, et en assumant une connaissance parfaite du canal au niveau récepteur (perfect Channel State Information, CSI).

En prenant en compte les résultats issus des analyses pratiques précédentes, le gain en terme de capacité, est évalué en s'orientant vers le domaine de la théorie de l'information. Plus particulièrement les débits globaux qui peuvent être atteints sont exprimés pour les systèmes à entrée et sortie unique (Single-Input Single-Output, SISO), à entrée unique et sorties multiples (Single-Input Multiple-Output, SIMO) et à entrées multiples et sorties multiples (Multiple-Input Multiple-Output, MIMO), en prenant en considération le nombre de couleurs. Ici la capacité ergodique obtenue avec un système à ré-utilisation de fréquence universelle (càd une seule couleur) est multipliée par un facteur 3 par rapport au système à trois couleurs. Le principe de la suppression successive des interférences est ensuite utilisé afin de dériver l'expression du débit pouvant être atteint au niveau utilisateur et l'impact de l'ordre (classement), avec lequel le processus de suppression des interférences est réalisé, est étudié. Dans cette thèse la maximisation du débit minimum par utilisateur est prise tout particulièrement en compte, entraînant, du fait de l'invariance du débit global MIMO à l'ordre avec lequel

les interférences sont supprimées, une amélioration du niveau d'équité entre les utilisateurs. Le meilleur classement pour atteindre ce critère max-min peut être trouvé en utilisant l'algorithme de Foschini et dans le cas du scénario satellite les gains obtenus sont de l'ordre de 30% par rapport à une suppression successive des interférences réalisée de façon non-ordonnée.

En considérant un système d'accès multiples avec une division dans le temps et à fréquences multiples (Multi-Frequency – Time-Division Multiple Access, MF-TDMA), l'allocation des ressources peut être optimisée de façon à améliorer les débits utilisateurs. Ceci peut être réalisé en modifiant la planification des ressources (ordonnancement) de sorte que les utilisateurs interférant de façon plus significative avec d'autres ne transmettent pas leurs données à la même fréquence et en même temps. Il a été montré que la modification de l'allocation des ressources n'a pas d'impact sur le débit global de l'allocation mais permet en fait d'influencer les débits utilisateurs dans chaque créneau (slot). Des algorithmes de recherche sont proposés et implémentés dans cette thèse. Une première proposition considère toutes les possibilités en terme d'allocation des ressources, qui constitue en réalité une recherche exhaustive (Exhaustive Search, ES). Une seconde proposition identifie toutes les combinaisons possibles d'utilisateurs dans chaque créneau. Pour cette dernière la théorie des graphes est utilisée, plus particulièrement une approche basée sur les graphes multipartites est prise en compte de façon à mieux représenter la distribution des ressources aux utilisateurs et aussi à réduire la complexité globale du calcul. Le critère de maximisation du débit minimum par utilisateur introduit précédemment est toujours considéré. Des algorithmes d'allocation des ressources sont ensuite conçus pour fonctionner avec des systèmes MIMO à grande échelle, tels que dans les communications satellites à faisceaux multiples. Un algorithme particulier, qui prend comme avantage le motif particulier des systèmes satellites à faisceaux multiples, offre des résultats similaires à ceux obtenus avec la recherche exhaustive, mais en réduisant considérablement la complexité. En prenant en compte le système satellite complet, qui est constitué de 96 faisceaux, cet algorithme améliore le débit minimal par utilisateur de 25% par rapport au système sans amélioration des ressources. L'impact de l'allocation optimisée des ressources, obtenue en utilisant la théorie de l'information, est ensuite analysé sur les taux d'erreurs en termes de bits non codés. A un taux de 10^{-4}, l'optimisation des ressources offre entre 4 et 7 dB de gain lorsque comparé à un système sans optimisation et en fonction de l'opération de classement réalisée par les récepteurs à suppression successive des interférences.

En utilisant tous les résultats obtenus précédemment, l'allocation des ressources est étudiée

en prenant en compte des contraintes de qualité de service (Quality of Service, QoS), telles que le débit de service, l'équité ou encore le délai. L'impact du nombre de faisceaux est tout d'abord examiné et l'effet du nombre d'utilisateurs sur les performances est étudié, représentant respectivement la taille du système et la profondeur avec laquelle l'optimisation des ressources est effectuée. De façon intéressante, mais logique, le débit minimum par utilisateur se détériore lorsque la taille du système augmente mais la tendance diminue lorsqu'un nombre de faisceaux particulier est atteint, principalement dû aux gains offerts par les multiples antennes de réception. Aussi, augmenter le nombre d'utilisateurs par faisceau qui sont pris en compte pour améliorer l'allocation des ressources permet d'augmenter le débit minimum par utilisateur mais le gain sature à un certain point, dû au nombre suffisant d'utilisateurs pour trouver une planification appropriée des ressources. Guidé par les observations précédentes, un nouvel algorithme d'allocation des ressources et qui vise à garantir un débit max-min particulier aux utilisateurs est conçu. Cet algorithme exploite les ressources disponibles dans le satellite et permet, grace à une stratégie basée sur l'allocation d'un slot vide (Free Slot Assignment, FSA), d'atteindre des performances identiques à l'algorithme précédent mais avec une profondeur plus réduite pour optimiser l'allocation des ressources. Plus particulièrement, il permet de respecter des contraintes en terme de débit au prix d'une faible perte en efficacité. Un autre algorithme innovant, basé sur le concept de fenêtres glissantes, est proposé de façon à prendre en compte les contraintes temporelles, plus particulièrement le délai introduit par le processus d'optimisation des ressources. Cela permet d'augmenter l'espace de recherche de l'ordonnanceur tout en évitant une dérive importante du temps entre la demande de ressources et l'allocation des ressources. Cet algorithme améliore le critère de maximisation du débit minimum pour des profondeurs d'allocation des ressources plus faibles au détriment d'une complexité de calcul plus importante. Finalement une combinaison des deux algorithmes est présentée. Cet algorithme hybride permet d'atteindre plus facilement la contrainte max-min du débit, tout en contrôlant la perte en efficacité et la profondeur d'allocation des ressources, et d'obtenir des résultats proches des résultats optimaux.

Les différentes recherches réalisées dans le cadre de cette thèse de doctorat sont toutes basées sur des hypothèses fortes puisque le but premier était d'évaluer les gains maximums théoriques pouvant être obtenus dans le lien retour tout en considérant le système satellite à faisceaux multiples comme un système MIMO et en optimisant l'allocation des ressources. Nous avons montré que l'utilisation d'une seule couleur et l'allocation contrôlée des ressources apportent des gains significatifs. Nous avons tout d'abord considéré des conditions de ciel dégagé (clear-

sky), une ligne de mire parfaite (perfect Line of Sight, LoS), et des terminaux satellites statiques avec des propriétés identiques. Nous avons ensuite considéré une synchronisation parfaite des terminaux satellites de façon à ce que des récepteurs MIMO puissent être pris en compte. Finalement une connaissance parfaite du canal de transmission et une passerelle virtuelle ont été pris en considération. En réalité les gains obtenus seront clairement plus bas, à cause des problèmes liés à l'implémentation en pratique de telles solutions, tous en rapport avec ces différentes suppositions. La matrice du canal ne reflétera pas les états réels du canal de transmission même si il a été montré que la valeur absolue des coefficients est suffisante pour optimiser l'allocation des ressources. Un système satellite à faisceaux multiples est généralement composé de plusieurs gateways (passerelles) ce qui implique en pratique un échange d'informations, plus particulièrement sur l'état actuel du canal et les données utilisateurs, de façon à mettre en place une collaboration. Cette collaboration est en fait nécessaire pour d'un côté optimiser l'allocation des ressources utilisateurs de manière efficace et d'un autre coté supprimer correctement les interférences. Ces hypothèses idéales ont été nécessaires de façon à comprendre de manière plus approfondie les systèmes satellites MIMO virtuels et à avoir un meilleur aperçu des gains pouvant être obtenus en optimisant l'allocation des ressources.

Comme indiqué précédemment, une connaissance parfaite de l'information sur l'état du canal (perfect Channel State Information, CSI), plus particulièrement de la valeur absolue des coefficients du canal coté réception, a été considérée. Ceci implique en pratique l'implémentation de mécanismes pour estimer l'état actuel du canal de transmission, ce qui peut être fait, par exemple, en transmettant des séquences connues d'entraînement (training sequences). En réalité la CSI sera imparfaite, ce qui entraînera une erreur pendant le calcul des débits pouvant être atteints par chaque utilisateur et par conséquent en premier lieu en optimisant l'allocation des ressources et ensuite en supprimant les interférences. La CSI imparfaite peut en fait être interprétée de plusieurs manières. Par exemple elle peut être liée aux conditions de transmission qui peuvent être influencées par l'atmosphère (pluie, nuages, etc.). Cette connaissance imparfaite peut aussi être vue comme un avantage pour de futurs travaux de façon à améliorer les algorithmes d'allocation de ressources présentés dans cette thèse et de concevoir de nouveaux algorithmes qui seraient basés sur des zones d'incertitudes. La zone couverte par un faisceau peut être sous-divisée en sous-zones dans lesquelles la même information sur l'état du canal est prise en compte et dans lesquelles les utilisateurs peuvent être regroupés puisqu'ils sont vus par le système comme ayant le même canal de transmission.

Cette stratégie implique une erreur dans l'information sur l'état du canal et, prenant cette erreur en compte, un algorithme d'allocation des ressources, basé sur des groupes d'utilisateurs, peut être conçu et devrait en principe réduire encore plus la complexité du calcul.

Bibliographie

[ABCCGD11] J. Arnau, M. Bergmann, E. .A. Candevra, G. E. Corazza, R. de Gaudenzi, B. Devillers, W. Gappmair, F. Lombardo, C. Mosquera, A. Pérez-Neira, I. Thibault, et A. Vanelli-Coralli, "Hybrid Space-Ground Processing for High-Capacity Multi-beam Satellite Systems", à *GLOBECOM*, Houston (Texas, USA), Dec. 2011.

[ADMN12] J. Arnau, B. Devillers, C. Mosquera, et A. Pérez-Neira, "Performance study of multiuser interference mitigation schemes for hybrid broadband mulibeam satellite architectures", dans *EURASIP Journal on Wireless Communications and Networking*, 132, 2012.

[AjHa05] W. Ajib, et D. Haccoun, "An overview of scheduling algorithms in MIMO-based fourth-generation wireless systems", dans *IEEE Network*, vol. 19, no. 5, pp. 43-48, Sep. 2005.

[AlMaTu10] G. Alfano, A. De Maio, et A. M. Tulino, "A Theoretical Framework for LMS MIMO Communication Systems Performance Analysis", dans *IEEE Transactions on Information Theory*, vol. 56, no. 11, pp. 5614-5630, Nov. 2010.

[ALBPCG11] P.-D. Arapoglou, K. Liolis, M. Bertinelli, A. Panagopoulos, P. Cottis, et R. De Gaudenzi, "MIMO over Satellite : A Review", dans *IEEE Communications Surveys and Tutorials*, vol. 13, no. 1, pp. 27-51, 2011.

[Bab52] W. C. Babock, "Intermodulation Interference in Radio Systems", dans *The Bell System Technical Journal*, pp. 63-73, Août 1952.

[BaCaZo08] N. Baldo, P. Casari, et M. Zorzi, "Cognitive spectrum access for underwater acoustic communications", dans *IEEE ICC*, Beijing (Chine), Mai 2008.

[BaMeLe03] J. R. Barry, D. G. Messerschmitt, et E. A. Lee, "Digital Communication", *Third Edition*, Springer, 2003.

[BBKNL07] H. Brandt, V. Boussemart, C. Kissling, C. Parraga Niebla, O. L ucke, R. Vilalta, E. Dupont, R. Schweikert, et T. W orz, "Resources Management using Adaptive Fade Mitigation Techniques in DVB-S2/RCS Multi-Beam Systems", à *ICSSC*, Seoul (Corée du Sud), Avr. 2007.

[BBRJ11] V. Boussemart, M. Berioli, F. Rossetto, et M. Joham, "On the Achievable Rates for the Return-Link of Multi-Beam Satellite Systems Using Successive Interference Cancellation", à *IEEE MILCOM*, Baltimore (MD, USA), Nov. 2011.

[BeCh02] N. Benvenuto, et G. Cherubini, "Algorithms for Communications Systems and their Applications", *First Edition*, Wiley, 2002.

[BeGaKa02] B. F. Beidas, H. El Gamal, et S. Kay, "Iterative Interference Cancellation for High Spectral Efficiency Satellite Communications", dans *IEEE Transactions on Communications*, vol. 50, no. 1, pp. 31-36, Jan. 2002.

[BoBeRo11] V. Boussemart, M. Berioli, et F. Rossetto, "User Scheduling for Large Multibeam Satellite MIMO Systems", à *ASILOMAR*, Pacific Grove (CA, USA), Nov. 2011.

[BoBr08] V. Boussemart, et H. Brandt, "A Tool for Satellite Communications", à *IWSPSC*, Rhodes Island (Grèce), Oct. 2008.

[BoBr09-1] V. Boussemart, et H. Brandt, "Performance Assessment using ACM in DVB-S2/Advanced DVB-RCS Satellite Systems", à *ICSSC*, Edinburgh (RU), Juin 2009.

[BoBr09-2] V. Boussemart, et H. Brandt, "A System Simulator for Advanced DVB-S2/RCS Multibeam Systems", à *DLRK*, Aachen (Allemagne), Sep. 2009.

[BoGr05] V. Boussemart, et O. Grémillet, "Investigation on the Self-Similarity of Web Traffic Generated by Aggregated Individual Browsers", à *ICSSC*, Rome (Italie), Sep. 2005.

[BoMaBe12-1] V. Boussemart, L. Marini, et M. Berioli, "Impact of Scheduling in the Return-Link of Multi-Beam Satellite MIMO Systems", à *GLOBECOM*, Anaheim (CA, USA), Dec. 2012.

[BoMaBe12-2] V. Boussemart, L. Marini, et M. Berioli, "Multi-Beam Satellite MIMO Systems : BER Analysis of Interference Cancellation and Scheduling", à *ASMS*, Baiona (Espagne), Sep. 2012.

[Bou05] V. Boussemart, "Investigations on Internet Traffic", *Rapport de Diplôme de Recherche Technologique (D.R.T.)*, DLR Munich (Allemagne) et Universitée de Valenciennes (France) - Ecole National Supérieure d'Ingénieurs en Informatique Automatique Mécanique énergétique Electronique (ENSIAME), Déc. 2005.

[CCFRV92] C. Caini, G. E. Corazza, G. Falciasecca, M. Ruggieri et F. Vatalaro : "A Spectrum- and Power-Efficient EHF Mobile Satellite System to be integrated with Terrestrial Cellular Systems", dans *IEEE Journal on Selected Areas in Communications*, vol. 10, no. 8, pp. 1315-1325, 1992.

[CCMO11] D. Christopoulos, S. Chatzinotas, M. Matthaiou, et B. Ottersten, "Capacity Analysis of Multibeam Joint Decoding over Composite Satellite Channels", à *ASILOMAR*, Pacific Grove (CA, USA), Nov. 2011.

[CeGa10] F. Di Cecca, et G. Gallinaro, "Cross-Polar Interference Cancellation for Earth Observation Data Downlink", à *Ka and Broadband Communications, Navigation and Earth Observation Conference*, Ka-band conf., Milan (Italie), Oct. 2010.

[ChChOt11] S. Chatzinotas, D. Christopoulos, et B. Ottersten, "Coordinated Multi-Point Decoding with Dual-polarized Antennas", dans le compte-rendu d'*IEEE IWCMC*, pp. 157-161, 2011.

[Clar45] A. C. Clarke, "Extraterrestrial Relays", dans le magazine *Wireless World*, 1945.

[Col85] R. E. Collin, "Antennas and Radiowave Propagation", *International Student Edition*, 1985.

[CoLeRi90] T. H. Cormen, C. E. Leiserson, et R. L. Rivest, "Introduction to Algorithms", *MIT Press*, Cambridge (MA, USA), 1990.

[Cou06] N. Courville, "Critical Issues of Resource Management in Geostationnary Satellite Systems with On-Board Switching", *Mémoire de Thèse de Doctorat*, DLR Munich (Allemagne) et SUPAERO Toulouse (France), Oct. 2006.

[DCMLC07] M. À. Díaz, N. Courville, C. Mosquera, G. Liva, et G. E. Corazza, "Non-Linear Interference Mitigation for Broadband Multimedia Satellite Systems", à *IWSSC*, Salzburg (Autriche), pp. 61-65, Sep. 2007.

[DGMRV06] M. Debbah, G. Gallinaro, R. M uller, R. Rinaldo, et A. Vernucci, "Interference Mitigation for the Reverse-Link of Interactive Satellite Networks", à *IWSPSC*, Noordwjik (Pays-Bas), Sep. 2006.

[DVB-RCS] Digital Video Broadcasting (DVB) : "Interaction channel for satellite distribution systems", dans *ETSI EN 301 790 V1.5.1*, European Standard (Telecommunication series), Jan. 2009.

[DVB-RCS2] Digital Video Broadcasting (DVB) : "Second Generation DVB Interactive Satellite System ; Part Lower Layers for Satellite standard", dans *DVB Document A155-2*, European Standard (Telecommunication series), Mars 2011.

[DVB-RCS2-P1] Digital Video Broadcasting (DVB) : "Second Generation DVB Interactive Satellite System (RCS2) ; Part 1 : Overview and System Level specification", dans *DVB Document A155-1*, European Standard (Telecommunication series), Mars 2011.

[DVB-S] Digital Video Broadcasting (DVB), "Framing structure, channel coding and modulation for 11/12 GHz satellite services", dans *ETSI EN 300 421 V1.1.2*, European Standard (Telecommunication series), Août 1997.

[DVB-S2] Digital Video Broadcasting (DVB) : "Second generation framing structure, channel coding and modulation systems for broadcasting, interactive services, new gathering and other broadband satellite applications", dans *ETSI EN 302 307 V1.1.2*, European Standard (Telecommunications series), Juin 2006.

[ESA-RM] Projet ESA : "Resources Management using Adaptive Fade Mitigation Techniques (FMT) in DVB-RCS Multi-Beam Systems", *Contract 18826/05/NL/US*, Jan. 2005 à Déc. 2008.

[FGVW99] G. J. Foschini, G. D. Golden, R. A. Valenzuela, et P. W. Wolniansky, "Simplified Processing for High Spectral Efficiency Wireless Communication Employing Multi-Element Arrays", dans *IEEE Journal on Selected Areas in Communications*, vol. 17, no. 11, pp. 1841-1852, Nov. 1999.

[GaVeRi07] G. Gallinaro, A. Vernucci, et R. Rinaldo, "Increasing Throughput of Wideband Satellite Systems Reverse-Link through Adjacent Channel Interference Mitigation", à *ICSSC*, Seoul (Corée), Avr. 2007.

[Gay09] J.-D. Gayrard, "Terabit Satellite : Myth or Reality", à *SPACOMM*, Colmar (France), Juil. 2009.

[GJJV03] A. Goldsmith, S. A. Jafar, N. Jindal, et S. Vishwanath, "Capacity limits of MIMO channels, dans *IEEE Journal on Selected Areas in Communications*, vol. 21, no. 5, pp. 684-702, Juin 2003.

[HeJoUt10] C. Hellings, M. Joham, et W. Utschick, "Power Minimization in Parallel Vector Broadcast Channels with Zero-Forcing Beamforming", à *GLOBECOM*, Miami (USA), Déc. 2010.

[HSBAG06] C. Antón-Haro, P. Svedman, M. Bengtsson, A. Alexiou, et A. Gameiro, "Cross-Layer Scheduling for Multi-User MIMO Systems", dans *IEEE Communications Magazine*, pp. 39-45, Sep. 2006.

[JaHaCh84] R. Jain, W. Hawe, et D. Chiu, “A quantitative measure of fairness and discrimination for resource allocation in shared computer systems”, *Digital Equipment Corporation*, Tech. Rep. DEC-TR-301, Sep. 1984.

[JiVaLi05] Y. Jiang, M. K. Varanasi, et J. Li, “Performance Analysis of ZF and MMSE Equalizers for MIMO Systems : An In-Depth Study of the High SNR Regime”, à *GLOBECOM*, St. Louis (MO, USA), Nov. 2005.

[KaViHa05] T. Kailath, H. Vikalo, et B. Hassibi, “MIMO Receive Algorithms”, dans *Space-Time Wireless Systems : From Array Processing to MIMO Communications*, Cambridge University Press, 2005.

[LeGr08] N. Letzepis, et A. Grant, “Capacity of the multiple spot beam satellite channel with rician fading”, dans *IEEE Transactions on Information Theory*, vol. 54, no. 11, pp. 5210-5222, Nov. 2008.

[LiPaAr09] K. P. Liolis, A. D. Panagopoulos, et P.-D. M. Arapoglou, “An analytical unifying approach for outage capacity achieved in SIMO and MISO broadband satellite channel configurations”, dans le compte-rendu d’*EuCAP*, pp. 2911-2915, Mars 2009.

[LPCR09] K. P. Liolis, A. D. Panagopoulos, P. G. Cottis et B. D. Rao, “On the applicability of MIMO principle to 10-66 GHz BFWA networks : capacity enhancement through spatial multiplexing and interference reduction through selection diversity”, dans *IEEE Transactions on Communications*, vol. 57, no. 2, pp. 530-541, Fév. 2009.

[LuWeJa00] E. Lutz, M. Werner, et A. Jahn, “Satellite Systems for Personal and Broadband Communications”, *First Edition*, Springer-Verlag, 2000.

[MaBo02] G. Maral, et M. Bousquet, “Satellite Communications Systems”, *Fourth Edition*, Wiley, 2002.

[Mar12] L. Marini, “Investigations on the Return-Link of Interference-Limited Multi-Beam Satellite Systems”, *Rapport de Master*, DLR Munich (Allemagne) et Université de Rome (Italie) Tor Vergata, Avr. 2012.

[MBBD07] J. P. Millerioux, M. L. Boucheret, C. Bazile et A. Ducasse, “Iterative interference cancellation and channel estimation in multibeam satellite systems”, dans *International Journal of Satellite Communications and Networking*, Wiley, vol. 25, no. 3, pp. 263-283, Mars 2007.

[MEGAAH11] D. Mignolo, R. Emiliano, A. Ginesi, A. B. Alamanac, P. Angeletti, et M. Harverson, “Approaching Terabit/s Satellite Capacity : A System Analysis”, à *Ka Broadband Conference*, Oct. 2011.

[NISIM05] "Novel Intra-System Interference Mitigation Techniques & Technologies for Next Generations Broadband Satellite Systems", *Rapport Final*, ESTEC Contract No. 18070/04/NL/US, 2005.

[Ogu83] T. Oguchi, "Electromagnetic Wave Propagation and Scattering in Rain and Other Hydrometeors", dans le compte-rendu d'*IEEE*, vol. 71, no. 9, pp. 1029-1079, Sep. 1983.

[PoBeBa09] M. Poggioni, M. Berioli et P. Banelli, "BER Performance of Multibeam Satellite Systems with Tomlinson Harashima Precoding", à *ICC*, Dresden (Allemagne), Juin 2009.

[Pro00] J. Proakis, "Digital Communications", *Fourth Edition*, McGraw-Hill Science, 2000.

[RaLiTa98] F. Rashid-Farrokhi, K. J. R. Liu, et L. Tassiulas, "Transmit beamforming and power control for cellular wireless systems", dans *IEEE Journal on Selected Areas in Communications*, vol. 16, no. 8, pp. 1437-1449, Oct. 1998.

[RyLi09] W. E. Ryan, et S. Lin, "Channel Codes - Classical and Modern", *First Edition*, Cambridge University Press, 2009.

[Sha49] C. E. Shannon, "Communication in the Presence of Noise", dans le compte-rendu de l'*Institute of Radio Engineers*, vol. 37, pp. 10-21, Jan. 1949.

[SSBHU09] D. A. Schmidt, C. Shi, R. A. Berry, M. L. Honig, et W. Utschick, "Distributed Resource Allocation Schemes", dans *IEEE Signal Processing Magazine*, vol. 26, no. 5, pp. 53-63, Sep. 2009.

[Tel99] E. Telatar, "Capacity of multi-antenna gaussian channels", dans *European Transactions on Telecommunications*, vol. 10, no. 6, pp. 585-596, 1999.

[TsVi08] D. Tse, et P. Viswanath, "Fundamentals of Wireless Communication", *University Press*, Fourth printing edition, Cambridge, 2008.

[VaGu97] M. K. Varanasi, et T. Guess, "Optimal decision feedback multiuser equalization with successive decoding achieves the total capacity of the gaussian multiple-access channel", dans le compte-rendu d'*ASILOMAR*, pp. 1405-1409, Nov. 1997.

[Vas00] H. Vasseur, "Degradation of Availability Performance in Dual-Polarized Satellite Communications Systems", dans *IEEE Transactions on Communications*, vol. 48, no. 3, pp. 465-472, Mars 2000.

[WuMi06] G. Wunder, et T. Michel, "Minimum Rates Scheduling for MIMO OFDM Broadcast Channels", dans le compte-rendu d'*IEEE International Symposium on Spread Spectrum Techniques and Applications*, Manaus (Brésil), Août 2006.

[YFVG11] T. Yoo, G. Foschini, R. Valenzuela, et A. Goldsmith, “Common rate support in multi-antenna downlink channels using semi-orthogonal user selection”, dans *IEEE Transactions on Information Theory*, vol. 57, no. 6, pp. 3449-3461, Juin 2011.

[YiLi02] H. Yin, et H. Liu, “Performance of Space-Division Multiple-Access (SDMA) with Scheduling”, dans *IEEE Transactions on Wireless Communincations*, vol. 3, no. 4, pp. 611-618, Oct. 2002.

[YoGo06] T. Yoo, et A. Goldsmith, “On the optimality of multiantenna broadcast scheduling using zero-forcing beamforming”, dans *IEEE Journal on Selected Areas in Communications*, vol. 24, no. 3, pp. 528-541, Mars 2006.

[ZCO11-1] G. Zheng, S. Chatzinotas, et B. Ottersten, “Generic Optimization of Linear Precoding in Multibeam Satellite Systems”, *CoRR*, vol. abs/1109.0681, 2011.

[ZCO11-2] G. Zheng, S. Chatzinotas, et B. Ottersten, “Multi-Gateway Cooperation in Multibeam Satellite Systems”, *CoRR*, vol. abs/1111.7094, 2011.

Annexe A

Acronymes and Notations

A.1 Acronymes

ACI Adjacent-Channel Interference

ACM Adaptive Coding and Modulation

AVBDC Absolute Volume-Based Dynamic Capacity

AWGN Additive White Gaussian Noise

BC Broadcast Channel

BCH Bose, Chaudhuri, and Hocquenghem

BER Bit Error Rate

BG B-partite Graph

BPSK Binary Phase-Shift Keying

BS Base Station

CCI Co-Channel Interference

CCM Constant Coding and Modulation

CDF Cumulative Density Function

CIR Carrier-to-Interference Ratio

CNR Carrier-to-Noise Ratio

COIN Communications in Interference-Limited Networks

CPCI Cross-Polarisation Channel Interference

CRA Constant Rate Assignment

CSI Channel State Information

DL Down-Link

DLR Deutsches Zentrum für Luft- und Raumfahrt

DPC Dirty Paper Coding

DRA Dynamic Rate Assignment

DSL Digital Subscriber Line

DVB-RCS Digital Video Broadcasting - Return Channel via Satellite

DVB-RCS2 Digital Video Broadcasting - Return Channel via Satellite version 2

DVB-S Digital Video Broadcasting via Satellite

DVB-S2 Digital Video Broadcasting via Satellite version 2

D.R.T. Diplôme de Recherche Technologique

EIRP Effective Isotropic Radiated Power

ENSIAME Ecole National Supérieure d'Ingénieurs en Informatique Automatique Mécanique énergétique Electronique

ER Error Rate

ES Exhaustive Search

ETSI European Telecommunications Standards Institute

FDL Forward Down-Link

FDM Frequency-Division Multiplexing

FL Forward-Link

FMT Fade Mitigation Technique

FSA Free Slot Assignment

FSL Free Space Loss

FUL Forward Up-Link

GEO Geostationary

GL Geo-Like algorithm

HPA High-Power Amplifier

I In-phase

IBO Input Back-Off

IC Interference Cancellation

ID Identifier

IEEE Institute of Electrical and Electronics Engineers

IMI Inter-Modulation Interference

IO Input-Output

IQ In-phase and Quadrature

ISAE Institut Supérieur de l'Aéronautique et de l'Espace

ISI Inter-Symbol Interference

IT Information Theory

i.i.d. independent and identically distributed

LDPC Low Density Parity Check Code

LEO Low Earth Orbit

LNA Low-Noise Amplifier

LoS Line-of-Sight

MAC Multiple Access Channel

MEO Medium Earth Orbit

MF-TDMA Multi-Frequency Time-Division Multiple Access

MIMO Multiple-Input and Multiple-Output

MIMO BC MIMO Broadcast Channel

MIMO MAC MIMO Multiple Access Channel

MISO Multiple-Input and Single-Output

MMSE Minimum Mean Square Error

ModCod Modulation and Coding

MRC Maximal Ratio Combining

MUD Multi-User Detection

MUT Mobile User Terminal

NCC Network Control Centre

NF Noise Figure

OBO Output Back-Off

OO Optimal Ordering

PAM Pulse Amplitude Modulation

PDF Probability Density Function

PER Packet Error Rate

Ph.D. Philosophiae Doctor

PSK Phase-Shift Keying

Q Quadrature

QoS Quality of Service

QPSK Quadrature Phase-Shift Keying

RBDC Rate-Based Dynamic Capacity

RDL Return Down-Link

RL Return-Link

RRM Radio Resource Management

RTT Round-Trip-Time

RUL Return Up-Link

SER Symbol Error Rate

SIC Successive Interference Cancellation

SIMO Single-Input and Multiple-Output

SINR Signal-to-Interference-plus-Noise Ratio

SISO Single-Input and Single-Output

SNIR Signal-to-Noise plus Interference Ratio

SNR Signal-to-Noise Ratio

ST Satellite Terminal

SUPAERO école nationale SUPérieure de l'AEROnautique et de l'espace

TBTP Terminal Burst Time Plan

TBTP2 Terminal Burst Time Plan version 2

TCP Transmission Control Protocol

TDM Time-Division Multiplexing

THP Tomlinson-Harashima Precoding

TUM Technische Universität München

TWTA Travelling Wave Tube Amplifier

UPC Up-link Power Control

UL Up-Link

UT User Terminal

VBDC Volume-Based Dynamic Capacity

VL Viterbi-Like algorithm

XPI Cross-Polarisation Interference

ZF Zero Forcing

A.2 Notations

A.2.1 Scalaires, Vecteurs et Matrices

- $\mathcal{N}\left(\mu, \sigma^2\right)$: variable Gaussienne avec valeur moyenne μ et variance σ^2
- $\mathcal{CN}\left(0, \sigma^2\right)$: variable Gaussienne complexe symétrique circulaire avec partie réelle et imaginaire $\mathcal{N}\left(0, \sigma^2/2\right)$ (i.i.d.)
- Vecteurs et matrices sont représentés par des caractères gras en minuscule et en majuscule, respectivement (par ex. $\boldsymbol{a}$ et $\boldsymbol{A}$)
- Element i du vecteur $\boldsymbol{a}$: a_i
- Element à la ligne i - colonne j de la matrice $\boldsymbol{A}$: $a_{i,j}$
- Vecteur colonne i de la matrice $\boldsymbol{A}$: $\boldsymbol{a}_i$
- Toutes les lignes, colonnes i à j de $\boldsymbol{A}$: $\boldsymbol{A}_{:,i:j}$

A.2.2 Opérateurs

- $|a_{i,j}|$: norme de $a_{i,j}$
- $\text{diag}\{a_1, a_2, \cdots, a_N\}$: matrice diagonale avec éléments a_1, a_2, ..., a_N
- $\boldsymbol{A}^{\mathrm{T}}$: transposée de la matrice $\boldsymbol{A}$
- $\boldsymbol{A}^*$: conjugué de la matrice $\boldsymbol{A}$
- $\boldsymbol{A}^{\mathrm{H}}$: Hermitien de la matrice $\boldsymbol{A}$ (transpose-conjugé)

A.2.3 Liste des Variables

Voir la partie A.2.3 du rapport de thèse rédigé en anglais.

Annexe B

Bases Mathématiques Utiles

Voir l'annexe B du rapport de thèse rédigé en anglais.

Annexe C

Bases Utiles sur les Communications et les Satellites

Cet annexe vise à fournir un contenu additionnel à la thèse de doctorat et est organisé selon la structure principal du document.

C.1 Satellite

Voir la partie C.1 du rapport de thèse rédigé en anglais.

C.2 Taux d'Erreurs Niveau Bit non Codé

Voir la partie C.2 du rapport de thèse rédigé en anglais.

C.3 Débit Atteignable

Voir la partie C.3 du rapport de thèse rédigé en anglais.

C.4 Ordonnancement

Voir la partie C.4 du rapport de thèse rédigé en anglais.

Annexe D

Informations Additionnelles

D.1 Liste des Publications, Brevets, et Autre(s)

Cette section résume les résultats de la thèse de doctorat, plus particulièrement les différents articles soumis à des conférences et journal, la participation à des workshops, école d'été, et les brevets déposés.

D.1.1 Article(s) de Conférences et Journal

[BBRJ11] : V. Boussemart, M. Berioli, F. Rossetto, et M. Joham, "On the Achievable Rates for the Return-Link of Multi-Beam Satellite Systems Using Successive Interference Cancellation", à *IEEE MILCOM*, Baltimore (MD, USA), Nov. 2011.
Status : *soumis, accepté et présenté.*

[BoBeRo11] : V. Boussemart, M. Berioli, et F. Rossetto, "User Scheduling for Large Multi-beam Satellite MIMO Systems", à *ASILOMAR*, Pacific Grove (CA, USA), Nov. 2011.
Status : *soumis, accepté et présenté.*

[BoMaBe12-1] : V. Boussemart, L. Marini, et M. Berioli, "Impact of Scheduling in the Return-Link of Multi-Beam Satellite MIMO Systems", à *GLOBECOM*, Anaheim (CA, USA), Déc. 2012.
Status : *soumis, accepté et présenté.*

[BoMaBe12-2] : V. Boussemart, L. Marini, et M. Berioli, "Multi-Beam Satellite MIMO Systems : BER Analysis of Interference Cancellation and Scheduling", à *ASMS*, Baiona (Es-

pagne), Sep. 2012.
Status : *soumis, accepté et présenté.*

[BoBe12] : V. Boussemart, et M. Berioli, "Scheduling in Virtual MIMO Multi-Beam Satellite Systems", dans *IEEE Journal on Selected Areas in Communications - Virtual MIMO (IEEE JSAC SI on Virtual MIMO)*, soumis le 15 octobre 2012.
Status : *soumis.*

D.1.2 Workshops, École d'Été et Autre(s)

L'auteur a donné les présentation suivantes dans le cadre de différents workshops, école d'été et autres événements, qui lui ont permis de décrire son travail et de recevoir des commentaires :
- Présentation du sujet de la thèse de doctorat et status au workshop du département à Munich (Allemagne), du 11 au 12 octobre 2010,
- Workshop Communications in Interference-Limited Networks (COIN) à Munich (Allemagne), du 12 au 13 octobre 2010,
- Présentation sur les communications satellites à large bande à la Technische Universität München (TUM), le 18 décembre 2010,
- Workshop COIN à Dresden (Allemagne), du 31 mai au 1 juin 2011,
- 2012 European School of Information Theory, IEEE Information Theory Society, à Antalya (Turquie), du 16 au 20 avril 2012.

D.1.3 Brevet(s)

L'auteur a déposé les brevets suivants dans le cadre de la thèse de doctorat :
- "Smart Free Slot Assignment Scheduling Algorithm for Interference-Limited Networks", Deutsche Patentanmeldung DE 10 2012 213 755.6, mai 2012,
- "Advanced Window Scheduling Algorithm for Interference-Limited Networks", Deutsche Patentanmeldung DE 10 2013 206 847.6, octobre 2012.